

Archaeological Chemistry—III

Publication Date: January 1, 1984 | doi: 10.1021/ba-1984-0205.fw001

In Archaeological Chemistry—III; Lambert, J.;
Advances in Chemistry; American Chemical Society: Washington, DC, 1984.

Publication Date: January 1, 1984 | doi: 10.1021/ba-1984-0205.fw001

ADVANCES IN CHEMISTRY SERIES **205**

Archaeological Chemistry—III

Joseph B. Lambert, EDITOR
Northwestern University

Based on a symposium sponsored by
the Division of the History of Chemistry
at the 184th Meeting
of the American Chemical Society,
Kansas City Missouri,
September 12–17, 1982

Publication Date: January 1, 1984 | doi: 10.1021/ba-1984-0205.fw001



American Chemical Society, Washington, D.C. 1984

In Archaeological Chemistry—III; Lambert, J.;
Advances in Chemistry; American Chemical Society: Washington, DC, 1984.



Library of Congress Cataloging in Publication Data

Archaeological chemistry—III.

(Advances in chemistry series 0065-2393; 205)

“Based on a symposium sponsored by the Division of the History of Chemistry at the 184th Meeting of the American Chemical Society, Kansas City, Missouri, September 12-17, 1982.”

“Seventh Symposium on Archaeological Chemistry”—Pref.

Includes bibliographies and index.

1. Archaeological chemistry—Congresses.

I. Lambert, Joseph B. II. American Chemical Society. Division of the History of Chemistry. III. American Chemical Society. Meeting (184th: 1982: Kansas City, Mo.) VI. Symposium on Archaeological Chemistry (7th: 1982: Kansas City, Mo.) V. Series.

QD1.A355 no. 205 [CC79.C5]
540s [930.1'028'5] 83-15736
ISBN 0-8412-0767-4

Copyright © 1984

American Chemical Society

All Rights Reserved. The appearance of the code at the bottom of the first page of each chapter in this volume indicates the copyright owner's consent that reprographic copies of the chapter may be made for personal or internal use or for the personal or internal use of specific clients. This consent is given on the condition, however, that the copier pay the stated per copy fee through the Copyright Clearance Center, Inc. for copying beyond that permitted by Sections 107 or 108 of the U.S. Copyright Law. This consent does not extend to copying or transmission by any means—graphic or electronic—for any other purpose, such as for general distribution, for advertising or promotional purposes, for creating a new collective work, for resale, or for information storage and retrieval systems. The copying fee for each chapter is indicated in the code at the bottom of the first page of the chapter.

The citation of trade names and/or names of manufacturers in this publication is not to be construed as an endorsement or as approval by ACS of the commercial products or services referenced herein; nor should the mere reference herein to any drawing, specification, chemical process, or other data be regarded as a license or as a conveyance of any right or permission, to the holder, reader, or any other person or corporation, to manufacture, reproduce, use, or sell any patented invention or copyrighted work that may in any way be related thereto. Registered names, trademarks, etc., used in this publication, even without specific indication thereof, are not to be considered unprotected by law.

PRINTED IN THE UNITED STATES OF AMERICA

**American Chemical
Society Library**

1155 16th St., N.W.

Washington, D.C. 20036

In Archaeological Chemistry—III: Lambert, J.
Advances in Chemistry; American Chemical Society: Washington, DC, 1984.

Advances in Chemistry Series

M. Joan Comstock, *Series Editor*

Advisory Board

Robert Baker
U.S. Geological Survey

Martin L. Gorbaty
Exxon Research and Engineering Co.

Herbert D. Kaesz
University of California—Los Angeles

Rudolph J. Marcus
Office of Naval Research

Marvin Margoshes
Technicon Instruments Corporation

Donald E. Moreland
USDA, Agricultural Research Service

W. H. Norton
J. T. Baker Chemical Company

Robert Ory
USDA, Southern Regional
Research Center

Geoffrey D. Parfitt
Carnegie-Mellon University

Theodore Provder
Glidden Coatings and Resins

James C. Randall
Phillips Petroleum Company

Charles N. Satterfield
Massachusetts Institute of Technology

Dennis Schuetzle
Ford Motor Company
Research Laboratory

Davis L. Temple, Jr.
Mead Johnson

Charles S. Tuesday
General Motors Research Laboratory

C. Grant Willson
IBM Research Department

FOREWORD

ADVANCES IN CHEMISTRY SERIES was founded in 1949 by the American Chemical Society as an outlet for symposia and collections of data in special areas of topical interest that could not be accommodated in the Society's journals. It provides a medium for symposia that would otherwise be fragmented, their papers distributed among several journals or not published at all. Papers are reviewed critically according to ACS editorial standards and receive the careful attention and processing characteristic of ACS publications. Volumes in the **ADVANCES IN CHEMISTRY SERIES** maintain the integrity of the symposia on which they are based; however, verbatim reproductions of previously published papers are not accepted. Papers may include reports of research as well as reviews since symposia may embrace both types of presentation.

ABOUT THE EDITOR

JOSEPH B. LAMBERT is Professor of Chemistry at Northwestern University, Evanston, Illinois. He was born in Fort Sheridan, Illinois, and grew up in San Antonio, Texas. He received his undergraduate education at Yale University (B.S., 1962) and carried out his graduate studies at the California Institute of Technology (Ph.D., 1965). In 1965, he returned to Illinois to begin his work at Northwestern. His research has been divided among the areas of nuclear magnetic resonance, conformational analysis, organic reaction mechanisms, and archaeological chemistry.



The editor has been an Alfred P. Sloan Foundation Fellow (1968–1970), a Guggenheim Fellow (1973), and a Fellow of the Japan Society for the Promotion of Science (1978). He was awarded the National Fresenius Award in 1976 and was elected a Fellow of the American Association for the Advancement of Science in 1981. He has been the author of four books, one ACS audio course, and over 180 publications in scientific journals. He has served on the editorial boards of *Organic Magnetic Resonance*, *Arts and Sciences*, and *International X-Ray Emission Spectrometry*. He is immediate past chairman of the ACS Subdivision of Archaeological Chemistry.

PREFACE

ARCHAEOLOGICAL CHEMISTS subject artifacts and other materials from Archaeological or art historical sources to the scrutiny of modern instrumental analysis. Workers in this field find these investigations always intensely interesting, seldom financially remunerative, and sometimes archaeologically useful. We have been organized in the United States as a Subdivision of the American Chemical Society since the Sixth Symposium, held in Chicago in 1977. We met for the Seventh Symposium in Kansas City, September 14–15, 1982. The papers presented at this Symposium form the basis for the chapters in this volume. They comprise a representative cross section of current activities of chemists and of scientists in related fields on behalf of archaeology and art history.

The workhorses of analytical chemistry (atomic absorption, x-ray fluorescence, and neutron activation analyses) continue to provide mainstream contributions to our understanding of pottery, glass, metal, and stone artifacts. Stronger attention is now also directed to archaeological soils, to bone and shell, to inks and pigments, and to organic materials such as gums, lacquers, and textiles.

Advances in chemical instrumentation make possible entirely new applications to archaeology, although the marketplace must demonstrate whether these developments are as much of use to the archaeologist as they are of interest to the chemist. This volume, for example, describes initial applications of Auger spectroscopy and of particle accelerators, respectively, for dating inks and for dating small samples of carbonaceous material. Instrumental advances, both for separation and analysis, have made organic materials more tractable, and applications described in this volume include gums, lacquers, and a shroud. Chemical analysis continues to provide key data on the subject of provenance and trade routes, illustrated herein with soapstone, obsidian, native copper, majolica, and Maya ceramics. Finally, chemical analysis provides the archaeologist or art historian with a fuller characterization of materials, whether they be human bone, medieval stained glass, Egyptian Blue, Roman coins, or textile fabric pseudomorphs, all of which are examined in this volume.

The Seventh Symposium on Archaeological Chemistry was supported by the donors of the Petroleum Research Fund, administered by the American Chemical Society.

JOSEPH B. LAMBERT
Northwestern University
Evanston, Illinois

December 1982

Use of Rare Earth Element Analysis to Study the Utilization and Procurement of Soapstone Along the Labrador Coast

RALPH ALLEN and HANY HAMROUSH

University of Virginia, Department of Chemistry, Charlottesville, VA 22901

CHRISTOPHER NAGLE

Brandeis University, Anthropology Department, Waltham, MA 02254

WILLIAM FITZHUGH

Smithsonian Institution, Anthropology Department, Washington, DC 20560

Neutron activation analysis provides the necessary sensitivity and accuracy to measure rare earth element (REE) concentrations in soapstone even when geochemical processes have left the soapstone very depleted in trace elements. The types of variation in REE concentrations expected from a single geological source were studied at the Fleur de Lys quarry in Newfoundland. Although the absolute concentrations varied, the chondrite-normalized distribution patterns remained parallel. Analysis of debitage indicates that most materials worked were from nearby outcrops, but there was some working of soapstone from more distant quarries. Artifacts representing various Eskimo and Indian cultures over the past 4000 years have been analyzed and many have been matched to geological outcrops on the basis of their REE patterns.

DESPITE ITS HARSH ARCTIC AND SUBARCTIC CLIMATE, the coast of present-day Labrador has been the home of peoples from several cultural traditions for over 7000 years. Most of the archaeological evidence—the tools and implements left by the prehistoric inhabitants of this area—consists of a variety of lithic (rock) artifacts. The variety of naturally occurring lithic materials utilized indicates that these prehistoric peoples were keen observers of their environment. As in many other parts of the world, the Indian and Eskimo peoples along the Labrador coast found and used the relatively soft, carvable soapstone. Soapstone is a hydrous

0065-2393/84/0205-0003\$06.00/0

© 1984 American Chemical Society

magnesium silicate containing the mineral talc and varying amounts of other minerals including chlorite and carbonate minerals. Soapstone deposits originated during episodes of regional or contact metamorphism and are thus found associated with mountainous areas. Although soapstone exposures or outcrops are not uncommon in certain types of terrain, these outcrops are often relatively small and may be difficult to identify. In late Maritime Archaic times (~ 4000 B.P.), these soapstone outcrops were identified and the soft rock was carved into plummets (1). During the Paleo-Eskimo and Neo-Eskimo times (after 4000 B.P.), this material became even more important as a resource when it was fashioned into a variety of lamps and cooking pots. Later, soapstone became (and remains) an important artistic medium for the Eskimo or Inuit.

Soapstone's unique properties are a result of the plate-like crystal structures of the talc and other minerals. These minerals are formed during the metamorphic alteration of several types of ultrabasic or sedimentary rocks. The geochemical process is a complex one, but previous work has indicated that the trace element contents are determined by the metamorphic process (2). The possibility of a unique set of trace element concentrations for each region where soapstone was formed makes this useful natural resource an attractive material for archaeologists to study. By identifying and characterizing the soapstone from outcrops that were used by prehistoric peoples, the archaeologist may be able to determine the source of soapstone artifacts found at habitation sites far from the outcrop. The fact that there are soapstone deposits scattered along the entire Labrador coast makes the study of soapstone procurement and utilization particularly interesting. Soapstone is certainly not a common type of rock and requires some effort to find; however, it was certainly more readily available to the prehistoric inhabitants of Labrador than was the Ramah chert that was used for chipped stone tools (1). Ramah chert from a single relatively localized source area makes up over 99% of the chipped stone from Dorset Paleo-Eskimo assemblages from the northern tip of Labrador to the areas south of Hopedale (Figure 1). This type of lithic material shows that there must have existed effective mechanisms for the dispersal of chert over long distances. The mechanism for resource procurement and dispersal is unknown, but the patterns in the dispersal of a more readily obtainable material like soapstone may help us understand this mechanism. The appearance of soapstone from nonlocal sources suggests population movements or group interactions. If interactions are the explanation, soapstone links two points in a network.

To show that a soapstone artifact originated from a particular outcrop, the trace element contents of the artifact must match the material from the outcrop. Like most naturally occurring materials, soapstone is some-

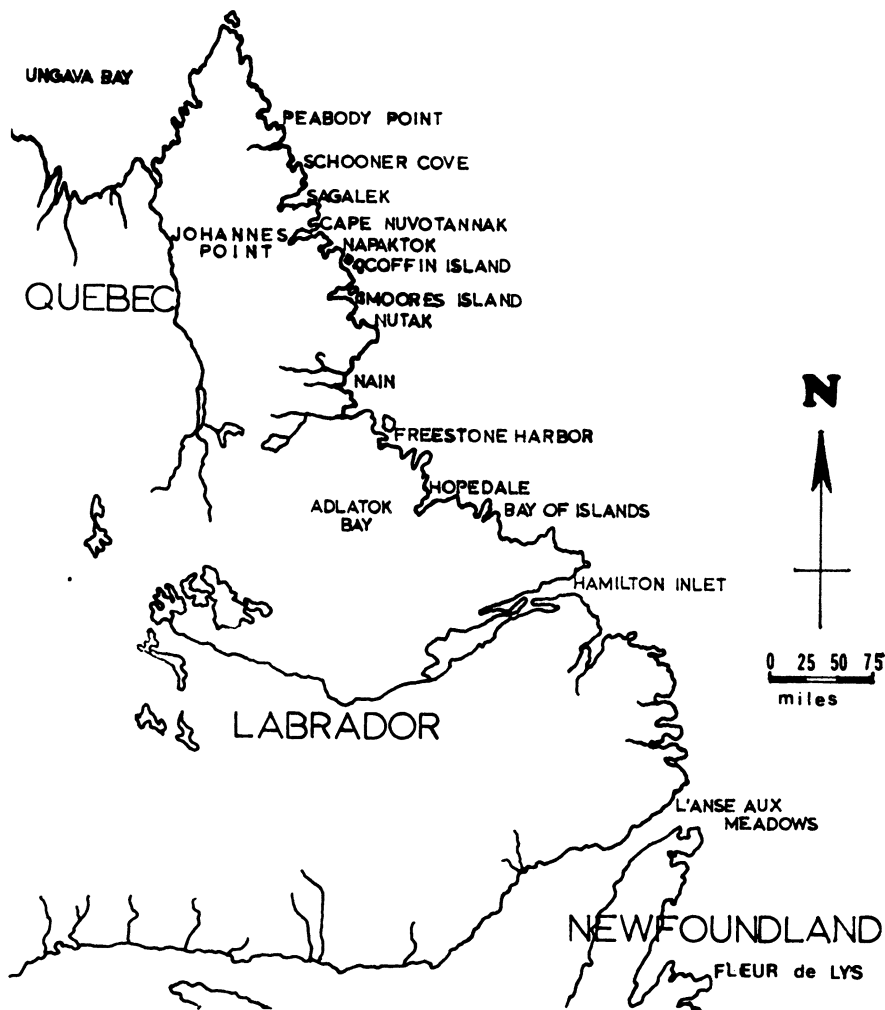


Figure 1. Map of Labrador coast and northern Newfoundland showing some of the soapstone outcrops and archaeological sites studied.

what inhomogeneous; therefore, a particular soapstone outcrop requires extensive sampling to determine the variability of the trace element contents for the material from a single geological formation. This type of extensive sampling was carried out for several soapstone outcrops in Labrador, including the best known aboriginal quarry in the region, located near Fleur de Lys in northern Newfoundland. The analysis of these samples helps to establish the variability expected for an outcrop and eliminates the uncertainty in matching artifacts with a particular quarry.

Background and Sampling

In Labrador, true prehistoric soapstone quarries—as opposed to geological outcrops—where clear evidence of mining or other extractive activities is preserved, have proved to be rather difficult to locate. An exception is the well-documented Fleur de Lys quarry, where Dorset Paleo-Eskimos apparently worked the deposits for many years (3). Quarried zones are found in two discrete localities, referenced as Localities 1 and 2, which are located about 0.5 km apart. The most intensively worked location (Locality 1) consists of a discontinuous series of areas where soapstone was removed, spaced over a distance of 200 m. Preliminary calculations based on the number of preform removal scars and unfinished preforms suggest that material for a minimum of 1000–2000 vessels was mined from this locality alone during the period of time that it was being quarried.

A total of 26 samples from locality 1 and 4 samples from locality 2 were selected for analysis to investigate intrasource variability in trace element content. Several other quarries along the Labrador coast, whose locations are shown in Figure 1, were sampled extensively. These samples include 16 from the Peabody Point (Seven Islands Bay area), 12 from a Coffin Island outcrop, 25 from Cape Nuvotannak, and 28 from the Bay of Islands. In addition, a total of over 20 other outcrops were sampled, including several outcrops in the Ungava Bay area. In some cases, only a few samples were obtained from a particular region. All outcrop samples were selected to be physically soft enough to have been material that could have been used during prehistoric times.

In addition to outcrop and quarry samples, we have analyzed debitage, preforms, and finished vessels to test the hypothesis that manufacturing took place in the proximity of the outcrops where the soapstone was obtained. Intuitively, this seemed logical, and evidence that Dorset (Paleo-Eskimo) sites near known outcrops contained substantial quantities of debitage and preform fragments bolstered this assumption. Trace element analysis of these materials and the nearby outcrops allowed this assumption to be tested. The most extensive test was for samples from Komaktorvik and other archaeological sites in the Peabody Point region. A total of 67 debitage samples and 16 preform fragments were analyzed from various sites in the Peabody Point area. In addition, 49 artifacts (cooking pots and lamps) were analyzed.

Over 650 soapstone samples from the Labrador region have now been analyzed. Of these, 400 samples are artifacts from a large number of different sites. The archaeological sites represent an extensive spatial distribution, but they also come from sites representing the different cultural traditions that span over 4000 years of human activity along the Labrador coast. The detailed discussion of these artifacts is not the subject

of this chapter, but our analysis has included artifacts from Maritime Archaic; Early, Middle, and Late Dorset; Thule, or Labrador Eskimo sites.

Materials and Methods

All samples were analyzed by instrumental neutron activation analysis (INAA) following procedures described previously (2,4). Because the rare earth elements (REEs) have proved to be most useful in characterizing the soapstone from the different quarries (5), the analysis was optimized for the measurement of these elements. Following a 2-h irradiation, with a flux of $\sim 2 \times 10^{12}$ neutrons $\text{cm}^{-2} \text{s}^{-1}$, the soapstone samples (0.3–0.7 g) were transferred to new counting vials for radioassay. The radioactivity was measured once with solid state Ge (Li) detectors 4–10 days after irradiation. The length of the count was determined by the activity of the ^{140}La , ^{153}Sm , ^{169}Yb , and ^{170}Lu that were being measured. In a second measurement, 40–50 days after the irradiation, ^{141}Ce , ^{152}Eu , ^{153}Gd , ^{160}Tb , ^{169}Yb , and ^{170}Yb were measured. Other long-lived radionuclides, such as ^{59}Fe , ^{46}Sc , ^{60}Co , and ^{51}Cr were measured at both times. In most cases, concentrations were determined by comparison to a soapstone standard prepared and analyzed in our laboratory. In some cases, other U.S. Geological Survey standard rocks (e.g., BCR-1) were also run as a cross check on the soapstone standard.

Results, including a measurement of the uncertainty due to counting statistics, were calculated, stored, and displayed with laboratory microcomputers.

The data display of particular interest is the normalized REE distribution pattern. The concentration of the particular REE is normalized by dividing it by the average concentration of that element found in chondritic meteorites. The geochemist assumes that the REE concentrations in chondritic meteorites represent undifferentiated primordial material. During the history of the earth, the REE and other elements have been partially separated from each other by geochemical processes on the basis of the charge and size of the ion (Goldschmidt's rule). In these natural processes, the REEs are normally all 3+ ions, so separations are the result of the decrease in ionic size (lanthanide contraction) with atomic number. The one exception is europium, which can be partially reduced to the 2+ ionic state during geochemical processes; this rare earth element behaves anomalously. In most studies of geochemistry of REE, the normalized concentrations have been plotted with the more convenient atomic number as the abscissa because the reciprocals of the rare earth element ionic radii are a linear function of atomic number (6). Although all 3+ ions (including scandium) could be plotted if ionic radii were used (e.g., Ref. 7), this chapter is concerned primarily with the REE. In the case of soapstone, the distribution of the concentrations of REE depends upon the metamorphic conditions as well as the original concentrations of REEs in the particular rocks being altered. Thus the distribution patterns of REE in soapstone show a great deal of variation among the different geological regions where the material is formed (5).

The key features in a normalized REE distribution plot are (1) the absolute magnitude of the concentrations; (2) the differentiation of the lighter REEs from each other in going from the radius of La^{3+} (1.14 Å) to Sm^{3+} (1.00 Å); (3) the differentiation of the heavier REEs as the size decreases from Gd^{3+} (0.97 Å) to Lu^{3+} (0.85 Å); and (4) the difference between the europium concentration measured and that predicted by a smooth variation in normalized concentrations between samarium and gadolinium. Because the REE distribution curves are

smooth functions of atomic number (or size), the essential features of the curve can be determined by accurate measurements of lanthanum, samarium, europium, gadolinium, and lutetium. We are fortunate that these elements are the ones where INAA data are the most precise, although at extremely low concentrations, the gadolinium measurements are subject to some analytical error owing to spectral interferences. These elements, where the results are most precise, were used to calculate five parameters that were used to describe the general features of the REE distribution plot. These parameters were (1) normalized lanthanum concentration; (2) normalized lutetium concentration; (3) slope, on a semilog plot, from lanthanum to samarium; (4) slope, on a semilog plot, from gadolinium to lutetium; and (5) the difference between the log of the measured europium concentration and that obtained by extrapolating between samarium and gadolinium on a semilog plot. These parameters as well as the concentrations of iron, scandium, cobalt, and chromium were evaluated using ARTHUR, a series of programs designed for pattern recognition and statistical algorithm development (8).

Results

The accuracy of the matching of artifacts to quarries depends upon the accuracy of the raw data, the variations in REE concentration within a geological formation or outcrop, and the uniqueness of the REE distribution pattern associated with each quarry. For soapstone from the Labrador area, the REE concentrations were often at or below the levels found in chondritic meteorites; these low concentrations are near the sensitivity limit for the INAA procedures utilized. The uncertainty in the analysis is based upon the counting statistics (Table I). In Figure 2 the results of the analysis of two typical soapstone samples from Labrador are shown normalized to chondritic meteorites. The standard deviation ($\pm 1\sigma$) due to counting statistics is indicated by the error bars for each element. It is clear from these results that at low concentrations the uncertainty in the analytical data must be considered in matching patterns. By focusing on the importance of the REE distribution pattern, the analytical uncertainty of a single element is not as critical. For the iron, cobalt, and scandium concentrations, the analytical uncertainties are generally less than $\pm 3\%$.

Previous work had indicated that the variations of REE contents within an outcrop were less than those between outcrops (4); this conclusion required further testing for the Labrador quarries. The large Fleur de Lys quarry offered an excellent opportunity for this study. Figure 3 shows the REE patterns typical of Fleur de Lys quarry. Over half of the samples are parallel to and fall between curves 1 and 2. Although this pattern is characteristic of the soapstone in this formation, the pattern shown by curve 3 is typical of the samples found at locality 2 and one worked area (B) at locality 1. The difference between these similar types of REE patterns is in the size of the europium anomaly. In early studies, this kind of difference between soapstone samples from

Table I. Some Representative INAA Data for Soapstone Outcrops Along Labrador Coast

Outcrop Sample	La (Norm.) ^a	Sm (Norm.) ^a	Eu (Norm.) ^a	Gd (Norm.) ^a	Lu (Norm.) ^a	Sc (ppm)	Co (ppm)	Fe ₂ O ₃ (%)
Saglek ^b	0.11	0.032	0.04	0.03	0.08	0.46	76.6	4.40
± σ ^c	(0.03)	(0.004)	(0.01)	(0.02)	(0.01)	(0.01)	(0.7)	(0.02)
Komaktorvik ^{b,d}	82.3	6.86	0.53	5.0	0.18	0.57	99.0	8.81
± σ ^c	(1.3)	(0.03)	(0.04)	(0.9)	(0.02)	(0.01)	(0.9)	(0.06)
Peabody Point	0.33	0.087	0.10	0.09	0.06	4.8	75.4	3.07
Bay of Islands	2.1	7.15	2.2	7.1	3.2	29.3	138	13.25
Johannes Point	39.7	11.2	2.7	3.0	3.9	42.6	35.1	10.25
Fleur de Lys	0.21	0.059	0.17	0.07	0.14	9.5	83	5.66
Fleur de Lys	0.45	0.044	0.22	0.05	0.21	6.3	167	7.72
Fleur de Lys	0.55	0.14	0.12	0.10	0.11	5.9	64	4.79
Fleur de Lys	0.39	0.11	0.15	0.09	0.10	10.6	101	6.42
Fleur de Lys	0.25	0.045	0.11	0.05	0.10	11.2	129	6.83

^a Rare earth elements normalized to chondritic meteorites. La = 0.33 ppm, Sm = 0.181 ppm, Eu = 0.069 ppm, Gd = 0.249 ppm, Lu = 0.034 ppm.

^b Samples plotted in Figure 2.

^c Uncertainty (± 1σ) due to counting statistics. These values are representative of the analytical uncertainty in the other samples.

^d Debitage from site 10 km from Peabody Point.

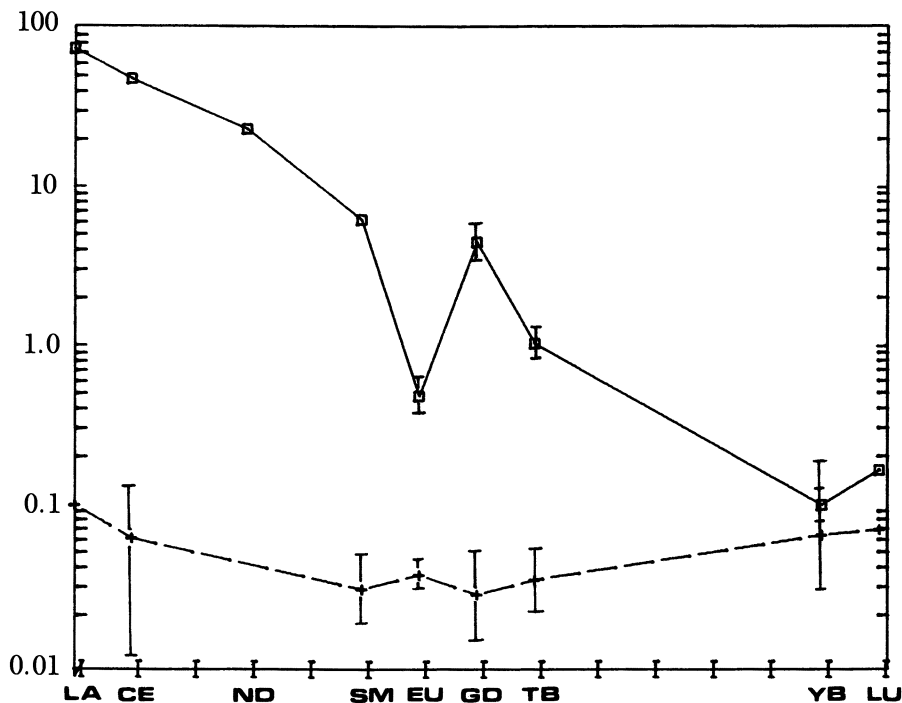


Figure 2. Chondrite-normalized REE distribution patterns for soapstone from Labrador showing analytical uncertainty based upon counting statistics.

similar areas had been observed. In one case, samples from southeastern Pennsylvania had parallel REE patterns but differed in the size of the europium anomaly because the samples came from two distinct geological settings (2). In the case of the Fleur de Lys samples, the sources of the soapstone represented by the two types of REE patterns were only a few meters apart, so the same explanation seems unlikely. The two types of patterns may more likely represent metamorphic reaction zones within the same geological formation. In geochemical studies of the alteration of serpentine to talc at Tamarack Lake (Calif.), a zone was observed where the europium anomaly changed dramatically over a distance of a meter. Although the other REE concentrations and the mineralogical compositions were very similar across this zone, the different behavior of the europium was attributed to changes in oxidation conditions as the hydrothermal solutions passed through the rocks causing the metamorphic alterations (2).

The observation of two similar but slightly different REE patterns for soapstone from the same outcrop was repeated for several other outcrops in Labrador. The geochemical reasons for different types of REE patterns in the same outcrops are not known. However, because

the trace elements are redistributed by the movement of hydrothermal solutions through the geological body and the mobility and "solubility" (partitioning between the mineral phase and solution) of each REE is a function of its ionic size (and oxidation state), the patterns observed probably reflect degrees of partial separation of the REEs from each other. An outcrop requires sufficient sampling to discover this type of inhomogeneity; this is especially true when there is overlap with REE patterns from other geological sources. There are significant differences between most of the soapstone outcrops studied (e.g., Table I); however, there are some differences that are difficult to distinguish. For instance, one of the two types of samples found at Peabody Point is indicated in Figure 3. Curves 4 and 5 represent the range of this type of Peabody Point soapstone.

Another type of variation, observed for outcrop samples in Labrador as well as in the eastern United States (9,10), is shown in Figure 4. In this case, each separate outcrop located within several miles of the other

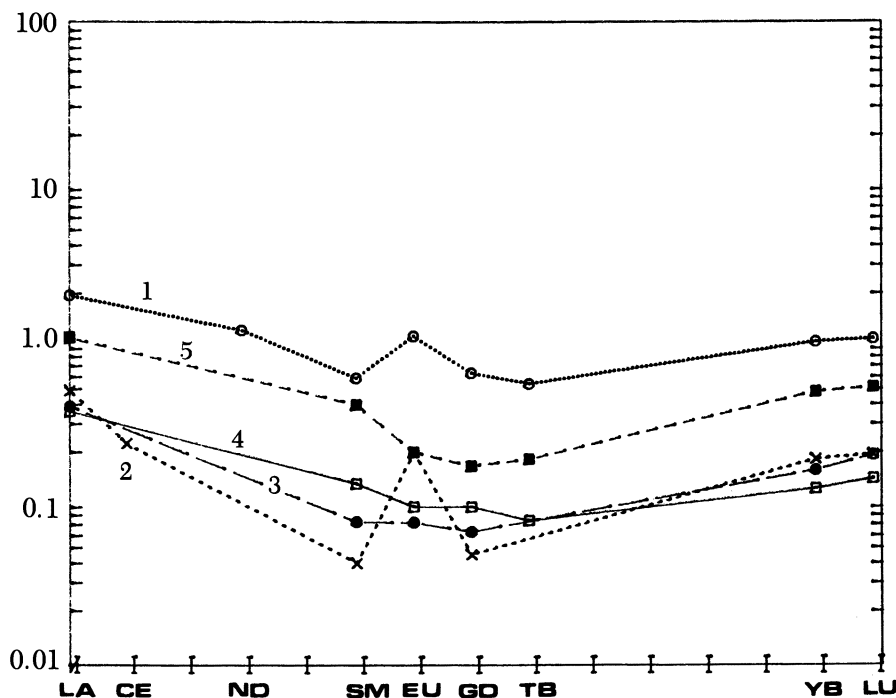


Figure 3. Chondrite-normalized REE patterns showing the range of patterns found for soapstone from the Fleur de Lys quarry in Newfoundland. Curves 1 (○) and 2 (×) represent range of concentrations for most of the samples; curve 3 (●) is the somewhat different pattern that was more typical of the Locality 2 soapstone. Range of REE patterns typical of the soapstone outcrops at Peabody Point is shown by curves 4 (□) and 5 (■).

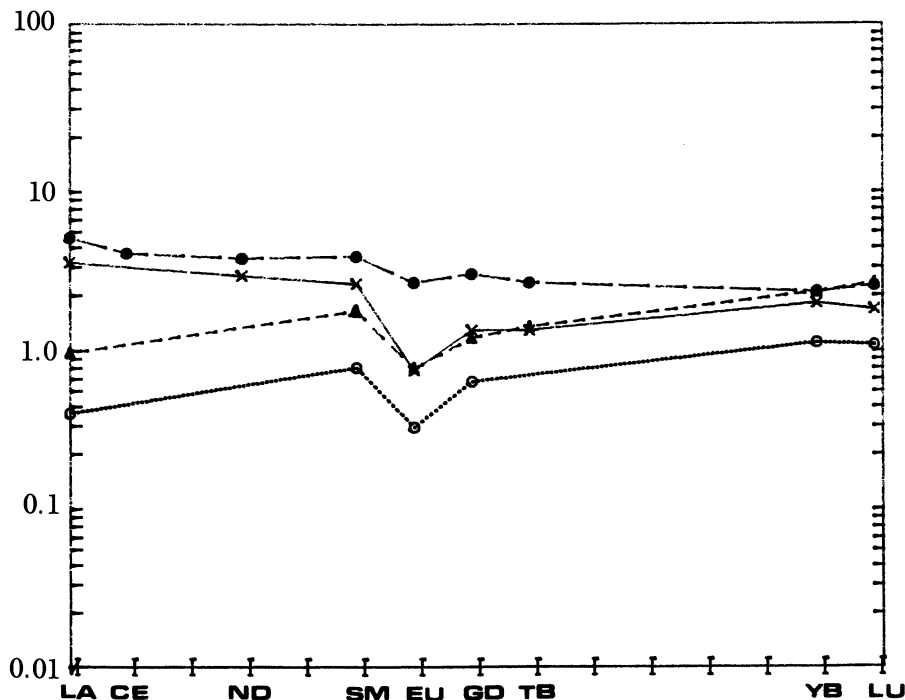


Figure 4. Chondrite-normalized REE patterns for representative soapstone samples from outcrops in the Okak area. Curves 1 (○) and 2 (●) are the types of patterns found at the Coffin Island outcrop; curve 3 (×) is an outcrop at Moores Island; curve 4 (▲) is typical of the Nutak outcrop.

outcrops in the region near Coffin Island has a similar pattern. The differences are due primarily to the size of the europium anomaly and the partitioning of the lighter REEs (the slope between lanthanum and samarium). Such "regional" changes could result from differences in the rocks that were metamorphically altered or differences in the extent of metamorphic activity throughout the region. Recognition of this type of regional variation may be valuable when it is impossible to find and analyze all of the soapstone outcrops in a region. For example, it may be reasonable to suggest that an artifact originated from soapstone in a given region if it is similar to, but not an exact match for, any of the outcrops sampled.

The matching of outcrop samples with debitage and other artifactual material is an ideal problem for computer-assisted pattern recognition techniques (8). The use of ARTHUR for the analysis of the soapstone from Labrador will be discussed in a future publication, but the important parameters for comparing soapstone are given in Table II. For this table, the samples from a given quarry were taken as one or two groups. The

Table II. Mean and Standard Deviation for Parameters Used to Distinguish REE Patterns in Soapstone

Quarry	Concentration ^a La	Concentration ^a Lu	Slope ^b La to Sm	Slope ^c Gd to Lu	Europium Anomaly ^d
Fleur de Lys A	0.73 ± 0.10	0.46 ± 0.11	-0.11 ± 0.02	0.028 ± 0.009	0 ± 0.03
Fleur de Lys B	0.55 ± 0.10	0.39 ± 0.14	-0.14 ± 0.02	0.064 ± 0.006	0.48 ± 0.04
Bay of Islands A	4.4 ± 0.7	2.3 ± 0.2	0.025 ± 0.009	-0.048 ± 0.005	-0.41 ± 0.03
Bay of Islands B	4.0 ± 0.8	3.7 ± 0.3	0.090 ± 0.009	-0.054 ± 0.003	-0.25 ± 0.04
Cape Nuvotannak A	2.8 ± 0.5	0.60 ± 0.10	-0.12 ± 0.01	-0.011 ± 0.010	-0.57 ± 0.03
Cape Nuvotannak B	1.7 ± 0.3	0.31 ± 0.05	-0.11 ± 0.01	-0.025 ± 0.010	-0.27 ± 0.01
Johannes Point	27.3 ± 5.0	6.9 ± 2.0	-0.06 ± 0.01	0.007 ± 0.006	-0.14 ± 0.04
Coffin Island	14.9 ± 2.9	5.2 ± 0.5	0 ± 0.008	-0.030 ± 0.003	-0.33 ± 0.03
L'Anse aux Meadows	0.68 ± 0.10	4.9 ± 0.8	0.17 ± 0.01	0.002 ± 0.008	0.11 ± 0.03
Napaktok Point	9.6 ± 2.0	2.3 ± 0.6	-0.08 ± 0.02	0.017 ± 0.006	-0.94 ± 0.01
Peabody Point	1.5 ± 0.2	0.48 ± 0.05	-0.11 ± 0.02	0.06 ± 0.01	-0.10 ± 0.06

^a Ratio of concentrations normalized to chondritic meteorites.^b Slope = $(\log [Sm] - \log [La])/5$.^c Slope = $(\log [Lu] - \log [Gd])/7$.^d Log [Eu] - [(log [Sm] + log [Gd])/2].

grouping was based upon the similarity of the samples using hierarchal dendrograms of feature correlations generated by the HIER routine in ARTHUR (8). Each of the five parameters used to characterize the REE pattern was averaged for all of the samples in the particular group. The number of samples included in determining the mean value as well as the standard deviation from the mean for each parameter is given. Only outcrops represented by five or more samples are included.

The outcrop samples from Peabody Point were compared to debitage, preforms, and finished vessels from the archaeological sites within 20 km. Much of the material analyzed had REE patterns similar to the Peabody Point outcrop (*see* Table II); however, there was a significant number of samples that were similar but had a lower degree of correlation (using hierarchal dendrograms) than did the outcrop samples. Many of the debitage samples were analyzed before the Peabody Point quarry had been completely characterized. The similarity with the analyzed outcrop samples was enough to suggest that there was another outcrop in the Peabody Point region that had not been sampled. Further sampling at Peabody Point did find this second REE pattern to be characteristic of some soapstone from this outcrop. About 64% of the debitage analyzed from Komaktorvik and all 12 debitage samples from the nearest archaeological sites match those from the Peabody Point outcrop. The other debitage from Komaktorvik includes samples with REE patterns that are very similar to samples from outcrops further south along the coast (e.g., Okak and Napaktok). There are several debitage samples that have a positive slope between lanthanum and samarium, and this particular REE pattern has not been found at the outcrops sampled to date. This characteristic REE pattern (positive La–Sm slope) was found for several artifacts from the Seven Islands Bay area (which included Peabody Point) as well as for the debitage.

Discussion

The Fleur de Lys soapstone quarry is unique in preserving considerable evidence of the methods used to extract soapstone. The worked areas at Fleur de Lys are almost certainly Dorset (11). There is no archaeological or historical evidence that the Neo-Eskimo population, which supplanted the Dorset peoples in Labrador, ever occupied the northern Newfoundland area (12). In more recent times, the 17th and 18th centuries, the Neo-Eskimos frequented the Strait of Belle Isle to trade with Europeans. The only other people who might have used the soapstone at Fleur de Lys were the Maritime Archaic Indians, who also lived in Newfoundland. However, these people used soapstone for plummets, so it is doubtful that they would have needed to employ any elaborate quarrying methods to extract the small amounts they needed.

Evidence of plummet manufacture was not observed from survey and test excavations at the quarry (3). There is no evidence for soapstone utilization by other Indian cultures in the area. Although no lithic tools, which are diagnostic of the Dorset culture, were found at Fleur de Lys, the preform morphology observed in the quarry corresponds to finished Dorset vessels in size and shape. Thus the consistent and uniform technology of soapstone extraction observed at Fleur de Lys is assumed to be only that of the Dorset people. Association of artifacts from dated archaeological sites may provide some indication of the length of time that the quarry was in use.

The amount of soapstone extracted from the Fleur de Lys quarry was large. In locality 1, there is a strong tendency for preforms, removal scars, and mounds of tailings from the quarrying operations to be clustered together in discrete groups over a 200-m length of the cliff face (Figure 5). The quality of the soapstone may have determined the locations of the worked areas, but other evidence at the site suggests an efficient technological reason for the intensive working of a particular area. Most partially carved but unremoved preforms found in place at

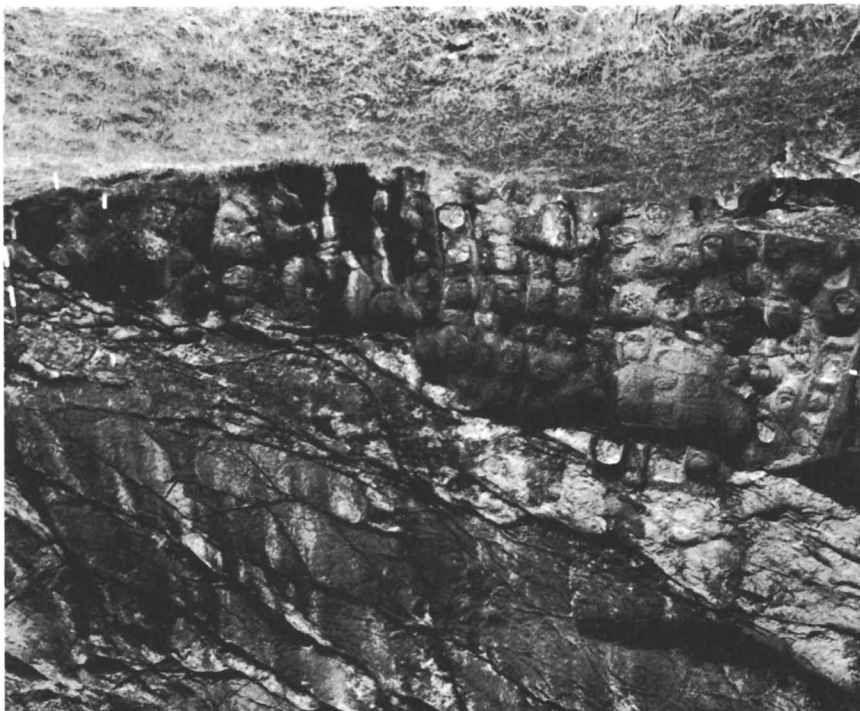


Figure 5. Photograph of prehistoric soapstone quarry at Fleur de Lys showing site of removal of preforms from the cliff face.

Fleur de Lys possess an "access zone" along one or more sides. Once a single preform has been removed the deep (15–20 cm) depression of the removal scar acts as one of the sides for the next preform if it is carved from the adjacent soapstone. The preform shapes are variable, but most are oval or subrectangular in the range of 20–25 cm in width and 25–30 cm in length. The outlines of the preform appear to have been carved using a semicircular scraping motion. The scrapers found in the test excavations were fashioned from thin tabular slabs of the hard neighboring bedrock. These "tools" were apparently shaped expeditiously to create an acute edge suitable for scraping the soapstone. After the preform was excavated all around the sides with the scrapers, it was removed by a clean break. There is no evidence of undercutting preforms to facilitate breaking them away from the outcrop. Although the removal method is not known, it may have been facilitated by the accessibility on one side.

Evidence for the next stage of soapstone manufacturing has not been found at Fleur de Lys. No Dorset habitation sites or soapstone processing sites with debitage were found or have been reported. There were very few fragments of partially worked vessel rejects in the tailings below the cliff face, which suggests that secondary reduction took place away from the quarry zones. Thus for information on this stage of manufacture, we must shift north to Komaktorvik, which appears to be a secondary reduction station for the material from the nearby outcrops at Peabody Point. Most of the debitage (78%) and preforms (62%) from Komaktorvik and the other sites in the area have REE patterns that fall within the range found at the Peabody Point outcrop. The debitage, and to a greater extent the preforms, at these sites were not derived exclusively from the Peabody Point outcrops, and some have REE patterns that match closely the patterns found in outcrops at Okak and Napaktok Point (5). This observation raises questions regarding the assumption that all manufacturing took place near the outcrops. The presence of nonlocal material may result from one of the following explanations: (1) After extraction and initial preforming, the soapstone can be transported and finished at another site where debitage and/or preform fragments can be deposited far from the quarry; (2) Dorset and later people often repaired and (or) reworked broken soapstone vessels to make them once again serviceable, and in the process they could produce debitage; (3) it is possible that blocks of soapstone or preforms were traded and (or) transported from considerable distances before being finished. In terms of the final explanation, it should be noted that some Dorset lamps are quite small and would not have required a very large piece of soapstone to be carried to a distant habitation site.

Although it is clear that the presence of "exotic" (nonlocal) soapstone will provide the best information about population movements and/or

contacts, the high percentages of local debitage at Peabody Point and Komaktorvik does show predominant use of local resources. Thus it should be possible to postulate that REE patterns for debitage (from sites where high quantities of debitage and preforms are found) represent a nearby "quarry" when none is known. Because we have analyzed only the relationship between Peabody Point and the surrounding sites, we feel that this assumption must be used with due caution.

Now that we have sufficient sampling of many soapstone outcrops, the variability of the trace elements within an outcrop region and among distant outcrops can help us to establish a statistical probability for the nearness of match for soapstone artifacts. While details of this matching will be the subject of a future publication, a few preliminary observations can be made. The most obvious finding is that the majority of the artifacts at a particular site originated from local or nearby outcrops. At Peabody Point, all the artifacts analyzed matched the nearby outcrops. However, in the entire Seven Islands Bay, only 36% of the 49 vessel fragments analyzed matched the Peabody Point outcrop. It should be recognized that these vessel fragments represent not only different geographical locations within the Seven Islands Bay area, but different cultural periods as well. The artifacts and debitage from Peabody Point were all from a late Dorset occupation, but in general the artifacts at other sites are from Pre- or Mid-Dorset times. When looking at the REE patterns for artifacts from this area, there appear to be at least four different sources of soapstone that were utilized but for which we have not sampled the outcrop. Those artifacts that match each other, but for which we have no matching quarry or where the quarry appears to be further south along the coast, tend to group by time period. For example, the six artifacts with one particular pattern are all from Late Dorset sites at Komaktorvik and Big Head.

By knowing the cultural context of an artifact, we will be able to determine the time frame for the utilization of a particular outcrop. Preliminary analysis indicates that the Fleur de Lys quarry was used during earlier Dorset periods, and some matching artifacts are found north along the Labrador coast. Although this is evidence for Dorset utilization of soapstone from Newfoundland (Fleur de Lys), these people apparently only populated the more northern regions of Labrador during the late Dorset (after A.D. 800) period. The one Dorset lamp from this period, which has been found south of the Nain area, was recovered from the suspected Norse (Viking) settlement at L'Anse aux Meadows on the northern tip of Newfoundland. Along with this late Dorset lamp, the most important soapstone artifact from this site was a spindle whorl (13). Earlier analysis indicated that this object could have been made from soapstone found at an outcrop within 2 km of the site (14). The analysis of a sample of the Dorset lamp, provided through the courtesy

of Parks Canada, indicates that it was not made from soapstone found at L'Anse aux Meadows. The best match for this Dorset artifact appears to be from a northern Labrador outcrop at Cape Nuvotannak. This unusual location for a late Dorset artifact from such a distant quarry raises the question of how the lamp came to Newfoundland. Could it have been brought from the northern coast by the Vikings? Single artifact-to-source matches are difficult to interpret, but large-scale studies such as this one can show how raw materials were distributed from sources. These patterns of resource procurement can suggest the mechanisms of distribution.

Literature Cited

1. Fitzhugh, W. W. *J. Field Archaeol.* **1976**, *3*.
2. Allen, R. O.; Pennell, S. E. In "Archaeological Chemistry II"; Carter, G. F., Ed.; ADVANCES IN CHEMISTRY SERIES No. 171; American Chemical Society: Washington, D.C., 1978; pp. 230-57.
3. Nagle, C. *Archaeol. in Newfoundland and Labrador* **1982**, 102-129.
4. Allen, R. O.; Luckenbach, A. H.; Holland, C. G. *Archaeometry* **1975**, *17*, 69.
5. Rogers, M.; Allen, R.; Nagle, C.; Fitzhugh, W. *Archaeometry* **1983**, *25*(2).
6. Masuda, A., Inst. Nucl. Study, Univ. Tokyo INSJ-54, **1963**.
7. Jensen, B. A. *Geochim. Cosmochim. Acta* **1973**, *37*, 2227.
8. Kowalski, B. R., Ed. "Chemometrics: Theory and Application"; ACS SYMPOSIUM SERIES No. 52; American Chemical Society: Washington, D.C., 1977.
9. Pennell, S. E. M.S. Thesis, University of Virginia, Charlottesville, Va., 1977.
10. Allen, R. O.; Hamrrouch, H.; Holland, C. G. *Proc. Int. Archaeometry Symp.* **1983**, in press.
11. Witemberg, W. *J. Am. Antiq.* **1940**, *4*, 309-33.
12. Linnaeae, U. *Tech. Pap. Newfoundland Museum* **1975**, *1*.
13. Ingstad, H., "Westward to Vinland"; St. Martins: New York, 1969.
14. Allen, R. O.; Allen, K. K.; Holland, C. G.; Fitzhugh, W. W. *Nature* **1978**, *271*, 5642.

RECEIVED for review November 3, 1982. ACCEPTED for publication March 28, 1983.

Provenance Studies of Middle Eastern Obsidian from Sites in Highland Iran

M. JAMES BLACKMAN

Smithsonian Institution, Conservation-Analytical Laboratory, Washington, DC 20560

Exchange of obsidian from a limited number of sources to most archaeological sites in the Middle East can be documented from the early Neolithic through the Bronze Age. Thus, precise provenance determinations for obsidian artifacts can provide important information concerning contacts among regions and clues to the nature of the exchange itself. Three regions, each with several discrete sources, have been identified as major suppliers of obsidian. Extensive sampling and chemical analysis of sources in Central Anatolia and the Greek Islands provide excellent coverage of these regions. The sources in the Eastern Turkish–Soviet Armenian region are, however, much less well known. The analysis, by instrumental neutron activation, of samples from three sources in this region and four sources in the Central Anatolian region are reported. The source data are compared with the analyses of artifacts from the important highland Iranian sites of Tal-e Malyan and Tepe Yahya. The methods of provenance identification and the implications for exchange in obsidian at these two sites are discussed.

THE EXCHANGE OF OBSIDIAN from a limited number of possible sources to most archaeological sites in the Middle East can be documented from the early Neolithic through the Bronze Age. Precise source provenance determinations for the obsidian artifacts can, therefore, provide important information concerning the nature and organization of exchange in obsidian, as well as in other goods moving in the same network, throughout this long period of cultural development. Obsidian is particularly well suited for use in the study of long-range exchange in the Middle East, for although the obsidian artifacts are widely distributed archaeologically, the geological occurrences are restricted to a relatively

This chapter not subject to U.S. copyright.
Published 1984 American Chemical Society

few sources located in geographically circumscribed regions. Moreover, obsidian (at least for the Middle Eastern sources so far examined) appears to be homogeneous within a given flow; precise chemical analysis shows significant elemental concentration differences among the flows, which allow differentiation with a high degree of certainty. The well-established and growing body of literature on obsidian analysis and exchange theory for the Middle East additionally provides a large data base which may be drawn upon to match sources and artifacts to test exchange models.

Users of chemical analysis to characterize obsidian and monitor long-range exchange have concentrated primarily on the earliest time periods from Neolithic to about 3500 B.C. It is, however, after about 3500 B.C. that state polities arose in the Middle East; such developments are postulated to have influenced and in turn have been influenced by long-distance exchange systems of the day. The use of exchanged items as a monitor to trace the direction and perhaps even the volume of exchange during this pivotal period is then of great interest to those attempting to assess the relationship between long-distance exchange and state development.

This investigation focuses on obsidian reaching two highland Iranian sites during the time period from roughly 3500 to 1800 B.C. Geological source samples from two major source regions in Western Asia were used to characterize possible sources of the artifacts.

Archaeological Sites and Obsidian Artifacts

Obsidian from two sites in highland Iran, Tal-e Malyan and Tepe Yahya, forms the basis of this investigation. The obsidian artifacts from these two sites were excavated from deposits dating from about 4500 B.C. to A.D. 400. It is, however, the period from 3500 to 1800 B.C., corresponding to the Middle Uruk through the Ur III to Isin Larsa periods in Mesopotamia (1,2), that is of primary concern.

The site of Tal-e Malyan (Figure 1), located in the Kur River Basin in Fars Province in southwestern Iran, was excavated by William Summer of Ohio State University. The first major occupation at Malyan occurred during the Banesh Phase (3400–2800 B.C.). The site reached its peak in size and population during the Kaferi Phase (2100–1800 B.C.), occupying about 200 hectares. During the subsequent Qaleh/Middle Elamite Phase (1600–1000 B.C.), Malyan declined, and it was abandoned sometime after 1000 B.C. (3). Confirmed as the ancient city of Anshan (4), co-capital with the lowland city of Susa of the Elamite polity, Malyan actively participated in a far-flung exchange system including lowland Elam and the Mesopotamian cities.

The site of Tepe Yahya, located in the Soghun Valley in south-

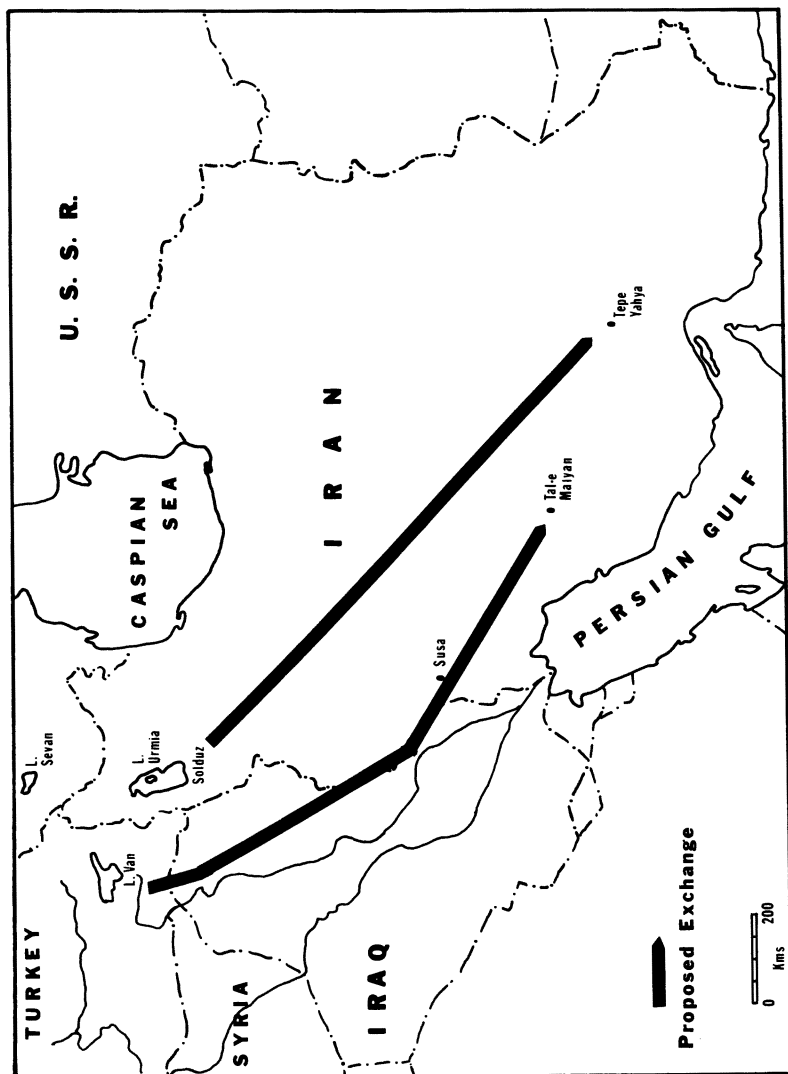


Figure 1. Location of archaeological sites.

central Iran, was excavated by C. C. Lamberg-Karlovsky of Harvard University. About 3 hectares in area, Tepe Yahya was occupied from the mid fifth to early second millenia B.C. (5). A site of manufacture of chlorite bowls, Tepe Yahya shows evidence for exchange links with Mesopotamia to the east and has been postulated to have had ties with the Harappian civilization in the Indus Valley to the west (6,7). Protoelamite tablets found at Tepe Yahya indicate the site's inclusion in the Elamite sphere of influence. It therefore seems likely that exchange links should exist between Tal-e Malyan and Tepe Yahya and between them and lowland Elam and Mesopotamia that might be monitored using obsidian provenance information.

Forty-seven obsidian objects, totaling 107 g, have been recovered from excavation at Tal-e Malyan. Two general categories of object may be defined based on function: utilitarian items—tools (mostly blades), cores, and debris; and luxury items—ground and polished bowls, bead/rings, and cylinders. The presence of spent cores and core trimming debris indicates that the blades were struck from the cores at the site rather than arriving as finished products. The manufacturing technology for the obsidian blades is identical to that used to make chert and jasper blades found in abundance and made of local material. The luxury items, ground and polished objects, may well have arrived at Tal-e Malyan as finished products. Although a ground stone industry was present at the site, only relatively soft stone materials such as talc, chlorite, marble, and limestone appear to have been worked. Obsidian, a much harder and more brittle material, would have required different working techniques. Large blocks of obsidian would also have had to be transported over great distances (~1500 km) to supply the raw material. It is likely that the luxury items and the raw material for the utilitarian items were being exchanged in terms of function rather than material type. As such, these two categories of object may have been included in different aspects of the exchange system.

Eleven obsidian objects from Tepe Yahya, composing about one-half of the excavated obsidian, were analyzed. The obsidian was an unsorted sample from two seasons of excavation, and is taken to be representative of the entire collection. All the Tepe Yahya obsidian, seven blades and four flakes, are of the utilitarian type. No obsidian luxury items were reported.

In addition to the Tal-e Malyan and Tepe Yahya artifacts, objects from two other archaeological sites were included in the analysis. The two selected pieces from earlier periods at Ali Kosh and Choga Safid were included to attempt to correlate the samples in this investigation with those analyzed by Renfrew and coworkers (8–10) by optical emission spectroscopy.

Geological Source Samples

Two geographically separate regions in Western Asia contain obsidian sources that might have contributed obsidian to archaeological sites in highland Iran. The smaller of the two regions, the Central Anatolian region, is located in central Turkey to the east and southeast of Lake Tuz (Figure 2). The second and by far the greater in area, the Eastern Turkish–Armenian S.S.R. region (ET–ASSR), encompasses most of eastern Turkey and Soviet Armenia stretching from Lake Van in the south to Lake Sevan in the north.

Thirteen samples from three general collection areas within the Central Anatolian region were available for analysis. The three areas, Hotmis Dağ, Göllü Dağ, and Hasan Dağ, are shown in Figure 2. Eight samples were collected from four localities in the area around Hotmis Dağ, three from three localities in the Göllü Dağ area, and two from the Hasan Dağ area.

Thirty-two samples from three general collection areas in the ET–ASSR region were available. Fifteen samples were collected from several localities at Nemrut Dağ on the southwestern shore of Lake Van; 10 samples were from several localities at Suphan Dağ on the northwestern shore of Lake Van; and 6 samples were from a source between the city of Razdan and the northwestern tip of Lake Sevan in the Armenian S.S.R. (Figure 2). A single sample from the Isle of Giali in the Aegean source region was also analyzed.

All of the source samples, except for the Lake Sevan material, were collected by Richard A. Watson of Washington University and Ibrahim T. Cakmak. This field work was facilitated by Saadettin Alpan, Director-General of the Maden Tetkik Arama Enstitutu, and funded by the National Science Foundation through support of the Turkish Prehistoric Project under the direction of Robert J. Braidwood and Halet Cambel. The Lake Sevan samples were provided by J. Allen of Dumbarton Oaks.

Methodology

The elemental analysis of the artifacts and geological source samples was performed by using instrumental neutron activation analysis at the National Bureau of Standards Reactor in Gaithersburg, Md. The geological samples and artifacts were prepared in the same manner. After cleaning in an ultrasonic bath and several washings alternately with distilled water and ethanol, the samples were dried at 105 °C, were wrapped in several thicknesses of clean polyethylene sheeting, and several small chips were struck off with an alumina pestle. The chips were further reduced to medium sand size, rewashed, dried, and about 100 mg was weighed into clean 0.5-mL polyethylene microcentrifuge tubes. About 95-mg replicates of the multielement standard, NBS SRM 1633–coal flyash, and two check standards were also encapsulated in microcentrifuge tubes.

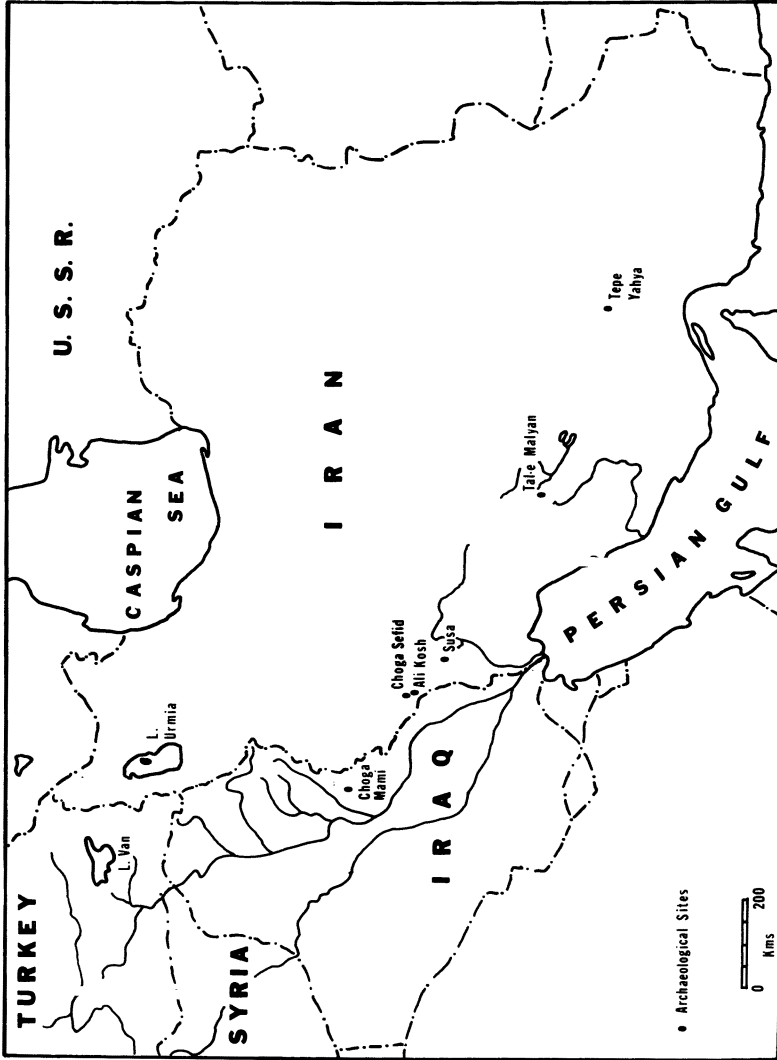


Figure 2. Geological source locations.

Samples and standards were irradiated for 8 h at a flux of 5×10^{13} n/cm²/s. Following a 6-day decay, the samples were counted for 2 h each using an intrinsic germanium detector (FWHM at 1333 ⁶⁰Co of 1.71 keV), and data were collected on an 8192-channel MCA. Data processing included corrections for pulse pileup and peak interferences. Samples were then allowed to decay for 30 days post-irradiation and were recounted for 4 h using the same system. Table I presents a summary of the elements sought and quantified.

Elemental concentration data for 19 elements were then used as input in a hierarchical aggregative clustering program (Table I). The clusters, presented as dendrograms plotted as a function of dissimilarity, were produced by "nearest neighbor" distance calculations on a mean character difference matrix (11). This method of data analysis is quite useful in sorting, grouping, and displaying

Table I. Experimental Parameters

<i>Elements</i>	<i>Nuclide Analyzed</i>	<i>Gamma Ray Energy (keV)</i>	<i>Count</i>	<i>Concentration in SRM 1633</i>
Na ^a	Na-24	1369	1	0.32%
K	K-42	1525	1	1.61%
Ca	Sc-47	159	1	4.70%
Sc ^a	Sc-46	889	2	27.0 ppm
Cr	Cr-51	320	2	131 ppm
Fe ^a	Fe-58	1099 and 1292	2	6.20%
Co	Co-60	1173 and 1333	2	41.5 ppm
Zn ^a	Zn-65	1115	2	213 ppm
As ^a	As-76	559	1	61.0 ppm
Br	Br-82	554	1	8.6 ppm
Rb ^a	Rb-86	1077	2	125 ppm
Sb	Sb-122	564	1	6.9 ppm
Sb ^a	Sb-124	1690	2	6.9 ppm
Cs ^a	Cs-134	796	2	8.6 ppm
Ba	Ba-131	496	1,2	2700 ppm
La ^a	La-140	1596	1	82.0 ppm
Ce ^a	Ce-141	145	2	146 ppm
Nd ^a	Nd-147	91	1,2	64.0 ppm
Sm ^a	Sm-153	103	1	12.9 ppm
Eu ^a	Eu-152	1408	2	2.5 ppm
Gd ^a	Gd-153	103	2	11.2 ppm
Tb	Tb-160	298	2	1.9 ppm
Yb	Yb-169	177	2	6.4 ppm
Yb ^a	Yb-175	396	1	6.4 ppm
Lu ^a	Lu-177	208	1	1.0 ppm
Hf ^a	Hf-181	482	2	7.9 ppm
Ta ^a	Ta-182	1221	2	1.8 ppm
Th ^a	Pa-233	312	2	24.8 ppm
U ^a	Np-239	106	1	11.6 ppm

^a Elements used in cluster.

quantities of sample data with large numbers of variables per sample. Cluster analysis is not, however, a statistical test, and the clusters formed by this technique must be further tested for statistical significance and geological and archaeological consistency.

Cluster Analysis of Source Samples

When the chemical concentration data from the geological source material were subjected to cluster analysis, several discrete clusters of geologically consistent samples were formed. The dendrogram in Figure 3 shows that the peralkaline obsidian from Nemrut Dağ is easily distinguished from the calc-alkaline to subalkaline obsidians from all the other sources. Finer-scale examination of the dendrogram reveals that all of the source areas sampled can be readily distinguished from one another, although obsidian samples from some source areas are clustered into more than a single group.

The three ET-ASSR source areas—Nemrut Dağ, Suphan Dağ, and Lake Sevan—are each composed of at least two chemically distinguishable groups (Appendix A), probably representing different eruptive events at the respective sources. The source group labeled Nemrut I in Figure 3 and Appendix A is quite homogeneous, with elemental dispersions of 4% or less. The Nemrut II source group is somewhat less homogeneous, particularly for scandium (28%), iron (11%), and europium (27%), and may consist of obsidian from more than one eruptive event. Two source samples from Nemrut Dağ (XNO522 and 525) do not cluster tightly with either Nemrut source group and may represent additional flows at Nemrut Dağ. Altinli (12) reported as many as 20 identifiable lava flows from Nemrut Dağ, indicating the likelihood of multiple obsidian occurrences that might be chemically distinguishable.

The Suphan Dağ source samples also cluster into two separate source groups. Chemically these two groups show much greater differences than did the Nemrut Dağ groups (Appendix A). The group designated Suphan I is less homogeneous than is the Suphan II group, and the former group may contain samples from more than one obsidian flow. Five of the six Lake Sevan source samples formed a homogeneous group, designated Sevan I in Figure 3. However, the sixth sample clustered closely with neither the Sevan I group nor with any other source sample. Based on its distinctive composition, this single sample has been tentatively given a separate source group assignment, Sevan II (Svn II in Figure 3).

The Central Anatolian region source samples present an equally intricate picture. The three Göllü Dağ area samples, plus two archaeological samples (XEO540 and 541) from the immediate area, formed a single group of chemically consistent composition. The Hasan Dağ source samples (Hsn in Figure 3) also cluster closely in a readily recognizable

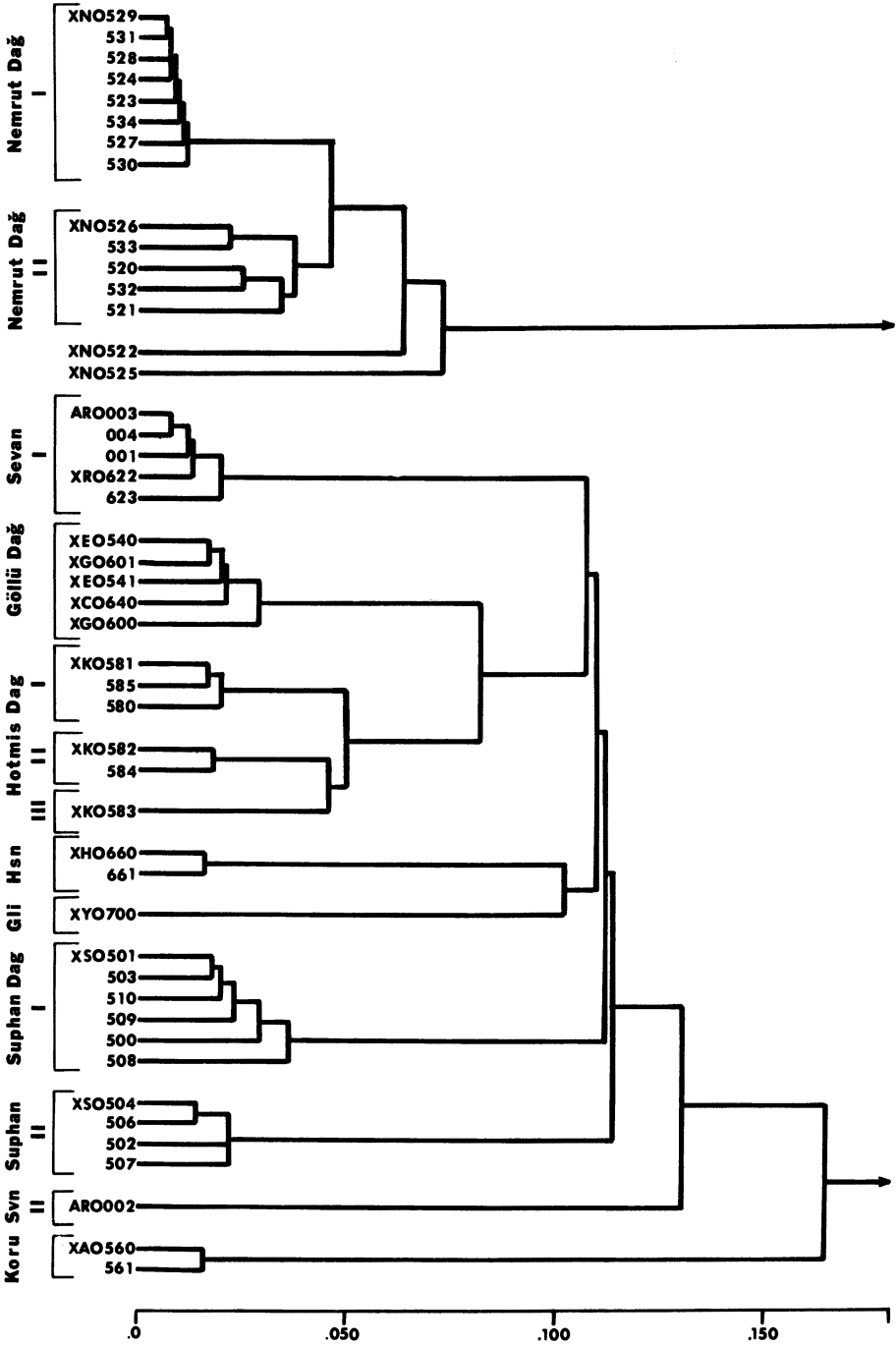


Figure 3. Clustering of source samples.

group. The eight Hotmis Dağ area samples, however, showed more complexity. Two samples clustered closely and were isolated from all other obsidian samples (this group is designated Koru in Figure 3). The remaining five Hotmis Dağ samples formed a loose but distinguishable cluster that may readily be subdivided into three groups, Hotmis I, II, and III. These groups most probably represent different eruptive events at Hotmis Dağ; the Koru group appears to be a separate source.

The single Aegean region sample from Giali is easily distinguished from the sources in both the Central Anatolian region and the ET-ASSR region. It has been placed in a separate group designated Gli in Figure 3.

The picture that emerges from the cluster analysis and direct comparison of concentration data is complex, but promising. Although several of the source areas consist of multiple occurrences of obsidian, all the source areas sampled have readily distinguishable source-specific compositions. At least 13 chemical groups from 7 collection areas can be identified (Table II). The collection areas of Suphan Dağ, Nemrut Dağ, Lake Sevan, and Hotmis Dağ each consist of two or more groups of distinct chemical composition. The presence of multiple chemical groups from what have been taken as single source areas points up the need for extensive and careful source sampling to avoid confusion in artifact source assignment.

Comparison with Previous Work

There is a large and growing literature on Middle Eastern obsidian studies that contains elemental data from the analysis of many hundreds of samples. Some effort is needed to reconcile the disparate terminology used to classify sources of both known and unknown provenance. The task is made difficult by the use of different analytical techniques of varying precision, the selection of different element sets in analysis and reporting, and the use of different secondary standards to quantify the concentration data.

The earliest work, by Renfrew and coworkers (8–10) using optical emission spectroscopic analysis, reported concentrations for 15 elements. The Ba/Zr ratios were the primary discrimination technique. Wright (13), Wright and Gordas (14), and Mahdavi and Bovington (15) used instrumental neutron activation analysis (INAA) as the analytical technique and Na/Mn ratios to make source discriminations. Work done at the University of Bradford by Warren, Aspinall, and their students (16–19) used INAA in reporting 16 elements. Plots of $1/Sc$ ($Cs + Ra + Rb/100 + (Th + La + Ce)/10$) vs. $\%Fe/Sc$ were used as the primary discrimination technique (16). Yellin and Perlman (20–23) at Hebrew University used high-precision INAA and based source discrimination on an element-by-element comparison of group means and root-mean-square deviations.

Table II. Geological Source Groups

<i>Source Groups</i>	<i>Hebrew Univ.</i>	<i>Bradford Univ.</i>	<i>Renfrew et al.</i>	<i>Location</i>
<i>Central Anatolian Obsidian Sources</i>				
1. Göllü	GLD	B1	2b (ÇİFTLİK)	Göllü Dağ
2. Hotmis I	HTMS-C	B5	1e-f (ACIGOL)	Hotmis Dağ
3. Hotmis II	HTMS-A	B5	1e-f	Hotmis Dağ
4. Hotmis III	HTMS-B	B5	1e-f	Hotmis Dağ
5. Koru	KRUD	—	—	Koru Dağ
6. Hasan	—	—	1h	Hasan Dağ
7. —	NNZD	—	—	Nenezi Dağ
8. —	—	—	4f	Kulaklikepez
<i>Eastern Turkish-Armenian S.S.R. Obsidian Sources</i>				
1. Nemrut I	NMRD 1	G1	4c	Nemrut Dağ
2. Nemrut II	NMRD 2 (?)	—	—	Nemrut Dağ
3. Nemrut III	—	—	—	Nemrut Dağ
4. Nemrut IV (?)	—	—	—	Nemrut Dağ
5. Suphan I	—	—	—	Suphan Dağ
6. Suphan II	—	—	—	Suphan Dağ
7. Sevan I	—	—	—	Lake Sevan
8. Sevan II	—	—	—	Lake Sevan
9. —	ZNKT	B4 (?)	3a (?)	Zarnaki Tepe
10. —	—	G2	4c	Bingöl Dağ
<i>Sources of Unknown Provenance</i>				
1. —	—	B2	1g	?

Direct correlation with the analysis done by optical emission spectroscopy and the early INAA work was not possible. However, correlations could be made with Hebrew University and the University of Bradford data. Because different standards were used at these two laboratories and in this investigation to quantify the elements, a set of correlation factors had to be calculated to convert the data to a comparable form. This task was done by intercomparison of the standards (24,25). When the converted group means of the Hebrew University and University of Bradford data were clustered with the means of the groups determined in this investigation, as shown in Figure 4, there was good correspondence for the groups from source areas known to be the same. The Göllü source group clustered closely with both the GLD (Göllü Dağ) source group of Hebrew University and the B1 (Çiftlik) source group of Bradford. The Koru source group likewise clustered with the KRUD (Koru Dağ) source group of Hebrew University and the three Hotmis

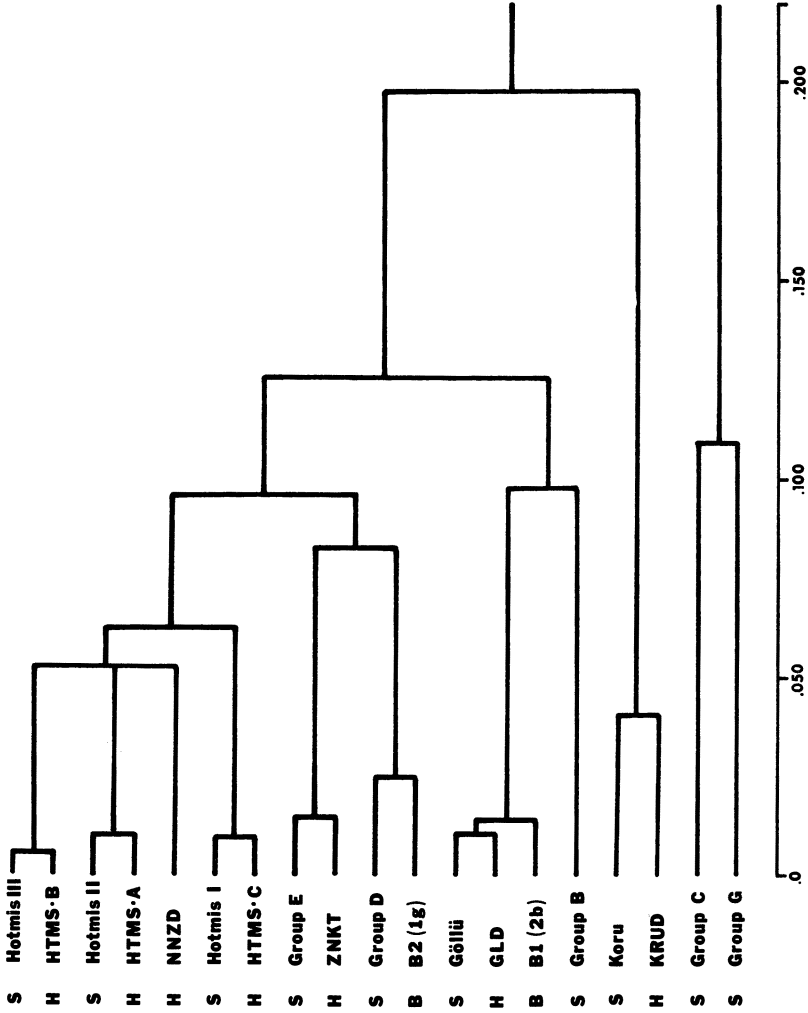


Figure 4. Clustering of converted mean data. Key: S, Smithsonian Institution; H, Hebrew University; B; University of Bradford.

source groups each clustered with one of the HTMS (Hotmis Dağ) source groups of Hebrew University. The close clustering of the converted source-group means from the same source area demonstrates the ability to use analytical data generated in other laboratories in the identification of artifact sources in this investigation. This fact is important because several known geological source groups that were not available for analysis in this investigation and artifact groups of unknown provenance from other archaeological sites have been analyzed at Hebrew University and the University of Bradford. The geological sources include the Nenezi Dağ source northwest of Göllü Dağ in the Central Anatolian region and the important Zarnaki Tepe source north of Lake Van in the ET-ASSR region; both were analyzed at Hebrew University. One of the artifact groups of unknown provenance, Bradford's B2 group, has been identified with the Renfrew et al. (10) 1g source. Table II presents a summary of the geological source groups outlined in this investigation and a correlation with the sources reported by the other investigators.

Archaeological Artifacts and Source Assignments

The elemental concentration data from the analysis of the artifacts from the highland Iranian sites of Tal-e Malyan and Tepe Yahya were subjected to the same cluster analysis as the geological source samples. Figure 5 shows that three major clusters were formed, representing significant geochemical differences. Each of these major clusters could be divided into two or more groups of distinctive chemical composition. The first major cluster contained artifact groups A and A', which appear to be closely related; the second major cluster contained artifact groups C and G; and the third major cluster contained groups E, D, F, and B. In all, eight artifact groups were identified, and each contained at least two samples. The elemental concentration data, presented in Appendix B, demonstrate the validity of these groups as chemically distinct entities.

When the geological source samples and the artifact groups were clustered together, as shown in Figure 6, three close matches between source and artifact group were observed. Group A artifacts and the Nemrut Dağ I source samples formed a single very tight cluster at a low level of dissimilarity. Although none of the artifacts clustered with the Nemrut Dağ II source, the two artifacts of Group A' formed a cluster with one of the Nemrut Dağ source outliers (XNO525 in Figure 3). This source sample and associated artifacts, now termed Nemrut Dağ III source group, demonstrate the need for a large and comprehensive sample of source material. Artifact Group F and the Sevan I source also formed a tight cluster at low levels of dissimilarity. Table III shows the close agreement, for selected elements, between the artifact group and the

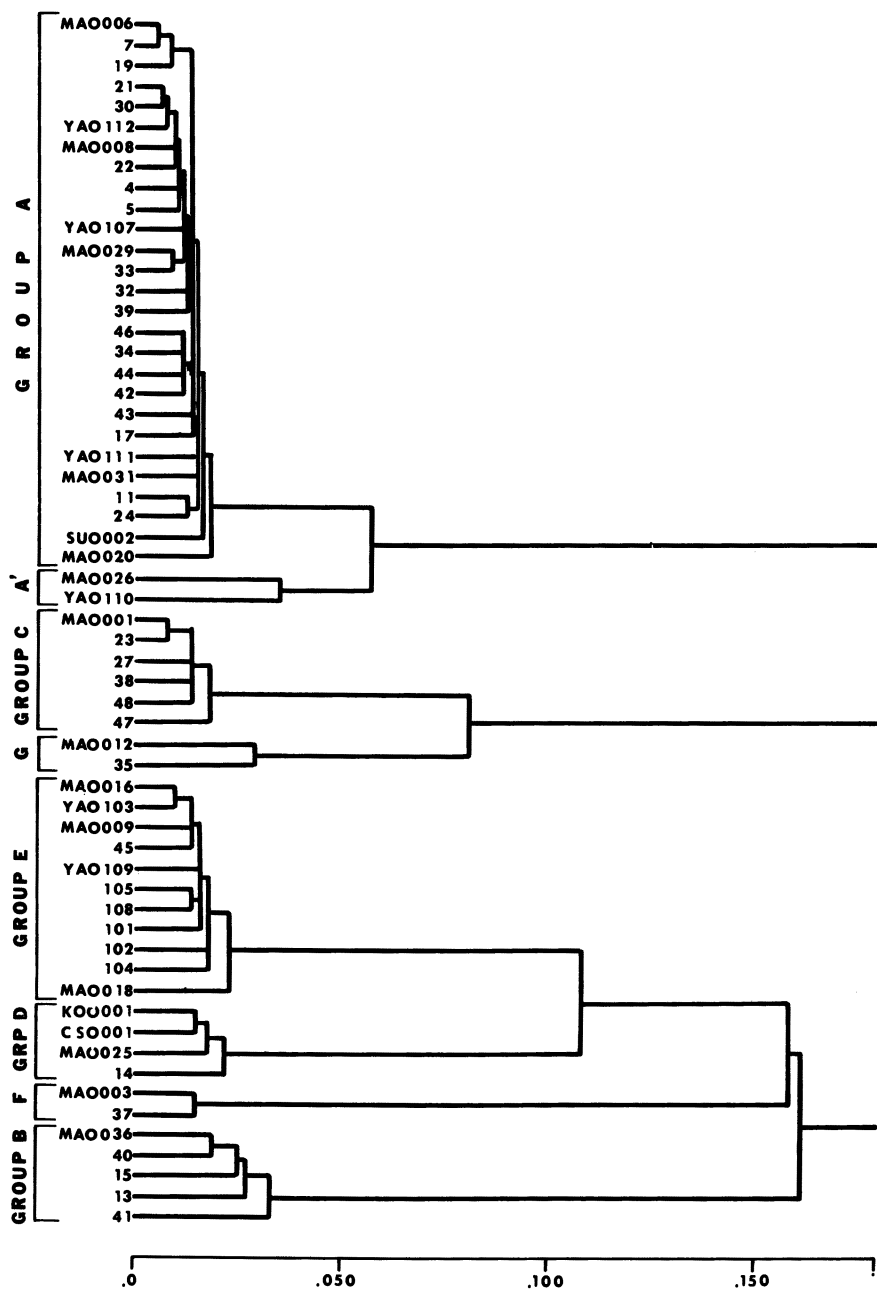


Figure 5. Clustering of archaeological artifact samples. Key: MAO, Tal-e Malyan; YAO, Tepe Yahya; SUO, Susa; KOO, All Kosh; CSO, Choga Safid.

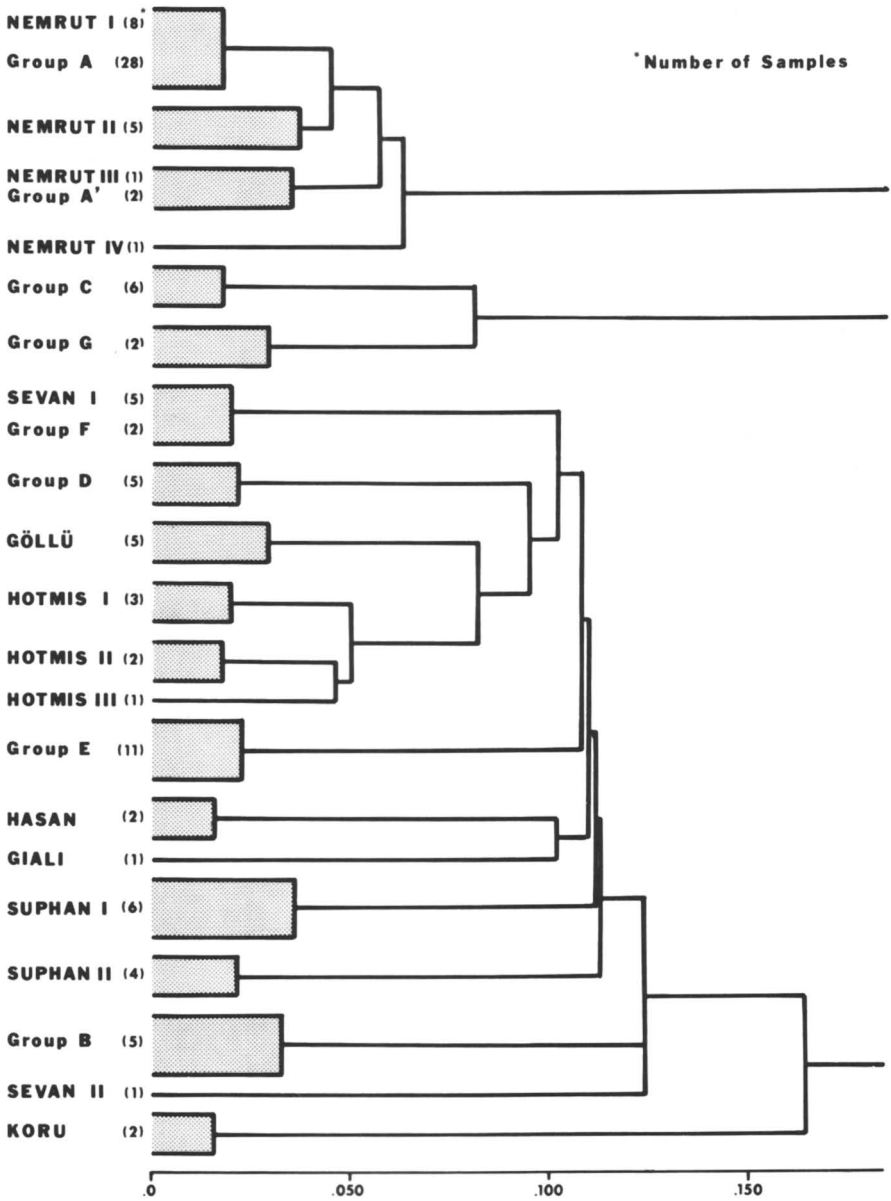


Figure 6. Clustering of geological source and archaeological artifact samples.

Table III. Comparison of Selected Elemental Concentrations Among Artifact Groups and Source Groups

<i>Elements</i>	<i>Nemrut I</i>	<i>Group A</i>	<i>Sevan I</i>	<i>Group F</i>
Na (%)	3.83 ± 0.03	3.89 ± 0.07	3.49 ± 0.05	3.45
Sc (ppm)	0.187 ± 0.005	0.193 ± 0.010	2.99 ± 0.03	2.95
Fe (%)	2.04 ± 0.02	2.03 ± 0.05	0.796 ± 0.011	0.802
Rb (ppm)	235 ± 5	229 ± 9	147 ± 6	145
La (ppm)	100 ± 0.5	103 ± 2	35.7 ± 0.4	35.4
Sm (ppm)	19.1 ± 0.3	19.2 ± 0.7	3.02 ± 0.04	3.00
Eu (ppm)	0.423 ± 0.011	0.419 ± 0.028	0.491 ± 0.026	0.488
Th (ppm)	26.7 ± 0.6	26.8 ± 0.9	17.8 ± 0.3	17.3

assigned source group. None of the remaining 5 artifact groups was clustered with any of the remaining 10 source groups.

The unassigned artifact-group means were then clustered with the converted means for the geological source from Nenezi Dağ and Zarnaki Tepe and artifact group B2 (1g) of unknown provenance. Figure 4 shows that none of the unassigned artifact groups clustered with the Central Anatolian source at Nenezi Dağ (NNZD). However, artifact Group E did form a very tight cluster with the Zarnaki Tepe source group (ZNKT) located in the ET-ASSR region, and artifact Group D clustered closely with Bradford's B2 (1g) artifact group of unknown provenance. As was shown earlier in this chapter, the agreement of the converted data among the three laboratories is excellent and lends credence to the contention that Group E artifacts originated at Zarnaki Tepe and that Groups D and B2 of Bradford are the same group. Group D artifacts included the samples from Ali Kosh and Choga Safid (KOO and CSO in Figure 5). Renfrew (26) found only Nemrut Dağ and source group 1g obsidian at these two sites, lending additional credence to the contention that artifact Group D obsidian is Renfrew's 1g obsidian.

Two important conclusions can be drawn from the source-artifact group assignments. First, none of the artifact groups originated at any of the known and analyzed Central Anatolian sources. As the analyzed sources from this region include the major sources (Göllü and Hotmis Dağ), it seems highly unlikely that new occurrences of obsidian will be discovered in this region that will prove to be the sources of the artifact groups of unknown provenance. Although central Anatolian obsidian has been found in very rare occurrences in lowland Mesopotamia (10,19), it does not appear to have penetrated into the Iranian highlands. The ET-ASSR region seems to be the origin of all obsidian from Tal-e Malyan and Tepe Yahya. Second, none of the artifact groups appears to originate from Suphan Dağ, a multiple source area only 60 km north of the important source at Nemrut Dağ. Much of the Suphan Dağ obsidian con-

tains large 2–4-mm plagioclase phenocrysts and is unsuitable for flaking; however, some of the Suphan Dağ material is of good quality. It is at present unclear why this material was not exploited.

Archaeological Implications

The source assignments, tabulated in Table IV, show that obsidian from eight chemically distinct sources reached Tal-e Malyan during all phases of occupation of the site. During a roughly comparable period of time, Tepe Yahya was receiving obsidian from three of these eight sources. At Tal-e Malyan, more than half of the artifacts were from the Nemrut Dağ I and III sources. The remaining artifacts were fairly evenly distributed among the other six source groups. Three artifacts, two from Nemrut Dağ and one from Group G, were surface finds of unknown provenance, and three additional artifacts, one each from Nemrut Dağ III, Zarnaki Tepe, and Group C, were from Qaleh/Middle Elamite context dating

Table IV. Artifact-to-Source Assignments at Tal-e Malyan and Tepe Yahya

<i>Tal-e Malyan</i>					
<i>Source Group</i>	<i>Banesh</i> 3400–2800 B.C.	<i>Kafteri</i> 2100–1800 B.C.	<i>Qaleh/M.E.</i> 1600–1000 B.C.	<i>Unknown</i>	<i>All-Phase Total</i>
Nemrut I	15 (88%)	7 (29%)	0	2	24
Nemrut II	0	0	1	0	1
Zarnaki	1 (6%)	2 (8%)	1	0	4
Sevan I	0	2 (8%)	0	0	2
Group D (1g)	1 (6%)	2 (8%)	0	0	3
Group B	0	5 (21%)	0	0	5
Group C	0	4 (17%)	1	1	6
Group G	0	2 (8%)	0	0	2
Total	17	24	3	3	47
<i>Tepe Yahya</i>					
<i>Source Group</i>	<i>VI</i> 4500–4000 B.C.	<i>VA-IVB</i> 3600–2600 B.C.	<i>Late/</i> <i>Unknown</i>	<i>All-Phase Total</i>	
Nemrut I	0	0	3	3	
Nemrut III	0	0	1	1	
Zarnaki	1	6	0	7	
Total	1	6	4	11	

from 1600 to 1000 B.C. Forty-one artifacts were from Banesh and Kafteri contexts and will be discussed at length later in this chapter. At Tepe Yahya, only about a third of the obsidian originated at Nemrut Dağ with both Nemrut Dağ I and III sources represented. Artifacts from these two sources were all from very late contexts or were surface finds of unknown provenance. All Tepe Yahya obsidian artifacts with firm archaeological provenance information, dating from 4500 to 2600 B.C., were assigned to the Zarnaki Tepe source, a relatively minor source at Tal-e Malyan.

When obsidian source assignments for comparable time periods, the Banesh Phase (3400–2800 B.C.) at Tal-e Malyan and periods VA to IVB (3600–2600 B.C.) at Tepe Yahya, are compared (Table IV), both sites show a heavy reliance on a single obsidian source. At Tal-e Malyan, the Nemrut Dağ I source contributes 88% of the obsidian; two other sources, Zarnaki Tepe and Group D (1g), contribute 6% each. At Tepe Yahya, however, the Zarnaki Tepe source contributes 100% of the analyzed obsidian.

Renfrew and Dixon (27) postulated an exchange network, the Zagros Interaction Zone, that included Nemrut Dağ (4c) obsidian and Group D (1g) obsidian (thought to be located west or southwest of Lake Van), operating along the western flanks of the Zagros Mountains as far south as Ali Kosh and Chogha Sefid on the Deh Luran Plain in 7500–5500 B.C. The proposed mechanism of the obsidian exchange was a reciprocal “down the line” exchange. After an apparent interruption in the flow of obsidian from these sources, the exchange resumed in about 5000 B.C., but with a third source, Group 3 (3a), replacing the 1g source. The redefined interaction zone, called the Tigris–Plateau Zone, now includes highland sites, and the mode of exchange is thought to have changed from reciprocal to central-place directional exchange (27). By 4000–3500 B.C., both Nemrut Dağ I (4c) and Group 3 (3a) had penetrated the southern highlands and are found at Tal-e Bakun, about 10 km from Tal-e Malyan in the same river basin. Renfrew et al. (10) and Dixon (28) postulated the Group 3 (3a) source to be located northeast of Lake Van and to have entered the system by way of Lake Urmia (Figure 7).

Epstein (19) analyzed obsidian from the lowland site of Choga Mish, dated to ca. 5500–4200 B.C. He found that 1g obsidian had not been replaced by Group 3 (3a) at Choga Mish, but that obsidian from these two sources coexisted with Nemrut Dağ (4c) obsidian. The Nemrut Dağ I (4c) source predominated with 1g, 3a, and possibly three other sources in subsidiary roles.

The source pattern for obsidian reaching Tal-e Malyan in 3400–2800 B.C. appears to have changed little from that reported by Renfrew et al. (10) and Epstein (19) for earlier lowland sites. Nemrut Dağ I obsidian predominates, with Group D (1g) and Zarnaki Tepe (3a?) present in minor

Publication Date: January 1, 1984 | doi: 10.1021/ba-1984-0205.ch002

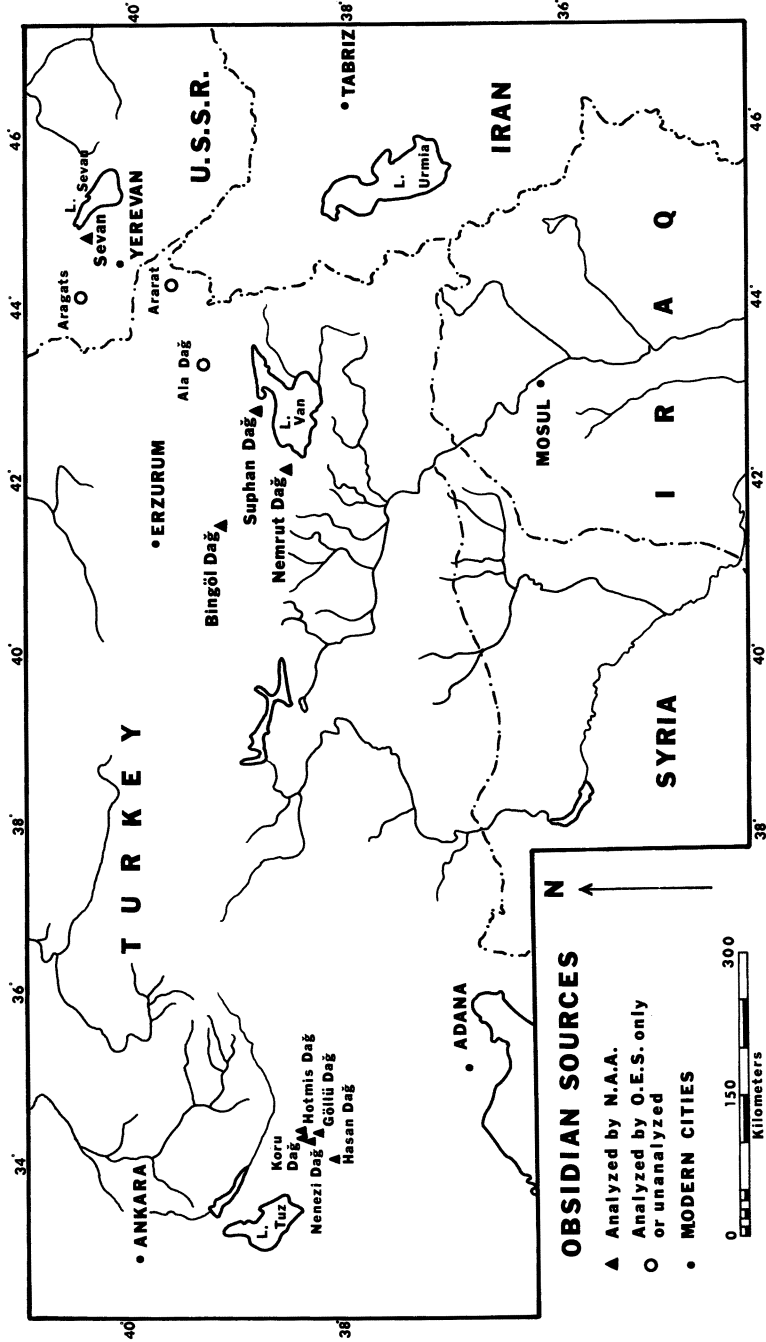


Figure 7. Postulated obsidian exchange routes.

amounts. However, the source pattern for obsidian from Tepe Yahya is quite different. Zarnaki Tepe (3a?) is the sole source of obsidian from good stratigraphic context for the periods from 3600 to 2600 B.C. No Group D (1g) obsidian is present and no Nemrut Dağ obsidian is from good context. Although the presence of Nemrut Dağ obsidian cannot be totally discounted, it would appear to be in a subsidiary role to the Zarnaki Tepe obsidian.

The Tepe Yahya sample is admittedly a small one; however, the distribution pattern argues against the inclusion of Tal-e Malyan and Tepe Yahya in the same obsidian exchange network during the period from 3500 to 2700 B.C. If, as Renfrew suggests, the exchange at this time took place between central places, obsidian moving along the western flanks of the Zagros Mountains should have moved through Susa and Tal-e Malyan before reaching Tepe Yahya (Figure 7). Were this the case, Nemrut Dağ obsidian should also be the predominant source at Tepe Yahya, as it is at Tal-e Malyan. It appears that the obsidian reaching Tepe Yahya may have taken a different route, more directly connected to the Zarnaki Tepe source north of Lake Van. This route could be from the Lake Urmia area, where Renfrew et al. (10,27) found Group 3 obsidian to predominate, via the valley systems east of the Zagros Mountains and thus to Tepe Yahya. Information on obsidian from archaeological sites in the valleys of the eastern Zagros is scarce or nonexistent and so this hypothesized exchange must await confirmation.

One-half of the obsidian recovered at Tal-e Malyan was from the Kaferi Phase ca. 2000 B.C., contemporaneous with Ur III in Mesopotamia. Comparison of the source distribution patterns between the earlier Banesh Phase and the later Kaferi Phase shows distinctly different patterns of source utilization. Unfortunately, contemporaneous obsidian artifacts from Tepe Yahya were not available, so these changes could not be monitored in the south central highlands.

During the Kaferi Phase, while the three sources present in the Banesh Phase continue to reach the site, four new sources have been added to the obsidian inventory. Three of these are of unknown provenance (Groups B, C, and G); however, the fourth is from the Sevan I source in the Armenian S.S.R. about 300 km north of Lake Van (Table IV). The distribution of artifacts among the sources also changes dramatically. The Nemrut Dağ I source contribution drops from 88% in the Banesh Phase to 29% in the Kaferi Phase; the contribution of the other sources rises from 12% in the Banesh to 71% in the Kaferi. Two of the sources introduced in the Kaferi Phase, Groups B and C, are 21% and 17%, respectively, of the assemblage. The distribution pattern has changed from heavy reliance on a single source in the Banesh to a more even reliance on at least three sources in the Kaferi.

In addition to these changes, it appears that luxury items made of obsidian were introduced during the Kaferi Phase. Two bowl fragments and a large highly polished bead/ring were recovered. One of the bowl fragments and the bead/ring were made of Nemrut Dağ I obsidian; the other bowl was of Zarnaki Tepe obsidian. If, as hypothesized earlier, these artifacts were not made at Tal-e Malyan, then one or more sites of bowl manufacture should exist, probably near Lake Van.

In summary, four major aspects of obsidian exchange have altered between Banesh and Kaferi times at Tal-e Malyan.

1. The number of sources utilized has increased twofold.
2. The reliance on a single source has been replaced by a more uniform distribution among the sources.
3. The geographical area exploited, which had centered on the Lake Van area, has expanded to include the most northerly known source on Lake Sevan in Soviet Armenia.
4. Luxury items make their appearance during the Kaferi Phase.

These changes argue for significant alterations in either the organization of the exchange, the political alignment in the source region, or both. During the Kaferi Phase, Tal-e Malyan together with Susa occupied an important and influential position as co-capital of Elam and as conduit for raw materials and finished goods moving out of the highlands and into lowland Mesopotamia. The position of importance held by Tal-e Malyan does not, however, explain the changes observed in the obsidian exchange. Although Tal-e Malyan might have been able to command a larger share of the exchange in many other types of goods, its distance from the obsidian sources makes its direct influence over events in the source region unlikely. One must look to developments in Ur III Mesopotamia for factors that effected the observed changes in the obsidian exchange. Expansion of Ur III influence into northern Mesopotamia or strictly local developments in the source region appear to have resulted in increased access to a larger number of obsidian sources. A tighter control over the exchange may be indicated, with the possibility of collection and transshipment locales resulting in the mixing of obsidian from different sources.

Conclusions

This study has demonstrated that precise chemical analysis is a powerful tool for the characterization and provenance determination of Middle Eastern obsidian. Thirteen to 15 chemically distinctive groups were distinguishable in geological source samples collected from eight source

areas. It appears that several of these groups represent different eruptive events at the same volcanic source. The presence of multiple chemical groups at the same volcano points out the need for extensive sampling at each potential source.

Eight chemical groups were identified within the artifact sample. Of these groups, four could be identified with known geological sources; however, the remaining four groups are of unknown provenance and three of the four do not appear to have been previously recognized. Clearly a great deal more field and analytical work needs to be done in the Eastern Turkish–Armenian S.S.R. region before a complete inventory of sources is available.

This investigation also demonstrates the potential of provenance studies to monitor exchange in both obsidian and other goods presumed to be flowing in the same network. There is a tendency to think of exchange as a unified phenomenon, i.e., a single network, organized along a single set of principles for each period of cultural development. Obsidian evidence from Tal-e Malyan and Tepe Yahya shows that exchange must be viewed as a much more complex procedure. Archaeological evidence indicates that these two sites should be linked in the exchange of several types of items. The obsidian source patterns point to the opposite conclusions for obsidian. Although obsidian reaching Tal-e Malyan during the period from 3400 to 2800 B.C. fits well with the central place redistributive model developed by Renfrew et al. (10) for the lowlands, Tepe Yahya does not seem to be participating in this obsidian exchange system. Tepe Yahya seems to have received its obsidian through a different system that may have been organized on a similar level, or may be a continuation of the reciprocal down-the-line system from earlier periods.

Coincident with Tal-e Malyan's expansion as a major local and regional power during the Kaferi Phase (2100–1800 B.C.), the level of organization and the scope of the obsidian exchange also appear to have undergone a significant change. The changes in the obsidian exchange system seem to be centered in the source region and possibly in northern Mesopotamia, but similar changes in exchange of other materials were also undoubtedly occurring. Whether long-range exchange was a factor contributing to, or the result of, increased sociopolitical organization in the region cannot be assessed from the study of a single material.

Extension of this study of obsidian into other sites in highland Iran is needed to outline more definitively the exchange routes in effect during the late fourth and early third millennia B.C. Expansion of precise provenance studies to include other types of exchange items is needed to provide the fine-grained information about the direction and nature of exchange not possible with more conventional archaeological techniques. It will, however, be the integration of provenance studies and the more

traditional archaeological techniques that will eventually determine the role of long-range exchange in the development of the Middle East.

Acknowledgments

I would like to thank Melinda A. Zeder for her critical reading of the manuscript and her helpful suggestions. I gratefully acknowledge William Sumner for providing the samples from Tal-e Malyan; C. C. Lamberg-Karlovsky for the Tepe Yahya samples; and Richard Watson and J. Allen for the geological source samples. Drs. Sumner, Lamberg-Karlovsky, and Watson's work was supported by various grants from the National Science Foundation. This work was supported by the Conservation-Analytical Laboratory of the Smithsonian Institution with substantial help from the personnel of the Activation Analysis Group, Division of Inorganic Analytical Chemistry, and the Reactor Operation Division of the National Bureau of Standards, Washington, D.C.

Appendix A

Elemental Concentrations in the Source Samples (Data given as ppm)

<i>Samples</i>	<i>Na</i> (%)	<i>Sc</i>	<i>Fe</i> (%)	<i>Zn</i>	<i>As</i>	<i>Br</i>	<i>Rb</i>	<i>Sb</i>	<i>Cs</i>	<i>Ba</i>
<i>Nemrut Dağ I</i>										
XNO523	3.82	.180	2.03	140	22.1	6.34	233	1.23	7.66	112
XNO524	3.82	.189	2.03	140	22.8	6.27	233	1.34	7.50	75.1
XNO527	3.82	.190	2.03	145	23.0	5.64	229	1.12	7.45	141
XNO528	3.87	.196	2.07	152	24.3	7.63	240	1.25	7.89	70
XNO529	3.86	.187	2.06	140	23.3	6.59	241	1.26	7.68	107
XNO530	3.83	.184	2.05	142	24.2	6.19	238	1.36	7.78	88.5
XNO531	3.81	.182	2.05	149	22.2	8.10	239	1.29	7.90	120
XNO534	3.78	.185	2.00	139	23.1	6.20	227	(1.48)	7.55	112
Mean	3.83	.187	2.04	143	23.1	6.62	235	1.26	7.68	108
± 1σ	.03	.005	.02	5	.8	.82	5	.08	.17	21
<i>Nemrut Dağ II</i>										
XNO520	4.26	.214	2.99	161	18.5	5.00	249	.805	8.78	114
XNO521	4.18	.352	2.49	135	20.9	4.93	243	1.11	9.13	120
XNO526	4.15	.198	3.19	163	20.6	4.50	268	1.20	9.62	123
XNO532	4.33	.241	2.81	147	19.1	5.83	256	.992	8.76	155
XNO533	4.24	.313	3.25	167	22.1	5.71	260	1.17	9.36	107
Mean	4.23	.257	2.93	154	20.2	5.16	255	1.05	9.12	123
± 1σ	.07	.072	.33	14	1.5	.58	10	.19	.38	19
<i>Nemrut Dağ III</i>										
XNO525	4.22	.106	3.01	173	33.3	18.8	252	2.42	14.7	175
<i>Nemrut Dağ IV</i>										
XNO522	4.30	.908	3.12	150	18.6	3.87	246	1.43	8.03	135
<i>Suphan Dağ I</i>										
XSO500	3.31	3.41	.816	32.4	13.6	n.d.	211	1.07	7.68	n.d.
XSO501	3.06	3.43	.817	26.7	11.6	n.d.	210	1.14	7.72	n.d.
XSO503	3.05	3.43	.814	24.8	12.6	n.d.	212	1.14	7.81	n.d.
XSO508	3.09	3.57	.954	39.1	12.0	n.d.	206	1.07	7.88	n.d.
XSO509	3.06	3.55	.841	37.8	13.2	n.d.	210	1.17	7.95	n.d.
XSO510	3.05	3.63	.906	26.6	13.0	n.d.	220	1.38	8.00	n.d.
Mean	3.10	3.50	.856	30.7	12.6	n.d.	211	1.16	7.84	n.d.
± 1σ	.10	.09	.059	6.6	.8	—	5	.11	.13	—
<i>Suphan Dağ II</i>										
XSO502	3.04	2.97	.862	27.5	8.12	n.d.	168	.626	5.13	602
XSO504	3.13	3.09	.910	25.9	8.48	n.d.	177	.608	5.30	577
XSO506	3.06	3.00	.886	26.1	8.48	n.d.	158	.602	5.02	573
XSO507	3.02	2.97	.894	36.1	10.0	n.d.	168	.578	5.21	620
Mean	3.06	3.01	.888	28.6	8.74	n.d.	168	.603	5.16	593
± 1σ	.05	.06	.020	4.9	.84	—	8	.020	.12	22

except where noted otherwise. N.D., not determined; n.d., not detected)

<i>La</i>	<i>Ce</i>	<i>Nd</i>	<i>Sm</i>	<i>Eu</i>	<i>Gd</i>	<i>Yb</i>	<i>Lu</i>	<i>Hf</i>	<i>Ta</i>	<i>Th</i>	<i>U</i>
<i>Source Group</i>											
100	189	92.0	19.1	.421	12.4	13.6	2.01	27.9	3.69	26.3	7.77
101	189	86.9	19.1	.426	12.1	13.8	2.08	28.1	3.81	26.3	8.11
101	188	85.3	18.6	.445	11.4	13.6	2.00	27.9	3.78	26.1	7.78
101	192	89.4	19.3	.428	12.1	14.0	2.10	29.4	3.91	27.5	8.37
100	190	87.7	19.4	.418	11.4	13.9	2.07	28.9	3.92	27.3	8.25
99.8		90.7	19.4	.423	10.4	13.8	2.06	28.8	4.01	27.2	8.34
	189	87.7	19.4	.416	10.9	14.2	2.10	29.0	3.93	27.0	8.63
99.3	186	87.0	18.8	.406	10.9	13.6	2.02	27.8	3.68	25.9	7.91
100	189	88.3	19.1	.423	11.5	13.8	2.06	28.5	3.84	26.7	8.15
.5	1.5	2.2	.3	.011	.7	.2	.04	.6	.12	.6	.31
<i>Source Group</i>											
115	209	98.6	20.0	.792	14.4	14.6	2.17	28.7	4.46	31.4	9.39
110	200	94.7	19.0	.453	12.6	13.7	2.07	28.0	4.22	31.9	9.67
121	222	103	20.7	.758	13.4	15.6	2.30	31.3	4.84	33.4	11.4
110	202	93.3	19.3	.656	11.3	14.1	2.17	28.3	4.40	30.9	9.91
119	220	102	21.6	.806	12.3	15.3	2.38	30.9	4.88	33.3	10.6
115	210	98.2	20.1	.678	12.5	14.6	2.19	29.4	4.55	32.2	10.2
5	10	4.4	1.1	.184	1.2	.8	.15	1.6	.30	1.1	.8
<i>Source Group</i>											
104	197	92.5	20.7	.670	14.1	15.2	2.22	30.3	4.18	33.1	11.8
<i>Source Group</i>											
115	210	96.4	19.3	1.02	12.2	14.1	2.13	28.4	4.25	30.2	8.63
<i>Source Group</i>											
20.5	38.4	16.4	4.49	.140	4.25	3.55	.660	3.64	1.34	14.8	5.55
20.7	41.3	17.6	4.35	.173	4.80	3.79	.626	3.34	1.38	15.6	6.83
19.4	39.1	15.1	4.14	.152	4.92	3.87	.620	3.26	1.43	14.8	6.99
23.9	48.3	17.3	4.88	.145	3.48	4.09	.644	4.06	1.33	17.5	7.27
19.0	39.1	17.9	4.27	.148	3.80	3.70	.625	3.35	1.43	15.4	7.17
18.1	36.9	13.5	4.10	.144	5.30	3.86	.621	3.26	1.36	14.7	7.09
20.2	40.4	16.4	4.36	.150	4.38	3.80	.633	3.47	1.38	15.3	6.79
2.0	4.0	1.9	.29	.012	.77	.19	.016	.31	.04	1.1	.79
<i>Source Group</i>											
32.3	59.8	22.9	5.00	.402	5.55	3.06	.510	3.79	.812	17.1	4.66
	62.8	22.1	5.28	.433	4.44	3.22	.548	4.42	.893	18.4	4.86
33.7	61.2	23.9	5.10	.439	4.57	3.19	.528	4.71	.895	17.6	4.87
33.1	60.0	22.5	4.89	.458	3.71	3.12	.503	3.75	.886	17.3	4.56
33.3	60.9	22.8	5.07	.433	4.52	3.15	.522	4.15	.871	17.6	4.74
.8	1.4	.8	.17	.024	.81	.07	.020	.50	.042	.6	.16

Continued on next page.

Elemental Concentrations in the

<i>Samples</i>	<i>Na</i> (%)	<i>Sc</i>	<i>Fe</i> (%)	<i>Zn</i>	<i>As</i>	<i>Br</i>	<i>Rb</i>	<i>Sb</i>	<i>Cs</i>	<i>Ba</i>
<i>Lake Sevan I</i>										
XRO622	3.43	3.02	.811	40.3	2.18	n.d.	158	.328	5.56	601
XRO623	3.46	3.01	.795	39.6	3.07	n.d.	143	.308	5.07	583
ARO001	3.47	2.96	.779	N.D.	N.D.	n.d.	142	.277	5.22	572
ARO003	3.55	2.98	.802	N.D.	N.D.	n.d.	148	.339	5.11	567
ARO004	3.54	2.96	.794	N.D.	N.D.	n.d.	145	.333	5.32	577
Mean	3.49	2.99	.796	40.0	2.63	n.d.	147	.317	5.26	580
$\pm 1\sigma$.05	.03	.011	—	—	—	6	.025	.20	13
<i>Lake Sevan II</i>										
ARO002	3.17	2.53	.392	36.9	3.84	n.d.	148	.493	3.69	162
<i>Göllü Dağ</i>										
XGO600	3.16	1.78	.559	23.4	8.07	n.d.	222	1.06	8.37	208
XGO601	3.01	1.70	.554	25.4	7.00	n.d.	208	1.04	7.67	369
XCO640	3.13	1.68	.542	19.4	6.20	n.d.	196	.859	7.30	305
XEO540	3.10	1.72	.569	22.7	7.09	1.84	204	.902	7.75	270
XEO541	3.05	1.69	.560	20.5	6.42	n.d.	199	.821	7.54	285
Mean	3.09	1.71	.557	22.3	6.96	—	206	.936	7.73	287
$\pm 1\sigma$.06	.04	.010	2.4	.73	—	10	.108	.40	58
<i>Hasan Dağ</i>										
XHO660	3.15	2.05	.580	20.5	6.39	2.31	145	.789	5.11	1004
XHO661	3.39	2.06	.586	21.0	6.03	1.48	144	.784	5.32	981
Mean	3.27	2.05	.583	20.8	6.21	1.90	145	.787	5.22	993
<i>Koru Dağ</i>										
XAO560	3.38	2.07	.568	24.9	11.3	n.d.	298	1.23	14.2	193
XAO561	3.35	2.09	.579	22.6	11.1	n.d.	298	1.35	15.0	157
Mean	3.37	2.08	.574	23.8	11.2	n.d.	298	1.29	14.6	175
<i>Hotmis Dağ I</i>										
XKO580	3.13	1.02	.738	32.8	5.00	2.82	201	.520	8.47	440
XKO581	3.20	1.04	.755	30.1	6.05	3.07	196	.683	8.39	431
XKO585	3.22	1.08	.749	30.5	6.48	2.76	196	.502	8.28	448
Mean	3.18	1.05	.747	31.1	5.84	2.88	198	.568	8.38	440
$\pm 1\sigma$.05	.03	.009	1.5	.76	.16	3	.100	.05	9
<i>Hotmis Dağ II</i>										
XKO582	3.41	1.30	1.23	41.2	4.67	1.96	171	.637	6.85	550
XKO584	3.48	1.31	1.22		5.63	3.31	176	.613	6.85	572
Mean	3.45	1.31	1.23	41.6	5.15	2.64	174	.625	6.85	561
<i>Hotmis Dağ III</i>										
XKO583	3.14	1.18	.944	34.5	5.07	2.81	194	.561	7.42	477
<i>Giali</i>										
XYO700	2.86	1.56	.667	18.7	9.26	7.14	155	.510	5.23	1032

Source Samples—Continued

<i>La</i>	<i>Ce</i>	<i>Nd</i>	<i>Sm</i>	<i>Eu</i>	<i>Gd</i>	<i>Yb</i>	<i>Lu</i>	<i>Hf</i>	<i>Ta</i>	<i>Th</i>	<i>U</i>
Source Group											
35.9	57.1	18.6	3.03	.508	n.d.	2.76	.403	5.18	3.10	18.3	9.47
35.2	56.4	28.0	3.07	.476	4.02	2.80	.406	4.75	3.10	17.7	9.32
35.4	55.3	18.5	2.98	.469	n.d.	2.69	.402	4.94	3.10	17.7	9.24
36.0	56.0	17.7	3.04	.528	n.d.	2.70	.400	4.93	3.03	17.7	9.40
36.1	55.9	17.4	2.98	.479	n.d.	2.68	.400	4.90	2.98	17.6	9.09
35.7	56.1	20.0	3.02	.491	—	2.73	.402	4.94	3.06	17.8	9.30
.4	.7	4.5	.04	.026	—	.05	.002	.15	.05	.3	.15
Source Group											
17.6	32.4	12.0	2.87	.238	N.D.	3.06	.439	3.40	2.42	14.7	8.19
Source Group											
25.7	45.4	14.8	2.83	.131	N.D.	2.61	.402	3.45	2.37	23.4	9.50
26.7	45.3	13.2	2.93	.148	N.D.	2.40	.372	3.49	2.06	23.0	8.40
26.0	43.4	13.2	2.59	.138	N.D.	2.44	.316	2.86	2.21	22.5	8.07
26.7	45.6	14.1	2.71	.155	N.D.	2.43	.375	3.20	2.13	23.4	8.53
25.9	44.4	15.3	2.91	.133	N.D.	2.43	.359	3.20	2.07	22.8	8.29
26.2	44.8	14.1	2.79	.141	N.D.	2.46	.365	3.24	2.17	23.0	8.56
.5	.9	.9	.14	.010	—	.08	.031	.25	.13	.4	.55
Source Group											
27.2	43.7	12.6	2.34	.418	n.d.	1.39	.280	2.86	1.35	14.3	3.95
27.0	44.6	12.0	2.38	.428	2.54	1.57	.257	2.92	1.40	14.6	4.21
27.1	44.2	12.3	2.36	.423	—	1.48	.269	2.89	1.38	14.5	4.08
Source Group											
15.2	31.8	12.8	3.62	.020	N.D.	4.58	.664	4.46	3.99	38.9	12.8
15.5	32.1	14.0	3.62	n.d.	N.D.	4.64	.652	4.51	3.68	33.8	12.4
15.4	32.0	13.4	3.62	.020	N.D.	4.61	.658	4.49	3.84	35.4	12.6
Source Group											
31.1	50.4	15.5	2.85	.276	N.D.	3.01	.434	4.10	2.25	28.9	8.24
31.7	51.1	16.0	2.90	.272	N.D.	3.00	.446	4.20	2.15	29.1	8.26
31.9	51.2	16.4	2.84	.295	N.D.	3.05	.459	4.32	2.20	30.1	8.33
31.6	51.0	16.0	2.86	.281	N.D.	3.02	.446	4.21	2.20	29.4	8.28
.4	.6	.5	.03	.012	—	.03	.013	.11	.05	.6	.05
Source Group											
37.7	60.6	19.7	3.47	.503	N.D.	3.12	.524	5.62	1.81	25.6	7.09
38.6	61.7	16.9	3.40	.517	3.88	3.10	.479	5.48	1.94	26.2	7.24
38.2	61.2	18.3	3.44	.510	3.88	3.11	.502	5.55	1.88	25.9	7.17
Source Group											
34.5	55.7	19.4	3.15	.386	N.D.	2.96	.507	4.81	1.96	27.1	7.59
Source Group											
42.9	64.5	16.7	2.69	.282	3.10	1.94	.317	3.37	1.57	18.8	5.02

Appendix B

Elemental Concentrations in the Artifact Samples (Data given as ppm)

<i>Samples</i>	<i>Na</i> (%)	<i>Sc</i>	<i>Fe</i> (%)	<i>Zn</i>	<i>As</i>	<i>Br</i>	<i>Rb</i>	<i>Sb</i>	<i>Cs</i>	<i>Ba</i>
<i>Artifact Group A:</i>										
MAO002	3.83	.181	1.97	147	N.D.	N.D.	217	1.32	7.32	99.5
MAO004	3.80	.208	2.04	138	24.8	6.45	227	1.42	7.53	83.7
MAO005	3.94	.208	2.09	123	23.9	5.90	224	1.26	7.74	n.d.
MAO006	3.82	.189	1.98	146	23.1	6.30	220	1.42	7.00	82.4
MAO007	3.83	.179	1.96	145	25.1	5.46	220	1.40	7.15	n.d.
MAO008	3.82	.202	2.09	146	23.0	6.88	227	1.23	7.52	n.d.
MAO011	3.89	.204	2.00	N.D.	N.D.	N.D.	226	1.26	7.68	96.5
MAO017	3.91	.192	2.12	N.D.	N.D.	N.D.	232	1.26	7.84	67.4
MAO019	3.84	.201	1.97	143	23.7	6.60	220	1.39	7.14	164
MAO020	3.85	.201	1.97	N.D.	N.D.	N.D.	221	1.17	7.86	79.0
MAO021	3.87	.200	2.08	142	26.2	7.15	224	1.32	7.46	88.9
MAO022	3.96	.190	2.09	148	25.8	7.10	231	1.43	7.57	110
MAO024	3.95	.194	1.99	N.D.	N.D.	N.D.	224	1.34	7.60	78.5
MAO029	3.90	.182	2.04	N.D.	N.D.	N.D.	228	1.41	7.50	81.6
MAO030	3.74	.202	2.08	150	26.8	7.28	229	1.32	7.67	n.d.
MAO031	3.95	.188	2.13	N.D.	N.D.	N.D.	241	1.33	7.01	n.d.
MAO032	3.81	.182	2.04	144	24.9	7.25	228	1.42	7.77	n.d.
MAO033	3.92	.181	2.03	N.D.	N.D.	N.D.	227	1.35	7.55	78.1
MAO034	3.93	.200	2.01	146	26.7	6.84	235	1.36	7.35	111
MAO039	3.98	.187	2.01	149	22.1	5.14	229	1.30	7.83	83.3
MAO042	3.98	.197	2.03	147	23.5	6.13	233	1.39	7.62	139
MAO043	3.96	.179	2.02	157	25.7	6.94	233	1.27	7.71	n.d.
MAO044	3.89	.199	1.98	149	22.9	6.26	238	1.25	7.41	n.d.
MAO046	3.92	.191	1.99	152	22.2	5.57	236	1.56	7.69	n.d.
YAO107	4.02	.203	2.13	152	26.2	6.49	248	1.45	7.86	n.d.
YAO111	3.87	.172	1.96	N.D.	N.D.	N.D.	202	1.46	7.74	57.7
YAO112	3.85	.192	2.07	142	24.0	6.49	236	1.36	7.50	n.d.
SUO002	3.97	.197	2.06	158	24.5	6.97	247	1.33	7.98	n.d.
Mean	3.89	.193	2.03	146	24.5	6.48	229	1.35	7.56	93.8
± 1σ	.07	.010	.05	7	1.5	.62	9	.08	.26	26.8
<i>Artifact Group A':</i>										
MAO026	3.97	.128	2.50	167	33.4	16.9	243	2.15	14.0	170
YAO110	4.25	.188	2.83	N.D.	N.D.	N.D.	219	2.14	13.8	86.8
Mean	4.11	.158	2.67	167	33.4	16.9	231	2.15	13.9	128
<i>Artifact Group B:</i>										
MAO013	3.13	1.59	.457	28.3	n.d.	n.d.	169	.181	3.87	173
MAO015	3.22	1.72	.467	32.6	n.d.	n.d.	187	.217	4.36	172
MAO036	3.21	1.69	.461	31.1	n.d.	n.d.	183	.143	4.23	200
MAO040	3.29	1.65	.472	30.0	n.d.	n.d.	184	.154	4.27	172
MAO041	3.31	1.84	.445	25.2	n.d.	n.d.	200	.241	4.87	170
Mean	3.23	1.70	.460	29.3	n.d.	n.d.	184	.184	4.30	177
± 1σ	.07	.10	.011	3.1	—	—	11	.045	.37	13

except where noted otherwise. N.D., not determined; n.d., not detected)

<i>La</i>	<i>Ce</i>	<i>Nd</i>	<i>Sm</i>	<i>Eu</i>	<i>Gd</i>	<i>Yb</i>	<i>Lu</i>	<i>Hf</i>	<i>Ta</i>	<i>Th</i>	<i>U</i>
<i>Nemrut Dağ I</i>											
99.7	188	81.8	N.D.	.417	21.3	13.5	N.D.	27.1	4.05	26.2	N.D.
103	191	86.5	19.2	.433	18.5	14.2	2.10	27.5	3.74	26.3	8.07
105	195	89.4	19.8	.417	17.4	14.5	2.15	28.3	3.80	26.7	8.62
98.3	189	85.1	18.5	.403	19.4	13.7	2.02	26.3	3.98	25.7	8.22
98.1	188	84.3	18.2	.408	18.2	13.4	2.02	26.3	3.97	25.4	8.11
104	196	92.0	19.8	.421	18.2	14.4	2.10	28.1	3.91	27.1	8.85
101	193	N.D.	N.D.	.422	N.D.	13.9	2.22	23.7	3.96	26.9	N.D.
103	N.D.	N.D.	19.5	.458	N.D.	14.3	2.22	30.8	4.37	28.3	N.D.
98.9	189	79.0	18.8	.420	15.7	13.5	1.99	26.3	3.87	25.6	8.39
102	184	N.D.	20.5	.426	N.D.	13.9	2.22	22.4	3.91	26.7	N.D.
104	195	92.7	19.5	.404	17.5	14.3	2.08	28.0	3.89	29.9	8.49
104	195	94.1	19.7	.427	16.3	14.3	2.12	28.1	4.05	27.0	8.78
103	193	N.D.	N.D.	.379	N.D.	14.3	2.24	21.4	3.81	27.1	N.D.
104	N.D.	N.D.	18.1	.417	N.D.	14.2	2.09	28.0	4.20	26.3	N.D.
104	197	92.2	19.7	.397	15.9	14.4	2.10	28.5	4.09	27.0	8.65
106	N.D.	N.D.	19.9	.491	N.D.	15.0	2.22	29.4	4.41	27.9	N.D.
100	189	86.6	19.0	.369	19.2	14.4	2.10	28.3	3.93	27.1	8.01
104	N.D.	N.D.	18.1	.360	N.D.	14.0	2.09	28.7	4.31	26.5	N.D.
104	192	83.5	18.7	.417	18.1	13.8	2.07	26.7	4.33	26.6	8.01
104	193	83.3	18.6	.440	18.5	13.8	2.10	26.8	4.30	26.7	8.08
103	193	82.8	18.8	.399	15.3	14.7	2.08	26.9	4.25	26.8	6.61
101	190	82.7	19.5	.472	14.3	13.7	2.13	27.4	4.42	27.3	7.88
101	192	78.6	19.1	.406	15.7	13.7	2.05	26.7	4.29	26.3	8.30
101	189	79.3	19.3	.446	16.1	13.9	2.08	27.2	4.38	26.9	8.08
107	199	91.2	20.3	.430	20.1	14.6	2.15	28.8	3.88	27.7	8.87
101	193	N.D.	N.D.	.400	N.D.	14.0	2.01	26.0	4.27	25.3	N.D.
103	193	90.9	19.4	.415	17.5	14.2	2.09	28.0	3.85	26.6	8.48
105	196	85.4	19.0	.451	18.2	14.4	2.07	28.5	4.13	27.2	8.37
103	192	86.1	19.2	.419	17.6	14.1	2.11	27.2	4.08	26.8	8.26
2	3	4.9	.7	.028	1.8	.4	.07	2.0	.21	.9	.50
<i>Nemrut Dağ III</i>											
100	192	84.7	19.4	.566	N.D.	14.4	2.10	27.8	4.07	32.4	11.8
102	197	N.D.	N.D.	.508	N.D.	14.6	2.09	25.4	4.46	29.9	N.D.
101	195	84.7	19.4	.537	N.D.	14.5	2.10	26.6	4.26	31.2	11.8
<i>Unknown Provenance</i>											
38.1	56.4	13.0	1.68	.175	n.d.	1.50	.256	3.80	2.17	31.7	9.64
36.0	54.2	13.8	1.58	.145	n.d.	1.52	.255	3.58	2.24	33.9	10.3
37.6	54.6	12.1	1.60	.158	n.d.	1.57	.248	3.64	2.32	33.7	9.60
40.4	58.6	15.0	1.75	.153	n.d.	1.59	.254	3.68	2.42	33.6	9.88
35.1	50.7	12.2	1.46	.134	n.d.	1.62	.264	3.63	2.53	35.3	10.9
37.4	54.8	13.2	1.61	.152	n.d.	1.56	.255	3.67	2.33	33.6	10.1
2.1	3.0	1.2	.11	.016	—	.05	.006	.08	.14	1.3	.5

Continued on next page.

**American Chemical
Society Library**

1155 16th St., N.W.

In *Archaeological Chemistry*, III; Lambert, J.;
Advances in Chemistry, American Chemical Society, Washington, DC, 1984.

20036

Elemental Concentrations in the

<i>Samples</i>	<i>Na</i> (%)	<i>Sc</i>	<i>Fe</i> (%)	<i>Zn</i>	<i>As</i>	<i>Br</i>	<i>Rb</i>	<i>Sb</i>	<i>Cs</i>	<i>Ba</i>
<i>Artifact Group C:</i>										
MAO001	3.86	.480	1.54	145	1.62	3.29	117	.379	1.30	616
MAO023	3.89	.480	1.58	142	n.d.	4.37	120	.364	1.30	631
MAO027	3.82	.469	1.55	140	n.d.	2.90	108	.347	1.10	636
MAO038	3.84	.483	1.54	138	n.d.	n.d.	117	.423	1.16	671
MAO047	3.93	.482	1.55	143	n.d.	2.58	122	.299	1.44	625
MAO048	3.77	.489	1.59	148	n.d.	3.29	123	.434	1.28	610
Mean	3.85	.480	1.56	143	1.62	3.23	118	.371	1.26	631
$\pm 1\sigma$.06	.007	.02	4	—	.70	6	.054	.13	21
<i>Artifact Group D:</i>										
MAO014	3.74	2.48	1.33	40.6	6.69	2.23	225	.949	10.5	576
MAO025	3.66	2.13	1.25	37.8	7.28	2.92	226	.994	10.4	487
KOO001	3.52	2.14	1.30	33.1	7.36	n.d.	251	.843	10.5	489
CSO001	3.56	2.16	1.30	39.3	7.67	n.d.	250	.961	10.2	511
Mean	3.62	2.22	1.30	37.6	7.24	2.55	238	.935	10.4	515
$\pm 1\sigma$.10	.17	.03	3.5	.43	—	15	.070	.1	42
<i>Artifact Group E:</i>										
MAO009	3.78	1.89	.940	60.8	n.d.	n.d.	218	.386	9.09	188
MAO016	3.77	1.90	.941	63.5	n.d.	n.d.	203	.435	8.75	n.d.
MAO018	3.68	1.81	.888	58.5	n.d.	1.13	199	.352	8.39	n.d.
MAO045	3.86	1.86	.943	61.0	n.d.	n.d.	216	.437	9.34	223
YAO101	3.84	1.90	.972	62.6	2.63	n.d.	226	.432	9.51	79.0
YAO102	3.81	1.89	.972	64.6	2.94	n.d.	226	.591	9.40	127
YAO103	3.84	1.88	.956	N.D.	N.D.	N.D.	219	.419	8.61	129
YAO104	3.79	1.93	.988	N.D.	N.D.	N.D.	234	.346	8.96	115
YAO105	4.02	1.83	.943	62.5	2.36	n.d.	205	.454	9.01	286
YAO108	3.73	1.85	.944	N.D.	N.D.	N.D.	212	.459	8.58	105
YAO109	3.79	1.86	.948	62.7	2.11	n.d.	228	.403	9.44	199
Mean	3.81	1.87	.949	62.0	2.49	1.13	217	.429	9.01	161
$\pm 1\sigma$.09	.03	.026	1.9	.38	—	11	.066	.39	67
<i>Artifact Group F:</i>										
MAO003	3.44	2.98	.795	37.3	2.20	n.d.	140	.370	4.71	567
MAO037	3.46	2.89	.810	38.8	n.d.	n.d.	150	.363	4.66	536
Mean	3.45	2.94	.802	38.1	2.20	n.d.	145	.367	4.69	552
<i>Artifact Group G:</i>										
MAO012	3.53	1.47	102	n.d.	4.90	113	.440	1.63	699	111
MAO035	3.77	1.49	108	n.d.	5.39	122	.459	1.23	702	116
Mean	3.65	1.48	105	n.d.	5.14	117	.449	1.42	700	113

Artifact Samples—Continued

<i>La</i>	<i>Ce</i>	<i>Nd</i>	<i>Sm</i>	<i>Eu</i>	<i>Gd</i>	<i>Yb</i>	<i>Lu</i>	<i>Hf</i>	<i>Ta</i>	<i>Th</i>	<i>U</i>
<i>Unknown Provenance</i>											
83.7	164	72.9	17.5	2.28	19.7	10.8	1.53	21.1	7.66	15.9	4.00
84.6	165	72.5	17.9	2.28	16.3	10.9	1.52	20.8	7.74	16.2	4.48
82.9	163	73.9	17.7	2.19	14.3	10.9	1.52	21.3	7.74	16.0	4.33
85.4	163	71.8	17.4	2.38	N.D.	10.9	1.57	20.9	8.23	16.3	3.77
84.2	163	69.7	18.2	2.32	N.D.	10.9	1.51	20.0	8.33	16.3	3.84
86.2	166	73.3	18.1	2.38	N.D.	11.0	1.56	21.1	8.38	16.8	3.40
84.5	164	72.3	17.8	2.30	16.6	10.9	1.54	20.9	8.01	16.2	3.95
1.2	1	1.5	.3	.07	2.9	.1	.02	.5	.34	.3	.42
<i>Unknown Provenance (1g)</i>											
42.8	72.8	24.9	4.61	.485	N.D.	3.68	.552	8.33	1.64	27.8	9.20
41.6	71.2	24.9	4.33	.396	N.D.	3.60	.529	7.96	1.69	28.1	9.40
42.9	71.1	24.5	4.51	.415	6.09	3.39	.604	8.21	1.44	28.9	9.44
42.6	70.5	26.2	4.48	.425	5.05	3.40	.546	8.22	1.50	28.8	9.49
42.5	71.4	25.1	4.48	.429	5.55	3.52	.557	8.18	1.56	28.4	9.38
.6	1.0	.7	.12	.039	—	.15	.033	.16	.12	.5	.15
<i>Zarnaki Tepe Source Group</i>											
35.2	70.1	29.9	6.73	.386	6.90	5.96	.934	8.46	2.28	25.3	8.74
35.5	70.0	31.4	7.24	.406	7.37	5.97	.949	8.45	2.45	24.2	8.65
33.1	67.0	29.4	6.82	.342	6.23	5.98	.927	8.14	2.21	23.4	7.94
35.2	69.6	30.3	7.22	.363	7.01	6.21	.993	8.43	2.61	25.1	8.67
35.8	71.1	33.7	7.65	.368	10.7	6.47	1.03	8.99	2.29	25.9	9.25
36.0	71.0	31.2	7.60	.337	7.17	6.60	.995	8.94	2.36	25.7	9.06
35.4	N.D.	N.D.	N.D.	.407	N.D.	5.72	.925	8.52	2.51	24.8	N.D.
34.4	N.D.	N.D.	N.D.	.361	N.D.	5.91	.959	8.82	2.48	25.7	N.D.
35.7	69.1	32.0	7.07	.333	7.05	6.13	.935	8.73	2.22	24.9	8.21
35.3	N.D.	N.D.	N.D.	.336	N.D.	5.61	.911	8.37	2.41	24.5	N.D.
35.8	69.8	32.9	7.52	.324	9.02	6.47	.999	9.08	2.44	25.3	9.00
35.2	69.7	31.3	7.22	.360	7.57	6.09	.960	8.63	2.39	25.0	8.65
.8	1.3	1.5	.36	.029	1.44	.32	.039	.30	.13	.7	.46
<i>Lake Sevan I Source Group</i>											
34.6	56.1	17.0	3.00	.457	5.34	2.80	.398	4.73	2.93	17.4	8.83
36.2	56.6	18.6	3.00	.518	N.D.	2.76	.371	4.72	3.11	17.1	8.44
35.4	56.4	17.8	3.00	.488	5.34	2.78	.385	4.73	3.03	17.3	8.64
<i>Unknown Provenance</i>											
111	203	81.4	16.8	1.80	13.8	8.92	1.25	14.2	7.42	18.2	4.92
116	203	80.1	17.3	1.88	n.d.	9.11	1.39	14.0	7.99	18.8	3.78
113	203	80.7	17.0	1.84	13.8	9.02	1.32	14.1	7.70	18.5	4.31

Literature Cited

1. Johnson, G. A. "Local Exchange and Early State Development in Southwestern Iran"; Anthropological Papers No. 38; Univ. Mich.: Ann Arbor, Mich., 1973.
2. Ehrich, R. W. "Chronology in Old World Archaeology"; Univ. Chicago Press: Chicago, Ill., 1965.
3. Sumner, W. M. *Iran* 1976, 14.
4. Reiner, E. *Iran* 1974, 12.
5. Lamberg-Karlovsky, C. C. *Iran* 1972, 10, 89–100.
6. Lamberg-Karlovsky, C. C. In "Ancient Civilization and Trade"; Sablott, J.A.; Lamberg-Karlovsky, C. C., Eds.; Univ. N.M. Press: Santa Fe, 1975.
7. Kohl, P. L. *Current Anthropology*, 1978, 19.
8. Cann, J. R.; Renfrew, C. "The Characterization of Obsidian and Its Application to the Mediterranean Region"; *Proc. Prehistor. Soc.* 30, 1964.
9. Renfrew, C.; Dixon, J. E.; Cann, J. R. "Obsidian and Early Cultural Contact in the Near East"; *Proc. Prehistor. Soc.* 32, 1964.
10. Renfrew, C.; Dixon, J. E.; and Cann, J. R. "Further Analysis of Near Eastern Obsidian"; *Proc. Prehistor. Soc.* 34, 1968.
11. Bieber, A. M.; Brooks, D. W.; Harbottle, G.; Sayre, E. J. *Archaeometry* 1976, 18(1).
12. Altinli, I. E. "Explanatory Text of the Geological Map of Turkey"; Van. Maden Tetkik ve Arama Enstitutu Vajinlarindan: Ankata, 1964.
13. Wright, G. A. "Obsidian Analysis and Prehistoric Near Eastern Trade: 7500 to 3500 B.C."; Anthropological Papers No. 37; Univ. Mich.: Ann Arbor, Mich., 1969.
14. Wright, G. A.; Gordas, A. A. *Isr. Explor. J.* 1969, 19.
15. Mahdavi, A.; Bovington, C. *Iran* 1972, 10.
16. Aspinall, A.; Feather, S. W.; Renfrew, C. *Nature* 1972, 237.
17. McDaniels, J.; Warren, S. E.; Moore, A. M. T. *Int. Symp. Archaeom. Archaeolog. Prospection*; Edinburgh, 1976.
18. McDaniels, J. M.A. Thesis, University of Bradford, 1976.
19. Epstein, S. M. M.A. Thesis, University of Bradford, 1977.
20. Perlman, I.; Yellin, J. HUAL 1 preprint, 1977, unpublished.
21. Yellin, J.; Perlman, I. SI-NBS Obsidian Workshop, Gaithersburg, Md., 1978.
22. Perlman, I.; Yellin, J. *Isr. Explor. J.* 1980, 30.
23. Yellin, J.; Perlman, I. *Rev. Archaeometrie* 1982, 111.
24. Blackman, M. J. *Symp. Archaeom. Archaeolog. Prospection*, Brookhaven National Laboratory, 1981.
25. Blackman, M. J., in preparation.
26. Renfrew, C. "Studies in the Archaeological History of the Deh Luran Plain"; *Memoirs of the Museum of Anthropology* No. 9; Univ. Mich., Ann Arbor, Mich., 1977.
27. Renfrew, C.; Dixon, J. E. In "Problems in Economic and Social Archaeology"; Sieveleing, G. deG.; Longworth, I. H.; Wilson, K. E., Eds.; Westview: Boulder, Colo., 1977.
28. Dixon, J. E. In "Advances in Obsidian Glass Studies"; Taylor, R.E., Ed.; Noyes: Park Ridge, N.J., 1977.

RECEIVED for review November 23, 1982. ACCEPTED for publication March 29, 1983.

The Application of Geochemical Techniques to the Investigation of Two Predynastic Sites in Egypt

RALPH ALLEN and HANY HAMROUSH

University of Virginia, Department of Chemistry, Charlottesville, VA 22901

Predynastic sites at Nagada and Hierakonpolis are important sources of information about the rise of Egyptian civilization. To identify areas related to prehistoric human activity, surface soil samples were analyzed for phosphate content and acidity. At Nagada, high phosphate concentrations were found in soils near storage pits; low phosphate contents characterized soils near what is believed to be the oldest tomb in human history. Grain size analysis allows differentiation between the various Nile sediment formations. Trace element analysis (particularly for rare earth elements) was also used to characterize the different silt formations at Hierakonpolis. Comparisons of trace element patterns in the silts to those in the sherds suggest that most of the pottery was made from the clay silts found in the immediate vicinity.

THE NILE RIVER VALLEY was one of the cradles of civilization and was characterized by the rich silts deposited along its length by regular episodes of flooding. The Nile River divides the desert area south of Cairo into two unequal geomorphic units. The Eastern Desert is characterized by its rugged mountains and steep scarps, which drain to either the Red Sea or the Nile; the Western Desert is characterized by the flat, monotonous pediplains between the Nile and a relatively high scarp in the west.

During Pliocene times, the overdeepened Nile Trench was invaded by the sea, which deposited thick beds of montmorillonitic clay interbedded with sand, organic rich detritus, and gravel (1-3). Later, during Late Pleistocene and Early Holocene times, the lower Nile Basin was overlain with a series of silt units as sediments were carried from the Upper Nile drainage basin. Some of the overlying silt formations along with the

0065-2393/84/0205-0051\$06.00/0
© 1984 American Chemical Society

approximate times of deposition are given on page 63. It is important to study these different Nile silt units because most Prehistoric and Predynastic settlements were located along the Nile Valley. The sedimentological events that accompanied the deposition of these silts had a great impact on the ecological environment and thus affected the different Prehistoric cultures along the Nile Valley.

Although there are numerous studies of Egypt during the Dynastic Period, there are far fewer of the Predynastic Period. The term Predynastic refers to the period of food-producing communities that immediately preceded the unification of Lower and Upper Egypt and the emergence of dynastic Egypt. The most important Predynastic sites known in Egypt are located at Nagada and Hierakonpolis. The Nagada area includes the important Predynastic areas of Nagada, Ballas, and Abadiyeh first investigated by Petrie (4). At Nagada, for example, a staggering total of 2149 graves were identified in a 17-acre area on the low desert spurs overlooking the cultivated land of the Nile Valley. Taking advantage of the soft ground on these spurs, the Prehistoric Nagadans placed their graves side by side until the area was literally saturated with tombs (5). The extensive site of Hierakonpolis apparently had great importance to early Egyptians and probably played an important role in Egyptian history, especially before and during the unification of the Egyptian state. The religious and political distinction of this town suggests that this may have been the capital of the Predynastic Kingdom of Upper Egypt (6).

Geological investigations of these two sites were started by Butzer in 1958 to permit the reconstruction of the geographical conditions of the Prehistoric settlements (7). These and other geomorphological studies have identified the Nile silt units upon which Paleolithic and Predynastic sites are found. At Nagada, seven Predynastic sites have been identified on silts ranging from the Sahaba formation to the Singari Member. At Hierakonpolis, several Predynastic sites existed on the top of the Masmara, Sahaba, and Arkin silt formations.

In the Nagada–Khattara region, geomorphological studies showed a relationship between the major trends of the wadis and the spatial distribution of the archaeological remains (8). These regional geomorphic studies are useful in identifying potential sites for seeking Predynastic archaeological remains, but more detailed local surveys are necessary to identify portions of a site that should be excavated. One problem confronting a geologist or archaeologist is to find and identify the Nile silt formation upon which Predynastic settlements and cemeteries were established. One approach is to use careful stratigraphic analysis of the area to determine the various levels of silt formations. Another approach is to use some distinguishing and discriminating geological or chemical feature to identify the various silt layers. We have investigated the use

of sedimentological techniques, including grain size analysis and trace element analysis, to distinguish among several of the silt formations at Nagada and Hierakonpolis. Other chemical techniques, mainly soil pH and phosphate analysis, have also been used to further establish the sites of prehistoric human activity upon a particular sediment layer. This chapter indicates the potential for the use of an interdisciplinary (geological and chemical) approach to prehistoric archaeology in Egypt and other similar areas.

Chemical Prospecting

Sites of prehistoric human activity may be evident where the human activity has disrupted natural chemical processes. This is particularly true in areas where the weathering processes do not include a great deal of leaching by aqueous solutions. For example, the ultimate source of all phosphates in soils is the breakdown of the phosphate minerals that are weathered from surrounding geological formations (9). Human activity may lead to decreases in the soil's phosphate levels (e.g., by agricultural activities) or increases in these levels when low-solubility phosphate compounds are deposited in the soil (e.g., by burials). The acidity of a soil may also be affected by human activities.

Surveys of soil pH and phosphate content are of proven value (e.g., 10), but it is important to recognize the effects of local geological conditions. For example, at Nagada the soil is highly alkaline due to Eocene limestone deposits (cliffs) near the site. When soils at the Predynastic site KH1 [occupied around 3700 B.C. (11)] at Nagada were analyzed for phosphate and pH, the alkalinity was dependent upon the amount of carbonate in the sample. Surface soil samples were taken from the corners of a grid (1 × 1 m units) imposed on the archaeological surface. For the phosphate analysis, 50 mg of sediment material finer than 0.5 mm was leached for 30 min in 5 mL of 7.5 N sulfuric acid. The phosphate was measured in the field by using a colorimetric technique based upon the phosphate reaction with molybdate (11,12). The pH measurement was made by placing 0.5 g of the soil into 5 mL of distilled water. After 3 min, the sediment had settled and the pH was measured using a calibrated glass electrode and pH meter.

The phosphate levels ranged from 0.7 to 7.0 mg P₂O₅/g soil, and the pH varied between 8.2 and 7.1. The highest pH values (8.0–8.2) were found for the sections in and near where a carbonate layer or horizon was identified during excavations (13). The pH was lower (7.4–7.6) in the soils from the areas where an intact and a looted Predynastic grave were found. However, the lowest values (pH 7.1–7.4) were from an area where the surface soil horizon was midden material from later occupations

(Dynastic times) of the area. The decay of organic materials in this midden material results in lower pH measurements. The midden material was partially transported by the wind and is covered in places by compact sand and scree. The irregular exposures of the midden material lead to significant variations in the large grid used.

The phosphate measurements at this Nagada site were useful in locating a Predynastic grave (> 2.5 mg P_2O_5/g) and what is interpreted as a hearth and storage pit ($2-3$ mg P_2O_5/g). The normal phosphate levels in the area were less than 1 mg/g. The phosphate levels around a looted grave were lower ($0.7-1.9$ mg P_2O_5/g), but this finding is consistent with the lack of bones in the grave. The low soil phosphate concentrations suggest that the bones were removed before they could contribute to the elevation of the phosphate levels. Petrie has contended that grave looting occurred even in Predynastic times (4). Clearly one of the problems at these Predynastic sites is the disruption caused by looting. In most cases, the results of chemical tests cannot be interpreted without stratigraphic information about the site.

At Hierakonpolis, the analyses of soil samples from some localities were of no value because of the great disruption of the materials. For example, a stone-cut tomb (Tomb 2), which is interpreted as being the oldest stone-cut structure of its kind in Egypt (Amaratian, ca. 3800–3500 B.C.), was surrounded by huge piles of looters' (and archaeologists') backdirt (6). The smaller graves that surround this stone-cut tomb may have been arranged around this larger tomb. In order to identify actual graves near the stone-cut tomb, the backdirt piles (containing pottery and animal bones) were cleared around the tomb. Once exposed, the hardened surface, into which the Amaratian and Protodynastic tombs had been cut, was sampled for phosphate determinations. In this case, the extensive work that went into eliminating the uncertainties of the stratigraphy were for naught because no new tombs were found in the immediate vicinity of Tomb 2. There were no anomalies in the phosphate levels.

The importance of stratigraphic studies and the identification of sedimentary units at extensively disrupted sites like Hierakonpolis can be illustrated by the excavations at locality 11, where there is evidence for habitation (trash mounds and pottery) as well as industry (pottery kilns). This locality offered a unique opportunity to study Predynastic ecology because of the excellent state of organic preservation in an area where there was a clustering of multi-functional components (6, 14). Four test pits were dug in one area through the site, in the direction $N10^\circ E-S10^\circ W$. The correlation profile is shown in Figure 1. The oldest unit identified was Nile silt (Masmis formation). In some areas, this silt was covered by eolian and/or wadi sands, which probably represents a local feature of sand accumulation under arid to semiarid conditions.

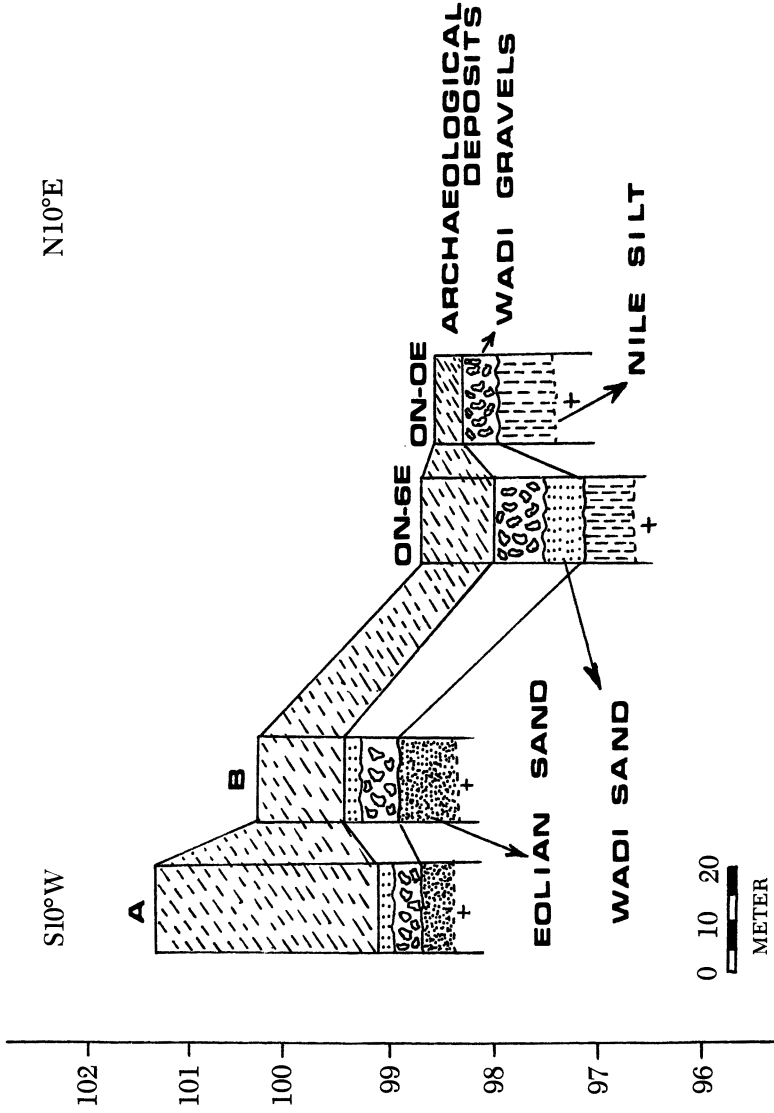


Figure 1. Correlation profile for the four studied sections at locality 11 in Hierakonpolis. Vertical scale is in meters above sea level.

There was initially thought to be great horizontal variation in the Nile silts because a dark brown silt was found at 0N-0E; a much lighter silt was at about the same level in test pit 0N-6E. The geological stratigraphy showed that this lighter material was not a Nile silt, but the filling of a depression with fine yellowish wadi sands. A comparison of the present topography of what has been interpreted as a trash mound and the paleotopographic profile shows that they are different. The human occupation and activity at this locality played an important role in creating the present topography, especially around the area of test (A). The cross section of the mound showed layers of different sediments, organic debris, and broken pottery. The paleotopographic profile suggests that this area was used for trash because it was a natural depression. The Predynastic topography sloped downward in the direction south of test pit A (not shown in Figure 1). Thus whether the disruption of the area is due to looters, erosion, or the inhabitants themselves, detailed stratigraphic studies are important to differentiate between the numerous silt formations and the various wadi deposits that might be present. Archaeological deposits are found on or in particular formations; therefore, the ability to recognize these particular sediment formations is important.

Identification of Sedimentary Units

The Quaternary stratigraphic features of the Nile Valley have been divided into a number of different silt units based upon field observations. However, it is sometimes difficult to define these silt units in the field because of their great geological similarities. In order to understand the differences in these silt units, it is instructive to look at how the Nile Valley has evolved with time. The Nile, 6800 km long, can be divided into three distinct river systems: (1) the White Nile between Lake Victoria and Khartum; (2) the Blue Nile between Lake Tana and Khartum; and (3) the Saharan Nile between Khartum and the Mediterranean. Thus the Nile silts in Egypt are deposits of materials from at least two distinctly different hydrogeological systems (i.e., the Ethiopian system and the Equatorial system). Over geological times, the contributions from these two systems to the Saharan Nile have changed; the various deposits [i.e., Dandara, Dibeira-Jer (Masmis), Sahaba, and Arkin formations] should reflect these different contributions. In addition, climatic conditions, and hence depositional conditions, have also changed and given rise to differences in the sediments (15). These differences (the contribution of each source and the climatic and depositional conditions) should be reflected in the geochemical characteristics of each unit.

Hassan (16) suggested that grain size parameters of sediments could be used to differentiate among the Nile silts deposited over the last 90,000

years from those deposited earlier when water from the Eastern desert made large contributions to the Nile sediments. This type of grain size analysis was applied to several of the older Nile formations in Nagada. The sediments were analyzed by standard methods by using settling velocities as measured with a hydrometer (17). The earliest of the Nile silts exposed at Nagada (the Giran el-Ful formation) had a mean grain size that is considerably larger (~ 0.5 mm, which is considered to be a medium sand) than that of the more recent silts. The next sedimentary period produced the Dandara, which is the oldest of the "modern" formations; it has a smaller mean grain size, that of a silt (~ 0.03 mm). Although the mean sizes of the two other "modern" formations were similar, the distribution of grain sizes was not. By taking sizes between 2 and 0.063 mm as sands, grains between 0.063 and 0.0039 mm as silts, and the smaller grains as clays, the sediments are quite different. The Dandara sediments are 45% sand, 30% silt, and 25% clay; the younger Dibeira-Jer formation sediments are 14% sand, 31% silt, and 55% clay. The Sahaba formation sediments were 35% sand, 21% silt, and 44% clay.

The differences in the grain size distribution for the various formations reflects the hydraulic conditions of deposition. The grain size parameters were used to determine these depositional conditions. The median (M) grain size was plotted as a function of the maximum (C) grain size (defined as the size of the largest 1% of the grains). The points on this CM diagram (Figure 2) correspond to particular modes of transportation and deposition (18, 19). Classes I, II, and III (Class III includes the older Giran el-Ful) in this figure represent rolled sediments where suspension is of little importance. Classes IV through VII were primarily suspended materials that were deposited by settling of the grains. Because the sediments of the "modern" Nile system fall into Class V, these materials were transported as a uniform suspension and were deposited as a rain of particles that were not sorted by bottom currents (20). The best explanation for these sediments is the deposition in swamps created when the Nile overflowed high banks. If such a depositional process occurred during the Predynastic occupation, then one might assume that the habitation sites were situated near swamps and far enough from the Nile to avoid flooding. These measurements of grain size fractionation were based upon a limited number of samples (20), but the precision is good enough to suggest that grain size distribution could be useful in characterizing and differentiating the various Nile sediment units.

In sediments of this type, the harder heavy minerals are usually found in the coarser (sand) fraction (along with the quartz). The differences in the amount of sand in a particular sample may therefore result in differences in the concentrations of those elements associated with the heavy minerals. In addition, the mineralogical composition of this heavy mineral fraction varies and is dependent upon the source of the

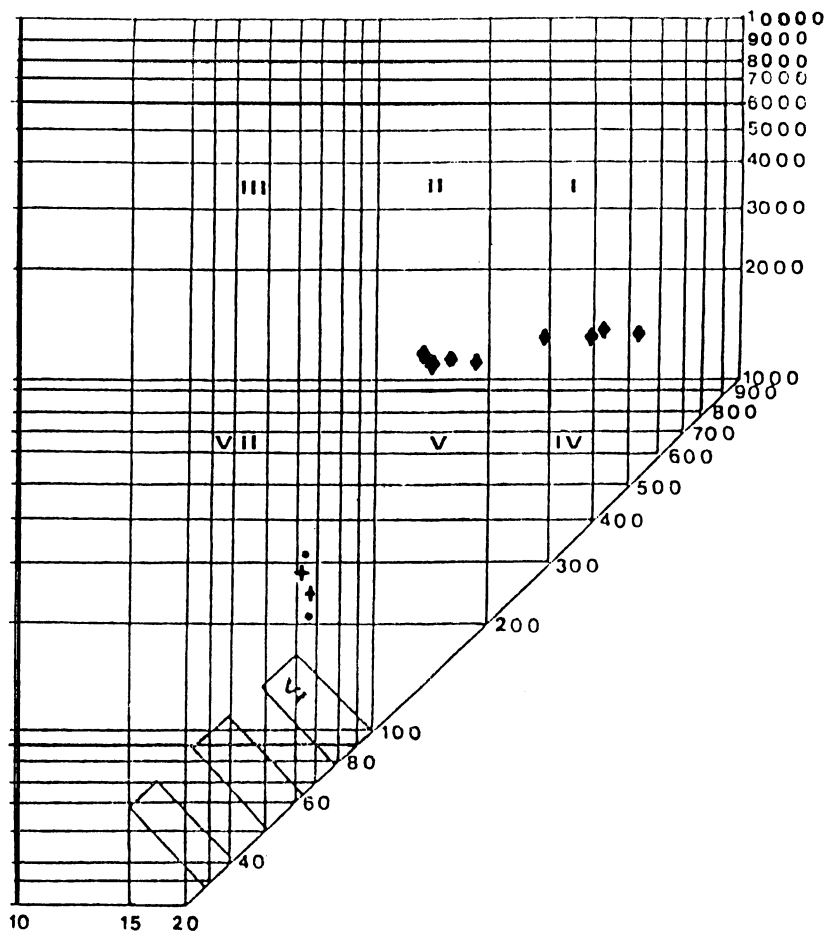


Figure 2. CM pattern of the modern and old Nile sediments. The abscissa (M) is the median grain size (in microns) for the sediments; the ordinate (C) is the size of the largest 1% of the grains. The Sahaba (+) and Dandara (●) formations are considered to be modern (since middle Pleistocene period) silts; the Giran el-Ful (◆) formation is from the older Nile regime. Significance of regions designated by roman numerals is discussed in the text.

sediment (16). Instrumental neutron activation analysis was used to measure some trace elements in sediments from the different formations at Hierakonpolis to show that trace element analysis could be used to identify the various sediment formations. This technique, which is described elsewhere (21,22), was used to analyze seven samples of sediment from the Masmis formation (equivalent to the Dibeira-Jer at Nagada), which was exposed by the excavations at locality 11 (Figure 3). Another Masmis

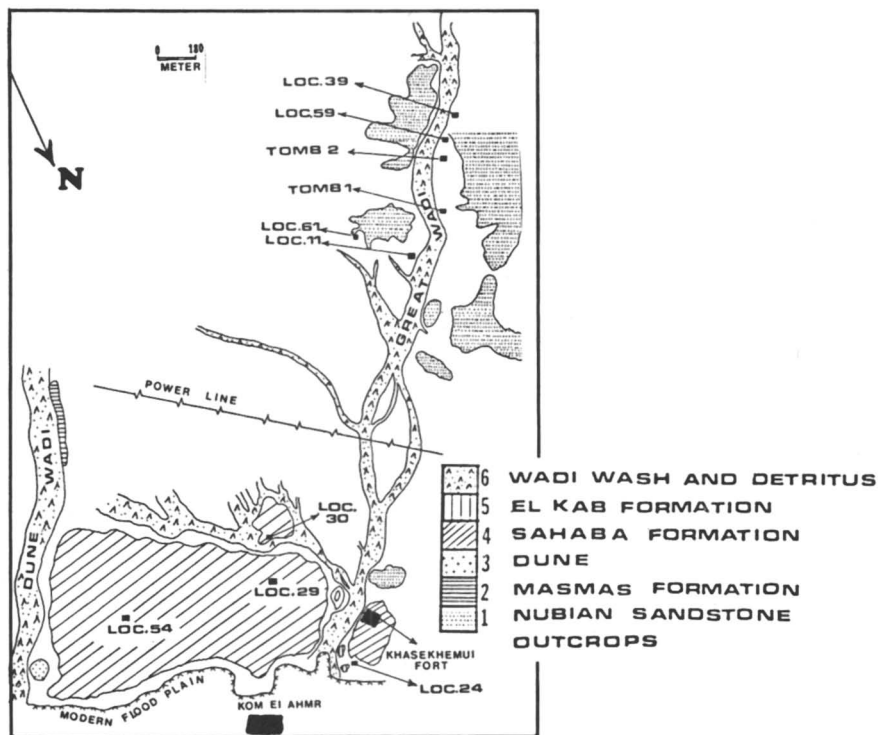


Figure 3. Map of Hierakonpolis showing the locations of some of the Predynastic sites studied and the geological descriptions of the surface.

formation sample was taken from a small exposure along the Dune wadi. Five samples from the younger Sahaba formation came from near localities 29 and 54 and the Khasekhemui fort. The Arkin formation is even younger, but at Hierakonpolis there are few exposures as most of it is covered by the cultivated area of the modern flood plain. Two samples of Arkin silt were collected from the small exposures between the fort and the flood plain. Another 30 samples of burned clay and pottery were taken from the archaeological sites where evidence of kilns was found. In examining the analytical results, it was clear that for many of the elements the actual concentration depended upon the amount of sand-sized material in the sample. The quartz contains few trace elements, but the heavy minerals associated with this same grain size fraction contain iron and many of the trace elements. The iron, cobalt, scandium, and chromium concentrations in the Arkin samples were similar to those in the Sahaba samples, but differed from those in the Masmias formation sediments. In Table I the averages (and standard deviations) are shown

Table I. Average Concentrations in Nile Silts and Pottery from Hierakonpolis

	<i>Masmas^a</i> <i>Silt(7)</i>	<i>Masmas^{a,b}</i> <i>Sherds(10)</i>	<i>Sahaba and</i> <i>Arkin^a Silt(8)</i>	<i>Sahaba^{a,c}</i> <i>Sherds(9)</i>
Fe ₂ O ₃ %	7.3 ± 0.4 ^d	8.2 ± 0.9 ^d	10.6 ± 0.8 ^d	10.9 ± 0.3 ^d
Co (ppm)	21 ± 1	29 ± 3	40 ± 5	38 ± 2
Sc (ppm)	13.7 ± 1.5	18.7 ± 2.0	23.7 ± 1.7	25.2 ± 0.7
Cr (ppm)	144 ± 13	—	270 ± 45	—
La ratio ^e	84 ± 8	103 ± 8	108 ± 10	130 ± 5
Lu ratio ^e	13.8 ± 1.0	13.7 ± 0.9	17.7 ± 0.9	18.2 ± 0.9
La-Sm ^f	-0.86 ± 0.008	-0.090 ± 0.008	-0.071 ± 0.005	-0.075 ± 0.004
Gd-Lu ^f	-0.025 ± 0.005	-0.030 ± 0.004	-0.051 ± 0.005	-0.050 ± 0.002
Eu ^g	-0.10 ± 0.02	-0.11 ± 0.03	-0.18 ± 0.03	-0.16 ± 0.01

^aNumber of samples included in average given in parentheses.

^bSherds and wasters from localities 11, 39, and 59.

^cSherds and wasters from localities 24, 29.

^dStandard deviation from the mean (uncertainty in individual analysis <2%).

^eNormalized to concentrations in chondritic meteorites: La, 0.33 ppm; Lu, 0.034 ppm.

^fSlope of REE curve using chondrite-normalized concentrations: La-Sm = (log[La] - log[Sm])/5; Gd-Lu = (log[Gd] - log[Lu])/7.

^gEu anomaly of REE curve using chondrite-normalized concentration: (log[Eu] - (log[Sm] + log[Gd])/2).

for the Masmas and Sahaba (including the two Arkin samples) sediments. The relative uncertainty in the analysis of iron, cobalt, scandium, and chromium was <2% for each sample. The two types of materials also differed from each other in the concentrations and relative distributions of the rare earth elements (REEs). Figure 4 indicates that although the REE distribution patterns [described elsewhere in this volume (22)] were the same for the Sahaba and Arkin samples, those for the Masmas silt differed. Not only did the REE patterns differ, but the absolute concentrations tended to follow the other elements measured. The average concentrations for lanthanum and lutetium for the two types of silt are shown in Table I. The samples plotted as chondrite-normalized patterns in Figure 4 show that there is some overlap in the absolute concentrations. The real differences are in the europium anomaly and the slope from gadolinium to lutetium. In Table II the slopes of the curves from lanthanum to samarium [(log[La] - log[Sm])/5] and from gadolinium to lutetium [(log[Gd] - log[Lu])/7] are shown along with the europium anomaly [(log[Eu] - ((log[Gd] + log[Sm])/2)).

The differences in iron and trace element concentrations are a result of differences in the source of the material (which minerals are present) and the depositional differences (heavy mineral fraction present). When the sediments were analyzed by x-ray diffraction techniques, the only minerals observable, besides the clays (montmorillonite and kaolinite), were the quartz and plagioclase (21). Most of the iron appears to be

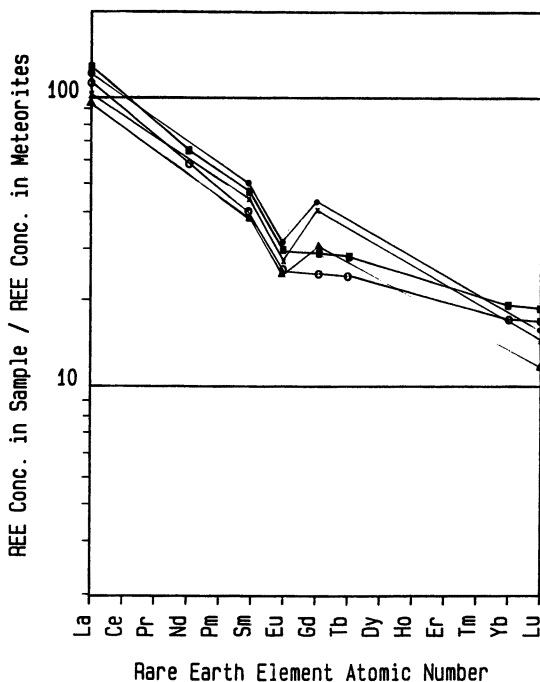


Figure 4. Normalized REE distribution curves for Masmis and Sahaba formations and ceramic materials from Hierakonpolis. Key: ○, typical pattern of Masmis silt; ■, ceramic plum red ware produced from this silt; ▲, typical pattern of the straw tempered ware; ●, a waster from the kiln where some of this straw tempered ware was produced; ×, silt from the Sahaba formation that was used at this kiln. (A silt from the Arkin formation was identical to the Sahaba silt in REE concentrations.)

present as amorphous ferroginous oxides coating all of the grains. There are heavy minerals present, and the differences in the mineralogy of this fraction may account for some of the compositional differences observed. Hassan (16) found that the heavy mineral fractions from the Sahaba formation contained larger amounts of opaque minerals (25–48%) and augite (21–31%) than did the fractions from the Dibiera-Jer (17–25% opaques, 3–28% augite) unit, which is comparable to the Masmis unit. The hornblende represented a higher fraction of the heavy minerals in the Dibiera-Jer (25–49%) than in the Sahaba (6–28%), with epidote being about the same (9–16%) for both fractions. Differences in the minerals present may account for the concentration differences as well as the REE patterns. The opaque minerals (magnetite and ilmenite) are iron-rich. The Sahaba materials contain more of the coarse fraction (hence more heavy minerals) and a larger proportion of the heavy minerals are opaques, which could account for the higher iron concentrations. Cobalt is geochemically as-

sociated with iron, but the ratio of cobalt to iron is different for the Masmias and Sahaba. The cobalt, scandium, and chromium in the Masmias are about half of what seems to be typical of the Sahaba silts. The chromium may be associated with the augite (23), which is more plentiful in the Sahaba sample. The REE distribution patterns may reflect the relative importance of hornblende, augite, plagioclase, or minor minerals like apatite (23).

The consequences of the differences in the REE contents of these sediments are greater than potentially allowing sediment formations to be identified by trace element analysis. Some of the numerous Predynastic ceramic artifacts from Hierakonpolis were also analyzed.

Pottery manufacture represents one of the earliest breakthroughs in chemical technology and is particularly important at a site like Hierakonpolis where ceramic production was perhaps a key factor in the initial settlement, development, and environmental degradation of the area in the 4th millennium B.C.. Although a variety of pottery types are represented at Hierakonpolis in Predynastic times, the most striking and extensively studied are those belonging to the untempered plum red ware category, found in abundance in cemeteries, and the straw tempered ware closely associated with settlement areas. The trace element data showed that the straw tempered ware and the untempered plum red ware were made using the local Nile sediments (21). The material used to make pottery was apparently taken from the immediate vicinity of the kiln. In Figure 4 the REE patterns of a sherd of straw tempered ware and a waster (overfired clay) from the vicinity of a kiln at locality 29 are shown. There were also sherds of the plum red ware near this ancient (Amratian) kiln, and these had REE patterns that were characteristic of the Sahaba formation silt on which the site was located. Another kiln was found at locality 11, and although the area was covered with later erosional material, the site was found on the Masmias formation silt. The plum red ware fragments, the wasters, and the straw tempered ware found in this area all had REE patterns like those of the Masmias silt (Figure 4). The sherds around the kilns at localities 39 and 59 were mostly plum red ware and they also match the Masmias silt. If all of the sherds and wasters from localities 11, 39, and 59 are averaged with the samples of Masmias silt, the average concentration and deviation are very similar to those of the sediment samples alone (Table I). The iron has somewhat lower and the cobalt and scandium have higher concentrations than average, but the REE distribution patterns are nearly parallel for all of the samples. When all of the sherds from sites located on the Sahaba sediments (localities 24, 29) were averaged with the Sahaba formation silts themselves, the results (Table II) confirm that all of these materials have essentially the same composition. The REE patterns were parallel for all of these materials. The only exception to this pattern of material

**Sedimentological Units Characteristic of the Nile Valley in the
Region Including Nagada and Hierakonpolis**

<i>Top</i>	<i>Approximate Radiocarbon Date</i>
Recent wadi scree	—
Singari member, Ineiba formation	8940 B.P.
el-Kab formation (or Arkin formation)	10,600–5600 B.P.
Malki member, Ineiba formation	12,070 B.P.
Sahaba silt	12,000–18,000 B.P.
Dibeira-Jer formation (Masmaš)	40,000 B.P.
Korosko formation	27,000 B.P. (?)
Dandara formation	Middle Pleistocene
Giran el-Ful formation	Early Pleistocene

utilization was a plum red ware sherd (not included in averages) that was found on the surface at locality 24. The composition and REE pattern suggest that this sherd was made further up the Great Wadi from Masmas formation material. It may have been transported to locality 24 at some later date.

Although the number of samples analyzed is limited, the inescapable conclusion to be drawn from our data is that some of the Nile silt formations can be differentiated on the basis of trace element contents and REE distribution patterns. In addition, we conclude that the Early Predynastic (Amratian) pottery was made from clays found in the immediate vicinity of the kiln. Older shales that are found layered with the much earlier sandstone deposits that were cut by the Great Wadi were also analyzed. The REE patterns as well as the scandium, chromium, and iron concentrations are different enough to suggest that these materials were not used to produce pottery (21). In a previous paper, we discussed the possibility that some of this shale, or the white salt found associated with it (anhydrite-CaSO₄), was mixed with the local clay to produce the finer, harder plum red ware (21). This addition could account for the slight difference in the average composition of the sherds from localities 11, 39, and 59 and the Masmas silt.

Conclusion

The studies at two Predynastic sites in Egypt have demonstrated the value of geological and geochemical techniques to aid the archaeologist.

It is often the combination of techniques that provides the best approach. The microstratigraphic studies along with pH and phosphate measurements made it possible to identify the location of different human activity in an archaeological site. The stratigraphic studies gave information about the processes that occurred at a site. Grain size analysis and chemical analysis of sediments offer some promise for determining which of the many Nile sediments is present without detailed stratigraphic studies. Trace element analysis has also been useful in tracking these silts as they were utilized for the Predynastic ceramic industry.

Acknowledgments

The assistance of M. Hoffman and F. Harland and the financial support of the Smithsonian Institution administered by the American Research Centre in Egypt for the collection of these materials are gratefully acknowledged. Neutron activation analysis was made possible through a grant from the U.S. Department of Energy to the University of Virginia Nuclear Reactor Facility and the assistance of P. Benneche.

Literature Cited

1. Chumakov, I. S. *Tr. Inst. Geol. Rudn. Mestorozhd., Petrogr., Mineral. Geokhim., Akad. Nauk SSSR* 1967, 1, 1–110.
2. Sandford, K. S.; Arkell, W. I., "Paleolithic Man and the Nile Valley in Lower Egypt"; Univ. of Chicago, Oriental Institute Publ., 1939, 49, 1–105.
3. Said, R. "The Geological Evolution of the River Nile"; Springer: New York–Heidelberg–Berlin, 1981; pp. 1–151.
4. Petrie, W. M. F. "Nagada and Ballas"; Br. Sch. Archaeol. Egypt: London, 1895; pp. 1–20.
5. Hoffman, M. A. "Egypt before the Pharaohs"; Knopf: New York, 1979; pp. 1–391.
6. Hoffman, M. A. "The Predynastic of Hierakonpolis"; Alden: Oxford, London, 1982; pp. 1–154.
7. Butzer, K. W. *Science* 1960, 132, 1617.
8. Hamrroush, H.; Wahab, S.; Allen, R. O. In *Proc. 22nd Symp. Archaeom.*, Bradford: U.K.; in press.
9. Proudfoot, B. In "Geoarchaeology: Earth Science and the Past"; Davidson, D. A.; Shackley, M. L., Eds.; Duckworth: London, 1976; p. 93.
10. Evans, G. J. "An Introduction to Environmental Archaeology"; Cornell Univ. Press: Ithaca, N.Y., 1978; pp. 1–154.
11. Hassan, F. A. *Am. Antiq.* 1979, 44, 267.
12. Drake, A. M.A. Thesis, Washington State Univ., 1980.
13. Hassan, F. A. *J. Field Archaeol.* 1978, 5, 197.
14. Hamrroush, H. In "The Predynastic of Hierakonpolis"; Hoffman, M., Ed.; Alden: Oxford, London, 1982; p. 93.
15. Shukri, N. M. *Q.J. Geol. Soc. (London)* 1950, 105, 511.
16. Hassan, F. A. In "Prehistory of the Nile Valley"; Wendorf, F.; Schild, R., Eds.; Academic: New York, 1976; p. 331.

17. Hamroush, H. M.Sc. Thesis, Cairo University, Egypt, 1980.
18. Passega, R. *Am. Assoc. Pet. Geol. Bull.* **1957**, *41*, 1952.
19. Passega, R. *J. Sediment. Petrol.* **1964**, *34*, 380.
20. Passega, R.; Byramjee, R. *Sedimentology* **1969**, *13*, 233.
21. Allen, R. O.; Rogers, M. S.; Mitchell, R. S.; Hoffman, M. A. *Archaeometry* **1982**, *24*, 199.
22. Allen, R. O.; Hamroush, H.; Nagle, C.; Fitzhugh, W. Chapter 1 in this volume.
23. Mason, B.; Allen, R. O. *N. Z. J. Geol. Geophys.* **1973**, *16*, 935.

RECEIVED for review November 3, 1982. ACCEPTED for publication April 11, 1983.

Soil Chemical Investigations in Illinois Archaeology: Two Example Studies

WILLIAM I. WOODS

Southern Illinois University at Edwardsville, Department of Anthropology,
Edwardsville, IL 62026-1001

The past decade has witnessed a significant increase in archaeological activity in the United States. Coupled with this trend has been a heightened interest in ancillary techniques of analysis. This chapter focuses on the author's experiences with one such technique; namely, soil chemical analysis. Specifically, discussion will be restricted to the aspects of this work related to Illinois archaeology. The results of two projects pertaining to both prehistoric and historic site contexts are reviewed in an effort to illustrate the potentialities of such investigations.

ARCHAEOLOGICAL SOILS ARE REPOSITORIES of information about past cultural activity. They not only contain artifactual remains and features, but also are themselves rewarding objects of study. A variety of physical and chemical changes occur in natural soils as a result of human occupation (1,2). Many of these changes are not long lasting, but others can be detected for millennia. Such physical modifications as soil compaction and textural change are evident to any experienced excavator. Less evident, but also of high interpretive value, are the chemical alterations that have been brought about by the addition of organic and inorganic debris to the soil matrix. The differential distribution of these alterations, among other things, can be used to determine site boundaries, define stratigraphic relationships, delimit intrasite activity areas and features, and aid in their functional interpretation.

The past decade has witnessed a significant increase in archaeological activity in the United States. Coupled with this trend has been a heightened interest in ancillary methodologies, including soil chemical analysis. A variety of studies involving archaeological soils have been conducted within the State of Illinois, and these can serve as a microcosm for the nation as a whole (3-17). Two of these applications will be discussed herein (Figure 1). In the first project, soil analysis was employed as a

0065-2393/84/0205-0067\$06.00/0
© 1984 American Chemical Society

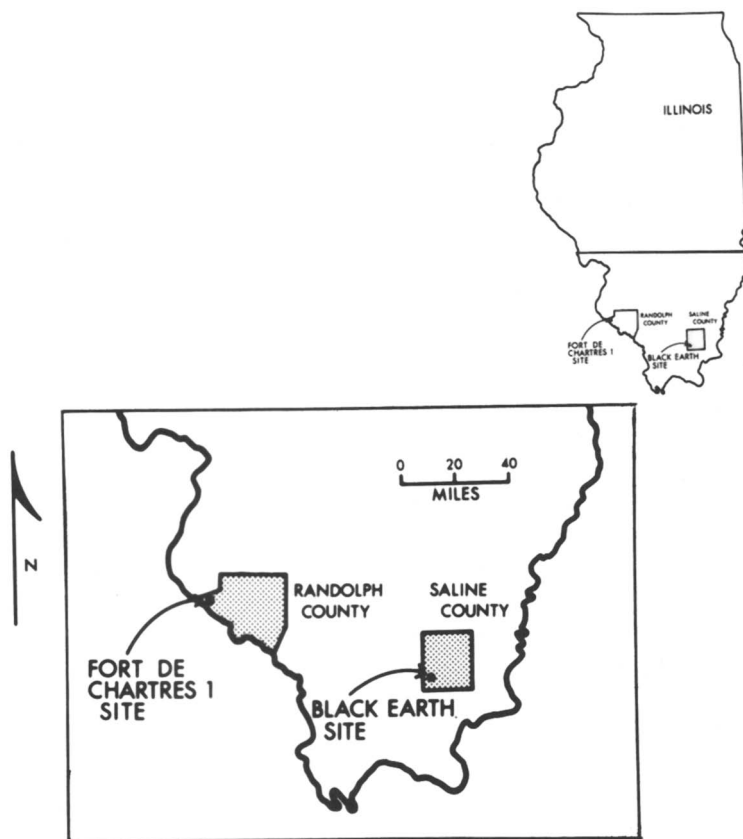


Figure 1. Regional site location.

technique to delineate and interpret the boundaries of an 18th century French fort for which no surface remains existed (11,15). In the second application, data derived from soils collected during the excavation of a prehistoric habitation midden were utilized to derive population parameters for a dated segment of the site's occupation (17). With the exception of those utilized for phosphorus determination, standard quantitative techniques of soil analysis were applied in both of these examples (see box).

Fort de Chartres 1 Site

In the first half of the 18th century, the French constructed a sequence of at least three forts named Fort de Chartres on the Mississippi River floodplain in Randolph County, Ill. (25). The first two forts were completed in the 1720s and had wooden palisades. Within less than a decade, each of these forts fell into disrepair and was abandoned. The final Fort

Experimental Methods

Sample Preparation

Pretreatment for all samples consists of air drying, mechanical grinding, and passage through a 2.0-mm sieve.

Analyses

Qualitative phosphate	Gundlach field test (18) as modified by Eidt (19) and Woods (20).
Inorganic phosphate	Sequential extraction with sodium hydroxide and hydrochloric acid reagents, spectrophotometric determination of the ascorbic acid reduced phosphomolybdate complex (6).
pH	Electrometric measurement of 1:2 soil: water mixture.
Organic carbon	Chromic acid digestion-titration (21-22)
Nitrogen	Semimicro Kjeldahl digestion-titration (23).
Calcium, potassium, magnesium	Hydrochloric acid extraction, determination by atomic absorption spectrometry.
Iron, copper, zinc	Sodium dithionite reduction, sodium citrate chelation, determination by atomic absorption spectrometry (23,24).

de Chartres, erected in the 1750s, was composed of stone. Although original portions of this fort still remain, the above-ground features of the first two forts disappeared and knowledge of their locations was lost until recently.

During the summer of 1980, examination of a 1928 U.S. Army Corps of Engineers aerial photograph revealed a dark rectangular stain situated approximately 1 km to the east of the stone fort (26). The shape and dimensions of the stain conformed closely to those indicated in documentary sources for the first Fort de Chartres. In the half-century since the photograph was taken, both a levee and a two-lane highway have been constructed over portions of the site area. The tract of land between the highway and levee that presumably contained the central portion of the fort is presently owned by the State of Illinois.

In an effort to ascertain the fort's precise location, delimit its external boundaries, and identify possible internal features and activity areas, the Illinois Department of Conservation sponsored a program of remote sens-

ing at the site. As part of that program the author and John Weymouth of the University of Nebraska were commissioned to conduct, respectively, a detailed soil chemical investigation and an intensive magnetic survey of the area utilizing the same site grid. Field activities carried out in November 1980 included topographic survey of the study area, establishment of a permanent site grid, and collection of soil samples. Unfortunately, conditions of extremely poor visibility did not allow for a surface survey of the area, which would have aided in formulating sample collection strategy. Consequently, samples were collected at 2-m intervals along a series of transects placed throughout the field (11). Soils were taken from a depth immediately below the plowzone through use of a 2-cm diameter core. The locations where cultural materials or feature fill were encountered during coring were recorded and were found to be contained within a 75-m-long area. Ultimately, 404 samples were recovered from the study area.

Immediately following fieldwork, the relative concentrations of phosphate in all of the samples were determined by means of a rapid qualitative test (18–20). Although not absolutely reliable, this test can be utilized as an initial screening device. The qualitative results were found to approximate closely the distribution of subsurface materials and feature fill. In order to depict the fort boundaries, as well as suspected internal features, more accurately, a series of 46 samples was selected for quantitative analysis. These samples were situated on three north–south-oriented transects between site grid lines N480 and N590. Phosphorus, calcium, and pH were determined for all of these samples and proved to be effective cultural indicators. Magnesium, potassium, iron, copper, and zinc testing were terminated after two transects due to the nondiagnostic nature of the results.

Figure 2 summarizes the distribution of the calcium, phosphorus, and hydronium ion concentrations along the three transects. Along all three transects, the hydronium ion concentration drops dramatically at N510 as the suspected boundary of the fort is approached from the south. By progressing northward, a distinct increase is noted in the vicinity of N580. The calcium and phosphorus results are similarly distributed along the first two transects, reaching their highest concentrations immediately on the inside of the boundaries exhibited by the hydronium ion and having relatively low levels in the area suspected to be the central portion of the fort. This distribution has been interpreted as indicating the locations of former structures along the interior margins of the palisade, separated by a parade ground. Significantly, feature fill and limestone were also evident at the locations of peak concentration. The results for the third transect are somewhat different, with peak calcium and phosphorus levels more closely spaced and centrally located. Again, these values correlate with feature fill and limestone. This transect is proximal

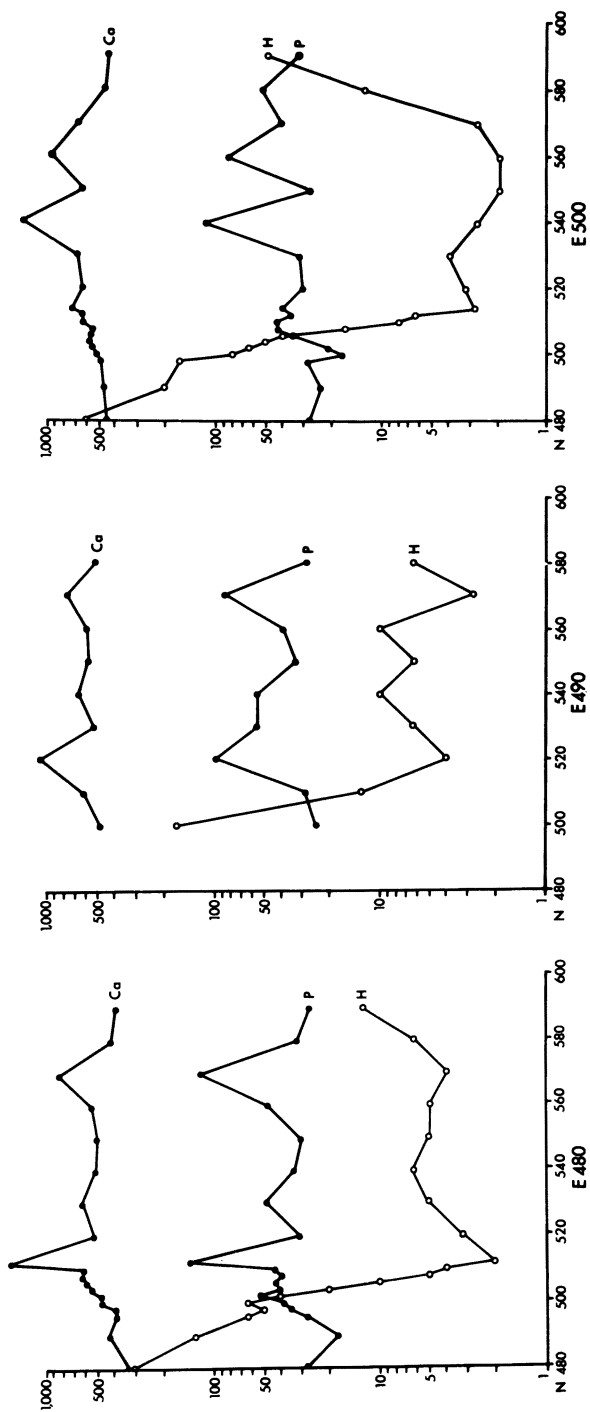


Figure 2. Transect sample results from the Fort de Chartres site. Key: Ca, ppm $\times 10^{-1}$; P, ppm $\times 10^{-1}$; and H, $[H_3O^+] \times 10^8$.

to the projected east wall of the fort and the two peaks may represent opposite ends of one structure approximately 20 m in length.

The results of Dr. Weymouth's magnetic survey are in accordance with the soil chemical analyses (15). The palisade lines, suspected interior structural features, and parade ground are clearly depicted on the line contour magnetic maps. Furthermore, the 1-m internal grid unit employed in that survey allowed for more accurate definition of the fort boundaries, and the 48-m inside dimension indicated by the magnetic results compares quite favorably with that suggested for the fort by documentary sources.

The Black Earth Site

The Black Earth site is one of three midden deposits in Saline County, Ill., that were excavated in 1978–79 as part of the Carrier Mills Archaeological Mitigation Project. Situated on a bluff overlooking the Saline River valley, the Black Earth site midden was approximately 80 m in diameter and reached a maximum thickness of 160 cm. In order to provide ancillary data relating to the origin and development of the midden, a series of 105 soil samples was collected from the excavations. Extreme care was exercised so as not to gather soil from feature or obviously disturbed contexts or from the immediate vicinity of burials. Upon recovery, samples were subjected to 13 basic physicochemical analyses. The results of these analyses demonstrated that when compared to the highly acid, infertile silt loams of the area, the midden deposit exhibited darker coloration, coarser texture, greatly increased pH levels, and higher concentrations of all elements tested.

One outgrowth of the soils work at the Black Earth site was the development of population parameters based on the analytical data. It was reasoned that because the midden was a wholly anthropogenic accretional phenomenon originating from habitation, certain aspects of its present chemical composition should be reflective of actual cultural additions. In an effort to estimate the number of individuals that would have been required to make these additions, soil physical and chemical data were examined for a 785-year segment of the Middle Archaic occupation at the site, which has been dated to between 5645 ± 70 B.P. and 4860 ± 85 B.P. (UGa 2705, UGa 2703, uncorrected). Initially, the volume and weight of the portion of the midden deposited during this period were determined. Then, population parameters were developed through utilization of various lines of evidence including the probable chemical contributions by standard resident communities and the total amounts of phosphorus and calcium found to have been present (Figure 3).

In order to determine the volume of the 90-cm extent of the midden between 50 and 140 cm below surface for which endpoints had been dated, the following standard formula was employed:

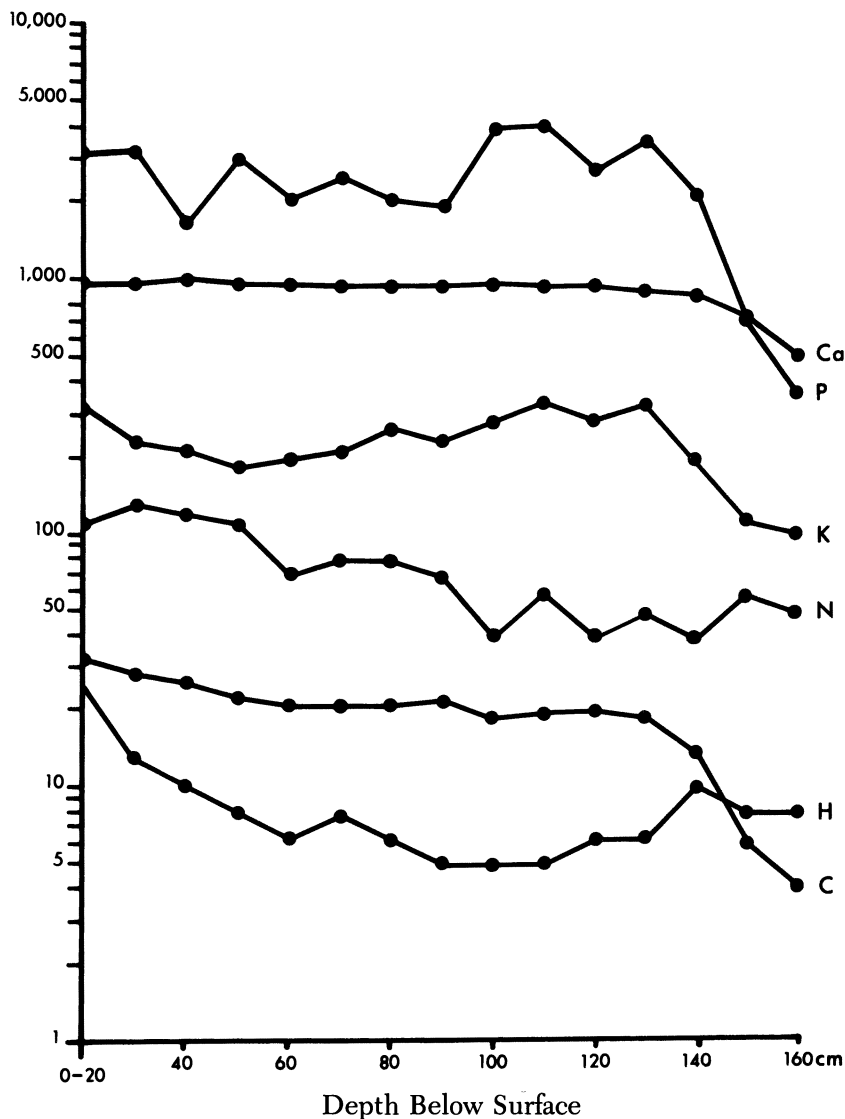


Figure 3. Column sample results from the Black Earth site, grid coordinates N267.0, E60.4. Key: Ca, ppm Ca $\times 10^{-1}$; P, ppm P; K, ppm K; N, % N $\times 10^3$; H, $[H_3O^+] \times 10^9$; C, % organic C $\times 10^1$.

$$\text{Volume} = (1/6) \pi h(h^2 + 3a^2)$$

where a is radius of base and h is maximum height. This formula assumes a roughly circular shape in plan view and an even curvature in profile from periphery to center, which was approximately attained by the mid-

den. For this analysis only two significant digits will be utilized, and the volume estimate was rounded to 2300 m³.

Bulk density was not analytically determined, but an estimate of 1.3 g/cc was arrived at after a review of literature concerning mollic epipedons of similar composition (27). By utilizing this figure, the total dry weight for the segment was determined to be 30×10^5 kg. Assuming a constant rate of accumulation, this yields total annual volume and dry weight depositions of 2.9 m³ and 3800 kg, respectively. Average elemental concentrations for the segment were determined from samples collected on a column in the core area of the midden.

The average concentration of phosphorus was found to be 3000 ppm. Given the calculated yearly material deposition rate, approximately 11 kg phosphorus would have been contributed each year. Cook and Heizer arrived at an annual deposition rate of 124 kg phosphorus to a site area by a standard population of 100 individuals (28). By utilizing this rate, a population of only nine individuals would have been required to account for the amounts of phosphorus found to be present. Because phosphorus as phosphate is the least mobile of the elements tested, this figure can be considered to represent an absolute minimum permanent population estimate for the site during the period of occupation under consideration. It should be remembered, however, that soil phosphate is also found in occluded forms and in organic combination and that these fractions were not totally measured by the procedure utilized (29). Consequently, the minimum population estimate should be increased, perhaps by as much as 50–60%, to about 15 individuals.

Given an average calcium concentration of 10,000 ppm and the same average annual deposition rate, approximately 38 kg calcium would have accumulated each year. For their standard permanent population of 100 individuals, Cook and Heizer projected an on-site per annum deposition of 55 kg calcium (28). Extension of this rate to the average amount of calcium present in the dated segment results in a population estimate of 69 individuals. In this regard, the mobility of calcium was not taken into consideration, because losses due to leaching are felt to have been roughly equaled by downward movement of additions from later occupations at the site.

Another line of evidence, the crude death rate and resultant burial population, was employed to assess the permanent resident population estimates derived from the phosphorus and calcium results. The per annum death rate of 3% postulated by Cook and Heizer (28) was utilized, and it was also assumed that all deceased individuals would have been interred on-site. Based on the community of 15 individuals and on the 3% per annum death rate, a burial population of 350 individuals would be expected. Similarly, a population of 69 would have resulted in the interment of approximately 1600 individuals during this period. The total

Middle Archaic burial population at the Black Earth site has been estimated on the basis of a 25% sample excavated area to have been approximately 550 individuals (30). This finding suggests that if Cook and Heizer's projections approximate reality, the phosphorus results most closely represent actual habitation intensity.

With a population of 15 individuals, the average weight of material contributed daily per person would have amounted to 0.69 kg on a dry weight basis. Again, assuming a permanent population with no periods of site abandonment, this does not appear to be an altogether unreasonable figure, especially considering the amounts of floral and faunal materials that would have been necessary to sustain the dietary requirements of such a population, not to mention the organic and inorganic items needed for food processing, fuel, heat retention, facility construction, tool manufacture, and clothing. Clearly, there are large uncertainties associated with these determinations. For example, the error values inherent in the radiocarbon dates were not considered. Furthermore, the assumption that the site was occupied continuously by an ideal standard population for 785 years is not acceptable. Anything less than permanent residence by the entire population or any periods of abandonment would, of course, increase the estimated population level. However, the projections do compare favorably with those arrived at after analysis of the data gathered through excavation, and, significantly, were determined solely through examination of the soil physicochemical characteristics.

Conclusions

Over the past half-century, the utility of soil chemical analysis to archaeology has repeatedly been demonstrated. Numerous investigations accomplished since 1972 have both reaffirmed previous findings and indicated directions for future applications. The prospect for continued expansion of this ancillary methodology is quite favorable.

Acknowledgments

The author gratefully acknowledges support received from American Resources Group; the Bureau of Land and Historic Sites, Illinois Department of Conservation; the Bureau of Location and Environment, Illinois Department of Transportation; the Archaeological Laboratory, University of Wisconsin—Milwaukee; the Center for Archaeological Investigations, Southern Illinois University at Carbondale; and the School of Social Sciences and the Graduate School, Southern Illinois University at Edwardsville. The encouragement and assistance provided by David Rands, Department of Chemistry, Southern Illinois University at Ed-

wardsville, during the development and testing of the rapid fractionation procedure is sincerely appreciated. Donald Meyer, Rock River Laboratory (Watertown, Wis.) is thanked for efficiently carrying out the numerous analyses requested over the past years. The cartography by Emily S. Brown of the three figures included in this chapter is also acknowledged.

Literature Cited

1. Cornwall, I. W. "Soils for the Archaeologist"; MacMillan: New York, 1958.
2. Limbrey, S. "Soil Science and Archaeology"; Academic: London, 1975.
3. Gregg, M. W. *The Wis. Arch.* 1975, 56(3), 174-200.
4. Williams, K. R., presented at the 41st Annual Meeting of the Society for American Archaeology, St. Louis, 1976.
5. Woods, W. I., "Soil Testing Report for the Proposed Interpretative Center at the Cahokia Mounds Historic Site, East St. Louis, Illinois," report submitted to the Archaeological Research Laboratory, Univ. of Wisconsin-Milwaukee, 1977.
6. Woods, W. I., presented at the Joint Meeting of the Illinois and Missouri State Academies of Science, St. Louis, 1977.
7. Williams, K. R.; Woods, W. I., "Archaeological Reconnaissance of FAP-410 (Bypass 50 to Pinckneyville)," report submitted to the Illinois Department of Transportation, Springfield, 1977.
8. Santeford, L. G.; Lopinot, N. H. In "Final Report on Archaeological Investigations at Frog City and Red Light: Two Middle Woodland Period Sites in Alexander County, Illinois"; Southern Ill. Univ. at Carbondale, Center for Archaeological Investigations Research Paper No. 6, 1978.
9. Woods, W. I., "Interim Report of Soil Analyses Conducted in Conjunction with the Carrier Mills Archaeological Mitigation Project," report submitted to the Center for Archaeological Investigations, Southern Ill. Univ. at Carbondale, 1979.
10. McElrath, D. L.; Williams, J. A. In "Archaeology in the American Bottom: Progress Report of the Illinois FAI-270 Archaeological Mitigation Project"; Bareis, C. J.; Porter, J. W., Eds.; Department of Anthropology, University of Illinois at Urbana-Champaign Research Report No. 6, 1981.
11. Woods, W. I., "An Archaeological Soils Investigation at the Fort I Site in Randolph County, Illinois," report submitted to the Illinois Department of Conservation, Springfield, 1981.
12. Woods, W. I., "Report of Soil Analyses for the McNitt 1 Site (11-Ca-31), Carroll County, Illinois," report submitted to the Archaeological Research Laboratory, University of Wisconsin-Milwaukee, 1981.
13. Woods, W. I., "Report of Soils Analyses for the Cahokia Mounds Historic Site Interpretive Center Tract," report submitted to the Archaeological Research Laboratory, Univ. of Wisconsin-Milwaukee, 1981.
14. Styles, T. R. In "Modoc Rock Shelter Archaeological Project Randolph County, Illinois 1980-81"; Styles, B. W., et al; report submitted to the Department of the Interior, Heritage Conservation and Recreation Service, and the Illinois Department of Conservation, 1981.
15. Weymouth, J. W.; Woods, W. I., *Hist. Archaeol.*, in press.
16. Lopinot, N. H.; Hutto, M.D.; Braun, D. P. "Archaeological Investigations at the Kingfish Site, St. Clair County, Illinois"; Southern Ill. Univ. at

- Carbondale, Center for Archaeological Investigations Research Paper No. 25, 1982.
17. Woods, W. I. In "The Carrier Mills Archaeological Project: Human Adaptation in the Saline Valley, Illinois"; Jefferies, R. W.; Butler, B. M., Eds.; Southern Ill. Univ. at Carbondale, Center for Archaeological Investigations Research Paper No. 33, 1982; pp. 1382-1407.
 18. Gundlach, H. *Mikrochim. Acta* 1961, 5, 735-37.
 19. Eidt, R. C. *Am. Antiq.* 1973, 38, 206-10.
 20. Woods, W. I. *Chesopiean* 1975, 13(1,2), 1-45.
 21. Allison, L. E. *Agronomy* 1965, 9, 1367-78.
 22. Allen, S. E.; Grimshaw, H. M.; Parkinson, J. A.; Quarmby, C. "Chemical Analysis of Ecological Materials"; Blackwell: Oxford, 1974.
 23. Soil Conservation Service. "Soil Survey Laboratory Methods and Procedures for Collecting Soil Samples"; Soil Survey Investigations Report No. 1; Washington, D.C., 1972.
 24. Mehra, O. P.; Jackson, M. L. In "Clays and Clay Minerals, Proceedings of the 7th National Conference," Earth Science Series Monograph 5; Pergamon: New York, 1960.
 25. Price, A. *Hist. Ill.* 1980, 3(1), 1-4.
 26. Downer, A. S. *Hist. Ill.* 1980, 3(2), 11.
 27. Soil Survey Staff. "Soil Classification—A Comprehensive System—7th Approximation"; *Soil Conservation Service, Dept. Ag. (U.S.)*, 1960.
 28. Cook, S. F.; Heizer, R. F. "Studies on the Chemical Analysis of Archaeological Sites"; Univ. Calif. Press: Berkeley, 1965; pp. 4-8.
 29. Woods, W. I. *Am Antiq.* 1977, 42(2), 249.
 30. Lynch, B. M. In "The Carrier Mills Archaeological Project: Human Adaptation in the Saline Valley, Illinois," Jefferies, R. W.; Butler, B. M., Eds., Southern Ill. Univ. at Carbondale, Center for Archaeological Investigation Research Paper No. 33, 1982, pp. 1116-1231.

NOTE: Submitted reports, such as References 5 and 7, are available upon request.

RECEIVED for review November 3, 1982. ACCEPTED for publication July 5, 1983.

Chemical Analysis of Archaeological Soils from Yagi Site, Japan

C. A. STIMMELL

University of Toronto, Department of Anthropology, Toronto, Ontario, Canada M5S 1A4

R.G.V. HANCOCK

University of Toronto, SLOWPOKE Facility and Department of Chemical Engineering and Applied Chemistry, Toronto, Ontario, Canada M5S 1A4

A.M. DAVIS

University of Toronto, Department of Geography, Toronto, Ontario, Canada M5S 1A4

Soils from archaeological sites have the potential to yield important information on natural and anthropogenic stratigraphy, resource availability, and site boundaries. Soil samples from Yagi, an Early Jomon site in southeastern Hokkaido, Japan, were analyzed. The stratigraphy there is composed of a series of paleosols accumulated during the Holocene from local volcanic activity. Archaeological and pedological techniques were used to classify soil units in the field. Instrumental neutron activation analysis was employed to generate multielement concentration profiles for 42 soil samples from six exposures. Chondrite normalized rare earth element (REE) patterns confirmed the validity of the field-designated stratigraphic sequence. A small number of potsherds from Yagi exhibited REE patterns similar to those of soil horizons of corresponding age. This approach can complement traditional pedological methods.

SINCE THE VERY BEGINNINGS of systematic archaeological research, when Boucher de Perthes searched the gravels of the Somme, stratigraphy has been a basic tool of prehistoric investigations. Archaeological soils have the potential to yield as much information about context, site boundaries, dating, resource availability, and past environments as the artifacts themselves. Over the past 30 years, archaeologists have begun to employ techniques borrowed from the soil sciences in an attempt to better under-

0065-2393/84/0205-0079\$06.00/0

© 1984 American Chemical Society

stand both natural and anthropogenic sediments. Conventional soil analysis techniques include a mixture of subjective field designations combined with relatively simple quantitative laboratory tests for important major elements such as carbon, calcium, nitrogen, phosphorus, aluminum, and iron (1,2).

These techniques are normally adequate to answer most of the questions encountered on archaeological sites; however, complex stratigraphy and unusual soil conditions can present a more difficult problem. In this chapter, we explore what additional information might be provided by a more comprehensive elemental analysis. Instrumental neutron activation analysis (INAA) was chosen because it provides concentration data for both the major elements usually obtained by conventional techniques and the trace elements used in many provenance studies.

Archaeological Setting

Yagi is located on the northern coast of the Oshima Peninsula in south-eastern Hokkaido. The site is located on a broad terrace that rises steeply 40 m above a narrow coastal strip. It is backed by a series of low, wooded mountains about 100 m in elevation and is circumscribed by two small rivers. Much of the terrain is very rugged. Most of the peninsula is andesitic highland, and its topography and geology are heavily influenced by local volcanic activity. The Oshima peninsula has two active volcanoes, Komagatake and Essan; both are within 30 km of the site.

The climate of the peninsula is cool-temperate maritime. Beech and oak forest is the dominant vegetation. Climate variation since the end of the Pleistocene has been slight, but has affected the vertical distribution of some plant communities (3).

Because flat areas in this region are scarce, all terraces on the peninsula are presently intensively utilized for either housing or cultivation. This was also true in the past. At least 84 other prehistoric sites are known within 10 km of Yagi. Most of these sites date to the Jomon period (11,000–300 B.C.). The Jomon period of Japanese prehistory is of special interest to archaeologists because Jomon people manufactured the first ceramics in the world—as early as 12,000 B.P. at sites in southern Japan (4).

The Yagi site was excavated under a project directed by William Hurley, Peter Bleed, and Masakazu Yoshizaki (5) (Figure 1). Archaeological remains of the Jomon period are scattered over 50,000 m² of the Yagi terrace. Excavated features include five semisubterranean houses, numerous large pits, middens, and living floors. On the basis of carbon-14 dates and ceramic typology, three major Jomon occupations are indicated (6). A late Initial Jomon occupation has been dated between 7000 and 5350 B.C. (The Jomon is traditionally subdivided into six periods:

Publication Date: January 1, 1984 | doi: 10.1021/ba-1984-0205.ch005

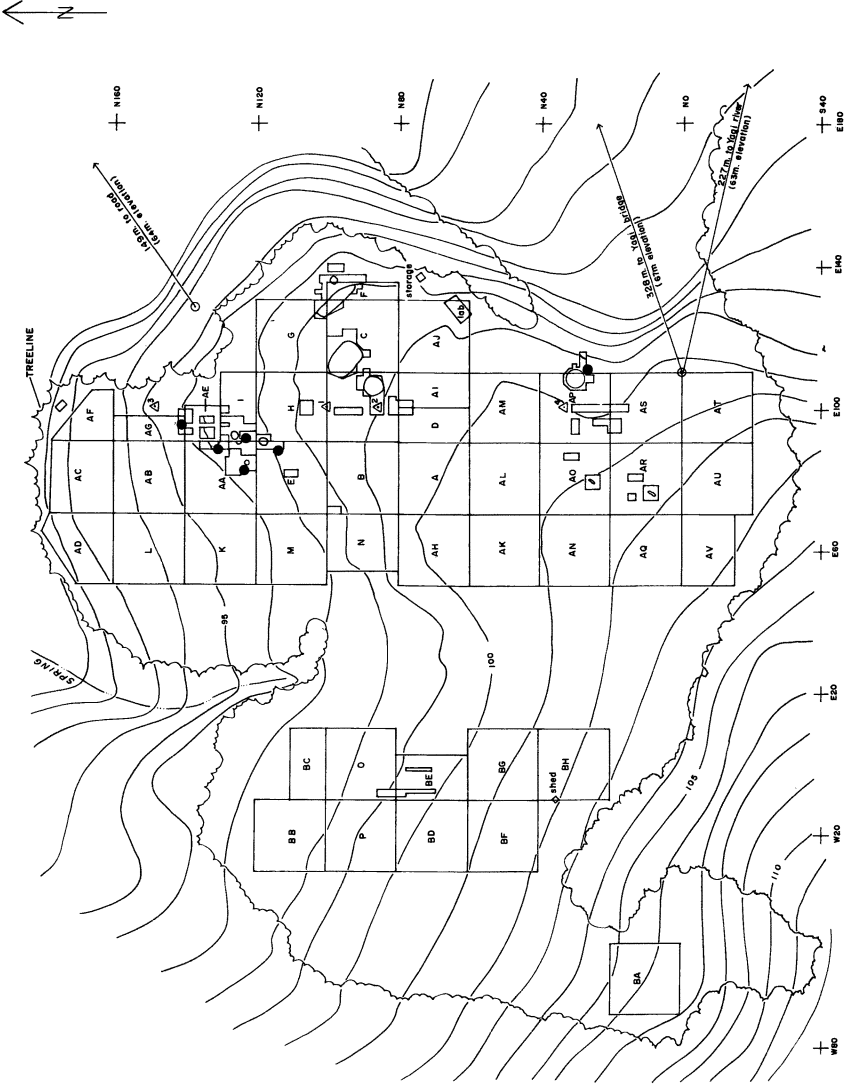


Figure 1. Excavation map of Yagi site, Hokkaido, Japan; Contour interval 1 m; arbitrary datum set at 100 m. Key: □, excavation units (1978–1980); ⊙, transit station; △, temporary bench marks (superscript 1, 1978; superscripts 2 and 3, 1979; superscript 4, 1980); ●, sampling sites.

Incipient, Initial, Early, Middle, Late, and Final.) Two Early Jomon occupations are represented: one between 4450 and 4000 B.C. and another between 3690 and 3190 B.C. The majority of features and artifacts date from these periods. The site was probably not continuously inhabited but was reoccupied at regular intervals. A limited Late Jomon component should date to around 1500–1000 B.C.

Interpreting the stratigraphic sequence at Yagi proved to be very difficult. Multiple archaeological horizons, layered between volcanic ash accumulations and interwoven with hundreds of subsurface features, obscured relationships between features and components. Relating Yagi to other Jomon sites in the region was also difficult because, traditionally, comparison often is based on a component's relationship to particular volcanic horizons. Yagi is on the periphery of most of the Komagatake ash falls; therefore not all volcanic episodes are represented at Yagi (Figure 2 and Table I). Although a stratigraphic framework for the archaeology at Yagi was evolved, a pedological analysis was also attempted to clarify the stratigraphy.

Pedological Methodology

Field descriptions of soil profiles include horizon designations and thicknesses, color, consistency, texture, structure, and boundary characteristics. The nomenclature used is that of the 7th Approximation (7). The

Table I. Volcanic Episodes During Jomon Occupations

<i>Eruption</i>	<i>Date</i>	<i>At Yagi</i>
<i>Komagatake</i>		
Ko-a	1929 A.D.	yes
Ko-b	1905 A.D.	no
Ko-c1	1856 A.D.	no
Ko-c2	1767 A.D.	no
Ko-d1	?	no
Ko-d2	?	no
Ko-e	1700 B.P.	yes
Ko-f	2750 B.P.	?
Ko-g	4780 B.P.	?
Ko-h	5750 B.P.	?
<i>Essan</i>		
Es-a	1750–1850 A.D.	?
Es-b		

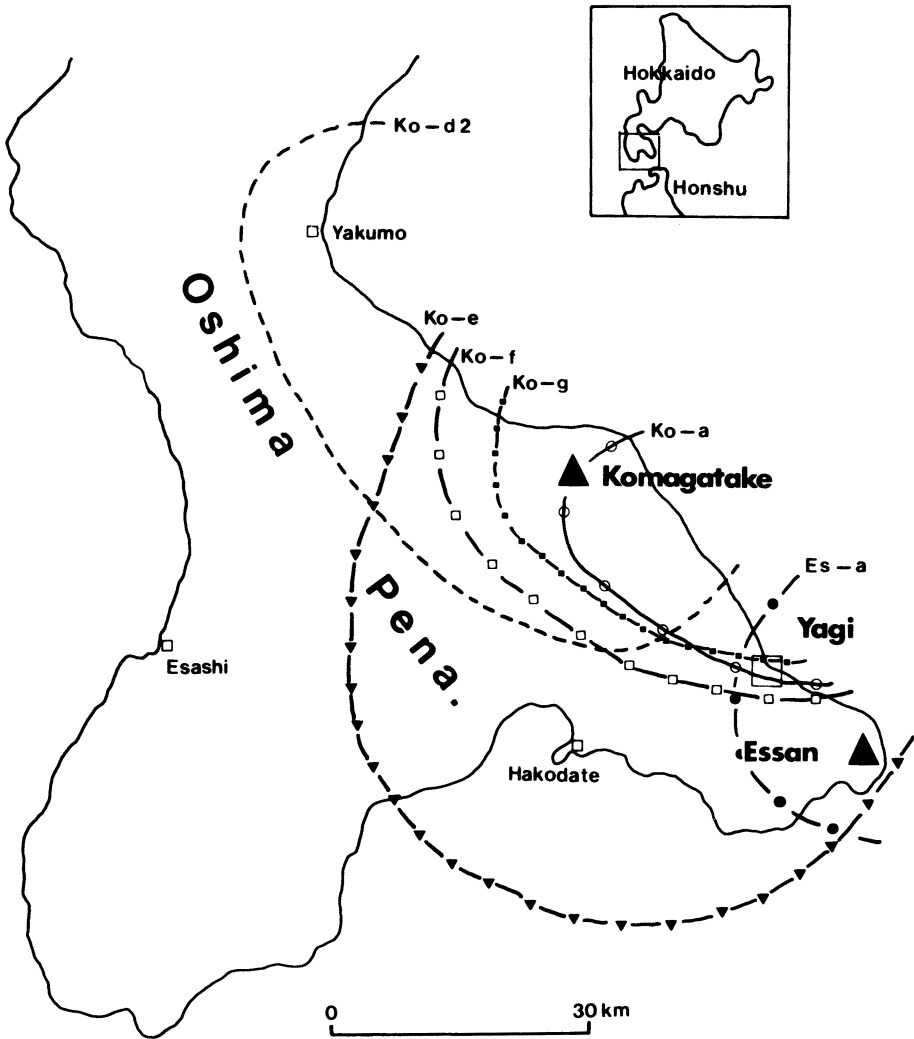


Figure 2. The Oshima Peninsula, Southern Hokkaido. The distribution of pyroclastic deposits from some of the Holocene eruptions of Komagatake and Essan (14).

pH was measured in the field with a narrow range pH testing kit. Detailed particle size analysis was performed in the laboratory: sand fractions were sieved, silt and clay fractions were separated by hydrometer (8). Organic carbon was determined by loss-on-ignition (9) rather than by sodium pyrophosphate solubility because the latter produced anomalous results. Phosphorus was measured colorimetrically after digestion in perchloric acid (10).

Results and Discussion

The soils of the Yagi site are andepts, immature soils developed in volcanic ash. Such soils are distinguished by their high organic carbon, high phosphorus retention, low bulk density, and high water-holding capacity (11). At Yagi, the soils have a high sand content (65–80%). Most soils fall into the sandy loam and sandy clay loam categories as determined by particle size analysis. However, in the field many horizons were designated as clay loam on the basis of texture and consistency. It is likely that the field designations are more accurate than laboratory determinations. The high cation exchange capacity of these soils makes it extremely difficult to disperse them for particle size distribution analysis (12,13).

The soils are generally dark except for the yellow-brown ash–pumice layers and the yellow initial materials below the archaeological horizons. The dark coloration (Munsell 10YR3/2–10YR2/1) is largely a function of organic carbon content. In the Yagi soils, organic carbon is generally high, occasionally over 20% by weight. It is lowest in the ash–pumice horizons and in the initial material below the archaeological layers.

The unusual thickness of the mollic and umbric horizons is caused by the accumulation of several paleosols formed from the multiple eruptions of two nearby volcanoes and by the stability of the humus–amorphous material complex.

The soils of the Yagi site were formed from the pyroclastic deposits of Komagatake and Essan. The former, about 25 km northwest of the site, has erupted frequently throughout the Holocene. Since ca. 6000 B.P., there have been 10 eruptions with substantial ejecta, although the materials from some were deposited very locally (Figure 2 and Table I). At Yagi, only Ko–a (1929) and Ko–e (1700 B.P.) are obvious in the stratigraphy as light-colored, gravel-like pumice, and even these are discontinuous across the site. Eruptions Ko–f and Ko–g should be evident at Yagi, but pedogenesis and disturbance have altered them sufficiently to make the initial material unrecognizable. Small inclusions of pumice evident in some exposures may represent one or both of these eruptions.

Figure 3 illustrates the relationships between the archaeological and pedological stratigraphy in one exposure (N124, E84, North Wall). Six major archaeological horizons have been recognized (5). The designations are partially site-specific, but do accommodate the stratigraphic scheme derived by local archaeologists. The horizons are based on their physical distinctiveness and associated artifacts and/or features. Horizon 1 is subdivided into 1a, the plowzone and Ko–a inclusions, and 1b, a black, sandy loam with no pumice. Horizon 2, Ko–e, is a thin discontinuous pumice layer. Horizon 3, containing the bulk of the artifacts, is subdivided into 3a and 3b. The lower section, 3b, sometimes occurs as dark, sandy

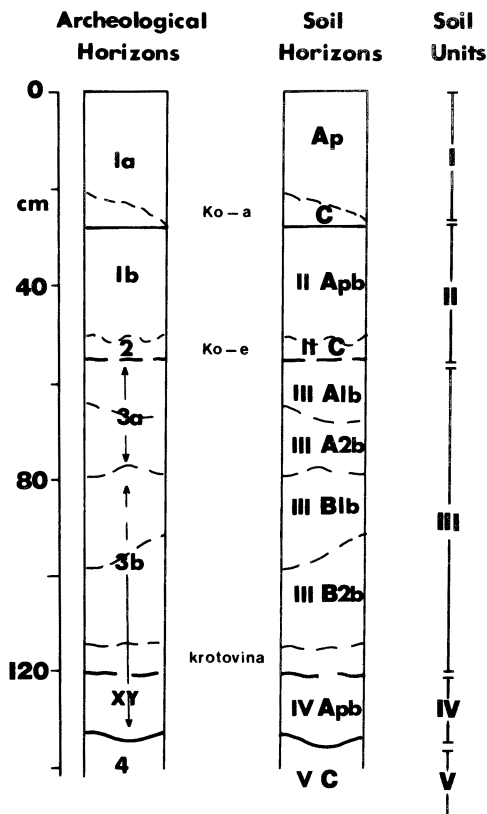


Figure 3. Comparison of the archaeological and pedological horizons at exposure N124, E88, north wall.

compact horizon, called XY, and is identified as an occupation zone. Horizons 4, 5, and 6 are light-colored sandy clay loams devoid of artifacts, which have features (storage pits, semisubterranean houses) intruded into them. Because the archaeological stratigraphy depends on the recognition of particular volcanic horizons and the appearance of the XY layer, both of which were discontinuous across the site, a pedological stratigraphy based on standard physical and chemical characteristics was derived.

Pedologically, several soil units can be recognized (Figure 3). Eruption Ko-a and above represents the modern soil (Unit I). However, much of Ko-a has been removed from areas where it interfered with modern cultivation. Unit II is composed of Ko-e and the Apb zone between it and Ko-a. Unit III, the most complex, was designated as one unit in the field. Its initial material is presumably Ko-f and Ko-g. The archaeological horizon, XY, constituted unit IV. It is only found in occupation areas and represents features such as house floors and sheet middens. Unit V

(Unit IV if XY is absent), the basal zone, is not physically or chemically uniform across the site, suggesting varying degrees of archaeological disturbance. Unit III appears to be composed of two physically and chemically distinct sections. Units I and II have reasonable internal consistency.

The soils at Yagi, then, are a series of paleosols accumulated during the Holocene. The stratigraphy of the upper sections is datable by the ash-pumice layers, Ko-a and Ko-e. Because initial material from earlier eruptions is unrecognizable, the time-scale must depend upon radiocarbon dating of the archaeological horizons.

The dark coloration of these paleosols has been attributed to the persistence of organic carbon. Normally organic carbon content declines rapidly after deposition (15). In Ireland, Gardiner and Walsh (16) have estimated that 75% of organic carbon in buried soils is depleted in about 4000 years. However, in andosols, organic carbon is persistent. Gibbs (17) stated that in buried andosols in New Zealand there is little or no color change over 20,000 years. Martini (18) noted that organic matter increases from incipient to mature andosols, then declines. This pattern may be related to the formation and diagenesis of morphous materials, particularly allophane, and to the stability of the humus-allophane complex.

Allophane is common in andosols of 6000–8000 years (19), but is rare in very young and older materials. Klages (20) attributed the decline of allophane in deposits of Quaternary age to replacement by metahalloysite.

Phosphorus content is also positively correlated to the amount of allophane (21,22). In Japan, retention of phosphorus is used as a crude criterion for distinguishing aluminous (volcanic ash) soils from siliceous soils derived from other parent materials (23). Phosphorus values in Yagi soils range from 0.13 to 1.22%. Values are highest in the modern soil, and in Unit III, particularly in the lower section. The lowest values occur in Unit II and in the materials below the archaeological horizons (Figure 3). The phosphorus loadings in all these soils are considerably higher than those recorded in anthropogenic horizons from nonvolcanic soils (24,25).

The similar behaviors of organic carbon and phosphorus suggest a common cause. Both are complexed with amorphous material. Their persistence appears to be determined by the temporal variation in the availability of amorphous material. The high values of phosphorus in the surface soil can probably be attributed to the current use of human excreta as fertilizer. The high carbon and high phosphorus levels in the lower section of Unit III coincide with the occurrence of many artifacts. If this unit represents midden material, high values would be anticipated. However, this unit is also of the correct age to have developed large amounts

of allophane. Clearly, the roles of diagenesis and human impact cannot be isolated. In the modern soil, the latter appears to be dominant. In Unit III, the two may be complementary.

The XY layer is anomalous. It is anthropogenic, but has relatively low organic carbon and phosphorus content. The complications caused by diagenetically controlled variations limit the use of phosphorus and organic carbon as indicators of human impact.

The laboratory tests normally used to confirm field designations and to establish the boundaries of archaeological occupation were inconclusive because of the nature of the soils at Yagi. A more complete chemical analysis of the soils was attempted by using neutron activation analysis.

Soil Sampling and Neutron Activation Analysis

Fifty grams of each soil sample was sieved to remove stones and gravel (>2.0 mm), then fired at 500 °C for 2 h to drive off excess moisture. The composition of the treated material would also approximate that of low-fired pottery.

Samplings of 250–350 mg of the fired materials were then analyzed by instrumental neutron activation analysis (INAA) by using the SLOW-POKE nuclear reactor at the University of Toronto. The concentrations of 31 elements were measured by means of three separate neutron irradiations and four sample countings (26). Short-lived isotope-producing elements (2 min–2.5 h) were measured with a short irradiation and rapid counting; medium-lived isotope-producing elements (9–15 h) were irradiated 15 × more and were counted the next day. Longer-lived isotope-producing elements were irradiated overnight and counted after 1 week for isotopes with half-lives of 26–100 h and after 2–3 weeks for the long-lived isotopes.

Results and Discussion

Forty-two soil samples were taken for analysis from different soil units of six exposures. The primary grouping of the analytical data was made by the soil units distinguished in the field (Figure 3). Table II contains the analytical data expressed as elemental concentration means and standard deviations for five major elements and nine minor and trace elements for the five soil units. Complete data are available from the authors on request. In addition, Units II and III have been subdivided on stratigraphic and chemical grounds. Unit II consists of Ko–e and its associated Apb. Because Ko–e is discontinuous, Unit II' is the second soil unit in those sections where Ko–e is missing from the exposure.

Unit III has been divided into III(upper) and III(lower). Unit III should represent at least two different volcanic episodes (Ko–f and Ko–

Table II. Distribution of Major and Trace Element Concentrations Among Soil Units

Element	Soil Units (number of samples)							
	I (4)	II' (7)	II (4)	III (upper) (9)	III (lower) (8)	IV (6)	Basal (4)	
Na ^a	1.2 ± 0.2	1.9 ± 0.3	1.0 ± 0.3	1.1 ± 0.3	1.2 ± 0.2	1.5 ± 0.3	1.5 ± 0.4	
Al ^a	8.2 ± 1.1	8.5 ± 1.0	8.7 ± 0.8	9.2 ± 1.6	9.8 ± 1.3	10.0 ± 0.7	10.0 ± 0.6	
Ca ^a	3.4 ± 0.7	2.5 ± 0.7	3.9 ± 1.3	3.4 ± 1.2	4.1 ± 0.9	5.0 ± 1.7	4.5 ± 2.0	
K ^a	0.7 ± 0.3	1.4 ± 0.4	0.5 ± 0.1	0.8 ± 0.3	0.5 ± 0.1	0.5 ± 0.3	0.6 ± 0.1	
Fe ^a	8.8 ± 1.3	6.4 ± 0.1	11.3 ± 1.5	9.0 ± 1.9	8.6 ± 1.3	7.3 ± 0.3	6.5 ± 2.0	
Sc ^b	29 ± 6	17 ± 3	37 ± 5	27 ± 3	28 ± 4	23 ± 3	20 ± 6	
V ^b	195 ± 40	114 ± 20	285 ± 83	217 ± 52	199 ± 37	154 ± 14	155 ± 83	
Cr ^b	32 ± 3	32 ± 9	29 ± 10	35 ± 16	21 ± 10	17 ± 12	23 ± 27	
Mn ^b	2500 ± 400	1700 ± 100	2700 ± 200	2700 ± 500	2400 ± 300	1900 ± 300	1700 ± 300	
Co ^b	22 ± 5	16 ± 7	29 ± 5	26 ± 17	21 ± 4	17 ± 3	17 ± 6	
Rb ^b	59 ± 11	90 ± 27	49 ± 11	59 ± 31	36 ± 11	33 ± 14	35 ± 17	
Cs ^b	4.0 ± 1.0	4.2 ± 1.0	2.4 ± 0.9	3.9 ± 1.2	2.3 ± 1.0	2.9 ± 2.1	2.6 ± 1.6	
Hf ^b	5.1 ± 1.6	16 ± 10	2.7 ± 0.6	4.1 ± 1.4	2.4 ± 0.5	2.5 ± 1.0	2.3 ± 1.8	
Th ^b	5.1 ± 1.1	11 ± 3	3.0 ± 1.0	4.2 ± 1.3	2.7 ± 0.7	2.6 ± 1.7	1.7 ± 1.8	

^aData are given as percentages.^bData are given as parts per million.

g), which could not be distinguished in the field. Unit III(upper) was probably produced by Ko-f materials and Unit III(lower) by Ko-g.

Table II suggests that the soil unit classification agrees quite well with the chemical concentration groupings, considering the heterogeneous nature of soil deposits, and forms reasonably precise (5–20%) groups.

The division of Unit II into II and II' is justified on the basis of both the major and the trace element concentrations. The splitting of Unit III into III(upper) and III(lower) is justified primarily by the concentration differences displayed by the higher atomic weight trace elements.

Of the elements listed in Table II, most were found either to be relatively unchanged in their concentrations (e. g., sodium and potassium) or to decrease by 25–50% with increased depth. However, aluminum and calcium appear to increase (by 15–50%) with depth. Calcium and aluminum are often leached out of the upper levels of acidic soils, and pH at Yagi varies from slightly acidic in upper levels (5.5–6.0) to neutral in the lower levels (7.0). The highest concentration of calcium is found in Unit IV, at the archaeological horizon, and may be caused by the addition of calcium-rich remains such as animal bone.

The soil units can be divided into two distinguishable groups (A and B). Unit IV and the basal unit have matching elemental concentrations and Unit III(lower) is quite similar except for slight elevations in the mean values of the medium atomic weight elements (iron to cobalt). These three soil units comprise Group B. Unit I and Unit III(upper) form a second chemically similar group (Group A). Unit II appears to be a mixture of these two distinct groups with approximately half of the elements favoring each group; most of the major constituents and all the high atomic weight elements show a Group B affiliation and the medium atomic weight elements show a Group A affiliation.

However, Unit II' exhibits the medium atomic weight element concentrations of Group B, but the high atomic weight elements produced mean values far higher than those of even the Group A units. The peculiarities of Units II and II' may be related to the addition of ash from the single modern eruption of Essan (Table I). All other volcanic horizons represent material ejected from Komagatake.

The rare earth element (REE) concentrations show similar patterns when the samples are grouped by soil units. Results, expressed as elemental concentration means and standard deviations, are displayed in Table III. There are three main points of interest:

1. The intergroup consistency of the mean europium concentrations.
2. The approximately 30% decrease in the mean concentrations of the heavy REE with depth. This parallels the changes found in other elements (Table II).

Table III. Distribution of REE Concentrations Among Soil Units

Element	Soil Units (number of samples)							
	I (4)	II' (7)	II (4)	III (upper) (9)	III (lower) (8)	IV (6)	Basal (4)	
La	21 ± 3	40 ± 10	10 ± 3	40 ± 19	10 ± 2	10 ± 6	9 ± 4	
Ce	45 ± 9	72 ± 35	29 ± 7	50 ± 29	21 ± 12	23 ± 9	26 ± 11	
Nd	18 ± 1	40 ± 7	10 ± 4	28 ± 17	10 ± 4	13 ± 10	10 ± 3	
Sm	5.6 ± 1.2	8.7 ± 3.0	3.7 ± 0.6	5.4 ± 2.0	3.9 ± 0.9	3.5 ± 1.1	3.7 ± 0.9	
Eu	1.4 ± 0.1	1.6 ± 0.2	1.4 ± 0.3	1.5 ± 0.2	1.6 ± 0.1	1.6 ± 0.4	1.4 ± 0.1	
Tb	0.75 ± 0.16	1.2 ± 0.4	0.74 ± 0.20	0.75 ± 0.21	0.63 ± 0.10	0.61 ± 0.20	0.51 ± 0.10	
Dy	5.4 ± 0.4	6.8 ± 2.0	4.3 ± 0.8	5.3 ± 1.4	3.7 ± 0.9	3.7 ± 0.7	3.3 ± 0.6	
Yb	2.8 ± 0.4	4.1 ± 0.7	2.5 ± 0.1	3.1 ± 0.8	2.7 ± 0.4	2.6 ± 0.3	2.3 ± 0.4	
Lu	0.41 ± 0.08	0.52 ± 0.08	0.34 ± 0.05	0.39 ± 0.09	0.34 ± 0.08	0.36 ± 0.08	0.30 ± 0.05	

NOTE: Data are given as parts per million.

3. The fractionation and subsequent enrichment of the light REE in Units I, II', and III(upper).

Comparison of the REE concentration profiles shows that Units II, III(lower), IV, and the basal unit are chemically very similar; Units I, II', and III(upper) form a less well defined but separate grouping. The REE groupings are in reasonable accord with those made using the other elements of Table II (Groups A and B).

To further investigate variations in the REE concentrations of all the samples, the concentrations were chondrite-normalized (27), and the chondrite-normalized patterns were plotted. Three basic patterns were observed (Figure 4). Pattern 1 is characterized by a high enrichment of

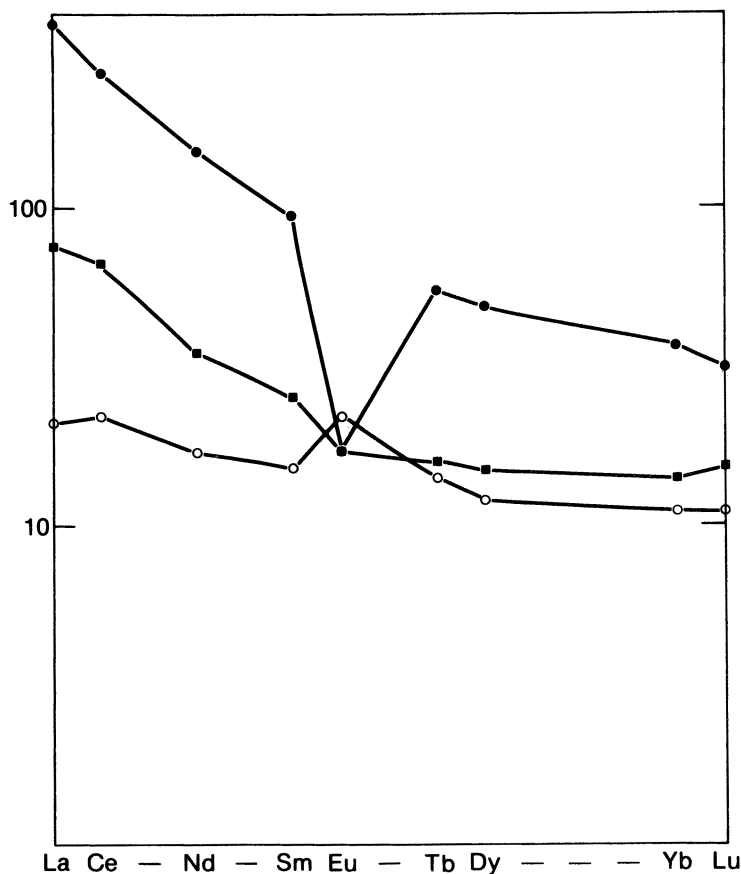


Figure 4. The three chondrite-normalized REE patterns characteristic of Yagi soil profiles: pattern 1 (●), pattern 2 (■), and pattern 3 (○). Pattern 2 is subdivided into 2a and 2b. That shown here is for 2a. Pattern 2b has a similar shape but has lower values.

light REE (with chondrite-normalized values of lanthanum >100), and a large negative europium anomaly. Pattern 2 is characterized by a decreased enrichment of the light REE with little or no europium anomaly. Because of the broad range of lanthanum values in pattern 2, it may be subdivided into 2a (chondrite-normalized values for lanthanum of 50–100) and 2b (chondrite-normalized values for lanthanum <50). Pattern 3 is characterized by a flatter REE profile with a positive europium anomaly. Through the arguments of Westgate and Gorton (28), these widely and subtly differing chondrite-normalized REE patterns may indicate sequential eruptions from two or more centers, although they may reflect temporal changes in the composition of ejecta from a single source. In the latter, magma may show elemental variability in response to changes in temperature and pressure via fractional crystallization. The major element and trace element composition of lava, ash, and pumice will reflect the elemental values of the magma.

The dominance of Komagatake ejecta at Yagi supports the concept of single source variability. The behavior of major elements and REE in the Yagi soil profiles is compatible (29). However, this will remain conjectural until analysis of dated stratigraphies at or close to both Komagatake and Essan have been completed.

After the REE patterns have been established, it is possible to check the reliability of the soil unit designations. The results in Table IV suggest that there is quite reasonable agreement between the REE patterns and the soil horizon units. Only 2 samples out of 42 do not appear to fit the various clusters. These two samples were obtained from an exposure where the basal stratigraphic sequence was undecipherable. This table confirms the similarity of Units II, III(lower), IV, and the basal unit (Group B) noted in Table III, and the similarity of Units I and III(upper) (Group A) with II'.

The sequence of the REE patterns observed with increasing depth

Table IV. Comparison of REE Patterns Found in Different Soil Units

<i>Unit</i> (number of samples)	<i>Pattern</i>			
	<i>1</i>	<i>2a</i>	<i>2b</i>	<i>3</i>
I (4)	—	4	—	—
II' (7)	5	2	—	—
II (4)	—	—	2	2
III upper (9)	2	5	1	1
III lower (8)	—	—	5	3
IV (6)	—	1	—	5
Basal (4)	—	—	2	2

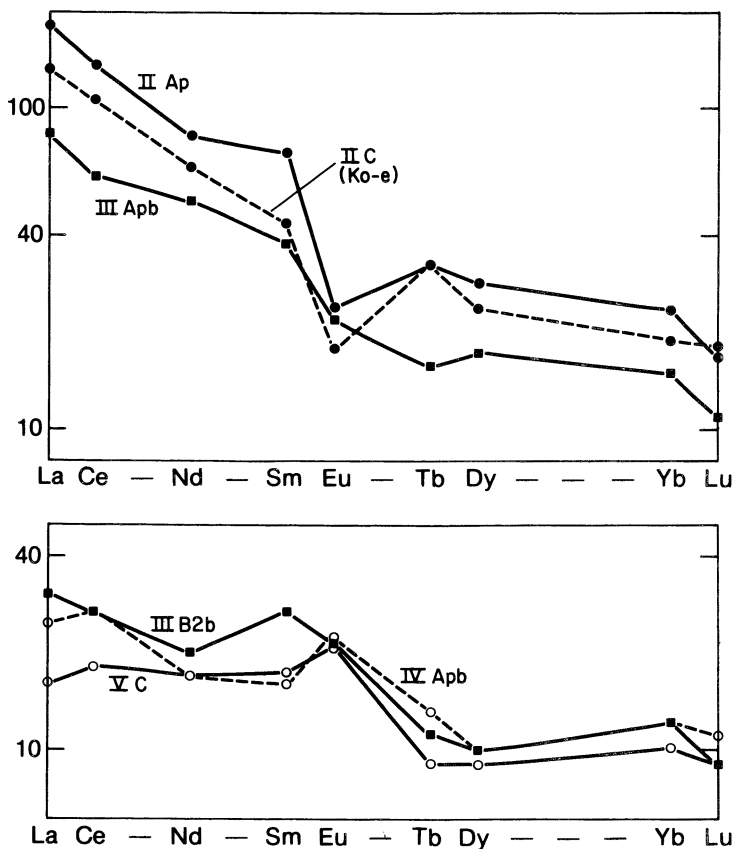


Figure 5. Chondrite-normalized REE patterns for the N124, E90 profile showing the change in pattern with depth. The figure has been divided into two sections for clarity. Key: ●, pattern 1; ■, pattern 2; ○, pattern 3.

for one exposure (N124, E90) is illustrated in Figure 5. The upper units, II Ap and IIC, exhibit REE pattern 1 and subsequently deeper soil units exhibit 2a (III Apb), 2b (IIIB2b), and 3 (IV Apb and VC).

Of the six exposures sampled with their combined 42 soil units, only one sample appears to be significantly misplaced. It is found in Unit IV with a pattern 2a rather than a pattern 3, and is one of the two possible outliers predicted from the expected REE pattern placement in Table III.

Eight ceramic samples from the Early Jomon occupations at Yagi were also analyzed as part of a continuing project involving both mineralogical and chemical analysis (30). Basal units at Yagi appeared to have adequate amounts of clay to manufacture pottery, and hence may have

provided a source of raw materials. While bearing in mind that pottery is made from mixtures of clays and tempers, and that additives may well distort the elemental concentration profiles, the chondrite-normalized REE patterns of these sherds (Table V) were found to be quite similar to those of the lower soil units—Unit III(lower) and IV, and the basal unit. These units would have been the contemporary surface when the site was occupied. The source of the REE patterns in the pottery could be derived from either the clays used or the volcanic glass used as temper. The REEs are very refractory; their relative distributions would not be affected by manufacturing.

Conclusions

The stratigraphic sequence at Yagi is formed from a series of paleosols accumulated from five volcanic episodes and modified by contemporary and prehistoric human activities. The entire sequence is about 8000 years old.

Archaeological and pedological stratigraphies were used to designate soil units in the field. However, conditions peculiar to volcanic soils limit the effectiveness of normal soil science laboratory tests.

Multielemental chemical analysis of soil samples by INAA produces elemental concentration profiles that may be used to confirm the original stratigraphic delineations of soil horizon units. The relationships between the various soil units may be explainable geochemically. Although the geochemical explanations may be of little direct interest to the archaeologist, they do imply that the observed differences are both real and expected. This finding provides reliability for stratigraphic analysis and for pottery provenance investigations.

Table V. REE Concentrations in Some Yagi Ceramics

<i>Element</i>	<i>Concentration (ppm)</i>
La	14 ± 4
Ce	40 ± 9
Nd	12 ± 4
Sm	2.4 ± 0.7
Eu	0.9 ± 0.2
Tb	0.37 ± 0.15
Dy	3.3 ± 0.9
Yb	2.3 ± 0.3
Lu	0.32 ± 0.05

This approach may be applicable in solving questions of archaeological dating and relative stratigraphy at sites where traditional pedological methods are inadequate.

Acknowledgments

We would like to acknowledge M. Hilgerdenaar, S. Glenn, and T. Wright for their assistance in the laboratory and Susan Aufreiter and Chris Robertson for their editorial help. The material was collected under a permit granted by Mayor S. Sato of Minamikayabe, Hokkaido. Local Japanese assistance was provided by T. Ogasawara. The neutron activation analysis was supported by a Natural Sciences and Engineering Research Council of Canada core grant to the University of Toronto SLOWPOKE Reactor Facility. We thank R. Allen, University of Virginia, for his insights.

Literature Cited

1. Cornwall, I. W. "Soils for the Archaeologist"; London: Phoenix House, 1958.
2. Limbrey, Susan. "Soil Science and Archaeology"; London: Academic, 1975.
3. Crawford, Gary. "Paleoethnobotany of the Kameda Peninsula Jomon"; Ann Arbor, Mich.: University of Michigan Museum Papers, in press.
4. Ikawa-Smith, Fumiko. *Am. Sci.* **1980**, *68*, 137–38.
5. Bleed, Peter; Yoshizaki, Masakazu; Hurley, William; Weymouth, John. *Technical Report No. 80-14*; Lincoln, Neb.: Univ. of Neb., Div. Arch. Research, 1978, pp. 10–12.
6. Hurley, William; Ralph, Elizabeth; Han, Mark; Yoshizaki, Masakazu. *Asian Perspectives* **1978**, *19*, 117–43.
7. Soil Survey Staff. "A Basic System of Soil Classification for Making and Interpreting Soil Surveys"; Washington, D.C.: GPO, 1975.
8. Day, P. R. "Methods of Soil Analysis"; Black, C. A., Ed.; Madison, Wis.: American Society of Agron., 1965; pp. 545–67.
9. Ball, D. F. *J. Soil Sci.* **1964**, *15*, 84–92.
10. McKeague, J. A. "Manual on Soil Sampling and Methods of Analysis"; Ottawa: Canada Soil Survey Committee, 1976.
11. Kawai, K. *Soil Sci. Soc. Am. J.* **1977**, *41*, 1171–75.
12. Soil Survey Staff. "A Basic System of Soil Classification for Making and Interpreting Soil Surveys"; Washington, D.C.: GPO, 1975.
13. Buol, S. W.; Hole, F. D.; McCracken, R. G. "Soil Genesis and Classification"; Ames, Iowa: Iowa State Univ. Press, 1973; pp. 112–13.
14. Sasaki, Tatsuo. "Distribution of the Late Quaternary Pyroclastic Deposits in Hokkaido, Japan"; Misc. Pub. Hokkaido Natl. Agric. Exp. Stn. **1974**, *4*, map.
15. Yaalon, D. H. "Paleopedology: Origin, Nature and Dating of Paleosols"; Israel Univ. Press: Jerusalem, 1971; pp. 29–39.
16. Gardiner, M. J.; Walsh, T. *Proc. R. Ir. Acad.* **1966**, *65*, Sect. C 29–35.
17. Gibbs, H. S. *N. Z. Soil News* **1969**, *3*, 73–82.
18. Martini, J. A. *Soil Sci. Soc. Am. J.* **1976**, *40*, 895–900.
19. Wada, Koji. In "Minerals in Soil Environments"; Dixon, J. B.; Weed, S. B., Eds.; *Soil Sci. Soc. Am. J.* **1977**, pp. 618–22.

20. Klages, M. G. *Soil Sci. Soc. Am. J.* **1978**, *42*, 830–33.
21. Saigusa, M.; Shoji, S.; Kato, T. *Geoderma* **1978**, *20*, 115–29.
22. Jones, J. P.; Singh, B. B.; Fosberg, M. A.; Falen, A. L. *Soil Sci. Soc. Am. J.* **1979**, *43*, 547–52.
23. Mizota, C.; Wada, K. *Geoderma* **1980**, *23*, 49–63.
24. Heidenreich, C. E.; Navratil, S. *Ont. Archaeol.* **1973**, *20*, 25–32.
25. Proudfoot, B. “Geoarchaeology: Earth Science and the Past”: Davidson, D. A.; Shackley, M. L., Eds.; London: Duckworth and Co., 1975; pp. 93–114.
26. Hancock, R. G. V. *J. IIC-CG.* **1978**, *3*, 21–27.
27. Haskin, L. A.; Haskin, M. A.; Frey, F. A.; Wildeman, T. R. “Origin and Distribution of the Elements”; Ahrens, L. H., Ed.; Elmsford, N.Y.: Pergamon, 1968, pp. 889–912.
28. Westgate, J. A.; Gorton, M. P. In “Tephra Studies”; Self, S.; Sparks, R. S. J., Eds.; Dordrecht, Netherlands: D. Reidel, 1981; pp. 73–94.
29. Allen, R., personal communication.
30. Stimmell, C. A. “1980 Yagi Report to the National Geographical Society”; in press.

RECEIVED for review November 3, 1982. ACCEPTED for publication April 18, 1983.

Analysis of Soil Associated with Woodland Burials

JOSEPH B. LAMBERT, SHARON VLASAK SIMPSON, JANE E. BUIKSTRA, and DOUGLAS K. CHARLES

Northwestern University, Departments of Chemistry and Anthropology, Evanston, IL 60201

We have analyzed the chemical composition of soil surrounding the femurs of five human skeletons buried during the Middle Woodland Period in west-central Illinois in order to document the movement of specific chemical elements between soil and bone. The use of elemental composition of bone as a measure of ancient diet is predicated on the absence of appreciable elemental flux between soil and bone. We found homogeneous concentrations of strontium and zinc in the soil, in agreement with the absence of any exchange activity for these elements. Concentrations of calcium, iron, aluminum, and potassium were inhomogeneously distributed, indicating flux out of (calcium) or into (iron, aluminum, potassium) bone.

ALTHOUGH THERE IS AN EXTENSIVE LITERATURE on the chemical analysis of soil (1,2), very little work has been done on the dynamics of soil composition associated with buried bone. The elemental content of human bone has been related to the ancient diet (3). Any significant transfer of specific elements from bone to soil or vice versa would vitiate the analysis of bone in terms of diet. Loss of trace or minor elements from bone could result in build-up of the elements in soil directly adjacent to the bone, unless the newly introduced elements are flushed away by the action of groundwater. Similarly, transfer of contaminative elements from soil to bone could be associated with depletion of elements in soil directly adjacent to the bone, unless groundwater maintains an equilibrium by reintroduction of the depleted materials. Thus, establishment of enhancement or depletion in the soil of elements found in bone should be an important aspect in our understanding of the relationship between

0065-2393/84/0205-0097\$06.00/0
© 1984 American Chemical Society

bone content and ancient diet. We report herein a multielement approach to the solution of this problem.

The most important element characterized to date in relation to diet is strontium. Discrimination by animals against strontium in favor of calcium results in decreased absolute strontium levels in animals compared with plants, and in carnivores compared with herbivores (3). Although the association of strontium with specific components of the diet is not yet established, decreased levels of strontium have been crudely associated with meat intake or protein level in the diet. Various authors have been able to relate the strontium level with the development of farming (4), with status as measured by the nature of grave goods (5), and with the sex and status of the individual as measured by burial location (6). Gilbert (7) and we (6) have examined other elements extensively for possible relationships with ancient diet. By consideration of elemental levels in soil compared with bone and of the relationship between elemental levels and the age of the individual at death, we (6) suggested that strontium, zinc, magnesium, calcium, sodium, and copper might be useful for dietary conclusions. Iron, aluminum, manganese, and potassium in bone are significantly contaminated by soil and are of no use. Gilbert (7) also concluded that strontium, zinc, magnesium, and copper would provide the best information on ancient diet. Our recent studies of elemental levels in rib and femur from the same population (8) confirmed that strontium, zinc, and magnesium, which have the same levels in the two bones, should be of greatest dietary use; iron, aluminum, manganese, and potassium, which show higher levels in the more contaminated ribs, are predominantly contaminants from the soil. A third group of elements (calcium, sodium, and lead) showed depletion in the ribs, presumably from leaching.

These results indicate that strontium, zinc, and magnesium, and possibly calcium, sodium, and lead, may be of use in understanding ancient diet, whereas iron, aluminum, manganese, and potassium clearly are of little use. If these conclusions are correct, iron, aluminum, manganese, and potassium should show depleted levels in the soil directly around buried bone, unless groundwater can reintroduce these ions from more distant soil. The remaining elements should show equal or enhanced levels in the adjacent soil. This proposition was tested briefly by Keeley et al. (9), who found depletion of manganese but no change in copper in soil adjacent to some entirely decomposed British burials. In the present study, we have examined levels of the three most important dietary elements (strontium, zinc, magnesium), as well as the clearly contaminative elements (iron, aluminum, manganese, potassium) and those possibly with mixed roles (calcium, sodium, lead), in order to obtain a complete understanding of the dynamics of elemental interchange between buried bone and the adjacent soil.

Materials and Methods

All burials were located at the Elizabeth site in west-central Illinois, dated approximately to the Middle Woodland Period (100 B.C. to 400 A.D.). Soil samples were taken at 5-cm intervals from the midpoint of the shaft of each femur, in horizontal and vertical directions. Approximately 50–100 g of soil was removed with a steel trowel from a 2-cm circle surrounding the measured position. The soil samples were air-dried and stored in sealed, polyethylene-lined paper bags.

The femur was chosen for its cylindrical symmetry, which permitted soil sampling in a full 360° solid arc around the bone without significant contamination from the effects of neighboring bones from the same skeleton. Furthermore, we have shown (8) that the femur is less sensitive to diagenetic effects than the rib, for example. The femurs appeared to have decomposed more on the underside than on any other surface. Soil sample sets were not usually complete because most skeletal discoveries could not be anticipated. Burials were normally located in a pit that had been backfilled at the time of interment. Consequently, soil within and outside the pit need not be of the same materials. Vertical samples well below the skeleton and horizontal samples well away from the skeleton may reflect a change in the type of soil. With one exception, only burials that had been located on a level surface were examined in order to avoid the effects of soil creep (10).

For chemical analysis of each sample, approximately 10 g of soil was transferred to a Gooch crucible. Surface debris such as twigs were removed, and the crucibles were heated in a muffle furnace at 500 °C for 24 h to remove organic components. The ashed soil was then pulverized with a pestle in a porcelain mortar. For each soil position, four 0.5-g portions of fine powder were analyzed separately, and the results were averaged. Soil analyses were performed in-house by atomic absorption spectrometry on a Varian Model 1250 spectrophotometer according to our previously reported method, which involves total dissolution of the sample in acid (11,12). The elements assayed were strontium, zinc, magnesium, calcium, sodium, lead, iron, aluminum, manganese, and potassium.

Results

In order to display and discuss the soil analyses, a coordinate system must be defined. With the femur extended in the z direction (feet always pointing toward the observer), the x axis is horizontal and the y axis vertical. Let us arbitrarily define the positive y direction as up and the positive x direction as away from the burial (hence, negative x is between the two femurs). In the data tables, $+5x$ then would indicate a soil sample located 5 cm away from the femur (i.e., away from the burial), $-5x$ would indicate a sample 5 cm from one femur inwards toward the other femur, and $-10y$ would indicate a sample 10 cm beneath the femur.

Soil was analyzed surrounding four separate burials, which we have designated by the letters A–D. Burial B contained two individuals represented by B1 and B2. Individual A (mound 3, burial 1) was a female of age 35–50; B1 (mound 3, burial 3) a female of age 50+; B2 (mound 3, burial 3) a female of age 40+; C (mound 3, burial 13) a female of age

25–35; and D (mound 11, burial 5) a male of age 20–21. Tables I–V display the results of our analyses.

Discussion

The distribution of elements around each femur was used as an internally calibrated measure of dynamic effects between bone and soil. The four analyses at each soil position were averaged, and the means for the various positions were compared to one another by the *F*-test (12, 13), which determines whether there is a significant difference among the means. A negative result indicates that all the means are statistically the same. A positive result indicates that at least one of the soil positions is distinct from the others. Thus, if the concentration of a given element decreases or increases with the distance from the bone (the result of leaching into or out of the bone), a positive result would be obtained. In addition, if the concentration above the bone is different from that below or on the side, a positive result also would be obtained. If only one soil point is anomalous, a positive result may be misleading.

These principles are best seen by application to burial A, the *F*-tests for which are given in Table VI. The distribution of zinc is seen to be entirely isotropic, as there are no differences in the means for all four soil positions around both femurs at the 95% confidence level. A homogeneous distribution of strontium also is seen around the left femur. The positive result for the right femur is caused by the single $-5x$ point, but there is no discernible overall trend in the strontium data. Except for this single point, the strontium distribution is essentially homogeneous around the right femur. Similarly for manganese, the distribution is homogeneous around the left femur, and the positive result for the right femur is caused by a single position, $-5x$.

We propose that a pair of criteria must be fulfilled in order to conclude that exchange effects are present. First, statistically significant (>95%) differences in elemental concentrations must be present for soil around both the right and the left femur. Secondly, the pattern of inhomogeneity must be the same for both femurs. In dealing with material as naturally heterogeneous as soil, it is necessary to utilize such extreme criteria. According to these criteria, in addition to strontium, zinc, and manganese, we observe the distributions of sodium and lead to be homogeneous around Burial A.

The distributions of magnesium, calcium, and iron are clearly anisotropic around the femurs, and aluminum and potassium are probably anisotropic. Within this set of five elements, however, there are two distinct patterns of leaching. The highest concentrations of magnesium and calcium are at positions $+5x$ and $-5x$ from the right femur and $-5x$ from the left femur. The lowest concentrations of these two elements

Table I. Soil Analyses for Burial A

	Right Femur				Left Femur			
	+5y	+5x	-5x	-5y	+5y	-5x	+5x	-5y
Sr	31 ± 1	31 ± 3	26 ± 1	30 ± 1	28 ± 4	26 ± 3	24 ± 2	30 ± 6
Zn	76 ± 33	50 ± 12	64 ± 7	61 ± 20	59 ± 21	46 ± 4	69 ± 9	53 ± 17
Mg	1.07 ± 0.02	1.10 ± 0.01	1.28 ± 0.03	0.94 ± 0.01	1.17 ± 0.04	1.31 ± 0.03	0.99 ± 0.01	0.92 ± 0.01
Ca	2.11 ± 0.03	2.27 ± 0.14	2.20 ± 0.03	1.80 ± 0.06	2.32 ± 0.09	2.67 ± 0.04	1.76 ± 0.04	1.73 ± 0.05
Na	309 ± 14	259 ± 17	283 ± 52	313 ± 26	302 ± 19	289 ± 25	197 ± 50	296 ± 12
Pb	21 ± 3	28 ± 3	30 ± 6	29 ± 2	27 ± 4	23 ± 3	39 ± 3	31 ± 2
Fe	2.21 ± 0.04	2.13 ± 0.06	2.08 ± 0.06	2.44 ± 0.07	2.24 ± 0.09	2.06 ± 0.10	2.29 ± 0.06	2.64 ± 0.01
Al	1.91 ± 0.06	1.69 ± 0.11	1.81 ± 0.11	1.95 ± 0.16	1.83 ± 0.14	1.74 ± 0.16	1.83 ± 0.10	2.13 ± 0.12
K	4340 ± 410	3170 ± 720	3000 ± 120	4110 ± 350	3720 ± 370	3670 ± 430	2870 ± 120	4060 ± 210
Mn	400 ± 82	375 ± 29	507 ± 68	339 ± 29	342 ± 25	375 ± 46	401 ± 29	358 ± 43

NOTE: Data are given as parts per million, except for Mg, Ca, Fe, and Al, which are as percentages (10⁴ ppm).

Table II. Soil Analyses for Burial B1

	Right Femur				Left Femur			
	+5y	+5x	-5x	-5y	+5y	-5x	+5x	-5y
Sr	24 ± 4	31 ± 3	28 ± 1	23 ± 3	29 ± 3	29 ± 5	26 ± 2	19 ± 2
Zn	80 ± 8	116 ± 34	85 ± 11	121 ± 32	117 ± 15	98 ± 16	94 ± 8	89 ± 8
Mg	1.29 ± 0.01	1.31 ± 0.01	1.38 ± 0.02	1.21 ± 0.02	1.44 ± 0.01	1.38 ± 0.02	1.15 ± 0.02	1.09 ± 0.02
Ca	2.38 ± 0.05	2.33 ± 0.05	2.73 ± 0.03	2.21 ± 0.05	2.70 ± 0.04	2.45 ± 0.06	1.94 ± 0.04	1.94 ± 0.08
Na	319 ± 12	302 ± 7	317 ± 17	317 ± 21	315 ± 18	337 ± 15	344 ± 10	284 ± 19
Pb	16 ± 2	17 ± 2	13 ± 2	19 ± 2	19 ± 1	17 ± 1	18 ± 1	19 ± 1
Fe	2.46 ± 0.06	2.51 ± 0.05	2.28 ± 0.07	2.77 ± 0.06	2.24 ± 0.06	2.36 ± 0.06	2.73 ± 0.05	2.59 ± 0.08
Al	1.83 ± 0.16	2.01 ± 0.11	1.77 ± 0.16	2.06 ± 0.13	1.74 ± 0.14	1.96 ± 0.17	2.15 ± 0.17	1.80 ± 0.06
K	4000 ± 250	4150 ± 200	3900 ± 360	4360 ± 170	3790 ± 280	4260 ± 280	4540 ± 200	3830 ± 230
Mn	506 ± 29	537 ± 40	504 ± 44	500 ± 10	510 ± 24	533 ± 25	522 ± 57	443 ± 21

NOTE: Data are given as parts per million, except for Mg, Ca, Fe, and Al, which are as percentages (10⁴ ppm).

Table III. Soil Analyses for Burial B2

	Right Femur			Between Femurs			Left Femur		
	+5x	-5y	-x	+5y	-5x	-5y			
Sr	30 ± 2	25 ± 3	26 ± 0.1	30 ± 0.1	24 ± 2	24 ± 3			
Zn	74 ± 18	117 ± 3	100 ± 11	91 ± 11	110 ± 16	93 ± 10			
Mg	1.22 ± 0.02	0.98 ± 0.03	0.96 ± 0.02	1.34 ± 0.03	1.07 ± 0.04	1.02 ± 0.05			
Ca	2.03 ± 0.04	1.54 ± 0.05	1.38 ± 0.04	2.52 ± 0.03	1.81 ± 0.08	1.72 ± 0.03			
Na	325 ± 18	373 ± 32	377 ± 22	360 ± 20	368 ± 18	357 ± 35			
Pb	17 ± 2	23 ± 1	22 ± 2	18 ± 2	20 ± 1	16 ± 1			
Fe	2.35 ± 0.05	2.56 ± 0.06	2.87 ± 0.09	2.32 ± 0.06	2.59 ± 0.10	2.63 ± 0.17			
Al	2.04 ± 0.17	1.98 ± 0.37	2.31 ± 0.23	1.85 ± 0.18	1.94 ± 0.26	1.96 ± 0.30			
K	4480 ± 260	4520 ± 630	5110 ± 400	4440 ± 300	4520 ± 460	4450 ± 540			
Mn	317 ± 11	317 ± 23	287 ± 19	350 ± 39	302 ± 40	316 ± 16			

NOTE: Data are given as parts per million, except for Mg, Ca, Fe, and Al, which are as percentages (10⁴ ppm).

Table IV. Soil Analyses for Burial C

	Right Femur					
	+15x	+10x	+5x	+5y	-5x	-10x
Sr	19 ± 1	18 ± 3	19 ± 0	18 ± 2	22 ± 2	19 ± 1
Zn	85 ± 34	95 ± 10	73 ± 14	65 ± 9	95 ± 22	98 ± 30
Mg	3560 ± 80	3380 ± 290	3570 ± 100	3420 ± 210	3480 ± 190	3520 ± 110
Ca	1260 ± 270	2030 ± 180	2030 ± 10	2010 ± 190	2020 ± 150	1720 ± 260
Na	285 ± 36	274 ± 39	293 ± 37	249 ± 34	256 ± 38	322 ± 35
Pb	25 ± 4	30 ± 2	34 ± 3	31 ± 4	30 ± 2	36 ± 9
Fe	1.99 ± 0.03	1.94 ± 0.09	2.05 ± 0.03	2.01 ± 0.06	2.08 ± 0.04	2.05 ± 0.05
Al	2.23 ± 0.06	2.17 ± 0.22	2.36 ± 0.11	2.22 ± 0.13	2.25 ± 0.14	2.29 ± 0.12
K	3540 ± 60	3240 ± 190	3670 ± 130	3410 ± 160	3540 ± 150	3320 ± 90
Mn	223 ± 17	265 ± 19	236 ± 33	231 ± 32	218 ± 13	276 ± 23

	Left Femur					
	+10y	+5y	+5x	+10x	+15x	
Sr	18 ± 2	17 ± 2	16 ± 1	18 ± 1	18 ± 0	
Zn	88 ± 33	61 ± 14	71 ± 15	65 ± 5	80 ± 19	
Mg	3310 ± 160	3440 ± 270	3360 ± 180	3610 ± 280	3380 ± 70	
Ca	2040 ± 260	2220 ± 100	2740 ± 180	2470 ± 130	2320 ± 100	
Na	313 ± 28	293 ± 64	345 ± 24	353 ± 38	359 ± 15	
Pb	21 ± 4	27 ± 7	32 ± 3	32 ± 7	27 ± 7	
Fe	1.94 ± 0.07	2.05 ± 0.07	1.96 ± 0.08	2.05 ± 0.06	2.01 ± 0.04	
Al	2.09 ± 0.14	2.07 ± 0.18	2.11 ± 0.16	2.30 ± 0.15	2.21 ± 0.06	
K	3430 ± 160	3310 ± 220	3470 ± 150	3690 ± 160	3520 ± 70	
Mn	339 ± 45	403 ± 43	373 ± 27	304 ± 75	353 ± 19	

NOTE: Data are given as parts per million, except for Fe and Al, which are as percentages (10⁴ ppm).

Table V. Soil Analyses for Burial D

Right Femur					
	+15x	+10x	+5x	+5y	-5y
Sr	32 ± 1	30 ± 3	32 ± 3	31 ± 1	33 ± 3
Zn	74 ± 32	54 ± 16	81 ± 23	63 ± 14	93 ± 19
Mg	2.53 ± 0.02	2.62 ± 0.04	2.23 ± 0.01	2.35 ± 0.01	2.41 ± 0.02
Ca	4.68 ± 0.05	5.08 ± 0.14	4.25 ± 0.05	4.31 ± 0.07	4.32 ± 0.11
Na	215 ± 31	239 ± 13	262 ± 23	166 ± 44	202 ± 33
Pb	35 ± 4	25 ± 3	32 ± 6	26 ± 4	29 ± 3
Fe	1.45 ± 0.04	1.33 ± 0.04	1.51 ± 0.06	1.53 ± 0.05	1.45 ± 0.07
Al	1.31 ± 0.08	1.11 ± 0.06	1.40 ± 0.07	1.46 ± 0.12	1.32 ± 0.13
K	2320 ± 140	2140 ± 90	2610 ± 180	2540 ± 240	2360 ± 250
Mn	363 ± 15	321 ± 10	376 ± 30	369 ± 33	352 ± 8

Left Femur					
	-5y	+5y	+5x	+10x	+15x
Sr	29 ± 4	24 ± 4	38 ± 5	31 ± 5	34 ± 4
Zn	338 ± 22	93 ± 27	82 ± 17	105 ± 54	55 ± 25
Mg	2.38 ± 0.01	2.19 ± 0.05	2.56 ± 0.01	2.63 ± 0.01	2.53 ± 0.07
Ca	4.55 ± 0.04	4.15 ± 0.12	5.08 ± 0.04	5.11 ± 0.06	4.93 ± 0.15
Na	289 ± 46	216 ± 29	272 ± 52	257 ± 27	244 ± 12
Pb	38 ± 5	29 ± 5	33 ± 7	37 ± 4	37 ± 7
Fe	1.40 ± 0.11	1.48 ± 0.10	1.45 ± 0.09	1.36 ± 0.08	1.35 ± 0.03
Al	1.19 ± 0.19	1.34 ± 0.13	1.24 ± 0.16	1.14 ± 0.12	1.12 ± 0.05
K	2120 ± 350	2520 ± 270	2220 ± 280	2150 ± 240	1960 ± 110
Mn	318 ± 21	404 ± 15	315 ± 28	295 ± 12	281 ± 12

Above and Between Femurs

	+35y	+25y	+15y	+10y	-x ^a
Sr	30 ± 4	29 ± 2	34 ± 1	33 ± 4	27 ± 2
Zn	61 ± 9	72 ± 20	74 ± 22	61 ± 4	69 ± 23
Mg	2.03 ± 0.01	2.09 ± 0.02	2.56 ± 0.02	2.74 ± 0.02	2.02 ± 0.02
Ca	4.29 ± 0.29	4.36 ± 0.09	5.29 ± 0.13	5.46 ± 0.10	3.89 ± 0.04
Na	144 ± 14	232 ± 61	207 ± 44	130 ± 30	284 ± 44
Pb	37 ± 14	31 ± 4	25 ± 5	20 ± 7	30 ± 4
Fe	1.61 ± 0.04	1.56 ± 0.03	1.37 ± 0.06	1.34 ± 0.08	1.50 ± 0.10
Al	1.48 ± 0.07	1.50 ± 0.04	1.27 ± 0.11	1.15 ± 0.11	1.45 ± 0.13
K	2790 ± 140	2810 ± 70	2500 ± 360	1940 ± 280	2680 ± 270
Mn	408 ± 27	405 ± 3	414 ± 66	356 ± 8	332 ± 26

NOTE: Data are given as parts per million, except for Mg, Ca, Fe, and Al, which are as percentages (10⁴ ppm).
^a Between femurs.

Table VI. Soil Analysis *F*-Test for Burial A

	<i>Right Femur</i> (+5y vs. +5x vs. -5x vs. -5y)	<i>Left Femur</i> (+5y vs. -5x vs. +5x vs. -5y)		<i>Right Femur</i> (+5y vs. +5x vs. -5x vs. -5y)	<i>Left Femur</i> (+5y vs. -5x vs. +5x vs. -5y)
Sr	9.89**	0.76	Pb	5.63++	16.95***
Zn	1.09	1.79	Fe	31.05***	30.24***
Mg	203.14***	188.27***	Al	4.24+	6.57*
Ca	27.63***	232.09***	K	8.71**	10.98***
Na	1.13	10.74**	Mn	6.40*	1.86

NOTES: *F*-test significances are indicated as follows: +, 95.0%; ++, 97.5%; *, 99.0%; **, 99.5%; ***, 99.9%.

For burial A, $m = 3$, $n = 12$ ($m + 1$ is the number of compared means; $n + m$ is the number of individuals).

are present directly below, $-5y$, both femurs. For iron and aluminum, however, the lowest concentrations are located at $+5x$ and $-5x$ from the right femur and $-5y$ from both femurs. Potassium follows this same pattern to a lesser extent. The most reasonable explanation for these divergent results is that magnesium and calcium are being released from the bone into the soil, whereas iron, aluminum, and potassium are being depleted from the soil into the bone. This conclusion is similar to the results obtained by comparison of rib analyses with femur analyses (8) and by analysis of concentrations as a function of the age of the individual at death (6). Fixation of iron and aluminum by phosphate, available from bone in this context, is a well-established phenomenon (14).

Thus three distinct patterns of elemental distribution emerge from the analyses of soil around burial A. The concentrations of strontium, zinc, manganese, lead, and sodium are relatively homogeneous in the soils above, beside, and below the femur. The concentrations of magnesium and calcium are high directly beside the femur and the concentrations of iron, aluminum, and potassium are low beside the femur. These results suggest that strontium, zinc, manganese, lead, and sodium are not involved in a significant dynamic interchange between soil and bone (or that the effects have been washed away), that magnesium and calcium are leached out of the bone into the soil, and that iron, aluminum, and potassium are removed from the soil into the bone. For burial A, these trends are more prominent for the right femur than for the left. In mound 3, all the burials contained two bodies. For burial A, the arrangement was such that the right femur was located next to the left femur of the companion, and soil effects on the right femur of A may be exaggerated by similar effects from the left femur of the companion.

The grave pits in mound 3 were prepared by removal of soil through the A and into the B horizon in order to form bowl-shaped holes in the ground. In soil science, the A horizon refers to the humus-rich top layer

that is most subject to the effect of washing. The B horizon is the region to which the washings from A can migrate. The C horizon is weathered but maintains chemical stability. The backfill process after burial would tend to homogenize the soil and mix the horizons. After the pit was filled, the mound was constructed over it. The hard clay beneath the hole would be less permeable to rain water, so that collection of water toward the bottom of the pit after rains could give rise to anisotropic distributions of elements.

Soil from burial B was sampled around both individuals, labeled B1 and B2. The analyses for B1 are given in Table II and the *F*-test comparisons in Table VII. The elemental distributions follow a similar pattern to that for burial A. The elements strontium, zinc, sodium, lead, and manganese again show relative homogeneity around the bones. For a positive result (i. e., anisotropy), significant differences must be observed around both femurs, and the same pattern must be present for both. Thus for B1, zinc is homogeneous around the right femur, but the positive result for the left femur is caused by the single point at +5*y*.

Significant inhomogeneity is observed for magnesium, calcium, and iron for B1. As for burial A, the highest calcium and magnesium concentrations are located at -5*x* and +5*y* from the left femur and at +5*y* and -5*x* from the right femur. The lowest concentrations are at -5*y* from both femurs. The lowest concentrations for iron and aluminum are at -5*x* and +5*y* from the left femur and at +5*y* and -5*x* from the right femur, and the highest concentrations are at -5*y* from both femurs. Thus the elemental distributions in the soil are very similar for both burials A and B1. Surprisingly, the distribution of potassium around B1 does not fulfill the criteria for inhomogeneity, although examination of the raw data does show similarities to the patterns for iron and aluminum.

Table VII. Soil Analysis *F*-Test for Burial B1

	<i>Right Femur</i> (+5 <i>y</i> vs. +5 <i>x</i> vs. -5 <i>x</i> vs. -5 <i>y</i>)	<i>Left Femur</i> (+5 <i>y</i> vs. -5 <i>x</i> vs. +5 <i>x</i> vs. -5 <i>y</i>)		<i>Right Femur</i> (+5 <i>y</i> vs. +5 <i>x</i> vs. -5 <i>x</i> vs. -5 <i>y</i>)	<i>Left Femur</i> (+5 <i>y</i> vs. -5 <i>x</i> vs. +5 <i>x</i> vs. -5 <i>y</i>)
Sr	7.33**	6.55 ^a ++	Pb	6.46*	1.33
Zn	3.05	4.00+	Fe	42.02***	49.64***
Mg	61.59 ^b ***	385.44***	Al	4.03+	6.93*
Ca	107.38***	156.61***	K	1.49	8.07**
Na	1.04	11.37***	Mn	1.08	5.45++

NOTES: *F*-test significances are indicated as follows: +, 95.0%; ++, 97.5%; *, 99.0%; **, 99.5%; ***, 99.9%.

For burial B1, *m* = 3, *n* = 12, unless otherwise indicated.

^a*m* = 3, *n* = 10 (see footnote, Table VI).

^b*m* = 3, *n* = 11 (see footnote, Table VI).

The generally higher solubility of potassium salts could promote reindroduction and homogenization of potassium in the soil around the burial. Local differences could explain why this process occurs more for B1 than for A.

Soil sampling was less extensive around burial B2 (Tables III and VIII). The *F*-test could be applied only to samples around the left femur, so our complete criteria, which require agreement for both femurs, could not be utilized. Again, however, the largest inhomogeneities are for magnesium, calcium, and iron. Furthermore, the highest magnesium and calcium concentrations are at $-5x$ and $+5y$ from the left femur and the lowest concentrations at $-5y$ from the left femur. Conversely, the lowest iron concentration is at $+5y$ and $-5x$ from the left femur and the highest at $-5y$. The patterns are the same as for burials A and B1. Again, homogeneous distributions are observed for strontium, zinc, sodium, lead, potassium, and manganese. The small amount of data for the right femur also follows the same patterns.

The conclusions from B1 and B2 parallel those from A. Leaching of calcium and magnesium occurs from the bone to the soil, and depletion of iron and aluminum occurs from the soil to the bone. All other elements show little or no leaching effect. Only potassium exhibits different properties; it appears not to be depleted from the soil around B1 and B2. As for A, the soils around B1 and B2 were a mixture of the A and B horizons.

For burial C, satisfactory statistical differences were found only for calcium (both femurs) (Table IX). Although several elements show significant anisotropy around the right femur (Table IX), the statistical conclusions in each case (except that of calcium) result from a single point and are not confirmed by the left femur. These results contrast with those for the burials described thus far, in that only calcium fulfills our criteria for inhomogeneity. The highest calcium concentrations are at $+5y$ and $+5x$ from the left femur and at $+5x$, $-5x$, and $+5y$ from the right femur. The calcium content decreases with increasing distance from both

Table VIII. Soil Analysis *F*-Test for Burial B2

	<i>Left Femur</i> ($+5y$ vs. $-5x$ vs. $-5y$)		<i>Left Femur</i> ($+5y$ vs. $-5x$ vs. $-5y$)
Sr	7.60++	Pb	7.68++
Zn	4.61+	Fe	8.88*
Mg	80.72***	Al	0.06
Ca	304.53***	K	0.03
Na	0.22	Mn	2.19

NOTES: *F*-test significances are indicated as follows: +, 95.0%; ++, 97.5%; *, 99.0%; **, 99.5%; ***, 99.9%.

For burial B2, $m = 2$, $n = 9$ (see footnote, Table VI).

Table IX. Soil Analysis *F*-Test for Burial C

	<i>Right Femur^a</i> (+15x vs. +10x vs. +5x vs. -5x vs. -10x)	<i>Left Femur^b</i> (+10y vs. +5y vs. +5x vs. +10x vs. +15x)		<i>Right Femur^a</i> (+15x vs. +10x vs. +5x vs. -5x vs. -10x)	<i>Left Femur^b</i> (+10y vs. +5y vs. +5x vs. +10x vs. +15x)
Sr	1.92	0.80	Pb	3.16+	2.92
Zn	1.36	1.25	Fe	3.44++	2.69
Mg	0.91	1.17	Al	0.89	1.67
Ca	9.84***	10.11***	K	5.51**	3.06
Na	2.12	2.30	Mn	3.67	2.58

NOTES: *F*-test significances are indicated as follows: +, 95.0%; ++, 97.5%; *, 99.0%; **, 99.5%; ***, 99.9%.

^aFor burial C, $m = 5$, $n = 18$ (see footnote, Table VI).

^b $m = 4$, $n = 15$ (see footnote, Table VI).

femurs in the + y , - x , and + x directions, in agreement with a process whereby calcium leaches from the bone only into the nearby soil.

There are two possible explanations for the lower sensitivity to elemental variation in the soil around burial C, compared with A, B1, and B2. First, we did not have a soil sample from the -5 y location, directly below the femurs, and this location is particularly sensitive to leaching effects. Without this point, the analysis may be less sensitive. Second, and possibly more important, the age of the individual in burial C (grave pit 3-13) was 25-35 years at the time of death; those in burials A, B1, and B2 (grave pits 3-1 and 3-3) were probably all over 40. The increased brittleness and porosity of the bones from older individuals have been shown to bring about increased contamination of chemical elements from the soil environment (6). Thus the younger age of the individual in burial C may have caused less elemental interchange with the environment.

The soil around burial D, located in a different mound (grave pit 11-5), was sampled very extensively (Table V). The expected trends are observed, for the most part, in the samples around the right femur (*F*-tests are given in Table X). Homogeneous distributions are found in both x and y directions for strontium and zinc. The remaining elements exhibited inhomogeneity, although many of these results are caused by a single, anomalous point. No expected patterns were observed in the soil around the left femur; these results were atypical compared with all others and may have been influenced by unknown soil anomalies or by decomposed burial artifacts.

The point located between the femurs, designated by - x in Table V (last section), is a useful control for other samples in the x direction, because it is >15 cm from each femur. Leaching effects should be tailing off at this distance. Indeed, concentrations of strontium, zinc, lead, sodium, and manganese at +15 x to +5 x from both femurs are similar to

Table X. Soil Analysis *F*-Test for Burial D

	<i>Above Femurs</i> ^a (+35y vs. +25y vs. +15y vs. +10y)	<i>Right Femur</i> ^b (+15x vs. +10x vs. +5x vs. +5y vs. -5y)	<i>Left Femur</i> ^b (-5y vs. +5y vs. +5x vs. +10x vs. +15x)
Sr	2.20	1.11	85.05***
Zn	0.82	1.94	52.58***
Mg	1750.00***	200.83***	73.84***
Ca	51.27***	60.51***	79.36***
Na	5.67++	5.46*	2.37
Pb	2.72	3.87++	1.74
Fe	23.23***	7.93**	1.64
Al	16.10***	8.06**	1.69
K	11.44***	3.81++	2.43
Mn	2.19	4.16*	25.53***

NOTE: *F*-test significances are indicated as follows: +, 95.0%; ++, 97.5%; *, 99.0%; **, 99.5%; ***, 99.9%.

^aFor burial D, $m = 3$, $n = 12$ (see footnote, Table VI).

^b $m = 4$, $n = 15$ (see footnote, Table VI).

the values at $-x$ (between the femurs). Magnesium and calcium concentrations are higher at $+15x$ to $+5x$ than at $-x$, and iron, aluminum, and potassium concentrations are lower. Thus, the three distinct patterns of elemental distribution observed for burials A and B are also observed in the x direction for D.

The vertical profile for burial D was the most extensive we obtained, from $+35y$ to $+5y$ in 5–10-cm increments, and showed the same trends we observed in the burials from mound 3. Thus the soil distributions for strontium, zinc, lead, and manganese are vertically homogeneous. Although the *F*-test for sodium is positive, the distribution is not monotonic and may not have been appreciably inhomogeneous. As usual, high *F* values are obtained for magnesium, calcium, iron, aluminum, and potassium. The magnesium and calcium concentrations decrease monotonically with increasing distance from the skeleton, whereas the iron, aluminum, and potassium concentrations increase monotonically with increasing distance from the skeleton. These results again are suggestive of loss of magnesium and calcium from the skeleton to the soil and loss of iron, aluminum, and potassium from the soil to the skeleton.

The soils in the vicinity of mound 11 were less developed than those around mound 3, with only a very weak B horizon. The pitfall was a mixture of soils from the A and C horizons. There was no actual mound over the pit, which was dug out from the side of a ridge. Thus the anomalies associated with the left femur may have been the result of soil creep.

Conclusions

Because of the normal heterogeneity of soil and because of possible unnatural alterations introduced at the time of burial, such as grave goods that have since decomposed, elemental analysis of soils and discernment of spatial trends of specific elements are fraught with difficulties. Nonetheless, we believe that we have documented permanent and diagnostic alterations in the soil composition as the result of elemental interchange with the skeleton. Furthermore, these observations correspond in almost every detail to those made in our study of the relative elemental compositions of excavated human ribs and femurs (8).

With few exceptions, we found that strontium and zinc are homogeneously distributed in the soil around the burials, so that there was no flux of these elements between soil and bone. These elements were found to be of equivalent proportions in the ribs and femurs (8) and have been classified as reliable indicators of ancient diet. Calcium was found in higher concentrations beside ($+x$ and $-x$) and above ($+y$) the skeleton, and this increased concentration clearly dies off in the $+y$ direction (gradient data were not available for $-y$). In agreement with the rib/femur study, these results suggest that calcium is leaching out of the bone and lodging permanently (on the time scale of the burial) in the soil around the skeleton. A similar observation for magnesium differs from the rib/femur result, in which magnesium was found in identical proportions in the two bones. The increased presence of magnesium in the soil around the bones may have resulted from effects of organic tissue, which we have not been able to consider.

The pattern whereby strontium is stable in buried bone but calcium clearly leaches out into the soil over time confirms that use of the strontium:calcium ratio in the analysis of buried bone is entirely inappropriate. Although valuable to the geologist and the biochemist, this ratio is dependent on diagenesis and is not reliable for the archaeologist looking at ancient bone. The absolute strontium and calcium percentages must be used in development of dietary inferences.

The elements sodium, manganese, and lead were generally homogeneous in their distribution in the soil around the skeleton. However, we have clearly demonstrated that sodium is lost from bone and manganese is gained during burial (6, 8) (lead effects were not entirely clear). Thus sodium and manganese may be relatively mobile within the soil, so that archaeological effects are too short term. The high solubility of sodium salts may promote the disappearance of any concentration inhomogeneities.

Finally, iron, aluminum, and potassium show unambiguous patterns of leaching from the soil into the bone. Their distributions are invariably anisotropic (except occasionally for potassium, another element with highly

soluble salts). Their concentrations are lower beside and above the skeleton; these decreased levels die off clearly in the $+y$ direction. These elements were found at higher levels in the rib than in the femur (8), as expected for contaminants.

In this study, we have not been able to focus on specific environmental effects, such as weathering, climate, bacteria, drainage, solifluction, grave goods, and the decomposed organic part of the body. Soil analysis can be a difficult and frequently unrewarding approach to understanding the effects of diagenesis of buried human bone. However, we believe that, at the least, we have shown that strontium and zinc in human bone undergo little or no flux with the soil during burial for the time period and conditions under study, that calcium leaches from the bone into the surrounding soil, and that iron, aluminum, and potassium move from the soil into the bone. The flux of magnesium, sodium, lead, and manganese is not clear from soil analyses alone, although their roles are clarified by comparison of their relative levels in rib and femur.

This study comprises an initial approach to understanding soil/bone dynamics. We have not been able to address the question of the actual mechanisms of elemental flux, which might be quite different for calcium, iron, and manganese, for example. Sites with other soil characteristics, such as pH, and other environmental characteristics, such as climate, might produce different results.

Acknowledgments

This work was supported by the Research Committee of Northwestern University and by funds from the local and national organizations of Sigma Xi, the Scientific Research Society, to S. V. S.

Literature Cited

1. Pickering, W. F. *CRC Crit. Rev. Anal. Chem.* **1981**, *12*, 233–66.
2. Smith, K. A. "Soil Analysis"; Marcel Dekker: New York, 1982.
3. Toots, H.; Voorhies, M. R. *Science* **1965**, *149*, 854–55.
4. Gilbert, R. I., Jr. Ph.D. Dissertation, University of Massachusetts, Amherst, Mass., 1975.
5. Schoeninger, M. J. *Am. J. Phys. Anthropol.* **1979**, *51*, 295–309.
6. Lambert, J. B.; Szpunar, C. B.; Buikstra, J. E. *Archaeometry* **1979**, *21*, 115–29.
7. Gilbert, R. I., Jr. In "Biocultural Adaption in Prehistoric America"; Blakely, R. L., Ed.; Univ. Georgia Press: Athens, Ga., 1977; pp. 85–100.
8. Lambert, J. B.; Vlasak, S. M.; Thometz, A. C.; Buikstra, J. E. *Am. J. Phys. Anthropol.* **1982**, *59*, 289–94.
9. Keeley, H. C. M.; Hudson, G. E.; Evans, J. J. *Archaeol. Sci.* **1977**, *4*, 19–24.
10. Bakkevig, S. *Norw. Archaeol. Rev.* **1980**, *13*, 73–100.

11. Szpunar, C. B.; Lambert, J. B.; Buikstra, J. E. *Am. J. Phys. Anthropol.* 1978, 48, 199–202.
12. Szpunar, C. B. Ph.D. Dissertation, Northwestern University, Evanston, Ill., 1977.
13. Sokal, R. R.; Rohlf, F. J. In "Biometry"; Freeman: San Francisco, Calif., 1969; pp. 201–9.
14. Eidt, R. C. *Science* 1977, 197, 1327–33.

RECEIVED for review November 3, 1982. ACCEPTED for publication May 4, 1983.

Modern Neutron Activation Analysis and Ancient History

I. PERLMAN

Hebrew University, Jerusalem

Neutron activation analysis (NAA) is an eminently suitable technique for obtaining the chemical profile of ancient pottery and artifacts made from other earthy materials. This technique can be used to determine where these articles originated. An NAA system that has proved to be adequate for this task is discussed. A brief review is also given of the way archaeologists have decided matters of provenance and the uses to which they put their knowledge. Finally, two examples of archaeological problems are given in which the new horizons opened by the laboratory work are stressed.

NEUTRON ACTIVATION ANALYSIS (NAA), as the title of this chapter suggests, has some relevance to the reconstruction of ancient history; to be more exact, we are dealing with the application of NAA to archaeology. Ancient writings that have been uncovered or handed down through the ages are of course invaluable, but much of what is known about ancient history comes from the work of the archaeologist.

This chapter focuses on the analysis of ceramics with the goal of learning where they originated—their provenance. Initially this seems to be a worthwhile but highly restricted objective; however, we shall see that it has much broader ramifications.

As archaeologists painstakingly uncover an ancient site they come upon a multitude of artifacts that are clues to who lived there, at what time, and to many aspects of daily life. It is not possible to discuss here the many facets of such problem solving, but it can be said that much of their attention is focused on the pottery. During one season of excavation at one site, more than 100,000 pottery fragments may be found. These fragments are quickly sorted, and a considerable number are kept for more thorough examination. Obviously, there is something to be “read” in the pottery.

The basis for reading pottery is the existence of pottery repertoires, each of which is recognized by a kinship among its members. The vessels

0065-2393/84/0205-0117\$06.00/0
© 1984 American Chemical Society

in each group may have different forms (e.g., bowls, jugs, plates, cups), but other characteristics are consistent. Details of the contours will recur among different forms within a repertory and will be different from those of another repertory. The archaeologist then looks at the quality of workmanship, the color and texture of the fabric, the color and quality of the finish, the decorative motifs, the technique of manufacture, and any other features that appear to be distinctive.

By performing such an analysis, an archaeologist can tell if pottery that he finds is a member of a particular group. To help remove ambiguities in the descriptions, drawings are available for each form with notes indicating which features are thought to be diagnostic.

The classification of pottery into recognizable groups is worth the effort only if other things can be learned by doing so. One of the important aspects of a pottery repertory is its relation to chronology. At one place or another, members of a group will be found in a stratum containing datable material. Among artifacts suitable for dating are coins, inscriptions, Egyptian scarabs, and seals. A stratum may also be a destruction layer that can be associated with an event mentioned in historical records.

Chronological associations of these kinds establish the dating of the pottery; therefore, similar pottery can be used for dating strata in sites where other dating evidence is absent. Because pottery is never absent, it is the most commonly used material for dating, either by itself or in a supporting role.

In addition to its function as a marker for chronology, a pottery repertory is always used to identify the people who made it and, by inference, its provenance. Pottery of local styles is to be expected, but more often than not vessels that are not indigenous to the area also appear—sometimes in large numbers. Pottery of foreign styles may simply reveal ancient trade patterns, which in itself is important. However, much more is learned from the full array of pottery when examined in conjunction with everything else noted in the stratum. In this connection, the architectural remains have a special importance.

Examination of fallen architecture may show that a city was destroyed in an earthquake. If such is the case, the indigenous pottery forms will continue in the stratum above because the same people would have rebuilt the city. Alternatively, a destruction layer may be completely permeated with ashes—a telltale sign that the city was razed by a conquering army. In such a case, there is an abrupt change to pottery styles of the conqueror. Not all cities had to be taken by violent means, but unless the occupation was transitory, the pottery style would still have changed.

An important question is whether the new forms of pottery were brought in from the homeland of the new occupants or whether they were made where they were found. Archaeologists try to answer this

question by a careful examination of the pottery in relation to similar forms found elsewhere. Their conclusions are often sheer guesswork.

The big problem in using typology to establish pottery provenance stems from the fact that discernible variations in a style are found in pottery from one place. Consequently, there is lack of precision in defining exactly what belongs in a pottery repertory and what should be excluded. Even when artifacts of pottery excavated at different places appear to be identical, there is no assurance that they were in fact made in one of the places.

The determination of provenance by laboratory methods, the subject of this chapter, has shown that such deductions, among others, are often completely in error.

A special type of problem afflicts archaeologists when an innovative pottery style appears that they cannot with confidence relate to any place of origin. Because the typological approach does not allow for such contingencies, the archaeologists have to resort to tortuous relationships. There are striking cases in which laboratory work showed that these guesses were without foundation.

Methodology for Provenance Determination

The basic premise in provenance determination is that each clay source can be distinguished by its chemical composition. The approach is often referred to as "fingerprinting." There is no a priori reason to favor any particular elements for measurement, but there is good reason to measure a cross section of the periodic table. Clay contains all elements found in nature, but relatively few elements account for more than 99% of the mass. Therefore, the analytical method should be sensitive to many elements that are present only in the parts-per-million range.

Another important consideration is the need for good precision. If clays from a single source are not uniform in composition, this approach is not appropriate; there will be a large spread in the pottery composition and it will not be possible to distinguish this source from the others. If clays from one source are reasonably homogeneous one must not introduce an artificial spread by using a technique with poor precision.

Although there has been continuous improvement in the equipment used for a number of analytical methods, we still feel that NAA is the most suitable technique for this kind of work. A more quantitative view of what is required will be given presently.

At the Hebrew University in Jerusalem, we employ two germanium detectors for measuring the gamma-ray spectra: a large detector with good efficiency for the high-energy gamma rays, and a small one with high resolution for the low-energy part of the spectrum, which is quite congested. Spectra are taken with each detector at two different times

in order to optimize data acquisition for long-lived and shorter-lived isotopes separately. A multielement standard is used to convert the counts in the unknowns to element abundances.

It is basic to this kind of work that a growing data bank must be kept and that many analyses must be made. Consequently, the analytical system is automated to change samples, accumulate spectra, and put the stored data on magnetic tape for computer processing.

The most demanding aspect of analysis of the spectral data comes from the fact that each spectrum contains patterns from literally hundreds of gamma rays. Many of these gamma rays may always be too weak to be of concern; nevertheless it is prudent to examine spectra from individual pure elements to obtain a quantitative view of which peaks can be ignored. The problem is essentially one of selecting peaks that are free of interferences and, where this is not possible, of making corrections. These interferences have different forms and are illustrated in the box.

1. The most common type of interference is the overlap between the peak of interest and those that come from other elements.

Gamma-Ray Interferences			
Cr^{51} (320.0 keV)			
<i>Interfering Gamma Ray and Energy</i>		<i>Monitor Peak</i>	
Nd^{147}	319.7 keV	Nd^{147}	531 keV
Cr^{51}	320.0 keV Made by Fe^{54} (n, α)	Fe^{54}	1292 keV
Ta^{182}	322.2 keV Pile up of 222.1 and 100.1 keV	Ta^{182}	1222 keV
$\text{Pa}^{233}(\text{Th})$ (311.9 keV)			
Co^{60}	310.5 keV Double escape peak from 1332.5 keV	Co^{60}	1332.5 keV
Sc^{46} (889.6 keV)			
Fe^{59}	1099.2 keV Compton edge	Fe^{59}	1099.2 keV

2. The same isotope can sometimes be made from more than one element. A good table of nuclear data, one in which the gamma rays are listed according to energy, is indispensable in locating possible interferences for both of the first two types of interference.
3. Pileup peaks come from two gamma rays that are coincident in a gamma-ray cascade. Such peaks cannot be found in a nuclear data table and are only discerned if the analyst notes that a peak is broader than it should be, and there is no other explanation. Once identified, a search can be made for possible candidates, with the ultimate goal of discovering the gamma rays involved.
4. In a few cases, the peak that is used sits right on the Compton edge of another gamma ray. This overlap causes a severe problem in determining the background under the peak. The way to handle this problem is to treat it as a background interference.

When any such interferences occur, it is necessary to use another peak that belongs to the interfering isotope but that is free of interference. The intensity of this peak serves as a monitor to determine the size of the correction.

The Cr^{51} 320.0-keV gamma ray has three interferences, all of different types. Nd^{147} (319.7 keV) falls under the chromium peak and the correction is monitored by the Nd^{147} 531-keV peak. Cr^{51} itself is made from the reaction $\text{Fe}^{54}(n,\alpha)\text{Cr}^{51}$. Ta^{182} has intense gamma rays of 222.1 and 100.1 keV, which pile up to give a peak at 222.1 keV that is not resolved from the chromium peak. Below this in the box is shown the 311.9-keV peak of Pa^{233} by which thorium is measured. This peak has under it a peak of 310.5 keV caused by the double escape from the 1332.5-keV gamma rays of Co^{60} (1332.5–1022 keV). The example of a Compton edge correction is that of the 889.6-keV peak of Sc^{46} , which lies on the Compton edge of the 1099.2-keV gamma ray of Fe^{59} . The photopeak of the 1099.2-keV peak serves as the monitor.

In a typical sample of pottery, the corrections to the chromium for neodymium, tantalum, and iron interferences were 0.9%, 0.2%, and 0.6%, respectively. For obsidian, in which chromium is very low, the respective corrections were 12.6%, 6.2%, and 17.2%. Because the corrections themselves are subject to a significant error, chromium is not a useful element for fingerprinting obsidians.

The system of NAA just outlined is capable of measuring well over 20 elements in samples of earthy materials such as clays, soils, and common rock types. The experience gained also permits calculation of how well these and other elements can be measured in different kinds of materials.

In NAA it is possible to study separately different sources of error and to come up with a good estimate of how they affect the accuracy of determination for each element. A basic source of error is introduced by the statistics of counting radioactive emissions and is called the counting error. The size of the error is calculated directly from all of the counts used in the analysis of each peak. These errors vary considerably from element to element, but for our purposes we are only interested in those peaks that have counting errors of a few percent or less.

The overall precision of measurement is indicated by the reproducibility in a set of identical samples that are irradiated together, and includes all random errors in the analytical process as well as the counting error. If the counting error is excluded, the residual error, which we call procedural uncertainty, remains. In our system, this uncertainty is less than 0.5%.

The procedural uncertainty is thus the resultant of all random errors excluding the counting error. The following steps are taken to minimize the sizes of these errors:

1. Powdered samples of the materials to be analyzed and standards, all of similar weight, are pressed into pills of constant dimension. For gamma-ray counting they are guided to a reproducible position above the detector. This ensures that the solid angle of each sample in relation to the detector is controlled. The maintenance of constant pill size is also involved in the following item.
2. A nuclear reactor has vertical and radial flux gradients that must be taken into account. The pills are placed on edge and in radial array in a jig that is sealed in a capsule; this assembly is rotated during irradiation. In this manner, all samples and standards are subject to the same neutron flux.
3. The precision of weighing the samples is a random error, which can be minimized by exercising care in the weighing procedure.
4. Because the peaks are integrated by preset instructions, any instability of the analyzer system during the runs will add to the observed dispersion. There is no way to guard against this ahead of time, but diagnostics are written into the computer program to signal any serious malfunction.

Most insidious are systematic errors that come from deficiencies in the application of interference corrections and from problems in getting proper backgrounds. We have internal checks in our analytical system for 12 elements. Each of these is measured in two or more independent ways. For example, different gamma rays from the same isotope provide results that are completely independent because the problems of spectral

analysis are different for each peak. Each set of problems therefore has been coped with successfully if the results agree about as well as they could from the counting errors alone.

The elements that can be determined in only one way present a more serious problem. One way of getting information is to compare results from the analysis of the same sample in different laboratories. No two equipment systems will produce identical spectra because the performance characteristics, which dictate how corrections are made and backgrounds taken, are not identical.

The background under the photopeaks is the envelope over all Compton distributions generated by all of the gamma rays. The estimation of the background under each peak is subject to error. Generally, the background in the vicinity of the peaks of interest is smooth enough that in a small segment of the spectrum it is well represented by a straight line. In this case, channels on both sides of the peak are summed and the background is determined by a linear interpolation.

In highly congested regions of a spectrum, there are peaks that are unsuitable for analyses because there is no room for measuring the background. For some peaks used, the background can be taken on one side of the peak and corrected by estimating the slope.

An interlaboratory study was made on six samples of rocks and pottery; analyses were performed in Berkeley and Jerusalem. Table I gives an abbreviated list of the results in which the error limits shown are the counting errors alone. From a practical viewpoint, the agreements among data are quite satisfactory. However, in terms of ultimate possibilities, there are still minor problems. For example, the scandium values for KERM1 have counting errors of only about 0.25%, yet the difference between the values is 2%.

The conclusion reached from this study is that NAA is capable of giving results that are much more reliable than has been generally supposed. The two laboratories employed the same standard materials; therefore, the only uncertainty in using the results as absolute values arises from how well this standard has been calibrated. The important dividend from this study is that each laboratory can use the data bank of the other.

Provenance of Obsidian

Obsidian is a volcanic glass which has fracturing properties that make it eminently suitable for fashioning implements such as knives, scrapers, and arrowheads. Obsidian sources are not found in every region and its use as an early article of trade is evidenced by its appearance far removed

Table I. Comparison of Hebrew University and Lawrence Berkeley Laboratory Abundance Measurements by Neutron Activation

<i>Elements</i>	<i>CIN5</i>	<i>CIN8</i>	<i>KERM1</i>	<i>BISH25</i>	<i>BISH26</i>	<i>BISH27</i>
Eu	1.468 ± 0.022	1.423 ± 0.021	1.975 ± 0.027	0.045 ± 0.007	0.344 ± 0.009	0.174 ± 0.007
	1.498 ± 0.013	1.432 ± 0.013	2.031 ± 0.018	0.047 ± 0.005	0.350 ± 0.005	0.172 ± 0.004
Sc	20.08 ± 0.04	19.19 ± 0.04	23.56 ± 0.05	3.049 ± 0.012	1.912 ± 0.009	1.863 ± 0.009
	20.10 ± 0.06	19.23 ± 0.06	24.07 ± 0.07	2.954 ± 0.013	1.854 ± 0.009	1.810 ± 0.009
Th	14.47 ± 0.08	13.67 ± 0.08	6.44 ± 0.06	19.87 ± 0.08	12.29 ± 0.06	12.82 ± 0.06
	14.58 ± 0.14	13.84 ± 0.13	6.21 ± 0.12	20.34 ± 0.07	12.23 ± 0.05	13.25 ± 0.05
Ta	1.336 ± 0.024	1.207 ± 0.023	1.438 ± 0.026	2.055 ± 0.033	0.811 ± 0.015	1.023 ± 0.018
	1.33 ± 0.01	1.24 ± 0.01	1.42 ± 0.01	2.01 ± 0.01	0.81 ± 0.01	1.02 ± 0.01
Fe(%)	5.35 ± 0.06	5.15 ± 0.06	7.04 ± 0.08	0.567 ± 0.008	0.845 ± 0.011	0.629 ± 0.008
	5.44 ± 0.07	5.15 ± 0.07	7.17 ± 0.09	0.547 ± 0.007	0.824 ± 0.008	0.594 ± 0.007

NOTE: Data are given as parts per million except for Fe, which is given as percentage. The top entries are the Hebrew University values and the lower entries are the Lawrence Berkeley Laboratory values. Data shown are taken from Ref. 1.

from any known sources. Fingerprinting this material represents provenance determination in its most rudimentary form.

The study of obsidian provenance differs from that of pottery. As compared with clays, there are a lot fewer obsidian sources; hence the search for chemical matches with artifacts is much simpler. The composition of obsidian is not altered in fashioning implements, whereas potters can refine a clay in different degrees, introduce additives, or blend different clays. Experience shows that obsidian flows are more uniform in composition than are clay beds; therefore, the chemical profiles are more distinctive for obsidian.

We can illustrate how these simplifying features manifest themselves by considering a study of obsidian artifacts found in sites in Israel. The closest overland sources of obsidian are in south-central Anatolia (Asiatic Turkey), more than 700 km away. Fortunately, we were able to obtain a meticulously sampled collection from this region.

Some of the characteristics of an obsidian group and the importance of thorough sampling can be seen in Table II. The flow is called Hotmis Dağ (HTMS), and the sampling area was about 7 km². The numbers for each element are the mean value, *M*, for the group, and the spread in values shown as the root-mean-square deviation, σ . The spreads in each group are only a few percent of the mean values.

The HTMS samples were divided into three groups (A, B, and C), which showed statistically valid separation although the compositions were not grossly different. Elements such as lanthanum and barium have values that decrease progressively, whereas those for tantalum and cesium increase. The reason for this variation might be learned from a

Table II. Obsidian Source Sampling (Hotmis Dağ)

	<i>HTMS-A</i> (18 samples)	<i>HTMS-B</i> (11 samples)	<i>HTMS-C</i> (32 samples)	<i>KRUD</i> (23 samples)
La	33.4 ± 0.7	30.4 ± 0.9	27.6 ± 0.7	12.6 ± 1.2
Ba	450 ± 19	384 ± 16	319 ± 20	0 ± 13
Ta	1.79 ± 0.03	1.95 ± 0.02	2.05 ± 0.03	3.28 ± 0.14
Cs	7.23 ± 0.09	8.05 ± 0.13	8.55 ± 0.21	14.09 ± 0.64
U	6.46 ± 0.16	6.99 ± 0.22	7.63 ± 0.21	10.86 ± 0.50
Th	25.3 ± 0.9	27.0 ± 1.1	29.0 ± 0.8	33.8 ± 1.7
Eu	0.546 ± 0.019	0.425 ± 0.017	0.321 ± 0.019	0.033 ± 0.011
Fe(%)	1.27 ± 0.02	1.03 ± 0.01	0.82 ± 0.03	0.63 ± 0.02
Yb	2.93 ± 0.07	2.95 ± 0.09	2.86 ± 0.07	4.19 ± 16
Sc	1.55 ± 0.08	1.42 ± 0.07	1.24 ± 0.06	2.30 ± 0.15
Hf	5.39 ± 0.08	4.78 ± 0.09	4.15 ± 0.10	4.34 ± 0.25

NOTE: Data are given as parts per million except for Fe, which is given as percentage. The data shown are taken from Ref. 2.

geochemical study, but for our interests it is enough to know that any of these three compositions represents obsidian from this place.

The last column in Table II demonstrates more dramatically the need for a thorough sampling. The obsidians labeled KRUD are also from this sampling area and can be seen to come from a completely different flow. Any artifact that matches this group therefore also came from the same small area as the HTMS material.

We next turn to Table III for the comparison of archaeological obsidian with sources. The first two data columns refer to sites in Israel (Beisamoun and Nahal Lavan). For economy of space, the individual values were grouped, which serves our purpose because their compositions agreed so closely that they must have come from a single source. These two groups agree with each other as well as they possibly could.

The third column refers to a source in Anatolia (Göllü Dağ) and gives an excellent match with the two groups of archaeological obsidian. The last column (Nenezi Dağ) is from a flow not too far distant from Göllü Dağ. The data are presented simply to show the contrast between two sources.

The provenance determination of the Beisamoun and Nahal Lavan obsidian is part of an interesting emerging story. These sites are dated by the prehistorians at about 6500 B.C. and 7000 B.C., respectively, a period termed Pre-Pottery Neolithic (PPN) because it precedes the making of pottery. Obsidian was analyzed from six PPN sites whose ages run from 8000 B.C. to about 6500 B.C. Curiously, it was determined that all of the obsidian came from one source, Göllü Dağ. If we accept the dating, this strange "monopoly" persisted for about 1500 years. The explanation for this cannot be that obsidian from other sources in Anatolia was unsuitable for making implements, because in more recent periods obsidian from a number of other sources appeared in the samples we analyzed from sites in Israel.

We found matches between our archaeological obsidians and five sources in Anatolia. However, we have six compositions that do not match any of the sources that we have analyzed. Some or all of these unknown sources may still be found in Anatolia because the sampling of flows was not exhausted.

It is also possible that obsidian came by land from more distant places, or by boat. Before our work started there was some evidence that boats traveled the open seas during Neolithic times. This evidence came from obsidian found in places that could only be reached by water from possible sources. Recently, we analyzed obsidian samples from two early Neolithic sites in Macedonia and found that they matched source material from the island of Milos. From Milos to the closest landfall on the mainland is more than 100 km, and if the obsidian was brought by water to Macedonia the distance would be 500 km.

Table III. Comparison of Archaeological Obsidian from Two Sites in Israel (Beisamoun and Nahal Lavan) and from Anatolian Sources (Göllü Dağ and Nenezi Dağ)

<i>Element</i>	<i>Beisamoun (24 samples)</i>	<i>Nahal Lavan (22 samples)</i>	<i>Göllü Dağ (60 samples)</i>	<i>Nenezi Dağ (18 samples)</i>
La	23.0 ± 0.6	22.9 ± 0.5	22.9 ± 0.4	39.3 ± 0.4
Eu	0.159 ± 0.009	0.160 ± 0.009	0.160 ± 0.011	0.545 ± 0.011
Yb	2.35 ± 0.07	2.34 ± 0.07	2.32 ± 0.08	2.33 ± 0.05
Ta	1.96 ± 0.02	1.94 ± 0.07	1.97 ± 0.03	1.56 ± 0.03
Fe (%)	0.609 ± 0.013	0.607 ± 0.011	0.607 ± 0.017	0.884 ± 0.010
Hf	3.19 ± 0.17	3.20 ± 0.12	3.22 ± 0.16	4.22 ± 0.07
Th	23.2 ± 0.4	22.4 ± 0.6	22.9 ± 0.4	27.6 ± 0.5
U	7.69 ± 0.23	7.76 ± 0.22	7.76 ± 0.20	6.84 ± 0.17
Na (%)	3.00 ± 0.05	2.93 ± 0.05	2.99 ± 0.11	3.21 ± 0.09
Cs	7.95 ± 0.11	7.78 ± 0.29	7.97 ± 0.14	6.95 ± 0.09
Sc	1.96 ± 0.06	1.96 ± 0.05	1.91 ± 0.03	1.50 ± 0.05
Ba	159 ± 14	152 ± 16	160 ± 14	550 ± 21

NOTE: Data given as $M \pm \sigma$, each data entry is the mean value (M) for an element in the group of samples shown in the column heading. Sigma (σ) is the root-mean-square deviation for the members of the group and relates to the spread of values encountered in group. The values for the elements are in units of parts per million except those indicated by the % sign, which are expressed as percentages. Data are from Ref. 3.

Eastern Terra Sigillata

By the year 336 B.C., Philip of Macedon had subdued the bickering city-states of Greece and welded them into an impressive fighting force. He had also completed plans to invade Asia Minor in order to take on the forces of the mighty Persian Empire. In the summer of 336 B.C., Philip was murdered and succeeded by his son Alexander, who went on with the project.

Alexander was a youth of 20. Twelve years later he died, but not until he conquered lands as far east as India and in other directions, making him master of an empire the size of which never had been seen before. He was not only an incredible military genius, but a consummate politician and administrator. Among other things, he fostered intermarriage between Greeks and the aristocracy of the conquered eastern lands, and the adoption of the ways of the East. During this brief interval, changes were wrought in bringing East and West together that profoundly affected world history.

Upon Alexander's death, the empire was divided among several of his generals, each of whom founded a dynasty whose leaders were more often than not doing battle with each other. The legacy of Alexander received its final blow with the Romans' domination. But the modified Greek culture of the Middle East did not disappear, and Greek was the lingua franca of the area for many centuries thereafter.

The interval between the conquest of the Persian forces and the demise of Alexander's empire is known as the Hellenistic Period. Volumes have been written through the ages about these turbulent times, and it would seem that the events are known in fine detail. However, many of the original information sources have been lost, and what has survived leaves much to be desired for understanding the interplay of complex forces that shaped the Hellenistic world, let alone the facts of daily life.

Sites of the Hellenistic Period are plentiful throughout the eastern Mediterranean. Under these circumstances, it is understandable that archaeologists will try to learn what they can. They have, in fact, been excavating such sites for almost 80 years. The reports of the excavations deal largely, of course, with such mundane matters as the classification of Hellenistic and Roman pottery, the chronology associated with the wares, questions of provenance, and association with other wares and artifacts.

The category of pottery most prominently dealt with is one that has been called Eastern Terra Sigillata (ETS). The repertory is vast both in the number of forms that have been included and in the numbers of such vessels that must have been made.

There have been many attempts to divide the repertory into sub-

groups based on one set of criteria or another. To review what various authors have concluded about these wares would be tedious and confusing, so just a few comments are offered.

1. That these wares were made in more than one place seems certain because distinctive differences can be seen without difficulty.
2. There is no consensus in answering the question of where any of these wares were made.
3. The modes of classification were not clear and decisive; therefore it became difficult to assign chronologies that could be agreed upon. A detailed examination of much-cited bench mark reports showed that even the datable evidence was sketchy and disjointed.

In short, after work spanning 80 years, Eastern Terra Sigillata has not provided the kind of firm information that makes a pottery repertory useful.

The work reported here was undertaken in an attempt to make the provenance determination of ETS found in Israel (4). The objective was more ambitious than just learning where various pieces of pottery came from, and included the possibility of reclassifying ETS in such a way that archaeologists would know what they were dealing with without having their pottery analyzed.

We proposed to analyze pottery from many sites and group those showing a common origin. Within a provenance group, the forms could be described without the trouble of extraneous factors. We hoped to establish a set of visual criteria that is unique for each provenance group. Finally, the chronology associated with each form could be delineated by assessing the stratigraphy at all sites where the form has been found and choosing the dates that seem most reliable.

The first and largest provenance group to be discussed comprises 157 vessels from 21 sites. We have given it a neutron designation, ETS-I. These vessels were divided into 20 basic forms, each of which was illustrated by a drawing accompanied by a brief note indicating the design features that set it apart from other forms. The range of fabric colors was given, the colors and quality of the slips, decorative features, and so on. For example, a number of the forms came in both red and black varieties, which were often put in separate categories. There is no need to do so if they were made at the same place and probably in the same potters' shops.

The earliest ETS-I forms found in Israeli sites started at about 180 B.C. and they did not go out of use simultaneously. The final existence of any ETS-I is A.D. 70, a date memorialized in the literature depicting the Roman destruction of Jerusalem. Because the various forms often

came into use and went out of use at different times, it is sometimes possible to bracket a stratum quite closely by the overlap interval.

The chronological table we offer is probably not the last word, but it is better than any other yet compiled. A major deficiency is that for some forms, the chronology is based on relatively few vessels. For example, one of our basic forms may only be represented by 5 specimens found in strata covering a time span of 120 years. Among these 5 having the same basic form, the details are not alike. If we had been dealing with 50 vessels instead of 5, it is likely that they could have been broken down into stylistic subgroups, each having a more restricted time span.

The data shown in Table IV are part of the evidence that ETS-I was made in eastern Cyprus. The ETS-I group matches Cypriot pottery from the site of Enkomi on the eastern plain of the island. Cyprus had not been mentioned in previous speculation about the pottery's provenance.

Earlier it was stated that provenance determination is inherently more complex for pottery than for obsidian. In general, pottery itself rather than clay is used as source material to establish the composition of pottery that was made locally.

Pottery as source material has some assets, one of which is the ancient potters' knowledge of which clays in an area were (and are) best for pottery making. If we were to search for these clays, we would be faced with a tedious, and largely blind, sampling. In addition, it is often unpractical or even impossible to mount clay-collection expeditious to distant places in which one is interested.

The drawback in using pottery as source material lies in the necessity of making a strong case that the pottery was indeed made locally. This

Table IV. Eastern Terra Sigillata

<i>Element</i>	<i>ETS-I (157 samples)</i>	<i>Cypriot Pottery (18 samples)</i>	<i>Cypriot Clay</i>	<i>ETS-II (48 samples)</i>
Fe%	5.66 ± 0.30	5.69 ± 0.27	5.88	5.41 ± 0.33
La	20.7 ± 1.4	20.5 ± 1.5	21.6	49.7 ± 4.1
Th	7.18 ± 0.45	6.76 ± 0.25	6.44	16.60 ± 6.6
Co	31.9 ± 2.2	31.5 ± 2.6	34.8	19.0 ± 1.2
Hf	3.05 ± 0.26	3.18 ± 0.22	3.17	6.79 ± 0.35
Cs	5.2 ± 0.6	4.6 ± 0.6	5.0	8.1 ± 0.7
Sc	22.8 ± 1.4	23.1 ± 1.5	25.5	18.1 ± 0.9
Yb	2.16 ± 0.18	2.26 ± 0.13	2.13	3.50 ± 0.15
Ta	0.71 ± 0.07	0.61 ± 0.04	0.65	1.93 ± 0.37
Eu	1.03 ± 0.06	1.06 ± 0.06	1.14	1.65 ± 0.05

NOTE: Data given as parts per million except for Fe, which is given as percentage.

goal is achieved by selecting a variety of styles and forms, all of which are in the tradition of the area. The position is fortified by also selecting pottery of different periods. If all of these samples are shown to be alike, it is highly unlikely that they were brought in from elsewhere.

The group of Cypriot pottery shown in Table IV consists of different typically Cypriot styles; this particular group is from a period about 1200 years earlier than ETS-I. Analysis of pottery samples of other periods showed them to be similar as well.

Finally, ETS-I is a case in which there was success in finding a matching clay. The data are shown in the third column of Table IV. This clay came from a present-day potter who said that he gets his clay from pits near the ancient site from which our pottery came.

A legitimate point can be raised that, after finding a match, we still do not know that all clay sources are distinguishable. There are very large numbers of possible sources, and it may never be possible to study all of them. This is a serious criticism if there is nothing more to counteract it than the sparse data that have been shown. However, we do have a large data bank consisting of 8000 or so analyses from a large number of sites in the eastern Mediterranean, and the Cypriot composition has not been seen among all of the local potteries.

ETS-I was made in large amounts and was widely distributed for at least 250 years, roughly between 180 B.C. and A.D. 70. The question arises whether this longevity is credible, bearing in mind that it was a period of great turmoil, in which parts of Alexander's empire changed hands repeatedly. The historical records should have something to say about this. These records are not necessarily complete or trustworthy but, such as they are, they indicate that Cyprus was under the dominion of the Ptolemies during this entire interval, although the later Ptolemies were vassals of Rome.

The last data column in Table IV pertains to a second ETS repertory, which we call ETS-II; the composition of ETS-II is greatly different from that of ETS-I. This pottery group consisted of 48 vessels from 9 sites. The numbers analyzed for ETS-II and ETS-I cannot be interpreted in terms of amounts found because only a very small percentage was sampled. This repertory was classified according to forms and other visual features, as was done for ETS-I, and the dating was established. Members of ETS-II are not difficult to distinguish by eye from those of ETS-I. ETS-II came into being only at about 50 B.C. and lasted until about A.D. 150.

The provenance of ETS-II has not yet been determined clearly, although it is fairly certain that this pottery came from a region in western Anatolia. The problem of giving a particular site stems from the fact that we were not able to get suitable reference material. What was available was a meager collection consisting of a few sherds from each of about 12

sites. An excellent match was found for ETS-II with a couple of sherds from one place, but this is not sufficient evidence for us to know that they were made where they were found.

At this point, we know that Eastern Terra Sigillata found in Israel is dominated by two categories; their chemical compositions are easily told apart and it is not difficult to give clues for visual identification. This is not quite everything, however, that was learned during this study. For one thing, we have a few sherds that do not fit into either the ETS-I or ETS-II repertory, although they clearly are Eastern Terra Sigillata. Among these pieces, three different compositions were encountered, which now means that at least five sites made such wares. Obviously there is much work to be done before we can fully understand how to handle all problems of Eastern Terra Sigillata.

Concluding Remarks

An attempt was made to convey a feeling for a subject that embraces such disparate disciplines as the techniques of nuclear physics and the processes used by archaeologists in reconstructing ancient history. I felt it necessary to go into some depth on archaeological problems, for which I gave two examples. In doing so, it became necessary to eliminate a review of the substantial literature on this subject. As it is, the discussion was confined to my experiences.

Literature Cited

1. Yellin, J.; Perlman, I.; Asaro, F.; Michel, H. V.; Mosier, D. F. *Archaeometry* **1978**, *20*, 95-100.
2. Yellin, J.; Perlman, I.; Payne, S. Unpublished data.
3. "Provenience of Obsidian from Neolithic Sites in Israel," *Israel Exploration Journal* **1980**, *30*, 83-88.
4. Gunneweg, J. Ph. D. dissertation, Hebrew University, Jerusalem, Israel, 1981 (Quedem Monograph Series, in press).

RECEIVED for review November 23, 1982. ACCEPTED for publication April 11, 1983.

Major, Minor, and Trace Element Analysis of Medieval Stained Glass by Flame Atomic Absorption Spectrometry

N. H. TENNENT

Glasgow Museums and Art Galleries, Kelvingrove, Glasgow G3 8AG,
Scotland

P. McKENNA, K. K. N. LO, G. McLEAN, and J. M. OTTAWAY

University of Strathclyde, Department of Pure and Applied Chemistry,
Glasgow G1 1XL, Scotland

Procedures are described for the analysis of 12 key elements (sodium, potassium, calcium, magnesium, aluminum, iron, manganese, lead, zinc, copper, cobalt, and nickel) in medieval stained glass by flame atomic absorption spectrometry (AAS). The method of choice involves dissolution of powdered glass samples (50–100 mg) in a hydrofluoric/perchloric acid medium. Alternative dissolution methods are discussed. Analytical data for the 10 synthetic medieval glasses prepared for the European Science Foundation are reported, and the accuracy and precision of the AAS method are evaluated in terms of these glasses and Corning Standard D. The compositions of 12 medieval stained glass fragments excavated from Scottish cathedral sites are presented and considered in terms of the source of plant ash and colorant materials. The results are consistent with the use of a mixture of fern and beech ash and the introduction of blue and green colors by means of colorants derived from copper-based alloys.

ATOMIC ABSORPTION SPECTROMETRY (AAS) has been extensively employed in the analysis of metallic and siliceous materials of archaeological and art historical significance. The scope and practical aspects of the technique of relevance to archaeology were comprehensively reviewed in 1976 (1); a more recent report focused on the application of atomic absorption analysis to archaeological ceramics (2). The technique carries the potential for analysis of a wide range of elements with good

0065-2393/84/0205-0133\$06.00/0

© 1984 American Chemical Society

accuracy and high sensitivity. Sample atomization can be accomplished by means of a flame or furnace (3). Although detection limits are generally several orders of magnitude lower for furnace atomization (1, p. 20), flame AAS, primarily for reasons of cost, is the more routinely employed method of analysis.

The analysis of modern glass is a well-established area of application of AAS (4). Analyses of archaeological glass include, for example, studies of Egyptian glass (5,6) and Venetian glass (7). Medieval stained glass compositions, determined by AAS, are also documented (8–10), but no published method developed specifically for the analysis of medieval stained glass was available when the program of analysis, reported in part in this chapter, was begun. Details of the analysis of silicates have since been reported by Hughes et al. (1), but well-evaluated procedures for the analysis of medieval stained glass by flame AAS remain undocumented.

Many analytical studies of ancient glass have yielded results of archaeological significance (11). Glass compositions have been interpreted primarily with a view to clarifying glass-making techniques (12), provenance (13), or corrosion phenomena (14). An extensive series of analytical studies has been critically assessed (15), but, despite some early investigations of stained glass (16,17), it is only in recent years that this field has become the subject of more intensive study. In a pioneering series of papers, Geilmann and his coworkers employed wet chemical techniques to determine specific elements of interest in understanding glass-making technology (18–20); more recently, the same approach has been adopted using x-ray fluorescence (21). This spectrometric technique has also enabled a relationship between the weathering and composition of medieval stained glass to be established (22). The importance of the analysis of major and minor constituents has been stressed by Brill (23) in a paper that suggests that data on five major constituents (the oxides of sodium, potassium, calcium, magnesium, and aluminum) are often sufficient to characterize a glass. Moreover, the levels of major, minor, and trace elements, determined by neutron activation analysis, have been shown to be consistent for glass from a single stained glass panel (and probably even from a particular workshop), despite the general heterogeneity of stained glass compositions (24). An understanding of the colorant role of elements in stained glass has also been advanced by several analytical studies (8,25,26), most recently by Mössbauer spectroscopy (27).

The purpose of this chapter is to outline the development of a reliable procedure that can be used to determine the elements that are the most significant constituents of medieval stained glass. The scope, accuracy, and precision of the method are evaluated in terms of standard glasses; the archaeological significance of the analyses, in terms of the criteria

outlined above, is assessed for medieval stained glass excavated from Scottish sites.

Experimental

Glasses. The standard glasses employed in this study consisted of the series of 10 glasses with typical medieval composition prepared for the European Science Foundation by Pilkington Brothers Ltd., with the aid of a grant from the Nuffield Foundation (28), and Standard D, prepared for the Corning Museum of Glass as part of an interlaboratory analytical investigation (29). Twelve fragments of medieval stained glass excavated from the sites of St. Andrews Cathedral (sample StA1), Melrose Abbey (sample MA1), Holyrood Abbey (sample HA1), and, principally, Elgin Cathedral (samples EC1–9) formed the basis of the investigation. The colors of these samples are described in Table IV and, in some cases, illustrated in Figure 1. The glass fragments had all undergone surface weathering due to burial, but the underlying glass remained in good condition. The weathering consisted of a fine corrosion film (EC1,2,9), deep pits (EC7, 8, and HA1), heavy encrustation (EC4–6), or a heavily pitted encrustation (EC3, StA1, and MA1), and was removed mechanically prior to analysis. In two instances (StA1 and HA1) there was evidence of painted designs on the fragments prior to treatment.

Apparatus. Perkin–Elmer (PE) 360 and 272 atomic absorption spectrometers, with an air–acetylene or a nitrous oxide–acetylene flame, were employed for the analyses. Standard hollow cathode lamps were used as light sources. In all cases, the instruments were operated as recommended by the manufacturer; gas pressures, gas flows, slits, wavelengths, and other controls were adjusted to the prescribed values. The readout was obtained directly using a 5-s integration in the concentration (PE 360) or absorbance (PE 272) mode.

Reagents. Reagents of the highest purity (Spectrosol or Aristar grades, BDH) were used throughout. Stock solutions of each element were prepared from an appropriate salt and stored in polythene bottles in 10^{-2} M hydrochloric acid. Cesium chloride (AnalaR grade, BDH) was added as an ionization suppressor to sodium and potassium standard solutions and glass sample solutions. Lanthanum oxide (Spectrosol grade, BDH) was added as a releasing agent to magnesium and calcium solutions and glass sample solutions and as an ionization suppressor to the aluminium solutions. Acetylene and nitrous oxide gases were supplied by BOC.

Sample Preparation. The glass samples (~100 mg) were carefully ground in an agate mortar and passed through a 200 British Standard mesh sieve. The finely ground samples (≤ 75 μm) were placed in an electric oven at 105 °C for 1 h, cooled in a desiccator, and weighed prior to dissolution. (Sample weights of 30–100 mg have been analyzed successfully.)

Dissolution was accomplished by the method of Langmyhr and Paus (30). Each finely ground sample (~100 mg) was transferred to an open 250 mL PTFE beaker, and 5 mL of 40% (v/v) hydrofluoric acid added, followed by 0.5 mL of perchloric acid. This mixture was taken to dryness on an electric hotplate and cooled. A further 5 mL of 40% hydrofluoric acid and 0.5 mL of perchloric acid were added, and the mixture again taken to dryness. The beaker was cooled, and 10 mL of 0.1 M hydrochloric acid was added. The salts were then brought into solution by heating. The clear solution was cooled and made up to 100 mL by the addition of distilled water to a polythene volumetric flask. Lanthanum

and cesium (1000 ppm) were added, where appropriate (as indicated in the following section), to the solutions at the final dilution stage prior to analysis.

Interferences. Each element under consideration was investigated for the effect of interference on the determination of all other elements. The effects of titanium, tin, and antimony, not analyzed in this study but known to be present in medieval stained glass, albeit at levels less than 1%, were also investigated. Silicon was not considered because it is removed by volatilization at the dissolution stage.

A solution of the element of interest, 1 ppm (10 ppm and 20 ppm for lead and aluminium, respectively) in $10^{-2}M$ hydrochloric acid was determined by AAS. A similar solution of this element was then prepared in the presence of 500 ppm of the "interfering" element and the atomic absorption signal compared with the blank solution. If the analytical signal did not change by more than $\pm 5\%$, then the element was regarded as not having a significant interference effect on the analyte element.

Only chemical interferences were observed; sodium and potassium ionized in the air-acetylene flame, and aluminum ionized in the nitrous oxide-acetylene flame; magnesium and calcium exhibited evidence of interference by both phosphorus and aluminum. All the other elements were found to be interference-free. The addition of 1000 ppm of cesium as an ionization suppressor effectively removed the ionization interference in the sodium and potassium solutions. Similarly, 1000 ppm of lanthanum removed the interference due to phosphorus and aluminum in the magnesium and calcium solutions and suppressed the ionization of aluminum.

Results and Discussion

Development of the Technique. The quality of analyses by AAS is highly dependent on procedures for sample treatment. Consequently, recent reports have recognized the need to focus on techniques designed to optimize the stages from sample removal to sample dissolution (1,2,31).

For stained glass, the removal of small chips, in a manner analogous to the grozing originally used to trim the glass to size, provides a straightforward means of sampling. For intact glass panels, it is usually possible to remove a sample unobtrusively from under the leading, most conveniently when the panel is undergoing conservation. In many cases, and virtually without exception for excavated glass, removal of the alteration products resulting from atmospheric weathering or burial is necessary. This removal can be accomplished by mechanical means using a variety of probes, scalpels, and fiberglass brushes. Vestiges of paint should also be removed. For the excavated glasses examined in this chapter, paint lines could be discerned in only two cases.

The samples were ground manually and when possible were sieved. In cases where only a small amount (≤ 50 mg) of glass was available, it has been found acceptable to omit the sieving step, particularly if the analyst has gained considerable experience in sample preparation. The merits of mechanical grinding have been discussed elsewhere (2).

For sample dissolution the method of Langmyhr and Paus (30), described above, offers an attractive combination of ease of handling and good reliability. The method suffers from the disadvantage that, because open beakers are used, volatilization of silicon tetrafluoride occurs, precluding the determination of silicon by this means. This has not proved to be a severe handicap; because 12 of the principal medieval stained glass components are determined in the reported method, silicon can be determined to a good approximation by difference. The removal of silicon interference in the determination of aluminum and magnesium (1) is an added virtue of this method. Scrutiny of the boiling points of the fluorides of the other elements of interest established that losses of these fluorides during dissolution would be insignificant.

Two additional hydrofluoric acid methods have been reported (1,2), and are similar to that described above. The method of Hughes et al. has also been the subject of two comparative studies relevant to the analysis of ceramics (2,31). Techniques that retain silicon have been discussed (1,2) and involve either fusion with lithium metaborate [or sodium carbonate (2)] or high pressure dissolution in a PTFE bomb. An alternative high pressure method, developed by Price and Whiteside (32), was evaluated in the course of this investigation but was found to be unreliable for stained glass of medieval composition; in many experiments dissolution was incomplete. Attempts to modify the procedure by varying the prescribed dissolution parameters produced insufficiently consistent results although superior conditions were established (Table I).

The importance of interferences in AAS has been stressed (2). We have observed only chemical interferences for stained glass of medieval composition. The interference due to ionization of sodium, potassium,

Table I. Data for the Variation of Dissolution Parameters

<i>Parameter</i>	<i>Prescribed Conditions^a</i>	<i>Variation</i>	<i>Optimum Conditions</i>
Water (mL)	2.5	0.5 – 3.0 ^b	0.5
Aqua regia (mL)	1.0	0.5 – 3.0 ^b	2.0
40% Hydrofluoric acid (mL)	0.5	0.5 – 4.0 ^b	3.0
Time of first heating stage (min)	30	20 – 70 ^c	60
4% Boric acid (mL)	5	0.5 – 6.0 ^b	2.5
Time of second heating stage (min)	20	10 – 40 ^c	30

^a 0.2 g samples were proposed (33). The reagents were scaled down for 0.1 g samples in this work, but the reaction times were kept constant.

^b Varied by increments of 0.5 mL.

^c Varied by increments of 10 min.

and aluminum has not been reported in the analysis of ancient glasses by AAS, but the ionization is effectively suppressed by the addition of an excess of cesium or lanthanum. In the analysis of calcium and magnesium, interferences were found to be due to the formation of compounds of aluminum and phosphorus with the analyte element in the flame, thereby decreasing the rates of atomization compared with those for the analyte element alone. The interference is removed by the addition of lanthanum, which acts as a releasing agent and avoids the necessity of using the nitrous oxide-acetylene flame as proposed by Hughes (1). In the AAS determination of copper, cobalt, and nickel in blue glasses described by Bettembourg (8), calibration was accomplished in a complex medium containing five elements (aluminum, potassium, calcium, magnesium, and phosphorus) at levels corresponding to the average concentrations in the glasses under investigation. The absence of interferences for copper, cobalt, and nickel established in this study obviates the need for this approach.

Standard Glasses. The accuracy of the AAS method has been assessed by analysis of the 10 synthetic glasses prepared for the European Science Foundation (ESF) and of Corning Standard D, which also served to determine the precision of the results. These standards were selected in preference to glasses with better-evaluated specifications because their compositions are representative of medieval stained glass.

The ESF standards were prepared primarily for the purpose of investigating glass durability and conservation methods. Their role as analytical standards has been secondary, but is important in view of the wide range of medieval stained glass compositions that they typify. In addition to the analysis initially reported (28, quoted in part in Table II), expressed conventionally as weight percentage of the oxide, determinations have been carried out by at least one additional laboratory (33) and the results provide a reasonable gauge of the accuracy of new analytical procedures. The results in Table II not only attest to the accuracy of the present AAS method, but also provide a sounder basis for the use of these glasses as standards for future analytical investigations. The AAS results are, for the most part, the means of three instrumental readings from two duplicate analyses carried out by two of the authors. The agreement is good in almost all instances; in those cases where a significant discrepancy from the published figures was found, repeat analyses were performed. The sodium analysis of standard 76-C-151 (Na_2O , 3.7%) is, for example, the mean of 10 samples, and the standard deviation (0.099) gives a good measure of confidence in the AAS result.

The tentative recommended figures for Corning Standard D (29, quoted in part in Table III) are based on the results of an interlaboratory analytical investigation, but, as a consequence of the Corning Museum flood in 1972, confidence levels for these figures have not yet been

Table II. Analyses of Synthetic Medieval Stained Glass Standards

Sample No.	Composition Determined (published)												
	Na ₂ O	K ₂ O	CaO	MgO	Al ₂ O ₃	Fe ₂ O ₃	MnO	PbO	ZnO	CuO	CoO	NiO	
76-C-144	0.1(0.1)	30.0(29.5)	20.6(20.6)	0.04(0.04)	3.7(3.9)	2.4(2.1)	0.03(0.05)	N.D.	N.D.	N.D.	N.D.	N.D.	
76-C-145	N.D.	24.2(24.9)	29.2(29.4)	0.06(0.05)	3.9(3.8)	N.D.	0.1(0.1)	0.16(0.16)	0.5(0.5)	N.D.	N.D.	0.1(0.1)	
76-C-147	0.1(0.1)	15.2(14.6)	30.2(30.1)	0.06(0.05)	3.9(3.8)	N.D.	N.D.	N.D.	0.08(0.07)	1.8(1.8)	N.D.	N.D.	
76-C-148	0.1(0.1)	14.6(14.6)	26.0(25.9)	0.07(0.05)	4.0(3.9)	0.4(0.4)	0.2(0.2)	1.0(0.9)	N.D.	0.08(0.07)	N.D.	0.08(0.08)	
76-C-149	0.1(0.1)	14.6(14.3)	21.2(21.5)	N.D.	4.0(4.2)	N.D.	1.4(1.8)	N.D.	N.D.	0.82(0.91)	0.25(0.24)	N.D.	
76-C-150	8.1(9.5)	1.6(1.5)	22.4(21.9)	6.5(6.6)	4.3(4.3)	0.7(0.3)	N.D.	N.D.	0.1(0.1)	N.D.	0.09(0.09)	N.D.	
76-C-151	3.7(5.0)	6.9(7.2)	19.9(19.0)	3.0(3.2)	3.8(3.9)	0.4(0.3)	0.3(0.5)	0.82(0.71)	N.D.	0.1(0.1)	N.D.	N.D.	
76-C-158	N.D.	23.2(24.2)	28.8(28.4)	0.10(0.06)	3.8(3.8)	N.D.	0.1(0.1)	0.16(0.14)	0.5(0.5)	N.D.	N.D.	0.1(0.1)	
76-C-159	N.D.	13.9(14.5)	34.0(34.9)	0.08(0.07)	3.8(3.9)	0.1(0.1)	0.6(1.0)	0.5(0.5)	N.D.	0.5(0.5)	N.D.	N.D.	
77-C-33	22.2(21.7)	N.D.	22.8(22.6)	0.06(0.05)	4.0(4.1)	2.8(2.5)	0.04(0.05)	N.D.	N.D.	N.D.	N.D.	N.D.	

NOTE: Data were determined (published in Ref. 28) as weight percentage. N.D., Not determined; these components were not present in the original batch constituents.

Table III. Analysis of Corning Glass Standard D

	Mean Composition (\bar{x})		Relative Standard Deviation [$(100\sigma/\bar{x})$]
	Determined (published)	Standard Deviation (σ)	
Na ₂ O	1.36 (1.39)	0.021	1.5
K ₂ O	11.01(11.56)	0.110	1.0
CaO	14.73(14.99)	0.138	0.9
MgO	4.89 (4.06)	0.101	2.1
Al ₂ O ₃	5.00 (5.42)	0.125	2.5
Fe ₂ O ₃	0.46 (0.51)	0.021	4.5
MnO	0.40 (0.55)	0.022	5.5
PbO	0.21 (0.25)	0.011	4.9
ZnO	0.10 (0.10)	0.002	2.0
CuO	0.37 (0.38)	0.011	3.0
CoO	0.03 (0.02)	0.002	6.7
NiO	0.06 (0.06)	0.001	2.1

published. The agreement of the AAS results with the published values is again good, although the discrepancies in magnesium and manganese analyses are surprising in the face of good agreement found with the ESF standards. The precision of the results for Standard D, based on the analysis of eight samples, is given in Table III.

It was the initial aim of this investigation that all elements of interest should be determined by AAS. Phosphorus is known to be an important elemental component of medieval stained glass (18,21) at levels ranging from about 1 to 7%. [Figures extracted from 90 published analyses (34,35) gave a mean P₂O₅ concentration of 3.6%.] Although direct determination of phosphorus by AAS has been reported, several practical difficulties are encountered in achieving low detection limits. Good sensitivity can be achieved by ensuring an intense phosphorus line source and a vacuum or inert-gas purged monochromator (36) but direct determination of phosphorus remains a field of development. Because the levels of phosphorus in medieval stained glass are generally >1%, it is hoped that the direct determination by flame AAS, currently under investigation, may be possible. It is intended that AAS determination of phosphorus as part of a program of trace element analyses with furnace techniques will also be evaluated. Analyses of certain glasses from Table IV, by using a scanning electron microscope with an energy dispersive x-ray fluorescence spectrometer attachment (37), gave P₂O₅ levels in the range 2.4–3.5%.

The tin concentration in the glasses under consideration lies close the detection limit (0.02%) for the flame AAS method described herein. Tin analyses were carried out but are not quoted because the proposed method does not offer sufficient accuracy for this element.

Table IV. Analyses of Medieval Stained Glass Fragments, Excavated from Scottish Sites

Sample No. (color, thickness ^a)	Composition (weight percentage)											
	Na ₂ O	K ₂ O	CaO	MgO	Al ₂ O ₃	Fe ₂ O ₃	MnO	PbO	ZnO	CuO	CoO	NiO
EC1 (sky blue, 1.7 mm)	0.6	12.2	19.7	4.5	3.4	1.1	0.9	0.10	0.17	0.07	0.05	<0.01
EC2 (sky blue, 1.8 mm)	0.6	10.2	26.6	3.7	3.4	1.0	0.6	0.14	0.31	0.17	0.07	0.02
EC3 (deep blue, 5.0 mm)	0.9	18.3	12.6	6.7	2.4	1.0	0.4	0.32	0.60	0.25	0.10	0.02
EC4 (deep blue, 3.0 mm)	1.3	17.8	21.0	6.9	3.0	0.8	0.7	0.22	0.20	0.28	0.16	<0.01
EC5 (amber, 2.1 mm)	1.7	19.4	15.8	6.3	1.9	0.6	0.9	0.08	0.09	0.05	<0.01	<0.01
EC6 (amber, 2.3 mm)	1.7	18.0	15.8	6.3	1.4	0.4	1.2	0.16	0.08	0.05	<0.01	0.02
EC7 (emerald green, 2.9 mm)	2.0	9.6	14.1	6.2	1.3	0.5	0.9	1.07	0.07	2.40	<0.01	<0.01
EC8 (emerald green, 2.7 mm)	3.1	11.2	14.9	9.1	1.2	0.6	0.8	1.23	0.07	3.07	0.01	0.01
EC9 (light green, 2.3 mm)	0.8	10.5	25.2	3.8	3.3	0.8	0.8	0.02	0.02	0.02	0.02	0.02
MA1 (light green, 3.7 mm)	0.3	18.8	21.1	5.3	3.3	0.5	0.8	0.01	0.03	0.01	<0.01	0.02
StA1 (purple, 5.1 mm)	2.0	20.9	12.2	6.3	1.5	0.6	1.4	0.01	0.07	0.01	<0.01	<0.01
HA1 (emerald green, 5.0 mm)	1.7	18.1	13.2	6.2	1.6	0.7	1.2	0.18	0.21	2.10	<0.01	<0.01

^a After removal of weathered layer; in most cases this approximates well to the original glass thickness, but in samples EC1, 2, 6, and 7, this is an underestimate by about 2 mm.

Excavated Glasses. Of the pre-Reformation cathedrals in Scotland, only two (Glasgow and Kirkwall) survive in anything resembling their original state, and virtually no intact medieval stained glass is in existence. Nonetheless, the extent of Scottish ecclesiastical patronage in the Middle Ages was far from insignificant, and in the 13th century, specifically, monastic and secular churches were constructed on a grand scale (38). The Reformation deprived most cathedrals and abbeys of their functions and revenues, resulting in extensive decay of the framework of the buildings. For art historical or technical information on medieval stained glass in Scotland, one must therefore rely on excavated material; in recent years, significant finds have been made at, for example, the sites of the Carmelite Friary at Aberdeen, the Dominican Friary at Ayr, and, most notably, Elgin Cathedral.

The glass considered in this work comes primarily from Elgin Cathedral, founded in 1224. The cathedral was damaged by a severe fire in 1270 and subsequently reconstructed to its present dimensions. It was viciously sacked by Alexander Stewart, "The Wolf of Badenoch," in 1390 and fell into decay and ruin after the Reformation (39). Approximately one thousand fragments, several with painted designs and many of colored glass, have been excavated from a pit some 100 m to the west of the Cathedral. The glass consists of whole quarries with well-defined grozed edges and little weathering (Figure 1, upper six pieces), broken fragments with varying degrees of weathering (Figure 1, second row from bottom, weathering removed), or totally devitrified glass, some with well-preserved painted designs (Figure 2). These designs are characteristic of 13th century glass painting. The glass may have been removed as part of a reglazing scheme (very little lead was found with the glass), probably in the 15th century. Glass from three other sites—St. Andrews Cathedral (founded in 1160), Holyrood Abbey (founded in 1128), and Melrose Abbey (founded in 1136)—is included for comparison. Of less certain date, these fragments can also be ascribed to the early medieval period.

The source of the glass is unknown. It is accepted that colored glass was not made in England in the 13th century, although the date at which colored glass was first manufactured is the subject of opposing views (40,41). Trade with France and Flanders during this period is known to have resulted in Scottish imports of manuscripts and metalwork, including enameled crucifixes and candlesticks from Limoges (39). It is also well documented that French master masons were associated with the work on Scottish cathedrals.

Uncertainties about the source and nature of the raw materials for glass-making provide an unpromising basis from which analyses may be used to draw conclusions on the location of glasshouses. The use of cullet, glass refuse, in the glass-making process would also be expected to cloud the issue. Nonetheless, a full statistical treatment of analytical data has



Figure 1. Six intact glass quarries, from Elgin Cathedral, and eight variously colored glass fragments from Elgin Cathedral (EC), Holyrood Abbey (HA), St. Andrews Cathedral (StAC), and Melrose Abbey (MA).

been shown to yield fruitful results in a paper that also points out the deficiency in reliable, published analyses (42). In this chapter, we confine discussion to the specific information that can be gained from inspection of the glass compositions obtained from a small group of samples by the flame AAS method described above.

The glasses under consideration are all “forest-type” potash glasses, typical of the medieval period, and reflect the change in plant ash from the maritime soda-rich plants of the Mediterranean to potash-yielding inland plants (Figure 3). The significance of plant ash components has been stressed by several authors and impurity levels have been used in an attempt to characterize the particular plant from which the ash was derived (9,19,21,43). Plots of two (21) or three (9) components have provided a successful means of grouping certain glasses. Figure 4 shows the distribution of the glass samples under investigation in terms of their potash and magnesia levels. This plot is based on that of Lehanier (21, Fig. 5, p. 220) using data for plant ash composition quoted by Turner (43, p. 289T). The K_2O/MgO ratio is consistent with use of a 1:1 mixture

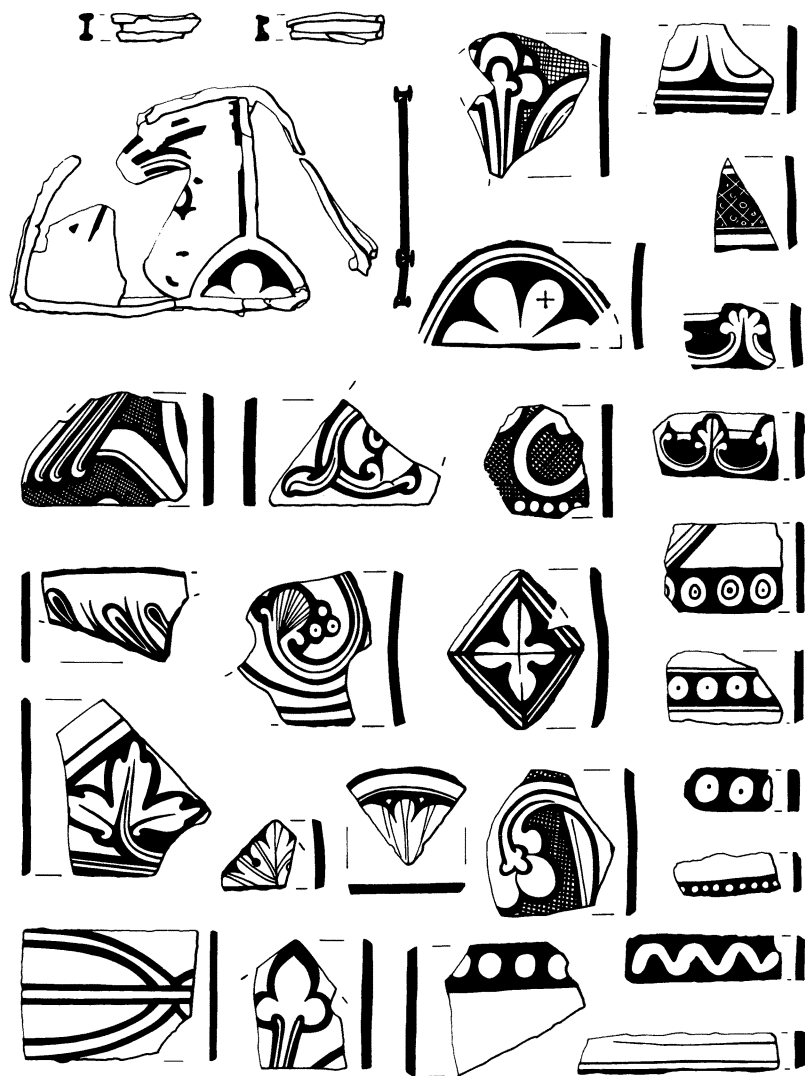


Figure 2. Painted designs from selected glass fragments from Elgin Cathedral. (Drawing reproduced by courtesy of W.J. Lindsay, Esq.)

of beech and fern ash. Other interpretations are possible, but the use of these plant ashes is in agreement with the medieval manuscript of Eraclius, variously ascribed to the 10th (44, p. 138) or 12th (45, p. xxxi) century, which recommends the use of a fern and beech ash, albeit in the ratio 6:1. Theophilus, however, advocates only beech ash (45); Agricola permits the use of oak or holmoak, hard oak, or Turkey oak or, if these are not available, beech or pine (46). A dramatic variability has been estab-

lished in the manganese content of the ash from beech trees, not only from different regions, but within a specific locality (19). Data were not available to enable us to determine if potash and magnesia concentrations display similar variability, but it is thought that manganese levels are more likely to be dependent on local soil conditions.

On the basis of close correspondence in the composition of two pairs of samples (EC2, 9 and EC5, 6), it is tempting to suggest that these glasses represent common glass-making sites. The equivalence of the



Figure 3. Illustration of 15th century Bohemian glasshouse. (Reproduced by permission of the British Library, Add Mss 24189, fl6.)

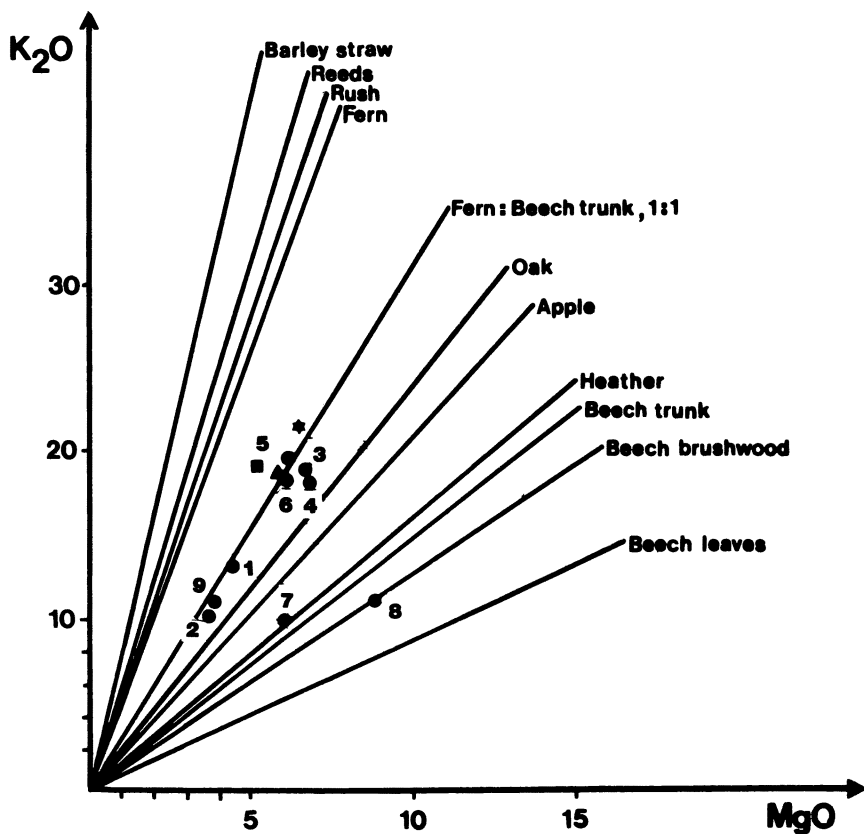


Figure 4. Correlation between the potash and magnesia level (as weight percentage) in plant ash and glass from Elgin Cathedral (●), Holyrood Abbey (▲), St Andrews Cathedral (★), and Melrose Abbey (■).

^{57}Fe Mössbauer parameters for EC2 and 9 (27, samples 6 and 5, respectively) establishes similar glass-making conditions for these glasses and adds weight to the postulate that the blue glass was produced from the same melt by the addition of copper- and cobalt-bearing materials that carried with them significant amounts of lead and zinc. The chapters dealing with the manufacture of blue glass are missing from the treatise of Theophilus (45), but from the composition of each of the blue glasses in Table IV it is clear that a combination of copper and cobalt is responsible for the blue color. [The colorant effect of copper is less pronounced than that of cobalt (47), and its purpose may be to mask the violet-blue tone imparted by cobalt alone (8,17).]

The precise nature of the colorant materials is unknown. The idea that oxidized or corroded bronze was used as a means of introducing copper as a colorant to ancient glasses was initially proposed by Geilmann

(20) and more recently by, among others, Sayre and Smith (48). It also appears from the blue and green glasses reported in this study that lead and zinc are likely to have been introduced by means of bronze or brass additions to the melt. The natural variability in lead and zinc levels for medieval glass makes conclusions of this kind difficult to confirm, but these observations find support in the unpublished results of other workers who have noted numerous examples of various combinations of lead, zinc, and tin in stained glass as well as in ancient Islamic and Venetian vessel glasses. The determination of tin concentrations is important in this connection and will be the subject of future investigations. On the present evidence, tin concentrations fall at or below the limit of detection (0.02%) for the glasses under consideration. Zinc concentrations greater than that of cobalt have been reported from an Egyptian cobalt-blue pigment (49). The possible introduction of zinc by means of a cobalt colorant material must therefore be kept in mind.

Copper is also responsible for the color of the emerald green glasses EC7, EC8, and HA1 at concentrations significantly higher than those found in blue glasses. [Data extracted from 16 published analyses (34,35) of green glasses gave a mean concentration of 2.1%.] Medieval documentary evidence supports the theory that copper was used to produce an emerald green color. Eraclius advocates the addition of copper filings burned until they are reduced to a powder (50, p. 214), but for green earthenware glazes, he asserts that brass is preferable (50, p. 206). The 16th century text of Neri, translated by Merrett (51), also suggests the use of calcined brass, but further stipulates the introduction of iron for emerald green colors. The iron concentration in the green samples from Table IV is no higher, however, than the levels in other glasses and arises from impurities in the sand. The high levels of lead in samples EC7 and 8 are worthy of comment, because they contrast with the emerald green glass HA1 and the other differently colored samples. In combination with the general consistency in the compositions of samples EC7 and 8, these high lead concentrations may reflect a common source for the Elgin emerald green glass. The exceptionally high lead levels may arise from a copper-lead alloy of the solder type. Although analyses of ancient glasses confirm the role of copper at levels of about 2–3% in producing a deep green color, the glass chemistry that results in this color is not well understood. Weyl comments that green colors are due to asymmetrical coordination of copper and are favored by higher concentrations (52), but the subject merits further study.

Conclusion

Although the salient features of medieval stained-glass-making techniques and composition were understood 50 years ago (17) and many

American Chemical
Society Library

1155 16th St., N.W.

Washington, D.C. 20036

subsequent studies have clarified specific aspects, our knowledge of the raw materials used, the glass-making conditions employed, and the chemistry of the glasses themselves remains imperfect. On the basis of analyses of 12 glass constituents by the flame AAS method described in this chapter, it is possible to ascribe, with good confidence, certain glass fragments to a common glass-making area, to infer the likely source of plant ash, and to appreciate the reasons for the glass color.

The AAS method has several limitations. For the trace elements, particularly the colorants cobalt and nickel, the dilution factor required for analyses of 12 elements by continuous nebulization places these elements close to the detection limits for flame AAS. More accurate data on these and other trace elements are necessary before conclusions can be drawn on the source minerals used to impart color. Phosphorus, a ubiquitous minor component of medieval stained glass, has not been determined by AAS in the course of this work, but has the potential to provide key information on sources of plant ash. A full understanding of the colorant role of the transition metal elements is not possible on the basis of analysis alone; UV-visible spectroscopy, electron spin resonance spectrometry, and Mössbauer spectroscopy, for example, are necessary adjuncts to achieve this aim. The results of the application of these techniques and the extension of the AAS method to trace element determination by pulse nebulization and furnace atomization will be addressed in future reports.

Acknowledgments

We wish to thank R. G. Newton for samples of the 10 European Science Foundation glasses, R. H. Brill for samples of the Corning Museum Standard Glass, and W. J. Lindsay and the Ancient Monuments and Historic Buildings Division of the Scottish Development Department for samples of the Elgin, St Andrews, Holyrood, and Melrose glasses. Information from Mr. Lindsay on the Elgin Cathedral site is acknowledged with particular thanks. We wish to acknowledge the gift of the Perkin Elmer 360 atomic absorption spectrophotometer from the British Steel Corporation, Ravenscraig Works, Motherwell. Color illustration is made possible by the award of a grant to N.H.T. from the Carnegie Trust for the Universities of Scotland.

Literature Cited

1. Hughes, M. J.; Cowell, M. R.; Craddock, P. T. *Archaeometry* **1976**, *18*, 19–37.
2. Gritton, V.; Magalousis, N. M. In “Archaeological Chemistry II”; Carter, G. F., Ed.; *ADVANCES IN CHEMISTRY SERIES* No. 171; American Chemical Society: Washington, D.C., 1977; pp. 258–70.

3. Price, W. J. "Analytical Atomic Absorption Spectroscopy"; Heyden: London, 1979.
4. Wise, W. M.; Burdo, R. A.; Sterlace, J. S. *Prog. Anal. A. Spectrosc.* **1978**, *1*, 201–23.
5. Cowell, M. R.; Werner, A. E. *Ann. Congr. Int. Étude Hist. Verre*, *6^e*, (Cologne) **1973** (pub. 1974), pp. 295–98.
6. Lambert, J. B.; McLaughlin, C. D. In "Archaeological Chemistry II"; Carter, G. F., Ed.; ADVANCES IN CHEMISTRY SERIES No. 171; American Chemical Society: Washington, D.C., 1977; pp. 189–99.
7. Brill, R. H. *J. Glass Stud.* **1973**, *15*, 93–97.
8. Bettembourg, J. M. *Int. Congr. Glass, Artistic Hist. Commun.*, *9th (Versailles)* **1971** (pub. 1972), 225–40.
9. Vassas, C. D. *Int. Congr. Glass, Artistic Hist. Commun.*, *9th (Versailles)* **1971** (pub. 1972), 241–66.
10. Foy, D. *Ann. Congr. Int. Étude Hist. Verre*, *7^e (Berlin-Leipzig)* **1977** (pub. 1978), 189–223.
11. Frank, S. "Glass and Archaeology"; Academic: London, 1982. (See, in particular, Ch. 3, p. 43–70.)
12. Turner, W. E. S. *J. Soc. Glass Technol.* **1956**, *40*, 162T–186T.
13. Newton, R. G. *Archaeometry* **1971**, *13*, 11–16.
14. Geilmann, W.; Beyerman, K.; Tölg, G. *Glastech. Ber.* **1956**, *29*, 145–68.
15. Caley, E. R. "Analyses of Ancient Glasses 1790–1957"; Corning Mus. Glass: New York, 1962.
16. Chesneau, M. G. *C. R. Hebd. Seances. Acad. Sci.* **1915**, *160*, 622–24.
17. Chesneau, G. *Bulletin Monumental* **1933**, 265–94.
18. Geilmann, W.; Jenemann, H. *Glastech. Ber.* **1953**, *26*, 259–63.
19. Geilmann, W.; Brückbauer, Th. *Glastech. Ber.* **1954**, *27*, 456–59.
20. Geilmann, W.; Beyerman, K.; Brückbauer, Th.; Jenemann, H. *Glastech. Ber.* **1955**, *28*, 146–56.
21. Lehanier, C. *Int. Congr. Glass, Artistic Hist. Commun.*, *9th (Versailles)* **1971** (pub. 1972), 209–24.
22. Cox, G. A.; Heavens, O. S.; Newton, R. G.; Pollard, A. M. *J. Glass Stud.* **1979**, *21*, 54–75.
23. Brill, R. H. *J. Glass Stud.* **1970**, *12*, 185–92.
24. Olin, J. S.; Sayre, E. V. In "Archaeological Chemistry"; Beck, C. W., Ed.; ADVANCES IN CHEMISTRY SERIES No. 138; American Chemical Society: Washington, D.C., 1974; pp. 100–123.
25. Sellner, C.; Oel, H. J.; Camara, B. *Glastech. Ber.* **1979**, *52*, 255–64.
26. Vassas, C. D. *Int. Congr. Glass, Artistic Hist. Commun.*, *9th (Versailles)* **1971** (pub. 1972), 267–94.
27. Longworth, G.; Tennent, N. H.; Tricker, M. J.; Vaishnav, P. P. *J. Archaeol. Sci.* **1982**, *9*, 261–73.
28. *Corpus Vitrearum News Letter* **1977**, *25*, Item 2, 3–5.
29. Brill, R. H. *Int. Congr. Glass, Artistic Hist. Commun.*, *9th (Versailles)* **1971** (pub. 1972), 93–110.
30. Langmyhr, F. J.; Paus, P. E. *Anal. Chim. Acta* **1968**, *43*, 397–408.
31. Bomgardner, D. L. In "Scientific Studies in Ancient Ceramics"; Hughes, M. J., Ed.; Br. Mus.: London, 1981; pp. 93–101.
32. Price, W. J.; Whiteside, P. J. *Analyst (London)* **1977**, *102*, 664–71.
33. *Corpus Vitrearum News Letter* **1978**, *28*, Item 5, 11–12.
34. *Corpus Vitrearum News Letter* **1976**, *21*, Item 5, 9–16.
35. *Corpus Vitrearum News Letter* **1977**, *24*, Item 5, 10–12.

36. Kirkbright, G. F.; Marshall, M. *Anal. Chem.* **1973**, *45*, 1610–13.
37. Tennent, N. H.; Placido, F. Unpublished observations.
38. Caldwell, D. H., Ed. "Angels, Nobles & Unicorns. Art and Patronage in Medieval Scotland"; Nat. Mus. Antiquities Scotland: Edinburgh, 1982.
39. Mackintosh, H. B.; Richardson, J. S. "Elgin Cathedral"; HMSO: Edinburgh, 1980.
40. Thorne, W. T. *J. Br. Soc. Master Glass-Painters 1955–57*, *XII*, 9–14, 108–16.
41. Lowe, J. J. *Br. Soc. Master Glass-Painters 1959–63*, *XIII*, 428–29.
42. Sanderson, D. C. W.; Hunter, J. R. *Revue d'Archéométrie, Supplément*, **1981**, 255–64.
43. Turner, W. E. S. *J. Soc. Glass Technol.* **1956**, *40*, 277T–300T.
44. Alexander, S. M. *Art Archaeol. Tech. Abstr.* **1969**, *7*, 123–61.
45. Hawthorne, J. G.; Smith, C. S. "Theophilus: On Divers Arts"; Dover: New York, 1979.
46. Hoover, H. C.; Hoover, L. H. "Georgius Agricola: De Re Metalica"; The Mining Magazine: 1912.
47. Brill, R. H. *J. Glass Stud.* **1962**, *4*, 127–38.
48. Sayre, E. V.; Smith, R. W. In "Archaeological Chemistry"; Levey, M., Ed.; Univ. Pennsylvania Press: Philadelphia, 1967; pp. 279–311.
49. Daton, J. "Minerals, Metals, Glazing and Man"; Harrap: London, 1978; pp. 457–61.
50. Merrifield, M. P. "Original Treatises, Dating from the XIIth to XVIIIth Centuries on the Arts of Painting"; John Murray: London, 1849; 2 vols.
51. Merret, C. "Neri's Art of Glass"; Sir T. Phillips, Bart., Ed.; privately printed, Middlehill, 1826.
52. Weyl, W. A. "Coloured Glasses"; Society of Glass Technology: Sheffield, 1976.

RECEIVED for review November 23, 1982. ACCEPTED for publication April 18, 1983.

Provenance and Technical Studies of Mexican Majolica Using Elemental and Phase Analysis

MARINO MAGGETTI

Institut für Mineralogie und Petrographie, Universität, Freiburg, Switzerland

HAROLD WESTLEY and JACQUELINE S. OLIN

Smithsonian Institution, Conservation Analytical Laboratory, Washington, DC 20560

One hundred nine majolica sherds from excavations at the Mexico City Cathedral and from Metro construction in Mexico City have been analyzed by d.c. plasma-optical emission spectrography. Many of the sherds have been studied petrographically and by x-ray diffraction. Earlier studies of majolica from Spain and from sites in Venezuela and in the Caribbean by instrumental neutron activation analysis did not involve complete determinations of major elements or extensive phase analysis. Subsequent work showed concentrations of calcium (as calcium oxide) of as much as 24% in both imported and locally produced pottery and the presence of calcium silicates diopside and gehlenite, which were produced during firing. This finding suggests that a calcareous clay was involved in majolica production both in Spain and in Mexico. Field work in Mexico has revealed that majolica is produced today using two kinds of clay, one calcareous, which are mixed together. Firing studies of these clays are reported.

THE STUDY OF TIN-GLAZED CERAMICS (majolica) by neutron activation analysis was previously reported (1). The sherds studied in that research were from Spanish-Colonial sites in the New World; a small number of sherds came as well from a suburb of Seville in Spain known as Triana. Although a small amount of x-ray diffraction and petrographic analysis was carried out in conjunction with that research, a number of questions remained which suggested that a much more extensive study

0065-2393/84/0205-0151\$11.25/0
© 1984 American Chemical Society

of the mineralogy would be appropriate. The present investigation is a result of such study.

The technology of majolica production was a Muslim contribution that was introduced into Spain and then diffused to the Western Hemisphere in the course of colonization. The majolica technique also diffused to other European countries from Spain. In the early Middle Ages, the Muslim occupation of Sicily brought to Italy the same majolica production as was present in Spain. Although the historical documentation of the production of majolica exists, there are few published accounts of chemical or mineralogical analysis (2–9). The studies of majolica ceramics from archaeological excavations in the Western Hemisphere have primarily concentrated on the decorative modes (10–14). Very little has been written about the firing temperatures and methods of production based on laboratory study of the archaeological material.

Our chemical and mineralogical investigation shows that the majolica from Spain can easily be differentiated from the Mexican products by the mineralogic–petrographic nature of the temper. The Spanish sherds contain the association of quartz and biotite and muscovite; the New World majolica is characterized by a volcanic-derived association of mostly plagioclase and amphibole. The x-ray diffractograms show that there are two groups of Mexican majolica: a calcareous group with calcsilicate phases such as gehlenite, wollastonite, and(or) diopside and a noncalcareous group without such calcsilicates. The Spanish sherds are also calcareous ones. The Mexican calcareous majolica was probably made by mixing a highly calcareous clay with a noncalcareous volcanic clay and firing at 900–1150 °C. The noncalcareous Mexican majolica would have been made from a volcanic clay and fired at lower temperatures of 800–1050 °C. These results will be discussed in the following sections.

Sources of Specimens

The majolica sherds studied in this investigation include those reported on earlier (1) as well as a set of 81 sherds excavated from beneath the Metropolitan Cathedral in Mexico City. In addition, two Aztec sherds from the excavations at the Metropolitan Cathedral have been studied. When the Spanish conquered the Aztec city of Tenochtitlan and began to build their colonial capital, they retained the general area of the Great Temple of the Aztecs. By the middle of the 16th century, efforts were begun to erect a cathedral. It is from beneath this cathedral that a large number of majolica sherds have been excavated. Those sherds from the Metropolitan Cathedral discussed here are from beneath a concrete and boulder foundation poured in 1573. The majolica types to which the sherds are assigned are from Goggin (10) or Lister and Lister (14).

In addition to the archeological materials, clay samples and contemporary ceramics from the present majolica production center in Puebla,

Mexico, are included in this study. These specimens were collected by one of the authors, M. Maggetti, on a field trip to Mexico in the fall of 1981.

Descriptions of all the specimens involved in the study are given in Appendixes A and B. Some of the concentrations of the oxides were published earlier (1) and the others appear in Appendix C.

Experimental Methods

Chemical Analyses. Two analytical methods were used in obtaining oxide concentrations. The first method used was instrumental neutron activation analysis (INAA). Neutron activation analysis was carried out in the Chemistry Department of Brookhaven National Laboratory using the standard procedures developed there (15). The data obtained using this method were reported (1) for 40 sherds from the Metro excavations in Mexico City and for 11 sherds from the excavations at the Metropolitan Cathedral in Mexico City as well as for a large sample of imported sherds excavated outside Mexico. The oxide concentrations determined using INAA were Na_2O , K_2O , BaO , MnO , Fe_2O_3 , Rb_2O , Cs_2O , La_2O_3 , Sc_2O_3 , CeO_2 , Eu_2O_3 , HfO_2 , ThO_2 , Cr_2O_3 , and CoO .

More recently, d.c. plasma-optical emission spectrography (DCP-OES) has been used to analyze the remaining sherds from the Metropolitan Cathedral excavations. This analytical method has been in use in the Conservation Analytical Laboratory for a number of years but we did not begin to do quantitative analysis of ceramic samples until October 1980.

Each sherd specimen is sampled along the edges using a 1/4-in. electric drill and 3/32-in. tungsten carbide bit. Approximately 200 mg of sample is removed, mixed by tumbling on glassine paper, and placed in Pyrex vials for storage.

A 25-mg sample of each specimen is weighed for the quantitative determination of the following constituent oxides: majors— SiO_2 , Al_2O_3 , CaO , MgO , Na_2O , and K_2O ; minors— TiO_2 , P_2O_5 , MnO , and BaO ; traces— Cr_2O_3 , CoO , HfO_2 , Sc_2O_3 , Eu_2O_3 , ThO_2 , La_2O_3 , Rb_2O , CeO_2 , Cs_2O , Sb_2O_3 , ZrO_2 , Lu_2O_3 , Ta_2O_5 , Sm_2O_3 , and Yb_2O_3 . A fusion technique using a lithium tetraborate ($\text{Li}_2\text{B}_4\text{O}_7$) flux is used. This chapter describes the analysis procedure employing a d.c. plasma (DCP) excitation source for simultaneous multielement determinations in sherd samples (16).

A mixture of 25 mg of sample and 175 mg of flux is placed in a 3.5% rhodium-platinum crucible, which is transferred to a Thermolyne Furnace and fused at 1000 °C for 20 min. The crucible is cooled and placed in a polyethylene beaker where the melt in the crucible is dissolved with 10 mL of Ultrex Grade dilute nitric acid (1:24), washed from the crucible, and transferred to a 100-mL volumetric flask. The volume is made up with dilute nitric acid (1:24) (17).

Each 100-mL solution is divided into two equal portions: solution A, undiluted, to be used for the determination of minor and trace elements, and solution B, diluted (1:3) with distilled water to be used for the determination of major elements.

A blank solution is made by first fusing 175 mg of lithium tetraborate in a rhodium-platinum crucible; further treatment is the same as that described for the samples.

Standard reference materials were chosen with matrices that matched those of the samples as nearly as possible. The standards used were a set of U.S. Geological Survey (USGS) silicates: G-2, GSP-1, PCC-1, DTS-1, AGV-1, and BCR-1. The elemental composition of these references was determined by DCP

using National Bureau of Standards (NBS) Glass Standards 610 and 612. Spex Industries Atomic Absorption Standards, in concentrations of 1000 g/L, were diluted and used to determine the concentrations of oxides not listed for the NBS standards, such as HfO_2 , ZrO_2 , Lu_2O_3 , and Cs_2O (18).

A mixture of 25 mg of each USGS standard and 175 mg of flux was placed in a rhodium-platinum crucible; further treatment is the same as that described for the samples.

Determinations were made by using a Spectra Span III multielement optical emission spectrometer (Spectrametrics, Inc.), which has a focal length of 0.75 m and is equipped with an echelle grating and prism, providing high dispersion and high resolution. The other components of the system are as follows: a DCP Argon Spectra Jet III excitation source equipped with a suction pump, nebulizer, and spray chamber and a microprocessor and printer equipped with multielement cassettes positioned in front of the 20 photomultiplier tubes. These multielement cassettes have been designed to determine preselected wavelengths for the measurement of specific elements.

The DCP source for spectrochemical excitation has temperatures of 5000–6000 K. It incorporates two graphite anodes and a tungsten cathode in an inverted “Y” configuration shown in Figure 1 (19), and exhibits the following features: (1) It reduces spectral background, (2) it lowers the detection limits, (3) it is stable and reproducible, (4) it reduces chemical interference, and (5) it produces a wide dynamic range.

To analyze an unknown solution in the multielement mode, the operator does the following:

1. Inserts the appropriate 20-element cassette in the detector housing.
2. Ignites the plasma.
3. Aligns the wavelengths of the cassette by peaking up (“profiling”) a factory-selected wavelength that automatically aligns the others.

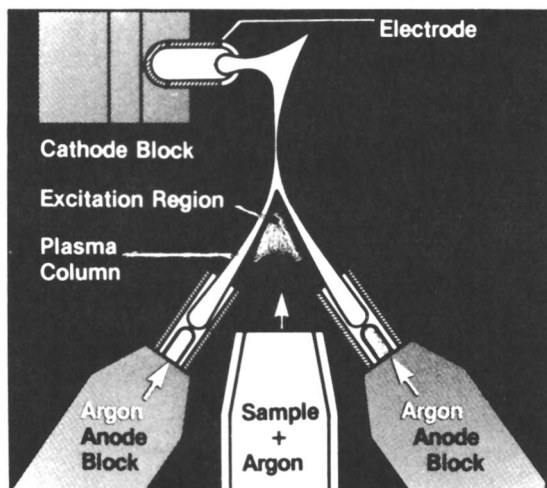


Figure 1. Block diagram of Spectra Jet III showing inverted “Y” configuration. Note area of excitation below plasma continuum.

4. Calibrates with standard solution containing the same elements as the cassette.
5. Calibrates with blank.
6. Corrects dilution if status messages indicate.
7. Repeats Steps 4 and 5.
8. If there are no further status messages, runs the unknown solution.
9. Notes concentration data for each element, including number of repetitions and average and standard deviation.

All solutions are run for a 10-s integration period.

The wavelengths of the elements to be determined by the multielement cassette are selected with the following considerations: sensitivity, intensity, and isolation from other spectral lines that could cause significant interference at that wavelength or from nearby background. Two cassettes were selected for the analysis of these samples and 20 elements were measured. Low detection limits for trace constituents were obtained by making careful and precise slit alignments as shown in Figure 2 (20).

Table I gives the values used for the USGS standard rocks both at Brookhaven National Laboratory and in the Conservation Analytical Laboratory of the Smithsonian Institution. The values reported for the Smithsonian were obtained by preparing the USGS standard rocks by using the method described earlier and analyzing them using NBS Glass Standards 610 and 612 and Spex Industries Atomic Absorption Standards. Twenty-four samples of majolica that had been analyzed by INAA were analyzed for comparison using DCP-OES. The data for three of these samples are given in Table II. Additional comparative data exist for SA 67, 76, 77, 84, and 94 and SC 03-21 for the 15 oxides that appear in Table II and in Reference 1.

Visual comparison of the values for these three samples shows excellent agreement between the data from the two methods, which suggests that DCP-OES data might be satisfactorily used in combination with INAA data. Further comparison of these two analytical techniques will be carried out.

Optical Microscopy. Of the specimens that were chemically analyzed by DCP-OES and INAA, 144 were selected for optical microscopy. From each a thin section was made, cross-cutting the sherd. Twenty-two specimens were prepared at the Department of Mineral Sciences, Smithsonian Institution, and

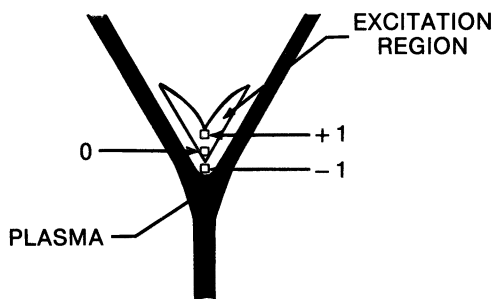


Figure 2. Plasma position as inverted image on slit.

Table I. Comparison of Value for Six USGS Standard Rocks Used at Brookhaven National Laboratory (BNL) and Smithsonian Institution (SI)

Oxides	G-2		GSP-1		AGV-1		BCR-1		PCC-1		DTS-1	
	BNL	SI	BNL	SI	BNL	SI	BNL	SI	BNL	SI	BNL	SI
Na ₂ O (%)	4.067	4.00	2.816	2.80	4.255	4.20	3.232	3.20				
K ₂ O (%)	4.500	4.50	5.507	5.50	2.909	3.00	1.689	1.70				
Fe ₂ O ₃ (%)	2.696	2.72	4.309	4.30	6.808	6.82	13.472	13.5	8.326	8.30	8.653	—
Rb ₂ O (ppm)	189.5	190.0	281.9	280.0	76.2	75.8	53.8	53.0				
Cs ₂ O (ppm)	1.320	1.30	1.100	1.15	1.334	1.32	1.280	1.20				
BaO (ppm)	2108	—	1515	1500	1418	1400	840	835				
MnO (ppm)	354.1	350	408.6	410	965.0	980	1816	1805	1172	1175	1227	—
CoO (ppm)	6.01	5.97	8.60	8.55	19.38	19.0	45.57	46.0	136	—	167.6	—
Sc ₂ O ₃ (ppm)	6.12	—	12.19	12.0	18.19	17.8	49.93	50.0	12.55	12.2	5.89	—
Cr ₂ O ₃ (ppm)	13.01	—	19.14	—	16.25	—	21.39	20.0	3909	4010	5885	5900
La ₂ O ₃ (ppm)	108.0	105.0	244.4	—	49.5	50.0	23.6	22.5				
Eu ₂ O ₃ (ppm)	1.73	1.80	3.18	3.00	1.882	1.72	2.461	2.50				
CeO ₂ (ppm)	204.5	202.0	553.8	548	95.2	93.8	56.9	57.2				
HfO ₂ (ppm)	8.84	9.00	14.56	—	6.05	6.00	5.13	5.00				
ThO ₂ (ppm)	28.77	28.5	125.6	123.0	7.66	7.52	7.07	7.00				

NOTES: Data for samples used at Brookhaven National Laboratory are from Ref. 15, pp. 88-89.

Samples of USGS rocks used at Smithsonian Institution were analyzed by Harold Westley, Conservation Analytical Laboratory, using DCP-OES with Spex Industries Atomic Absorption Standards.

Table II. Comparison of the Composition of Spanish Colonial Majolica Analyzed by Instrumental Neutron Activation Analysis (INAA) and Direct Current Plasma-Optical Emission Spectrography (DCP-OES)

Oxides	SA66		SA74		SA18	
	INAA ^a	DCP-OES ^b	INAA ^a	DCP-OES ^b	INAA ^a	DCP-OES ^b (conc. ± SD)
Na ₂ O (%)	1.46	1.50	2.08	2.00	1.81	1.83 ± 0.00
K ₂ O (%)	1.57	1.50	0.75	0.78	2.0	2.1 ± .01
Fe ₂ O ₃ (%)	5.3	5.0	4.3	4.5	3.8	3.9 ± .01
Rb ₂ O (ppm)	55	54	43	43	73	72 ± .10
Cs ₂ O (ppm)	4.6	5.0	2.8	3.1	6.5	6.7 ± .02
BaO (ppm)	43	45	58	60	57	60 ± .00
MnO (ppm)	39	42	72	75	42	50 ± .00
CoO (ppm)	11.0	12.0	15.3	15.5	13.3	13.6 ± .00
Sc ₂ O ₃ (ppm)	22.0	21.3	16.0	15.8	15.7	16.0 ± .00
Cr ₂ O ₃ (ppm)	135	130	92	98	77	79 ± .10
La ₂ O ₃ (ppm)	25	27	23	24	28	28 ± .00
Eu ₂ O ₃ (ppm)	1.25	1.20	1.42	1.47	1.32	1.40 ± .00
CeO ₂ (ppm)	41	40	50	50	43	43 ± .10
HfO ₂ (ppm)	6.3	6.2	5.7	5.6	4.3	4.7 ± .01
ThO ₂ (ppm)	5.5	5.4	5.5	5.3	6.4	6.8 ± .02

Note: Comparative data on samples were obtained from 24 sherds, of which 3 are reported here.

^a Data given are from Ref. 1.

^b Data given are from Ref. 52. The standard deviation shown for SA 18 was calculated by taking three separate readings of the blank, standard and unknown at the wavelength chosen for each element and determining the standard deviation of the calculated concentrations.

the rest were made at the Institute for Mineralogy and Petrography of the University of Freiburg. For comparison, thin sections were prepared from two sherds from Teotihuacan (17, I-1 and I-2).

x-Ray Diffraction. A total of 111 sherds have been analyzed by x-ray diffraction using a Philips diffractometer ($5-45^\circ 2\theta$, CuK_α radiation). The clays were studied in the same manner, including oriented samples of the fine-grained clay fraction, by using the standard procedure ($2-30^\circ 2\theta$, air-dried, glycolated 60°C for 24 h, fired 550°C for 1 h).

Firing Experiments. From the clays SD 28, SD 47, and SD 48 as well as the mixtures in a ratio of 1:1 of SD 27 + SD 28 and SD 38 + SD 39 small specimens ($3.5 \times 6.5 \times 1$ cm) were formed. The clays were used as collected, without sieving, but with thorough homogenization. These specimens were fired in an electric kiln under oxidizing conditions at 600, 700, 800, 900, 1000, 1100, and 1200°C ($10-11^\circ\text{C}/\text{min}$ heating rate, 1 h at maximum temperature, no temperature control during cooling). Additionally, the mixtures were fired at 850, 950, and 1050°C . The fired clays were thin-sectioned and were analyzed by x-ray diffraction, except for the specimens fired at 950°C , which were only thin-sectioned.

Experimental Results

Chemical Data. The oxide concentrations given in Appendix C were obtained by DCP-OES. This method of analysis allows easy determination of the oxides of silicon, aluminum, magnesium, calcium, and phosphorus in addition to the 15 oxides originally analyzed by INAA. In the study presented here, this additional concentration data on major constituents was very useful in conjunction with the study of the mineralogy by microscopic examination and by x-ray diffraction analysis.

The oxide concentrations of cerium, lanthanum, and thorium given in Appendix C can be used to identify sherds of Spanish origin. These include the sherds identified as Sevilla White and as Columbia Gun Metal in Appendix C; all have higher concentrations of these three oxides than do sherds of Mexican origin. Another distinction can be made on the basis of the calcium oxide concentration. The two groups labeled Valle Ware and Romita Sgraffito have, with one exception, SC 61, concentrations of calcium expressed as calcium oxide well below 10%. These two groups of sherds can be recognized as being Spanish-Colonial on the basis of their surface decoration, but they are not true majolica in the sense that one identifies the majolica from Triana, Spain, in Appendix C as having calcium oxide concentrations well above 10%. The concentrations of the oxides of cerium, lanthanum, and thorium in the Valle Ware and Romita Sgraffito are the lower values characteristic of sherds of Mexican origin.

Optical Microscopy. The analyzed sherds can be divided, based on the nature of the temper minerals, into three main groups: (1) sherds with temper of sedimentary origin; (2) sherds with temper of volcanic origin; or (3) sherds with temper of plutonic origin.

Temper Classification of the Sherds

Group 1—Sedimentary Temper

SA 1, 3, 11, 15, 18, 27, 58

SB 30, 31, 52, 56, 60–62, 65, 66, 70, 73, 86–90, 93

SC 2–9, 19, 26, 86–89, 91

Group 2—Volcanic Temper

a) fine-grained in a more or less calcitic matrix (sherds with ignimbritic fragments appear in boldface type)

SA 65, 66, 68, 70–73, 75–77, 79, 80, 81, 82, 83, 86–88, 90, 93–99

SB 20, 26, 27, 32, 33, 36, 37

SC 12, 13, 14, 15, 17, 18, 21, 22–25, 28, 29, 30, 31, 32, 33, 35, 37, 38, 40, 42–44, 46–48, 50–52, 56, 57, 61

SD 2

b) coarse-grained in a siliceous matrix
only volcanic elements SB 38, 39

mixed volcanic with granitic elements SB 41, 42, 44

c) medium- to fine-grained in a siliceous matrix (sherds with ignimbritic fragments appear in boldface type)

SC 55, 58–60, 62, 63, 67, 69–72, 74–80, 92–94, 96, 98, 99

SD 1, 3, 4

Group 3—Plutonic Temper

SB 43

1. SHERDS WITH TEMPER OF SEDIMENTARY ORIGIN. These sherds have a very fine-grained matrix, either calcitic or more or less isotropic, and some small calcite grains. The coarser temper particles have a maximum diameter of 0.3 mm and are composed predominantly of quartz with a few red oxidized biotites and colorless muscovites (Figure 3). The remaining minerals include some grains of plagioclase and epidote. In addition, red amphibole occurs in SA 11. Fossil fragments (spicules of sea-urchins) are found in SB 30, 31, and 89 (Figure 4). Many little round calcitic fragments can be observed, especially in the sherds with calcitic matrix. Other rock fragments present include rare quartzites. The pores of sherds with calcitic matrix, especially, are often filled with secondary calcite.

2. SHERDS WITH TEMPER OF VOLCANIC ORIGIN. They can be divided into three subgroups: (a) fine-grained sherds with calcitic matrix,

(b) coarse-grained sherds with siliceous matrix, and (c) medium- to fine-grained sherds with siliceous matrix.

Subgroup a has either a light brown matrix with a lot of fine-grained calcite grains dispersed in it or an anisotropic red to brown matrix with minor or apparently no calcite grains. The coarser fragments with a maximum diameter of approximately 0.4 mm are of volcanic origin and contain primarily plagioclase with small amounts of amphibole, and very minor amounts of orthopyroxene, clinopyroxene, brown biotite, olivine, quartz, pumice, red glass, andesite, and basalt (Figure 5). Especially in the sherds with a dominant calcitic matrix, we found a large number of small and irregularly shaped or rounded calcitic fragments, and the pores are often filled with secondary calcite grains of euhedral habit.

In a very few sherds, the diameter of these fragments measured 2.4 mm, but diameters of most of these particles do not exceed 0.1–0.2 mm. Glassy, colorless fragments of ignimbritic aspects are found to be an intrinsically important temper (Figure 6). The plagioclase is strongly oscillatory zoned and often contains trapped glassy inclusions, colorless to red or brown in color. The shapes of the feldspars are often idiomorphic or nearly idiomorphic with rounded edges. The amphibole has a strong pleochroism (X = yellow; Y,Z = red to deep red-brown) and is usually idiomorphic to subidiomorphic. The pyroxenes and olivines also are often idiomorphic and show red surfaces. Secondary calcite could be detected in almost all sherds as a pore filling.

The sherds of **subgroup b** have a mostly red matrix and more temper fragments than the ones from subgroup a (Figure 7). The diameter of these fragments is usually greater and can be as large as 0.6–2 mm. The volcanic amphibole can be red (SB 38, SB 39) or red with green patches (SB 41, SB 42). The pyroxenes do not have red surfaces.

The sherds of **subgroup c** have a red matrix and contain no secondary calcite. The maximum diameter of the temper fragments lies between 0.4 and 0.7 mm. The sherds contain much more temper than do the sherds from subgroup a. Some sherds contain typical ignimbritic colorless glass, very often as triangular Y-like forms, but mostly as thin rectangular or slightly curved plates or needles (Figure 8). As for the sherds from subgroup a, these glass fragments are frequently not preserved and were probably destroyed during the manufacture of the thin sections, but their identification is possible due to the characteristically curved or Y-shaped form of the pores preserved. The dominant temper mineral is plagioclase, followed by red amphibole, pyroxene, and, rarely, olivine and platy hematite. The pyroxenes sometimes have red surfaces, sometimes do not. Both varieties can be seen in the same thin sections. The Aztec sherds SC 98 and SC 99 match this group. Contrasting with this homogeneous group are sherds SC 92, SC 93, SC 94, SC 96, SC 98 and SC 99, which have less temper than do the other specimens. They

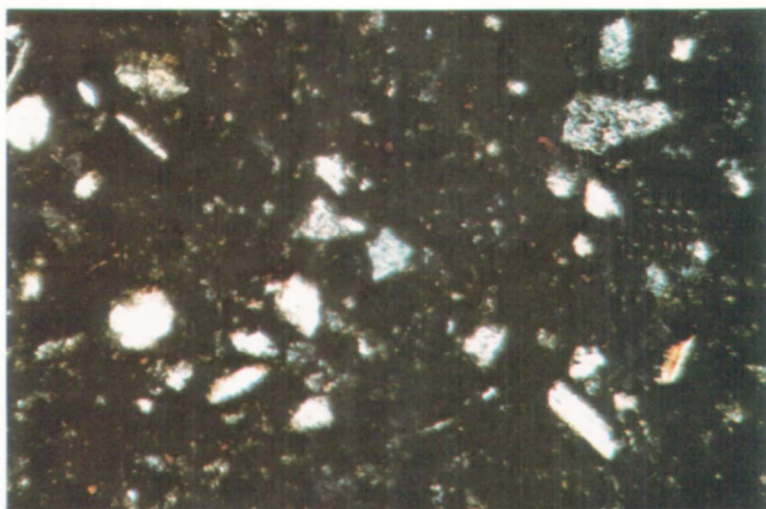


Figure 3. Typical aspect of a thin section of an imported majolica, SA 27, from Spain with characteristic sedimentary temper. The colorless fragments are quartzes, the brown lathes biotites. In the bottom right corner a colorless lath of a muscovite/illite can be seen. 1 Nicol. Length of the image area is 0.82 mm.

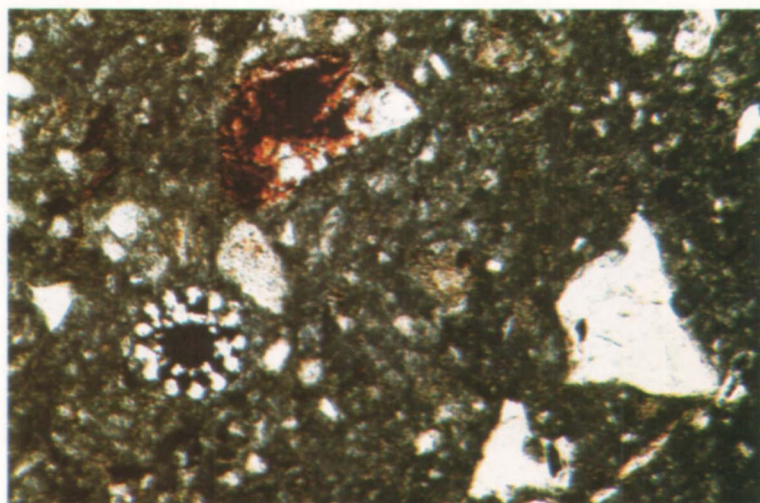


Figure 4. Characteristic fragment of a spicule of a sea-urchin beside colorless quartzes, brown biotites and yellowish rounded carbonaceous fragments in sherd SB 30 from Genoa, Italy. 1 Nicol. Length of the image area is 0.82 mm.

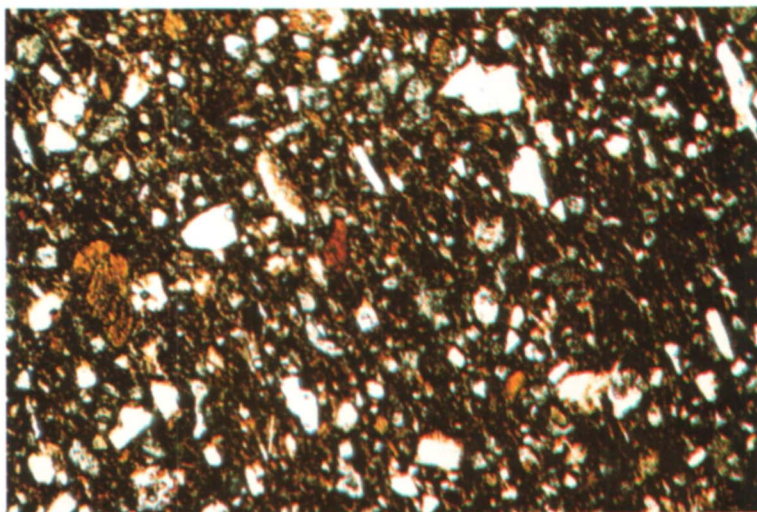


Figure 5. Typical aspect of a Mexican majolica, SA 68, with volcanic temper. In a light brown matrix, red or yellow amphiboles and colorless plagioclases can be identified. 1 Nicol. Length of the image area is 2 mm.

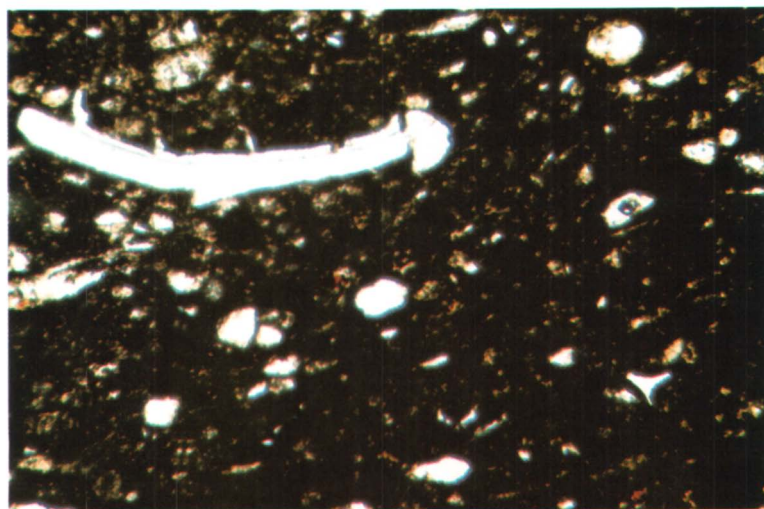


Figure 6. Characteristic bended colorless ignimbritic glass fragment with a rest of the part from which a Y-like form of the original fragment can be deduced in sherd SC 29, see Figure 7. A small fragment of the central part of a Y-like ignimbritic fragment can be seen at the bottom right corner. In the dark matrix only plagioclases and yellowish calcitic inclusions can be found. 1 Nicol. Length of the image area is 2 mm.

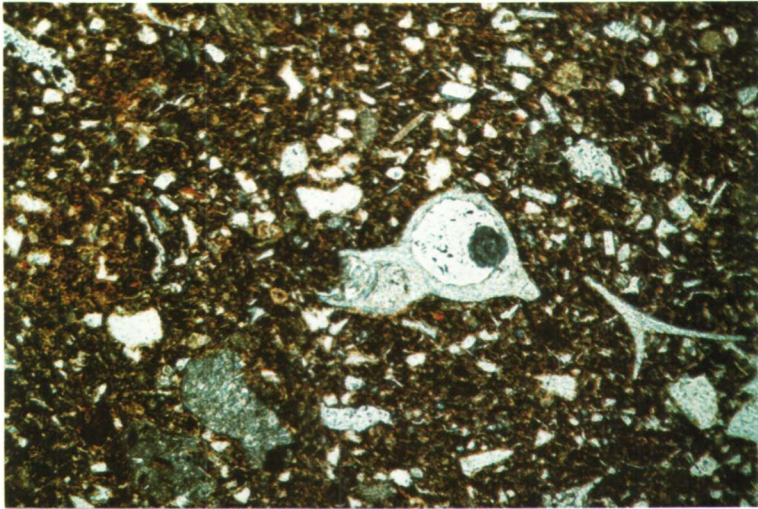


Figure 7. Colorless ignimbritic glass fragments in sherd SC 72. In the center an irregular-shaped fragment with a round hole can be seen; at the right of this temper element is another typical Y-like ignimbritic particle. Two andesitic grains are at the left below the central ignimbritic grain. The rest are plagioclases in the brownish matrix. 1 Nicol. Length of the image area is 2 mm.

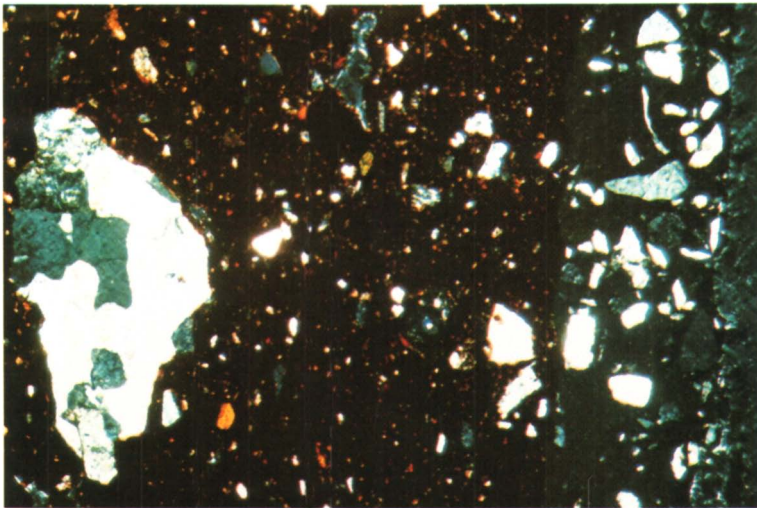


Figure 8. Majolica, SB 41, from Peru. Under crossed polars two parts can be distinguished: at the left, the red sherd matrix with a big granitic fragment; at the right, the black glaze with quartz inclusions. In the matrix, colorless to greyish plagioclases as well as colored little amphiboles can be seen. Length of the image area is 2 mm.

contain no ignimbritic glassy fragments, rather yellowish recrystallized glass particles. The proportion of rock fragments present is higher than in the other sherds. Amphibole is very rare.

3. **SHERDS WITH TEMPER OF PLUTONIC ORIGIN.** Only one sherd belongs to this group; it shows coarse-grained granitic temper fragments, in a red, siliceous matrix.

x-Ray Diffraction Analyses. Based on the presence or absence of calcsilicate phases such as gehlenite, diopside, and wollastonite, the specimens can be grouped into two main populations: group I, sherds with calcsilicate phases; and group II, sherds without calcsilicate phases. All of the sherds with temper of sedimentary origin as well as the sherds from subgroup a with volcanic temper have calcsilicate phases; subgroups b and c of the sherds with temper of volcanic origin and the one with temper of plutonic origin do not have calcsilicate phases. With respect to the chemical analyses, the sherds of group I have a high CaO content (mostly 10–24 wt %), but the ones from group II have a low CaO content (<8 wt %). The low CaO content derives from the plagioclases; the high CaO values are due to the presence of calcsilicates, formed during firing from preexisting calcite reacting with other oxides, as will be shown further on.

The detailed phase associations are summarized in Figures 9 and 10; Table III attributes each sherd to one of these associations. From this table it appears that the majority of the analyzed sherds belong to group I (with calcsilicate phases), and that in both groups there is one association that is predominant. In group I this is I_h; in group II it is II_a. A detailed inspection of Figure 9 shows the following significant characteristics:

- predominantly quartz in I_a.
- the presence of amphibole in I_b–I_e, absence of this phase in I_a and I_f–I_i.
- among the calcsilicates, only gehlenite can be identified in I_b and I_f; only diopside in I_e and I_i; gehlenite as well as wollastonite in I_c and I_g; gehlenite and diopside in I_a, I_d, and I_h.
- more quartz than plagioclase in I_a, I_c, I_f, and I_g.

Of special interest is the presence of quartz in the associations I_b–I_i, a phase that could only rarely be identified in the corresponding thin sections as a temper constituent. Therefore, it is to be assumed that quartz is present as a fine-grained component of the matrix.

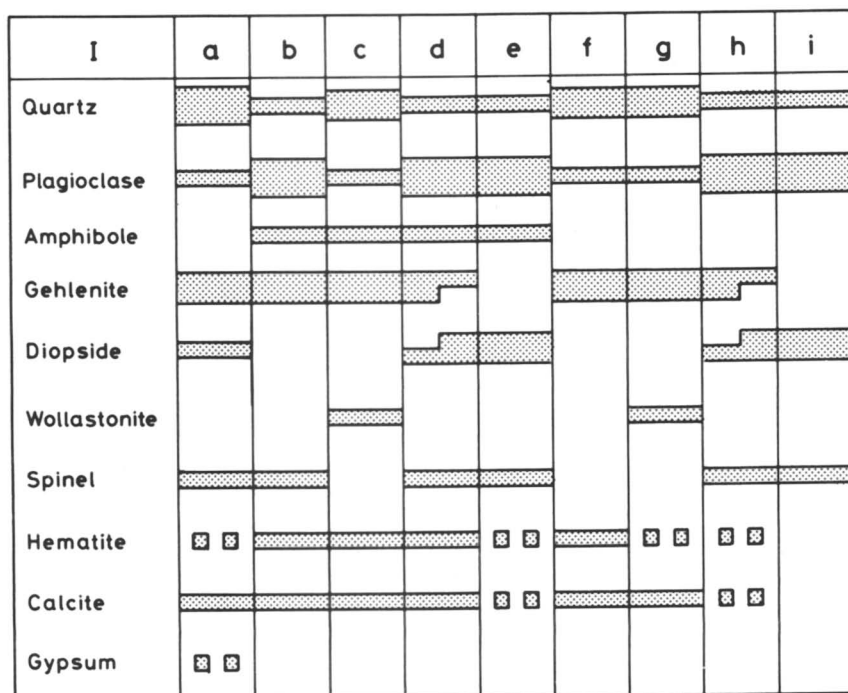


Figure 9. Phase associations of the calcareous majolica as deduced from x-ray analysis. The relative amounts of the phases present are based on the comparison of the peak heights in the x-ray diffractograms and are expressed by varying widths: narrow, medium, and wide.

Interpretation of Origin on the Basis of Mineralogical Data

The chemical composition of imported, European-made majolica is different from that of majolica made in Mexico (1). The differences in the concentrations of the oxides of cerium, lanthanum, and thorium are easily recognized; the Spanish majolica contains approximately twice as much of each of these oxides as the Mexican majolica. The mineralogical composition, too, of the pottery products of each area is fundamentally different and can easily be identified. The ceramic types and their origins, based on archaeological arguments, can be found in Table I.

Majolica of European Origin. The sherds of true European manufacture, SC 2–SC 9 from Jerez, Spain, have characteristic sedimentary temper with predominant quartz. These specimens belong microscopically to group 1 (p. 159) and by x-ray classification to the mineral association Ia of Table III. These findings confirm the observations of Olin et al. (1). All other majolica found in the Caribbean area fall—with respect to mineralogical composition—into this group and have, there-

II	a	b	c	d
Quartz				
Plagioclase				
Amphibole				
Cristobalite	☐ ☐			
Spinel				
Hematite				
Magnetite				
Calcite	☐ ☐			

Figure 10. Phase associations of the noncalcareous majolica as deduced from x-ray analysis.

fore, also been imported. This deduction was confirmed by the chemical composition. The Columbia Gunmetal variant (specimens SC 86–SC 89, SC 91) have also been imported. However, the exact place of fabrication of all these sherds of European origin can not be precisely located, principally because we have few comparative mineralogical data from the known European manufacturing sites. It seems to be quite difficult to make a distinction, for example, between the Italian and Spanish majolica. Analyzed sherds SB 30 and SB 31, identified by Lister as late 16th-century Italian (probably from Genoa, Ref. 21) are mineralogically not very different from the Spanish majolica. Both sherds contain characteristic sea-urchin fragments, but an identical fragment has been found in specimen SB 89, which belongs to the Spanish group. Archaeological evidence indicates that Triana, a suburb of Seville, is the manufacturing place of almost all imported Spanish sherds. More chemical and mineralogical analysis of European majolica is needed.

Majolica of American Origin. In contrast to the sherds definitely known to be European, with their characteristic sedimentary temper, there are specimens that contain volcanic or—as for SB 43—granitic temper. This observation corroborates the chemical arguments, which support distinctions based on the volcanic temper and quartz temper. The petrographic characteristics of the volcanic temper fragments (e.g.,

Table III. Classification of the x-Rayed Sherds with Respect to the Phase Association Shown in Figures 9 and 10

<i>Phase association</i>	SA	SC	SD
Ia	1,3,11,18,51,58	2-5,7-9,10,19 26,27	
Ib	68,71	57,61	
Ic		22,40	
Id (Ge>Di)	69, 88	18, 70, 73, 80, 93	2
(Ge<Di)	74, 76, 81	25, 30	
Ie	65, 82, 86		
If	66, 84		
Ig	90, 91	12, 31, 35, 38, 41-44,51, 53	
Ih (Ge>Di)	67, 77-79, 85, 87, 92, 93, 95, 96, 97, 99	37, 45, 48, 50, 56	
(Ge<Di)	72, 75	13, 14, 16, 17, 20, 23, 24, 28, 29, 32-34, 36, 49, 54, 65	
Ii		11, 21, 46, 52	
IIa		55, 58-60, 63, 64, 66, 67	
IIb	89		1, 3, 4
IIc		62	
IID		68, 98, 99	

NOTE: In Id and Ih the ratio of diopside (Di) to gehlenite (Ge) varies.

prevailing plagioclase associated with amphibole, ignimbritic flakes, few basalts, and olivines), suggest a volcanic source of prevailing andesitic composition with associated rhyolitic-ignimbritic parts and smaller basaltic elements, as is the case for the surroundings of both Mexico City and Puebla (22-35).

Therefore, the mineralogical analyses add additional arguments to the archaeological evidence for a Mexican majolica production (10, 14). In detail, the New World majolicas show differences among the individual sherds. First, it is interesting to notice that specimens SB 38, SB 39, SB 41, SB 42, SB 43, SB 44, and SB 45, which were found in Guatemala, Panama Viejo, Peru, and Ecuador, differ by their coarse temper fragments from the fine- to medium-grained majolica. These specimens are also chemically different from the other sherds (1). A Latin American origin—as denoted by the volcanic temper—is obvious; this is probably also valid for sherd SB 43, which has the same granitic temper as SB 44, here combined with volcanic temper and therefore of Latin American provenance. It is therefore very probable that in the 16th century majolica was made in South America, too (14).

Second, two specimens shown in Table I—one believed to have been made in Europe (SB 33), the other of questionable Mexican origin (SB 32)—contain volcanic temper and, therefore, belong to the New World production. Both specimens contain the cerium, lanthanum, and thorium oxide concentrations characteristic of Mexican majolica.

Third, the Valle Ware specimens form a distinct group. With one exception (SC 61), they belong microscopically to subgroup 2c; in the x-ray diffractograms they show no calcsilicates, indicating therefore a calcium-poor composition. The ignimbritic fragments in the temper are very characteristic and probably highly diagnostic, which indicates use of a raw material containing andesitic as well as ignimbritic fragments. The microscopic similarities within the locally made Teotihuacan material (15) are in good agreement with the assumption of Lister and Lister (14) that the Valle Ware was made in the Valley of Mexico. To locate the place of manufacturing exactly would require a major petrographic investigation into the specific composition of the volcanic deposits of the Valley of Mexico. However, the close mineralogical relationships among almost all analyzed Valle Ware sherds indicate the use of an identical clay and manufacture at the same site. Exceptions such as SC 61 and SD 3, which contain calcsilicate phases and are calcium-rich sherds, must have been made from another type of clay and come probably from another site. The calcsilicate-free Romita Sgraffito Ware must have been made from a different clay from the Valle Ware, as indicated by its lack of ignimbritic temper elements. In this they resemble the Aztec sherds and are probably locally made.

Fourth, a distinction between the Mexico City and Puebla majolica seems to be very difficult to make, on mineralogical arguments alone. This is not very surprising, considering the similar geological environment of both manufacturing areas. However, there are still some differences that could potentially allow discrimination. It is indeed very interesting to note that many Mexico City sherds contain the same ignimbritic fragments as do the Valle Ware; both are believed to be true Valley of Mexico products (14). However, one Puebla sherd (SA 81) contains identical fragments. Further work is needed on more specimens to show how valid the petrographic argument will be.

Manufacturing Technique of the Mexican Majolica

The technique of manufacture of majolica pottery has been discussed in many publications. A thorough discussion is given by Caiger-Smith (36) and, for Mexican majolica, by Lister and Lister (14). Majolica can be made either directly from a calcitic, calcareous white-burning clay which is plastic enough, or from a mixture of a chalky clay and a noncalcareous or slightly calcareous red-burning clay. The body of this type of raw

material hardens at low temperatures: its high calcium content is responsible for the great amount of shrinkage of the sherd during cooling, putting the glaze under compression and overcoming the tendency of low-temperature glazes to craze. It provides considerable porosity, and the white clay does not contrast with the white tin glaze; therefore less tin is needed to cover the sherd body. However, a disadvantage of the high-lime clays is that they contain large particles of limestone that turn to quicklime (CaO) in firing. On subsequent hydration to portlandite [$\text{Ca}(\text{OH})_2$], they will expand and destroy the glaze and even the body itself. Screening of these clays was therefore essential, and is still done today. Another negative point, the distortion of lime-rich clay bodies at high temperatures due to the action of lime as a flux, could be overcome by adding an alkaline flux and powdered flint or quartz. In places where the chalky clay was not plastic enough or had a high calcium content, blending with one or more red-burning plastic clays was commonly done, e.g., at Valencia, Delft, and many other manufacturing sites.

In order to establish how majolica potters of Mexico work, a field trip to Mexico City and Puebla was undertaken in October 1981. It was assumed that the modern technology reflects the ancient one and that the methods did not change too much in time, as was also assumed by Catala (36).

Modern Majolica Pottery Technique in Puebla

From inquiries among Mexican archaeologists and ethnologists it became evident that no majolica is presently produced in the Valley of Mexico, but we found that there is still a small majolica production in Puebla. The majolica manufacturers visited in this city were the La Trinidad factory (Guevara sisters) and the Santa Maria factory (Padierna family). Both manufacturers work in an identical manner and use a clay body blended from a mixture of equal amounts of a black and a white clay.

The black clay comes from the site of manufacture itself or from just outside the town, from the Loreto hill or Cerro de los Fuentes. Geologically, this clay belongs to the widespread formation of "tepetate," group of Chichinautzin, a Cenozoic deposit of volcanic tuffs and ashes of primary eolian nature, which underwent secondary fluvial lacustrine resedimentation (23, 38, 39). This is also the basic material used for local adobe and brick fabrication (23, 40). Samples from ancient brick-clay excavations near the road between Puebla and Cholula were shown by mineralogical and chemical inspection to be similar to the black clays collected at the manufacturing sites. The black clays are composed of montmorillonite (small peaks in the x-ray diffractograms indicate either small amounts or poor crystallization); large amounts of plagioclase, strongly zoned with trapped glass inclusions; and small amounts of light-green to

yellow amphibole, augites, orthopyroxenes, quartz, and rock fragments as tuffs, basalts, andesites, and glass in different colors, mostly red or yellow-brown. The optical characteristics of these minerals are in good agreement with the published descriptions of the volcanic products (38). As indicated by the absence of calcite, the black clay is a typical red-burning, noncalcareous or slightly calcareous clay.

The white clay comes from outcrops about 10 km southeast of Puebla, from the hills surrounding the small village of Santo Tomas Chiautla near Totimehuacan. It belongs geologically to the marine marly clay sediments of the Cretaceous Maltrata formation of Albian (38) or Turonian (23) age. The mineralogical composition of these marls is montmorillonite, predominant calcite as finely dispersed crystals in the matrix, some quartz, a few tiny plagioclase fragments that show no volcanic features such as strong zoning or trapped glass inclusions, a very few biotites and zircons, and some rounded calcitic fragments of small dimensions. From these findings it is quite obvious that this type of clay belongs to the highly calcareous clays, which is in agreement with the chemical composition.

According to the publications of Comermex (41) and Catala (37) and discussions with the potters of Puebla, the following steps are used in majolica production:

- Mixing of both clays in a 1:1 ratio in a wet bath;
- Sieving and drying slowly during a 60-day period;
- Shaping;
- Drying for 50–90 days;
- First firing for 8–12 h in an oil-burning kiln at 600–800 °C;
- Glazing and decorating;
- Second firing for 8–14 h at high temperatures (these temperatures could not be exactly identified, but the La Trinidad factory staff believed them to be around 1200 °C);
- Slow cooling for 24 h.

Technology of Mexican Majolica of the 16th and 17th Centuries

Little can be said about the technique of Spanish majolica based on the present knowledge from the mineralogical composition of these products. For instance, it is not known if two clays were mixed or if only one single clay was used. However, the basic material must have been a marl, as inferred by the presence of calcsilicate phases and the chemically determined high calcium content. If blending of two or more clays did not occur, the addition of quartz sand is probable because a calcareous clay would not be likely to contain quartz in such high amounts as identified. This addition would explain the high amount of this phase in the sherds.

Work in progress on typical majolica clays from Spain will give evidence about the ancient technique used in this part of the world.

Treatment of the Raw Materials. Based on the field expedition to Mexico in 1981 and the subsequent mineralogical and chemical analyses of the collected clays and modern majolica, much more can be worked out on the technique of ancient Mexican majolica production. The low calcium content of the Valle Ware specimens points to the use of a noncalcareous clay. The observed mineralogical matching of these specimens with modern black clays from Puebla (SD 47 and SD 48) and ancient Pre-Columbian pottery (I-1, I-2, SC 98, SC 99) suggests that these objects have been made from the locally available common red-burning volcanic clays, which were used extensively in Pre-Columbian time. There is no further evidence from microscopic inspection that supplementary addition of another material took place. These clays were therefore used, possibly after a sieving, as they have been found.

The chemically determined high calcium content of many of the majolica sherds demonstrates the use of a calcium-rich clay; a previous assumption was that secondary calcite was deposited during burial (1). The calcium is fixed in the calcsilicate phases, which form only at a high firing temperature (as explained later in this chapter), and must therefore have been present in the primary clay before firing, probably as calcite. The calcite present in the sherds is not of primary but rather of secondary origin; its formation will be discussed later. Mineralogical arguments strongly support the archaeological arguments that, in contrast to the Valle Ware, the Mexican majolica was made by blending two clays, as the modern potters do in Puebla. As shown later, the volcanic clays SD 47 and SD 48 do not contain any calcite, and the Cretaceous clay SD 28 contains no volcanic elements. The presence of true volcanic temper fragments in the calcium-rich majolica sherds is therefore a sound proof that the potters of the 16th and 17th centuries mixed two clays, a white-burning calcareous and a red-burning noncalcareous one, exactly as modern potters do. From this fact and the chemical similarity between modern and ancient majolica of Puebla (*see* Appendix C), the assumption can be made that the modern potters use a technique identical with that of their ancestors. It is quite probable that the first European potter who introduced the majolica fabrication to Mexico used the same methods as were employed in Europe, including mixing two chemically and mineralogically different clays. As for the Valle Ware, a sieving of both clays must have occurred also as a step in the majolica production. The maximum diameter of the temper grains found in the majolica sherds is much less than that of the clays and the Valle Ware, indicating a better processing of clays for the very fine-grained majolica pottery.

Origin of the Raw Materials. The sources of these clays were very close to Puebla. The city rests on a base of volcanic red-burning clay and

the hills at the southeast contain the white-burning calcareous clay. Major problems would have confronted the Spanish-Colonial majolica potters in Mexico City. Red-burning clay had been used since Pre-Columbian time and was easy to find. But where would the potters have dug a calcareous clay? The nearest suitable outcrops¹ lie 50–60 km away from Mexico City and are (a) in the region of Tepeji del Rio, province of Hidalgo, 50 km NNW of Mexico City (42); (b) in the region 60 km SSE of Mexico City in the province of Morelos (43); and (c) in the region N and NE of Pachuca, province of Hidalgo, 110 km NE of Mexico City (44, 45). If the Mexico City majolica potters used these clays, transportation of the raw materials over a great distance would have been necessary. This factor would have served, among others, as a reason for the decline of majolica production in Mexico City and the rise of it in Puebla, where the raw material was readily available.

The coarse-grained particle size of majolica from other sites in South America contrasts strikingly with the Mexican majolica and must have been made, as indicated by the absence of calcsilicates, from a silicatic clay. The grain-size distribution indicates a much poorer processing of the clays and therefore a lower degree of technology.

Firing Temperatures. The firing temperatures of the ancient majolica can be estimated by the firing experiments carried out on the clays collected in Puebla and by comparing the resulting mineralogy with that of the majolica sherds. A ceramic sherd is actually an association of three genetically different phase groups: primary or pre-firing, firing, and secondary or post-firing minerals or phases (46, 47).

The marl SD 28 (Figure 11) shows as primary minerals montmorillonite, calcite, quartz, and plagioclase. The clay mineral montmorillonite loses its intracrystalline water at low temperatures, and the peak at 10Å in the diffractograms disappears between 700 and 800 °C. Calcite decomposes between 800 and 900 °C. Calcium oxide, mineralogically lime, can be seen in all firing steps as a dissociation product of calcite. Portlandite, which is a rehydration product of lime and therefore a secondary mineral, is seen as well. The formation of portlandite so soon after firing is not astonishing, because lime is very hygrophilic. Quartz is stable in the whole range of firing temperatures. Calcsilicates are found between temperatures of 700 and 800 °C (gehlenite) and 800 and 900 °C (wollastonite) and forms by recombination of free CaO, from the decomposition of calcite, with free alumina and silica, from the breakdown of montmorillonite. The increase of the plagioclase peak between 800 and 900 °C is probably caused by the formation of a high-temperature plagioclase of presumed anorthitic composition. The combined increase of wollastonite and decrease of quartz at 1000–1100 °C indicate the participation of quartz in the wollastonite-formation process, perhaps due to the ex-

¹ The Upper Cretaceous Mexcala and Mendez formations, which contain marls.

haustion of available silica from the montmorillonite breakdown. A glassy phase must be present at higher temperatures. At 1200 °C, the specimen is completely molten. The experiments show that not all CaO could combine with other oxides to form new firing calcsilicate phases; this free CaO will rehydrate and recarbonate to secondary calcite in normal conditions.

The slightly calcareous volcanic clays SD 47 and SD 48 show a similar behavior during firing (Figure 11); this behavior is profoundly different from that of the marl SD 28. Montmorillonite, present only in small amounts or perhaps poorly crystalline, is stable up to 800 °C. Quartz disappears between 1000 and 1100 °C; plagioclase decreases slightly at 1100–1200 °C; amphibole breaks down at 900–1000 °C. The primary pyroxene could not be detected in all specimens. The newly formed firing minerals include mullite and cristobalite, which form in the temperature range 1000–1100 °C, and hematite (700–800 °C). The presence of spinel is probable, but not certain due to the coincidence of the peaks in the diffractograms with the one of plagioclase. Contrasting with the calcareous bodies, these sherds are mechanically stable up to 1200 °C and show no sign of collapsing. They, too, contain a glassy phase at higher firing temperatures.

The mixtures show mineralogical behavior different from that of the clays discussed until now (Figure 12). The primary minerals montmorillonite and calcite both break down at 800–900 °C, with formation of lime and free oxides as alumina and silica. Amphibole is stable up to 900–1000 °C for SD 38 + SD 39 or 1000–1050 °C for SD 27 + SD 28. This stability is perhaps a grain-size effect, although the thin sections do not show differences in the grain-size of this mineral between the mixtures. Gehlenite (800–850 °C), diopside (1000–1050 °C), and anorthitic plagioclase (850–900 °C) are formed as new-firing calcsilicates. In these experiments, the growth of diopside occurs at higher temperatures than in the highly calcareous illitic clays (48). Diopside probably forms either as a dehydration product of the volcanic iron–magnesium amphibole or by a complex reaction involving gehlenite and quartz, as shown by the decrease of these phases at high temperatures. Other firing minerals are hematite (900–1000 °C) and iron–magnesium spinel (1050–1100 °C).

Under the microscope the following changes were observed with increasing firing temperatures: The matrix of the marl SD 28 is calcitic up to 700 °C and becomes isotropic at higher temperatures. The coarser calcitic fragments resist dissociation up to 800 °C, but are completely destroyed at 900 °C.

The matrix of the volcanic clays SD 47 and SD 48 changes to an isotropic red at 800 °C and becomes black at about 1100 °C. The amphibole shows a color change: The initial homogeneously green specimens develop red borders due to increasing oxidation at 700 °C, a process

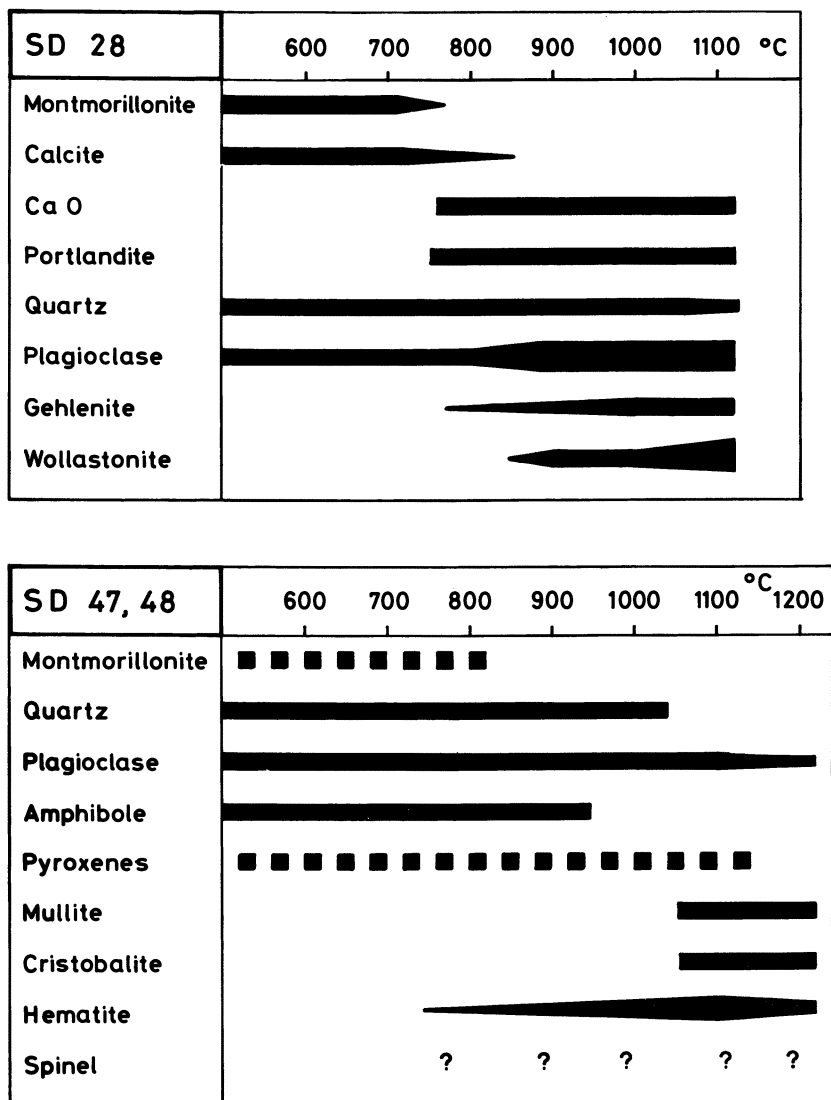


Figure 11. Mineralogical changes during firing of the marl SD 28 and the volcanic noncalcareous clays SD 47 and SD 48.

which is terminated at 800 °C when the amphiboles are homogeneously red. The pyroxenes have oxidated borders from 800 to 950 °C and upward. At 1200 °C both specimens show signs of strong melting process. All observable and recognizable mineral species have rounded shapes and are surrounded by or embedded in a light brown glass.

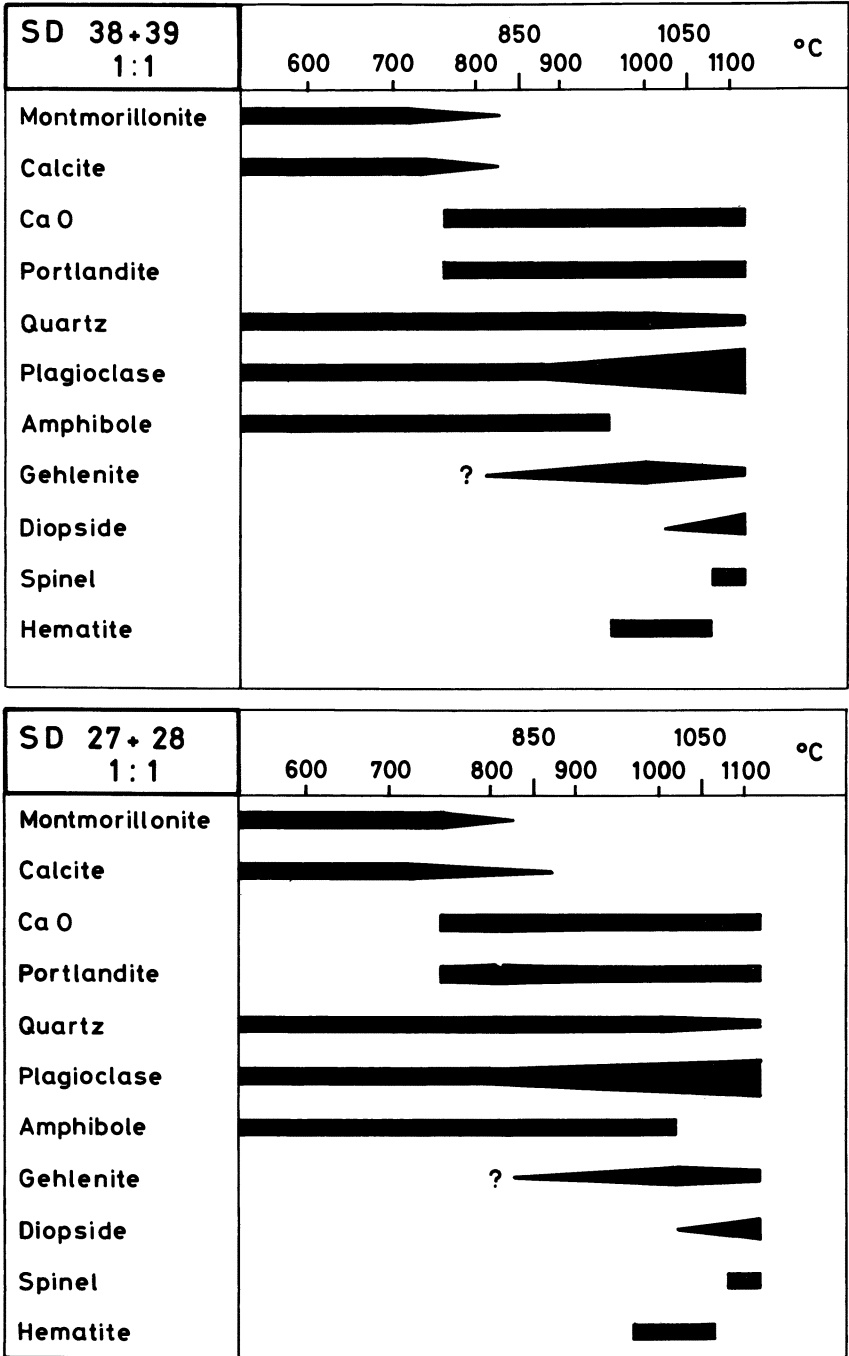


Figure 12. Mineralogical changes of the 1:1 mixture of a calcareous and a noncalcareous clay.

A similar behavior is shown by the mixtures. By combining the microscopic and x-ray results, a scheme for estimating their ancient firing temperatures can be established (Figure 13). Here it should be stressed that the resulting firing temperatures are only rough approximations, because the conditions of the firing experiments are surely different from those used by the ancient artisans. A firing procedure identical to that used by modern potters in Puebla is made difficult by the design of modern laboratory electrical kilns, where, for example, the temperature rise rate cannot easily be equaled. However, from the presence of hematite in many sherds it can be deduced that the firing atmosphere in ancient time was oxidizing, exactly as it was for the firing experiments.

The mineralogy of the low calcareous sherds can be compared with the firing series of the volcanic clays SD 47 and SD 48 (Figure 11). The sherds of the mineral association IIa in Table III therefore have been fired at 800–850 °C to 950–1000 °C. The lower temperature limit is given by the breakdown of montmorillonite, which was not detected in the diffractograms of the sherds; the upper limit is given by the breakdown of amphibole, which was detected. Similarly, the absence of amphibole in the sherds belonging to the phase association IIb stresses an inferior firing temperature of 900–950 °C; the absence of mullite as well as cristobalite implies a superior firing temperature of 1000–1050 °C. Compared with this association, the sherds of IIc denote probably slightly higher firing temperatures, due to the presence of cristobalite and the absence of mullite. The majority of the Valle Ware and the majolica from South America and meso-America have been fired at comparatively low temperatures. Only one sherd from the Valle Ware, in addition to the Romita Sgraffito and the Mexico City majolica, indicates higher firing temperatures. The association IId in Table III denotes a reducing firing followed by an oxidizing process, as indicated by the black core and the red surfaces of these sherds as well as by the presence of hematite and magnetite. There is not sufficient experimental data for this assemblage to determine a precise firing temperature.

The interpretation of the phase assemblages of the highly calcareous majolica is ambiguous. The upper firing temperature limit of the Mexican majolica is at least 1200 °C, when the firing runs are completely molten and warped. This limit can be reduced to about 950–1050 °C for the amphibole-bearing associations Ib–Ie. The presence of gehlenite in all these specimens indicates a minimum temperature of about 850 °C. A reasonable approximate firing temperature of these sherds would lie between 850 and 1050 °C, probably in the upper range, as can be deduced from the oxidated borders of the pyroxenes and the combined presence of gehlenite and diopside. The absence of amphibole in the x-ray diffractograms of the assemblages If–Ii limits the firing temperatures to a minimum of 950–1050 °C, the upper limit being 1100–1200 °C, when

SD 27+28 } SD 38+39 } 1:1	600	700	800	900	1000	1100	1200 °C
Matrix	carbonatic light brown		isotropic, red			isotropic black	molten
Amphibole	green	green core red border	totally red				
Pyroxene					Oxidated border		
Montmorillonite	X	X	X				
Gehlenite				X	X	X	
Diopside						X	
				X	X	X	

Figure 13. Combined scheme showing the mineralogic changes in firing of both mixtures as deduced from optical microscopy (matrix + amphibole + pyroxene) and x-ray diffraction analysis (montmorillonite + gehlenite + diopside).

warping occurs. In all these sherds, the pyroxenes are strongly oxidized. The behavior of the calcsilicates in the sherds is puzzling. Why do certain sherds contain only diopside or only gehlenite, and why do others show the combination of diopside and gehlenite or gehlenite and wollastonite? This is perhaps due to chemical and technological factors. The gehlenite-wollastonite association could be explained by the use of a highly calcareous clay with very minor addition of volcanic temper. But the chemical and mineralogical analyses show Fe_2O_3 concentrations, for instance, as high as in the other sherds containing another calcsilicate assemblage, so this cannot be a decisive factor. It is perhaps only the MgO content or the MgO/ Fe_2O_3 ratio that influences the formation of diopside instead of wollastonite. The wollastonite-bearing sherds have very low MgO concentrations (1.5–4 wt %), but other sherds with diopside have comparably low MgO contents. However, these sherds show little diopside so it could be a factor, although not a decisive one.

The specimens with only diopside, or with more diopside than gehlenite (seen by comparing the height of the main peaks of both phases in the diffractograms) probably either were fired at a longer maximum temperature than the other specimens or were made from finer-grained raw materials, allowing a speedier establishment of mineralogical equilibrium. In effect, as previously discussed (49–51) and shown in the firing experiments, gehlenite is a metastable phase and tends to disappear during long firing; thus a stable phase assemblage of diopside + plagioclase + quartz + hematite is formed for these highly calcareous sherds. This is somewhat corroborated by the observation that the secondary calcite is very rare in these sherds, indicating that most of the CaO reacted with the other oxides to form new firing calcsilicates. In the other phase assemblages that show strong gehlenite peaks there is more secondary calcite, indicating that after firing of this pottery, more free CaO was left than in the diopside-rich majolica. This result matches well with the findings of the firing experiments, where in all runs free CaO was left in amounts diminishing with increasing temperature. This free CaO combines quickly with water to form portlandite and thereafter in a slow process with carbon dioxide to form calcite. The high porosity and small particle size of these secondary phases prevented destruction of the pottery during rehydration of the CaO particles. Another secondary phase, found only in one sherd of European origin, is gypsum.

Looking at the distribution of the possible Puebla and Mexico City majolica on the mineral assemblages and comparing these results with the firing experiments, we propose the following:

- The majority of the specimens were fired to temperatures of 950–1150 °C.

- The specimens from Mexico City belong to the diopside-rich association type and therefore indicate a probable higher firing temperature or a finer-grained starting material. In both cases, the technology of the Mexico City majolica seems to be slightly different and indicates a more refined technique, better kilns, or better processing than was used to produce the majolica from Puebla. This would not be surprising, considering that the majolica was first produced in Mexico City by a European potter and that the newer majolica of Puebla was possibly made by non-Europeans who were less familiar with the traditions of the majolica technique.

Conclusions

The mineralogic–petrographic compositions of European- and Mexican-made majolica differ markedly. Both products can be easily distinguished based on microscopic and x-ray analyses. Microscopic analysis shows that the temper of the imported European majolica is of sedimentary origin and is predominantly quartz; the temper fragments of the locally made Mexican majolica are of a volcanic nature and consist of minerals such as plagioclase and amphibole with additional volcanic rock fragments such as andesites and ignimbrites. The x-ray diffractograms show that there are two groups of Mexican majolica: a calcareous group with calcsilicate phases such as gehlenite, diopside, and(or) wollastonite and a noncalcareous group without such calcsilicates. Both groups are chemically different in their calcium contents. By comparing the mineralogic features of these ceramics with modern majolica from Puebla and with the firing experiments of modern clays used at Puebla, it can be deduced that the calcareous majolica was made by mixing a white-burning calcareous clay with a red-burning noncalcareous clay. The firing temperature was between 950 and 1150 °C. The noncalcareous majolica was made from the common noncalcareous volcanic clays used by Pre-Columbian potters. Their firing temperatures were in the range of 800–1050 °C. Both majolicas were made from sieved clays. In contrast, the noncalcareous majolica from South America is much coarser and evidences a poorer technology.

Acknowledgments

We acknowledge the interest of Florence and Robert Lister (University of Arizona), who provided the sherds from the Metro excavations in Mexico City and those gathered at Jerez de la Frontera and attributed to the potters at Triana, Spain. They were also instrumental in securing

sherds from Patrimonial Nacional, which were obtained from beneath the Metropolitan Cathedral in Mexico City. We also acknowledge Hugo Nutini (Veracruz, Mexico) for his help in providing introductions to potters in Puebla, Mexico, and the Guevara and Padierna families of Puebla for explaining the techniques of modern majolica production. We are indebted to Robert Johnson (Department of Mineral Sciences, Smithsonian Institution) and Paul Bourqui (Institut für Mineralogie und Petrographie, Freiburg, Switzerland) for preparing the thin sections. Our geological knowledge of Mexico was greatly improved through discussions with Max Suter and Fernando Ortega (Istituto de Geologia, Universidad, Mexico City). Additional information was provided by Costanza Vega-Sosa (Museo Nacional de Antropología, Mexico City) and Isabel Kelly (Mexico City). We thank Giulio Galetti and Odette Marbacher (Institut für Mineralogie und Petrographie, Freiburg, Switzerland) for chemical analyses of the clays and Jean Charrière (of the same institute) for the drawings. Further analyses of the clays are underway. Martha Goodway and Timothy Padfield (Smithsonian Institution, Conservation Analytical Laboratory) were of great help in all photographic and laboratory problems. The research was supported by the Conservation Analytical Laboratory, Smithsonian Institution.

Appendix A

Description of Ancient Ceramic Samples

Sample Number	Majolica Type and Source	Comments
SA 1-20	Columbia Plain (10,14) excavated at	The place of manufacture is probably Seville (Triana), Spain (7, 14). Chemical data in Ref. 1.
SA 32-41	Convento de San Francisco, Juandolio,	
SA 50-59	and La Vega Vieja, Dominican Republic;	
SB 59-68	and Jerez, Spain.	
SB 86-SB 99		
SC 1, 8-9		
SA 21-23	Yayal Blue on White (10, 14) excavated	As above.
SA 31	at Convento de San Francisco and	
SA 46	Juandolio, Dominican Republic; Nueva	
SA 60-64	Cadiz, Venezuela; and Jerez, Spain.	
SB 46-57		
SB 69-78,		
SB 80,		
SB 82-85		
SC 2-7		
SA 24-26	Isabela Polychrome (10, 14) excavated	
SA 42-45	at Juandolio and Isabela, Dominican	
SA 47-49	Republic; and Nueva Cadiz, Venezuela.	

Description of Ancient Ceramic Samples—Continued

<i>Sample Number</i>	<i>Majolica Type and Source</i>	<i>Comments</i>
SA 27–30	Caparra Blue (10, 14) excavated at Nueva Cadiz, Venezuela. This type has been identified as a plain version of Guadalquivir Ware (14).	As above.
SB 33	This sherd, which came from the subway excavations in Mexico City, has been identified as a copy of Ligurian Blue on Blue made in Spain (14).	The place of manufacture is probably Spain (14). Chemical data in Ref. 1.
SC 10	Sevilla White (14) excavated beneath the Metropolitan Cathedral in Mexico City.	The place of manufacture is probably Spain (14). Chemical data in Appendix C.
SC 19		
SC 26–27		
SC 86–91	Columbia Gun Metal (14) excavated beneath the Metropolitan Cathedral in Mexico City.	As above.
SB 30–31	These sherds came from the subway excavations in Mexico City.	The place of manufacture may be Genoa, Italy (10). Chemical data in Ref. 1.
SA 65–67 SC 36–54	Fig Springs Polychrome (10); San Juan Polychrome (14) excavated from subway and Metropolitan Cathedral, Mexico City.	The place of manufacture is probably Mexico and may be Mexico City (14). Chemical data in Ref. 1 and Appendix C.
SA 68–70 SB 36–37	Los Angeles Polychrome (10) excavated from subway, Mexico City.	The place of manufacture is probably Mexico and may be Mexico City (14). Chemical data in Ref. 1.
SA 71–73	San Luis Blue on White (10, 14) excavated from subway, Mexico City.	As above.
SA 82–83	San Luis Polychrome (10, 14) excavated from subway, Mexico City.	As above.
SA 86–88	Aucilla Polychrome (10) excavated from subway, Mexico City.	As above.

Continued on next page.

Description of Ancient Ceramic Samples—Continued

<i>Sample Number</i>	<i>Majolica Type and Source</i>	<i>Comments</i>
SB 26–27 SC 16	Copy of Columbia Plain (14) excavated from subway and Metropolitan Cathedral, Mexico City.	The place of manufacture is probably Mexico and may be Mexico City (14). Chemical data for SB 26 in Ref. 1 and for SC 16 in Appendix C.
SB 32	Caparra Blue (7, 14) excavated from subway, Mexico City.	Chemical data in Ref. 1.
SC 11–15 SC 17–18 SC 20–25 SC 28–35 SC 56–57	Mexico City White (14) excavated from Metropolitan Cathedral, Mexico City.	The place of manufacture is probably Mexico and may be Mexico City (14). Chemical data in Appendix C.
SC 55 SC 58–85 SD 1–2	Tlalpan White, Valle Ware (14) excavated from Metropolitan Cathedral, Mexico City.	As above.
SC 92–97 SD 3–4	Romita Sgraffito (14) excavated from Metropolitan Cathedral, Mexico City.	As above.
SA 74–77	Puebla Polychrome (7, 14) excavated from subway, Mexico City.	The place of manufacture is probably Puebla, Mexico (7, 14). Chemical data in Ref. 1.
SA 78–81	Abo Polychrome (7, 14) excavated from subway, Mexico City.	As above.
SA 84–85	Castillo Polychrome (7, 14) excavated from subway, Mexico City.	As above.
SA 89–92	Puebla Blue on White (7, 14) excavated from subway, Mexico City.	As above.
SA 93–94	San Elizario Polychrome (21) excavated from subway, Mexico City.	As above.
SA 95–96	San Agustin Blue on White (7, 14) excavated from subway, Mexico City.	As above.
SA 97–98	Unnamed type, excavated from subway, Mexico City.	As above.
SA 99 SB 1	Huejotzingo Blue on White (7, 14) excavated from subway, Mexico City.	As above.

Description of Ancient Ceramic Samples—Continued

<i>Sample Number</i>	<i>Majolica Type and Source</i>	<i>Comments</i>
SB 20	Excavated from subway, Mexico City.	As above.
SB 38–39	Excavated at Santiago de los Caballeros (Antigua) Guatemala.	Chemical data in Ref. 1.
SB 40–42	Excavated at Panama Viejo.	As above.
SB 43–44	Excavated at Cuzco, Peru.	As above.
SB 45	Excavated at Quito, Ecuador.	As above.

NOTE: Aztec sherds from the Metropolitan Cathedral excavations in Mexico City were studied. They are sample numbers SC 98 and 99.

Appendix B

Description of Clay and Modern Majolica Samples

<i>Sample Number</i>	<i>Type (Source)</i>	<i>Factory</i>
SD 27	Black clay (Cerro de los Fuentes, Loreto Hill, Puebla).	La Trinidad/Puebla
SD 28	White clay (Totimehuacan).	As above.
SD 29	Modern Majolica, first firing.	As above.
SD 30	As above.	As above.
SD 31	As above.	As above.
SD 32	As above.	As above.
SD 33	As above.	As above.
SD 34	As above.	As above.
SD 35	As above.	As above.
SD 36	As above.	As above.
SD 37	As above.	As above.
SD 38	Black clay (soil of the factory).	Santa Maria/Puebla.
SD 39	White clay (St. Thomas, Chiautla).	As above.
SD 47	Gray clay (old excavations for brick production on the road from Puebla to Cholula).	As above.
SD 48	Brown clay (old excavations for brick production on the road from Puebla to Cholula).	As above.

Appendix C

Concentrations of Oxides Obtained by Direct

<i>Specimen Number</i>	<i>SiO₂ (%)</i>	<i>Al₂O₃ (%)</i>	<i>MgO (%)</i>	<i>P₂O₅ (%)</i>	<i>CaO (%)</i>	<i>Na₂O (%)</i>	<i>K₂O (%)</i>	<i>BaO (%)</i>	<i>MnO (%)</i>	<i>Fe₂O₃ (%)</i>
<i>Majolica from Puebla</i>										
SA 74	45	18.6	8.30	0.120	19.2	2.00	0.78	0.060	0.075	4.5
SA 76	45	21.9	3.20	0.120	19.9	1.90	2.00	0.055	0.080	4.5
SA 77	49	16.5	2.35	0.120	22.9	2.00	1.10	0.100	0.060	4.5
<i>Castillo</i>										
SA 84	51	15.1	2.36	0.150	23.0	1.20	1.25	0.050	0.050	3.9
<i>San Elizario</i>										
SA 94	45	21.7	1.79	0.100	22.0	1.80	1.00	0.060	0.065	4.7
<i>Mexico City</i>										
SC 11	55	16.4	6.6	0.106	12.2	1.93	1.61	0.054	0.027	3.3
SC 12	47	13.2	3.9	0.114	26.5	1.76	1.60	0.058	0.055	3.8
SC 13	52	11.3	7.1	0.104	21.1	1.96	1.26	0.046	0.040	3.1
SC 14	50	15.2	5.1	0.100	19.4	2.34	2.06	0.058	0.056	4.1
SC 15	48	14.6	7.9	0.107	20.4	1.80	0.72	0.045	0.055	4.0
SC 17	47	13.8	8.8	0.115	22.9	1.14	0.98	0.050	0.039	3.0
SC 18	50	14.9	4.4	0.108	20.3	1.87	2.04	0.060	0.046	3.9
SC 20	56	15.5	5.1	0.246	14.1	3.28	1.88	0.061	0.030	4.9
SC 21	58	13.0	6.3	0.305	15.0	1.57	1.34	0.060	0.037	4.5
SC 22	56	14.0	4.0	0.272	18.2	1.80	1.44	0.058	0.042	4.3
SC 23	45	19.0	8.1	0.382	19.0	2.34	1.67	0.087	0.063	4.3
SC 24	51	12.8	8.9	0.284	21.4	1.63	1.38	0.084	0.054	3.0
SC 25	54	14.2	5.9	0.330	16.0	2.50	1.61	0.086	0.055	5.1
SC 28	56	15.0	5.1	0.318	14.0	2.90	2.14	0.075	0.055	3.8
SC 29	49	15.0	5.8	0.200	21.0	1.72	1.51	0.069	0.050	4.3
SC 30	52	15.8	5.3	0.385	18.5	2.20	1.71	0.076	0.052	4.4
SC 31	52	14.0	3.7	0.315	22.0	2.07	1.90	0.072	0.043	3.7
SC 33	53	14.4	6.0	0.245	16.1	2.08	1.21	0.067	0.083	5.2
SC 34	54	14.0	4.7	0.300	16.1	3.20	1.70	0.072	0.092	4.4
SC 35	49	14.0	4.7	0.302	24.0	2.15	1.54	0.082	0.072	3.8
SC 56	55	13.5	2.7	0.174	19.4	1.56	1.71	0.067	0.109	4.0
SC 57	54	13.3	2.9	0.164	19.0	1.69	2.36	0.064	0.052	4.7
<i>Mexico City Copies</i>										
SC 16	47	13.0	5.5	0.107	25.5	1.26	1.46	0.059	0.051	3.9
SC 32	50	15.0	6.0	0.290	19.2	2.11	1.81	0.069	0.050	5.4
<i>Fig Springs Polychrome</i>										
SA 66	50	17.1	1.50	0.130	21.6	1.50	1.50	0.045	0.042	5.0
SA 67	46	19.6	2.70	0.100	23.0	1.40	1.70	0.050	0.050	3.5
SC 36	55	15.7	1.84	0.307	18.5	1.74	1.14	0.060	0.050	5.1
SC 37	55	16.0	1.80	0.301	17.7	1.89	1.21	0.062	0.056	5.0
SC 38	54	16.1	2.18	0.245	18.6	2.20	1.41	0.067	0.050	5.0

Current Plasma-Optical Emission Spectroscopy

TiO_2 (%)	Rb_2O (ppm)	La_2O_3 (ppm)	Cs_2O (ppm)	Sc_2O_3 (ppm)	CeO_2 (ppm)	Eu_2O_3 (ppm)	HfO_2 (ppm)	ThO_2 (ppm)	Cr_2O_3 (ppm)	CoO (ppm)
Excavations in Mexico City										
<i>Polychrome</i>										
1.00	43	24.2	3.1	15.8	50	1.47	5.6	5.3	98	15.5
1.00	47	23.4	2.1	22.3	47	1.34	5.7	5.4	107	15.7
0.87	45	21.5	4.4	21.2	45	1.37	4.9	5.2	130	21.0
<i>Polychrome</i>										
0.87	50	17.0	6.1	15.7	33	1.00	3.5	5.0	97	11.4
<i>Polychrome</i>										
1.00	52	21.4	3.5	19.0	40	1.40	4.1	5.3	133	16.0
<i>White</i>										
1.03	59	36	4.0	19.5	57	1.68	4.3	8.3	81	8.8
0.86	51	26	5.3	15.3	42	1.16	4.1	6.2	71	12.0
0.81	44	18	2.0	11.3	27	0.82	3.4	4.9	62	7.4
0.92	79	30	5.5	17.4	45	1.29	4.4	6.5	76	12.7
0.96	50	23	4.1	15.9	37	1.20	3.9	5.2	87	12.7
0.92	42	17	3.0	11.3	27	0.86	2.9	3.7	60	10.3
1.03	73	28	6.3	16.0	41	1.28	4.4	6.5	78	13.7
0.30	65	23	3.5	12.2	36	0.99	4.1	6.4	61	10.0
0.30	68	26	5.4	12.5	40	1.09	4.3	6.6	75	14.2
0.30	68	24	4.6	14.4	41	1.12	4.2	6.1	104	17.1
0.40	73	24	5.4	12.3	42	1.07	4.4	5.9	94	14.5
0.30	74	25	4.5	12.7	39	1.15	4.5	6.0	92	14.5
0.47	60	24	4.7	12.7	35	1.22	4.6	6.4	102	7.0
0.31	62	22	4.0	12.7	36	1.20	4.9	6.1	114	10.3
0.23	62	25	3.5	12.9	38	1.08	4.3	5.9	87	20.4
0.33	63	25	4.8	13.2	40	1.14	4.5	5.8	103	19.7
0.33	63	23	4.9	12.8	41	1.17	4.2	5.9	90	20.2
0.37	63	24	4.7	13.2	42	1.15	4.2	5.9	90	17.2
0.38	61	22	3.7	12.9	38	1.18	4.6	6.2	90	17.7
0.40	63	24	4.8	13.2	41	1.09	4.6	5.9	96	18.0
0.88	81	28	7.0	18.1	56	1.31	4.4	6.7	101	12.4
0.96	84	31	6.8	17.8	58	1.42	4.8	8.4	85	13.8
<i>of Columbia Plain</i>										
0.87	41	41	4.0	19.0	53	1.17	7.5	1.3	68	12.5
0.36	63	24	4.7	13.2	41	1.15	4.2	5.9	115	15.3
<i>(San Juan Polychrome)</i>										
1.02	54	27.1	5.0	21.3	40	1.20	6.2	5.4	130	12.0
0.92	75	18.5	3.8	16.7	28	1.00	4.6	5.1	90	40.0
0.42	70	24	4.9	12.8	39	1.15	4.1	5.9	96	16.6
0.44	68	23	4.6	12.5	40	1.17	4.1	5.9	95	10.4
0.54	69	24	4.8	13.0	41	1.09	4.4	5.9	105	10.3

Continued on next page.

Concentrations of Oxides Obtained by Direct

<i>Specimen Number</i>	<i>SiO₂ (%)</i>	<i>Al₂O₃ (%)</i>	<i>MgO (%)</i>	<i>P₂O₅ (%)</i>	<i>CaO (%)</i>	<i>Na₂O (%)</i>	<i>K₂O (%)</i>	<i>BaO (%)</i>	<i>MnO (%)</i>	<i>Fe₂O₃ (%)</i>
Majolica from										
<i>Fig Springs Polychrome</i>										
SC 39	55	18.0	1.95	0.200	16.0	1.96	1.51	0.070	0.035	5.1
SC 40	57	14.9	2.50	0.300	15.9	1.73	1.27	0.055	0.041	5.1
SC 41	52	15.1	3.72	0.304	20.7	1.57	1.51	0.057	0.045	5.1
SC 42	51	16.0	3.05	0.306	20.6	2.10	1.56	0.069	0.047	5.1
SC 43	53	16.0	2.67	0.295	19.0	2.00	1.43	0.068	0.040	5.4
SC 44	55	16.3	2.00	0.163	18.0	1.70	1.44	0.054	0.050	3.9
SC 45	47	16.3	3.37	0.172	22.4	1.55	2.00	0.065	0.091	5.6
SC 46	50	17.5	6.24	0.182	16.0	2.06	1.90	0.070	0.045	4.1
SC 47	50	17.5	3.52	0.172	17.0	1.50	1.67	0.071	0.087	6.4
SC 48	50	15.4	2.71	0.165	19.3	1.86	2.78	0.066	0.050	5.6
SC 49	50	18.0	2.44	0.172	19.5	1.59	2.48	0.082	0.049	5.2
SC 50	53	13.3	3.10	0.179	20.9	1.45	1.70	0.064	0.091	4.5
SC 51	56	13.5	3.55	0.183	16.0	1.30	1.92	0.056	0.091	5.4
SC 52	51	17.0	6.20	0.177	16.1	2.02	2.02	0.062	0.038	4.0
<i>Sevilla</i>										
SC 10	45	16.0	6.2	0.124	22.0	0.91	2.59	0.050	0.056	4.1
SC 19	46	15.8	4.1	0.107	22.7	0.95	3.42	0.071	0.040	4.3
SC 26	49	16.4	5.7	0.206	18.3	1.00	3.00	0.073	0.055	5.4
SC 27	51	15.9	5.0	0.198	17.9	1.26	2.59	0.070	0.050	4.6
<i>Columbia</i>										
SC 86	55	12.7	3.8	0.168	16.5	1.20	2.36	0.076	0.056	5.7
SC 87	39	13.0	4.3	0.156	32.5	1.00	2.17	0.076	0.076	5.3
SC 88	52	12.0	4.1	0.160	20.5	1.10	2.00	0.082	0.060	5.8
SC 89	54	11.8	4.0	0.169	19.6	1.19	2.10	0.054	0.048	4.9
SC 91	54	11.7	4.0	0.204	20.0	0.91	2.48	0.061	0.051	5.0
<i>Valle</i>										
SC 55	64	20.0	1.88	0.185	4.1	2.07	1.72	0.007	0.081	4.6
SC 58	64	18.2	1.88	0.178	4.0	2.49	1.91	0.068	0.085	5.2
SC 59	62	20.3	2.32	0.160	4.0	2.34	1.83	0.067	0.098	5.2
SC 60	62	19.0	2.25	0.157	3.7	2.71	1.62	0.074	0.074	6.0
SC 61	52	18.5	2.11	0.143	17.0	1.92	1.87	0.072	0.008	4.8
SC 62	56	24.0	2.40	0.162	3.7	2.18	1.13	0.076	0.155	8.0
SC 63	61	22.0	1.97	0.159	3.9	2.50	1.73	0.064	0.113	4.8
SC 64	61	23.0	1.82	0.172	3.6	2.39	1.70	0.074	0.090	4.7
SC 66	58	21.0	1.89	0.148	7.6	2.31	2.06	0.077	0.090	4.8
SC 67	59	23.0	1.85	0.143	4.4	2.53	2.22	0.084	0.120	5.1
SC 68	57	23.0	1.78	0.154	7.7	2.21	1.84	0.080	0.100	4.7
SC 69	64	17.4	2.4	0.191	5.0	2.58	1.65	0.078	0.065	4.9
SC 70	62	17.5	2.4	0.212	5.4	2.78	1.70	0.072	0.077	5.7
SC 71	65	17.0	2.3	0.200	4.5	2.68	1.59	0.070	0.051	4.8
SC 72	60	20.8	2.7	0.173	4.0	2.87	1.63	0.074	0.061	5.3
SC 73	63	18.0	2.2	0.183	5.4	2.40	1.59	0.076	0.060	4.8
SC 74	64	17.0	2.4	0.187	5.2	2.52	1.15	0.070	0.070	5.5
SC 75	64	17.0	2.5	0.182	4.1	2.86	1.54	0.076	0.063	5.4
SC 76	63	17.5	2.5	0.232	4.9	2.77	1.69	0.082	0.069	5.2
SC 77	63	17.8	2.4	0.176	5.0	2.49	1.67	0.082	0.072	5.2

Current Plasma-Optical Emission Spectroscopy—Continued

TiO ₂ (%)	Rb ₂ O (ppm)	La ₂ O ₃ (ppm)	Cs ₂ O (ppm)	Sc ₂ O ₃ (ppm)	CeO ₂ (ppm)	Eu ₂ O ₃ (ppm)	HfO ₂ (ppm)	ThO ₂ (ppm)	Cr ₂ O ₃ (ppm)	CoO (ppm)
Excavations in Mexico City—Continued (San Juan Polychrome)—Continued										
0.40	62	24	5.0	12.5	41	1.13	4.5	5.9	90	10.3
0.65	71	24	4.7	12.4	40	0.99	4.2	6.0	105	14.2
0.30	63	25	5.1	12.3	40	1.02	4.1	6.2	110	10.5
0.31	71	24	4.7	13.0	41	1.07	4.6	6.0	111	10.6
0.30	71	23	4.8	12.5	40	1.09	4.0	6.0	115	14.0
0.97	60	35	4.3	13.0	56	1.11	4.2	8.7	130	17.1
1.06	77	34	7.1	14.3	55	1.70	4.1	8.6	116	14.5
0.98	73	38	5.9	12.2	56	1.20	4.0	8.6	93	12.7
1.04	82	33	7.8	16.2	58	1.25	4.8	8.0	112	12.5
1.02	80	39	7.4	14.0	58	1.47	4.3	8.5	132	15.0
0.95	78	34	4.6	13.5	57	1.23	4.3	8.6	98	12.6
1.05	81	39	7.4	14.0	57	1.69	3.7	8.4	130	12.3
1.42	83	35	4.5	13.0	56	1.12	4.4	8.1	93	13.7
0.95	83	29	7.4	13.8	56	1.48	4.0	8.5	105	13.0
White										
0.98	147	60	10.9	18.3	105	1.46	8.1	21.9	69	13.6
0.97	170	53	11.7	18.6	161	1.45	6.7	19.4	72	13.1
0.41	67	35	4.8	17.0	57	1.19	5.3	10.1	95	11.0
0.31	68	35	4.9	17.2	57	1.20	5.1	9.8	98	9.5
Gun Metal										
1.30	63	44	5.3	18.0	77	1.27	4.7	10.8	95	14.5
1.29	60	48	5.1	16.0	76	1.37	5.8	14.0	135	13.2
1.37	67	41	4.3	17.1	80	1.60	6.9	10.3	92	12.7
1.35	65	40	7.0	17.4	73	1.18	6.0	10.4	94	15.7
1.27	50	40	5.1	16.8	71	1.31	6.1	10.8	82	16.2
Ware										
0.91	60	34	5.1	13.0	58	1.24	4.4	8.5	123	13.8
1.02	84	28	7.7	12.9	58	1.35	4.0	8.4	70	13.0
1.00	83	33	7.3	19.4	57	1.40	4.0	7.8	122	13.0
1.07	81	27	7.2	13.5	57	1.27	4.0	7.8	79	14.5
1.02	70	30	6.4	16.3	54	1.32	3.9	6.7	79	15.0
1.04	84	34	7.2	13.3	51	1.35	4.0	6.4	80	15.3
1.00	67	39	7.8	13.9	55	1.27	4.1	6.8	80	17.0
0.96	72	40	7.7	13.7	58	1.52	4.0	6.4	75	12.2
1.00	81	39	6.7	13.4	58	1.25	3.9	5.8	92	12.3
1.06	81	31	7.4	13.6	55	1.30	4.0	6.9	92	15.8
1.02	81	37	6.1	13.1	54	1.21	3.8	6.0	88	15.5
1.23	71	23	5.6	18.5	38	1.20	6.0	7.0	92	13.0
1.42	70	23	5.2	17.5	37	1.08	6.1	6.5	81	15.5
1.36	57	24	5.2	16.7	38	1.02	6.1	5.9	81	16.5
1.42	56	24	5.0	16.8	38	1.11	6.2	6.9	88	18.0
1.13	71	23	4.8	19.9	40	1.38	6.4	7.0	88	16.0
1.28	62	24	5.0	18.2	39	1.17	6.0	6.5	71	12.0
1.36	63	24	4.8	17.5	40	1.21	6.1	6.1	84	16.3
1.39	60	32	4.7	17.8	42	1.28	6.3	8.9	84	17.0
1.42	59	24	4.8	16.2	43	1.12	6.0	6.4	80	17.3

Continued on next page.

Concentrations of Oxides Obtained by Direct

<i>Specimen Number</i>	<i>SiO₂ (%)</i>	<i>Al₂O₃ (%)</i>	<i>MgO (%)</i>	<i>P₂O₅ (%)</i>	<i>CaO (%)</i>	<i>Na₂O (%)</i>	<i>K₂O (%)</i>	<i>BaO (%)</i>	<i>MnO (%)</i>	<i>Fe₂O₃ (%)</i>
Majolica from Valle										
SC 78	63	17.8	2.5	0.153	4.9	2.53	1.39	0.068	0.051	5.4
SC 79	62	17.1	3.0	0.200	5.4	2.42	1.57	0.082	0.072	5.5
SC 81	61	17.9	2.7	0.195	5.4	2.82	1.45	0.071	0.077	5.7
SC 82	64	16.8	2.4	0.205	4.9	2.82	1.57	0.066	0.036	5.0
SC 84	62	18.1	2.4	0.188	3.1	1.47	1.08	0.054	0.127	9.4
SC 85	60	18.0	2.7	0.204	4.5	2.55	1.41	0.072	0.092	8.0
SD 1	63	18.9	1.9	0.327	5.1	2.81	1.35	0.073	0.103	4.9
SD 2	53	18.9	1.9	0.256	14.4	3.06	1.47	0.068	0.106	5.1
Romita										
SC 92	64	18.2	1.16	0.196	3.2	1.12	1.09	0.058	0.104	8.5
SC 93	63	19.7	1.00	0.179	1.6	1.16	1.00	0.067	0.086	9.6
SC 94	65	18.0	1.08	0.195	2.9	1.20	1.07	0.061	0.082	8.2
SD 2	57	22.0	0.90	0.301	2.1	2.56	1.37	0.072	0.116	11.5
SD 4	65	21.3	0.82	0.315	1.2	1.87	1.34	0.074	0.126	5.7
Majolica from Yayal										
SC 2	49	15.9	3.1	0.100	23	1.00	1.50	0.050	0.085	5.5
SC 3	52	13.0	3.8	0.100	22	0.50	2.25	0.060	0.060	4.5
SC 4	54	12.4	4.5	0.130	20	0.80	2.05	0.090	0.070	5.0
SC 5	52	13.0	4.3	0.110	22	0.60	1.70	0.065	0.060	5.0
SC 6	48	16.3	2.4	0.110	23	1.00	1.70	0.092	0.062	5.5
SC 7	49	15.7	3.3	0.120	23	0.65	2.07	0.100	0.065	5.0
Columbia										
SC 8	52	13.8	2.1	0.133	23	0.65	2.10	0.080	0.070	4.5
SC 9	52	13.5	2.9	0.150	23	0.70	1.75	0.065	0.050	4.8
Aztec Sherds from Metropolitan										
SC 98	63	19.3	1.8	0.337	4.0	2.81	1.31	0.072	0.102	5.3
SC 99	63	19.3	1.9	0.346	4.5	2.78	1.28	0.068	0.098	5.0
Modern Majolica Ceramics										
SD 29	57	15.8	2.04	0.23	16.0	1.95	1.08	0.037	0.053	4.6
SD 30	56	16.1	2.01	0.23	15.7	2.06	1.16	0.038	0.061	4.6
SD 31	56	16.3	2.11	0.23	16.2	1.89	1.08	0.039	0.064	4.8
SD 32	57	15.8	2.09	0.20	16.0	1.84	1.02	0.040	0.064	4.8
SD 33	56	16.0	2.08	0.23	15.7	2.11	1.15	0.035	0.065	4.6
SD 34	56	15.7	2.11	0.23	16.0	1.94	1.33	0.039	0.057	4.9
SD 35	51	18.5	2.49	0.27	16.0	2.04	1.32	0.041	0.078	6.4
SD 36	52	18.2	2.36	0.29	15.7	2.02	1.27	0.042	0.070	6.3
SD 37	51	19.2	2.41	0.28	16.0	2.07	1.22	0.041	0.078	6.1

Current Plasma-Optical Emission Spectroscopy—Continued

<i>TiO</i> ₂ (%)	<i>Rb</i> ₂ <i>O</i> (ppm)	<i>La</i> ₂ <i>O</i> ₃ (ppm)	<i>Cs</i> ₂ <i>O</i> (ppm)	<i>Sc</i> ₂ <i>O</i> ₃ (ppm)	<i>CeO</i> ₂ (ppm)	<i>Eu</i> ₂ <i>O</i> ₃ (ppm)	<i>HfO</i> ₂ (ppm)	<i>ThO</i> ₂ (ppm)	<i>Cr</i> ₂ <i>O</i> ₃ (ppm)	<i>CoO</i> (ppm)
--------------------------------	--	---	--	---	----------------------------------	---	----------------------------------	----------------------------------	---	---------------------

Excavations in Mexico City—Continued*Ware—Continued*

1.37	63	24	5.3	17.7	42	1.41	6.3	6.9	81	16.7
1.40	61	26	5.3	16.0	42	1.35	6.0	7.0	86	18.2
1.42	60	24	4.8	20.6	38	1.42	6.0	6.8	81	18.0
1.36	58	24	4.9	18.0	40	1.37	6.3	6.2	79	17.0
1.36	62	22	5.7	17.6	39	1.45	6.7	6.8	82	12.7
1.39	65	23	5.9	17.3	40	1.05	5.0	6.3	90	18.0
0.94	73	29	5.5	16.0	43	1.35	5.4	6.5	91	14.5
0.83	74	28	5.1	16.5	44	1.30	5.3	6.9	91	14.3

Sgraffito

1.41	60	22.0	4.8	17.5	38	1.00	5.9	6.2	75	12.0
1.40	69	17.5	5.0	17.5	41	1.28	6.1	6.1	87	15.0
1.22	67	17.5	4.6	16.7	38	1.12	6.1	5.9	66	16.2
0.93	75	29.5	4.9	15.8	43	1.27	4.3	6.2	90	13.6
0.93	72	29.8	4.8	15.7	45	1.30	5.0	6.0	91	13.8

Jerez (Triana), Spain*Blue-on-White*

1.00	73	39	4.3	21.3	90	1.56	6.8	12.2	120	17.4
1.20	90	41	5.9	18.8	80	1.41	4.9	11.0	106	15.0
0.88	105	45	7.8	20.0	80	1.44	6.1	12.1	130	15.3
0.68	99	44	7.7	20.3	80	1.45	5.8	11.6	133	13.6
1.20	79	44	4.7	20.3	75	1.40	5.3	10.2	188	15.2
1.00	84	50	5.0	15.7	90	1.52	5.7	12.0	120	19.3

Plain

1.10	100	44	6.1	20.0	78	1.61	5.1	11.0	115	16.0
1.00	101	44	8.1	19.3	78	1.45	5.3	11.0	107	16.0

Cathedral, Mexico City

0.91	77	29	5.1	15.8	42	1.33	5.1	6.3	90	14.2
0.93	72	29	5.2	15.5	43	1.40	4.3	5.9	92	13.8

from Puebla, Mexico

0.82	67	25	4.1	17.6	33	1.10	5.8	6.6	81	17.8
0.81	61	23	3.8	17.8	33	1.17	6.0	7.0	81	16.4
0.82	60	24	4.1	18.0	31	1.20	5.9	5.8	81	16.5
0.79	60	24	3.9	18.7	35	1.16	5.9	6.9	73	17.0
0.77	62	24	4.1	18.1	34	1.14	6.0	6.5	68	16.0
0.76	59	26	4.1	18.2	32	1.21	6.0	6.7	68	17.7
1.06	57	30	3.9	18.3	33	1.17	6.2	6.5	90	16.3
1.06	87	46	4.0	18.8	57	1.19	6.6	9.2	86	17.4
1.06	62	30	4.1	19.0	36	1.14	6.4	6.7	86	16.9

Literature Cited

1. Olin, J. S.; Harbottle, G.; Sayre, E. V. In "Archaeological Chemistry II"; Carter, G. F., Ed.; ADVANCES IN CHEMISTRY SERIES No. 171; American Chemical Society: Washington, D.C., 1978; pp. 200–229.
2. Olin, J. S.; Sayre, E. V. *Bull. Am. Inst. Conserv.* **1975**, *15*, 57–62.
3. Demians d'Archimbaud, G.; Lemoine, C. *Colloq. Int. C. N. R. S.* **1978**, 359–72.
4. Bastenaire-Daudenart, F. "L'art de fabriquer la Faience"; Dessain et Tolra: Paris, 1828.
5. Brongniart, A. "Traite des Arts Ceramiques"; Dessain et Tolra: Paris, 1844.
6. Picon, M.; Demians d'Archimbaud, G. *Colloq. Int. C. N. R. S.* **1978**, 125–35.
7. Vallauri, L.; Vichy, M.; Broecker, R.; Salvaire, M. C. *Colloq. Int. C.N.R.S.* **1978**, 413–27.
8. Vaz, J. E.; Cruxent, J. M. "Gamma-ray induced thermoluminescence of majolica pottery as an indicator of its provenience"
9. Vaz, J. E.; Cruxent, J. M. *Am. Antiq.* **1975**, *40*(1).
10. Goggin, J. M. "Spanish Majolica in the New World, Types of the Sixteenth to Eighteenth Centuries"; Yale Univ. Publications in Anthropology No. 72, Yale Univ. Press: New Haven, Conn., 1968.
11. Lopez Cervantes, G. *Bol. INAH* **1976**, *18*, 33–38.
12. Lopez Cervantes, G. *Coleccion Cientifica Arqueologia* **1976**, *38*, 7–67.
13. Lister, F. C.; Lister, R. H. *El Palacio* **1975**, *81*(2), 25–48.
14. Lister, F. C.; Lister, R. H. "Sixteenth Century Majolica Pottery in the Valley of Mexico"; Anthropological Papers of the University of Arizona No. 39; Univ. Ariz. Press: Tucson, Ariz., 1982.
15. Abascal, M. R.; Harbottle, G.; Sayre, E. V. In "Archaeological Chemistry"; Beck, C. W., Ed.; ADVANCES IN CHEMISTRY SERIES No. 138; American Chemical Society: Washington, D.C., 1974, pp. 81–99.
16. Zander, A. T. *Ind. Res./Dev.* **1982**, February, 146–50.
17. Johnson Matthey Chemical Ltd. "Spectoflux (prefused Borate Fluxes)"; Manuf. Lit., JMC Publication 2765.
18. Miller, W.; DeMenna, G. *Spex Speaker* **1980**, September, 1–4.
19. Spectrametrics, Inc. "Plasma Emission Spectrometers for Atomic Analysis"; Manuf. Lit., 1980, pp. 1–16.
20. Spectrametrics, Inc. "Handbook of Spectral Line Characteristics for DC Plasma Echelle Systems"; Andover, Mass., 1982.
21. Lister, F. C., personal communication.
22. Freudenberg, W. "Geologie von Mexico"; Borntraeger: Leipzig, 1921.
23. von Erffa, A.; Hilger, W.; Knoblich, K.; Weyl, R. *Das Mexiko-Projekt der Deutschen Forschungsgemeinschaft* **1977**, *XI*.
24. von Erffa, A.; Hilger, W. *Das Mexiko-Projekt der Deutschen Forschungsgemeinschaft* **1975/1977**, *XI*.
25. Guenther, E. W. *Schr. Naturwiss. Ver. Schleswig-Holstein* **1972**, *42*, 21–34.
26. Guenther, E. W. *Das Mexiko-Projekt der Deutschen Forschungsgemeinschaft* **1973**, *VI*, 1–20.
27. Gunn, B. M.; Mooser, F. *Bull. Volcanol.* **1971**, *34*, 577–616.
28. Mooser, F. *Congr. Int. 22 Sess. Sec. 1*, Mexico D. F., **1957**, *2*, 337–48.
29. Mooser, F. "Informe sobre la Geologia de la cuenca del Valle de Mexico y

- zonas colindantes”; Comisión hidrológica de la cuenca del Valle de México, Secretaría de Recursos Hidráulicos: México, D.F., 1961.
30. Mooser, F.; Seele, E. *Geofisica Int.* **1972**, *12*, 67.
 31. Negendank, J. F. W. *N. Jb. Miner. Abh.* **1972**, *116*, 308–20.
 32. Negendank, J. F. W. *Bull. Volcanol.* **1973**, *37*, 292–303.
 33. Negendank, J. F. W. *Muenstersche Forsch. Geol. Palaeontol.* **1973**, *31/32*, 289–302.
 34. Weyl, R. *Natur und Museum* **1974**, *104*, 137–52.
 35. Weyl, R. *Bol. Asoc. Mex. Geol. Pet.* **1974**, *25*, 375–424.
 36. Caiger-Smith, A. “Tin-glazed pottery in Europe and the Islamic World”; Faber: London, 1973.
 37. Catala, E. “Mexican Folk Ceramics”; Blume: Barcelona, 1975.
 38. Bunde, H. *Das Mexiko-Projekt der Deutschen Forschungsgemeinschaft* **1973**, *VI*, 21–93.
 39. Aeppli, H.; Schoenhals, E. *Das Mexiko-Projekt der Deutschen Forschungsgemeinschaft* **1975**, *VIII*.
 40. Seele, E. *Das Mexiko-Projekt der Deutschen Forschungsgemeinschaft* **1968**, *I*, 194–208.
 41. Grupo financiero Comermex. “Talavera de Puebla”; Comermex: Mexico City, Mexico, 1973.
 42. Carta Geologica de Mexico, Serie de 1:1000,000, Hoja Guernavaca, 14Q–h (8), Universidad Nacional Autonoma de Mexico, Instituto de Geologia, 1965.
 43. Carta Geologica de Mexico, 1:2,000,000, Mexico 1976.
 44. Carta Geologica de Mexico, Serie de 1:100,000, Hoja Pachuca, 14Q–e (11), Universidad Nacional Autonoma de Mexico, Instituto de Geologia, 1962.
 45. Segerstrom, K. “Geology of south central Hidalgo and northeastern Mexico, Mexico”; Bulletin 1104–C; U.S. Geological Survey: Washington, D.C., 1962.
 46. Maggetti, M. *Br. Mus. Occas. Pap.* **1981**, *19*, 33–49.
 47. Maggetti, M. In “Archaeological Ceramics”; Olin, J. S.; Franklin, A. D., Eds.; Smithsonian Institution: Washington, D.C., 1982; pp. 121–33.
 48. Kuepfer, T.; Maggetti, M. *Schweiz. Mineral. Petrogr. Mitt.* **1978**, *58*, 189–212.
 49. Heimann, R.; Maggetti, M. *Br. Mus. Occas. Pap.* **1981**, *19*, 163–67.
 50. Maggetti, M.; Heimann, R. *Schweiz. Mineral. Petrogr. Mitt.* **1979**, *59*(3), 413–17.
 51. Peters, T.; Jenni, J. P. *Beitr. Geol. Schweiz, Geotechn. Serie* **1973**, *50*, 1–59.
 52. Westley, H. Conservation Analytical Laboratory Reports 2700 and 2701; The Smithsonian Institution: Washington, D.C.

RECEIVED for review November 23, 1982. ACCEPTED for publication March 25, 1983.

Provenance Determination of Fine Orange Maya Ceramic Figurines by Flame Atomic Absorption Spectrometry

A Preliminary Study of Objects from Jaina (Campeche) and Jonuta (Tabasco), Mexico

LUIS M. TORRES and ANA W. ARIE

Universidad Nacional Autónoma de México, Instituto de Investigaciones Antropológicas, Ciudad Universitaria, 04510 México, D.F.

BEATRIZ SANDOVAL

Instituto Nacional de Antropología e Historia, Dirección de Restauración del Patrimonio Cultural, Exconvento de Churubusco, 04020 México, D.F.

The provenance of Fine Orange Maya figurines from Jaina and Jonuta, Mexico, is studied by correlation of their major, minor, and trace-element compositions, analyzed by flame atomic absorption spectrometry (AAS). Ten figurine samples from Jonuta, five from Jaina, and three clays used in brick factories in the Jonuta region were analyzed. Preliminary interpretation is that the Jonuta figurines form a compositional group indicating the probability of a single manufacturing place. The Jaina figurines present great variability in composition, indicating inadequate sampling, contamination, or several provenances; results are not yet conclusive. Clays seem related to both places, probably because of a common geologic origin. Ground samples were dissolved by the alkaline fusion methods, and elemental compositions were determined by gravimetry, flame emission AAS, or flame AAS. Further analyses are advised.

SINCE LIBBY'S DEVELOPMENT of the radiocarbon dating method, which made the determination of absolute dates—or of dates with a known degree of precision—possible, archaeology has undergone a subtle and continuous transformation toward greater precision and reliance on quantitative data. Dating has become one of the milestones of modern ar-

0065-2393/84/0205-0193\$06.25/0

© 1984 American Chemical Society

chaeology as provenance studies only developed in the later years. If a country wants to improve its archaeological research, it has to establish a radiocarbon dating laboratory and an elemental analytical method to determine provenance. Although producing a date is a straightforward process, determining provenance is not.

The provenance of an artifact by chemical analyses is based on what has been called the "provenance postulate" (1) described in the following terms (2): "In many instances there will exist differences in chemical composition between pottery from different sources that will exceed, in some recognizable way, the differences observed within pottery from a given source." It is thus assumed that artifacts with similar elemental chemical composition have the same origin, or at least were manufactured with the same raw materials. From this assumption, the archaeologist is able to infer trade and, in general, cultural contacts among groups that have artifacts of similar composition, although other cultural, technological, and historical facts could also be inferred. However, it must be realized that the elemental chemical analyses of an artifact do not of themselves constitute the determination of its origin. To be able to distinguish different or similar provenances, chemical types, or compositional categories of artifacts, a broad research program specific to each kind of artifact is essential in each particular region and even subregion in order to be able to establish a link between two particular artifacts or between an artifact and a source of raw material.

Therefore, besides having an analytical method capable of producing accurate and replicable results with a large number of elements, the research program must enable the investigators to answer the two questions discussed in the following two paragraphs.

Do different sources of raw materials in the area of interest really have a different chemical composition? It is not only necessary to find that the ceramic objects were made with clays coming from the same or different sources, but also to know the extent of the area from which these raw materials were obtained by a particular group. Definition of the "resource procurement zone" (3), "resource zone" (4), or "catchment area" (5) has been recognized as of great importance (6,7) for understanding trade in the past. Variations on the compositional pattern or changes in the fingerprinting of a given source may show up through its geological profile, so "fingerprinting" should be one. Ideally, each of the geologic and geographic areas of interest (8) would be profiled, although so many analyses might be impractical because of the great amount of labor required in some cases. In other cases, incomplete knowledge of the area would make profiling impossible.

Are the clay samples and ceramic pastes adequate for analysis? It is often assumed that the proportions of the analyzed elements are not changed during burial, exposure to the environment, manufacturing

technique (tempers, slips, paint), use, and even washing, handling, and packing by the archaeologist. This assumption may be true for some elements and in some cases, but not always. Bishop et al. (2) state that in preparing the clay—in particular fine pastes—the potter levigates it to remove the coarser particles; they found no difference between coarser and finer fractions. However, Attas et al. (9) found substantial difference in the composition of levigated and coarse fractions of clays from other sources. In fact, Magalousis (10) was able to show in some preliminary analysis that washing sherds with river water introduced contamination detected by an increase in the proportions of calcium, magnesium, potassium, and sodium, measured versus the sherds washed with distilled and deionized water. In addition to these two requirements, the research program requires

1. That the chosen analytical method should have sufficient resolution to separate very close chemical compositions; otherwise the grouping of artifacts that are not so similar might result.
2. That a data bank of elemental chemical analyses of artifacts of the area of interest and its vicinity be formed.
3. That there be a mathematical procedure capable of distinguishing different compositional categories or chemical types of artifacts and capable at the same time of grouping the similar ones.

Such a research program requires a great investment of time and money (11). Therefore, the choice of analytical method to be used is a critical one. Until now, neutron activation analysis (NAA) has been the most popular method and the one that has produced the best results. In countries where a neutron source with enough energy is available, NAA is widely and successfully used. Although neutron reactors exist in many developing countries, the facilities are beyond practical reach for an NAA program geared toward determination of archaeological provenances, and another analytical method must be selected.

The research described herein is part of the program of the Instituto de Investigaciones Antropológicas of the Universidad Nacional Autónoma de México. Although atomic absorption spectrometry (AAS) is a method that can have a high degree of precision and very low detection limits, it has not been a popular analytical method for provenance studies.

Analysis of ancient artifacts by AAS is exemplified by the interlaboratory comparison study published by Chase (12), in which, of 36 laboratories surveyed, 5—around 15%—were using AAS for analysis of ancient metals, and probably had been as early as 1965, when Gettens (13) initiated the program. The importance of AAS for archaeology is recognized in an early paper by Bowers et al. (14). Probably the first and

most enthusiastic user was the British Museum Research Laboratory, as is shown by its publication *Scientific Studies in Ancient Ceramics* (15), in which several of the more important applications of AAS for provenance studies of ancient ceramics have been published (16, 17). The advantages of the method have been stressed by Magalousis and Gritton (18, 19), and in spite of their enthusiasm and success, AAS is not the method most used for the study of ancient ceramics. [In the seminar on archaeological ceramics organized by the Smithsonian Institution and the National Bureau of Standards in 1980 (20), not a single paper on AAS appears.] The main shortcomings of AAS for ceramic provenance studies are the great amount of human labor involved and a need for proficiency in wet chemical techniques that our instrumental analytical technology is making obsolete. The shortcomings described above may not be so important in countries where modern instruments are expensive or beyond the budgets of archaeological research institutions, and where the costs of employing talented wet chemists are still low.

In Mexico a fair number of other analytical instruments are in use, but their time is primarily used for research and production priorities in which the humanities have a very low rating.

Our decision to use AAS for provenance studies is supported by several facts. A large number of atomic absorption spectrometers are in use in Mexico; thus good service, maintenance, and supplies are generally available. It is economically feasible to hire several chemists, but almost prohibitive to acquire new and expensive instruments. Also, it would be difficult to obtain chemicals, literature, and the other supplies needed for the operation of these new instruments.

AAS has been used in Mexico for examination of artifacts and art objects since 1976. It was applied, for example, in the analysis of the faked metal objects of the suspected tomb of Cuauhtemoc, last of the Aztec rulers (21), and by 1977 Pre-Columbian metals were analyzed by Franco (22). At meetings of the Sociedad Mexicana de Antropología, AAS has become a frequently used term (24); in Mexico there are at least three institutions with AAS equipment and permanent programs of analysis: the Laboratory of Applied Chemistry of the Instituto de Investigaciones Antropológicas of the Universidad Autónoma de México, which analyzes metals, bone, obsidian, ceramics, and soils; the Chemistry Department of the Universidad Autónoma Metropolitana Azcapotzalco, which applies AAS to the study of Pre-Columbian metallurgy; and the Laboratory of the Departamento de Prehistoria of the Instituto Nacional de Antropología e Historia, which analyzes obsidian for dating purposes by the hydration method. From 7 to 10 chemists are continuously using AAS for analysis of archaeological artifacts. At the internal meeting of the Instituto de Investigaciones Antropológicas in 1981, four of the six papers read by the symposium on archaeological chemistry presented

applications of AAS to archaeological ceramics, metals, and bone; some of these papers will be published (24, 25). The use of AAS for provenance studies is, however, a later development in Mexico.

The choice of Fine Orange ceramics for one of the initial studies on the development of our analytical method is significant. In addition to the archaeological importance of this ceramic type, it was one of the two ceramic types analyzed by Sayre in his pioneer work on the provenance studies (26), which were the practical breakthrough for provenance determination through chemical analyses.

Archaeological Background

Fine Orange ware was made by the Maya from the Classic through the late Post-Classic periods (6th to 16th centuries), and is characterized by a fine texture and compact paste with little or no temper. Together with Plumbate it is one of the more important diagnostic ceramic types for the Mayan culture in Mesoamerica.

Many kinds of objects were produced in this ware, but the best known and most remarkable are the figurines, which are usually small mold-made sculptures, 10–20 cm tall, representing warriors, priests, gods, peasants, animals, and the like. They are found all through the Mayan area, and date, according to some researchers, from the 3rd through the 16th centuries. Of them all, the most impressive figurines, because of their realistic representation and great beauty, are those found on the island of the Jaina, located just off the northwestern shore of the state of Campeche on the western side of the Yucatan Peninsula (Figure 1). The Jaina apparently did not have plastic clays, and probably because of limited resources to sustain a permanent population, give no evidence of a ceramic industry. The island is a ceremonial center and cemetery, covered by hundreds of graves, in which the precious figurines were deposited as offerings.

The figurines have been the subject of several publications (27–29), and they form an important part of many exhibits of Pre-Columbian art throughout the world. The lack of a ceramic industry in the island raises the question of the place of manufacture of the figurines, and this topic has been the concern of several research projects (30). Other Fine Orange figurines that closely resemble those from Jaina have been found in Jonuta, a town located some 300 km southwest of the island, in the state of Tabasco. Jonuta has been recognized as a center of manufacture and distribution of Fine Orange ware (31). For this reason, and because of the resemblance between some Jonuta and Jaina figurines, it has been assumed that Jonuta was the place of manufacture of the Jaina figurines. Sanchez Caero's (32) study of Jonuta ceramics, he found that the maximum development of ceramic manufacture (the greatest number of types)

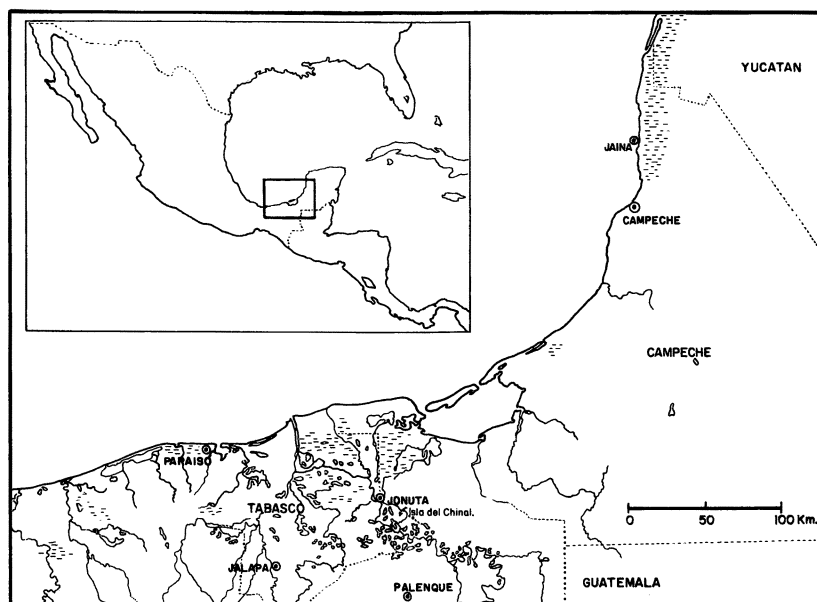


Figure 1. Map of the area from which the samples originated. (Courtesy of the Universidad Nacional Autónoma de Mexico.)

occurred during the “Jonuta” phase, and concludes that Jonuta was a manufacturing and distribution center of Fine Orange ceramics for a wide area.

Since the original analysis of Sayre et al. published in 1958 (26), the Brookhaven National Laboratory has been analyzing fine paste ceramics from the Mayan area, including not only Fine Orange but also Fine Gray pastes. The Brookhaven Fine Paste Ceramic Project was described recently by Sabloff (33), and a large volume has been published as the culmination of two decades of research, presenting conclusions from the archaeological and scientific points of view. Originally, Sayre and co-workers concluded that Fine Orange sherds from the Mayan city of Piedras Negras closely resembled in chemical composition those produced in the Mayan highlands of Guatemala, and differed from the other domestic ware found in the city. As a further step, Sayre and Chan (34) analyzed a larger number of Fine Orange sherds from a vast area in Belize, Guatemala, and the Mexican Southeast, including the sites of Chichen Itza, Carlos Green place, Cintla, Jonuta, and Nueva Esperanza in Mexico; Piedras Negras, Uaxactum, Seibal, Altar de Sacrificios, and Kixpech in Guatemala; and San José and El Cayo in Belize. They found great uniformity in composition among the different types of Fine Orange ware from these localities coming from the late Classic and Post-Classic

Mayan periods, and concluded that all were made from the same clay.

The Chontalpa, the area where Jonuta is located, was a very important region during the 16th and 17th centuries (35), and according to archaeological data this importance predates the Spanish Conquest. The area was on the borderline between the lowland Mayan-speaking and highland Nahuatl-speaking groups, and as such was a frontier between the Maya region and Teotihuacan, Tula, Cholula, and, of course, the Aztec regions in later periods. "Chontal," the word for a Mayan language, is in fact an Aztec or rather Nahuatl expression that means foreigner. The Usumacinta River adds another important feature to the region by facilitating communication between the Mayan lowlands and the highlands of Chiapas and Guatemala, and by connecting such important archaeological centers as Yaxhilan, Piedras Negras, Altar de Sacrificios, and Bonampak, as well as the Cuchumatanes area in Guatemala and Palenque via the Grijalva River.

Environment

The climates of Jaina and Jonuta are quite similar (36): tropical, with a rainfall of about 1500 mm/year. High temperatures are above 18 °C during most of the year, reaching 45 °C in the shade during May and June. Rainfall is distributed throughout the year, with a short dry period in Jaina in the winter and heavier rains during the summer. Vegetation is mostly savanna and tropical rainforest, but it has been modified by farming and excessive lumber exploitation. Jaina is a small island located a few meters from the shore, some 750 m in diameter and no more than 20 m above sea level, a height that actually is due to the ceremonial pyramids found in the center of the island. It is practically submerged by waves during cyclones. Its soil is sandy and saline, on a limestone bedrock, and it has been covered artificially by a layer of sascab—a natural clay mortar—and contains many saline ponds.

Jonuta is nearly 100 m above sea level. It is located on a point of land a little before the junction of the two branches of the Usumacinta River that forms Chinal Island. It is surrounded by swamps, ponds, rivers, and creeks, bordered to the north by Palisada County of the state of Campeche. Soils in the area are arcillous; it is also possible to find some lateritic and red soils, but they are being transformed by erosion to sandy soils. The bedrock is an Eocene limestone covered by a 20-cm-thick layer of flint (36).

The Samples

The clays and samples of figurines from Jonuta used for this study were obtained during the "Research Project on the Northwestern Lowland of

the Maya area," sponsored by the Centro de Estudios Mayas of the Universidad Nacional Autónoma de México since 1973. The excavation was conducted by Carlos Alvarez and Luis Casasola during 1977.

The Jonuta ceramics recovered were studied by Sánchez Caero (32), and the figurines were studied extensively by Casasola and Alvarez (37). This study is a consequence of their work. The samples for analysis were selected by looking for the least possible contamination during burial and by trying to find the largest spans of time, appearance, and site. Of the 10 samples analyzed, 3 were found in the archaeological site of Jonuta, 2 more came from the archaeological site of Paraíso, located some 25 km from Jonuta downstream of the Usumacinta River, and 1 came from an excavation at La Tejería, located almost in front of Paraíso on the other side of the river. The other four samples were recovered in excavations carried out at two archaeological sites in the nearby Palisada County in the state of Campeche, some 3 km north of Jonuta; two of them are from El Ocotlán and the other two from San Joaquín. The layers from which the samples were recovered were dated by carbon-14 techniques at Teledyne Isotopes Laboratories of Westwood, N.J., by using Libby's half-life for carbon-14 of 5568 years. Jonuta layer IV, quadrant 3, was dated A.D. 665 ± 85 ; layer V, quadrant I produced a date of A.D. 505 ± 80 ; and layers III and IV of el Ocotlán were dated A.D. 540 ± 85 and 515 ± 100 , respectively. It was not possible to find good samples of charcoal to date San Joaquín, although the epochs are evidently the same as those of the other sites. We can then be certain that the samples from Jonuta date from the late 5th or early 6th century to the end of the 8th or the early 9th century.

The 10 samples from Jonuta are Jonuta 1, JO-9-1-IV; Jonuta 2, JO-9-2-2-IV, Jonuta 3, JO-9-3-IV; Paraíso 1, JO-9-1-II, Paraíso 2, JO-9-2-II; La Tejería, JO-12-2-II; El Ocotlán 1, PL-1-I-D-IV; El Ocotlán 2, PL-1-I-A-IV; San Joaquín 1, Pl-I-A-IV; San Joaquín 1, PL2-1-D-III; and San Joaquín 2, PL-2-2-A-III. The numbers are those assigned by Alvarez and Casasola in their excavations.

The three clay samples were taken from places where the local brick factories obtained their raw materials. These clays are not used to make pottery, but with some processing and preparation they could produce good ceramic clays. Sites from which the clay samples were obtained are Sitio Lerma (2.5 m deep), Finca Canul (0.5 m deep), and Chinal Island (0.4 m deep). The clay samples are good only for purposes of general comparison; they may only represent a typical analysis of the arcillous soils of the area of Jonuta, and—as has been discussed before—contamination, variability of soil profile, and preparation may introduce changes in their chemical composition. These considerations should be taken into account in interpreting results. The samples taken by the archaeologist were from an actual "blend" prepared by the brick maker. It was im-

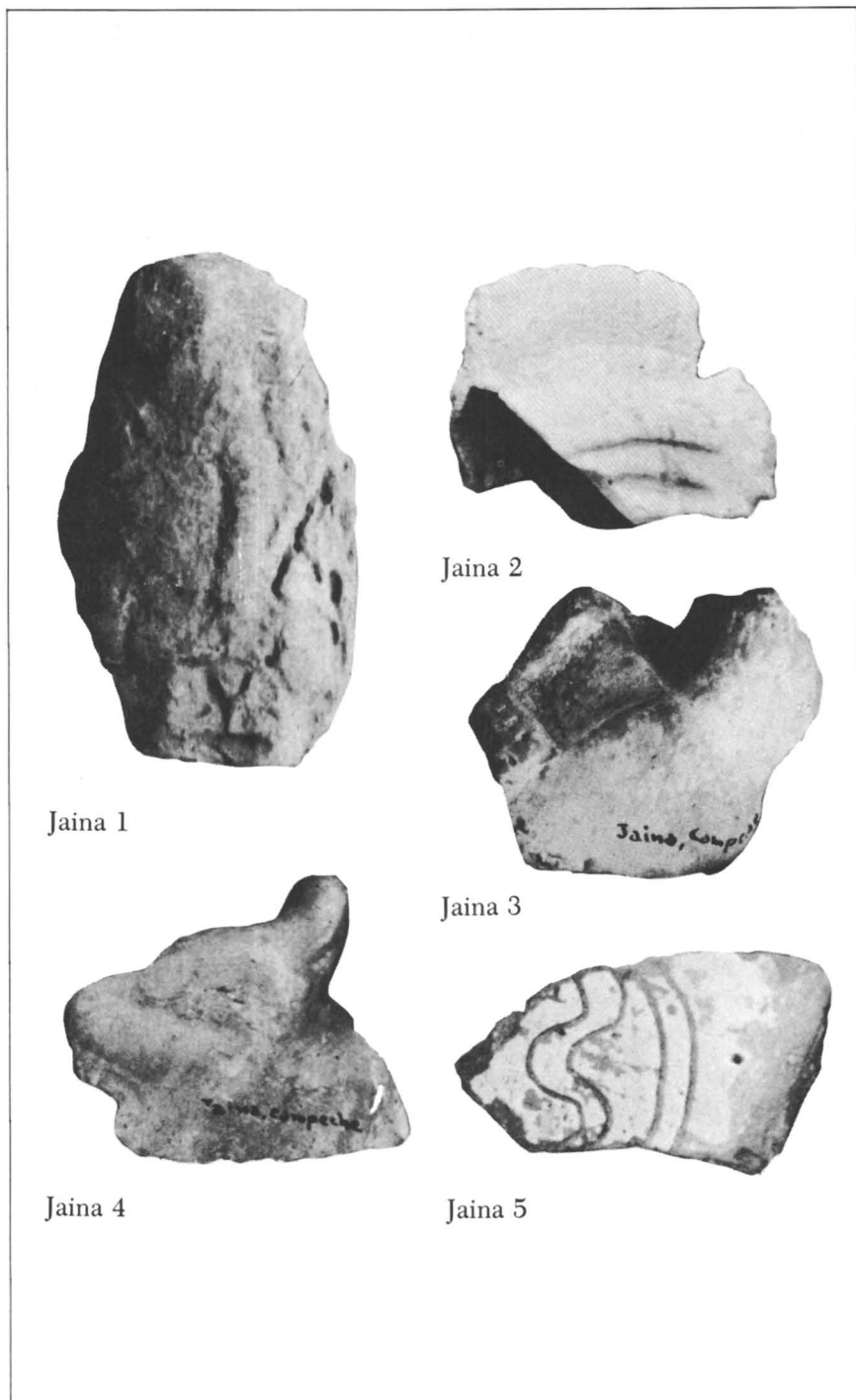
possible to know if only one or more than one layer of the profile were taken; in addition, the blend was mixed with water from the river or a well.

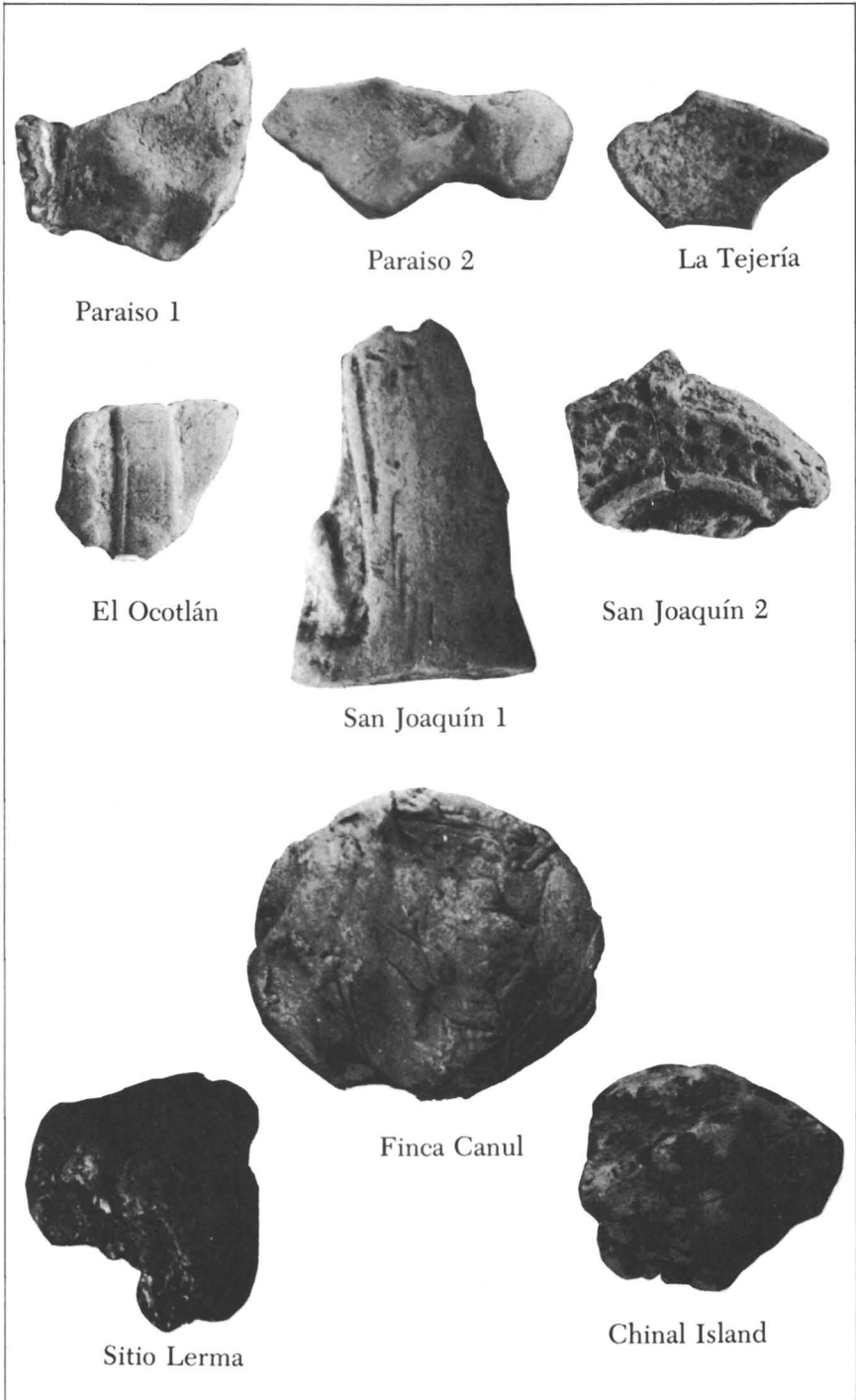
The five samples of figurines from Jaina (*see* the photograph on page 202) form part of the collection of the Museo Nacional de Antropología de México: the sherds were recovered by R. Piña Chan during his 1964 season. According to him (38), the Jaina figurines were produced between the 3rd and 10th centuries. He gives earlier dates than other archaeologists. Because the figurines included in this study lack excavation numbers, they cannot be assigned a more precise date during this span of time. We are aware that the data on them are not very good, but there has not been another better-controlled excavation on the island in recent times. It should be remembered that Jaina soil is saline and is partially covered by sascab—a natural puzolanic mortar—so that contamination of the sample by salt and lime will be detected in the analysis. The sherds from Jonuta (*see* the photograph on page 203) were classified as similar to the Fine Orange ware of the Altar variety, and one of the samples from Jaina was similar to the ones from Jonuta.

Analytical Procedure

The analytical technique can be outlined as follows: Samples were washed by the archaeologists after excavation, using whatever water supply was available to them near their camp or excavation area. In the laboratory, the samples were photographed, washed two times with distilled water—for an hour each time, dried overnight, and cleaned superficially with a brush at 10 times magnification to remove any concretions adhering to the surface. Because only sample No. 5, from Jaina, had a white “kaolin” slip, samples for analysis were taken without scraping the surface. This method followed the procedure and point of view of Gritton and Magalouis (39), who considered that “if the entire shard is crushed, finely ground and well mixed, then the analytical sample taken will represent the best estimate possible of the composition of the entire object.” This procedure affected the analysis, as will clearly be shown in the difference in the analysis of sample No. 5 from Jaina.

Samples were ground in an agate mortar and weighed in a semimicroanalytical balance. Two samples of 250 mg each were weighed with up to 0.01 mg of precision; samples were then dried in an oven at 100 °C for 4 h, weighed again, and calcinated at 600 °C to destroy organic matter. The samples were then fused in a platinum crucible with 1 g of a mixture of 1:1 sodium carbonate: sodium dioxide. The fused portion was dissolved in 50 mL of 1:1 hydrochloric acid and evaporated to dryness. When redissolved in 2% hydrochloric acid, a precipitate of silica and alumina forms and is filtered and washed out with more 2% hydrochloric acid to extract all the iron. One of the portions was diluted with distilled water to 250 mL in a volumetric flask. The other portion was diluted to 50 mL. These solutions were used to determine the following elements by AAS: iron, calcium, magnesium, potassium (a diluted aliquot was used; potassium was determined by flame emission), copper, cobalt, chromium, manganese, nickel, silver, gold, platinum, scandium, indium, europium, lanthanum, and terbium. The precipitate was calcinated, weighed, and, to determine silica and





alumina, the silicon was redissolved and evaporated in the following way: 5 mL of hydrofluoric acid with 2 drops of concentrated sulfuric acid was added and evaporated to dryness; the difference in weight was silica lost by evaporation, the remainder was alumina.

The idea behind using two different concentrations for the analyses was to increase the concentration of the elements present in trace quantities and to compare the concentrate with the diluted portion. In general in AAS, working with concentrations higher than 1000 ppm produces faulty signals because of matrix problems. However, in these techniques due to the precipitation and separation of two major components, a solution with a small amount of solids was produced. Therefore, it was possible to avoid the matrix problems by having a better signal-to-noise ratio.

In the comparison, a substantial difference in the signal-to-noise ratio was observed, and with the increase of concentration it was possible to reach detection limits for some elements, such as scandium and indium, not detected in the dilute solution. By increasing the concentration of the trace elements five-fold, we obtained signals 1 order of magnitude higher, while background and standard deviation remained essentially the same. The degree of precision was also increased tenfold; the increase in precision was critical for analysis of silver and gold. The gold detected is probably an interference and not a true presence, but further studies should be made to resolve this problem, as some high silicon and low aluminum values were abnormal. Several decomposition procedures have been developed for analyzing major, minor, and trace elements in aluminosilicate minerals, some of which have been used in analysis of cultural artifacts. Eighteen elements have been determined after a single decomposition method by using hydrofluoric acid and aqua regia, adding the digested sample to boric acid (40). Because digestion is accomplished in a sealed Teflon bomb, the evaporation of volatile fluorides is eliminated, which allows the determination of silicon, aluminum, and titanium. No fluxes are used, so it is possible to analyze the alkali and alkaline earth elements in the same solution.

Another procedure uses an alkaline flux method with lithium metaborate (41), and involves diluting the fused portion in nitric acid. Interferences and interelement effects must be eliminated by calibration of samples and standards of similar composition. A procedure used successfully in the analysis of archaeological ceramics is described by Gritton (19). The sample is decomposed with hydrofluoric acid and perchloric acid, fumed to a moist residue, treated twice more with perchloric acid, dissolved in more perchloric acid, and diluted with water.

In the initial analysis we performed, the first two methods described above were compared with the sodium carbonate: sodium dioxide flux method and a very close similarity in the results for more of the elements analysed was found. It is felt, however, that the values reported in this study are only valid for comparative purposes. They should not be considered as absolute values. Comparison of the three methods is still under study and it is not possible yet to give a final evaluation of them. The use of a rock standard in a destructive method still under study does not seem wise, considering the problems faced in obtaining these standards in Mexico. It is possible to find some elements that give high readings due to interference or emission from the matrix, and to find some others, which may be absorbed in the precipitate, that give abnormally low results.

In the sodium carbonate: sodium dioxide flux method a possible side reaction has to be taken into account. Molten sodium hydroxide, which may form from

moist air and sodium dioxide, could slightly attack the platinum crucible. Use of iron or nickel crucibles is a recommended alternative, but considering the importance of these two elements in the analysis of ceramics and the fact that platinum should not be found in the clays, we decided to do the fusing in platinum crucible.

Not all the silica is precipitated in a single boiling after the addition of the hydrochloric acid; the mixture must be evaporated to dryness in the presence of hydrochloric acid or fumed with sulfuric or perchloric acids. In a single evaporation, 97–99% of the silica present is rendered insoluble (42). If magnesium is present, some silica may be pseudosoluble in presence of the magnesium chloride. Except potassium, all the metal perchlorates are soluble in water or dilute perchloric acid solution, which is an advantage of the Gritton method of digesting silicates.

The analyses were performed with a 373 Perkin-Elmer atomic absorption spectrophotometer; the readings were taken at the wavelength recommended by the manufacturer in the standard conditions for analysis of each element. Two standards were run for each element, generally, one 5 ppm and the other 1 ppm.

Discussion

The results of our analyses are given in Table I. Scandium and indium were detected at about 0.004%, but it was not possible to determine precise concentrations. Platinum, lanthanum, and europium were not detected. (Platinum actually was detected, but when a zero reading was taken against a blank, its presence was shown to be caused by attack of the crucible.) The results were processed by means of a microcomputer to obtain Pearson correlation coefficients. The correlation was done between the major and minor elements, and again between the trace elements; thus two different coefficients were obtained. A high degree of variation is seen with calcium, which did not correlate well with the major and minor elements. Calcium was eliminated by considering it to be a contaminant. Zinc did not correlate well either, but it could not be thus eliminated. The correlation coefficients for the trace elements are given in Table II.

The correlation for all samples of four major and minor elements (iron, potassium, silicon, and magnesium) higher than 0.95, reaching a maximum of 0.98. In interpreting the correlation values for the trace elements given in Table II, recall that one sample was compared against the others. An "average sample" composition was not used to obtain the coefficients. It is expected that by using such an average composition for each group, the group would be more coherent and the coefficient should be higher. By using the high values of the first four elements mentioned, the coefficient is further increased in all cases. In this study we are then considering a correlation to be fairly good when the coefficient in Table II is on the order of 0.70.

In the Jonuta figurines, two different groups with good correlation

Table I. Elemental Compositions of Samples

<i>Sample</i>	<i>SiO₂</i>	<i>Al₂O₃</i>	<i>Fe</i>	<i>Ca</i>	<i>Mg</i>	<i>K</i>	<i>Co</i>
Jonuta 1	49.24	10.40	5.34	0.191	0.170	2.45	0.009
Jonuta 2	47.88	9.28	4.95	0.286	0.178	2.41	0.013
Jonuta 3	49.96	15.76	6.07	0.654	0.188	2.18	0.011
Paraiso 1	67.48	11.88	5.02	0.269	0.112	2.22	0.006
Paraiso 2	63.76	12.60	4.38	0.066	0.176	2.15	0.018
La Tejería	53.64	28.40	5.15	0.122	0.170	2.63	0.011
El Ocotlán 1	46.16	15.72	6.12	0.840	0.197	2.45	0.017
El Ocotlán 2	43.92	17.88	4.20	0.054	0.217	3.35	0.010
San Joaquín 1	65.28	13.56	5.85	0.225	0.194	2.47	0.009
San Joaquín 2	59.64	13.96	5.55	0.076	0.154	2.55	0.020
Finca Canul	56.36	4.21	5.53	0.050	0.155	2.07	0.013
Sitio Lerma	51.78	5.04	5.52	1.108	0.277	2.17	0.015
Chinal Island	67.88	11.56	6.20	0.284	0.178	2.40	0.011
Jaina 1	58.08	10.52	13.93	0.742	0.282	2.70	0.014
Jaina 2	55.04	10.84	4.67	3.283	0.125	2.95	0.008
Jaina 3	54.20	12.84	7.98	2.133	0.180	4.07	0.011
Jaina 4	51.72	18.36	3.88	0.915	0.070	1.92	0.011
Jaina 5	54.13	11.54	4.52	0.029	0.131	2.58	0.074
<i>Sample</i>	<i>Cr</i>	<i>Cu</i>	<i>Mn</i>	<i>Zn</i>	<i>Ag</i>	<i>Au</i>	<i>Ni</i>
Jonuta 1	0.045	0.007	0.071	0.022	0.004	0.016	0.032
Jonuta 2	0.043	0.012	0.085	0.075	0.002	0.026	0.034
Jonuta 3	0.059	0.009	0.069	0.058	0.002	0.028	0.028
Paraiso 1	0.046	0.007	0.101	0.012	0.004	0.024	0.036
Paraiso 2	0.064	0.005	0.120	0.019	0.002	0.044	0.032
La Tejería	0.037	0.063	0.067	0.101	0.003	0.046	0.038
El Ocotlán 1	0.040	0.008	0.109	0.021	0.002	0.032	0.049
El Ocotlán 2	0.047	0.008	0.102	0.256	0.004	0.032	0.040
San Joaquín 1	0.060	0.031	0.067	0.046	0.001	0.025	0.061
San Joaquín 2	0.048	0.009	0.175	0.033	0.001	0.032	0.069
Finca Canul	0.064	0.009	0.110	0.247	0.001	0.005	0.063
Sitio Lerma	0.039	0.010	0.068	0.056	0.002	0.013	0.038
Chinal Island	0.072	0.008	0.050	0.024	0.001	0.028	0.034
Jaina 1	0.052	0.006	0.052	0.223	0.002	0.019	0.031
Jaina 2	0.012	0.015	0.025	0.039	0.006	0.032	0.021
Jaina 3	0.022	0.027	0.053	0.145	0.005	0.026	0.016
Jaina 4	0.019	0.000	0.043	0.040	0.003	0.023	0.031
Jaina 5	0.050	0.009	0.053	0.061	0.003	0.032	0.015

NOTE: Data are given as percentages.

in composition were obtained. The first group was formed with the three samples from Jonuta, the two from Paraiso, the El Ocotlán 1, the two from San Joaquín, and the clays from Sitio Lerma and Chinal Island. Sample 4 from Jaina has a rather high correlation with the members of this group. The second group is made up of the sample from La Tejería, El Ocotlán 2, and Finca Canul. The members of this group have a fairly high similarity with the samples 1, 2, 3, and 4 from Jaina. As a group, the Jaina samples do not correlate well among themselves.

Jaina samples 1 and 3 are somewhat similar, sample 2 is about 70% similar to sample 4, and sample 5 is different from all the clays and samples from both Jonuta and Jaina. Jaina 4 is somewhat close to both groups of Jonuta figurines, except for the clay sample from Chinal Island.

Several samples from Jonuta, of the Altar type of Fine Orange, have been analyzed by NAA at the Brookhaven National Laboratory and the results have been published. One sample is from a figurine named XCII by Goldstein (30), another is named sample 53 by Sayre et al. (34), and the last two are identified as samples 4 and 6 by Sabloff (43). The elements analyzed by both NAA and AAS were potassium, iron, chromium, manganese, and cobalt. The concentrations of these elements expressed as oxides, are given in Table III for all the samples analyzed by NAA and AAS. Again, recall that the concentrations of the elements analyzed by AAS do not represent absolute values; they are only used for comparative purposes.

In Figures 2–4 are presented the concentrations of, respectively, the minor elements—iron, magnesium, calcium, and potassium; the trace elements; and the elements analyzed by NAA and AAS. The concentrations are presented in groups. Group 1 is from Jonuta: Jonuta 1, 2, and 3; Paraiso 1 and 2; El Ocotlán 1; and San Joaquín 1 and 2; group 2 is from Jonuta, with La Tejería, and El Ocotlán 2. Plotted separately are the clays from brick factories; Jaina 1, 2, 3, and 4; and Jaina 5.

Preliminary Interpretations

Both groups from Jonuta (*see* Figures 2–4) are so closely related that they can be considered as forming a single group in which some elements have more variability in their concentrations (potassium, chromium, copper, and zinc). Some clays compare fairly well with the samples from both Jonuta and Jaina; however, considering the wide variation in composition, it is only possible to assume that the clays and the figurines from both places are probably from the same general geologic region. It seems rather clear that figurine Jaina 4 was made at Jonuta and taken to the island. The decision to analyze Jaina 5 by including the white slip most likely caused its composition to be different from the composition of the other four Jaina samples. By sampling only the core, the figure's composition possibly will be close to the others.

The number of Jaina samples seems to be quite inadequate for this study, but the Jonuta samples were adequate. The wide variation in the composition of Jaina clay may indicate the need for more and better samples. Until now, there were more questions posed than answers supplied. For example, were the figurines manufactured with several clays, as had been stated previously, (30), or was the paste badly con-

Table II. Pearson Correlation

	Jonuta 1	Jonuta 2	Jonuta 3	Paraiso 1	Paraiso 2	La Tejería	El Ocotlán 1	El Ocotlán 2
Jonuta 1	1.00	0.81	0.87	0.97	0.97	0.35	0.95	0.31
Jonuta 2	0.81	1.00	0.94	0.72	0.72	0.75	0.76	0.80
Jonuta 3	0.87	0.94	1.00	0.76	0.78	0.63	0.76	0.68
Paraiso 1	0.97	0.72	0.76	1.00	0.99	0.27	0.98	0.17
Paraiso 2	0.97	0.72	0.78	0.99	1.00	0.25	0.98	0.17
La Tejería	0.35	0.75	0.63	0.27	0.25	1.00	0.32	0.81
El Ocotlán 1	0.95	0.76	0.76	0.98	0.98	0.32	1.00	0.24
El Ocotlán 2	0.31	0.80	0.68	0.17	0.17	0.81	0.24	1.00
San Joaquín 1	0.88	0.84	0.93	0.78	0.78	0.64	0.75	0.51
San Joaquín 2	0.93	0.78	0.74	0.97	0.95	0.35	0.99	0.28
Finca Canul	0.39	0.83	0.72	0.24	0.26	0.79	0.29	0.99
Sitio Lerma	0.85	0.99	0.95	0.75	0.74	0.69	0.78	0.76
Chinal Island	0.83	0.61	0.84	0.72	0.78	0.25	0.67	0.22
Jaina 1	0.19	0.70	0.61	0.02	0.03	0.76	0.08	0.98
Jaina 2	0.26	0.69	0.57	0.23	0.27	0.83	0.32	0.78
Jaina 3	0.20	0.73	0.58	0.07	0.06	0.87	0.14	0.98
Jaina 4	0.72	0.96	0.87	0.67	0.69	0.79	0.74	0.79
Jaina 5	0.41	0.55	0.55	0.29	0.38	0.23	0.39	0.47

Table III. Concentration of Elements Analyzed by AAS and NAA

	Fe_2O_3	K_2O	Cr_2O_3	MnO	CoO
Jonuta 1	7.64	2.95	658	917	114
Jonuta 2	7.08	2.90	628	1098	165
Jonuta 3	8.68	2.63	862	891	140
Paraiso 1	7.18	2.67	672	1304	89
Paraiso 2	6.26	2.59	935	1550	228
La Tejería	7.36	3.17	541	865	140
El Ocotlán 1	8.75	2.95	585	1408	216
El Ocotlán 2	6.15	4.04	687	1317	127
San Joaquín 1	8.36	2.98	877	865	114
San Joaquín 2	7.94	3.07	701	2260	252
Finca Canul	7.91	2.49	935	1420	165
Sitio Lerma	7.89	2.61	570	878	191
Chinal Island	8.86	2.89	1052	646	140
Jaina 1	19.92	3.25	760	671	178
Jaina 2	6.68	3.55	175	322	102
Jaina 3	11.41	4.90	322	684	140
Jaina 4	5.57	2.31	278	555	140
Jaina 5	6.46	3.11	731	684	940
XCII ⁺	6.0	2.0	672	1620	57
Sample 53 ⁺	7.8	—	720	1580	38
Sample 4 ⁺	7.71	2.23	641	1140	39.5
Sample 6 ⁺	8.10	2.09	654	1450	40.1

NOTE: Fe_2O_3 and K_2O as percentages; all others as parts per million.

+, Analyzed by NAA.

Coefficients of Trace Elements

San Joaquin 1	San Joaquin 2	Finca Canul	Sitio Lerma	Chinal Island	Jaina 1	Jaina 2	Jaina 3	Jaina 4	Jaina 5
0.88	0.93	0.39	0.85	0.83	0.19	0.26	0.20	0.72	0.41
0.84	0.78	0.83	0.99	0.61	0.70	0.69	0.73	0.96	0.55
0.93	0.74	0.72	0.95	0.84	0.61	0.57	0.58	0.87	0.55
0.78	0.97	0.24	0.75	0.72	0.02	0.23	0.07	0.67	0.29
0.78	0.95	0.26	0.74	0.78	0.03	0.27	0.06	0.69	0.38
0.64	0.35	0.79	0.69	0.25	0.76	0.83	0.87	0.79	0.23
0.75	0.99	0.29	0.78	0.67	0.08	0.32	0.14	0.74	0.39
0.51	0.28	0.99	0.76	0.22	0.98	0.78	0.98	0.79	0.47
1.00	0.73	0.57	0.87	0.85	0.43	0.45	0.45	0.76	0.37
0.73	1.00	0.33	0.79	0.59	0.11	0.31	0.19	0.75	0.37
0.57	0.33	1.00	0.81	0.29	0.97	0.67	0.96	0.78	0.51
0.87	0.79	0.81	1.00	0.66	0.67	0.57	0.68	0.91	0.59
0.85	0.59	0.29	0.66	1.00	0.19	0.20	0.11	0.51	0.42
0.43	0.11	0.97	0.67	0.19	1.00	0.71	0.98	0.68	0.47
0.45	0.31	0.67	0.57	0.20	0.71	1.00	0.80	0.83	0.28
0.45	0.19	0.96	0.68	0.11	0.97	0.80	1.00	0.74	0.39
0.76	0.75	0.78	0.91	0.51	0.68	0.83	0.74	1.00	0.54
0.37	0.37	0.51	0.59	0.42	0.47	0.28	0.39	0.54	1.00

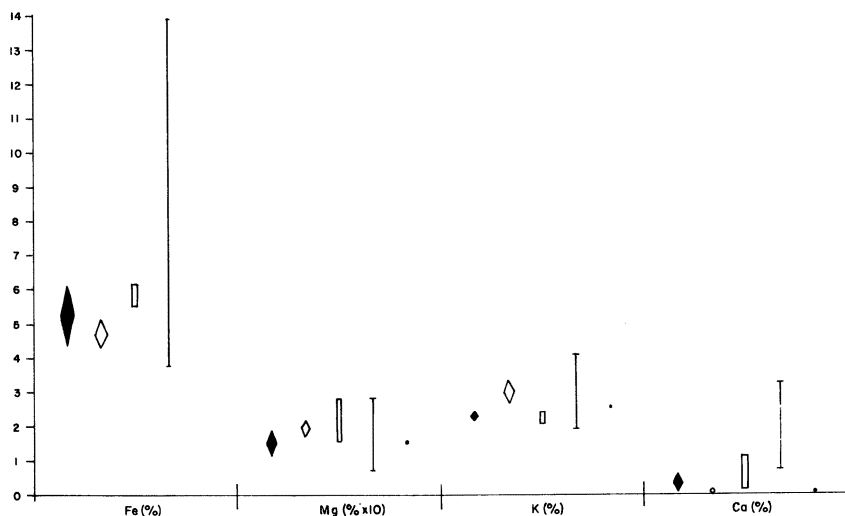


Figure 2. Concentration of iron, magnesium, potassium, and calcium in the analyzed samples. Key: \blacklozenge , group 1 from Jonuta; \diamond , group 2 from Jonuta; \square , clays from brick factories; $|$, Jaina 1-4; $*$, Jaina 5.

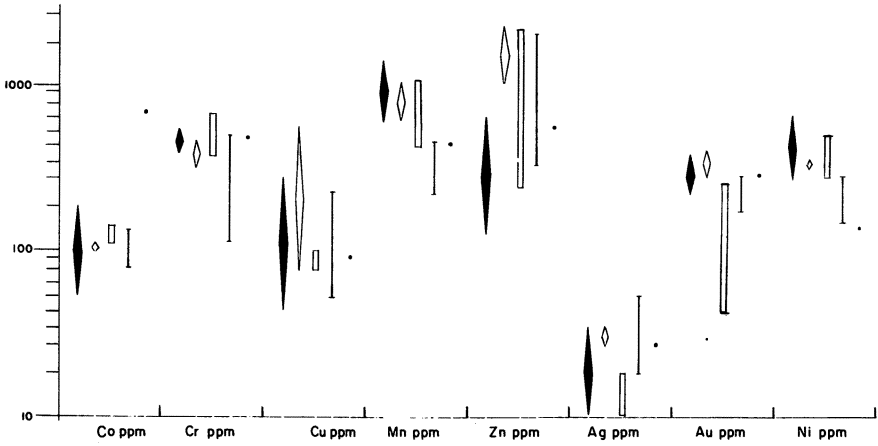


Figure 3. Trace element concentrations in the analyzed samples. Key: \blacklozenge , group 1 from Jonuta; \diamond , group 2 from Jonuta; \square , clays from brick factories; ∇ , Jaina 1-4; $*$, Jaina 5.

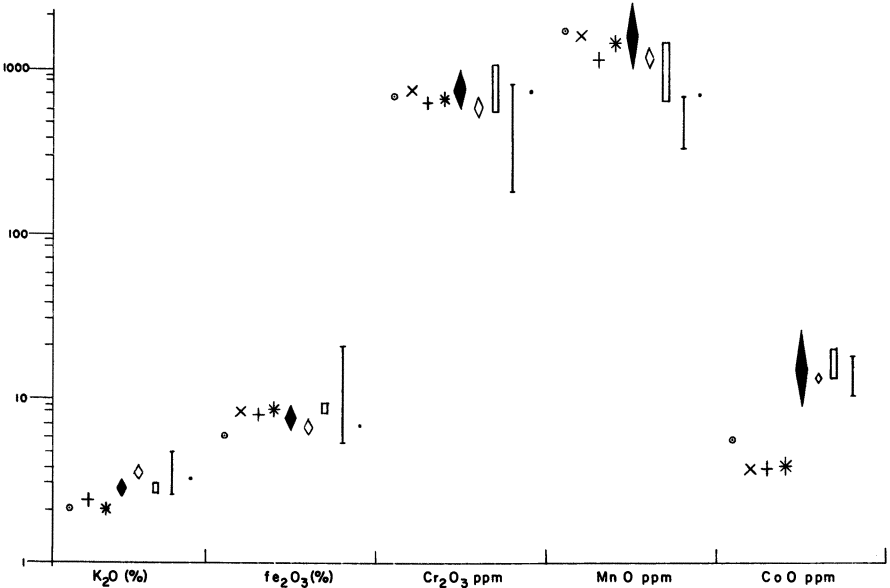


Figure 4. Comparison of samples analyzed by NAA and AAS. Key: \blacklozenge , group 1 from Jonuta; \diamond , group 2 from Jonuta; \square , clays from brick factories; ∇ , Jaina 1-4; $*$, Jaina 5; \circ , sample XCII (30); \times , sample 53 (34); $+$, sample 4 (43); $*$, sample 6(43).

taminated by salt and sascab during burial in the Island? Was Jaina 4 manufactured at Jonuta? Yes, probably it was. With this in mind, we can see in the comparison of analysis by NAA and AAS (considering the obvious high values for potassium and cobalt) that Jonuta samples may belong to the same composition group as the one assigned in the work of Sabloff (44) to the Fine Orange ware of the Altar type.

From the point of view of the analytical method, we can conclude that it is possible to increase the number of elements analyzed by using a higher concentration of sample. However, the linearity of the results has to be further analyzed to determine to what extent the concentration can be increased. Certainly, a better signal-to-noise ratio is obtained; in turn, a lower standard deviation results. Some elements are detected by this increase in concentration, but only in special cases are results produced that can be used quantitatively. However, the use of AAS with flameless technique may be advantageous.

Acknowledgments

We would like to thank Carlos Alvarez and Luis Casasola, of The Centro de Estudios Mayas of The Universidad Nacional Autónoma de México, who furnished the samples and the original idea for this research. They also discussed with us the archaeological implications. The samples from Jaina were furnished by Nohemi Castillo Tejero, Head of the Department of Archaeology of The Museo Nacional de Antropología of México City. We also would like to express our gratitude to Francisca Franco from The Universidad Autónoma Metropolitana-Azcapotzalco for the technical assistance in the development of the wet chemistry and to Fernando Botas and Humberto Arrieta for the drawings and photographs. Finally, we would like to mention the invaluable help we obtained from Paul Schmidt, who helped us with the use of the microcomputer and the translation of our text into English. He also contributed the discussion of archaeological and methodological aspects of our chapter.

Literature Cited

1. Weigand, P. C.; Harbottle, G.; Sayre, E. V. In "Exchange Systems in Prehistory"; Earle, T. K.; Ericson, J., Eds.; Academic: New York, 1977; pp. 15-34.
2. Bishop, R. L.; Harbottle, G.; Sayre, E. V. In "Analyses of Fine Paste Ceramics"; Sabloff, J. A., Ed.; *Memoirs Peabody Mus. Archaeol. Ethnol.* 1982, 15(2), Chap. 2.
3. Rands, R. L.; Bishop, R. L. In "Models and Methods in Regional Exchange"; Fry, R. E., Ed.; Society for American Archaeology Papers No. 1, 1980; pp. 19-46.
4. Arnold, D. E. In "The Espatial Organization of Culture"; Hodder, I., Ed.; Duckworth: London, 1978; pp. 39-60.

5. Vita-Finzi, C.; Higgs, E. S. *Proc. Prehistoric Soc.* **1970**, *36*, 1–17.
6. Bishop, R. L.; Rands, R. L.; Holley, G. R. In "Advances in Archaeological Method and Theory"; Academic: New York, 1982; Vol. **V**, pp. 275–330.
7. Roper, D. C. In "Advances in Archaeological Method and Theory"; Shiffer, M. B., Ed.; Academic: New York, 1979; Vol. **II**, pp. 119–40.
8. Magalousis, N. M.; Flint, A.; Gritton, V.; Miller, G. E. *J. Syro-Mesopotam. Stud.* **1980**, *3(4)*, 1–32.
9. Attas, M.; Yaffe, L.; Fossey, J. M. *Archaeometry* **1977**, *19*, 33–43.
10. Magalousis, N. M. *J. Syro-Mesopotam. Stud.* **1980**, *3(4)*, 12–14.
11. Bishop, R. L.; Rands, R. L.; Holley, G. R. In "Advances in Archaeological Method and Theory"; Academic: New York, 1982; Vol. **V**, p. 175.
12. Chase, W. T. In "Archaeological Chemistry"; Beck, C. W., Ed.; ADVANCES IN CHEMISTRY SERIES No. 138; American Chemical Society: Washington, D.C. 1974; Chap. 9, pp. 148–85.
13. Gettens, R. S., private commun., 1965.
14. Bower, N. Y.; Bromund, R. H.; Smith, R. H. *J. Field Archaeol.* **1975**, *2*, 389–98.
15. Hughes, M. J., Ed. In "Scientific Studies in Ancient Ceramics"; Br. Mus. Occas. Pap. No. 19, 1981.
16. Bomgardner, D. L. In "Scientific Studies in Ancient Ceramics"; Hughes, M. J., Ed.; Br. Mus. Occas. Pap. No. 19, 1981; pp. 93–101.
17. Magalousis, N. M.; Gritton, V. In "Scientific Studies in Ancient Ceramics"; Hughes, M. J., Ed.; Br. Mus. Occas. Pap. No. 19, 1981; pp. 103–16.
18. Magalousis, N. M. *Archaeo-Phisica Band 10, Proc. 18th. Int. Symp. Archaeometry Archaeol.* Prosp. (Bonn) **1978**, 173.
19. Gritton, V.; Magalousis, N. M. In "Archaeological Chemistry II"; Carter, G. F., Ed.; ADVANCES IN CHEMISTRY SERIES No. 171; American Chemical Society: Washington, D.C., 1978; pp. 259–79.
20. Olin, J. S.; Franklin, A. D., Eds. "Archaeological Ceramics"; Smithsonian: Washington, D.C., 1982; 256 pp.
21. Torres, L. "Examen de los objetos metálicos de la Tumba de Ixcateopan, Gro.," in press.
22. Grinberg, D. M. K.; Franco, F. In "Toniná, Une Cité Maya du Chiapas"; Boudezz, C.; Becquelin, P., Eds.; Mission Arqueologique et Ethnologique Francaise au Mexique: México, 1982; Vol. **II**.
23. Franco de Torres, F. "XV Mesa Redonda"; Sociedad Mexicana de Antropología, México; Tomo **II**.
24. Mountjoy, J. B.; Torres, L. M. "The Production and Use of Prehispanic Metal Artifacts in the Central Coastal Area of Jalisco, México"; Weigand, P. C., Ed.; in press.
25. Torres, L. M.; Rojas, J. In "Antropología y Técnica No. 2"; in press.
26. Sayre, E. V.; Murrenhoff, A.; Weick, C. F.; "The Nondestructive Analysis of Ancient Potsherds Through Neutron Activation"; Brookhaven National Laboratory Report No. 508, Upton, 1958.
27. Groth-Kimball, I. "Mayan Terracotas"; New York, 1961.
28. Corson, C. "Maya Anthropomorphic Figurines from Jaina Island, Campeche"; Ballena: Ramona, Calif., 1976.
29. Cook, deLeonard C. *Int. Congr. Americanist 35th.*, México 1964. pp. 361.
30. Goldstein, M.; Ph. D. Thesis, Columbia University, New York, 1979.
31. Berlin, H. "Late Pottery Horizon of Tabasco México"; Contributions to American Anthropology and History No. 59, Pub. 606; Carnegie Inst.: Washington, D. C., 1956; pp. 95–153.

32. Sánchez Caero, O. Thesis, Escuela Nacional de Antropología, México, 1979.
33. Sabloff, J. A. *Memoirs Peabody Mus. Archaeol. Ethnol.* **1982**, *15*(2), Chap. 1.
34. Sayre, E. V.; Chan, L. H.; Sabloff, J. A. In "Science in Archaeology"; Brill, R. H., Ed.; MIT Press: Cambridge, Mass., 1971; pp. 165–181.
35. Ochoa, L., Ed. "Estudios Preliminares sobre los Mayas de las Tierras Bajas Noroccidentales"; Universidad Nacional Autónoma de México: México, 1978.
36. Tamayo, J. L. "Geografía Económica y Política de México"; UNAM: México, 1962.
37. Alvarez, C.; Casasola, L. "Las Figurillas de la Zona de Jonuta, Tabasco"; Centro de Estudios Mayas, UNAM: in press.
38. Piña Chan, R. "Jaina. La Casa del Agua"; Instituto Nacional de Antropología e Historia: México, 1968.
39. Gritton, V.; Magalousis, N. M. *J. Syro-Mesopotam. Stud.* **1980**, *13*(4), 11.
40. Buckley, D. F.; Cranston, R. E. *Chem. Geol.* **1981**, *7*, 273–84.
41. Ingamels, C. O. *Anal. Chim. Acta* **1970**, *42*, 323–34.
42. Kolthoff, I. M.; Sandell, E. B. "Textbook of Quantitative Inorganic Analysis", 3rd ed.; Macmillan: New York, 1952.
43. Sabloff, J. A. *Memoirs Peabody Mus. Archaeol. Ethnol.* **1982**, *15*(12).
44. Sabloff, J. A., Ed. *Memoirs Peabody Mus. Archaeol. Ethnol.* **1982**, *15*(2).

RECEIVED for review November 23, 1982. ACCEPTED for publication April 25, 1983.

Technological Examination of Egyptian Blue

M.S. TITE, M. BIMSON, and M.R. COWELL

British Museum Research Laboratory, London WC1B 3DG

The chemical composition, microstructure, hardness, and color of a series of ancient Egyptian Blue samples from Egypt, Mesopotamia, and Western Europe (Roman period) have been investigated using principally atomic absorption spectrophotometry and scanning electron microscopy. Egyptian Blue has been produced in the laboratory by using a range of compositions and firing procedures and has been compared with the ancient material. From these results, information on the techniques used in antiquity to produce Egyptian Blue has been obtained. In particular, it seems probable that a two-stage firing cycle with grinding and molding to the final shape between the first and second firing was used in the production of small objects.

EGYPTIAN BLUE first occurs in Egypt during the 3rd millennium B.C., and during the subsequent 3000 years, its use as a pigment and in the production of small objects such as beads, scarabs, inlays, and statuettes spread throughout the Near East and the Eastern Mediterranean and to the limits of the Roman Empire.

Egyptian Blue was not only the first synthetic pigment, it was one of the first materials from antiquity to be examined by modern scientific methods. A small pot containing some of the pigment was found during the 1814 excavations at Pompeii; it caused considerable interest and was examined by several scientists of the day, including Sir Humphrey Davy. In 1884, Fouqué (1) published his analysis, which identified the compound as the calcium-copper tetrasilicate $\text{CaCuSi}_4\text{O}_{10}$ and defined the optical characteristics of the crystals. In the latter part of the 19th century, he and several other chemists, including Dr. W. J. Russell, believed that they had synthesized the pigment. Subsequently, a comprehensive series of syntheses was undertaken by Laurie et al. (2), who systematically investigated the effect of firing temperature and the concentration of alkalis. However, it was the application of x-ray diffraction powder analy-

0065-2393/84/0205-0215\$08.00/0

© 1984 American Chemical Society

sis (3,4) that made it possible to positively identify Egyptian Blue as $\text{CaCuSi}_4\text{O}_{10}$; to establish that Egyptian Blue and the natural mineral cuprorivaite are the same material; and to differentiate easily between Egyptian Blue and other blue pigments, such as blue glass frit and cobalt blue.

Recently there have been several extended research programs into the manufacture of Egyptian Blue. Chase (5) investigated the firing temperature range over which Egyptian Blue could be produced and the effect of different firing atmospheres. Bayer and Wiedemann (6) employed differential thermal analysis to investigate the formation and stability of Egyptian Blue and published SEM micrographs of single crystals. Ullrich (7) also successfully reproduced Egyptian Blue in the laboratory and investigated the variation in yield for different firing temperatures, firing times, alkali concentrations, and grain sizes of the raw materials used.

In the work reported in this chapter, which follows from a preliminary investigation (8), samples of Egyptian Blue from Egypt and Mesopotamia (Nimrud and Nineveh) together with samples of the Roman period from Western Europe (Appendix A) have been examined in order to characterize the wide range of observed fabrics (from soft and friable to hard and semivitrified and from light to dark blue) and to obtain information on the materials and techniques used in their manufacture. At the same time, any geographical or chronological differences in the range of fabrics produced and the techniques of manufacture employed have been sought.

The chemical compositions of the ancient Egyptian Blue samples (reported in the following section) were determined by atomic absorption spectrophotometry using the hydrofluoric acid digestion method together with the lithium metaborate fusion method for the silica determination (9). Some 20–30 mg of powder drilled from the objects was used for these analyses. Additionally, the arsenic concentrations were determined by x-ray fluorescence spectrometry. The precision of the analytical data was 1–2% for the major elements (>10% concentration) and deteriorated to 5–20% for the trace elements (<0.1% concentrations). However, due to the inhomogeneity of the material, variations in elemental concentrations (i.e., major, minor, and trace) of 10–15% can be expected within a single object.

The microstructures were investigated by examining in the scanning electron microscope (SEM) polished, resin-impregnated sections, prepared from small fragments (typically 2–3 mm diameter) taken from the objects. When necessary, x-ray diffraction was used to confirm the identification of the crystalline phases. The hardness values were determined by using the Mohs' scratch test, and the color groupings were defined

on the basis of direct visual comparison. Egyptian Blue was also produced in the laboratory by using a range of compositions and firing procedures; the laboratory-produced samples were compared with the ancient Egyptian Blue in terms of microstructure, hardness, and color. The production and comparative testing are described in this chapter.

Chemical Composition

The results of the chemical analyses of the ancient Egyptian Blue samples are presented in Appendix B. The concentrations of the major components (i.e., SiO_2 , CaO , and CuO) are plotted on a ternary diagram (Figure 1) after normalization to 100%. The position of the Egyptian Blue mineral ($\text{CaCuSi}_4\text{O}_{10}$ or $\text{CaO}\cdot\text{CuO}\cdot 4\text{SiO}_2$) is also plotted on the ternary diagram.

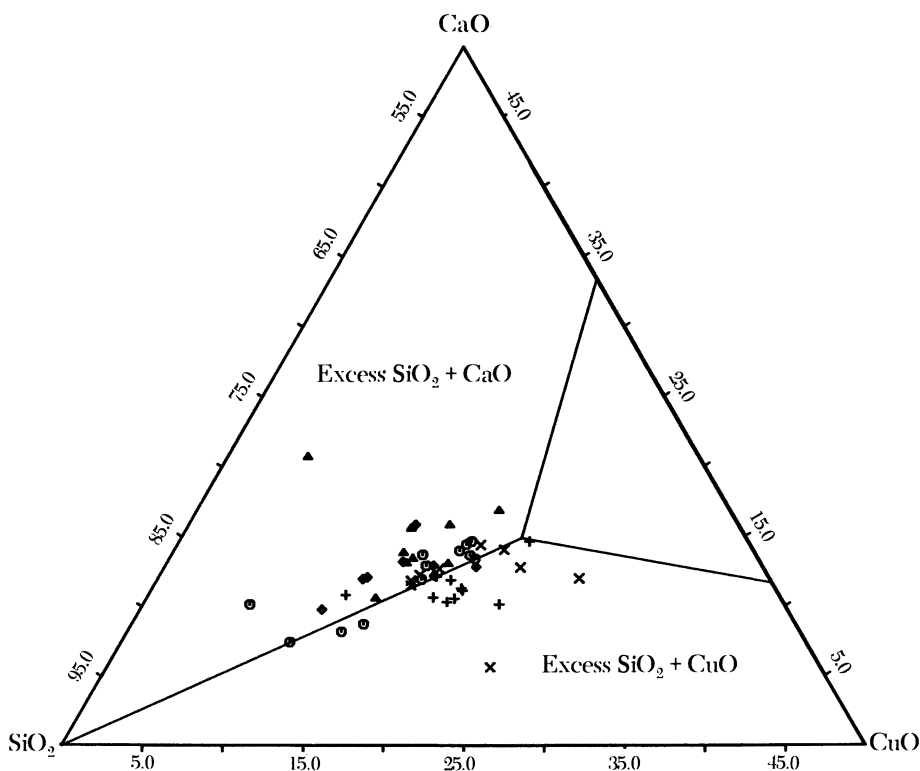


Figure 1. Ternary plot of silica, calcium oxide, and copper oxide concentrations for ancient Egyptian Blue (after normalization to 100%). The point towards the center of the ternary plot from which the three lines radiate towards the pure component positions represents the composition of the stoichiometric Egyptian Blue mineral. Key: ○, Egypt; ▲, Amarna; +, Nimrud; ×, Ninevah; ◆, Roman.

The lines radiating from this point toward the three pure component positions mark out three compositional zones. Samples falling within a zone can be considered as the Egyptian Blue mineral with an excess of two of its components; which two depends on the particular zone involved. Samples falling on, or close to, one of the lines have excess amounts of only one of the three components. The calculated percentages of the Egyptian Blue mineral (EBLU), which assume complete reaction, are given in Appendix B, together with the percentages of the excess components (SIEX, CUEX, CAEX; SiO₂, CuO, and CaO, respectively).

From the data plotted on the ternary diagram, it can be seen that none of the samples analyzed were deficient in SiO₂; that is, none contained an excess of both CaO and CuO. Instead, the majority contained moderate excesses of SiO₂ (10–30%) together with small excesses of either CaO (1–6%) or CuO (1–8%). Which of these latter components is in excess depends to some extent on the provenance of the samples. For example, the Egyptian (including Amarna) and Roman material are mainly characterized by excess CaO, whereas for the samples from Nimrud, excess CuO occurs more frequently. The material from Nineveh contains an excess of either CaO or CuO.

The concentrations of calcium oxide in the samples are rarely more than a few percent greater or less than that required to produce the Egyptian Blue minerals. Therefore, if, as is the situation for contemporary glass from Egypt and Mesopotamia, the calcium oxide was introduced into the Egyptian Blue as an impurity in the silica sand and alkali, these materials must have been carefully selected. Furthermore, because the concentration of calcium oxide in the Egyptian Blue (typically 9–15%) exceeds that in contemporary glass (5–10%), and because the alkali concentration is much lower in the Egyptian Blue (typically 4%) than in the glass (10–20%), the sands used for the Egyptian Blue must have contained significantly higher concentrations of calcium carbonate than those used for the glass. In spite of this difference, it seems unlikely that calcium oxide was added as a separate component, especially because there is no mention of this component in the description of the manufacture of Egyptian Blue given by the Roman architect Vitruvius (10).

The presence of small amounts of tin (0.1–1%) in a high proportion of the Egyptian (including Amarna) and Roman material suggests that scrap metal rather than copper ores provided the source of the copper oxide. Further, the concentrations of tin (0.5–6%), arsenic (0.05–0.15%), and lead (0.5–2%) relative to that of copper in these groups are reasonably consistent with the compositions of copper alloys for the respective periods. It is important to realize that, if corroded scrap metal had been used, the corrosion products would not exactly follow the composition of the metal. In contrast, the samples from Nimrud and Nineveh generally contain little or no tin (<0.1%) and also significantly less lead and

arsenic, which suggests the use of copper ores or copper ingots rather than scrap metal.

The concentrations of the alkali oxides (i.e., K_2O and Na_2O) are plotted in Figure 2, from which it can be seen that, with one exception (No. 14123), the Nimrud and Nineveh samples are characterized by low-alkali contents ($<0.4\%$ K_2O and Na_2O). In contrast, the majority of the Egyptian (including Amarna) and Roman material contains significantly higher concentrations of the alkali oxides (0.2 – 2.0% K_2O and 0.4 – 4.0% Na_2O). It seems possible that, in the samples containing very low alkali concentrations (less than about 1.0% K_2O plus Na_2O and with the molar concentrations of Na_2O plus K_2O less than or equal to that of Al_2O_3), the alkalis were introduced with the silica sand as feldspars and clay minerals. However, when present in higher concentrations the alkalis almost certainly represent a deliberate addition. The possible sources of the alkalis

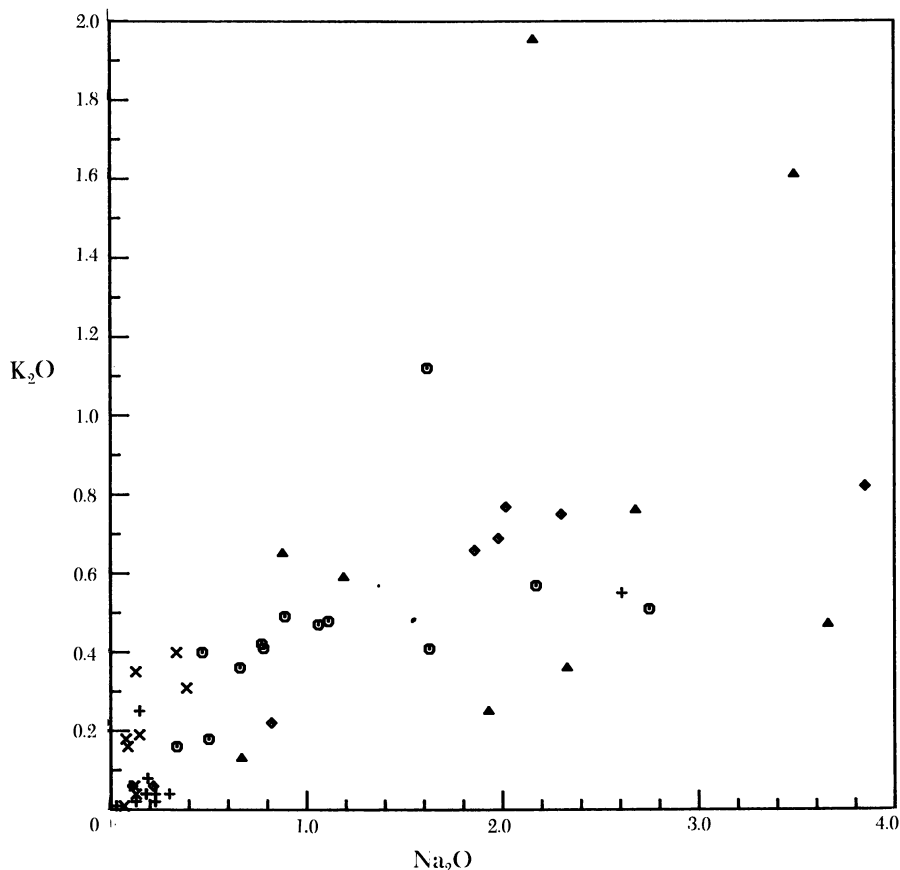


Figure 2. Potassium oxide vs. sodium oxide concentrations for ancient Egyptian Blue. Key: \odot , Egypt; \blacktriangle , Amarna; $+$, Nimrud; \times , Nineveh; \blacklozenge , Roman.

in this latter case are natron, the residues from evaporated river water, and ashes from desert or sea coast plants. Sayre and Smith (11) have suggested that the concentrations of K_2O and MgO provide a basis for identifying the source of the alkali used in ancient glass. Silica sands rarely contain more than about 1% K_2O and about 2% MgO ; therefore, higher concentrations of these oxides in ancient glasses were probably derived from the soda-rich alkali used in the production of the glass. Natron is reported to contain only very low concentrations of K_2O and MgO , whereas a few percent of each oxide is typically present in the residue from evaporated Nile and Jordan river water and in desert or sea coast plant ash. Sayre and Smith (11) therefore suggest that these latter two alkali sources were used in the production of the high K_2O (1–3%), high MgO (3–8%) glasses made in Egypt and Mesopotamia during the second and first half of the first millennia B.C. Because the concentration of Na_2O in Egyptian Blue (typically <4%) is much smaller than that in the contemporary glass (typically 10–20%), any K_2O and MgO introduced with the soda-rich alkali will not significantly alter the base level concentrations of these oxides. Therefore, K_2O and MgO concentrations are less useful as criteria for identifying the alkali source for Egyptian Blue than for glass. However, there was no obvious increase in the MgO concentration when alkali was deliberately added to the Egyptian Blue (i.e., no increase greater than about 0.5% Na_2O) (Figure 3). This finding suggests that the added alkali did not contain significant amounts of MgO and that natron could therefore have been the source of the alkali used in the production of Egyptian Blue.

Cobalt was detected in a high proportion of the samples from Nimrud and Nineveh and in an occasional sample from Egypt. However, although the concentration of cobalt (0.01–0.1%) would in some cases be high enough to produce a blue color in a glass, the glass phase present in Egyptian Blue is probably both insufficient and too fragmented for the cobalt to contribute significantly to the overall blue color. The concentration of cobalt in copper-based artifacts is typically less than 0.01% and only exceptionally as high as 0.1–0.2%. Therefore, because the Egyptian Blue only contains about 15% CuO , its cobalt concentration, if introduced with the copper, should be less than 0.002%. Similarly, the concentration of cobalt in contemporary blue glass is typically in the range 0.1–0.4%. Because of the low concentration of Na_2O in the Egyptian Blue from Nimrud and Nineveh (typically <0.5%) as compared with the glass (10–20%), at most some 5% of blue glass could have been added to the Egyptian Blue. The resulting cobalt concentration, if introduced by the addition of a normal blue glass, should be less than 0.01%. Therefore, the cobalt probably was introduced into the Egyptian Blue as a cobalt-rich glass frit analogous with zaffre or smalt, perhaps in the form in which it was added to a colorless glass to form a dark blue glass.

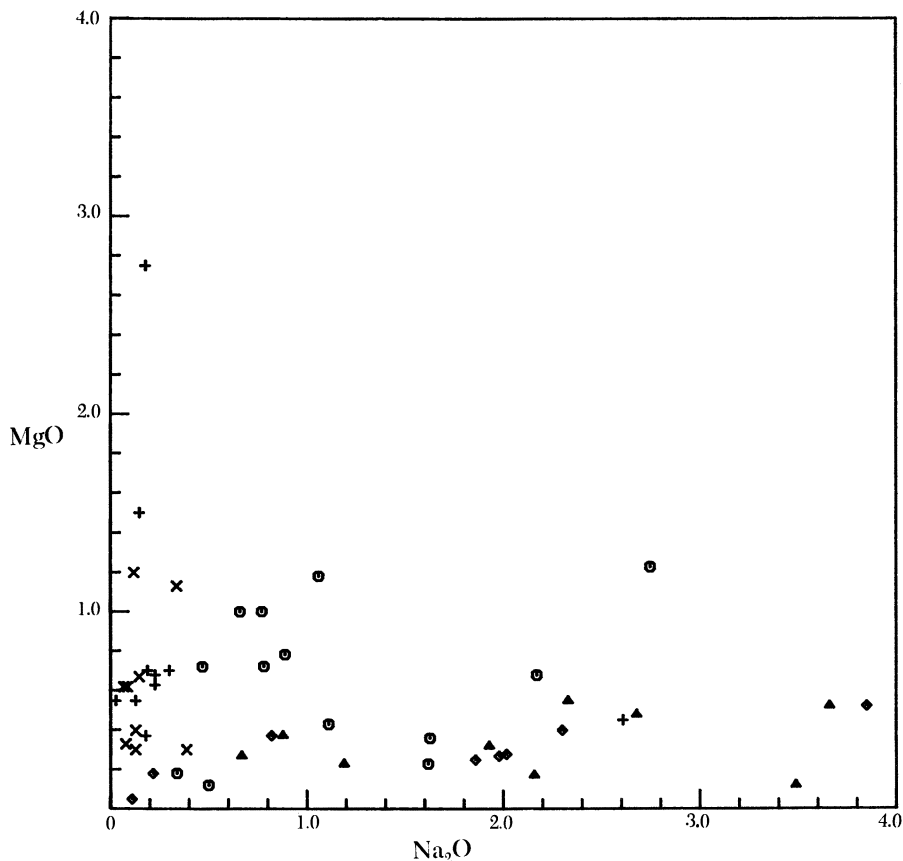


Figure 3. Magnesium oxide vs. sodium oxide concentrations for ancient Egyptian Blue. Key: \odot , Egypt; \blacktriangle , Amarna; +, Nimrud; \times , Ninevah; \blacklozenge , Roman.

Laboratory Reproduction

The following raw materials were used for the laboratory reproduction of Egyptian Blue: coarse-grained quartz (quartz sand $<250\ \mu\text{m}$, Pilkington Brothers Ltd.) or fine-grained quartz (ground flint $<53\ \mu\text{m}$, Fulham Pottery Ltd.); calcium carbonate ($<53\ \mu\text{m}$, Analar); malachite ($<53\ \mu\text{m}$); and anhydrous sodium carbonate ($<53\ \mu\text{m}$, Analar).

On the basis of the analytical data for the ancient Egyptian Blue (*see* the section entitled "Chemical Composition"), mixtures were prepared using either coarse- or fine-grained quartz such that if complete reaction occurred, the Egyptian Blue mineral ($\text{CaCuSi}_4\text{O}_{10}$) with 25% unreacted quartz would be produced. In each case, the equivalent of either 0.3 or 3% Na_2O was added to reproduce the low- and high-alkali ancient material, respectively. To achieve intimate mixing of the components, the calcium carbonate, malachite, and sodium carbonate were first ground

together under acetone and the mixture was then reground after the addition of the quartz. The four mixtures prepared in this way (see Table I) were pre-fired at 850 °C in air for 1 h in order to immobilize the alkali and decompose the carbonates. They were then ground to pass through either 250- μm or 53- μm sieves (coarse- and fine-grained quartz, respectively), dampened with water, and pelleted by using either hand pressure or a screw press.

Egyptian Blue was then produced by using either a single firing or a two-stage firing cycle. In the former case, the pelleted samples were fired in air in a laboratory furnace at either 900 or 1000 °C for up to 27 h. For the two-stage firing cycle, the Egyptian Blue produced from fine-grained quartz plus 0.3% Na_2O by firing at 1000 °C for 27 h was reground to pass through a 53- μm sieve. The resulting powder was repelleted using the screw press and fired for a second time at temperatures of 850–1000 °C for 1.5 h [Fine (R) in Table I]. To investigate the effect of a two-stage firing cycle on high-alkali material, a sample taken from the block of Egyptian Blue from Nimrud (No. 14123) was similarly ground, pelleted, and refired [Nim (R) in Table I].

Microstructure

A selection of the ancient Egyptian Blue samples and all the samples produced in the laboratory were examined in polished section in the SEM. The different phases present were distinguished on the basis of their atomic number contrast. The Egyptian Blue crystals ($\text{CaCuSi}_4\text{O}_{10}$), the glass phase, and the unreacted quartz are visible as increasingly dark areas in the photomicrographs (Figures 4–17).

Ancient Egyptian Blue. In the majority of the samples examined, abundant Egyptian Blue crystals and unreacted quartz, together with varying amounts of glass phase and only occasional unreacted calcium- and copper-rich areas, were observed. The lengths of the tabular Egyptian Blue crystals ranged from 10 to 100 μm and the diameters of the essentially equiaxial quartz grains ranged from 10 to 300 μm .

The microstructures observed were first classified as coarse- or fine-textured (c or f, respectively, in Appendix B: TEX) according to the degree of aggregation of the Egyptian Blue crystals. In the coarse-textured samples, the Egyptian Blue crystals aggregate to form definite large clusters, some of which adhere to the unreacted quartz (Figures 4, 5, 8, and 9). In the fine-textured samples, the Egyptian Blue crystals tend to be smaller, do not form large clusters, and are more uniformly interspersed between the unreacted quartz grains (Figures 6, 7, and 10). The majority of the samples classified in this way as coarse-textured also contain coarse-grained quartz (50–300- μm diameter) (Figures 4, 5, and 8); those classified as fine-textured contain fine-grained quartz (10–50-

Table 1. Laboratory-Produced Egyptian Blue

Quartz	Na ₂ O (%)	Pelleting ^a	Firing Temperature (°C)	Firing Time (h)	Texture ^b	Hardness (Mohs) ^c	Color ^{c, d}
Coarse	3.0	sp	900	5	c/C	3	1
Coarse	3.0	hp	900	27	c/C	3	1
Coarse	3.0	hp	1000	27	c/C	3	1
Fine	3.0	sp	900	5	c/F	1/2	1
Fine	3.0	hp	900	27	c/F	1	1
Coarse	0.3	sp	900	27	—	—	—
Coarse	0.3	sp	1000	27	c/C	2	1
Fine	0.3	sp	900	27	—	1	—
Fine	0.3	sp	1000	27	c/F	2/3	1/2
Fine	0.3	hp	1000	27	c/F	1/2	1/2
Nim (R)	—	sp	850	1.5	f/F	1	2/3
Nim (R)	—	sp	900	1.5	f/C	2/3	2/3
Nim (R)	—	sp	950	1.5	f/C	3	1/2
Nim (R)	—	sp	1000	1.5	f/C	3	1/2
Fine (R)	0.3	sp	850	1.5	f/F	1	2
Fine (R)	0.3	sp	900	1.5	f/F	1/2	2
Fine (R)	0.3	sp	950	1.5	f/F	2/3	2
Fine (R)	0.3	sp	1000	1.5	f/C	2/3	2

^a sp, screw press; hp, hand pressure.^b c, coarse; f, fine; C, continuous; F, fragmented.^c 1/2 and 2/3 are intermediate between 1 and 2 and 2 and 3, respectively.^d 1, dark blue; 2, light blue; 3, diluted light blue.

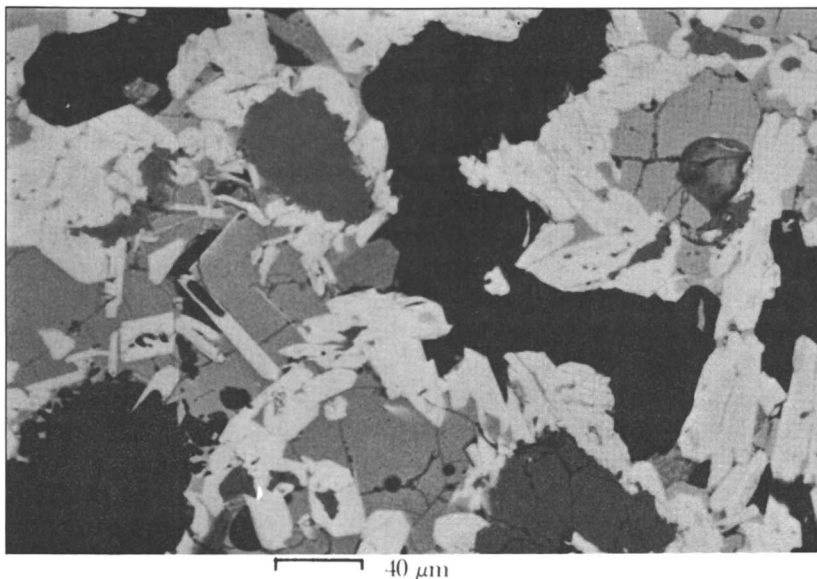


Figure 4. Sample No. 14122 (Roman): high alkali, coarse texture, continuous, hardness >3 Mohs, dark blue. The following phases can be identified: Egyptian Blue (white), glass (light gray), and quartz (dark gray).

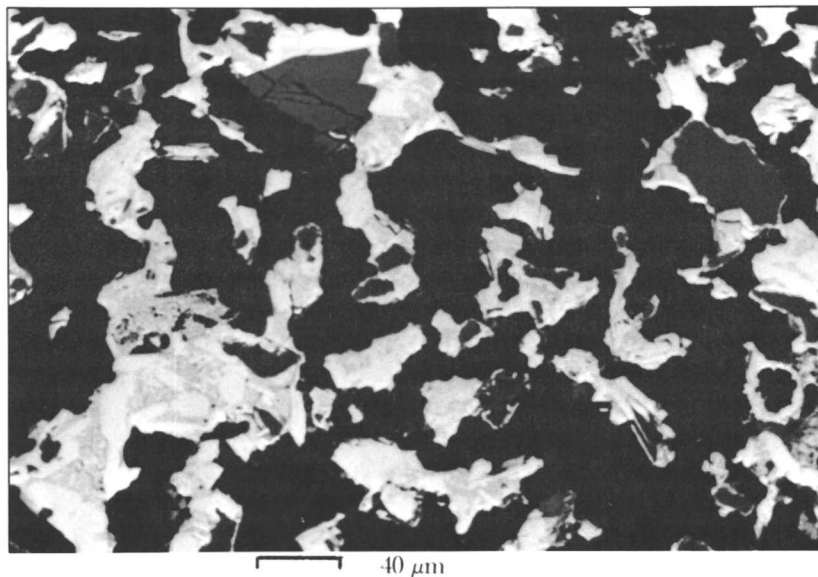


Figure 5. Sample No. 14123 (Nimrud): high alkali, coarse texture, fragmented, hardness 1 Mohs, dark blue. The following phases can be identified: Egyptian Blue (white), glass (light gray), and quartz (dark gray).

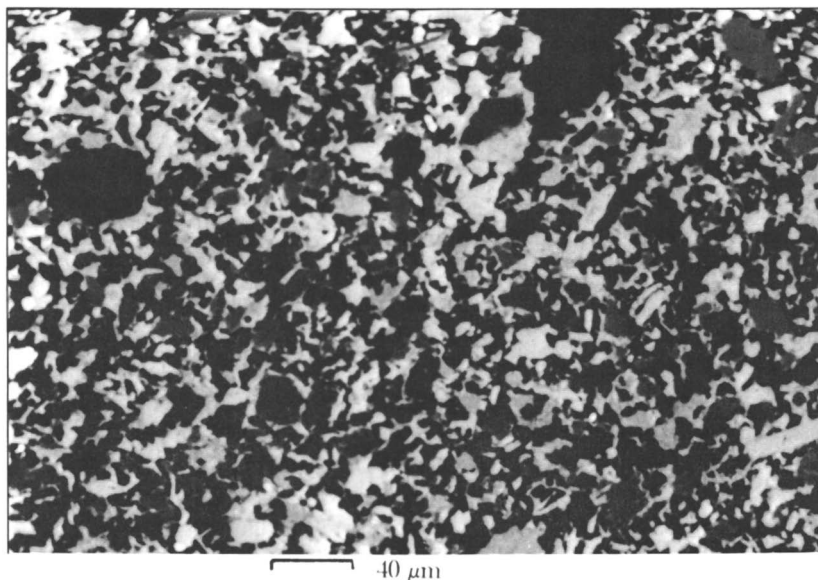


Figure 6. Sample No. 16299 (Amarna): high alkali, fine texture, continuous, hardness 2/3 Mohs. The following phases can be identified: Egyptian Blue (white), glass (light gray), and quartz (dark gray).

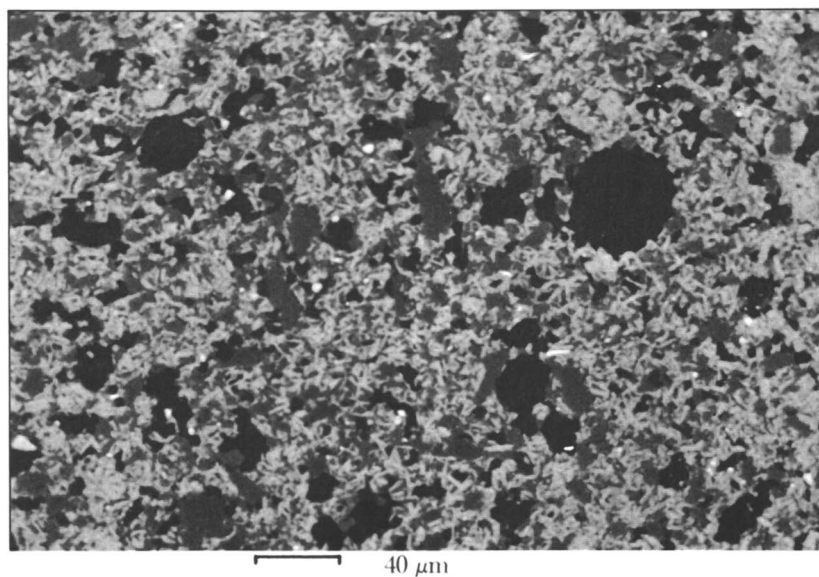


Figure 7. Sample No. 14414 (Egypt): high alkali, fine texture, continuous, hardness >3 Mohs, diluted light blue. The following phases can be identified: Egyptian Blue (white) and quartz (gray). No clearly defined areas of glass are visible.

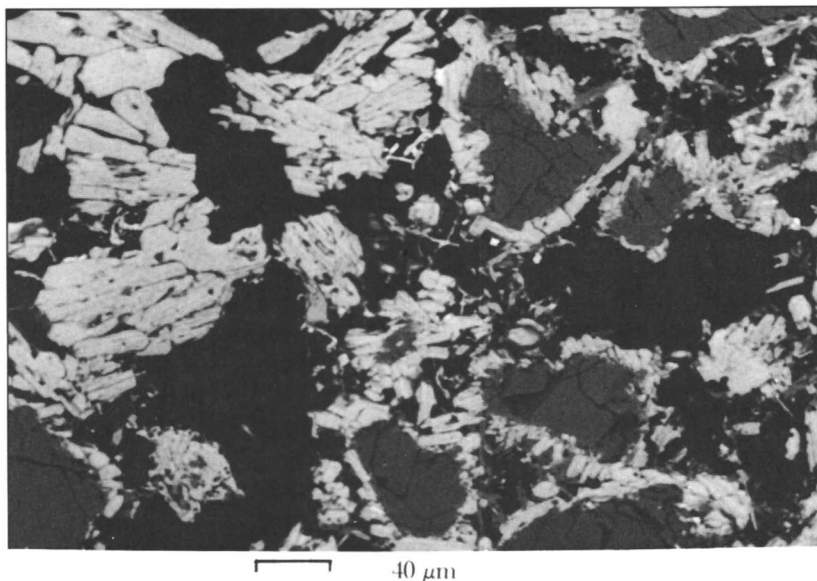


Figure 8. Sample No. 14121 (Roman): low alkali, coarse texture, fragmented, hardness 1 Mohs, dark blue. The following phases can be identified: Egyptian Blue (white) and quartz (gray). No areas of glass are visible.

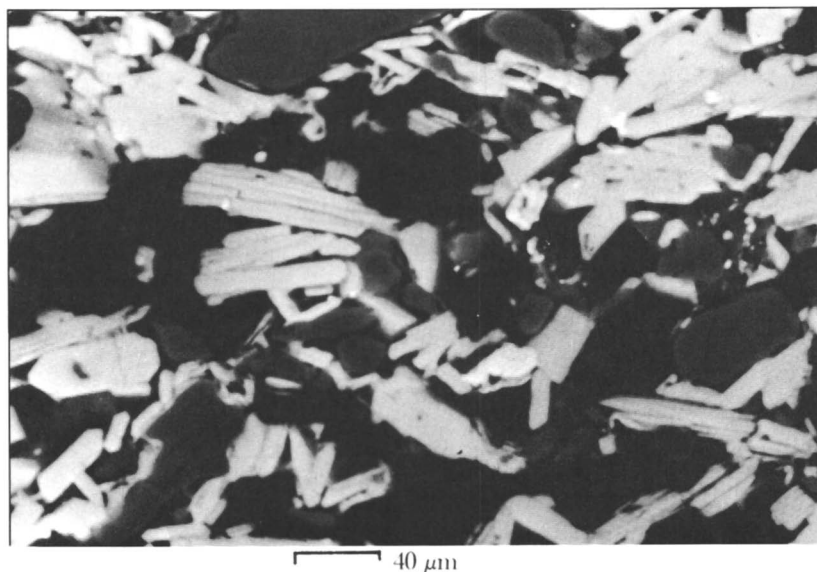


Figure 9. Sample No. 14125 (Egypt): low alkali, coarse texture, fragmented, hardness 1/2 Mohs, dark/light blue. The following phases can be identified: Egyptian Blue (white) and quartz (gray). No areas of glass are visible.

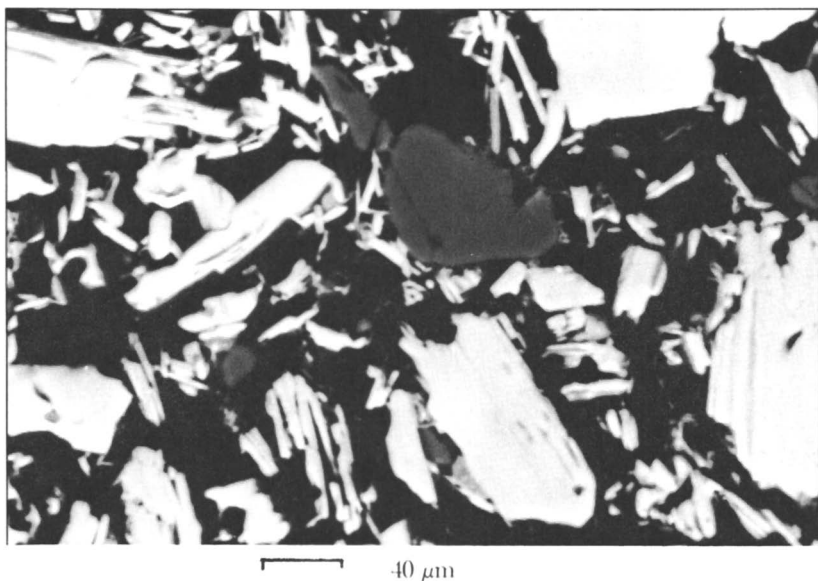


Figure 10. Sample No. 13714 (Nineveh): low alkali, fine texture, fragmented, hardness 1 Mohs, light blue. The following phases can be identified: Egyptian Blue (white) and quartz (gray). No areas of glass are visible.

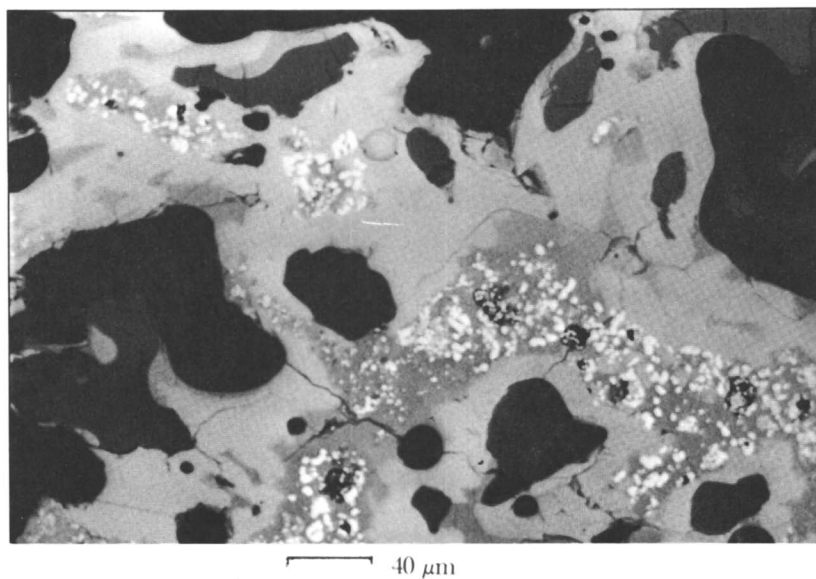


Figure 11. Laboratory sample (single firing, coarse-grained quartz, 3% Na₂O, hand pelleted, 900 °C 27 h): coarse texture, continuous, hardness 3 Mohs, dark blue. The following phases can be identified: copper oxide (white spots) in glass matrix (medium gray), Egyptian Blue (extended areas of whitelight gray), and quartz (dark gray).

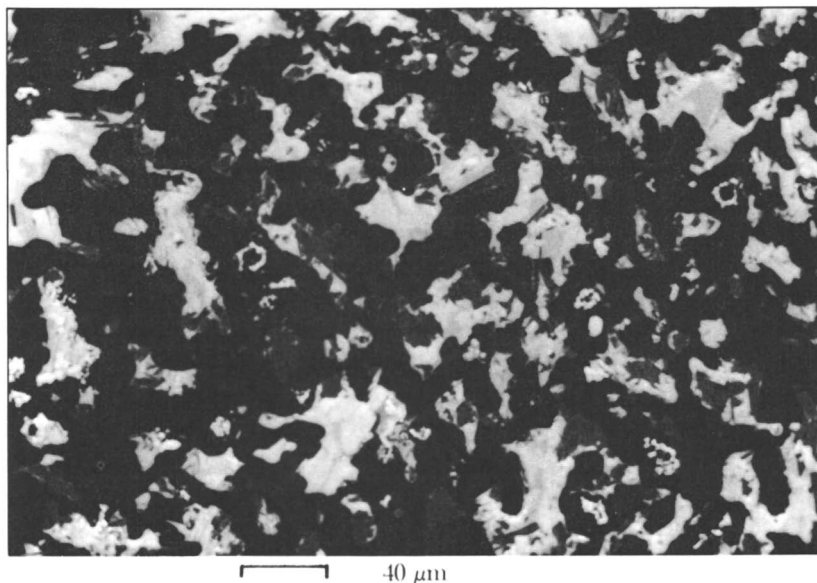


Figure 12. Laboratory sample (single firing, fine-grained quartz, 3% Na₂O, hand pelleted, 900 °C 27 h): coarse texture, fragmented, hardness 1 Mohs, dark blue. The following phases can be identified: Egyptian Blue (white), glass (light gray), and quartz or tridymite (dark gray).

μm diameter) (Figures 6, 7, and 10). Therefore, this classification additionally provides some measure of the macroscopic texture of the samples.

The microstructures were further classified as continuous or fragmented (C or F, respectively, in Appendix B: TEX) according to the extent of the long-range interconnection between the different phases. In the samples with the higher alkali contents (greater than about 1% Na₂O plus K₂O), the Egyptian Blue crystals and unreacted quartz are embedded in a glass matrix. This glass phase also normally produces long-range continuity between these reaction zones (Figures 4, 6, and 7); the exceptions are samples No. 14123 (Figure 5) and No. 13730. In contrast, in the samples with the lower alkali contents (less than about 1% Na₂O plus K₂O), a glass phase is not normally formed, and there is little or no long-range interconnection between the Egyptian Blue crystals and unreacted quartz (Figures 8–10).

Laboratory-Produced Egyptian Blue. The Egyptian Blue produced in the laboratory using a single firing was classified as coarse-textured in that, with all four mixtures specified in the “Laboratory Reproduction” section, the Egyptian Blue crystals had aggregated to form definite large clusters (Figures 11–14). However, with the high-alkali mixtures (3% Na₂O), firing at 900 °C for 5 h was sufficient to produce a significant quantity of Egyptian Blue, but with the low-alkali mixtures (0.3% Na₂O), the higher firing temperature of 1000 °C was required.

Also with the low-alkali mixtures, more Egyptian Blue crystals were produced when the samples were pelleted by using a screw press than when using hand pressure.

Although a glass phase was only formed with the high-alkali mixtures, the microstructures observed, and in particular the extent of the long-range interconnection, differed in a number of respects from those observed in the equivalent coarse-textured ancient material. With the high-alkali mixture based on coarse-grained quartz, the microstructure resembled that of the high-alkali ancient material fairly closely (Figure 11 compared with Figure 4). However, the angular morphology of the Egyptian Blue crystals was less clearly defined on the laboratory-produced material and the glass phase contained significant amounts of recrystallized copper oxide. The precipitation of copper oxide probably occurred because the mixing of the raw materials and the amount of quartz that had reacted were insufficient. With the high-alkali mixture based on fine-grained quartz, the extent of the long-range continuity was considerably reduced, and recrystallized tridymite, which was observed in only one ancient sample (No. 13731), was present in significant amounts in the glass phase even after firing to only 900 °C (Figure 12). With the low-alkali mixture based on coarse-grained quartz, a second phase consisting of calcium silicate and recrystallized copper oxide was observed;

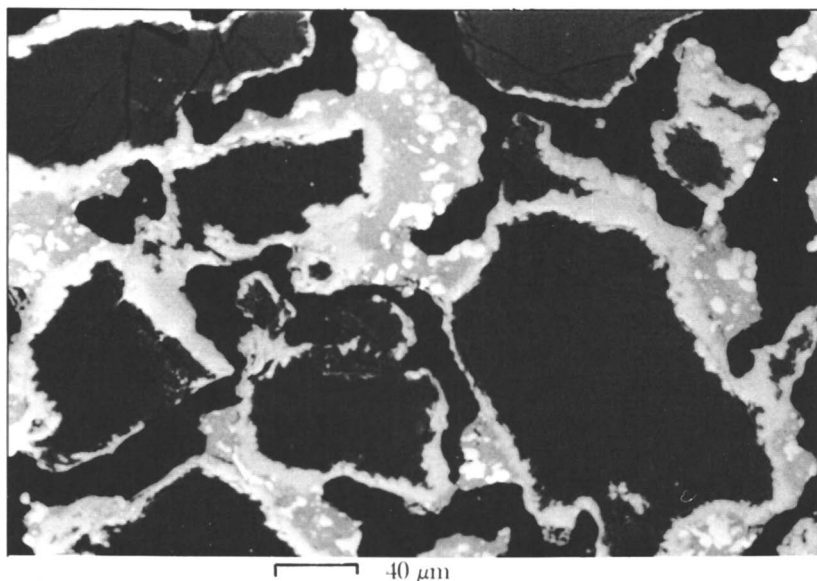


Figure 13. Laboratory sample (single firing, coarse-grained quartz, 0.3% Na₂O, screw press, 1000 °C 27 h): coarse texture, continuous, hardness 2 Mohs, dark blue. The following phases can be identified: copper oxide (white spots) in calcium silicate matrix (medium gray), Egyptian Blue (white/light gray), and quartz (dark gray).

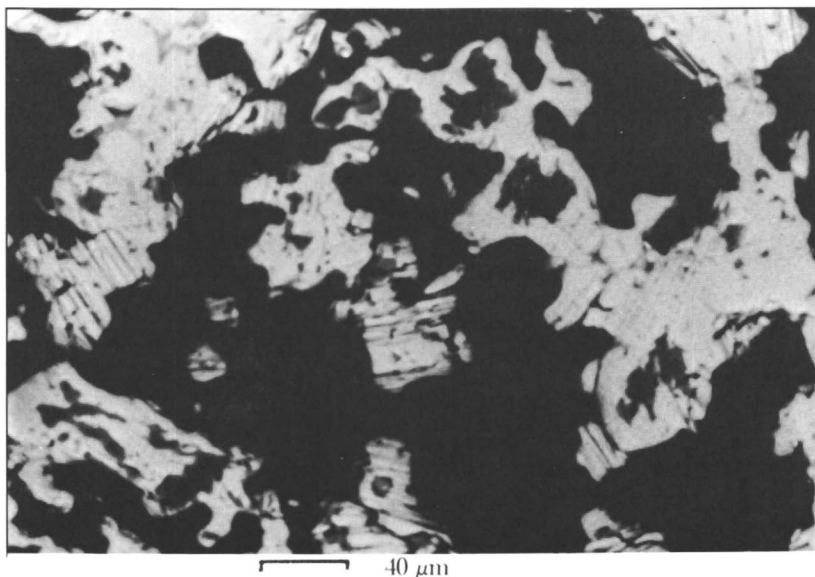


Figure 14. Laboratory sample (single firing, fine-grained quartz, 0.3% Na₂O, screw press, 1000 °C 27 h): coarse texture, fragmented, hardness 2/3 Mohs, dark/light blue. The following phases can be identified: Egyptian Blue (white) and quartz (gray). No areas of glass are visible.

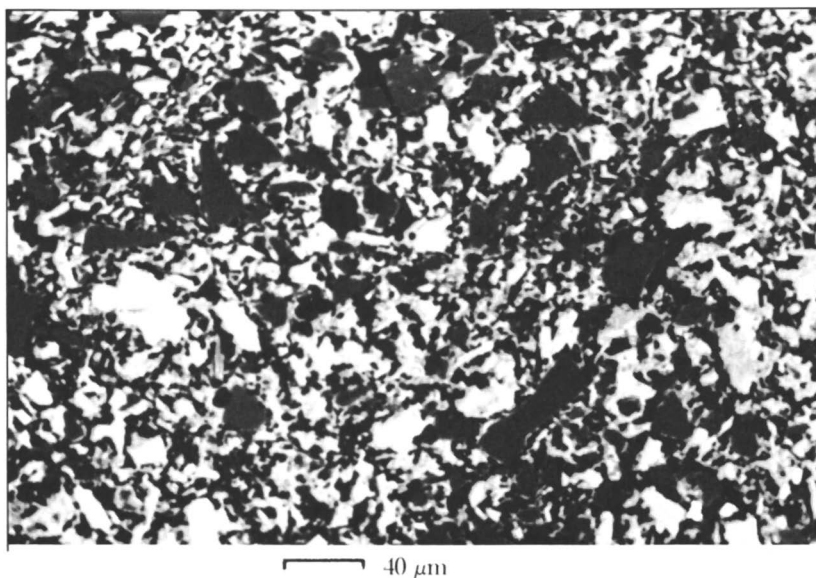


Figure 15. Laboratory sample (two-stage firing, Nim (R), 900 °C 1.5 h): fine texture, continuous, hardness 2/3 Mohs, undiluted/diluted light blue. The following phases can be identified: Egyptian Blue (white) and quartz (gray). No clearly defined areas of glass are visible.

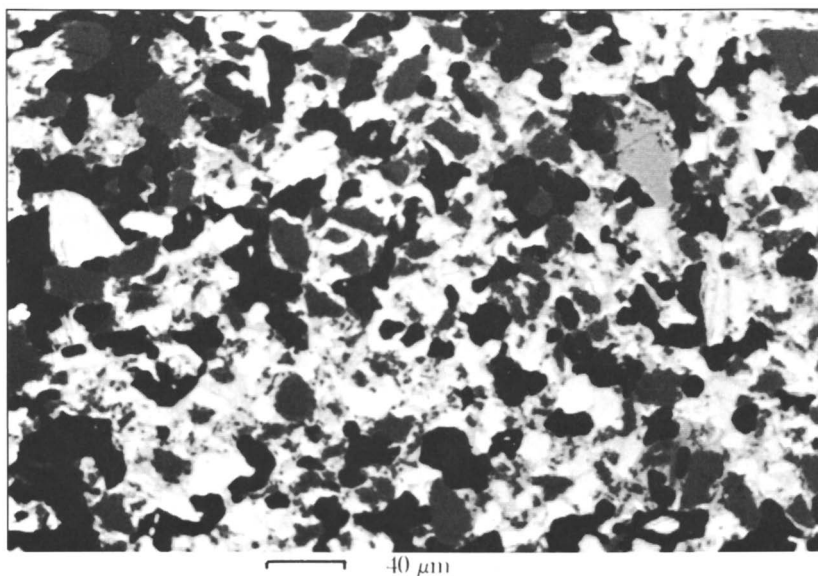


Figure 16. Laboratory sample (two-stage firing, Nim (R), 1000 °C 1.5 h): fine texture, continuous, hardness 3 Mohs, dark/light blue. The following phases can be identified: Egyptian Blue (white) and quartz (gray). No clearly defined areas of glass are visible.

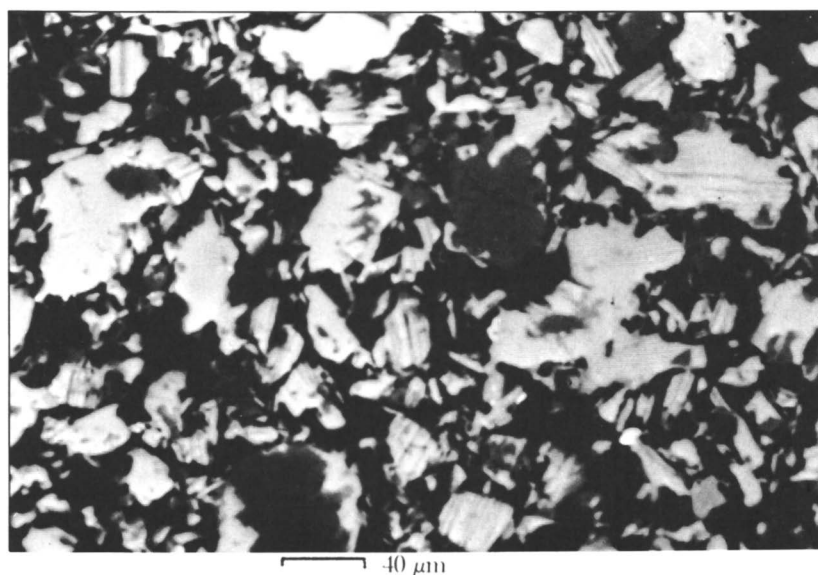


Figure 17. Laboratory sample (two-stage firing, fine (R), 900 °C 1.5 h): fine texture, fragmented, hardness 1/2 Mohs, light blue. The following phases can be identified: Egyptian Blue (white) and quartz (gray). No areas of glass are visible.

this provided some long-range interconnection (Figure 13). The formation of this second phase again probably occurred because the mixing of the raw materials and the amount of quartz that had reacted were insufficient. However, this second phase was much less pronounced within the low-alkali mixture based on fine-grained quartz; the microstructures observed in these samples resembled fairly closely those of the low alkali ancient material (Figure 14 compared with Figures 8 and 9).

The Egyptian Blue produced in the laboratory by using a two-stage firing cycle with regrinding between the first and second firings was classified as fine textured because the Egyptian Blue crystals were no longer aggregated into large clusters but were uniformly interspersed among the unreacted quartz grains (Figures 15–17). With the high-alkali samples [Nim (R)] derived from the block of Egyptian Blue from Nimrud (No. 14123), the extent of the long-range interconnection increased progressively, due to remelting and redistribution of the glass phase, as the refring temperature was increased from 850 to 1000 °C (Figures 15 and 16). However, with the low-alkali samples [Fine (R)], in which there was no glass phase, only limited long-range interconnection had developed even after refring to 1000 °C.

Thus the microstructures observed in the samples produced using the two-stage firing cycle resemble fairly closely those observed in many of the fine-textured ancient samples (Figure 15 compared with Figure 6, Figure 17 compared with Figure 10). The principal difference is that in the ancient material the angular morphology of the Egyptian Blue crystals is more clearly defined and there is less Egyptian Blue adhering to the unreacted quartz. However, the microstructure of the high-alkali ancient material, in which closely packed and very small Egyptian Blue crystals (~10 μm in length) are embedded in an essentially continuous glass matrix (Figure 7), has not been reproduced. Although the glass matrix is reasonably continuous in the laboratory-produced high-alkali sample refired at 1000 °C, the Egyptian Blue crystals are very much larger (20–40 μm in length) than in the corresponding ancient material and they are beginning to coalesce (Figure 16). This result suggests that the grinding between the first and second firing was much finer for this group of ancient material. It is also possible that the refring time was much shorter so that remelting of the glass occurred without any significant further reaction between the constituent phases.

Discussion. The primary characteristics of the vast majority of the microstructures observed in the ancient Egyptian Blue (i.e., degree of aggregation of Egyptian Blue crystals and extent of long-range interconnection between the different phases) have been successfully reproduced in the Egyptian Blue samples made in the laboratory. Further, the results of the laboratory reproduction suggest that the Egyptian Blue mineral ($\text{CaCuSi}_4\text{O}_{10}$) is formed as a result of a solid state reaction between the three principal components (silica, lime, and copper oxide). For this solid

state reaction to proceed, intimate mixing of and contact between the three components is necessary, and the formation of a glass phase such as occurs when sufficient alkali is present clearly facilitates the reaction. Thus with the high-alkali samples (3% Na₂O), significant quantities of Egyptian Blue crystals are formed at 900 °C; with the low-alkali samples (0.3% Na₂O), a firing temperature of about 1000 °C is necessary. Also with the low-alkali samples, pelleting with a screw press, as compared with hand pressure, increases the quantity of Egyptian Blue crystals produced. The reaction results in the formation of definite clusters of Egyptian Blue crystals, some of which adhere to the unreacted quartz. With a high alkali content, the Egyptian Blue crystals and unreacted quartz are embedded in a glass matrix, which also provides long-range continuity between the reaction zones.

Thus the coarse-textured ancient material could have been produced with a single firing. However, it seems most unlikely that the fine-textured ancient material could have been produced in this way; a two-stage firing cycle probably was used. The Egyptian Blue formed by the first firing would have been ground to a fine powder, thus breaking up the clusters of Egyptian Blue crystals and mixing them more uniformly with the unreacted quartz. This powder would then probably have been dampened with water and molded to the required shape before firing for a second time at 850–950 °C, which would have been sufficient to achieve coherence without any significant further reaction between the constituent phases. The microstructure of the Egyptian Blue produced in this way in the laboratory was sufficiently similar to that of the corresponding fine-textured ancient material to justify this hypothesis. Our laboratory results also established that the addition of a glass frit to the ground powder prior to refiring, as suggested by Chase (5), would not have been necessary.

Possible exceptions to this hypothesis of a single firing for the coarse-textured material and a two-stage firing cycle for the fine-textured material are the two high-alkali, coarse-textured samples (Nos. 14123 and 13730). The microstructures of these samples do not exhibit long-range interconnection between the reaction zones (Figure 5). For these samples, it seems probable that a two-stage firing cycle was employed but that the grinding between the first and second firings was only sufficient to destroy the long-range continuity and did not completely break up the clusters of Egyptian Blue crystals.

Hardness

Hardness measurements using the Mohs' scratch test were undertaken on the complete range of ancient and laboratory-produced Egyptian Blue samples (Appendix B: HAR and Table I, respectively).

The results show that the hardness clearly correlates with the extent of the long-range interconnection between the constituent phases as observed in polished section in the SEM. Thus the low-alkali samples in which there is no interconnecting glass phase (Figures 8–10) have hardnesses at the lower end of the range (1–2 Mohs). The principal exception is the fine-textured sample No. 13709 (hardness >3 Mohs) in which an extensive copper-rich glass phase has formed as a result of its 13.6% overall excess of copper oxide. In contrast, values over the full range of hardnesses (1–>3 Mohs) are observed for samples with high alkali content. The high values are associated with samples exhibiting long-range continuity (Figures 4, 6, and 7) and the low values with samples in which the Egyptian Blue/quartz reaction zones are fragmented (Figure 5).

Similarly, with the laboratory-produced samples, the high-alkali material exhibits greater hardness than does the equivalent low-alkali material. Also, the high-alkali material made by using coarse-grained quartz exhibits greater hardness than does that made by using fine-grained quartz in which the extent of long-range continuity is considerably reduced (Figure 11 compared with Figure 12). Finally, with the samples produced using a two-stage firing cycle, the hardness increases with increasing refring temperature as the long-range interconnection increases (Figure 15 compared with Figure 16).

Color

On the basis of direct visual comparison of the body, as opposed to the original surface, the ancient and laboratory-produced Egyptian Blue samples were grouped into three broad color categories: dark blue, light blue, and diluted or pale light blue (Appendix B: COL and Table I).

The results show that the change from dark blue to light blue is associated with a decrease in the overall dimensions of the clusters of Egyptian Blue crystals. Thus, samples classified as coarse-textured (Figures 4, 5, 8, 9, 11–14) and normally produced by a single firing tend to be dark blue, whereas those classified as fine-textured (Figures 7, 10, and 15–17) and produced by a two-stage firing cycle tend to be light blue.

The distinction in terms of microstructure between undiluted and diluted light blue is less obvious, but it appears that the diluted light blue is observed in fine-textured samples when the color of the Egyptian Blue phase is effectively masked by the presence of a glass phase. Thus, a high proportion of the fine-textured low-alkali samples in which there is no obvious glass phase (Figures 10 and 17) are undiluted light blue. The vast majority of the fine-textured, high-alkali samples that contain

a significant amount of a glass phase (Figures 7 and 15) are diluted or pale light blue.

Conclusions

Our results show that the range of textures, hardnesses, and colors observed in ancient Egyptian Blue can be satisfactorily explained in terms of the composition of the mixture used, the particle size of its constituents, and the firing procedures employed. The common parameter of the great majority of the ancient Egyptian Blue samples is an excess of silica (10–30%) over and above that necessary to produce the Egyptian Blue mineral ($\text{CaCuSi}_4\text{O}_{10}$) and a somewhat smaller excess of either calcium oxide or copper oxide. Further, at the microscopic level, the majority of the samples examined consist of an intimate mixture of Egyptian Blue crystals and unreacted quartz together with varying amounts of glass phase and only occasional unreacted calcium- and copper-rich areas. The amount of glass phase present is determined primarily by the alkali content (i.e., Na_2O and K_2O) of the samples, which varies from less than 0.2% to about 5%.

From the results of the laboratory reproduction of Egyptian Blue, it seems probable that both a single firing and a two-stage firing cycle were employed in the production of the ancient material. A single firing, at about 900 °C for the high-alkali material and about 1000 °C for the low-alkali material, would normally have been used to produce the coarse-textured Egyptian Blue. In contrast, a two-stage firing cycle with grinding and molding to the required final shape between the first and second firings would normally have been used to produce the fine-textured Egyptian Blue. The temperature of the second firing typically would have been 850–950 °C. The hardness of the Egyptian Blue, which depends on the extent of the long-range interconnection between the constituent phases, varies according to the temperature used in the final firing and the alkali content. Similarly, the color depends on both the overall dimensions of the clusters of Egyptian Blue crystals and the amount of glass phase present, and varies according to the firing procedure (i.e., single firing or two-stage firing cycle) and the alkali content.

The three principal groups of ancient material studied differ from each other in a number of respects. The Roman material, which consists only of pigment balls and mosaic tesserae, is entirely coarse-textured but spans the full range of alkali contents (<0.2–5%); it was probably produced using a single firing. It is dark blue in color but exhibits the full range of hardnesses (1–>3 Mohs). In contrast, the Nimrud and Nineveh material consists primarily of fragments from small objects, is almost entirely fine textured, and has only low alkali contents; it was probably

produced using a two-stage firing cycle. This material is predominantly light blue in color with a high proportion of undiluted light blue samples and exhibits hardnesses at the lower end of the range (1–2 Mohs). The principal exceptions are the two massive blocks of Egyptian Blue (Nos. 14123 and 13712), which probably represent the material used to make small objects; these samples are coarse-textured and hence dark blue in color. The Egyptian material that, except for the Amarna samples, again consists primarily of fragments from small objects, but in this case spanning a chronological range of about 1000 years, is more heterogeneous. The fragments from Amarna include both coarse- and fine-textured material with predominantly high alkali contents but exhibit hardnesses chiefly at the lower end of the range (1–2 Mohs). The objects made from Egyptian Blue are mainly fine-textured with high alkali contents; they were most probably made using a two-stage firing cycle. The light blue color predominates, with a higher proportion being diluted light blue, and the hardnesses are mainly at the upper end of the range (2–>3 Mohs).

Additionally, for the Nimrud and Nineveh material, the consistently low concentrations of tin, arsenic, and lead suggest that copper ores or copper ingots were the source of the copper oxide. Scrap metal was probably used for the majority of the Roman and Egyptian material, which contains higher concentrations of these impurities. Further, as discussed in the section on chemical composition, the analytical data suggest that where alkali was deliberately added, as in the case of a high proportion of the Roman and Egyptian material, natron was used. Thus the reported compositions are consistent with the description of the manufacture of Egyptian Blue given by Vitruvius (10), who states that sand and natron were first powdered together and copper filings were then added.

In spite of the obvious differences in the manufacturing procedures used for the three principal groups of Egyptian Blue, the number of samples studied and their chronological range were insufficient to establish whether the production of Egyptian Blue represents a single invention that subsequently spread through the Near East or whether parallel technological developments occurred independently in different parts of the Near East. Similarly, there are insufficient data available to fully establish to what extent the manufacturing procedures were varied according to the purpose for which the Egyptian Blue was being produced. However, it would appear that the small objects of Egyptian Blue, which are almost invariably fine-textured, were made using a two-stage firing cycle. Also, the massive blocks of Egyptian Blue such as those from Nimrud and Nineveh (Nos. 14123 and 13712) probably represent the material from which these objects would have been produced by grinding, molding, and refiring.

Acknowledgments

We are most grateful to T. G. H. James, Keeper, Department of Egyptian Antiquities, for suggesting this project. We are also indebted to the Departments of Egyptian and Western Asiatic Antiquities and to the Petrie Collection, University College, London, for providing the Egyptian Blue samples that have been examined. Assistance from S. La Niece and N. D. Meeks in the preparation and preliminary examination of the polished sections is gratefully acknowledged. We thank I. C. Freestone for his advice and comments during the progress of the work.

Appendix A

Egyptian Blue Samples

Sample Number	Cat/Reg	Description	Provenience	Date
14413	1926 11-11 20	Fragment of disc-shaped cover	Egypt	ca. 1350 B.C.
14412	1876 11-30 229	Pigment slab	Egypt	ca. 1350 B.C.
14128	1885 11-1 31	Vessel fragment	Naucratis, Egypt	ca. 600 B.C.
14414	1886 10-9 163	Fragment of figure	Egypt	ca. 600 B.C.
14125	1873 6-9 123	Head of a lion	Tell el Yahudja, Egypt	6-5 Century B.C.
14233	1902 4-12 194	Columnn drum	Egypt	ca. 300 B.C.
14232	1902 4-12 195	Columnn drum	Egypt	ca. 300 B.C.
14231	1902 4-12 197	Columnn drum	Egypt	ca. 300 B.C.
14230	1902 4-12 196	Columnn drum	Egypt	ca. 300 B.C.
14127	1946 12-14 146	Figures of Bes	Egypt	ca. 300 B.C.
14126	1902 4-12 193	Columnn drum	Egypt	ca. 300 B.C.
16298	UC25155	Fragment	Amarna, Egypt	14 Century B.C.
16299	UC25156	Fragment	Amarna, Egypt	14 Century B.C.
13728	UC25153c	Fragment	Amarna, Egypt	14 Century B.C.
13729	UC25154	Fragment	Amarna, Egypt	14 Century B.C.
13730	UC8987	Fragment attached to pottery jar	Amarna, Egypt	14 Century B.C.
13731	UC24686	Fragment	Amarna, Egypt	14 Century B.C.
13726	UC25153a	Fragment	Amarna, Egypt	14 Century B.C.
13727	UC25153b	Fragment	Amarna, Egypt	14 Century B.C.
13717	N769	Fragment of hair	Nimrud	9-7 Century B.C.
13719	1946 11-4 289	Vessel fragment	Nimrud	9-7 Century B.C.

13720	N775	Fragment of curl	Nimrud	9-7 Century B.C.
13721	N770	Fragment of plaited wig	Nimrud	9-7 Century B.C.
13722	N778	Pendant fragment	Nimrud	9-7 Century B.C.
13723	N776	Corrugated fragment	Nimrud	9-7 Century B.C.
13724	N767	Lion's head, fragment of beard	Nimrud	9-7 Century B.C.
13725	N781	Plaque, fragment depicting sacred tree	Nimrud	9-7 Century B.C.
13726	N768	Fragment of wig	Nimrud	9-7 Century B.C.
14123	RLab	Block of raw material	Burnt Palace, Nimrud	9-7 Century B.C.
13708	1855 12-5 92	Vessel fragment	Kouyunjik, Nineveh	9-7 Century B.C.
13710	1905 4-9 432	Fragment of curl	Kouyunjik, Nineveh	9-7 Century B.C.
13711	1905 4-9 431	Cylinder	Kouyunjik, Nineveh	9-7 Century B.C.
13712	1855 12-5 345	Block of raw material	Kouyunjik, Nineveh	9-7 Century B.C.
13713	1880 7-19 239	Octagonal handle, fragment	Kouyunjik, Nineveh	9-7 Century B.C.
13714	1885 2-5 87	Cylinder fragment	Kouyunjik, Nineveh	9-7 Century B.C.
13715	1885 12-5 91	Decorated motif	Kouyunjik, Nineveh	9-7 Century B.C.
13716	1882 5-22 322	Fragment	Kouyunjik, Nineveh	9-7 Century B.C.
13709	RM2 451	Vessel fragment	Kouyunjik, Nineveh	9-7 Century B.C.
13982	BR1972 769 ACW	Ball of pigment?	Braughing, Herts	Romano-British
14118	RLab	Pigment?	Cow Roast, Berkhamstead	Romano-British
14120	RLab	Ball of pigment	Wreck of Planter III, Marseilles	Roman
14121	RLab	Ball of pigment	Wreck of Melueha, Malta	3 Century A.D.
16356	RLab	Ball of pigment	Wreck, Malta	2 Century A.D.
14119	RLab	Mosaic	Dormus Augustana, Palatine	A.D. 81-96
14122	RLab	Mosaic	Hadrian's Villa, Tivoli	A.D. 117-138
14124	RLab	Mosaic	Hadrian's Villa, Piazzadoro	A.D. 117-138

Appendix B
Analyses of Egyptian Blue

Sample Number	HAR#	TEX#	COL#	Cu	Ca	Si	Fe	Na	K	Mg	Al	Pb	Zn	As	Sn	Co	Total	EBL ^b	SIEX ^c	CUEX ^c	CAEX ^c
14413	>3	f/C 1/2	13.3	8.03	70.9	0.370	2.17	0.570	0.680	1.20	—	—	—	<0.01	<0.10	<0.01	97.30	53.9	36.5	1.90	—
14412	1/2	f/C 3	10.0	7.10	78.6	0.5	1.11	0.480	0.430	1.40	—	—	—	<0.01	<0.10	<0.01	99.60	47.2	48.5	—	—
14128	2	c/F 1/2	18.1	13.3	66.0	0.830	0.340	0.160	0.180	0.4	0.020	0.010	0.010	<0.01	<0.10	<0.01	99.30	85.4	11.4	—	0.6
14414	>3	f/C 3	11.4	7.0	67.3	0.760	1.63	0.410	0.360	1.0	—	—	—	<0.01	<0.10	<0.01	89.80	47.0	37.3	1.40	—
14125	1/2	c/F 1/2	14.9	10.8	65.0	0.590	0.5	0.180	0.120	0.6	0.330	<0.01	<0.01	0.010	0.5	<0.01	93.40	70.3	20.1	—	0.3
14233	3	2	16.5	13.3	61.0	0.8	0.770	0.420	1.0	0.9	0.260	0.010	0.010	0.010	0.9	<0.01	95.90	77.8	11.3	—	1.70
14232	3	f/C 3	13.9	12.2	63.0	0.890	0.890	0.490	0.780	0.8	0.230	<0.01	<0.01	0.010	0.8	0.030	94.0	65.6	21.2	—	2.40
14231	>3	f/C 3	17.0	12.0	60.5	0.830	0.660	0.360	1.0	1.0	0.250	<0.01	<0.01	0.025	0.9	<0.01	94.50	80.2	9.30	—	—
14230	>3	2	16.1	12.9	60.5	0.8	1.06	0.470	1.18	0.8	0.230	0.010	0.010	0.010	0.8	<0.01	94.90	75.9	12.0	—	1.60
14127	1/2	1/2	16.4	12.9	63.0	0.8	0.470	0.4	0.720	0.6	0.040	0.050	<0.01	<0.10	<0.01	<0.01	95.40	77.4	13.6	—	1.40
14126	>3	f/C 2/3	14.1	11.2	61.5	0.740	0.780	0.410	0.720	0.7	0.220	<0.01	<0.01	0.010	0.8	<0.01	91.20	66.5	19.0	—	1.30
16298	2		13.9	12.3	65.5	0.710	2.68	0.760	0.480	0.5	0.010	<0.01	<0.01	<0.01	0.5	0.010	97.30	65.6	23.6	—	2.50
16299	2/3	f/C	13.1	12.6	65.5	0.410	2.33	0.360	0.550	0.5	0.020	<0.01	<0.01	<0.01	0.6	<0.01	96.0	61.8	26.0	—	3.40
13728	2		17.1	15.3	58.5	0.540	1.93	0.250	0.320	0.6	0.020	<0.01	<0.01	—	0.1	<0.01	94.70	80.7	7.0	—	3.30
13729	1		14.5	12.7	70.0	0.430	1.19	0.590	0.230	0.6	0.010	<0.01	<0.01	<0.01	0.8	<0.01	101.1	68.4	26.3	—	2.50
13730	1/2	c/F	13.3	14.8	67.0	0.3	2.16	1.95	0.170	0.4	0.010	<0.01	<0.01	<0.01	1.0	<0.01	101.1	62.7	26.9	—	5.50
13731	1/2	c/C	13.1	9.70	69.0	0.190	3.49	1.61	0.120	<0.10	0.2	<0.01	<0.01	<0.01	<0.10	<0.01	97.40	61.8	29.5	—	0.5
13726	2		16.5	12.3	65.5	0.240	0.670	0.130	0.270	0.6	0.020	<0.01	<0.01	<0.01	0.5	<0.01	96.70	77.8	15.8	—	0.7
13727	2		15.4	15.0	64.5	0.640	0.880	0.650	0.370	0.8	0.010	0.010	0.010	<0.01	<0.10	<0.01	98.30	72.6	18.1	—	4.20
13717	1	f/F 2	17.4	11.3	66.5	0.660	0.230	0.040	0.630	0.7	0.030	<0.01	<0.01	<0.01	<0.10	0.1	97.60	75.8	18.0	1.30	—
13719	1	f/F 3	15.5	10.9	63.5	0.830	0.180	0.040	2.75	0.9	0.050	<0.01	<0.01	0.010	0.4	<0.01	95.10	73.1	16.8	—	—
13720	1	3	18.1	10.4	65.0	0.360	0.030	0.010	0.550	0.3	0.020	<0.01	<0.01	<0.01	<0.10	<0.01	94.80	69.8	20.4	3.30	—
13721	1	f/F 2	20.4	13.7	59.5	0.330	0.130	0.020	0.550	0.3	0.020	<0.01	<0.01	<0.01	<0.10	0.080	95.0	91.9	0.7	0.9	—

13722	1	2	18.4	10.8	66.5	0.630	0.230	0.020	0.680	0.7	0.030	0.010	<0.01	<0.10	0.010	98.0	72.5	20.2	3.0	—
13723	1	fF 2	18.0	9.90	66.0	0.470	0.150	0.250	1.50	0.5	0.030	0.030	<0.01	<0.10	0.010	96.80	66.4	23.5	3.90	—
13724	1/2	2/3	17.9	9.80	67.5	0.5	0.190	0.080	0.7	0.6	0.030	<0.03	<0.01	<0.10	<0.01	97.30	65.8	25.5	4.0	—
13725	1/2		19.6	9.0	60.0	0.290	0.180	0.040	0.370	0.6	0.010	0.010	<0.01	<0.10	<0.01	90.10	60.4	21.4	6.80	—
13718	1	2	17.5	10.5	70.5	0.540	0.3	0.040	0.7	0.7	0.030	0.030	<0.01	<0.10	0.010	100.8	70.5	25.5	2.60	—
14123	1	c/F 1	11.0	9.70	69.0	2.46	2.61	0.550	0.450	1.10	0.140	0.240	0.150	<0.10	0.010	97.40	51.9	35.8	—	2.0
13708	1	fF 2/3	14.9	11.3	66.0	0.560	0.390	0.310	0.3	0.9	0.060	<0.01	<0.01	0.9	<0.01	95.60	70.3	21.2	—	0.8
13710	1	2	20.4	11.8	60.0	0.8	0.130	0.040	0.4	0.9	0.080	<0.01	<0.01	0.1	0.030	94.70	79.2	9.40	3.60	—
13711	1	2	16.5	12.2	67.5	0.340	0.070	0.010	0.620	0.2	0.020	<0.01	<0.01	<0.10	<0.01	97.50	77.8	17.8	—	0.6
13712	1/2	c/F 1	15.0	11.2	68.5	0.210	0.130	0.350	0.3	0.4	0.020	<0.01	<0.01	<0.10	<0.01	96.10	70.8	23.3	—	0.7
13713	1	2	15.0	10.8	68.0	0.540	0.080	0.180	0.330	0.5	0.010	<0.01	<0.01	<0.10	<0.01	95.40	70.8	22.8	—	0.3
13714	1	fF 2	18.4	14.0	65.0	0.370	0.090	0.160	0.620	0.4	0.020	<0.01	<0.01	<0.10	0.010	99.10	86.8	9.50	—	1.10
13715	1	3	18.5	12.7	59.0	0.560	0.150	0.190	0.670	0.6	0.050	<0.01	<0.01	0.1	0.030	92.50	85.2	4.50	0.4	—
13716	1	fF 2	21.4	9.80	50.5	0.690	0.340	0.4	1.13	0.7	0.020	<0.01	<0.01	<0.10	<0.01	85.0	65.8	8.50	7.50	—
13709	>3	f/C 3	20.6	4.90	61.0	0.240	0.120	0.060	1.20	0.3	0.020	0.040	<0.01	<0.10	0.030	88.50	32.9	40.0	13.6	—
13982	1/2	c/F 1	18.0	11.9	63.0	0.470	0.110	0.060	0.050	0.6	0.270	0.010	<0.01	<0.10	<0.01	94.50	79.9	12.0	1.10	—
14118			11.6	10.9	68.5	1.03	2.30	0.750	0.4	3.40	0.270	<0.01	<0.01	0.4	<0.01	99.60	54.7	33.5	—	2.70
14120	1/2	1	13.1	14.7	65.0	0.560	0.220	0.060	0.180	0.4	0.150	<0.01	0.065	0.1	<0.01	94.60	61.8	25.5	—	5.50
14121	1	c/F 1	15.7	11.2	65.0	1.50	0.822	0.220	0.370	0.7	0.130	<0.01	0.025	0.1	<0.01	95.70	74.1	17.7	—	0.3
16356			11.4	10.6	65.8	1.53	3.85	0.820	0.520	2.71	0.240	0.030	<0.01	0.5	<0.01	98.50	53.8	31.4	—	2.60
14119	2	1	15.4	11.9	65.0	0.890	1.98	0.690	0.270	1.90	0.1	0.050	<0.01	0.4	<0.01	96.50	72.6	18.6	—	1.10
14122	>3	c/C 1	13.1	11.8	64.5	0.640	1.86	0.660	0.250	1.70	0.050	<0.01	<0.01	0.1	<0.01	94.70	61.8	25.0	—	2.60
14124	2	c/C 1	10.5	9.10	73.5	0.890	2.02	0.770	0.280	1.90	0.280	<0.01	<0.01	0.3	<0.01	98.60	49.5	41.9	—	1.70

NOTE: Data are given as percent weight of oxides unless otherwise indicated.
^a HAR, hardness in Mohs; TEX, texture—c: coarse; f: fine; C, continuous; F, fragmented; COL, color—1, dark blue; 2, light blue; 3, diluted light blue. 1/2 and 2/3 are intermediate between 1 and 2 and 2 and 3, respectively.
^b Calculated percentages of the Egyptian Blue mineral.
^c Excess components: SIEX, SiO₂; CUEX, CuO; CAEX, CaO.

Literature Cited

1. Fouqué, F. *Bull. Soc. de Mines de France* 1884, 12, 36–37.
2. Laurie, A. P.; McLintock, W. F. P.; Miles, F. D. *Proc. Roy. Soc.* 1914, A89, 418–29.
3. Pabst, A. *Acta Crystallogr.* 1959, 12, 733–39.
4. Mazzi, F.; Pabst, A. *Am. Mineral.* 1962, 47, 409–11.
5. Chase, W. T. “Science and Archaeology”; Brill, R. H., Ed.; MIT Press: Cambridge, Mass., 1971; pp. 80–90.
6. Bayer, G.; Wiedemann, H. G. *Bull. Sandoz* 1976, 40, 19–40.
7. Ullrich, D. Diploma Thesis, Freien Universität, Berlin, 1979.
8. Tite, M. S.; Bimson, M.; Meeks, N. D. *Rev. d'Archéométrie* 1981, 5 (Supplément), 296–301.
9. Hughes, M. J.; Cowell M. R.; Craddock, P. T. *Archaeometry* 1976, 18, 19–37.
10. Vitruvius. “The Ten Books on Architecture”; Bk. 7, Chap. 11.
11. Sayre, E. V.; Smith, R. W. “Archaeological Chemistry”; Levey, M., Ed.; Univ. Pennsylvania Press: Philadelphia, 1967; pp. 279–311.

RECEIVED for review October 6, 1982. ACCEPTED for publication March 18, 1983.

Analysis of Medieval Pigments from Cilician Armenia

DIANE E. CABELLI

Brookhaven National Laboratory, Upton, NY 11973

MARY VIRGINIA ORNA, O.S.U.

College of New Rochelle, New Rochelle, NY 10805

THOMAS F. MATHEWS

New York University, Institute of Fine Arts, New York, NY 10021

Chemical and physical analysis of the pigments found in four Cilician manuscripts show a remarkable consistency from manuscript to manuscript. From the mid 13th through the 14th centuries, the palette of this region is most notable for its use of ultramarine as the standard blue pigment and for the lack of a true green pigment. Indications are that the Cilician palette was continuous with that of an earlier tradition dating from the mid 11th century, and that this painting tradition continued with the Lake Van School into the 15th and 16th centuries.

ESTABLISHING EMPIRICALLY the range of pigments in use in Armenia from the 10th century to the 16th century is the goal of a larger project (1) of which this chapter is a part. From the pioneering work of Thompson (2) to the more recent studies of Roosen-Runge and Werner (3, 4), the discussion of pigments in medieval manuscripts has generally been based on a close reading of the painters' manuals joined with a minute observation of the works of art. Analytical data that might indicate the varieties of palette available in different centers at different times are still very scarce. In Byzantine art, moreover, where painters' manuals that antedate that of Dionysius of Fourna, an 18th century work (5), are missing, discussion of pigments in manuscripts is largely speculative. The present project was designed to fill some of these gaps by analyzing pigments from representative manuscripts through the conventional techniques of small particle analysis.

Armenian material was chosen for this project because a large percentage of Armenian manuscripts are dated and located by inscriptions,

0065-2393/84/0205-0243\$06.00/0

© 1984 American Chemical Society

permitting the establishment of chronological and geographical distribution patterns. In Byzantine material, by contrast, dates and places would be largely conjectural. Armenia seems to promise a wide diversity of evidence because it was, at different periods in its history, in close contact with the Latin world, Byzantium, Islam, and civilizations even farther east (6).

The first, pilot phase of the project consisted of a thorough analysis of the pigments of a single manuscript, the gospel from Glajor, near Lake Sevan, ca. 1300 (Los Angeles, U. C. L. A. MS Arm. 1). After distinguishing on the basis of style five artists belonging to two distinct workshops, the palette of each artist was examined separately. Results indicated slight differences from artist to artist and significant differences between the two workshops. One workshop had not only wider range, but also a better quality of pigments (7).

The second phase of the study (8, 9) comprised the analysis of the pigments of 22 manuscripts in the United States and Israel representing four distinct developments in the history of Armenian art: 1) manuscripts of Greater Armenia and Melitene in the 10th and 11th centuries, 2) manuscripts of the Armenian Kingdom of Cilicia in the 13th and 14th centuries, 3) manuscripts in the vicinity of Lake Sevan in the 12th to 14th centuries, and 4) manuscripts in the vicinity of Lake Van in the 14th and 15th centuries. In this chapter we report on data under the second heading. Our aim is to describe the pigments available to the artists of this period and locale; to determine, if possible, the techniques that were used in fabricating the wide range of hues found in these manuscripts; and to provide the groundwork for future studies of Armenian illuminated manuscripts from both earlier and later periods and different locales.

Description of the Manuscripts

Armenians began settling in Cilicia (*see* Figure 1) in the second half of the 10th century in territory from which the Moslem population had been expelled by the Byzantine emperor. This process was accelerated in the 11th century when the Turkish invasion drove larger numbers of Armenians out of their territorial home in Greater Armenia. In their new state on the Mediterranean, they found themselves in immediate alliance with the Latin kingdoms established by the Crusaders in the Levant, but their commercial and diplomatic contacts reached much farther—from Constantinople to the court of the Mongol Khan (10). The cosmopolitan character of the Cilician Kingdom is reflected in the sophisticated painting of surviving illuminated manuscripts.

Three of the four manuscripts that comprise this study come from Hromkla, which was the seat of the patriarch and the most important

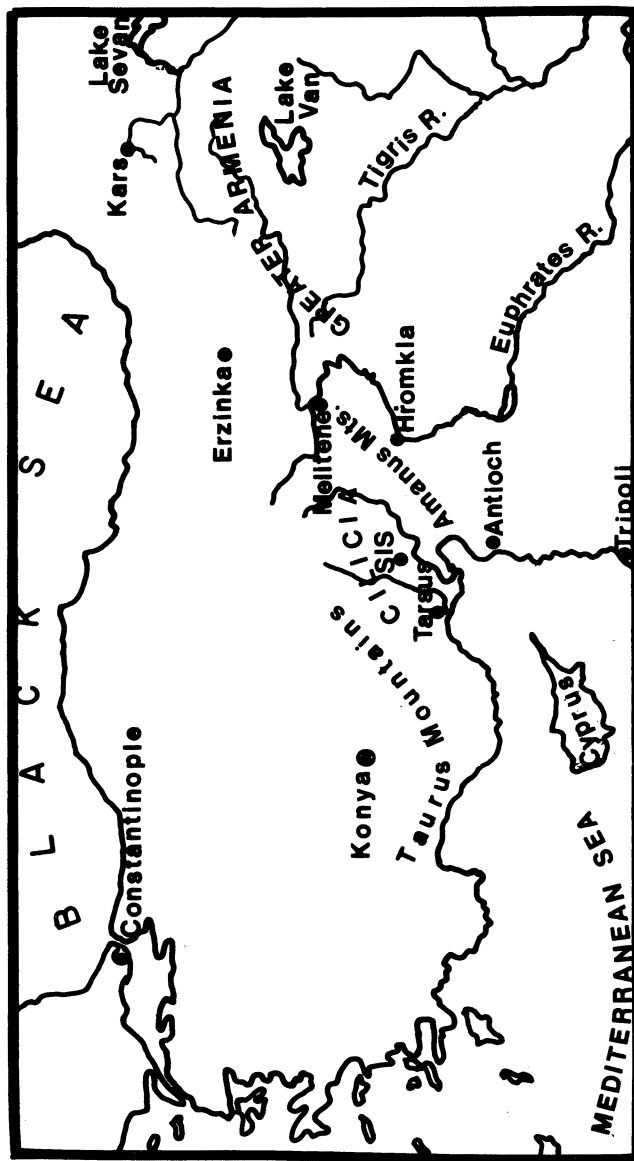


Figure 1. Cilicia and neighboring lands.

scriptorium in Cilicia. The first is a gospel manuscript on vellum (Washington, Freer Gallery of Art, MS 44.17) executed by the monk Hohannes for the Catholicos Constantine I in 1253.

The second manuscript, also a gospel on vellum (Washington, Freer Gallery of Art, MS 32.18), is one of the finest and most extensively illuminated Cilician manuscripts. Although its dedicatory inscription is missing, Der Nersessian (11, 12) assigned the manuscript to the atelier of T'oros Roslin, the master of the scriptorium at Hromkla during the second half of the 13th century. The name of its owner, the Baron Vasak (d. 1284), is written in gold letters on the marginal medallion of page 52.

The inscriptions of the third manuscript (Baltimore, Walters Art Gallery, MS W. 539) document its completion at Hromkla at the hands of T'oros Roslin in 1262. A gospel on vellum, it was executed for the priest T'oros, nephew of Constantine I. The extensive narrative illuminations make this manuscript in many ways a twin of the preceding gospel (12).

The fourth manuscript (New York, Pierpont Morgan Library MS M. 622) is the second volume of a two-volume menologium containing the abridged lives of 193 Armenian, Greek, and Latin saints. The manuscript, on paper, was executed at Sis, the capital of Cilicia, by Sargis Pijak, who is the most accomplished Cilician painter of the 14th century (13).

Experimental Procedure

Over 150 pigment samples covering the spectrum of hues used in Cilician art were taken from the four manuscripts described above. The hues were differentiated both by visual assessment and by comparison with color chips from the Munsell Book of Colors (14). In addition, because both MS Freer 32.18 and MS W. 539 were painted by workshops, pigment samples were taken from all of the miniatures of recognizably different styles in these two manuscripts.

The samples were abstracted with a fine surgical scalpel (Sterisharps No. 11 blade) under a 40 \times binocular microscope, stored for transport between two precleaned 75 \times 25 mm microscope slides (Fisher), and sealed with transparent tape. In many instances, samples were taken from smudges of pigment offset from the miniatures onto the facing pages of the manuscripts, allowing for most sampling to take place without touching the painting of the miniatures themselves. When such offset samples of a specific hue were unavailable, particles were removed only from the borders or from already damaged parts of the miniature in question. The curatorial and conservation staffs of the collections have provided close guidance on the best way to handle each manuscript.

Each sample was coded according to hue, page number, and $y-x$ coordinates in millimeters as measured from the bottom and outer edges of each page. For example, a code of R,109v (173,126) identifies a red sample taken from folio 109 verso, 173 mm from the bottom and 126 mm from the outer (left) edge of the page. The location of each sample was also marked on photographs made of each sampled page. Figure 2 shows the locations of samples taken from folio 13 verso,



Figure 2. MS W. 539, folio 13 verso, "St. Matthew, the Evangelist"; locations from which samples were taken for analysis are indicated. Reproduced with permission from the Walters Art Gallery, Baltimore, Md.

the Portrait of the Evangelist Matthew, from MS W. 539, and Table I identifies each sample according to hue–location code and Munsell color notation.

The samples were analyzed by polarized light microscopy and x-ray diffraction according to the methods outlined by McCrone and coworkers (15, 16). The microscope (Olympus Model POS-1) was equipped for photomicrography in transmitted light. The opaque samples were photographed at 180 \times magnification in reflected light on a Reichert Me F 2 metallograph.

**American Chemical
Society Library**

1155 16th St., N.W.

Washington, D.C. 20036

Table I. Hue and Location of Pigment Samples from Folio 13 Verso, MS. W. 539 (A.D. 1262)

<i>Number^a</i>	<i>Hue</i>	<i>Hue-Location Code</i>	<i>Munsell Color Notation</i>
1	Black	BL13v (60, 156)	
2	Blue	B13v (183, 70)	5 PB 4/12
3	Flesh	FL13v (135, 130)	10 R 8/2
4	Green	G13v (207, 46)	7.5 GY 4/2 to 3/2
5	Light blue	LB13v (186, 73)	5 BP 7/8
6	Magenta	M13v (237, 62)	10 P 7/6 to 5/10
7	Orange	O13v (99, 154)	5 YR 7/8
8	Orange	O13v (115, 145)	5 YR 8/4
9	Purple	P13v (252, 129)	2.5 P 4/6
10	Red	R13v (252, 129)	5 R 6/4
11	White	W13v (60, 156)	

^aCorresponds to numbers on Figure 2.

The x-ray diffraction patterns were obtained by mounting the sample particles on a glass filament in a 114.59-mm diameter powder camera (Debye-Scherrer) and irradiating with Cu-K α x-rays at 30 kV and 15 mA for periods of time ranging from 8 to 24 h.

The data taken for each sample included refractive index relative to the mounting medium (Aroclor, $n_D = 1.66$), average particle size, behavior in polarized light, and x-ray diffraction pattern. A photomicrograph of each sample was also taken on tungsten film (Ektachrome ASA 160) with a single lens reflex 35-mm camera (Olympus OM-1) equipped with a FK3.3 \times eyepiece adapter through a 40 \times objective (55 \times for the samples photographed in reflected light). These photographs were particularly helpful in examining the purple, brown, flesh-colored, and green pigments, which were mixtures.

The samples thus studied have been placed on permanent file at the Conservation Center, Institute of Fine Arts, New York University, for consultation or for comparison with samples to be taken in the future.

Results

The general results of the analyses according to hue and manuscript are presented in Table II. The overall palette of Cilician manuscripts of the 12th–13th centuries as gleaned from these data is presented in Table III.

Several interesting observations can be made upon examination of information contained in Table II:

1. Ultramarine as a blue pigment and vermilion as a red pigment are common to all four manuscripts.
2. No true green pigment has been found in these Cilician manuscripts (nor for that matter, in the vast majority of the manuscripts studied in this project); the green hue was

Table II. Identity by Hue of the Pigments Used in Four Cilician Manuscripts of the 12th–13th Centuries

<i>Hue</i>	<i>MS FGA 44.17</i> (A.D. 1253)	<i>MS FGA 32.18</i> (13th Century)	<i>MS W. 539</i> (A.D. 1262)	<i>MS M. 622</i> (A.D. 1348)
Blue	Ultramarine	Ultramarine	Ultramarine	Ultramarine
Brown				White lead, orpiment, vermilion, and black pigment
Flesh	Vermilion, white lead, and organic yellow		Vermilion, white lead, and organic yellow	
Green	Orpiment and organic blue	Orpiment and organic blue	Orpiment and organic blue; ultramarine and organic yellow	Orpiment and organic blue
Magenta	Organic red lake	Organic red lake	Organic red lake	
Olive			Vermilion, white lead, organic blue, and yellow	
Orange	Vermilion, white lead, and organic yellow	Vermilion, white lead, and organic yellow	Vermilion, white lead, and organic yellow	
Pink	Vermilion and white lead	Vermilion and white lead		
Purple	Vermilion, organic red, and blue	Vermilion, organic red, and blue	Vermilion, ultramarine, and organic red; vermi- lion, organic red, and blue	
Red	Vermilion	Vermilion	Vermilion	Vermilion
White	White lead	White lead	White lead	
Yellow	Orpiment and organic yellow	Orpiment and organic yellow	Orpiment and organic yellow	Orpiment

NOTE: Several samples also contained varying amounts of the minerals muscovite, wollastonite, and calcined bone; in addition, gold and silver were used in all of the manuscripts.

Table III. The Cilician Palette of the 12th and 13th Centuries

<i>Pigment Name</i>	<i>Chemical Identity</i>	<i>Comments</i>	<i>Method of Identification</i>
Calcined Bone	$\text{Ca}_3(\text{PO}_4)_2$	Made from animal bone ash	XRD ^a
Gold	Au		XRD
Organic pigments		Organic blues, reds, and yellows were widely used in manuscript painting	M ^b
Orpiment	As_2S_3	Ancient pigment; naturally occurring in many places	XRD, M
Silver Ultramarine	Ag Clathrate compound of sulfur in silicate mineral	Obtained from semi-precious stone, lapis lazuli	XRD, M
Vermilion	HgS	One of the most ancient of the synthetic pigments; also found as cinnabar ore	XRD, M
White lead	$2\text{PbCO}_3 \cdot \text{Pb}(\text{OH})_2$	Widely used in ancient times	XRD, M

^a x-Ray diffraction analysis.

^b Polarized light microscopy.

achieved in these manuscripts by mixing an organic blue pigment of uncertain identity and orpiment.

3. The purple hues were obtained by mixing varying amounts of vermilion with organic blue pigments or with ultramarine; the organic red pigment visually identified as "magenta" was also used in these mixtures.
4. The magenta, purple, and red hues, which were distinguishable both visually and through comparison with Munsell chips (*see* Table I), were chemically distinct.
5. The brown, flesh, olive, and orange tones were all achieved by skillful mixing of more basic colors. For example, the flesh tones in MS FGA 44.17 and MS W. 539 were achieved by mixing varying amounts of vermilion, white lead, organic yellow, and organic red.
6. Use of organic pigments was extensive. In this project, they were not identified chemically, but were identified tentatively through comparison with known microscopic samples. For example, on this basis, it was concluded that the organic yellow samples were probably not saffron.

Discussion

The palette we have thus established in Cilician Armenia shows a remarkable consistency from manuscript to manuscript and within any given manuscript. Der Nersessian observed that the two great gospels from the atelier of T'oros Roslin (MSS FGA 32.18 and W. 539) are the products of the collaborative work of several artists (11, 12). In our study of these manuscripts, samples were taken that would represent the palettes of the different artists, but the range and the quality of the pigments proved to be quite uniform. The kind of differences observed in the Glajor gospel (7) are not found, and this may be an indication of greater control in the manufacture of the pigments and the application of more rigid standards for the work of the individual artist.

Unfortunately, until comparable data has been developed on contemporary manuscript painting in Europe, Byzantium, and Islam, it will not be possible to situate exactly the palette of Cilician Armenia in respect to those traditions. However, some interesting contrasts can be observed. Although ultramarine is the standard blue in Cilicia, in Europe it seems to have been the exception. The pigment comes from mines located in present-day Afghanistan; therefore, it was evidently more readily available in the Near East than in Europe (17, 18). At the same time, the Cilician artists lacked a natural green and had to resort to mixtures, but in Europe, the use of verdigris (a collective term for copper acetates of various compositions) can be dated to at least the 13th century (19), and the use of malachite, $\text{Cu}_2\text{CO}_3(\text{OH})_2$, by the Chinese can be demonstrated as early as the 9th and 10th centuries (20).

Nevertheless, although the precise relationship of the Cilician palette to other traditions remains obscure, data already available from other Armenian manuscripts allows us to discuss its position in the larger picture of the Armenian tradition. Most important in this respect are our data from the gospel of King Gagik of Kars (Jerusalem, Patriarchate of St. James, MS 2556). This manuscript from Greater Armenia, dated 1045–64, revealed an identical range of pigments and pigment mixtures (9). The palette of Cilician Armenia was therefore continuous with earlier Armenian painting practice and was not borrowed from Armenia's new contacts in Cilicia. In the light of Armenia's many borrowings from her Latin neighbors, this continuity in painting practices deserves more attention.

On the other hand, the style of painting in Cilicia had a strong normative effect on subsequent Armenian painting. Cilician manuscripts were treasured and frequently copied in later periods. Our examination of manuscripts from the vicinity of Lake Van in the 15th and 16th centuries showed that the palette was also copied here. Although the Lake Van manuscripts indicate less interest in the subtleties of mixed colors

and a preference for large areas of unmodulated hue, the overall coloristic effects are very similar to those of the earlier Cilician tradition. The major hues of all of the manuscripts described above are summarized in Table IV.

Upon examination of Table IV, it may be seen that one notable exception to the traditional Armenian palette was the work of the priest Khatchatur of Khizan (MS W. 543). Khatchatur was both traditional and innovative. He followed the traditional Cilician palette in that he used all of the pigments listed in Table III, but he also expanded the range and use of his pigments. With respect to range, in particular, Khatchatur was most innovative: for the first time in the manuscripts that we have studied, we encounter the use of realgar and smalt. Realgar, an orange pigment generally found in the same deposits as orpiment (As_2S_3), has the formula As_2S_2 . This pigment is rare in Armenian manuscript illumination because the traditional method of achieving orange consisted of mixing vermilion with orpiment (and/or organic yellow) and shading the resultant hue with white lead until the desired tonality was obtained (8). Another rare pigment used by Khatchatur was smalt, a finely ground cobalt-containing glass that produces a pale, transparent blue. Although its discovery has been attributed to a Bohemian glassmaker of the mid 16th century (21), a more recent review of the literature sources reveals that smalt may have been produced in the Near East several centuries before the alleged European discovery (22, 23). The presence of smalt in Khatchatur's 15th-century manuscript seems to bear this latter opinion out.

The scientific study of medieval painting is still in its infancy. Until we can define the range of materials and techniques in use in the surrounding Islamic principalities, as well as the options open in late Byzantine painting, the true measure of Khatchatur's innovations and the traditionalism of the later artists of the Lake Van region will remain an unanswered quantity.

Acknowledgments

We would like to thank Esin Atil, Curator of Near Eastern Art, the Freer Gallery of Art; Archbishop Norayr Bogharian, Librarian, the Armenian Patriarchate of St. James; John Plummer, Curator of Manuscripts, the Pierpont Morgan Library; and Lilian Randall, Curator of Manuscripts, the Walters Art Gallery. In addition, we thank the staffs of the Conservation Center, Institute of Fine Arts, New York University, and the Department of Objects Conservation of the Metropolitan Museum of Art, New York City, for the use of their equipment and for their generous assistance. This work was supported in part by grants from the National Museums Act and the New York University Research Challenge Fund.

Table IV. Comparison of the Palette of the Cilician Manuscripts with Other Armenian Manuscripts

Pigment or Pigment Mixture	MS Jerusalem 2556 (1045-64)			Cilician MSS FGA 44.17 FGA 32.18 W. 539 M. 622 (1253-1348)			Lake Van Region MSS W. 543 (1455)			W. 540 (1475)		Jer. 135 (1575)	
	Blue:	Ultramarine	X		X			X ^a		X			X
Green:	Smalt			X			X		X			X	
	Orpiment and organic blue Organic yellow and ultra- marine	X		X		X	X		X		X	X	
Magenta:	Organic red lake	X		X			X		X		X	X	
	Vermilion, white lead, and organic yellow	X		X			X		X		X	X	
Purple:	Realgar						X		X				
	Vermilion, organic blue, and red	X		X			X		X		X	X	
Red:	Vermilion, ultramarine, and organic red	X		X			X		X		X	X	
	Vermilion	X		X			X		X		X	X	
White:	White lead	X		X			X		X		X	X	
	Orpiment and organic yellow	X		X			X		X		X	X	
Yellow:	Orpiment						X					X	

^a Visually identified without sampling.

Literature Cited

1. Mathews, T.F. *Jahrbuch der Österreichischen Byzantinistik* 1981, 31, XVI *Internationaler Byzantinistenkongress Akten*, Vol. I, section 3.2, pages unnumbered.
2. Thompson, D.V., Jr. "The Materials and Techniques of Medieval Painting"; Geo. Allen and Unwin: London, 1936.
3. Roosen-Runge, H.; Werner, A.E.A. "The Pigments and Medium of the Lindisfarne Gospels, *Codex Lindisfarnensis*"; Deutscher Kunstverlag: Basle, 1960, Vol. II, p. 263 f.
4. Roosen-Runge, H. "Farbgebung und Technik Frühmittelaltlicher Buchmalerei"; Deutscher Kunstverlag: Munich, 1967, Vol. I; p. 11.
5. Dionysius of Fournä. "The Painter's Manual"; Hetherington, P., Tr.; Sagittarius; London, 1974.
6. Velmans, T.; *Revue des Études Arméniennes* 1980, 14, 415-33.
7. Orna, M.V.; Mathews, T.F. *Stud. Conserv.* 1981, 26, 57-72.
8. Cabelli, D.E.; Mathews, T.F. *J. Walters Art Gallery* 1982, 40, 37-40.
9. Cabelli, D.E.; Mathews, T.F. "The Armenian Palette of the 10th and 11th Centuries"; in preparation.
10. Der Nersessian, S. "The Armenians"; Praeger: New York, 1969; p. 44f.
11. Der Nersessian, S. "Armenian Manuscripts in the Freer Gallery of Art"; Smithsonian Institution: Washington, D.C., 1963; p. 18f.
12. Der Nersessian, S. "Armenian Manuscripts in the Walters Art Gallery"; Trustees of the Walters Art Gallery: Baltimore, 1973; p. 10f.
13. Sanjian, A.K. "A Catalogue of Medieval Armenian Manuscripts in the United States"; University of California Press: Berkeley, 1976, p. 520f.
14. "The Munsell Book of Color"; Neighboring Hues Edition, Matte Finish Collection; Macbeth Division of Kollmorgen Corporation: Baltimore, 1976.
15. McCrone, W.C.; Delly, J.G. "The Particle Atlas"; 2d Ed.; Ann Arbor Science: Ann Arbor, Mich., 1974-78.
16. McCrone, W.C.; McCrone, L.B.; Delly, J.G. "Polarized Light Microscopy"; Ann Arbor Science: Ann Arbor, Mich., 1978.
17. Orna, M.V.; Low, M.J.D.; Baer, N.S. *Stud. Conserv.* 1980, 25, 53-63.
18. Plesters, J. *Stud. Conserv.* 1966, 11, 62-91.
19. Kühn, H. *Stud. Conserv.* 1970, 15, 12-30.
20. Gettens, R.J.; FitzHugh, E.W. *Stud. Conserv.* 1974, 19, 2-23.
21. Mühlenthaler, B.; Thissen, J. *Stud. Conserv.* 1969, 14, 47-61.
22. Gettens, R.J.; Stout, G.L. *Stud. Conserv.* 1957-58, 3, 107-19.
23. Harley, R.D. "Artists' Pigments: c. 1600-1835"; Butterworths: London, 1970.

RECEIVED for review November 3, 1982. ACCEPTED for publication March 18, 1983.

Scanning Auger Microscopy for Dating of Manuscript Inks

RODERICK J. McNEIL

Bio/Environmental Research Group, New Milford, CT 06776

Although quite accurate tests exist for dating of writing supports (paper or vellum), the question of when the ink was applied could not be separately addressed by the same techniques. In a study of the ink edge profile it was noted that a skewed "tail" extended beyond the dried capillary drawn ink area. Further, the area of this tail seemed to increase with time. Eight paper documents in the period 1200–1972 were examined in 10 separate areas by iron spectrum scanning auger microscopy. A regression analysis of the data (area values) versus time showed a correlation coefficient of 0.95. The documents were each of known date from a large private collection. Seven vellum documents were also examined and the correlation was significant at the $P = 0.90$ level. It proved more difficult to select adequate test areas on vellum owing to surface irregularities such as hair follicles. Some proposals are offered for the correlation between time and area, the sensitivity limits are discussed, and the lack of sensitivity to environmental extremes is described.

THE HYPOTHESIS THAT SECONDARY ION MIGRATION might take place in textiles dyed with inorganic dyes was suggested while Alan D. Adler, John H. Heller,¹ and the author of this chapter were discussing the chemical testing of the Shroud of Turin. The discussion had turned to the retting process for linen and the selective absorption of inorganic species to the cellulosic base material. It seemed possible that if such secondary migration took place, the process would also occur in manuscripts where inorganic inks are used.

The basic concept is that the migration of ions from the ink is directly proportional to time. This would allow dating the application of ink rather than dating the writing support, which seemed to have merit. Although

¹ Alan D. Adler and John H. Heller are coauthors of Chapter 22 in this volume.

good destructive (^{14}C) and nondestructive (particle accelerators) techniques exist for dating the support, neither technique addresses the question of when the ink was applied. The hypothesis, if valid, would have value in detecting forgeries as well as use for dating.

Preliminary Experimentation

As a preliminary experiment, several documents from the author's collection spanning the period 1722–1972 were evaluated by using x-ray energy dispersive analysis as well as scanning auger microscopy (SAM). A literature survey had shown that iron gallotannate was likely to be the most prevalent ink in the 1200–1600 period; it was therefore felt that elemental iron would be a good atomic species for investigation. Figures 1, 2, and 3 show the vellum surface at $50\times$, $150\times$, and $1000\times$, respectively. A background spectrum was taken $500\ \mu\text{m}$ to the left of the ink area and an x-ray spectrum was taken of the left limb of the letter (Figures 4 and 5, respectively).

Although a number of unique elements, including phosphorus, calcium, potassium, iron, and zinc, are present to some extent, only iron is present in sufficient quantities (greater than 1%) and has high enough

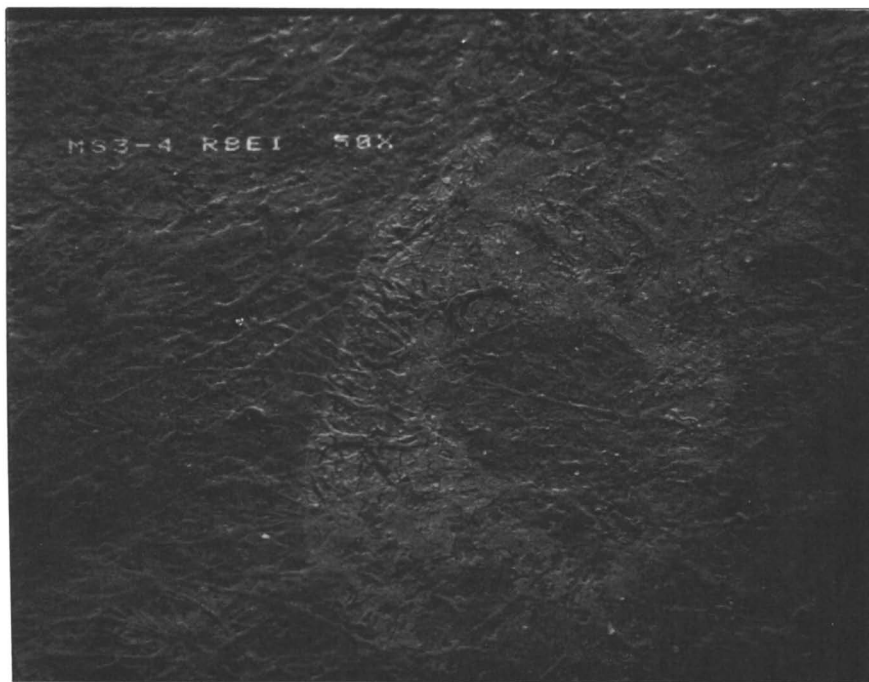


Figure 1. Vellum surface photographed at $50\times$ in Robinson Backscatter emission. Letter "O" from 1722 cartographic document.

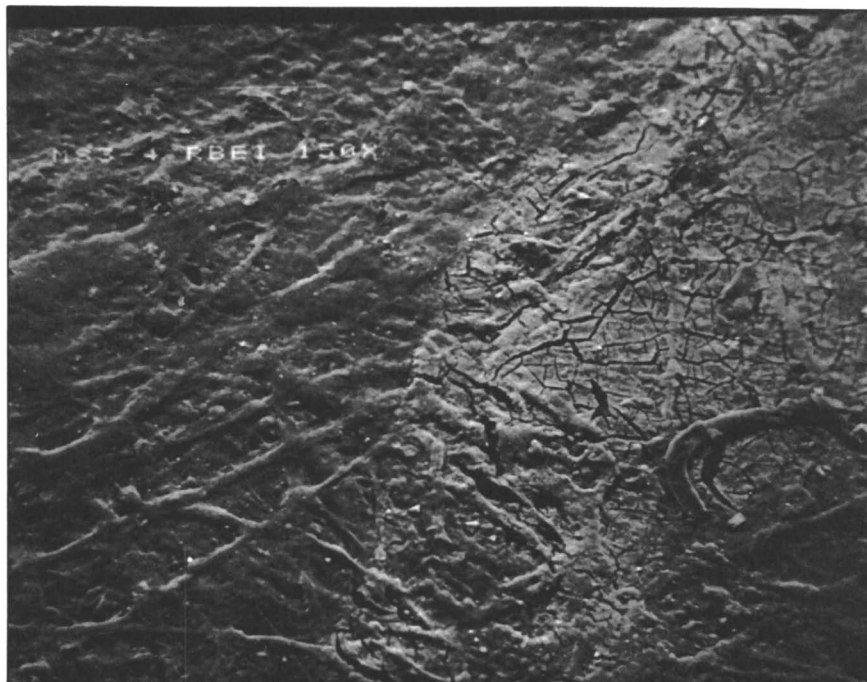


Figure 2. Same as Figure 1, photographed at 150 \times ; upper left limb of character.

atomic weight ($Z \geq 20$) to make auger spectroscopy feasible. A survey of 12 additional documents on vellum, parchment, and paper showed similar results.

In order to detect the small amount of ionic migration suspected at the periphery of the ink margin, SAM was employed to improve spatial resolution and elemental specificity. Auger spectroscopy differs from electron spectroscopy for chemical analysis (ESCA) in that the former uses electrons instead of x-rays for specimen excitation.

Both electron microprobe analysis and SAM use an electron beam for excitation of the specimen. The difference between these techniques is in the detection of emitted x-rays in the microprobe technique while SAM measures emitted electrons. For both techniques, the energy of the detected particles is characteristic of the parent atom and thus identifies the atomic species present. The lateral spatial resolution in SAM is superior due to the much shorter mean free path of the emitted energy (electrons). The escape depth of auger electrons is approximately 10 Å versus 1000 Å in microprobe analysis. This phenomenon makes SAM a highly specific surface analysis technique.

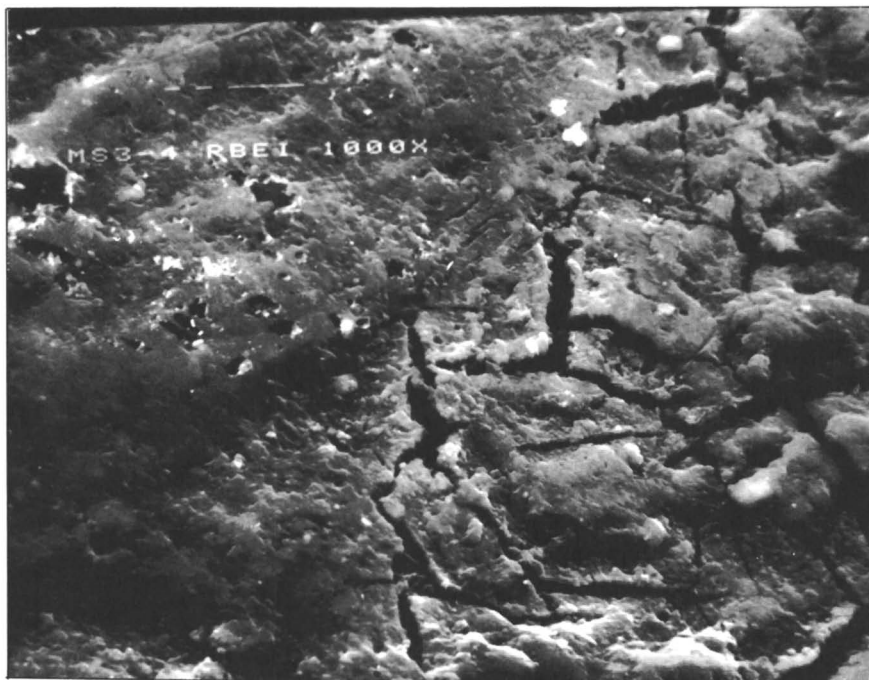


Figure 3. Same as Figure 1, photographed at 1000 \times ; ink boundary and capillary diffusional area.

Auger electrons are caused by the ejection of an electron in an outer shell to a state in the continuum. If a primary vacancy exists in the K shell, the vacancy is filled from the L_2 shell and the energy released in this transition results in the expulsion of an electron from the L_3 shell; the electron will be denoted as an auger electron of the KL_2L_3 type. Thus, there are nine forms of radiationless transition in the KLL group, each with a specific energy unique to the element.

In Figure 6 we see the relative energies of various auger transitions versus Z , the atomic weight of the element. Obviously, the transition

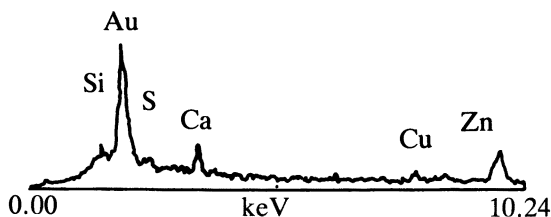


Figure 4. Background spectrum taken in x-ray energy dispersive mode.

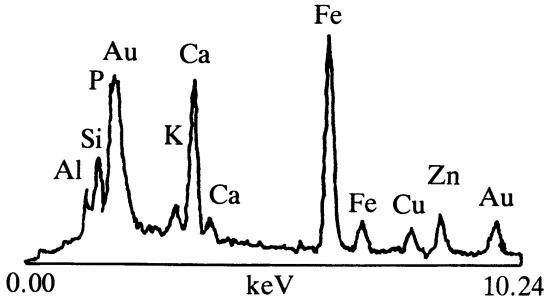


Figure 5. Ink spectrum from left limb in x-ray energy mode.

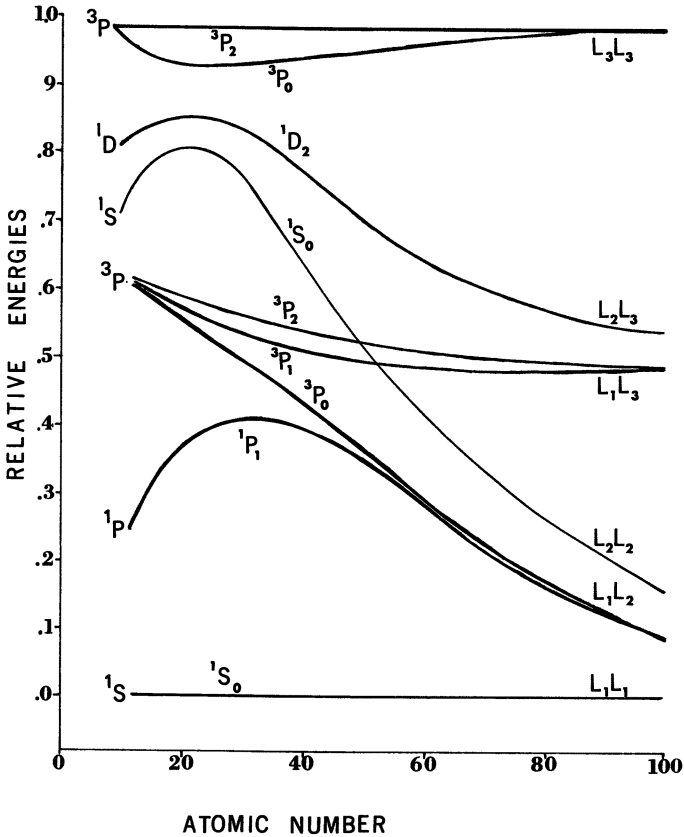


Figure 6. Relative energies of Auger transitions vs. atomic weight. (Reproduced with permission from Ref. 1.)

auger line may be selected to yield maximum sensitivity. In the case of iron, the L_1L_2 line at 5.519 KeV and the L_2L_3 line at 5.619 KeV were monitored. An initial low resolution ($1.0 \mu\text{m}$) lateral scan of the ink profile in sample MS3-4 yielded the results shown in Figure 7. Note the parallel valleys created by the nibs of the quill pen and the shoulder at either side that represents the diffusion by capillary action at the surface in the parchment.

If the area count is normalized to 100% at the capillary shoulder, a "tail" becomes evident (*see* Figure 8). The area integration of this tail was found to vary with time. Seven paper documents dating from 1272 to 1972 were then run by the same technique to confirm the relationship of area increase with time. An averaging of three replicate measurements from five different sites on each document is shown in Figure 9.

Because the phenomena seemed to lend credence to the secondary ion migration hypothesis, a detailed study of a number of documents began.

Materials and Methods

Twenty-two paper documents were evacuated to 1×10^{-9} torr and examined by SAM. The samples underwent no prior surface preparation, as the "dust of ages" was present to varying amounts on each, and the effect of this debris on the quality of the measurements was of interest. The documents, loaned by three private libraries, covered the period of 1272-1972, and all carried "unequivocal" dates. The KL_1L_2 and KL_2L_3 transitions in iron were monitored in the high spatial resolution mode, $\sim 1500 \text{ \AA}$. Each document was scanned in five locations and three replicates were made for each. The SAM used was a PHI590 with an analog signal output directed to a Bascom-Turner 8120 recorder-integrator. The integral of the slope was used to define the point of inflection for initiation of area summation (*see* Figure 8).

Area counts were statistically evaluated for intrasample coefficient of variance and a linear regression analysis for the line of fit for area versus time was prepared. The same evaluation protocol was then used for seven vellum documents and eight parchment documents.

Controls were established by using Whatman Elephant Grade writing paper as well as vellum and parchment of unknown manufacture. An iron gallotannate ink was prepared according to the method of Skelton (2). Controls were maintained at 20, 100, 150, and 200 °C at varying degrees of atmospheric saturation. The ambient control sets were controlled at 92% relative humidity with saturated sodium carbonate, 55% over saturated calcium nitrate, 1.4% over cupric sulfate, and 0.005% over silica gel and anhydrous calcium sulfate. Two differing 0% controls were used to determine the effect of competitive cations associated with the

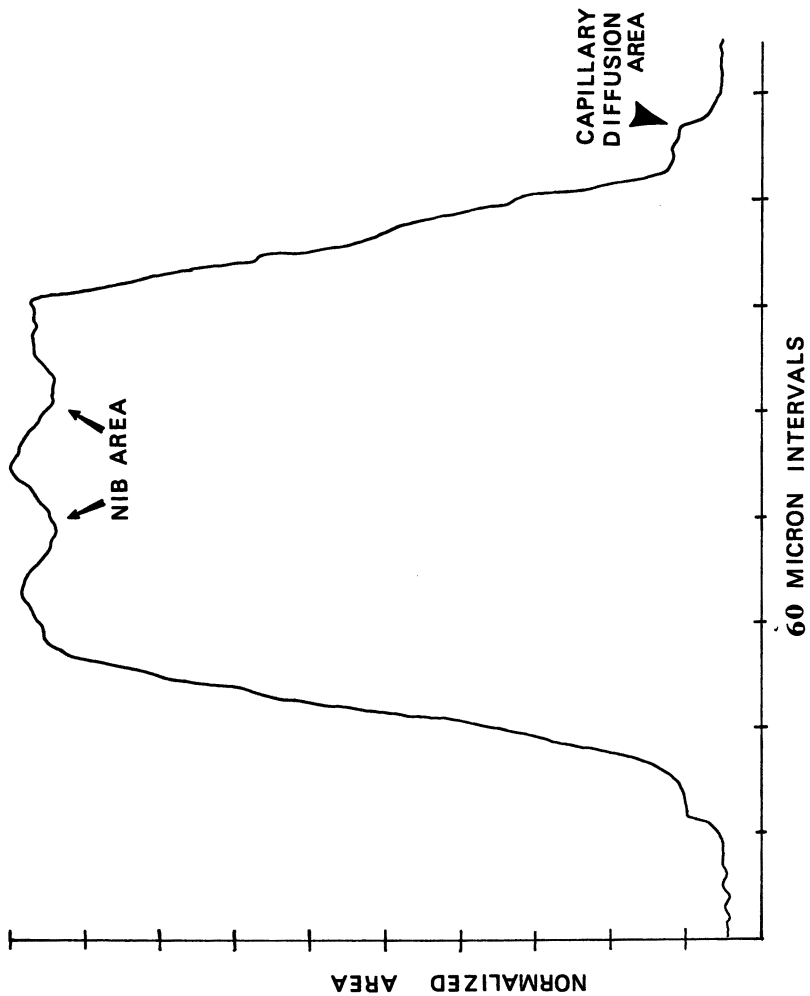


Figure 7. Low-resolution lateral scan of ink profile from sample MS3-4-21.

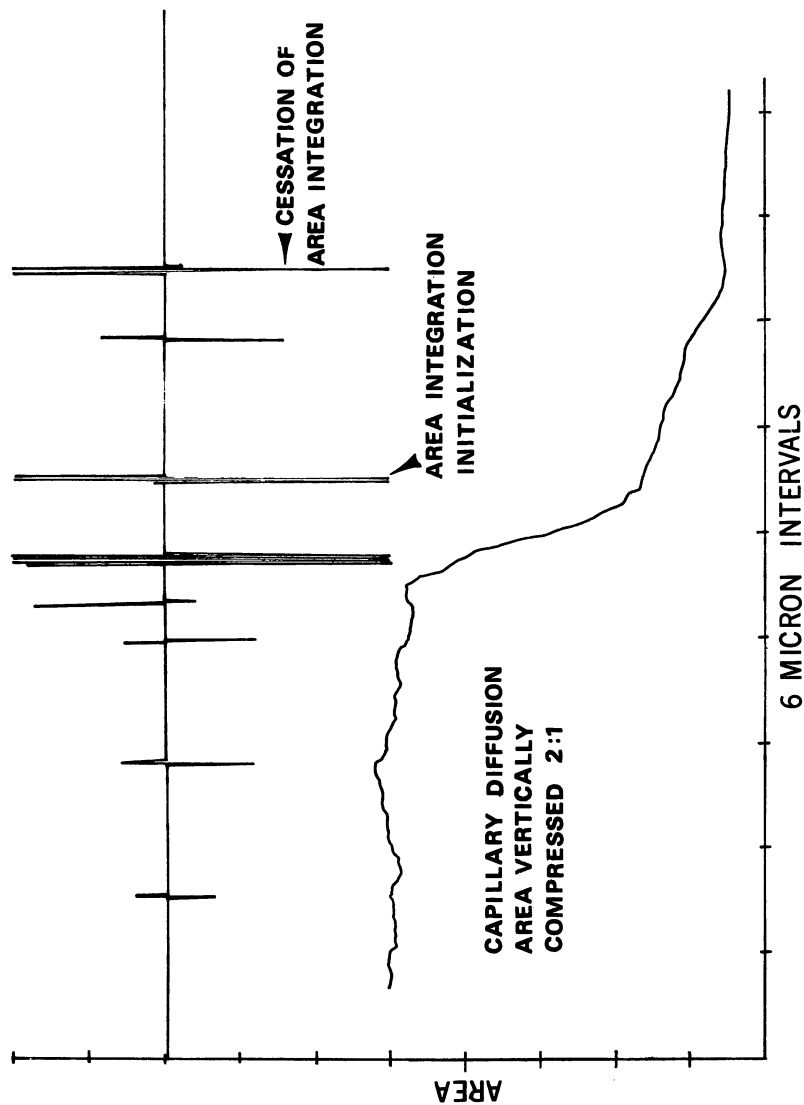


Figure 8. Capillary diffusional area normalized to 100% full scale. Upper scale depicts first-order slope integral of the scan.

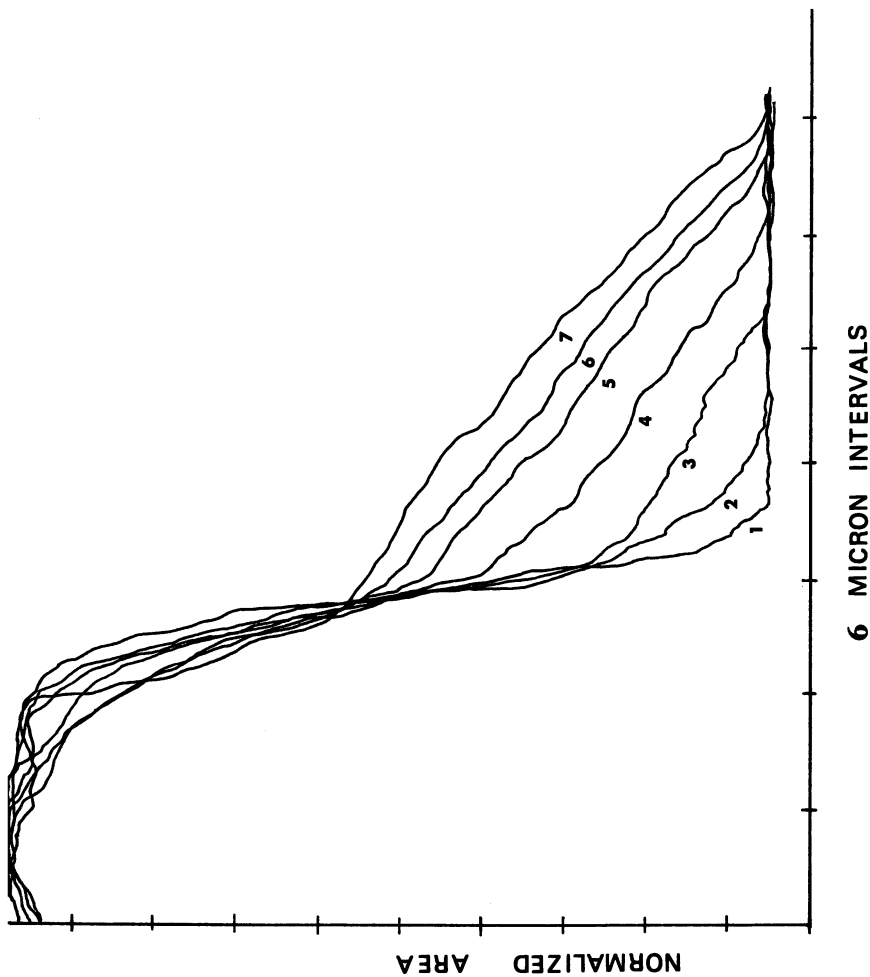
**6 MICRON INTERVALS**

Figure 9. Normalized capillary diffusional areas for seven paper documents from 1272 to 1972. Scans represent three replicates of five measurement sites on each document. Key: 1, 1972; 2, 1904; 3, 1857; 4, 1747; 5, 1457; 6, 1354; 7, 1272.

support. The controls at 100, 150, and 200 °C were maintained at the saturated dew point for these temperatures. Each set of samples has now been maintained under these conditions for 6 months.

After the initial curve calibration, four documents from the Bishop Collection (scientific and cartographic documents) were measured as double-blind samples.

Results

The intrasample error for paper, vellum, and parchment is summarized in Table I. Note that the coefficient of variance is significantly higher for vellum and parchment than for paper. The selection of test site was far more difficult on "skin" than on paper. For paper sampling, a fibril was selected which ran perpendicular to the ink line so that the electron beam would scan the surface of a single fibril without falling into the "valley" between fibers. With skin, the presence of hair follicles and anomalies in surface texture introduced more sampling error.

Figure 10 depicts the regression plot for the 22 paper samples. Each sample point represents an average triplicate measurement for each of the five points measured on each document. The relationship appears to be linear. The dotted line in Figure 11 represents the computer projection of the 90% confidence limit (by using the inflection point of the tailing and direct integral) for acceptable time resolution. Also depicted in Figure 10 are the data from the parchment documents as well as the vellum data. Unlike the paper data, this information suggests a curvilinear relationship. In all probability, the number of points presently available is insufficient to adequately define the area versus time relationship.

Table I. Relative Standard Deviation Produced in Intersample and Intrasample Testing as Related to Document Age Dependence

	<i>Relative Standard Error (%)</i>	
	<i>Intersample</i>	<i>Intrasample^a</i>
Paper (22 samples)		
Date dependent maxima	7.93	7.50
Date independent average	4.67	1.62
Vellum (7 samples)		
Date dependent maxima	11.42	10.86
Date independent average	8.91	7.61
Parchment (8 samples)		
Date dependent maxima	12.02	11.44
Date independent average	7.55	7.80

^a Five samples from each document, averaged from triplicate measurements.

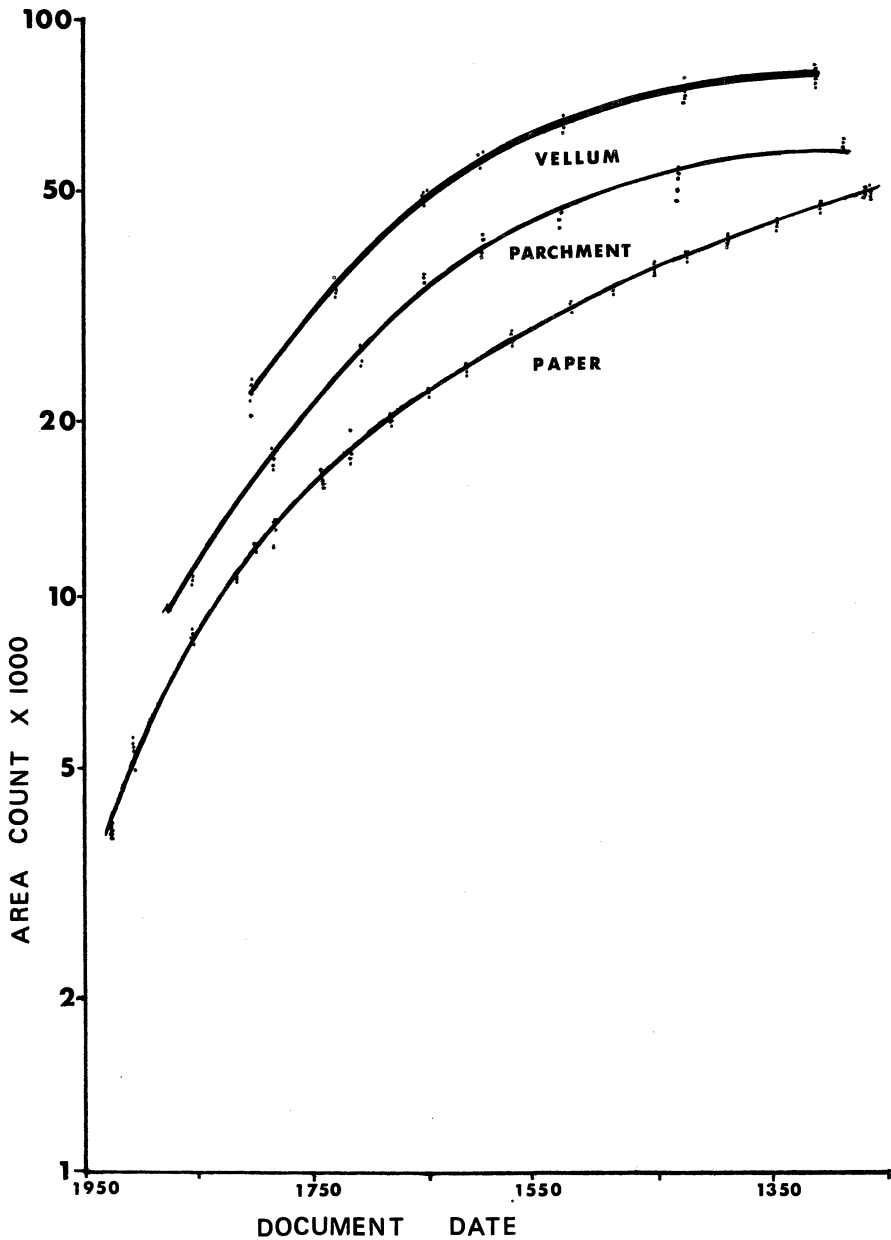


Figure 10. Regression plot for paper (22 samples), vellum (7 samples), and parchment (8 samples) writing supports. Information regarding sampling intervals is shown with the figure. Each sample was tested in five areas, and the measurements were made in triplicate for each test site.

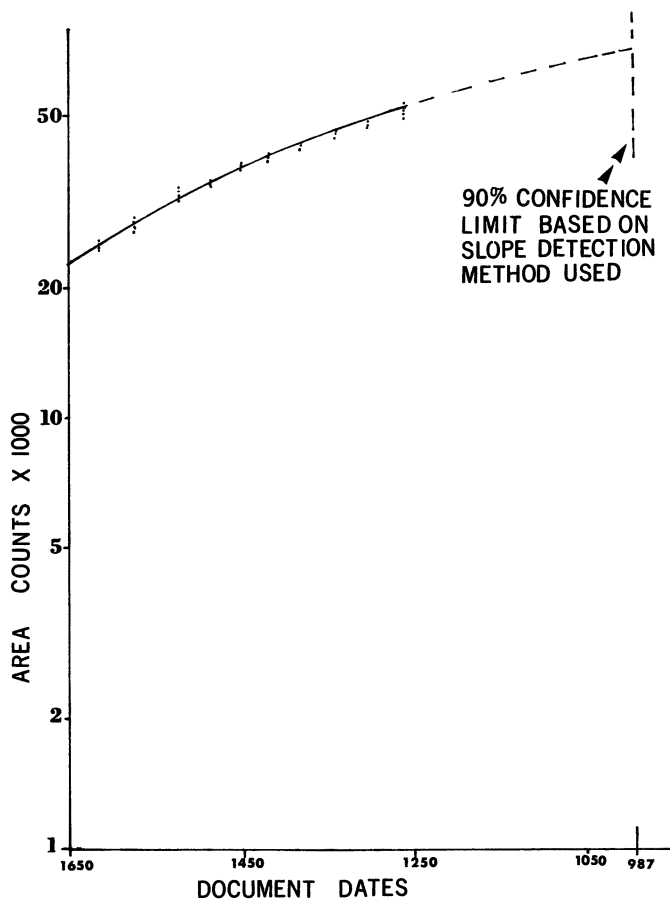


Figure 11. Regression analysis of paper data showing 90% confidence limit for maximum dating limit based on first-order slope integration.

The four double-blind samples were measured by the paper techniques previously described and were found to have dates of 1450, 1630, 1680, and 1730 by fitting analysis. With the exception of the earliest date, the dates proved to be within ± 22 years of the actual dates: 1637, 1692, 1751. The first document was supposedly from ca. 1275 based on the script and handwriting analysis. It is not known at this time which date is the more accurate.

Ten months into the control period there has been no detectable area increase dependent on temperature or humidity. Thus far, no environmental conditions have been found that could produce the tailing effect described.

The mechanism for ion migration is currently under investigation, but data are as yet inadequate to describe the phenomena accurately.

Discussion

Numerous problems were encountered in preparation of the documents for SAM analysis. Large bound documents took more than a week to de-gas to 1×10^{-7} torr. This necessitated de-gassing all documents in advance and transporting them to the test site under vacuum. The high degree of vacuum necessary for SAM produced significant glue embrittlement, resulting in some binder damage. In addition, the large size of many of the documents precluded measurements in all but a very few SAM instruments.

To generate a sufficiently accurate regression expression that would be applicable to the general case will require far more truly dated samples, particularly on vellum and parchment.

A statistical analysis of the 110 points sampled on paper indicates a correlation coefficient of 0.90 for the regression analysis. The significantly different curve fit for vellum and parchment as well as the far smaller number of samples does not allow any statistically valid assumptions to be made regarding the accuracy of SAM as a dating technique for these supports. It was noted in document reviews that the illuminated documents used mercury in the red dyes. The use of mercury rather than iron might provide significantly higher sensitivity due to the higher auger energy and the higher concentration of mercury apparently used in illuminated manuscripts (*note* Figures 12 and 13). This would extend the usefulness of SAM as a dating technique back to 3200 B.P., assuming no improvements are made in discrimination of the tail as a fused peak. However, significant improvements in fused peak inflection should be possible by using more sophisticated techniques.

The use of the current technique on paper should allow an absolute accuracy of ± 30 years back to 1050 B.P.. As fused peak inflection detection methods improve, we should be able to date considerably earlier documents.

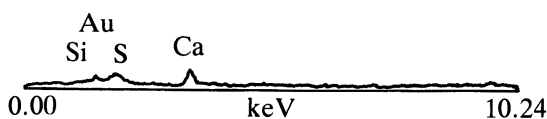


Figure 12. Background spectrum from MS3-36 adjacent to illuminated manuscript area. x-Ray energy mode; note that the attenuation is $8 \times$ greater than that used with iron (*i.e.*, Hg is $8 \times$ more sensitive than Fe).

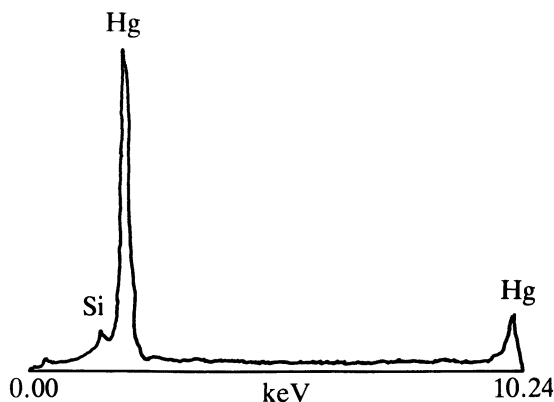


Figure 13. Red ink area on MS3-36. x-Ray energy mode. The attenuation used was the same as for Figure 12.

The original preparation of the support may also affect the sensitivity of the technique. Several documents were encountered with high iron background. In such cases the signal-to-noise ratio for discrimination of the inflection point was reduced sufficiently to produce counting errors as well as reducing time sensitivity.

The "dust of ages" seems to have had little effect on the accuracy of the measurements. It was necessary, however, to make each measurement in triplicate with five samples from each document to achieve a satisfactory critical value (see Table I).

Summing both lead and trailing tails did not statistically improve the accuracy of the technique.

It was also noted that it was easy to detect that an ink line had been overwritten. A "staircase" results in the capillary action area of the lateral line SAM scan. For those documents where overwriting is suspected in restoration, it should be possible to determine which portions of the document have been altered.

As was noted earlier, there is at present no explanation for the nature of ion migration taking place in the document. It is hoped that other techniques, such as scanning electron stimulated desorption (SESD), may throw light on the ion transition phenomena.

Conclusions

The measurement of ion migration trailing by SAM seems to allow accurate dating of manuscripts using iron-based inks. The use of this technique may be valid for vellum and parchment, but insufficient data are currently available to allow statistical confidence in the results.

Although the current technique with iron works back to 1000 B.P., use of better fused peak discrimination or a higher concentration/sensitivity element such as mercury would increase the time sensitivity of the technique significantly.

The mechanism for ion transition which allows the utilization of this technique is at present undefined.

Literature Cited

1. "Alpha-, Beta-, and Gamma-Ray Spectroscopy"; North-Holland: Amsterdam, Vol. 2, p. 1530.
2. Skelton, R. A. "The Vinland Map and the Tartar Relation"; Yale Univ. Press: New Haven, 1965.

Trace Element Discrimination of Discrete Sources of Native Copper

GEORGE RAPP, JR., and JAMES ALLERT

University of Minnesota, Archaeometry Laboratory, Duluth MN 55812

EILER HENRICKSON

Carlton College, Department of Geology, Northfield MN 55057

Activation analysis is used to establish trace element "fingerprints" of geologic deposits of native copper. By using the statistical techniques of discriminant analysis and K-means cluster analysis and the trace element concentrations in artifact copper, an assignment of probable geographic and(or) geologic source of the artifact raw material can be made.

THE USE OF TRACE ELEMENT ANALYSIS to determine the provenance of archaeological materials has expanded rapidly in the last decade. It is now a well-established technique for the identification of obsidian source deposits (1), and is nearly as established for turquoise (2), steatite (3), and some ceramic materials (4). Native copper has received much less attention. Friedman et al. (5), Fields et al. (6), and Bowman et al. (7) used trace element analyses to determine the type of geological ore from which copper was extracted. However, only our efforts (8) and the work of Goad and Noakes (9) have focused on collecting and analyzing native copper from all potential deposits of a given region to provide a data base for statistical comparison with artifact trace element compositions.

Our trace element data base now contains analyses of 586 samples of native copper from deposits throughout the world. However, the sample sources are skewed toward the northern United States, especially the Lake Superior region. Trace elements can be considered as those normally found in concentrations below 100 ppm (i.e., below the 0.01% normally used as the lower limit of standard rock and mineral analyses). Trace elements do not play a major part in the physicochemical reactions that take place in the formation of geologic deposits. They are either concentrated in or dispersed throughout rock, mineral, and ore deposits

0065-2393/84/0205-0273\$06.25/0

© 1984 American Chemical Society

by virtue of their residence in the bulk chemical system and involvement in certain phases of geochemical alteration. It would be highly unlikely that two unsmelted (or otherwise chemically altered) artifacts would have coincident trace element concentrations of eight or more geochemically independent elements unless they were made of material from the same rock or ore body.

Background information on "fingerprinting" native copper published in Reference 8 will not be repeated here. Our first neutron activation analyses were done in the mid 1960s at Argonne National Laboratory. Most of the analyses reported here were done at the nuclear reactor facility at the University of Wisconsin, Madison (Richard Cashwell, director). A thermal neutron flux of about 10^{12} neutrons/cm²/s was used. The gamma radiation was counted using a Ge(Li) detector and the spectra were analyzed by Wisconsin's NAA CALC program. Initially we used a variety of standards. From 1973 through 1980, gold was the only internal standard used. Since 1981 a new standard, the Canadian Reference Soil Sample, has been used.

Our initial analyses sought only eight elements: silver, cobalt, chromium, iron, mercury, antimony, scandium, and selenium. Beginning in 1973 arsenic, gold, cadmium, cerium, cesium, europium, hafnium, indium, iridium, lutecium, nickel, ruthenium, tin, tantalum, tellurium, thorium, tungsten, ytterbium, and zinc were added, and in 1981 molybdenum was added. The number and variety of elements examined were largely a function of the capabilities of the analytical instrumentation used and the evolution of techniques over the course of time. Changes in the standards, the gamma wavelengths used for given elements, the elements sought, and the computer programs used to measure gamma radiation intensities have made the data unhomogeneous. However, it is our contention that the inherent heterogeneity of the raw materials and the lack of any ancient technology to remove impurities probably combine to make measured differences in trace element concentrations of less than one-third of an order of magnitude (i.e., concentration differences from 0.3 to 3 times) insignificant in provenance studies of pre-historic copper and bronze artifacts.

The Archaeometry Laboratory trace element data base contains 1980 analyses, all undertaken by the laboratory with assistance from personnel at the reactor facilities at the University of Wisconsin, Madison, or at Argonne National Laboratory. The distribution of analyses by material analyzed is presented in the box on the next page.

Statistical Analyses

A wide variety of statistical techniques has been used in archaeometry to assign artifacts to sources or to similarity groups based on trace chem-

<i>Material</i>	<i>Number of Analyses</i>
Metal artifact	716
Native copper	586
Cassiterite	172
Ceramic artifact	156
Chalcopyrite	86
Ceramic clay	74
Azurite	39
Malachite	34
Bornite	24
Chalcocite	23
Cuprite	12
Other	58
Total	<u>1980</u>

ical data. We have used two techniques primarily, a discriminant function and a K-means cluster analysis. Discriminant analysis can be used when the investigator has a priori knowledge of the specific group to which an unknown must belong. The discriminant function is then a decision rule that assigns the unknown to one group on the basis of a set of measurements. The coherence and uniqueness of each group can be tested by removing members from groups to check if the decision rule returns them to their (known) group. Incorrect or overlapping groups can be uncovered by such tests.

Cluster analysis is a statistical technique for determining relationships in a large matrix of measurements. We have found that the common agglomerative-hierarchical dendrograms expressing relationships among trace element patterns in copper deposits are not helpful in assigning unknowns (artifacts) to probable sources. However, by using cluster analysis as a simple form of correlation analysis, the results can be presented in a two-dimensional diagram where group separations and overlaps are easily seen. This method can be an important tool in provenance studies. K-means cluster analysis uses standard Euclidean distance as a measure of similarity between reference groups or between unknowns and the reference groups (in our case, copper deposits). The technique allows the operator to seek natural groups of any desired level of similarity.

The Discriminant Function d^* . In order to assign a copper artifact to the copper deposit of most probable origin, it is necessary to use statistical techniques compatible with the data. Several discriminant func-

tions were tested by Rapp et al. (8) in order to come up with an appropriate design. We decided to use a simple univariate product function wherein the trace element concentrations in an artifact are compared to all trace element analyses from specified coherent geographical sources, anywhere in size from a single deposit (mine) to a large region, which form a population defining a trace element "fingerprint." For each specified geographic source, the trace element data are arranged in a two-dimensional matrix with the analytical data for each chemical element recorded in five concentration intervals, I_1 to I_5 . The intervals are different for each chemical element and are chosen from an inspection of the data base to maximize the discriminating power of the function. The concentration intervals and the measured concentrations for 27 elements are given in the Appendix.

The product function d^* compares the unknown (artifact) with each possible source fingerprint by

$$d^* = \prod_{i=1}^j \frac{N_{ij}}{n}$$

where n is the number of analyses and N_{ij} is the number of analyses falling into the i th concentration interval of the j th element. The potential locality with the highest product value is the indicated source. *The viability of this simple linear discriminant function is totally dependent on a priori knowledge that any unknown is a member of one of the source sets.* In other words, if not all potential sources are represented in the data base, then the d^* will assign as the source that locality where the product value is maximum. No part of d^* is designed to reject a provenance determination because the unknown is insufficiently similar to all given sources in trace element abundances.

A fingerprint of any of the sources listed in the Appendix can be assembled from the information presented. The Appendix is organized such that others may compare results with our data. The concentration ranges in parts per million for the elements are given in the Appendix. A six-element fingerprint for Snake River, Minn., would be as follows:

	<i>Co</i>	<i>Te</i>	<i>Fe</i>	<i>Hg</i>	<i>Sb</i>	<i>W</i>
I_1	4	10	3	4	5	9
I_2	0	0	0	0	0	1
I_3	0	7	0	0	1	9
I_4	15	2	8	15	12	0
I_5	0	0	8	0	1	0
	19	19	19	19	19	19

This means, for example, that of the 19 analyzed specimens from Snake River, 4 of the cobalt trace element concentrations were in the

range I₁ and 15 were in the range encompassed by I₄. The other ranges contain no values. The reason for the bimodality in the Snake River abundances shown above is not known. For the six-element Snake River fingerprint above, an unknown whose analysis placed cobalt in I₄, tellurium in I₃, iron in I₃, mercury in I₅, antimony in I₃, and tungsten in I₂ would have a d* value for Snake River of

$$\left(\frac{15}{19}\right)\left(\frac{7}{19}\right)(0.005)(0.005)\left(\frac{1}{19}\right)\left(\frac{1}{19}\right) = 0.000000201$$

to be compared with d* values for all other potential sources (for examples, *see* Tables II, III, IV, and V). It should be noted that the sample calculation given in Reference 8 is incorrect.

The test for the uniqueness of a fingerprint is accomplished by randomly removing specimen analyses one by one from a locality fingerprint, reconstituting the fingerprint without the test specimen values in the fingerprint, then using d* to assign the test specimen to a source. If all or nearly all are returned to the known source, then the fingerprint has a high level of uniqueness. Attempts to distinguish individual mines in northern Michigan provide the toughest test. The northern Michigan deposits are all of the same age and have similar geologic origins. Hence there is more overlap in fingerprint characteristics among these sources than between them and deposits in Alaska, Illinois, or Arizona. In a test of Isle Royale copper samples versus Kingston Mine samples, 17 of 20 randomly selected samples were returned to the known source.

Data for 10 sources in the United States are presented in the Appendix. Our Kingston Mine fingerprint is based on analyses of 159 specimens from throughout the modern mine. The trace element abundances vary with level in the mine. Prehistoric humans did not have the technology to engage in deep mining; therefore, the most appropriate fingerprint would be from samples taken only from the surface or at shallow depth.

Statistically, 159 analyses from one source is a more than adequate number. However, the number of analyses from the Champion mine is 9, which is statistically inadequate. For a 16-element fingerprint, 20 analyzed specimens is a marginal number; 25–40 are recommended. Our work thus far indicates that the discriminant function seems to succeed if there are 20 or more analyzed samples in each locality fingerprint.

The concentration intervals I₁ through I₅ for each element were chosen by inspecting the range of abundances using all 1027 analyses of native copper. By using the data shown in Table I, the intervals were chosen to distribute the concentrations as evenly as possible throughout the five I cells. Because many concentrations were below the detection limit, the lowest concentration interval (which includes “not detected”)

Table I. Concentration of 27 Elements from Analyses of Native Copper and Native Copper Artifacts

<i>I</i>	<i>Ag</i>	<i>As</i>	<i>Au</i>	<i>Cd</i>	<i>Ce</i>	<i>Co</i>	<i>Cr</i>	<i>Cs</i>	<i>Eu</i>
<i>I</i> ₁	212	352	238	519	450	115	356	488	480
<i>I</i> ₂	310	87	51	14	185	232	354	19	24
<i>I</i> ₃	206	50	225	29	121	39	31	21	17
<i>I</i> ₄	141	41	74	12	14	532	249	25	32
<i>I</i> ₅	158	49	214	5	35	109	37	25	25
Total	1,027	579	802	579	805	1,027	1,027	578	578
<i>I</i>	<i>Fe</i>	<i>Hf</i>	<i>Hg</i>	<i>In</i>	<i>Ir</i>	<i>Lu</i>	<i>Ni</i>	<i>Ru</i>	<i>Sb</i>
<i>I</i> ₁	354	481	202	509	428	520	482	525	393
<i>I</i> ₂	291	10	164	214	197	16	36	16	215
<i>I</i> ₃	85	217	37	21	46	16	20	6	59
<i>I</i> ₄	86	62	552	32	99	16	13	28	212
<i>I</i> ₅	211	19	72	26	30	11	27	4	148
Total	1,027	789	1,027	802	800	579	578	579	1,027
<i>I</i>	<i>Sc</i>	<i>Se</i>	<i>Sn</i>	<i>Ta</i>	<i>Te</i>	<i>Th</i>	<i>W</i>	<i>Yb</i>	<i>Zn</i>
<i>I</i> ₁	341	445	518	528	479	496	334	520	422
<i>I</i> ₂	247	248	7	4	3	13	142	24	26
<i>I</i> ₃	155	211	11	22	67	21	29	20	73
<i>I</i> ₄	163	89	17	18	26	48	33	14	20
<i>I</i> ₅	120	34	26	7	4	0	41	0	38
Total	1,026	1,027	579	579	579	578	579	578	579

NOTE: Data are given as parts per million.

tends to be more populous than the other intervals. The ability of *d** to function as a discriminator depends on the choice of trace elements and intervals used. For specific problems, the effectiveness of *d** can be maximized by refining the intervals and the choice of elements by using only the data from relevant localities.

To illustrate the range of trace element abundances throughout the intervals *I*₁ through *I*₅ for all native copper in the data base, Table I combines the 586 analyses of native copper samples from deposits throughout the world with the 441 analyses of native copper artifacts from North America.

Restructuring Table II into locality fingerprints in the form of the six-element fingerprint given above for Snake River illustrates which trace elements are important in establishing the degree of uniqueness of each locality. For example, high iron, zinc, europium, iridium, and nickel concentrations make the Illinois fingerprint unique in the data base.

Table II. Summary of Unknown vs. Fingerprints (Specimen No., 34-1-82A; McKinstry, Minn.; bar artifact)

<i>Area</i>	<i>Discriminant Function</i>
Kingston, Mich.	0.000006439059
Champion, Mich.	0.000000000000
Centennial, Mich.	0.000000000000
Isle Royale, Mich.	0.000000028666
Snake River, Minn.	0.000105815251
Arizona	0.000003576278
Alaska	0.000000000111

NOTE: Fingerprint best fit, Snake River, Minn.

Table III. Summary of Unknown vs. Fingerprints (Specimen No., 34-1-82A)

<i>Area</i>	<i>Discriminant Function</i>
Kingston, Mich.	0.00000007475
Champion, Mich.	0.000000000000
Centennial, Mich.	0.000000000000
Isle Royale, Mich.	0.000000000000
Snake River, Minn.	0.000007125975
Arizona	0.000000000000
Alaska	0.000000000000
Wisconsin	0.000000000000
Illinois	0.000000000000
Lake Michigan	0.000000000000

NOTE: Fingerprint best fit, Snake River, Minn.

Rapp et al. (8) presented five examples of the use of d^* that indicated that artifacts from Petaga Point, McKinstry, and Snake River, Minn., all came from native copper outcrops or stream pebbles along Snake River. By using additional analyses and making some changes in both the concentration ranges (I) and the elements used, the artifact (34-1-82A) from McKinstry that was assigned (8) to a Snake River source with the values shown in Table II is now (Table III) assigned d^* much more positively to a Snake River source. The major differences in d^* values for localities listed in Tables II and III illustrate the sensitivity of d^* to changes in I and in the trace elements used.

The Snake River fingerprint is not unique. Table IV shows a Snake River native copper specimen that barely returns to the Snake River group, being nearly assigned instead to Arizona or the Kingston, Mich., mine. Table V shows a typical example of the proper return by d^* of a Kingston specimen to the Kingston group.

Table IV. Summary of Unknown vs. Fingerprints (Specimen No., 34-1-80T; Snake River Native Copper)

<i>Area</i>	<i>Discriminant Function</i>
Kingston, Mich.	0.000000539299
Champion, Mich.	0.000000000002
Centennial, Mich.	0.000000000000
Isle Royale, Mich.	0.000000000549
Alaska	0.000000002519
Arizona	0.000000733383
Snake River, Minn.	0.000000746059
Wisconsin	0.000000000009
Illinois	0.000000000000
Lake Michigan	0.000000000001

NOTE: Fingerprint best fit, Snake River, Minn.

Table V. Summary of Unknown vs. Fingerprints (Specimen No., 34-21-35DP; Kingston Mine Sample)

<i>Area</i>	<i>Discriminant Function</i>
Kingston, Mich.	0.000000625352
Champion, Mich.	0.000000000000
Centennial, Mich.	0.000000000001
Isle Royale, Mich.	0.000000004080
Alaska	0.000000000741
Arizona	0.000000000049
Snake River, Minn.	0.000000000634
Wisconsin	0.000000000000
Illinois	0.000000000000
Lake Michigan	0.000000000016

NOTE: Fingerprint best fit, Kingston, Mich.

Nine copper artifact samples from the Houska Point excavation site in northern Minnesota were recently analyzed and run against the data base using d^* . Table VI presents the results. Houska Point is located in northern Minnesota along the Canadian border. From the analyses it appears that the earliest prehistoric inhabitants of the site may have secured their copper from deposits along the Snake River in Central Minnesota, then later imported raw copper or finished products from sources on Isle Royale in Lake Superior (approximately the same distance away as Snake River) and from the extremely abundant surficial deposits in the Upper Peninsula of Michigan. The Kingston mine can be considered a surrogate for the Upper Michigan deposits. Although analyses of additional artifacts from Houska Point would be necessary before the

Table VI. d* Assignments of Copper Artifacts, Houska Point Site, Minn.

<i>Excavation Level</i>	<i>Sample Number</i>	<i>Discriminant Assignment</i>
Level I	83D	Isle Royale, Mich.
Level II	83E	Upper Michigan
Level III	83F	Upper Michigan
	83G	Upper Michigan
	83H	Isle Royale, Mich.
	83I	Isle Royale, Mich.
Level IV	83J	Isle Royale, Mich.
	83K	Isle Royale, Mich.
Level V	83L	Snake River, Minn.

copper source pattern is firmly established, the potential of the d* function is evident.

K-Means Cluster Analysis. K-means cluster analysis is an iterative clustering technique with reallocation capability. [See Doran and Hodson (10, pp. 180–85) for a general discussion of the application of K-means procedures to archaeological data sets.] The most important advantage of K-means clustering over the hierarchical–aggregative techniques more often used in NAA data analysis (11) is its ability to continuously review cluster membership and to reallocate members by an optimizing criterion. In the K-means program used here (12), BMDPKM, the reallocation algorithm minimizes the Euclidean distance between the members of a given cluster and the cluster centroid. Initially all samples are members of a single cluster (i.e., $K = 1$); this cluster is subsequently subdivided until the final number of clusters specified by the user is attained. Samples are then iteratively reallocated to the cluster whose centroid is closest to them. The optimum K-number for any clustering operation is determined both quantitatively, by finding the K-number with the smallest mean of average intracluster Euclidean distances, and qualitatively, by examining the scatter plot of the orthogonal projection of samples into the plane defined by the centroids of the three most populous clusters.

K-means cluster analysis was found to be an effective way to discriminate among a limited number of provenances. Figure 1 illustrates the clarity with which cluster divisions between two geographic provenances (float copper specimens from various locations within Illinois and native copper specimens from the Snake River area in Minnesota) are displayed by the program output. Figure 1 is an orthogonal projection of the specimens making up each cluster into the plane passing through the center of the three most populous clusters. The ordinate and the abscissa represent positive and negative distances from the centroid of the initial cluster. Table VII lists the sample identifiers indicating the cluster assignment for each sample and the distance of the sample from

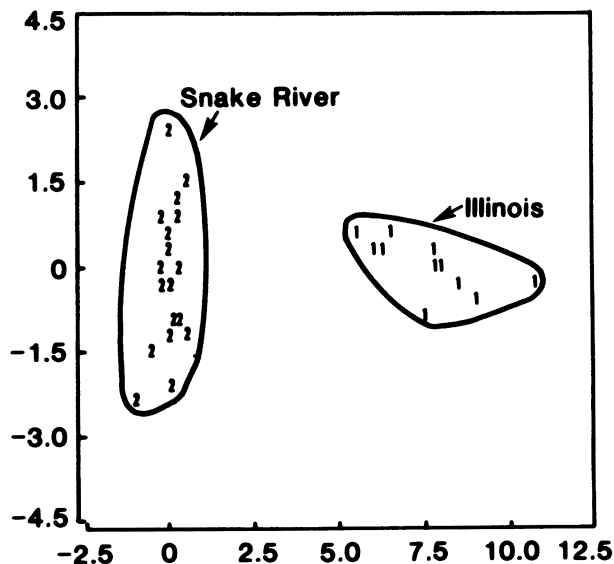


Figure 1. Projection into plane through the centers of clusters 2, 1, and 3.

Table VII. Illinois (IL) and Snake River, Minn. (SR), Cluster Composition

Cluster 1 (11 Cases)		Cluster 2 (21 Cases)			
Case	Distance	Case	Distance	Case	Distance
IL-40A	2.4405	IL-45B	2.5053	SR-80K	4.7280
IL-41A	1.7755	IL-50A	2.5053	SR-80L	3.2164
IL-41B	1.4472	SR-80A	1.9143	SR-80M	1.8948
IL-44A	1.3196	SR-80B	1.9245	SR-80N	2.2841
IL-45A	1.1780	SR-80C	1.6576	SR-80O	2.7832
IL-46A	3.2341	SR-80D	1.9374	SR-80P	2.4516
IL-46B	2.8372	SR-80E	2.9347	SR-80Q	1.5592
IL-46C	0.9107	SR-80F	1.2840	SR-80R	1.9222
IL-46D	0.7805	SR-80G	5.8925	SR-80S	1.7175
IL-48A	1.3032	SR-80I	3.4061	SR-80T	1.8935
IL-49B	0.7112	SR-80J	1.4870		

the center of that cluster. Cluster 1 is composed exclusively of Illinois float coppers; cluster 2 contains all the Snake River coppers and two anomalous Illinois samples.

Perfect clustering, such that no heterogeneous clusters would occur, was rarely achieved, yet overlap such as occurs in cluster 2 above does not pose a major threat to interpretation or application of this form of cluster analysis.

Where sample overlap does become a problem, further clarification was often achieved by increasing the number of clusters. Table VIII

Table VIII. Five Midwestern Localities Cluster Composition Comparisons

	<i>Snake River</i>	<i>Illinois</i>	<i>Wisconsin</i>	<i>Lake Michigan</i>	<i>Isle Royale</i>
<i>Five Clusters</i>					
Cluster 1	0	11	0	0	0
Cluster 2	4	0	0	0	0
Cluster 3	2	0	0	0	0
Cluster 4	11	0	1	0	5
Cluster 5	2	2	18	20	25
<i>Nine Clusters</i>					
Cluster 1	0	10	0	0	0
Cluster 2	4	0	0	0	0
Cluster 3	2	0	0	0	0
Cluster 4	4	0	1	0	4
Cluster 5	0	0	0	0	1
Cluster 6	2	0	2	0	24
Cluster 7	2	2	18	18	3
Cluster 8	0	1	0	0	0
Cluster 9	5	0	0	0	0

NOTE: Modal values are in boldface type.

compares the cluster compositions of analyses made on float copper specimens from Illinois with specimens from the Lower Peninsula of Michigan, with specimens from Wisconsin, with native copper from sources on Isle Royale, and with specimens from Snake River in central Minnesota. Ideally, five clusters should be enough to separate out these five distinct localities. However, specimen outliers (a function of total sample size as well as of trace element composition similarity) make it impossible to distinguish between groups at this level and at succeeding levels 6, 7, and 8. When the same group was separated into nine clusters, however, homogeneous groups began to emerge. Table VIII indicates the number of samples from each locality within each of the clusters and demonstrates the benefit derived from increasing the number of clusters. Even with nine clusters, however, the program was unable to distinguish between Wisconsin and lower Michigan float coppers. The trace element compositions of samples within those groups appear to be very similar. Curiously enough, the Illinois float copper specimens, although geographically close and geomorphically related to the Lower Michigan and Wisconsin specimens, were, for the most part, easily separated from them. This grouping is apparent even in the five-cluster analysis and is indicative of the unique composition of float coppers from Illinois.

After grouping specimens from five localities into nine clusters, it was necessary to recombine the clusters to evaluate the success of the

program in distinguishing among localities. All Illinois samples except two were found in homogeneous clusters 1 and 8. As previously mentioned, Wisconsin and Lower Michigan were lumped together and comprised the bulk of cluster 7. Isle Royale samples clearly dominated cluster 6, entirely made up cluster 5, and shared cluster 4 with samples from Snake River. Snake River specimens exclusively made up clusters 2, 3, and 9, in addition to making a strong showing in cluster 4. The complexity of these relationships is shown on the planar projection of the clusters (Figure 2), where Illinois clusters 1 and 8 are shown widely separated from the rest. Within the non-Illinois clusters, the division into localities is discernible yet difficult to illustrate on the planar projection diagram.

As a tool to trace artifact copper material to its most likely geographic and(or) geologic source, cluster analysis is useful, although the inability of this technique to distinguish easily among more than two or three localities at any one time makes it less valuable than the discriminant analysis. In an attempt to use cluster analysis in this manner, three artifact samples from the Lower Peninsula of Michigan were added individually to a cluster analysis of Illinois and Lower Michigan float copper specimens. All three samples clustered with the Lower Michigan float coppers.

A further demonstration of K-means clustering uses samples from two copper mines in the Upper Peninsula of Michigan. The Champion

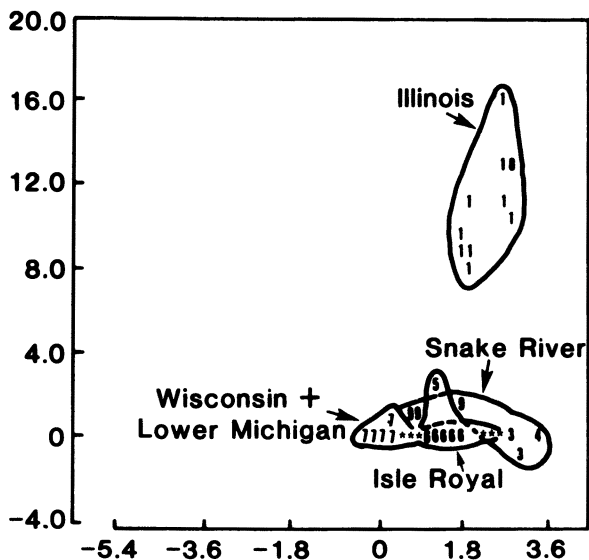


Figure 2. Projection into plane through the centers of clusters 7, 6, and 1.

Table IX. Cluster Composition Comparisons

	<i>Champion</i>	<i>Centennial</i>
<i>Two Clusters</i>		
Cluster 1	9	10
Cluster 2	0	1
<i>Six Clusters</i>		
Cluster 1	3	5
Cluster 2	4	1
Cluster 3	1	0
Cluster 4	0	2
Cluster 5	0	3
Cluster 6	1	0

NOTE: Modal values are in boldface type.

and Centennial mines were chosen for comparison because of their close proximity and geologic similarity. Of six clusters, five could be assigned to one mine or the other on the basis of cluster homogeneity and dominance of one mine; the sixth cluster (cluster 1) was mixed (Table IX). The relationship is evident, although not entirely explicit, in Figure 3. Two clusters, overlapping in only one area, emerged from the analysis, although the initial separation into two clusters was not definitive.

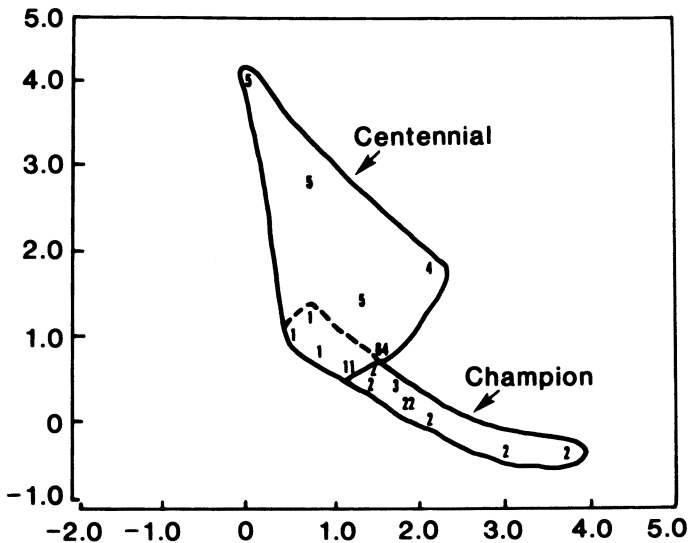


Figure 3. Projection into plane through the centers of clusters 1, 2, and 5.

Summary and Conclusions

We have presented trace element data and statistical analyses using these data. The data base needs to be expanded with analyses of samples from the many additional known localities in North America. Other statistical techniques, such as the one used by Sigleo (2) for turquoise, will also be examined. It appears that the discriminant function d^* is an important tool for archaeologists in provenance studies and that K-means cluster analysis can be very helpful in studying the singularity of trace element patterns for given localities.

Acknowledgments

The neutron activation analyses were done as part of the Reactor Sharing Program under U.S. Department of Energy Contract E-(11-1)-2144 to the University of Wisconsin Reactor Facility (Richard Cashwell, director). Robert Woodhams assisted with the securing and sampling of some of the native copper samples. Gregg Deutsch assisted with many of the computer calculations. S.E. Aschenbrenner provided valuable assistance in the development and maintenance of the data base. This project has been funded in part by Carleton College with a grant from the Bush Foundation and in part from private contributions to the University of Minnesota from the William A. Kings, the George Gibsons, and the Charles McCrossans.

Appendix**Concentration Intervals and Distribution of Abundances Throughout These Intervals for 27 Elements and 10 Source Localities**

<i>Range^a</i>	<i>King^b</i>	<i>Cham</i>	<i>Cent</i>	<i>Isle</i>	<i>Alas</i>	<i>Ariz</i>	<i>Snak</i>	<i>Wisc</i>	<i>Illn</i>	<i>Lomi</i>
<i>Silver (Ag)</i>										
<1.00000	2	0	0	13	0	2	0	17	2	13
100.00000	8	0	2	6	6	22	4	0	0	6
200.00000	53	0	7	1	11	1	6	0	6	1
300.00000	61	6	2	0	2	0	4	0	5	0
999999.00000	35	3	1	0	12	4	5	1	0	0
Totals	159	9	12	20	31	29	19	18	13	20
<i>Arsenic (As)</i>										
<.00010	8	0	0	18	14	18	0	16	2	18
50.00000	10	0	0	2	8	2	1	1	0	2
200.00000	12	0	1	0	0	0	0	0	7	0
1000.00000	22	0	0	0	1	0	2	0	4	0
999999.00000	19	0	0	0	0	0	16	0	0	0
Totals	71	0	1	20	23	20	19	17	13	20
<i>Gold (Au)</i>										
<.00010	43	0	1	6	19	11	0	15	4	10
.01000	2	0	0	0	0	1	0	0	0	0
.05000	20	0	0	1	6	6	10	1	0	1
.10000	5	0	0	7	0	1	7	1	0	9
999999.00000	1	0	0	0	0	1	2	0	9	0
Totals	71	0	1	14	25	20	19	17	13	20
<i>Cadmium (Cd)</i>										
<.00010	61	0	1	20	23	20	12	16	13	20
1.00000	0	0	0	0	0	0	0	1	0	0
50.00000	3	0	0	0	0	0	3	0	0	0
100.00000	4	0	0	0	0	0	4	0	0	0
999999.00000	3	0	0	0	0	0	0	0	0	0
Totals	71	0	1	20	23	20	19	17	13	20
<i>Cobalt (Co)</i>										
<.01000	1	0	0	5	2	1	4	6	2	5
.05000	54	9	11	0	10	8	0	1	0	0
1.00000	18	0	0	0	0	1	0	1	0	0
50.00000	86	0	1	15	19	18	15	10	0	15
999999.00000	0	0	0	0	0	1	0	0	11	0
Totals	159	9	12	20	31	29	19	18	13	20

Footnotes are at end of table.

Continued on next page.

**Concentration Intervals and Distribution of Abundances Throughout
These Intervals for 27 Elements and 10 Source Localities—Continued**

<i>Range^a</i>	<i>King^b</i>	<i>Cham</i>	<i>Cent</i>	<i>Isle</i>	<i>Alas</i>	<i>Ariz</i>	<i>Snak</i>	<i>Wisc</i>	<i>Illn</i>	<i>Lomi</i>
<i>Cerium (Ce)</i>										
<.00010	16	0	0	18	21	20	14	17	13	18
1.00000	3	0	0	1	4	0	0	0	0	1
50.00000	41	0	1	1	0	0	5	0	0	1
100.00000	7	0	0	0	0	0	0	0	0	0
999999.00000	6	0	0	0	0	0	0	0	0	0
Totals	73	0	1	20	25	20	19	17	13	20
<i>Chromium (Cr)</i>										
<.00010	31	0	0	18	16	11	13	16	2	18
.01000	84	7	10	0	2	5	0	1	0	0
1.00000	0	2	0	0	7	1	0	1	0	0
50.00000	44	0	2	2	6	12	6	0	0	2
999999.00000	0	0	0	0	0	0	0	0	11	0
Totals	159	9	12	20	31	29	19	18	13	20
<i>Cesium (Cs)</i>										
<.00010	59	0	1	13	23	20	14	16	2	13
.50000	1	0	0	1	0	0	0	0	0	1
1.00000	8	0	0	0	0	0	3	1	0	0
50.00000	3	0	0	6	0	0	2	0	0	6
999999.00000	0	0	0	0	0	0	0	0	11	0
Totals	71	0	1	20	23	20	19	17	13	20
<i>Europium (Eu)</i>										
<.00010	52	0	1	19	23	18	16	17	2	19
.05000	2	0	0	0	0	2	0	0	0	0
.10000	2	0	0	1	0	0	0	0	0	1
1.00000	15	0	0	0	0	0	3	0	0	0
999999.00000	0	0	0	0	0	0	0	0	11	0
Totals	71	0	1	20	23	20	19	17	13	20
<i>Iron (Fe)</i>										
<.00010	34	0	0	18	20	15	3	17	2	18
1.00000	51	9	9	1	2	6	0	1	0	1
300.00000	6	0	2	1	8	4	0	0	0	1
1000.00000	26	0	0	0	0	1	8	0	0	0
999999.00000	42	0	1	0	1	3	8	0	11	0
Totals	159	9	12	20	31	29	19	18	13	20

Footnotes are at end of table.

**Concentration Intervals and Distribution of Abundances Throughout
These Intervals for 27 Elements and 10 Source Localities—Continued**

<i>Range^a</i>	<i>King^b</i>	<i>Cham</i>	<i>Cent</i>	<i>Isle</i>	<i>Alas</i>	<i>Ariz</i>	<i>Snak</i>	<i>Wisc</i>	<i>Illn</i>	<i>Lomi</i>
<i>Hafnium (Hf)</i>										
<.00010	50	0	1	20	23	20	14	17	2	20
.50000	4	0	0	0	0	0	0	0	0	0
1.00000	7	0	0	0	2	0	1	0	0	0
50.00000	10	0	0	0	0	0	4	0	3	0
999999.00000	0	0	0	0	0	0	0	0	8	0
Totals	71	0	1	20	25	20	19	17	13	20
<i>Mercury (Hg)</i>										
<.00010	14	0	1	14	10	9	4	13	2	14
.50000	5	0	2	1	4	0	0	1	0	1
1.00000	3	2	5	0	1	2	0	0	0	0
50.00000	134	7	4	5	16	18	15	4	0	5
999999.00000	3	0	0	0	0	0	0	0	11	0
Totals	159	9	12	20	31	29	19	18	13	20
<i>Indium (In)</i>										
<.00010	68	0	1	20	22	19	13	17	2	20
50.00000	3	0	0	0	2	1	6	0	0	0
200.00000	0	0	0	0	1	0	0	0	0	0
750.00000	0	0	0	0	0	0	0	0	4	0
999999.00000	0	0	0	0	0	0	0	0	7	0
Totals	71	0	1	20	25	20	19	17	13	20
<i>Iridium (Ir)</i>										
<.00010	60	0	1	11	23	20	12	14	2	11
.00100	0	0	0	0	2	0	0	1	0	0
.05000	10	0	0	0	0	0	2	0	0	0
.50000	1	0	0	9	0	0	5	2	0	9
999999.00000	0	0	0	0	0	0	0	0	11	0
Totals	71	0	1	20	25	20	19	17	13	20
<i>Lutecium (Lu)</i>										
<.00010	46	0	1	20	23	20	16	17	13	20
.05000	4	0	0	0	0	0	0	0	0	0
.10000	6	0	0	0	0	0	2	0	0	0
.50000	8	0	0	0	0	0	1	0	0	0
999999.00000	7	0	0	0	0	0	0	0	0	0
Totals	71	0	1	20	23	20	19	17	13	20

Footnotes are at end of table.

Continued on next page.

**Concentration Intervals and Distribution of Abundances Throughout
These Intervals for 27 Elements and 10 Source Localities—Continued**

<i>Range^a</i>	<i>King^b</i>	<i>Cham</i>	<i>Cent</i>	<i>Isle</i>	<i>Alas</i>	<i>Ariz</i>	<i>Snak</i>	<i>Wisc</i>	<i>Illn</i>	<i>Lomi</i>
<i>Nickel (Ni)</i>										
<.00010	62	0	1	20	21	16	13	17	2	20
50.00000	1	0	0	0	1	3	1	0	0	0
100.00000	7	0	0	0	1	0	2	0	0	0
750.00000	1	0	0	0	0	0	3	0	0	0
999999.00000	0	0	0	0	0	1	0	0	10	0
Totals	71	0	1	20	23	20	19	17	12	20
<i>Ruthenium (Ru)</i>										
<.00010	64	0	1	19	23	20	14	16	13	19
.50000	0	0	0	1	0	0	0	0	0	1
1.00000	0	0	0	0	0	0	0	0	0	0
50.00000	7	0	0	0	0	0	5	1	0	0
999999.00000	0	0	0	0	0	0	0	0	0	0
Totals	71	0	1	20	23	20	19	17	13	20
<i>Antimony (Sb)</i>										
<.00010	44	0	1	17	20	16	5	15	2	17
.01000	85	7	11	0	3	7	0	1	0	0
1.00000	10	2	0	2	6	1	1	1	0	2
50.00000	20	0	0	1	2	4	12	1	0	1
999999.00000	0	0	0	0	0	1	1	0	11	0
Totals	159	9	12	20	31	29	19	18	13	20
<i>Scandium (Sc)</i>										
<.00010	25	0	0	10	20	15	14	13	2	10
.01000	8	9	2	0	10	9	0	2	0	0
.10000	56	0	2	7	1	3	4	2	0	7
.50000	57	0	4	3	0	2	1	1	0	3
999999.00000	12	0	4	0	0	0	0	0	11	0
Totals	158	9	12	20	31	29	19	18	13	20
<i>Selenium (Se)</i>										
<.00010	60	0	1	19	19	10	12	16	2	19
.10000	29	9	11	0	10	5	0	1	0	0
1.00000	59	0	0	0	1	5	0	0	0	0
50.00000	10	0	0	1	1	9	7	1	0	1
999999.00000	1	0	0	0	0	0	0	0	11	0
Totals	159	9	12	20	31	29	19	18	13	20

Footnotes are at end of table.

**Concentration Intervals and Distribution of Abundances Throughout
These Intervals for 27 Elements and 10 Source Localities—Continued**

<i>Range^a</i>	<i>King^b</i>	<i>Cham</i>	<i>Cent</i>	<i>Isle</i>	<i>Alas</i>	<i>Ariz</i>	<i>Snak</i>	<i>Wisc</i>	<i>Illn</i>	<i>Lomi</i>
<i>Tin (Sn)</i>										
<.00010	63	0	1	20	23	17	14	17	13	20
50.00000	0	0	0	0	0	0	0	0	0	0
100.00000	6	0	0	0	0	0	0	0	0	0
200.00000	1	0	0	0	0	1	2	0	0	0
999999.00000	1	0	0	0	0	2	3	0	0	0
Totals	71	0	1	20	23	20	19	17	13	20
<i>Tantalum (Ta)</i>										
<.00010	61	0	1	20	22	18	15	17	13	20
.10000	0	0	0	0	0	1	0	0	0	0
.50000	4	0	0	0	1	0	2	0	0	0
1.00000	5	0	0	0	0	1	1	0	0	0
999999.00000	1	0	0	0	0	0	1	0	0	0
Totals	71	0	1	20	23	20	19	17	13	20
<i>Tellurium (Te)</i>										
<.00010	56	0	1	20	22	16	10	17	2	20
1.00000	0	0	0	0	0	1	0	0	0	0
50.00000	15	0	0	0	1	3	7	0	1	0
100.00000	0	0	0	0	0	0	2	0	10	0
999999.00000	0	0	0	0	0	0	0	0	0	0
Totals	71	0	1	20	23	20	19	17	13	20
<i>Thorium (Th)</i>										
<.00010	34	0	1	20	23	20	13	17	13	20
.50000	3	0	0	0	0	0	0	0	0	0
1.00000	7	0	0	0	0	0	1	0	0	0
50.00000	27	0	0	0	0	0	5	0	0	0
999999.00000	0	0	0	0	0	0	0	0	0	0
Totals	71	0	1	20	23	20	19	17	13	20
<i>Tungsten (W)</i>										
<.00010	10	0	0	11	4	17	9	14	9	13
50.00000	16	0	1	3	14	3	1	3	2	7
100.00000	5	0	0	0	0	0	9	0	1	0
300.00000	19	0	0	0	1	0	0	0	1	0
999999.00000	21	0	0	0	4	0	0	0	0	0
Totals	71	0	1	14	23	20	19	17	13	20

Footnotes are at end of table.

Continued on next page.

**Concentration Intervals and Distribution of Abundances Throughout
These Intervals for 27 Elements and 10 Source Localities—Continued**

<i>Range^a</i>	<i>King^b</i>	<i>Cham</i>	<i>Cent</i>	<i>Isle</i>	<i>Alas</i>	<i>Ariz</i>	<i>Snak</i>	<i>Wisc</i>	<i>Illn</i>	<i>Lomi</i>
<i>Ytterbium (Yb)</i>										
<.00010	51	0	1	19	23	20	15	17	13	19
.50000	2	0	0	0	0	0	1	0	0	0
1.00000	9	0	0	0	0	0	2	0	0	0
50.00000	9	0	0	1	0	0	1	0	0	1
999999.00000	0	0	0	0	0	0	0	0	0	0
Totals	71	0	1	20	23	20	19	17	13	20
<i>Zinc (Zn)</i>										
<.00010	57	0	1	16	20	15	12	17	2	16
1.00000	0	0	0	4	0	0	0	0	0	4
50.00000	10	0	0	0	3	4	4	0	0	0
400.00000	1	0	0	0	0	0	3	0	0	0
999999.00000	3	0	0	0	0	1	0	0	11	0
Totals	71	0	1	20	23	20	19	17	13	20

^a Upper limits of concentration intervals.

^b Column headings are as follows: King, Kingston Mine, Northern Michigan; Cham, Champion Mine, Northern Michigan; Cent, Centennial Mine, Northern Michigan; Isle, Isle Royale, Michigan; Alas, Alaska; Ariz, Arizona; Snak, Snake River, Central Minnesota; Wisc, Wisconsin; Illn, Illinois; Lomi, Lower Michigan.

Literature Cited

1. Asaro, F.; Michel, H. V.; Sidrys, R.; Stross, F. *Am. Antiq.* **1978**, *43*, 436.
2. Sigleo, A. C. *Science* **1975**, *189*, 459.
3. Allen, R. O.; Luckenbach, A. H.; Holland, C. G. *Archaeometry* **1975**, *17*, 1.
4. Brooks, D.; Bieber, A. M., Jr.; Harbottle, G.; Sayre, E. V. In "Archaeological Chemistry"; Beck, C. W., Ed.; ADVANCES IN CHEMISTRY No. 138, American Chemical Society: Washington, D.C., 1975.
5. Friedman, A. M.; Conway, M.; Kastner, M.; Milsted, J.; Metta, D.; Fields, P. R.; Olson, E. *Science* **1966**, *152*, 1504.
6. Fields, P. R.; Milsted, J.; Henrickson, E.; Ramette, R. "Science and Archaeology"; Brill, R., Ed.; MIT Press: Cambridge, 1971.
7. Bowman, R.; Friedman, A. M.; Lerner, J.; Milsted, J. *Archaeometry* **1975**, *17*, 157.
8. Rapp, G., Jr.; Henrickson E.; Miller, M.; Aschenbrenner, S. E. *J. Met.* **1980**, *32*, 35.
9. Goad, S.; Noakes, J. In "Archaeological Chemistry II"; Carter, G. F., Ed.; ADVANCES IN CHEMISTRY No. 171; American Chemical Society: Washington, D.C., 1977.
10. Doran, J. E.; Hodson, F. R. "Mathematics and Computers in Archaeology"; Harvard University Press: Cambridge, 1975.
11. Bieber, A. M., Jr.; Brooks, D. W.; Harbottle, G.; Sayre, E. V. *Archaeometry* **1976**, *18*, 59.
12. Engleman, L.; Hartigan, J. A. "K-Means Clustering"; Dixon, W. J., Ed.; BMDP Statistical Software 1981; Univ. Calif. Press: Berkeley, 1981.

RECEIVED for review October 6, 1982. ACCEPTED for publication April 18, 1983.

Mass Spectrometry as a Historical Probe: Quantitative Answers to Historical Questions in Metallurgy

B. I. KRONBERG

University of Western Ontario, Department of Geology, London, Ontario, Canada N6A 5B7

L. L. COATSWORTH and M. C. USSELMAN

University of Western Ontario, Department of Chemistry, London, Ontario, Canada N6A 5B7

Although platinum was introduced to Europe in the mid-18th century, it was first made commercially available in large quantities and in malleable form in 1805 by the English chemist William Hyde Wollaston. Previous attempts at consistently producing malleable metal were hindered by chemical purification techniques that gave platinum contaminated with deleterious metallic impurities. Richard Knight's improved process of 1800 was carried out on a suitable sample of crude ore, and analysis of the purified platinum by spark source mass spectrometry (SSMS) indicates an impurity level of about 6%. Reconstruction of Wollaston's purification procedures, coupled with SSMS analysis, indicates that his product was over 98% pure. His superior chemical purification techniques, coupled with improvements in the powder consolidation method, explain Wollaston's success.

MALLEABLE BAR PLATINUM became generally available to the European scientific community for the first time in the early months of 1805. The new noble metal, known in Europe only since the mid-18th century, had resisted all prior efforts by experimenters to transform consistently the crude alluvial ore into a chemically pure, malleable metal. Bar platinum was a product of the chemical and metallurgical researches of the English natural philosopher William Hyde Wollaston, who had spent much of the previous 5 years developing and improving a satisfactory production process. The details of his chemical and tech-

0065-2393/84/0205-0295\$06.00/0

© 1984 American Chemical Society

nological investigation were concisely recorded in his laboratory notebooks, but were not published until 1829, a few weeks after his death (1). During the period of secrecy, Wollaston held a virtual monopoly on the production and sale of platinum in Europe, and the profits from the small industrial enterprise allowed him to pursue his other scientific interests from a position of financial security.

The reasons for Wollaston's success, however, are not obvious from the details provided in his published account. Although the literature process was successfully exploited with little modification by several others throughout the 19th century, a technical rationale for Wollaston's success has eluded historians. His chemical purification procedures, it has been assumed, must have yielded a product with reduced levels of impurities, but their nature and amounts have only been guessed at. Metallurgists have emphasized the critical innovations to powder compaction techniques introduced by Wollaston, with little idea of the chemical composition of the powder to which the techniques were applied.

The importance of metallurgical innovations for the success of the production process varies inversely with the purity of the platinum. If the metal contains relatively high concentrations of impurities, then the metallic powder that results from chemical purification will be very difficult to consolidate and work; consequently, the technical processes involved in compaction are of prime importance. If, however, chemical purification yields a relatively pure metallic powder, then consolidation becomes a facile process, and Wollaston's success owes more to chemistry than to metallurgical technique. For historians of science and technology, then, an assessment of the factors that allowed the metal platinum to become an item of commerce in the 19th century requires answers to the following interrelated questions. For what reasons did those who sought to produce malleable platinum prior to Wollaston fail to develop a process that yielded compact metal of consistent physical and chemical properties? What discoveries or innovations enabled Wollaston to produce malleable platinum in large quantities? Why did Wollaston have no serious competitors in the platinum business during his lifetime? Compelling answers to these questions are not to be found easily either in Wollaston's published papers or in his laboratory notebooks, for nowhere is the secret of his process explicitly stated. We can doubt whether Wollaston himself knew which facet of his process, or combination of factors, was responsible for success. Techniques of modern analytical chemistry can become tools of historical analysis when they are used to resolve such problems. In the case under consideration, experimental details as recorded in Wollaston's laboratory notebooks permit representative purification procedures to be carried out on similar samples of alluvial platinum deposits. Elemental analysis by spark source mass spectrometry (SSMS) of the metal at various stages of purification would then

allow an assessment to be made of the efficacy of Wollaston's purification process, and subsequently of the relative importance of the chemical versus the technological aspects.

Platinum as a New Noble Metal

Although low-melting platinum alloys were fashioned into jewelry by the Pre-Colombian Indians of Ecuador (2), platinum became known in Europe only in the mid 18th century when the Spanish naval officer Don Antonio de Ulloa mentioned the substance in an account of his voyage to the Spanish colonies in South America (3). The platinum he described was found intermixed with gold as an alluvial deposit extracted principally from the gravels of the San Juan and Atrato rivers, both in the district of Choco on the western fringe of New Granada, now Colombia (4). The platinum grains were separated from the gold and were routinely discarded because of fear of the potential debasement of coinage through the alloying of gold with the similarly inert, and dense, platinum. The possibility of such platinum alloys led the Spanish Minister for the Indies in the late 18th century to reconfirm the prohibition of platinum exports from New Granada to Europe, although interested investigators could obtain samples of alluvial platinum from Spain. For those who would wish to obtain larger amounts of the metal, a more important source was the vigorous smuggling trade, which moved the platinum separated in the Choco region to the Port of Cartagena, and then to Jamaica, where it was available for purchase by interested parties at 5–10 Spanish dollars per pound (5).

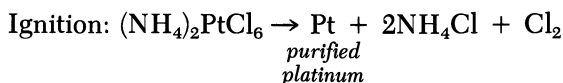
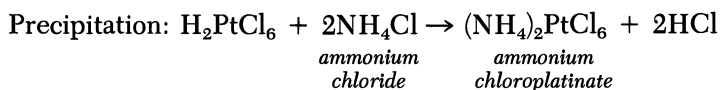
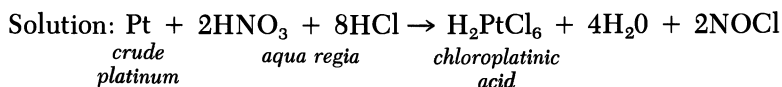
The first platinum to be subjected to experimental investigation was brought to England in 1741 by Charles Wood, an assayer from Jamaica. He determined that the metal could not be fused by the force of any fire then available, formed low-melting alloys with several metals, and had a density similar to that of gold. His results were communicated in 1750 to the Royal Society of London by William Watson and later were published in the *Philosophical Transactions* (6). This publication sparked interest throughout Europe, for the discovery of a new noble metal was as much a surprise to chemists as the discovery of the new planet Uranus by Herschel was to be to astronomers 30 years later.

Several investigators sought to establish the characteristic physical and chemical properties of platinum and to develop the fundamentals of a purification process (7). Their key discoveries were that the heterogeneous alluvial platina was largely soluble in aqua regia, was precipitated from such a solution as a yellowish-orange powder by addition of sal ammoniac (ammonium chloride, NH_4Cl), and that relatively pure platinum powder could be obtained by strong heating of the precipitate. This chemical procedure, modified in minor details by various workers,

produced a product whose specific gravity after consolidation and hammering sometimes exceeded 20 (the modern value for platinum is 21.45), and which occasionally could be hammered into small articles, such as jewelry items or laboratory crucibles. The most notable platinum production of this period is a large chalice (now in the Treasury at St. Peter's, Rome) made late in the 18th century by Pierre Chabaneau for King Charles III of Spain, who subsequently presented it to Pope Pius VI. Such large platinum items remained rare, however, for the purification of platinum remained a little understood process, and the quality of the product varied widely. Malleable metal, it seemed, resulted more from chance circumstances than from chemical art.

State of the Art in 1800

In February 1800, a British mineralogist named Richard Knight published what he termed a "new and expeditious process" for rendering platinum malleable (8). According to Knight, his process enabled him "to reduce any quantity of crude platina to a perfectly malleable state entirely free from impurity and capable of being wrought into any form whatever" (9). The chemical details of the process were, however, quite unoriginal. The crude platinum was boiled in a glass retort with a 15-fold excess of aqua regia until the acid took on a deep saffron color. The solution was then decanted and more aqua regia was added to the undissolved metal and brought to a boil again until all the metal entered solution. An aqueous solution of sal ammoniac was then added in portions to the combined solutions until precipitation ceased, and the precipitate was washed free of adsorbed acid with water and evaporated to dryness. In his treatment of this dried powder, however, Knight introduced an important innovation. The yellow platinum precipitate was placed in a hollow, inverted cone of crucible earth and heated to a strong white heat, which served to reduce the precipitate to a spongy metallic powder. While still in the furnace, the spongy metal was compressed with a ceramic plug to a compact mass, which, after cooling, could be forged into an ingot of malleable metal. The chemical processes involved in this purification sequence are as follows:



The stoichiometry of solution predicts that a 1:4 molar ratio of nitric acid to hydrochloric acid is most efficient. Knight, however, in keeping with the practice of his time, used a 1:1 volume ratio of nitric (70% HNO₃) and hydrochloric (25% HCl) acids, which gives an aqua regia with a molar ratio of 2:1 (HNO₃:HCl). The large deficiency of hydrochloric acid is the principal reason why Knight was forced to use such a large excess of aqua regia for solution of the crude ore.

Compression of the hot, spongy metal before cold-working is the novel feature of Knight's method and it represents an important advance in the history of platinum metallurgy. However, even the improved process failed to give consistent results. Knight never produced malleable platinum himself, nor did anyone else who used his published procedure.

We decided to apply Knight's purification sequence to a similar sample of crude platinum, hoping to gain insight into the efficacy of the process by SSMS analysis of the metallic component at various stages of the procedure. Through the generosity of Matthey Bishop, Inc. of Malvern, Pa., a small sample of alluvial platinum from Colombia was made available for our studies. The modern Colombian alluvial platinum appears to differ little in physical appearance from that described by 19th century metallurgists, being a heterogeneous mixture of flattened metallic grains ranging up to 1 mm² in size. Although the grains of gold clearly visible in the modern sample would have been removed from the platinum smuggled out of New Granada in the early 19th century, SSMS analysis, the results of which are summarized in Table I, indicates a chemical composition comparable to the ore worked by Wollaston and others.

The literature averages recorded in Table I are representative values

Table I. Percent Elemental Composition of Colombian Alluvial Platinum

<i>Element</i>	<i>Modern Colombian (by SSMS)</i>	<i>Wollaston's Analysis^a</i>	<i>Literature Averages^b</i>
Pt	68.40	75.0	76.82–86.20
Pd	1.76	0.5	0.50– 1.66
Ir	1.27	1.5	0.85– 2.52
Rh	2.63	0.5	1.22– 3.46
Os	—	1.5	0.19– 1.13
Au	0.78	—	0.30– 3.15
Ag	1.05	—	—
Fe	19.67	16.0	2.30– 9.78
Cu	3.92	3.0	0.21– 5.20
Pb	0.42	—	—
As	0.11	—	—
(Sand)	—	3.0	—

^a Data are from Ref. 11.

^b Data are from Ref. 10.

taken from several 19th century analyses (10), and the SSMS analysis is an average of two independent determinations. Wollaston's values are taken from data recorded in his laboratory notebooks as average figures calculated in 1815 after the processing of 24,000 troy oz of crude platinum (11). The modern alluvial deposit contains slightly less platinum and more iron and silver than did that worked by Wollaston, but the other constituent metals are present in comparable quantities. (Although Wollaston gave no figures for gold and silver, he did extract both precious metals from his raw material, and estimated that the recovered gold would pay for the aqua regia used in the refining process). For our purposes of historical reconstruction, then, the modern Colombian platinum is sufficiently similar to the 19th century material to give useful results.

Knight's purification sequence was applied to a 500-mg sample of crude platinum and the analytical results for the metallic constituents (taken as 100%) are given in Table II. Although Knight reported that all the ore was soluble in excess aqua regia, we were unable to achieve complete solution, and the metallic composition of the residue was shown by SSMS to consist largely of silver (in the form of silver chloride, only marginally soluble in aqua regia), iridium and rhodium (both of which are insoluble as bulk metals in aqua regia), and iron. It was from similar residues that Smithson Tennant was later to isolate and characterize the metals osmium and iridium (12). The composition of the undissolved residue is surprising only in the high percentage of iron, for which we have no obvious explanation. Analysis of the metallic content of the aqua regia solution shows, as expected, a composition similar to that of the impure ore with some depletion of the undissolved elements. The aqua

Table II. Platinum Purified by Knight's Procedure

<i>Element</i>	<i>Crude Ore</i>	<i>Undissolved Residue</i>	<i>Aqua Regia Solution</i>	<i>Purified Platinum</i>
Pt	68.40	—	64.42	94.04
Pd	1.76	—	1.59	0.17
Ir	1.27	10.50	0.90	1.99
Rh	2.63	6.45	1.65	0.58
Au	0.78	—	0.45	—
Ag	1.05	64.90	0.31	0.29
Fe	19.67	18.15	26.93	2.08
Cu	3.92	—	3.32	—
Pb	0.42	—	0.44	0.86
As	0.11	—	—	—

regia solution should give a more trustworthy analysis of the ore, for the powder that remains after drying would have a more homogeneous distribution of metals than is the case with the heterogeneous crude ore.

The most important composition is that of the purified platinum obtained by ignition of the sal ammoniac precipitate. Analysis of the fine platinum powder indicates a platinum content of 94.04%, with the principal impurities being iridium (1.99%) and iron (2.08%). This result indicates, firstly, that the simple purification procedure does remove the greater part of the metallic impurities present in the crude ore and, secondly, that the purified platinum would be very difficult to consolidate and work because the impurities that remain are sufficient to increase considerably the hardness of the consolidated metal. Very pure (99.99%) platinum in the annealed condition is only slightly harder than gold and is very malleable and ductile, but impurities and cold-working adversely affect these properties. For example, the Vickers hardness (VHN) of very pure platinum increases from 40VHN to 80VHN for a 6% iridium alloy (13). Cold-working increases the hardness of annealed platinum from 40VHN to 76VHN after 25% reduction in thickness and to 108VHN after 75% reduction in thickness (14). Thus Knight's platinum would be rather hard initially due to the contained impurities, and would become increasingly intractable as it was worked further. For these reasons, it seems unlikely that Knight's product would be suitable for any application that required much working of the metal; consequently, its commercial potential would be limited.

Wollaston's First Purification Process

William Hyde Wollaston (1766–1828) came from a distinguished scientific family and, after taking his degree at Cambridge, practiced medicine until 1800 when, liberated by a large inheritance, he turned his attention to chemistry. In partnership with Smithson Tennant, another disenchanted physician with a growing reputation in chemistry, he purchased nearly 6000 troy oz of crude alluvial platinum in December 1800 (15). The two men were well aware that a reliable process for rendering platinum malleable would be both scientifically and financially rewarding, for the metal would give a substantial profit even if sold at £1 per troy oz, which would be about one-quarter of the price of gold, with which it would compete in most commercial applications. Wollaston and Tennant had experimented with platinum during their student days together at Cambridge in the 1780s and Wollaston, who was to carry out much of the platinum research himself, had purchased small amounts of crude platinum in 1799 and early 1800 for investigative studies. Although un-

doubtedly familiar with Knight's process, at the time of the large platinum purchase in late 1800, Wollaston had not even attempted the consolidation of platinum into malleable ingots. His early experiments were devoted entirely to the most economical solution of platinum by a standardized formulation of aqua regia.

Wollaston's earliest notebook entries relating to the purification of platinum begin in the fall of 1800 (16), and from the outset his concern for establishing the purification process on a quantitative basis is apparent. He carefully measured the strengths and quantities of acids used in the preparation of aqua regia by neutralizing acid samples with Iceland spar (calcium carbonate), with the clear intent of fixing precisely the acid ratios required for the most efficient solution of platinum. When the data recorded in the notebooks are compared with modern stoichiometry, it becomes apparent that Wollaston rapidly settled on acid ratios and amounts very close to the optimum stoichiometric values. His investigation, motivated as much by a concern for the economics of solution as by chemical effectiveness, yielded a recipe for aqua regia very different from contemporary literature values, and Wollaston kept the details secret until his posthumous 1829 paper. In addition to using aqua regia of a 4:1 (HCl:HNO₃) molar ratio, Wollaston used only enough acid to dissolve half of the crude platinum and diluted it with an equal volume of water before addition to the crude ore, in an effort to minimize the solution of unwanted contaminants. It is important to remember that in 1800 none of the other platinum metals had yet been discovered. It was only later that Wollaston was able to isolate and characterize palladium (1802) and rhodium (1804), while Tennant, in his investigation of the insoluble residues, discovered osmium and iridium (1804). In 1800, however, the existence of these new elements was unsuspected, although both men likely believed that metallic impurities of uncertain nature were the primary cause of the intractability of platinum.

Concurrent with the solution trials were precipitation and decomposition experiments, for which Wollaston's numerical data again approached those predicted by modern stoichiometry. Thus Wollaston's innovations to the chemical purification process were principally of a quantitative nature, but they brought to the process a consistency that had previously been lacking, and yielded platinum much purer than had earlier been possible. His initial production runs, on 12-troy-oz quantities of crude platinum, began in February 1801 and yielded spongy platinum that was first consolidated and worked in April. The purification process was similar to Knight's published procedure, except for the details noted herein, and the analytical details of the reconstructed process are given in Table III.

It is immediately obvious that the small ore sample used for the repetition of Wollaston's process was much richer in platinum than is

**Table III. Wollaston's First Production Process for Platinum
(% Composition of Metals)**

<i>Element</i>	<i>Crude Ore</i>	<i>Undissolved Residue</i>	<i>Aqua Regia Solution</i>	<i>Purified Platinum</i>	<i>Iron Precipitate</i>
Pt	68.40	93.01	83.43	98.57	52.60
Pd	1.76	0.74	0.30	—	3.38
Ir	1.27	0.41	0.96	0.22	0.33
Rh	2.63	0.31	1.01	0.05	2.69
Au	0.78	—	0.63	0.05	5.98
Ag	1.05	—	0.03	—	0.03
Fe	19.67	5.01	11.76	0.85	32.07
Cu	3.92	0.38	1.24	—	2.76
Pb	0.42	0.06	0.43	0.27	0.03
As	0.11	—	0.21	—	0.14

the bulk sample, for platinum comprised 83.43% of the metallic content of the aqua regia solution. Although such compositional anomalies are unavoidable when dealing with small samples of a heterogeneous mixture, they do not detract seriously from the value of the results; the important observation is the relative difference in metallic composition between the aqua regia solution and the purified platinum. Wollaston's process yields platinum significantly purer than did Knight's (98.57% versus 94.04%), with a much reduced proportion of the troublesome impurities iridium, rhodium, silver, and gold. It is clear that the smaller volume of diluted aqua regia, although not significantly more selective in its dissolving power, does give a much cleaner precipitate with sal ammoniac. The major, and unexpected, impurity in both Wollaston's and Knight's purified platinum is iron. The undissolved residue is richer in platinum than the aqua regia solution because the acid, present in limited amounts, more readily dissolves the base metals. Wollaston saved the residues from his batch processes until all the crude ore being purified at the time had been treated once with aqua regia; then he resubmitted the residues to chemical purification.

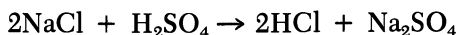
In order to extract all the platinum and other noble metals from the solution that remained after sal ammoniac treatment, Wollaston inserted clean iron bars into the neutralized solution to precipitate all metals of lower affinity (or, in modern terms, of lower oxidation potential). From this "first metallic precipitate," as he called it, Wollaston separated gold, more platinum and later, large quantities of palladium and rhodium (17). We immersed iron wire in the solution remaining after sal ammoniac treatment of the aqua regia solution and analyzed the metallic precipitate displaced. The analytical results, also given in Table III, reveal the expected mixture of noble and base metals, with platinum representing only 52.60% of the total. The percentage of iron is unusually high due

to the inclusion of pieces of iron wire, much of which disintegrated in the displacement reaction.

The spongy platinum remaining after strong heating of the ammonium chloroplatinate was first consolidated into bar metal by Wollaston in 1801, although the preparation of malleable metal remained plagued with difficulties. His early recorded attempts make frequent mention of ingots that "snapped," or were "broken to pieces" (18). Thus it is clear that platinum with an impurity level of about 2% is difficult to consolidate from a spongy powder, and Wollaston then paid more attention to improvements in the powder consolidation technique. Wollaston used the purification technique described above only for a few months before he altered the solution chemistry because of his dissatisfaction with the variable quality and high price of the muriatic acid required.

Wollaston's Second Purification Process

As mentioned previously, many of Wollaston's innovations were prompted by economic considerations. He kept a careful record of the economic efficiency of the solution process by calculating the cost of aqua regia per ounce of purified platinum produced, and calculated that the cost could be reduced from 4 pence per oz to 2 pence per oz by substituting salt and vitriolic acid for muriatic acid (19). Thus the proper mixture of nitric acid, vitriolic acid and salt would give an aqua regia stoichiometrically equivalent to that obtained by directly mixing nitric and hydrochloric acids, for vitriolic acid reacts with salt to give muriatic acid:



This alternative preparation of aqua regia was used for all production runs from mid 1801 to 1808. In 1808, Wollaston reverted to his first purification process for two reasons: (1) The sodium sulfate produced often formed a cake over the residual, undissolved ore and made its further processing difficult, and (2) the solution process was lengthened from 3 to 6 days, requiring expenditures on charcoal (for heating) and reaction vessels that exceeded the saving on acid costs.

Because much of Wollaston's platinum was produced by this second process, we decided to purify a crude platinum sample by this method to see if the purity of the product was adversely affected. The analytical results are given in Table IV and indicate that the platinum purified by the second process did not differ in any important respects from that obtained by the first process. The slight decrease in platinum content (98.57% to 97.35%) is balanced by small increases in the levels of the metallic impurities. Given the inherent uncertainties in the sampling procedure, the compositional differences between the platinum produced by the two methods are insignificant. The relative proportions of

**Table IV. Wollaston's Second Production Process for Platinum
(% Composition of Metals)**

<i>Element</i>	<i>Crude Ore</i>	<i>Undissolved Residue</i>	<i>Aqua Regia Solution</i>	<i>Purified Platinum</i>	<i>Iron Precipitate</i>
Pt	68.40	69.66	63.98	97.35	56.33
Pd	1.76	1.29	2.67	—	0.63
Ir	1.27	4.46	0.99	0.44	0.03
Rh	2.63	3.93	2.40	0.24	1.34
Au	0.78	—	2.12	0.23	3.91
Ag	1.05	—	0.51	—	0.12
Fe	19.67	18.66	21.75	0.93	36.24
Cu	3.92	1.52	4.78	—	1.13
Pb	0.42	0.16	0.80	0.81	0.11
As	0.11	—	—	—	0.16

**Table V. The Purification of Residual Platinum
(% Composition of Metals)**

<i>Element</i>	<i>Undissolved Residue</i>	<i>Aqua Regia Solution</i>	<i>Purified Platinum</i>
Pt	40.47	73.63	98.52
Pd	1.10	1.54	0.09
Ir	4.87	0.96	0.36
Rh	4.38	1.95	0.11
Au	—	0.01	—
Ag	—	0.22	0.03
Fe	45.05	18.25	0.77
Cu	4.14	3.30	—
Pb	—	0.10	0.12

the metals contained in the undissolved residue, and in the metallic precipitate displaced by iron, are also comparable for the two processes.

As noted earlier, Wollaston collected the undissolved residue from each batch process, and resubmitted the combined residues to a second purification sequence. The purified platinum obtained from the residues was also worked successfully, and we checked the purity of such platinum by combining the residues from both of the procedures we repeated, and purified the crude residue by the second chemical sequence; the analytical results are given in Table V. As might be expected, this second treatment with aqua regia much reduces the proportion of platinum in the undissolved residue, and increases the relative amounts of iridium and rhodium.

The purified platinum is quite similar in types and levels of impurities to that produced by the primary purification sequences. It is therefore apparent why Wollaston found no consistent differences in the metallurgical characteristics of the platinum powder produced from the crude ore or the retreated residuum by either of his two purification processes.

Experimental Details

Analyses. All samples were analyzed on a JEOL-JMS-O1BM-2 spark source mass spectrometer fitted with Ilford Q2 photoplates. For each sample, a series of 8 exposures was deposited on the photographic emulsion; the intensity varied over a factor of 10^5 . The ion intensities were scanned (from m/e 45 to m/e 220) and digitized from the photoplates with an Optronics International Stripsan System S-2000 microdensitometer. The data were then treated by computer to generate the relative abundances of all metallic ions using the ^{195}Pt and ^{196}Pt isotopes as internal standards for calibration by the Churchill two-line method (24). The relative abundances were converted to percentages by assuming the metallic content of the sample to be 100%.

For sample preparation, 20–40 mg of metallic powder was triturated with approximately 250 mg carbon and compacted into small rods 1 cm in length, which served as electrodes in the ionization chamber of the mass spectrometer. Elements other than those listed in the tabular results were detected, but their intensities lay outside the lower limit of the calibration curve and they were ignored in calculations of percent composition.

Colombian Alluvial Platinum. The analytical results are an average of two determinations. Each sample consisted of approximately 500 mg ore in 1 g carbon.

Knight's Method. A 7.5-g aliquot of aqua regia (consisting of a 1:1 volume ratio of 25% HCl and 70% HNO_3) was added to 500 mg crude platinum in a 25-mL round-bottomed flask fitted with a reflux condenser. The contents were then heated at reflux temperatures for 3 h, at which time the deep-amber-colored solution was decanted off and replaced by another 7.5-g weight of aqua regia. After further refluxing for 6 h the acid solution was separated and combined with the first solution; a 1-mL aliquot of this solution was evaporated to dryness to yield 55.8 mg of black residue, which was analyzed. The undissolved residue (4.1 mg) was washed, dried, and analyzed. A 3.7 M ammonium chloride solution was added dropwise to the aqua regia solution until formation of precipitate ceased (2.5 mL added), and the orange-colored precipitate was filtered off, washed with water until the pH of the washings exceeded 5, and dried. A 410-mg portion of this precipitate (total weight 610 mg) was placed on a Pyrex watch glass and heated strongly over a Bunsen burner for 20 min, at which time 162 mg of a very porous, feathery platinum powder remained. A 29-mg sample of this powder was analyzed.

Wollaston's First Process. Aqua regia consisting of 2.7 mL hydrochloric acid (25%), 0.3 mL nitric acid (70%), and 1.7 mL water was added to 0.99 g crude platinum, and the mixture, in a 10-mL round-bottomed flask, was heated at 55 °C in a sand bath for 3 days. The undissolved residue (299 mg) was then filtered off, washed, dried, and 33 mg was separated for analysis. A 1-mL aliquot of the aqua regia solution was evaporated to dryness to yield 83 mg of residue, which was analyzed. Ammonium chloride solution (3.7 M) was added dropwise to the remaining aqua regia solution until precipitation ceased (2.0 mL added).

The dark yellow precipitate was separated, washed free of acid, and dried; 890 mg (total weight 972 mg) was reduced over a Bunsen burner to yield 340 mg metallic powder, of which 22 mg was analyzed. Pure iron wire (90 cm, 300 mg) was immersed in the ammonium chloride filtrate, and after 24 h, the very fine metallic powder displaced by iron was filtered off, dried, weighed (16 mg), and analyzed.

Wollaston's Second Process. A solution of 0.73 mL nitric acid (35%), water (6 mL), sodium chloride (1.32 g) and 0.51 mL sulfuric acid (96%) was added to 1.00 g crude platinum in a 10-mL round-bottomed flask and heated at 55 °C in a sand bath for 6 days. Further treatment and sample preparation were similar to the procedures described above for Wollaston's first process.

Purification of Platinum Residuum. The procedure was identical to that described above for Wollaston's second process, with all quantities scaled down to an initial weight of 0.77 g residual platinum. There was, however, insufficient material displaced by iron in the final stage to permit its analysis.

Conclusion

In their thorough, and expert, analysis of the history of platinum, McDonald and Hunt wrote that Wollaston's was "the best platinum so far made and that it was many, many years, perhaps as long as a century, before its equal was seen again" (20). Certainly Wollaston's contemporaries recognized that his product was far superior to that which had previously been available. Our analysis suggests that the principal reason for his successful production of malleable platinum was the efficacy of his chemical purification. He was able to consistently produce platinum of about 98% purity, which made the subsequent consolidation into malleable ingots possible. Previous workers, if their methods of purification were as good as Knight's, worked with platinum containing 6% or more of various impurities. It is also clear that no one impurity was principally responsible for the intractibility of platinum. Iridium, the principal culprit in the eyes of most historians of metallurgy, was probably equalled by iron in its deleterious effects, but rhodium and lead also contributed.

Of course, Wollaston's purification process was only an enabling condition. As he himself was aware, it yielded a spongy powder that still required careful techniques for consolidation into malleable metal. Although the present study is not concerned primarily with Wollaston's metallurgical innovations, parallel work has indicated that his advances owed more to improvement of existing techniques than to novel discovery. In the first place, precipitation of platinum from a dilute solution of aqua regia produces small metallic agglomerations of maximum surface area. Secondly, Wollaston washed the fine spongy platinum repeatedly with water to remove undecomposed salts and to partition the platinum into fractions of similar particle sizes. The finest particles were used for the most demanding applications, such as crucibles and very fine wires. Finally, in 1812, Wollaston designed and built a powerful lever press

capable of compressing spongy platinum to a compact solid before subsequent heating and forging. Such technological innovations were as essential to the ultimate success of the process as were the chemical ones.

The validity of the historical conclusions drawn rests on the reliability of the SSMS analyses and, although our results are internally consistent (to the extent allowed by the variation in composition of the platinum samples subjected to purification), the results become more compelling when compared with analyses of Wollaston's own platinum. Fortunately a number of authentic Wollaston artifacts are held by the Science Museum, London, and small samples of fine platinum wires produced by him were made available for analysis. Analyses by SSMS of four platinum wires (21) gave average values for the principal metallic constituents as follows: platinum (99.32%), iridium (0.22%), rhodium (0.03%), iron (0.35%), copper (0.03%), and lead (0.01%). The composition of Wollaston's platinum thus correlates well with the values obtained by repetition of his purification procedures on similar samples of alluvial Colombian platinum.

The techniques of analytical chemistry used in our investigations of early platinum processing allow answers to be framed for the questions posed at the outset of the study. Workers prior to 1800 were unable to consistently produce malleable platinum because their purification techniques yielded a metal with total impurity levels too high to permit cold-working of the consolidated mass. If by chance a sample of crude platinum of unusually high purity was worked, then a malleable product would result, but success rested more upon good fortune than upon chemistry. Wollaston's purification process, in both modifications, yielded a product that generally was over 98.5% pure and that, after being subjected to a careful consolidation technique, gave malleable metal of consistent metallurgical properties.

Although we have identified the basis for Wollaston's success in his careful attention to detail, rather than in novel discovery, contemporaries were convinced that he had discovered some critical factor essential for success. Through his silence on the matter, Wollaston encouraged this false assumption and thus protected the viability of his platinum business. The award to him of one of the two Royal Medals of the Royal Society of London in 1828 for his platinum process was, nonetheless, criticized by a Fellow of the Society (22):

—the adjudication of a Royal medal to a philosopher who had already enriched himself by the very discovery which the council thought proper thus to reward, and of which death alone seems to have compelled the promulgation, was truly unjust. —By keeping that discovery to himself for many years—like a medical empiric, who dares not to purchase a patent

lest he should be compelled to give a specification of his remedy—Dr. Wollaston retarded the course of investigation and discovery respecting one of the most useful metals in nature. I say retarded advisedly, for what chemist or metallurgist would have ventured to undertake any series of experiments on the same subject, respecting which it was known, that every difficulty had already been conquered by Wollaston, who might at any moment divulge his secret to the world, and thus thwart at once the pretensions of any other successful experimentalist?

The criticism is correct when it accuses Wollaston of retarding the progress of investigation into the production of malleable platinum, for that was his prime motive for secrecy. He was well aware that his process was not novel enough to be patented, and could easily be mastered by a good chemist. As Berzelius wrote after learning of the process (23):

We are now re-casting all our old soldered platinum crucibles by Wollaston's method of making platinum pliable; it goes like a dance. I think Wollaston must have laughed inside over the many elaborate methods which have been used in vain for this purpose, when his is so simple.

Acknowledgments

We would like to thank David Lundy and Matthey Bishop, Inc., for provision of Colombian alluvial platinum and the Social Sciences and Humanities Research Council of Canada for a grant (to M. C. Usselman), which made this research possible.

Literature Cited

1. Wollaston, W. H. *Philos. Trans. Roy. Soc. London* **1829**, *119*, 1–8.
2. Bergsoe, P. "The Metallurgy and Technology of Gold and Platinum among the pre-Colombian Indians": *Naturvidenskabelige Samfund*: Copenhagen, Denmark, 1937.
3. Juan, J.; de Ulloa, A. "Relacion historica del viaje a la America Meridional hecho de orden de S. Mag.," 2 vols.; Antonio Martin: Madrid, 1748; Vol. 1, Book 6, Chap. 10, p. 606.
4. McDonald, D.; Hunt, L. B. "A History of Platinum and Its Allied Metals"; Johnson Matthey: London, 1982; pp. 13–27.
5. Usselman, M. C. *Ann. Sci.* **1980**, *37*, 256.
6. Watson, W. *Philos. Trans. Roy. Soc. London* **1751**, *46*, 584–96.
7. McDonald, D.; Hunt, L. B. "A History of Platinum and Its Allied Metals"; Johnson Matthey: London, 1982; pp. 29–53.
8. Knight, R. *Philos. Mag.* **1800**, *6*, 1–3.
9. *Ibid.*, p. 1.

10. Mellor, J. W. "A Comprehensive Treatise on Inorganic and Theoretical Chemistry", 16 vols.; Longmans, Green: London, 1922–37; Vol. 16, p. 6.
11. Usselman, M. C. *Platinum Met. Rev.* 1978, 22, 106.
12. Tennant, S. *Philos. Trans. Roy. Soc. London* 1804, 94, 411–18.
13. Vines, R. F.; Wise, E. M., Eds. "The Platinum Metals and Their Alloys"; International Nickel: New York, 1941; p. 28.
14. *Ibid.*, p. 25.
15. Usselman, M. C. *Ann. Sci.* 1980, 37, 253.
16. Wollaston MSS; Cambridge Univ. Library; Notebook J, pp. 17–18.
17. Kronberg, B. I.; Coatsworth, L. L.; Usselman, M. C. *Ambix* 1981, 28, 20–35.
18. Usselman, M. C. *Platinum Met. Rev.* 1978, 22, 105–106.
19. Wollaston MSS; Cambridge Univ. Library; Notebook G, p. 82.
20. McDonald, D.; Hunt, L. B. "A History of Platinum and Its Allied Metals"; Johnson Matthey: London, 1982; p. 173.
21. Coatsworth, L. L.; Kronberg, B. I.; Usselman, M. C. *Hist. Tech.* 1981, 6, 91–111.
22. Granville, A. B. "The Royal Society in the XIXth Century"; London, 1836; p. 70.
23. Wallach, O. "Briefwechsel zwischen J. Berzelius und F. Wohler"; Wilhelm Engelmann: Leipzig, 1901; Vol. 1, p. 253.
24. Ahearn, A. J., Ed. "Mass Spectrometric Analysis of Solids"; Elsevier: Amsterdam, 1966; pp. 84–86.

RECEIVED for review October 6, 1982. ACCEPTED for publication March 18, 1983.

Chemical Compositions of Copper-Based Roman Coins: Claudian Quadrantes A.D. 41–42

GILES F. CARTER

Eastern Michigan University, Chemistry Department, Ypsilanti, MI 48197

Ninety-nine Claudian quadrantes have been analyzed for iron, nickel, copper, silver, tin, antimony, and lead by x-ray fluorescence spectroscopy. The coins are the purest copper of any Roman coins analyzed to date. Fifteen coins were made from small, thick flans; these coins usually contain less nickel but comparatively much more lead, antimony, and silver than do the 84 coins having normal, thin flans. All the thick-flan coins were struck in A.D. 41; normal flans were used for coins struck in both A.D. 41 and 42. Compositions of the quadrantes are very similar to those of Claudian asses (a denomination of larger copper coins) and also to Caligulan quadrantes and asses. However, the compositions are significantly different from Tiberian coins of about A.D. 34 and Neronian coins of A.D. 64–66.

SEVERAL HUNDRED COPPER-BASED ROMAN COINS have been analyzed by wet chemistry (1–5), x-ray fluorescence spectroscopy (6–11), and atomic absorption spectroscopy (12). Consequently, a general understanding of the compositions of copper-based Roman coins is developing. For instance, the debasement of orichalcum (Roman brass) coins by substituting tin and lead for zinc during the late first and second centuries is well known (1,12).

The following three paragraphs contain examples of knowledge gained through determination of the major and trace element compositions of Roman coins:

As the first Emperor, Augustus instituted a brilliant new copper-based coinage comprising four denominations: the sestertius and dupon-

This chapter is the seventh in a series of articles on the chemical composition of copper-based Roman coins.

0065-2393/84/0205-0311\$06.00/0

© 1984 American Chemical Society

dius, both made of orichalcum, and the as and quadrans, made of nearly pure copper. Furthermore, the major Roman mint at Lugdunum (Lyons, France) used essentially the same compositions as did that at Rome under Augustus. However, less important mints in the Roman colonies produced coins having miscellaneous low concentrations of several percent tin and lead (6). This coinage policy was, indeed, brilliant and is evidence of Augustus' perception of the favorable propaganda value of good quality copper-based coins.

So-called imitations, or "military copies," of copper coins of Claudius, probably minted in France, Germany, and England for the Roman army, have small, but significant, differences in trace element concentrations from Claudian coins minted in Rome (10).

The presently accepted chronology of Augustan quadrantes is probably wrong. Both chemical analyses and size measurements indicate that the "8 B.C." quadrantes are likely to be older than the "9 B.C." quadrantes. Also some Augustan asses have been dated to 7 and 6 B.C., but their compositions are different from those of the quadrantes. It is concluded that the quadrantes, now tentatively dated at 9, 8, 5, and 4 B.C., were made in a 4–6 yr period during which no asses were minted (8).

It is necessary to analyze large numbers of coins to solve most numismatic problems because of variations in composition within any given period of time and among mints. In fact, the variation itself is important in many instances because it reflects the degree of quality control exercised in producing the coin flans at a given time. Obviously, it is not possible to use wet chemical or other destructive techniques to analyze large numbers of coins. Therefore, methods such as neutron activation analysis, x-ray fluorescence, or atomic absorption spectroscopy are favored. Atomic absorption spectroscopy, however, requires small samples obtained from drilling into the coin edges. Hence it is usually restricted to large coins.

Because x-ray fluorescence analysis determines a rather thin surface layer of metal in coins (*see* Table I for calculations), the surface must be representative of the entire coin or misleading results are obtained. Carter and Kimiatek (13) compared the compositions of Augustan quadrantes at the surfaces and in the interiors. Usually only small and irregular differences were noted. It was concluded that for nearly pure copper coins, x-ray fluorescence analysis is capable of providing good analyses provided the coins are cleaned properly. Proper cleaning involves removing oxides by electrolytic reduction followed by rubbing with a pencil eraser. Then, 10–15 μm of metal is removed from each surface of the coin by means of an air blast containing fine abrasive particles of chemically pure aluminum oxide (Al_2O_3) (14).

The quadrans was the lowest denomination of Roman coins; slightly worn quadrantes have roughly about the same weight as a U.S. penny, a little over 3 g. Quadrantes, however, are usually smaller in diameter

Table I. Transmittance of x-Rays by Copper Coins

Element	Surface Thickness of Copper (μm)							
	1	5	10	15	20	25	30	40
Fe	0.91	0.63	0.40	0.25	0.16	0.10	0.06	0.02
Ni	0.94	0.74	0.55	0.41	0.31	0.23	0.17	0.09
Cu	0.95	0.79	0.62	0.49	0.39	0.30	0.24	0.15
Ag	0.98	0.88	0.78	0.69	0.61	0.54	0.48	0.37
Sn(L α_1)	0.62	0.09	0.01	0	0	0	0	0
Sb(L α_1)	0.65	0.12	0.014	0	0	0	0	0
Pb(L α_1)	0.84	0.42	0.18	0.07	0.03	0.013	0.006	0

NOTE: All values are the transmittance, namely I/I_0 .

Lead L α_1 x-rays are heavily absorbed by copper because they have moderately higher energy than the absorption edge of copper.

and thicker than a new penny. They were first struck by Augustus in approximately 9–4 B.C.; no other quadrantes were struck until the reign of Caligula in the late 30s A.D. A large number of quadrantes was struck by Claudius in A.D. 41–42. In this chapter we report the results of our analysis of a group of 99 Claudian quadrantes and compare these analyses with those of Augustan quadrantes, Tiberian asses, Caligulan quadrantes and asses, Claudian asses, and Neronian quadrantes and asses.

Experimental

Two x-ray fluorescence spectrometers were used for the analyses: a General Electric XRD–6 for iron, copper, tin, and antimony, and a General Electric XRD–5 for nickel, silver, and lead (the latter machine has updated electronics and gave superior results for these three elements). Four certified standards from the National Bureau of Standards were used for each element to obtain a straight line calibration curve using linear regression (10). The experimental conditions used for the determination of each element were given by Carter et al. (10).

Each coin was weighed, and its physical dimensions and properties, such as maximum and minimum diameter, maximum thickness, density, and die orientation, were obtained. These results are summarized in Appendix A.

Physical Properties of Claudian Quadrantes

The density of pure copper is 8.93 g/cm³, and the densities of the Claudian quadrantes average about 8.91 ± 0.04 g/cm³. None of the coins has any appreciable quantity of voids or internal pores. Die orientations were determined by rotating each coin about its obverse vertical axis. The reverse vertical axis was then found to point in a given direction, which was identified by the equivalent direction of the hour hand of a clock. All of the 84 Claudian quadrantes in the chemical compositional group,

A.D. 41 group 41 #B (*see* the section on chemical compositions) have a die orientation very close to 6:30 (Appendix A). The mean orientation is $6:27 \pm 0:22$. This means that great care was taken to orient the reverse die with respect to the obverse die during striking. This is in marked contrast to the striking of Augustan quadrantes in 9–4 B.C. (8), where the die orientations clustered about the four orientations, 1:00, 4:00, 7:00, and 10:00 (1:00 and 7:00 predominate).

Five of the 15 coins in the compositional group 41 #A have die orientations close to 12:30. The significance of this fact is unknown, although it may indicate that the compositional group 41 #A comprises coins struck in a different workshop, or even possibly that these coins were merely copies of the other Claudian quadrantes. However, there is no other evidence to indicate that quadrantes were copies. Large numbers of copies of Claudian asses (large copper coins about 3 cm in diameter) and dupondii (brass coins about the size of asses) are known.

On the average, coins from group 41 #A are appreciably thicker than quadrantes from group 41 #B. However, this general rule does not apply to every coin. There are a few thick coins in group 41 #B and a few thin coins in group 41 #A. Almost every coin whose very poor condition makes its complete identification impossible belongs to the small group 41 #A. This finding is surprising, and again may indicate that group 41 #A are copies that were poorly struck.

All groups of coins have roughly the same average ellipticity (maximum diameter divided by the minimum diameter; *see* Appendix A). The weights of the quadrantes vary considerably and are not representative of weights for all Claudian quadrantes because these coins were dredged from the Tiber River and subsequently cleaned. Coins in museum collections are usually outstanding specimens and have a much higher average weight than the Claudian quadrantes in this study. Museum coins are on the average at least 0.5 g heavier. The weights of quadrantes in private collections are unknown. Corrosion will change the weight of a coin far more than it will affect the maximum or minimum diameter or the maximum thickness. Hence the weights of these coins are useful primarily to identify the coins in the future (most are being sold to collectors, but some may enter eventually into museum collections).

No significant differences in size or physical properties could be correlated with catalog numbers of the quadrantes. Figure 1 illustrates the different varieties of Claudian quadrantes, namely BMC [British Museum Catalog number (15)] 174, 179, 181, 182, and 182 variety.

Chemical Compositions of Claudian Quadrantes

Ninety-nine Claudian quadrantes made in A.D. 41 or 42 were analyzed for several elements (approximate standard deviations are in parenthe-



Coin 1150
BMC 174 A.D. 41



Coin 1098
BMC 179 A.D. 41



Coin 1144
BMC 182 A.D. 42

Figure 1. Claudian quadrantes; magnification is 2×; BMC, British Museum Catalog (15). Coin no. 1164 is the only coin from compositional group 41 #A. All other coins are from group 41 #B. BMC 182 variety is the same as BMC 182 except "PP" is omitted from its reverse legend. Continued on next page.



Coin 1164
BMC 174 A.D. 41



Coin 1143
BMC 181 A.D. 42



Coin 1101
BMC 182 var. A.D. 42

Figure 1—continued. Claudian quadrantes: magnification is 2×; BMC, British Museum Catalog (15). Coin no. 1164 is the only coin from compositional group 41 #A. All other coins are from group 41 #B. BMC 182 variety is the same as BMC 182 except “PP” is omitted from its reverse legend.

ses): iron (0.003%), nickel (0.003%), silver (0.007%), tin (0.003%), antimony (0.003%), and lead (0.02%) (Appendix B). Sixty-one quadrantes were produced in A.D. 41, 31 in A.D. 42; 7 are of unknown date. In A.D. 41 there were apparently two groups of quadrantes: 15 quadrantes appear to belong to one compositional group, called group 41 #A, and these coins tend to have relatively low concentrations of iron and nickel as well as high concentrations of silver, antimony, and sometimes lead:

0.086 ± 0.043% Fe (thick flans) vs. 0.141 ± 0.064% Fe (thin flans);
0.008 ± 0.005% Ni (thick flans) vs. 0.015 ± 0.005% Ni (thin flans);
0.029 ± 0.014% Ag (thick flans) vs. 0.004 ± 0.003% Ag (thin flans);
0.049 ± 0.016% Sb (thick flans) vs. 0.009 ± 0.004% Sb (thin flans);
0.11 ± 0.06% Pb (thick flans) vs. 0.04 ± 0.02% Pb (thin flans).

These quadrantes almost always are smaller and thicker than those in the other group (*see* Appendix A), and occasionally the size of the letters in the inscription is significantly smaller than it is in the second group. The second compositional group comprises 84 quadrantes, and it is called group 41 #B.

Compositions of the group 41 #B quadrantes made in A.D. 41 are experimentally indistinguishable from the compositions of A.D. 42 quadrantes, all of which also belong to the compositional group 41 #B (Appendix B). This observation leads one to believe that the group 41 #B coins were struck continuously from A.D. 41 into A.D. 42. Compositional group 41 #B is characterized by moderate iron and nickel concentrations compared with other Roman coins of nearly pure copper. Also, their copper concentrations are comparatively high—in fact, they are the highest known for any group of Roman coins. The silver, tin, antimony, and lead concentrations of this compositional group are the lowest known for any group of Roman copper-based coins.

Coin no. 1159 has an unusually high tin, as well as antimony and lead, content. This coin is the only one having a composition quite different from those of either group 41 #A or 41 #B.

Comparison of Compositions with Those of Other Roman Coins of About the Same Age

Table II summarizes previous analyses and compares them with the present two compositional groups 41 #A and 41 #B (the quadrantes made in A.D. 42 all belong to the compositional group 41 #B). Nine Claudian asses, which are large-diameter coins of nearly pure copper, have been analyzed (9), and the analyses are very close to the compositions of the group 41 #B coins. Four of the asses were minted in A.D. 41, and five in A.D. 42.

Table II. Comparison of Compositions of Claudian Quadrantes with Compositions of Tiberian, Caligulan, and Neronian Coins

Emperor	Denomination	Date, Number A.D. Coins	Fe	Ni	Cu	Zn	Ag	Sn	Sb	Pb
Augustus	Quadrans	4 B.C. 86	m 0.194	0.010	99.5	—	0.038	0.016	0.084	0.17
Tiberius	As	34-37 14	s 0.137	0.005	0.2	—	0.015	0.043	0.042	0.07
			m 0.129	0.007	99.6	—	0.068	0.012	0.076	0.075
Caligula	As and Quadrans	37-41 6	s 0.06	0.006	0.18	—	0.017	0.009	0.038	0.04
			m 0.087	0.020	99.8	0.005	0.022	0.012	0.016	0.02
Claudius	As	41-42 9	s 0.071	0.011	0.1	0.012	0.029	0.013	0.016	0.02
			m 0.085 ^a	0.017	99.9 ^a	0 ^a	0.007	0.006	0.009	0.01
Claudius	Quadrans (group 41 #A)	41 15	s 0.045	0.010	0.1	0	0.005	0.004	0.003	0.02
			m 0.098 ^b	0.008	99.6 ^b	—	0.029	0.018 ^b	0.054 ^b	0.15 ^b
Claudius	Quadrans (group 41 #B)	41 52	s 0.062	0.005	0.2	—	0.014	0.042	0.023	0.16
			m 0.148 ^b	0.017	99.8 ^b	—	0.004	0.004	0.009	0.04
Claudius	Quadrans (group 41 #B)	42 31	s 0.074	0.005	0.1	—	0.003	0.002	0.004	0.02
			m 0.166 ^c	0.012	99.8 ^c	—	0.004	0.005	0.008	0.04
Nero	As	64-66 4	s 0.101	0.004	0.1	—	0.003	0.002	0.003	0.02
			m 0.146	0.008	99.2	0.002	0.092	0.019	0.089	0.49
			s 0.080	0.004	0.3	0.005	0.017	0.010	0.037	0.21

NOTE: m, mean; s, standard deviation.

^a One coin contained 0.58% iron and 0.22% zinc and was omitted from the group in calculating m and s for iron, copper, and zinc.

^b Omits one outlying determination.

^c Omits outliers.

Seven previously analyzed Claudian quadrantes (9) are fairly close in composition to the ones reported in this chapter. However, improved analytical techniques and use of a better x-ray fluorescence spectrometer for nickel, silver, and lead analyses have produced results that are probably more accurate than the previous ones.

The Claudian quadrantes group 41 #A (thick flans) have nearly the same composition as the imitation Claudian asses. The primary difference is in silver concentration, but the difference is large enough to indicate that there is probably no connection between Claudian imitation asses and group 41 #A quadrantes.

Augustan quadrantes, attributed to 9–4 B.C., have compositions similar only to the group 41 #A coins (*see* Table II). They are quite different from the large group 41 #B. However, usually the group 41 #A Claudian quadrantes have less iron, more copper, and less silver, antimony, and lead than Augustan quadrantes. It is possible, but not too probable, that Augustan quadrantes were restruck as Claudian quadrantes group 41 #A. An alternate possibility is that Augustan quadrantes or asses were melted along with some new copper to produce the Claudian 41 #A quadrantes.

The Caligulan asses and quadrantes (six analyses) of A.D. 37–41 have nearly the same composition as Claudian quadrantes group 41 #B (Table II). This finding would indicate that the group 41 #A quadrantes either were copies or were produced at a separate workshop, because apparently Caligulan coins and Claudian quadrantes and asses were produced throughout A.D. 41 and into A.D. 42, all with about the same compositions, namely those of group 41 #B.

Fourteen Tiberian asses dating from A.D. 34–37 have been analyzed (9). These coins are different in trace element composition from either group 41 #A or 41 #B (Table II). For instance, the Tiberian asses have significantly higher silver contents and usually more antimony and less lead than group 41 #A coins. The Tiberian asses are quite different from the group 41 #B Claudian quadrantes.

Neronian asses were produced in A.D. 64–66, long after the Claudian quadrantes, but essentially no copper-based Roman coins were produced in the interim period, A.D. 43–63. It is, therefore, of interest to compare the trace element compositions of nearly pure copper coins of Claudius and Nero to determine whether significant changes occurred, indicating different ore sources or conditions of smelting and refining. Indeed, there are significant differences: The silver contents of the Neronian asses are very high, namely $0.092 \pm 0.017\%$, versus $0.029 \pm 0.014\%$ in the group 41 #A Claudian quadrantes. (However, only four Neronian coins minted in Rome have been analyzed.) Also, the antimony and lead contents of the Neronian asses are significantly higher in most of the coins (Table II). Copper ores and(or) conditions of smelting and refining were different for the Neronian asses. Perhaps the catastrophic great fire in Rome just

prior to the striking of Nero's copper coins meant that the new copper was prepared in great haste and was not desilvered by using liquid lead.

Numismatic Questions

The chemical analyses and physical properties of Claudian quadrantes raise several questions for future study:

1. Why are there two major compositional groupings of Claudian quadrantes?
2. Is the compositional group 41 #A different because the coins are copies or because they were made in a separate workshop?
3. Why are the issues of BMC 181 and BMC 182 variety so small in numbers of coins? Is BMC 181 merely a hybrid coin made from an obverse die produced in A.D. 41 and a reverse die from A.D. 42? Is BMC 182 variety simply an engraver's mistake in omitting "PP" from the reverse legend (*see* Figure 1)?
4. Why is there more than one issue per year?
5. Why are all the thick-flan group 41 #A coins limited to A.D. 41? (Why were not some made in A.D. 42?)
6. Were the A.D. 42 coins minted for only part of the year?

Conclusion

There are two broad compositional groups of Claudian quadrantes. Claudian asses have compositions essentially the same as those of the larger of these groups. Also, Caligulan quadrantes and asses are very similar to this compositional group, but additional Caligulan copper coins must be analyzed to enable an investigator to tell whether these coins represent a different compositional group. Tiberian and Neronian copper coins are significantly different in trace element compositions from the Claudian quadrantes. The large number of Claudian quadrantes analyzed has provided ample evidence for two rather close-knit compositional groups. It is to be hoped that numismatists will be able to deduce reasons for the existence of the relatively small compositional group 41 #A, which has smaller and thicker flans than the other group, group 41 #B. Because group 41 #B coins have a higher purity than other Roman coins, they were probably made from virgin copper.

Acknowledgments

I am grateful to the Kelsey-Hayes Research and Development Laboratory in Ann Arbor, Mich., and to the Lewis Research Center of NASA in Cleveland for the use of their x-ray fluorescence spectrometers. Appreciation is also given to Simon Bendall and to A.H. Baldwin & Sons Ltd. in London for supplying the coins for analysis.

*Appendix A***Dimensions and Physical Properties of Claudian Quadrantes**

<i>Coin Number</i>	<i>Catalog Number</i>	<i>Weight (g)</i>	<i>Maximum Diameter (cm)</i>	<i>Minimum Diameter (cm)</i>	<i>Maximum Thickness (cm)</i>	<i>Density (g/cm³)</i>	<i>Die Orientation</i>	<i>Ratio of Maximum to Minimum Diameter</i>
A.D.41 Group 41 #A								
1117	174	3.4145	1.649	1.522	0.257	8.95	11:30	1.083
1120	174	2.4916	1.753	1.654	0.206	8.90	6:30	1.060
1146	174	1.8130	1.767	1.614	0.150	8.88	7:00	1.095
1164	174	3.4335	1.602	1.449	0.293	8.90	7:30	1.106
1190	174?	2.5328	1.684	1.582	0.185	8.91	1:00	1.064
		m 2.737	1.691	1.564	0.218	8.91		1.082
		s 0.689	0.070	0.080	0.057	0.03		0.020
1094	179	2.8675	1.602	1.530	0.235	8.93	5:30	1.047
1127	179	2.0448	1.767	1.642	0.167	8.90	6:30	1.076
1132	179	2.6115	1.825	1.725	0.182	8.91	6:00	1.058
1189	179	2.7885	1.787	1.625	0.243	8.92	5:30	1.100
		m 2.578	1.745	1.630	0.207	8.92	5:52	1.070
		s 0.371	0.098	0.080	0.038	0.01	0:29	0.023
1097	174 or 179	3.1692	1.441	1.348	0.309	8.93	6:00	1.069
1148	174 or 179	2.5800	1.510	1.435	0.266	8.85	8:00	1.052
1152	174 or 179	2.6525	1.538	1.289	0.259	8.91	12:30	1.193
1159	174 or 179	2.7095	1.444	1.346	0.255	8.88	6:30	1.073
1163	174 or 179	2.4521	1.494	1.426	0.241	8.82	1:00	1.048
1169	174 or 179	1.8252	1.639	1.487	0.186	8.85	1:00?	1.102
		m 2.565	1.511	1.388	0.253	8.87		1.090
		s 0.437	0.073	0.073	0.040	0.04		0.054
For all of group 41 #A		m 2.626	1.633	1.512	0.229	8.90		1.082
		s 0.490	0.129	0.129	0.047	0.03		0.037

Footnotes are at end of table.

Continued on next page.

Dimensions and Physical Properties of Claudian Quadrantes—Continued

Coin Number	Catalog Number	Weight (g)	Maximum Diameter (cm)	Minimum Diameter (cm)	Maximum Thickness (cm)	Density (g/cm ³)	Die Orientation	Ratio of Maximum to Minimum Diameter
A.D. 41 Group 41 #B								
1095	174	2.2160	1.640	1.597	0.173	8.93	6:30	1.027
1099	174	1.8077	1.695	1.648	0.139	8.94	6:00	1.029
1104	174	3.0063	1.750	1.690	0.204	8.92	6:30	1.036
1107	174	2.1016	1.708	1.524	0.170	8.96	6:00	1.121
1110	174	2.3239	1.749	1.671	0.170	8.88	6:30	1.047
1113	174	2.2600	1.707	1.627	0.173	8.97	6:30	1.049
1123	174	2.9115	1.647	1.543	0.226	8.90	7:00	1.067
1125	174	2.7566	1.842	1.705	0.183	8.94	6:30	1.080
1128	174	2.0076	1.775	1.571	0.152	8.94	6:00	1.130
1130	174	2.1328	1.649	1.585	0.182	8.94	6:30	1.040
1133	174	2.6968	1.601	1.565	0.205	8.92	6:30	1.023
1136	174	0.8457	1.591	1.571	0.098	9.04	6:00	1.013
1142	174	2.4590	1.775	1.629	0.210	8.89	7:00	1.090
1150	174	3.2274	1.746	1.613	0.223	8.91	6:00	1.082
1154	174	2.4342	1.647	1.568	0.194	8.91	7:00	1.050
1157	174	1.9598	1.760	1.519	0.183	8.93	6:30	1.159
1161	174	1.7860	1.639	1.549	0.150	8.92	6:00	1.058
1167	174	2.1169	1.786	1.621	0.167	8.88	7:00	1.102
1171	174	1.9928	1.604	1.532	0.168	8.93	7:00 ^p	1.047
1175	174	1.5368	1.957	1.617	0.119	8.91	6:30	1.210
1177	174	2.5781	1.866	1.769	0.181	8.90	7:00	1.055
1179	174	1.9297	1.691	1.583	0.178	8.79	6:30	1.068
1183	174	1.5517	1.715	1.616	0.133	8.92	6:00	1.061
1185	174	2.2696	1.642	1.528	0.180	8.91	6:30	1.075
1187	174	1.6139	1.690	1.602	0.136	8.92	6:00	1.055
1188	174	1.5771	1.672	1.597	0.146	8.90	6:30	1.047
1192	174	1.8863	1.603	1.503	0.162	8.91	6:30	1.067
		m 2.148	1.688	1.598	0.171	8.92	6:28	1.070
		s 0.521	0.152	0.062	0.030	0.04	0:22	0.044

A.D. 41 Group 41 #B									
1098	179	2.5338	1.733	1.563	0.191	8.93	6:30	1.109	
1103	179	1.9460	1.980	1.668	0.153	8.89	7:00	1.187	
1106	179	2.9630	1.881	1.753	0.226	8.90	6:00	1.073	
1109	179	2.0843	1.617	1.532	0.183	8.80 ^a	6:00	1.055	
1112	179	3.0947	1.659	1.520	0.242	8.95	6:30	1.091	
1116	179	3.1233	1.886	1.786	0.190	8.94	6:00	1.056	
1119	179	2.5955	1.733	1.666	0.194	8.86	6:00	1.040	
1122	179	1.7832	1.817	1.682	0.149	8.79	6:30	1.080	
1124	179	3.1871	1.677	1.622	0.237	8.95	6:00	1.034	
1129	179	2.1617	1.803	1.725	0.177	8.93	7:00	1.045	
1135	179	2.8678	1.673	1.622	0.213	8.93	6:30	1.031	
1137	179	2.4843	1.825	1.734	0.167	8.93	6:30	1.052	
1141	179	2.5423	1.682	1.556	0.199	8.91	6:30	1.081	
1145	179	2.3433	1.799	1.645	0.197	8.91	7:00	1.094	
1149	179	1.8117	1.679	1.601	0.168	8.91	6:30	1.049	
1153	179	2.6029	1.804	1.604	0.181	8.91	6:00	1.125	
1156	179	2.8025	1.754	1.618	0.224	8.91	6:30	1.084	
1160	179	2.4835	2.017	1.646	0.190	8.89	6:30	1.225	
1166	179	3.0431	1.755	1.657	0.214	8.89	6:30	1.059	
1170	179	2.7243	1.730	1.577	0.233	8.92	6:30	1.097	
1174	179	2.1549	1.816	1.541	0.201	8.90	7:00	1.178	
1178	179	2.2208	1.817	1.599	0.200	8.85	6:00	1.136	
1182	179	2.8131	1.709	1.650	0.224	8.89	6:00	1.036	
1186	179	1.3862	1.880	1.693	0.113	8.88	6:00	1.110	
1191	179	1.9254	1.680	1.600	0.174	8.93	6:30	1.050	
		m 2.467	1.776	1.634	0.194	8.90	6:24	1.087	
		s 0.477	0.100	0.069	0.030	0.04	0:21	0.051	

Continued on next page.

Footnotes are at end of table.

Dimensions and Physical Properties of Claudian Quadrantes—Continued

Coin Number	Catalog Number	Weight (g)	Maximum Diameter (cm)	Minimum Diameter (cm)	Maximum Thickness (cm)	Density (g/cm ³)	Die Orientation	Ratio of Maximum to Minimum Diameter
A.D. 42 Group 41 #B								
1143	181	1.9059	1.666	1.549	0.155	8.94	6:30	1.076
1096	182	2.8243	1.790	1.576	0.216	8.93	6:00	1.136
1100	182	3.0966	1.776	1.643	0.221	8.94	6:00	1.081
1105	182	2.4785	1.783	1.681	0.209	8.93	6:30	1.061
1108	182	3.1234	1.721	1.593	0.230	8.93	6:00	1.080
1111	182	2.6194	1.868	1.634	0.185	8.94	6:30	1.143
1114	182	2.2810	1.807	1.728	0.161	8.96	7:00	1.046
1118	182	1.9348	1.652	1.580	0.175	8.95	7:00	1.046
1121	182	1.9627	1.662	1.580	0.176	8.95	6:30	1.052
1126	182	2.5469	1.720	1.613	0.193	8.92	7:00	1.066
1131	182	1.4397	1.600	1.544	0.156	8.96	6:00	1.036
1134	182	1.5558	1.807	1.618	0.158	8.96	6:30	1.117
1138	182	2.4626	1.784	1.648	0.196	8.88	6:30	1.083
1139	182	1.8708	1.736	1.643	0.154	8.93	6:30	1.057
1140	182	2.0763	1.702	1.638	0.176	8.91	7:30	1.039
1144	182	2.4612	1.833	1.715	0.176	8.89	7:00	1.069
1147	182	2.9402	1.727	1.566	0.221	8.90	6:30	1.103
1151	182	2.2606	1.699	1.605	0.179	8.93	6:00	1.059
1158	182	2.7232	1.736	1.698	0.172	8.91	6:30	1.022
1162	182	2.5054	1.721	1.536	0.206	8.91	6:30	1.120
1165	182	1.2066	1.613	1.481	0.148	8.91	6:30	1.089
1168	182	2.5599	1.763	1.632	0.195	8.92	7:00	1.080
1172	182	2.1088	1.688	1.519	0.178	8.87	6:30	1.111
1173	182	2.4085	1.659	1.611	0.179	8.91	6:00	1.030
1176	182	1.9164	1.706	1.581	0.161	8.91	6:30	1.079
1180	182	2.2939	1.810	1.592	0.176	8.91	6:30	1.137
1184	182	1.7698	1.670	1.578	0.175	8.93	6:30	1.058
		m 2.225	1.730	1.609	0.180	8.92	6:32	1.076
		s 0.457	0.070	0.060	0.020	0.02	0:23	0.035

1101	182 var.	2.6314	1.706	1.621	0.200	8.93	6:30	1.052
1102	182 var.	1.6258	1.724	1.593	0.143	8.94	6:00	1.082
1155	182 var.	2.3104	1.623	1.553	0.182	8.91	6:30	1.045
		m 2.189	1.684	1.589	0.175	8.93	6:20	1.060
		s 0.514	0.054	0.034	0.029	0.02	0:17	0.020
1115	?	2.5785	1.726	1.596	0.212	8.95	6:00	1.081
1181	?	2.5032	1.710	1.618	0.185	8.90	6:30	1.057

NOTE: m, Mean; s, standard deviation; catalog number, British Museum Catalog number (15); var., variety.
^a Rough surface on this coin; air bubble could cause a slightly low result.

Appendix B

Chemical Compositions of Claudian Quadrantes

Coin Number	Catalog Number	Fe	Ni	Cu	Ag	Sn	Sb	Pb
A.D. 41 Group #A								
1117	174	0.154	0.001	99.6	0.042	0.008	0.067	0.13
1120	174	0.064	0.003	99.8	0.015	0.007	0.031	0.07
1146	174	0.071	0.014	99.6	N	0.014	0.019	0.28
1164	174	0.168	0.007	99.7	0.034	0.003	0.036	0.04
1190	174?	0.438 ^a	0.004	99.3 ^a	0.035	0.007	0.064	0.15
		m 0.114	0.006	99.7	0.025	0.008	0.043	0.13
		s 0.054	0.005	0.1	0.017	0.004	0.021	0.09
1094	179	0.132	0.020	99.7	0.016	0.005	0.050	0.10
1127	179	0.048	0.011	99.8	0.015	0.003	0.048	0.08
1132	179	0.065	0.007	99.7	0.038	0.006	0.070	0.16
1189	179	0.102	0.007	99.7	0.021	0.006	0.058	0.12
		m 0.087	0.011	99.7	0.022	0.005	0.056	0.12
		s 0.038	0.006	0.05	0.011	0.001	0.010	0.03
1097	174 or 179	0.259 ^a	0.008	99.5 ^a	0.037	0.013	0.047	0.12
1148	174 or 179	0.037	0.011	99.8	0.040	0.007	0.060	0.07
1152	174 or 179	0.043	0.005	99.8	0.041	0.008	0.036	0.11
1159	174 or 179	0.088	0.014	98.9 ^a	0.024	0.170 ^a	0.116 ^a	0.69 ^a
1163	174 or 179	0.051	0.003	99.8	0.034	0.013	0.067	0.06
1169	174 or 179?	0.094	0.002	99.7	0.049	0.006	0.037	0.08
		m 0.063	0.007	99.8	0.038	0.009	0.049	0.09
		s 0.026	0.005	0.05	0.008	0.003	0.014	0.03
All of group 41 #A		m 0.086	0.008	99.7	0.029	0.008	0.049	0.11
		s 0.043	0.005	0.08	0.014	0.003	0.016	0.06
A.D. 41 Group 41 #B								
1095	174	0.188	0.019	99.7	0.011	0.002	0.004	0.03
1099	174	0.095	0.018	99.8	0.008	0.006	0.010	0.04
1104	174	0.155	0.016	99.8	0.007	0.007	0.020	0.03
1107	174	0.199	0.019	99.7	0.002	0.002	0.011	0.04
1110	174	0.230	0.018	99.7	N	0.005	0.011	0.04
1113	174	0.191	0.018	99.8	0.014	N	0.008	0.02
1123	174	0.074	0.014	99.8	0.009	0.001	0.021	0.04
1125	174	0.142	0.017	99.8	0.005	0.002	0.009	0.02
1128	174	0.194	0.021	99.7	N	0.003	0.005	0.03
1130	174	0.082	0.018	99.9	0.003	0.002	0.002	0.03
1133	174	0.782 ^a	0.016	99.1 ^a	0.006	0.006	0.007	0.07
1136	174	0.069	0.010	99.8	0.009	0.005	0.024	0.03
1142	174	0.082	0.019	99.8	N	0.005	0.009	0.06
1150	174	0.132	0.013	99.8	N	0.003	0.011	0.06
1154	174	0.160	0.013	99.8	N	0.004	0.005	0.02
1157	174	0.207	0.022	99.7	N	N	0.009	0.03
1161	174	0.207	0.014	99.7	0.002	0.001	0.009	0.03
1167	174	0.061	0.021	99.9	0.004	0.005	0.008	0.03
1171	174	0.168	0.029	99.8	0.008	0.003	0.009	0.02
1175	174	0.210	0.021	99.7	0.003	0.003	0.014	0.06

Footnotes are at end of table.

Chemical Compositions of Claudian Quadrantes—Continued

<i>Coin Number</i>	<i>Catalog Number</i>	<i>Fe</i>	<i>Ni</i>	<i>Cu</i>	<i>Ag</i>	<i>Sn</i>	<i>Sb</i>	<i>Pb</i>
A.D. 41 Group 41 #B—Continued								
1177	174	0.084	0.003	99.8	0.004	0.001	0.011	0.05
1179	174	0.081	0.018	99.8	N	0.004	0.003	0.05
1183	174	0.228	0.030	99.7	0.006	0.002	0.017	0.06
1185	174	0.231	0.014	99.7	N	0.002	0.011	0.03
1187	174	0.186	0.012	99.8	N	0.005	0.004	0.04
1188	174	0.344	0.020	99.6	0.006	0.006	0.011	0.04
1192	174	0.210	0.017	99.7	N	0.003	0.006	0.06
		m 0.162	0.017	99.8	0.004	0.003	0.011	0.04
		s 0.069	0.005	0.07	0.004	0.002	0.008	0.015
A.D. 41 Group 41 #B								
1098	179	0.121	0.016	99.8	N	0.004	0.011	0.05
1103	179	0.070	0.010	99.9	0.005	0.001	0.009	0.03
1106	179	0.075	0.015	99.8	0.004	0.008	0.006	0.05
1109	179	0.053	0.003	99.9	N	0.004	0.008	0.03
1112	179	0.144	0.023	99.8	0.005	0.004	0.009	0.02
1116	179	0.173	0.020	99.8	N	0.004	0.009	0.04
1119	179	0.054	0.014	99.9	0.002	0.008	0.016	0.04
1122	179	0.627 ^a	0.021	99.3 ^a	0.005	0.004	0.015	0.05
1124	179	0.090	0.010	99.9	0.004	0.002	0.012	0.02
1129	179	0.064	0.020	99.9	0.005	0.001	0.006	0.03
1135	179	0.292	0.019	99.6	0.004	0.007	0.007	0.05
1137	179	0.377 ^a	0.019	99.5 ^a	N	0.005	0.011	0.06
1141	179	0.080	0.020	99.8	0.008	0.006	0.006	0.08
1145	179	0.156	0.015	99.8	N	0.002	0.011	0.04
1149	179	0.150	0.020	99.8	0.002	0.004	0.006	0.02
1153	179	0.177	0.020	99.7	0.008	0.005	0.008	0.05
1156	179	0.130	0.017	99.8	N	0.002	0.009	N
1160	179	0.083	0.006	99.9	0.006	N	0.006	N
1166	179	0.119	0.017	99.8	0.004	0.006	0.007	N
1170	179	0.245	0.015	99.7	0.004	0.004	0.011	0.03
1174	179	0.120	0.013	99.8	0.003	0.006	0.008	0.02
1178	179	0.085	0.010	99.9	0.001	0.008	0.008	0.03
1182	179	0.101	0.014	99.8	0.007	0.004	0.009	0.05
1186	179	0.118	0.020	99.8	0.001	0.003	0.008	0.02
1191	179	0.125	0.016	99.8	N	0.002	0.006	0.02
		m 0.123	0.016	99.8	0.003	0.004	0.009	0.03
		s 0.059	0.005	0.08	0.003	0.002	0.003	0.02
A.D. 42 Group 41 #B								
1143	181	0.143	0.013	99.8	0.006	0.008	0.009	N
A.D. 42 Group #B								
1096	182	0.149	0.009	99.8	0.002	0.005	0.008	0.02
1100	182	0.113	0.006	99.8	0.006	0.005	0.012	0.05
1105	182	0.118	0.011	99.8	0.001	0.003	0.013	0.02
1108	182	0.251	0.016	99.7	N	0.006	0.004	0.01
1111	182	0.390 ^a	0.010	99.5 ^a	0.009	0.007	0.011	0.03

Footnotes are at end of table.

Continued on next page.

Chemical Compositions of Claudian Quadrantes—Continued

<i>Coin Number</i>	<i>Catalog Number</i>	<i>Fe</i>	<i>Ni</i>	<i>Cu</i>	<i>Ag</i>	<i>Sn</i>	<i>Sb</i>	<i>Pb</i>
A.D. 42 Group #B—Continued								
1114	182	0.122	0.007	99.8	0.004	0.003	0.007	0.01
1118	182	0.346 ^a	0.012	99.6 ^a	N	0.006	0.008	0.06
1121	182	0.094	0.010	99.8	0.010	0.003	0.020	0.06
1126	182	0.198	0.011	99.7	0.003	0.006	0.007	0.03
1131	182	0.157	0.009	99.8	N	0.004	0.006	0.02
1134	182	0.104	0.019	99.9	0.002	0.005	0.007	0.01
1138	182	0.066	0.011	99.9	0.003	0.005	0.011	0.03
1139	182	0.168	0.013	99.8	0.007	0.003	0.008	0.01
1140	182	0.087	0.010	99.8	N	0.005	0.008	0.04
1144	182	0.085	0.013	99.9	0.005	0.003	0.005	0.02
1147	182	0.089	0.004	99.9	N	N	0.005	0.05
1151	182	0.093	0.010	99.9	0.008	0.007	0.008	0.01
1158	182	0.150	0.014	99.8	0.007	0.008	0.008	0.06
1162	182	0.335 ^a	0.016	99.6 ^a	0.006	0.009	0.007	0.05
1165	182	0.226	0.016	99.6	0.007	0.005	0.008	0.11
1168	182	0.136	0.005	99.8	0.002	0.004	0.002	0.04
1172	182	0.048	0.008	99.9	0.008	0.002	0.004	0.04
1173	182	0.179	0.009	99.8	N	0.008	0.009	0.03
1176	182	0.134	0.023	99.8	N	0.005	0.008	0.05
1180	182	0.138	0.009	99.8	0.006	0.005	0.012	0.04
1184	182	0.439 ^a	0.012	99.5 ^a	0.002	0.008	0.009	0.06
		m 0.135	0.012	99.8	0.004	0.005	0.008	0.04
		s 0.052	0.004	0.08	0.003	0.002	0.004	0.02
A.D. 42 Group 41 #B								
1101	182 var.	0.089	0.019	99.8	0.003	0.007	0.008	0.02
1102	182 var.	0.106	0.016	99.8	0.007	0.004	0.006	0.03
1155	182 var.	0.323	0.016	99.6	0.005	0.008	0.008	0.08
		m 0.173	0.017	99.7	0.005	0.006	0.007	0.04
		s 0.130	0.002	0.12	0.002	0.002	0.001	0.03
1115	?	0.127	0.011	99.8	0.005	0.002	0.008	0.03
1181	?	0.119	0.010	99.8	0.006	0.003	0.010	0.04
All of group 41 #B (82 coins)		m 0.141	0.015	99.8	0.004	0.004	0.009	0.04
		s 0.064	0.005	0.08	0.003	0.002	0.004	0.02

NOTE: All determinations are weight percent. m, Mean; s, standard deviation; catalog number, British Museum Catalog number (15); var., variety; N, none detected.

^a Outlying result is omitted from calculation of the mean and standard deviation.

Literature Cited

1. Caley, E. R. "Orichalcum and Related Ancient Alloys"; Numismatic Notes and Monographs No. 151; American Numismatic Society: New York, 1964.
2. Caley, E. R. "Analysis of Ancient Metals"; Macmillan: New York, 1964.
3. Cope, L. H.; Billingham, H. N. *Bull. Hist. Metall. Group* 1967, 1, 9 1-6.
4. Cope, L. H. *Methods Chem. Metall. Invest. Ancient Coinage, Symp., Spec. Publ. R. Numis. Soc.* 1972, 8, 49-66.
5. Cope, L. H. *Numismatic Chronicle* 1968, 7, 115-49.
6. Carter, G. F. In *Sci. Archaeol., Symp. Archaeol. Chem., 4th, 1968*; MIT Press: Cambridge, Mass., 1971; pp. 114-30.
7. Carter, G. F.; Buttrely, T. V. *Amer. Numis. Soc. Mus. Notes* 1977, 22, 49-65.
8. Carter, G. F. In "Archaeological Chemistry II", Carter, G. F., Ed.; ADVANCES IN CHEMISTRY SERIES No. 171; American Chemical Society: Washington, D.C., 1978; pp. 347-77.
9. Carter, G. F.; King, C. E. In "Metallurgy in Numismatics I"; R. Numis. Soc.: London, 1980; pp. 157-67.
10. Carter, G. F.; Kimiatek, M. H.; Klupacs, F. J.; Giard, J. B. *Rev. Numismatique* 1978, 6 (XX) 69-88.
11. Carter, G. F.; Theodory, E. S. In "Scientific Studies in Numismatics"; Occasional Paper No. 18, Br. Mus. Research Lab.: London, 1980; pp. 65-80.
12. Riederer, J. *Jahrbuch Numismatik Geldgeschichte* 1974, 24, 73-98.
13. Carter, G. F.; Kimiatek, M. H. *Archaeo-Physika* 1979, 10, 82-96.
14. Carter, G. F. *Archaeometry* 1965, 7, 106-13.
15. Mattingly, H. "Coins of the Roman Empire in the British Museum", Vol. 1; Br. Mus.: London, 1923; reprinted 1965.

RECEIVED for review November 23, 1982. ACCEPTED for publication May 9, 1983.

Radiocarbon Dating by Particle Accelerators: An Archaeological Perspective

R. E. TAYLOR—University of California, Riverside, Department of Anthropology, Institute of Geophysics and Planetary Physics, Riverside, CA 92521

DOUGLAS J. DONAHUE and T. H. ZABEL—University of Arizona, Department of Physics, Tucson, AZ 85721

P. E. DAMON and A. J. T. JULL—University of Arizona, Department of Geosciences, Tucson, AZ 85721

In archaeological and paleoanthropological contexts, the most important aspect of the introduction of accelerator or high energy mass spectrometry (AMS/HEMS) for ion or direct ^{14}C analysis is the major reduction in sample size into the milligram and microgram range as well as the potential of extending the maximum ^{14}C range. The reduction in sample size results in the increased practicality of obtaining more precise ^{14}C determinations on samples containing extremely small amounts of organic carbon, e.g., ceramics, as well as multiple analysis on different chemical fractions from the same sample, e.g., bone, as a means of enhancing the reliability of the ^{14}C age estimates. Using the AMS/HEMS system at the University of Arizona, direct counting of three organic fractions of bone from a human skeleton from the Sunnyvale Site in California, previously dated by the amino acid racemization technique at about 70,000 years, resulted in a revised date of between 3500 and 5000 ^{14}C years B.P.

THE RADIOCARBON DATING METHOD was developed by Willard F. Libby and his coworkers James R. Arnold and Ernest C. Anderson between 1946 and 1949 at the University of Chicago. The now well-known physical model on which the method rests had been conceived by Libby during the period of his tenure with the Manhattan Project at Columbia University during World War II (1,2). The first critical test of the model

0065-2393/84/0205-0333\$07.00/0

© 1984 American Chemical Society

occurred in late 1946. It followed from Libby's prediction that there would be a significant difference between the ^{14}C activity of living biological materials and organics of great geological age, e.g., fossil fuels such as coal and natural gas (3). Unfortunately, the instrumentation available at that time was not sensitive enough to accurately measure the extremely low concentration of natural ^{14}C even in living materials. Libby, nevertheless, devised an experiment that would test his prediction.

Samples of biological methane ("biomethane") obtained from a sewage disposal plant in Baltimore, Md., and of petroleum methane ("petromethane") from an oil refinery were enriched by equal amounts of ^{14}C in a thermal diffusion column. Whereas the ^{14}C activity of the biomethane increased in direct proportion to the amount of ^{14}C enrichment, there was no significant increase in the ^{14}C counting rate of the petromethane with enrichment (4). The confirmation of Libby's prediction initiated an extensive study of the distribution of ^{14}C in nature. However, the use of a thermal diffusion column for this research would have made progress slow and expensive. A method to measure natural ^{14}C concentrations on a routine basis without the necessity of costly enrichment procedures was needed. Libby turned to a counting technique with which he was familiar from his graduate days at Berkeley (5) and in so doing ushered in the first generation of instrumental methods employed in ^{14}C research—decay counting using a screen-wall Geiger counter containing the sample in a solid form as elemental carbon.

In the more than 30 years that have followed, radiocarbon studies have evolved through two generations of instrumental methods. Libby employed solid carbon counting (combined with an application of the anticoincidence principle to reduce background count rate) to establish the fundamental validity of the method (6). This goal was achieved in December 1949 with the publication of the famous "Curve of Knowns," which demonstrated that the residual ^{14}C content of a series of samples was directly related to their age (7).

During the first half of the 1950s, solid carbon counting instrumentation was installed in eight other institutions in the United States, Canada, New Zealand, and Sweden. A number of other investigators who attempted to utilize solid carbon counting for routine low-level ^{14}C analysis experienced moderate to severe problems in obtaining reproducible values. Most frustrating at this time was the problem of avoiding contamination of the elemental carbon sample during processing by artificial ^{14}C produced as a result of fallout from the detonation of nuclear and thermonuclear devices in the atmosphere. As a result, by the end of the decade, all laboratories that had begun operations with solid carbon counting along with those that were contemplating the establishment of ^{14}C facilities had decided to move to second generation counting systems employing either gas or liquid scintillation detectors.

Initially, the majority of ^{14}C laboratories adopted carbon dioxide proportional counting although both acetylene and, somewhat later, methane were also used as counting gases. The potential of employing liquid scintillation for natural ^{14}C measurements was demonstrated very early by Arnold (8) and was used for several years in the late 1950s at Trinity College, Dublin (9). However, its use did not begin to be widespread until late in the 1960s, following the resolution of problems in the preparation of benzene and increasing experience with commercially available liquid scintillation instruments. Besides avoiding fallout contamination of sample preparations, the most significant advantage of gas and liquid scintillation instrumentation was the substantial increase in operational as well as counting efficiency. Increase in maximum dating range, reduction in statistical errors, and, in general, a reduction in the amount of sample material required resulted from these improvements.

Table I provides a summary of the characteristics of the counting systems employed in the measurement of natural ^{14}C in dating applications. Currently, *standard, high precision, extended range, and microsample* decay counting using both gas and liquid scintillation systems is employed in over one hundred ^{14}C laboratories worldwide. For example, high precision ^{14}C detectors can achieve 1σ counting statistics on the order of ± 20 years on samples less than about 1 half-life old (10). However, the sample size requirements and counting times required are greatly in excess of what was required even with solid carbon counting. On the other end of the scale, microsample detectors have made measurements on as little as 10 mg of carbon. However, counting times are on the order of months and the maximum age range is significantly limited (11).

Extending the maximum age range and(or) decreasing the typical sample requirement of decay counting face constraints that derive from the reality of the physical characteristics of this carbon isotope. One of the most important constraints is that although there are approximately 5.9×10^{10} atoms of ^{14}C in 1 g of contemporary "prebomb" carbon, over a 1-min period on the average less than 14 of them will decay. On this basis alone, decay counting for ^{14}C , as for all relatively long-lived isotopes, is inherently inefficient (12). A logical alternative would be to measure ^{14}C on an atom-by-atom basis, as can be accomplished on a mass spectrometer. One intensively pursued attempt to accomplish this for ^{14}C unfortunately was largely unsuccessful. Michael Anbar, then at the Stanford Research Institute, employed a conventional mass spectrometer specifically designed to attempt to measure ^{14}C in natural concentrations. The failure of the experiment was largely due to the inability of the spectrometer to distinguish the signal from interfering stable ions with similar charge-to-mass ratio to a degree that would permit a reasonable resolution of the ^{14}C signal (13).

Table I. Radiocarbon Dating: Generation, Mode, and Type of Instrumentation

Instrument	Counting Mode	Type	Typical Sample Size ^a (mg carbon)	Typical Precision ^b (%)	Typical Counting Period (h)	Maximum Range (years × 10 ³)
Generation I	Decay	Solid ^c	2,000 – 5,000	3 – 5	48 – 120	25
Generation II						
Standard	Decay	Gas/liquid scintillation	250 – 2,000	0.5 – 1.5	24 – 72	30 – 50
High precision	Decay	Gas	2,000 – 20,000	0.2 – 0.5	72 – 168	—
Extended range	Decay	Gas/liquid scintillation	10,000 – 20,000	2 – 3	72 – 168	70 – 75
Microsample	Decay	Gas	10 – 250	1 – 2	960 – 2,760	—

^a After pretreatment.^b One sigma counting error.^c Obsolete.

Third Generation Radiocarbon Measurements

The potential for measuring ^{14}C by direct rather than by decay counting has now been realized by the development of accelerator or high energy mass spectrometry (AMS/HEMS). In AMS/HEMS, ions are accelerated to energies at least three to four orders of magnitude greater than in conventional mass spectrometers, i.e., to several million electron volts rather than to several thousand. At these energies, discrimination of the interfering molecular ions (for electrostatic accelerators) and very high mass resolutions (for cyclotrons) can be accomplished.

The fascinating history of the events associated with the development of HEMS for direct detection of ^{14}C has been outlined by the earliest principals, Luis W. Alvarez (14) and a former graduate student of Alvarez, Richard A. Muller (15). Briefly stated, before 1977 there were only two publications reporting on experiments using a particle accelerator (the 60-in. University of California, Berkeley, cyclotron) as a mass spectrometer. Both of these were notes published in 1939 by Alvarez and a graduate student, Robert Cornog. The basic idea was revived in 1974 by Alvarez's suggestion to use the 88-in. Berkeley sector-focused cyclotron as a mass spectrometer to search for those elusive subatomic particles, quarks. In March 1976, during the period that the UC Berkeley group were pursuing their quark studies, Kenneth Purser of the General Ionex Corporation filed for a patent for a system employing a tandem electrostatic accelerator as part of an ultrasensitive spectrometer for making mass and elemental analyses.

An early suggestion to use an accelerator to measure ^{14}C directly was contained in the July 4, 1976, issue of *Astrophysical Notes*, an internal publication of the UC Berkeley Space Sciences Laboratory, written by Muller and entitled "Radioisotope Dating with a Cyclotron." An article with the same title appeared in the March 1977 issue of *Science* (16). In November 1977, simultaneous publication of the initial results of the ^{14}C Van de Graaff measurements by a Simon Fraser-McMaster University collaborative effort (17) and a University of Toronto-General Ionex Corporation-University of Rochester consortium (18) appeared in *Science*. The culmination of the initial demonstrations of the possibility of direct ^{14}C measurements was the First Conference on Radiocarbon Dating with Accelerators held at the University of Rochester in April 1978 (19).

Since 1978, a dramatic expansion of activity has characterized developments in AMS/HEMS research as applied to the measurement of a number of radioisotopes including ^{14}C . Several major symposia on the general subject of accelerator mass spectrometry for ^{14}C analysis have occurred over the last 5 years, including those that have been held as part of the last two International Radiocarbon Conferences (20-22). A series of review papers on AMS/HEMS radioisotope dating has appeared

(15,23–26). As a result, radiocarbon dating is now entering a third generation of research effort. Over the next decade, direct or ion counting by using particle accelerators will provide an increasing percentage of the ^{14}C determinations employed by archaeologists and paleoanthropologists in their research. New areas of research are being opened along with new questions, concerns, and problems. All of these will confront the archaeologist as he moves to utilize this new technology.

HEMS: Basic Principles

The central concept behind HEMS is that practical direct detection of ^{14}C can be accomplished by accelerating sample atoms in the form of ions to high energy. For energies on the order of 0.5 MeV per nucleon, ions of the same mass and energy but differing nuclear charge (e.g., ^{14}C and ^{14}N) can be distinguished by measuring the total energy (E) of each ion as well as its rate of energy loss (dE/dx). In electrostatic accelerators, another important advantage of going to highly charged states is that all molecules are essentially destroyed in the stripping process. Unfortunately, the extremely sensitive detectors employed in such nuclear physics experiments cannot function with beams in excess of a few thousand particles per second. Because of this, elimination of as many unwanted particles as possible must be accomplished before or during acceleration.

The operation of an HEMS system to measure natural ^{14}C concentrations involves four steps: production of ions from a sample, acceleration of the ionized particles, separation of the ^{14}C from all other isotopes and molecules, and counting of individual ^{14}C atoms. As we have noted, two types of particle accelerator have been used in experiments in direct ^{14}C measurements: cyclotron and electrostatic systems. Each system employs different isotope separation and identification strategies. For each system, a significant amount of attention has been focused on the design of the ion source because its performance plays a crucial role in the efficient operation of an HEMS system. Characteristics of an ion source that must be considered include beam current (the number of ions produced per unit time), which must be relatively high to minimize run times; the source's efficiency, which must be relatively high to minimize sample size; stability; ability to avoid isotopic fractionation; and ability to avoid memory effects (27).

Cyclotron Systems

In cyclotrons, high energies are imparted to particles by accelerating ions through two semicircular high voltage electrodes within a magnetic field. An alternating accelerating voltage is applied between the electrodes and repetitive acceleration continues until the particles reach a

high enough energy to move to the edge of the magnet where a beam can be extracted. An important characteristic of the cyclotron is that magnetic separation of different ions takes place simultaneously with acceleration, i.e., the process of acceleration in the cyclotron itself acts as a charge-to-mass ratio filter. When the cyclotron frequency is tuned to accelerate ^{14}C , the only other ion present is ^{14}N . Other ions with the wrong charge-to-mass ratio quickly drop out of phase and are lost from the beam. To remove the ^{14}N from the beam, a "range separation" method has been employed. This method takes advantage of the fact that the range of ^{14}N in a solid or gas is about 30% less than that of ^{14}C . A xenon gas cell operated at pressures of between 0.2 and 0.5 atm or a metal foil has been used to discriminate against ^{14}N . The ^{14}C ions are detected by an ionization chamber and a solid state device to ascertain the total energy and energy loss of the particles (28).

Experiments performed to date with cyclotrons have used positive ions obtained from carbon dioxide and a gas ion source. This is an advantage in the sense that it permits standard pretreatment practices developed over the last 30 years at decay counting laboratories to be routinely employed up to the point of measurement (29). On the other hand, beam currents using gas ion sources are characteristically significantly less than those from the solid samples currently used with electrostatic type accelerators. In addition, memory effects, which make comparisons of a standard to an unknown difficult, have been reported. The first cyclotrons used for radioisotope measurements had previously been used extensively for nuclear physics experiments and the production of high energy ions. Because of these experiments, some cyclotron systems have apparently been contaminated. For the 88-in. Berkeley cyclotron, the construction of an external ion source was designed to attempt to overcome this problem. Unfortunately, the efficiency of the beam transport system in the external ion source introduced other problems (30).

Electrostatic Accelerator Systems

The majority of laboratories currently actively involved in the development of HEMS ^{14}C counting employ some type of tandem electrostatic accelerator. The high voltage required to accelerate the ^{14}C ions to high energies is provided either by a moving belt or chain or by a solid state voltage multiplier (Cockroft-Walton type). Negative ions are accelerated toward a positively charged terminal and then stripped of their electrons by passage through a stripper to create positively charged ions, which are then accelerated away from the terminal. In the stripping process, all molecules are destroyed. The total energy of the ion is a result of the energy acquired during acceleration both toward and away from the

terminal. Because the acceleration occurs in two stages, such an instrument is referred to as a tandem accelerator. The use of tandem accelerators for HEMS is known as tandem accelerator mass spectrometry (TAMS).

In this discussion, we will illustrate the characteristics of a TAMS system using the tandem accelerator operating at the National Science Foundation Regional Accelerator Facility at the University of Arizona. This system was constructed by General Ionex Corporation. The design of this system is based on the design proposed by Purser in his 1976 patent application. Figure 1 provides a schematic of the beam line arrangement. Figure 2 provides a photographic view of the accelerator components oriented as in Figure 1 with the beam proceeding from right to left.

One of the important advantages of a tandem accelerator is that $^{14}\text{N}^-$ apparently does not form negative ions that live long enough to pass through the accelerator to the terminal (18,31). Thus a primary source of background is essentially eliminated. Another important characteristic of a TAMS is the fact that it is a relatively simple operation to sequence the acceleration of the various isotopes of carbon through the system in a reproducible manner. Thus measurements can be made of $^{14}\text{C}/^{13}\text{C}$ and $^{13}\text{C}/^{12}\text{C}$ ratios in times that are short compared to the times of change of system transmission. Experiments at the University of Arizona have demonstrated that this sequencing time can be as long as several minutes (32).

The Arizona TAMS source produces negative ions by cesium sputtering of a solid carbon target. Wood cellulose and charcoal have been directly reduced to elemental carbon. In cases where we wish to ensure sample homogeneity, it may be advantageous to first convert to carbon dioxide and then to produce elemental carbon by reduction on magnesium. Our efforts to optimize the preparation of the target materials have included preparing mixtures such as Ag-C, Pb-C, Cu-C, and KBr-C, and compounds such as Fe_3C and Mn_3C . Tests with irradiated spectroscopic graphite indicate that these materials, at least following neutron activation, appear to be very sensitive to properties of the target. For these targets, $^{14}\text{C}/^{13}\text{C}$ ratios have changed by as much as a factor of 2 after prolonged sputtering. The ratio changes even before any obvious surface defects appear. At the present time, Fe_3C beads appear to give the most reproducible ion yields. Targets of Fe_3C from wood hewn in A.D. 1890 consistently yield from 1 to 3 μA of $^{12}\text{C}^-$ (approximately 20% of the yield of irradiated spectroscopic graphite) and exhibit from 1 to 3 counts/s (cps) of ^{14}C activity. The fabrication of more satisfactory targets is a subject of continuous study at the University of Arizona. In a cooperative effort, the Arizona TAMS facility and the University of California, Riverside, ^{14}C laboratory are currently investigating high tem-

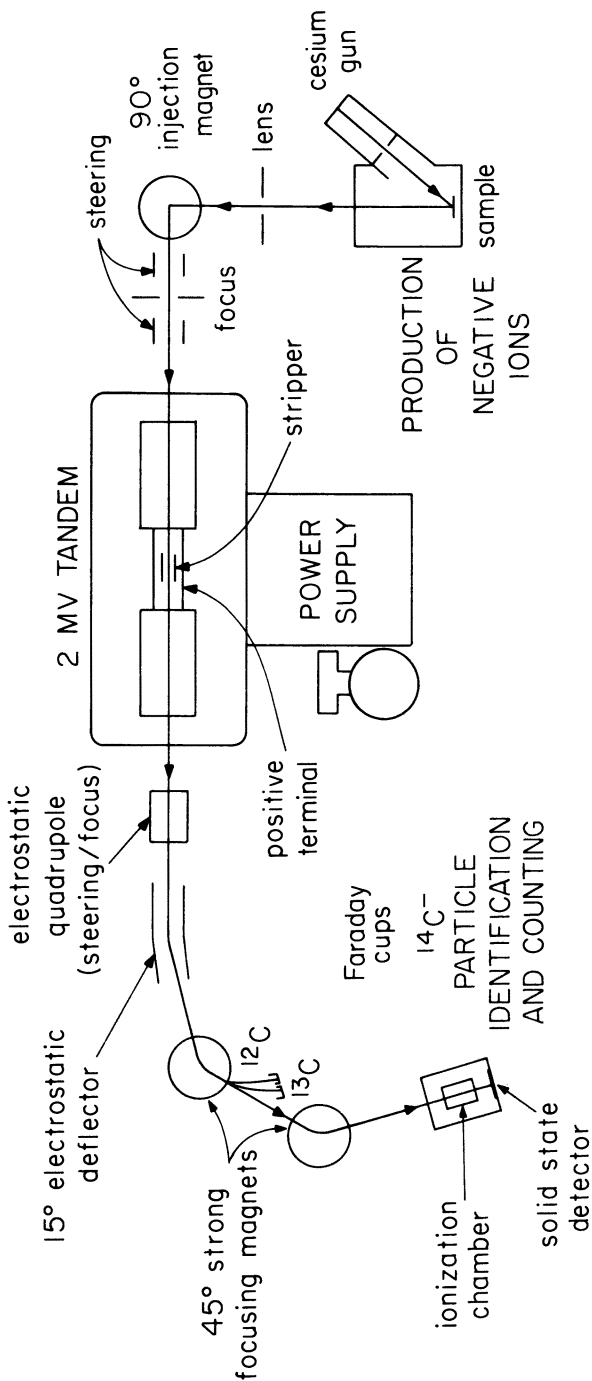


Figure 1. Schematic of beam line arrangement of the TAMS system operating at the National Science Foundation Regional Accelerator Facility at the University of Arizona.

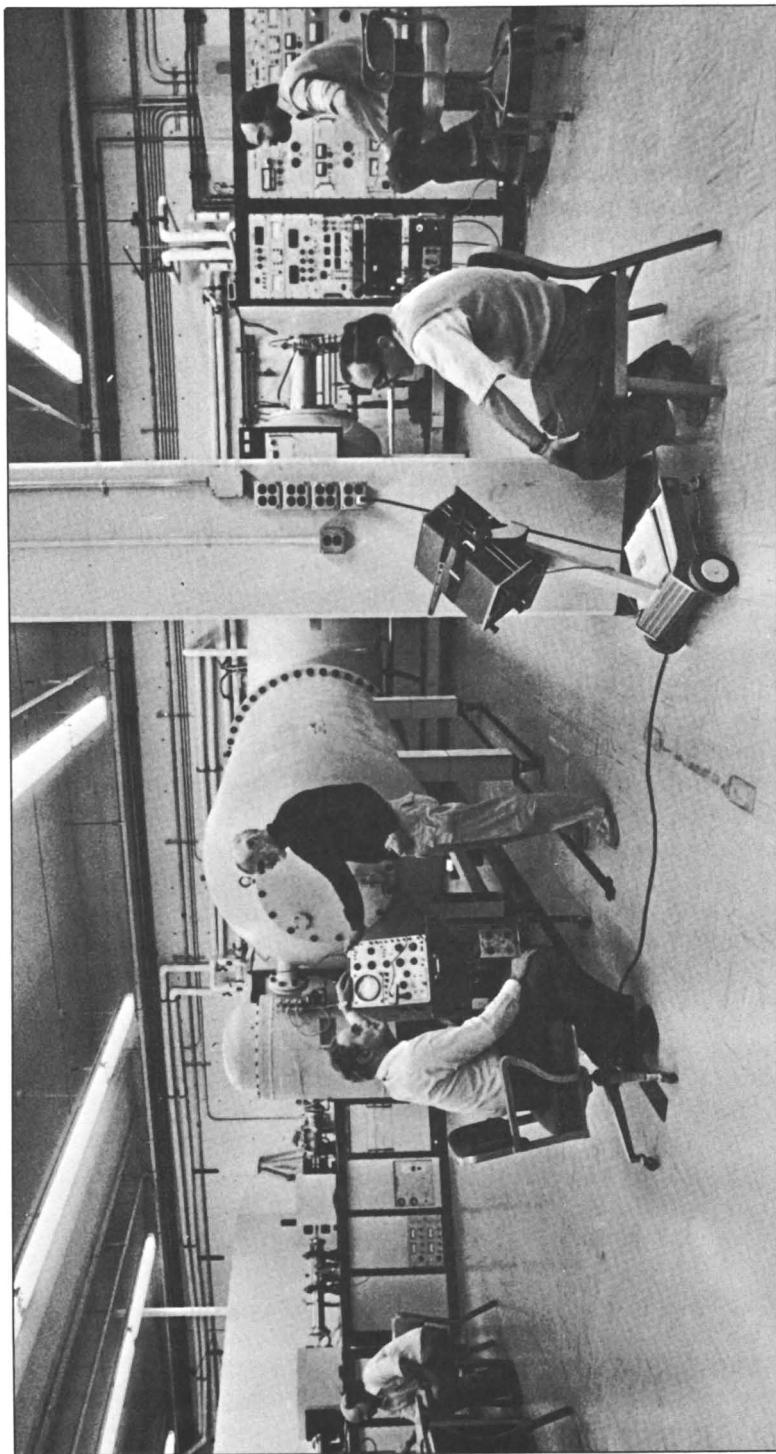


Figure 2. Photographic view of TAMS system operating at the National Science Foundation Regional Accelerator Facility at the University of Arizona. From left: A. J. T. Jull, Kenneth Purser, Paul E. Damon, Douglas J. Donahue, and T. H. Zabel. Photograph courtesy of G. Kew.

perature methods of preparing graphite from elemental carbon prepared from carbon dioxide sample combustions (33).

The measurement procedure currently employed at the Arizona TAMS facility is as follows (32):

1. With a graphite target activated to 1.6 times modern ("pre-bomb") ^{14}C activity, ion source controls, lenses, and other electrostatic and magnetic elements are set to optimize the ^{14}C rate in the detector.
2. A standard of known ^{14}C content is moved into position in the ion source and the injection magnet set to accelerate mass 14.
3. The ^{14}C count rate is measured at the detector. Counting times range from 2 to 4 min.
4. To normalize the ^{14}C measurement, the injection magnet is set to accelerate mass 13. The ^{13}C current is measured with a Faraday cup on the high energy side of the accelerator. The counting times are from 10 to 30 s.
5. A sample of unknown age is moved into position in the ion source.
6. Steps 3 and 4 are repeated.
7. A ratio is calculated using the formula

$$R = \frac{(^{14}\text{C}/^{13}\text{C})_{\text{sample}}}{(^{14}\text{C}/^{13}\text{C})_{\text{standard}}}$$

8. An age is calculated using the known age of the standard as the reference value.

A series of tests has demonstrated that measurements on targets prepared from Fe_3C by following the procedure set forth above are reproducible to about $\pm 2\%$ (32).

An example of application of the Arizona TAMS instrument to a sample of archaeological interest is given in Table II. Radiocarbon determinations obtained on the basis of both carbon dioxide gas proportional decay counting and TAMS direct counting measurements have been obtained on bones from a morphologically modern human skeleton excavated from an archaeological site in Sunnyvale, southern San Francisco Bay, California. Portions of this skeleton had been dated by the aspartic acid racemization dating method to approximately 70,000 years (34). If this age assignment was correct, it would make the Sunnyvale skeleton one of the oldest *Homo sapiens sapiens* in the world. The validity of the racemization-derived assignment of age for this sample had been previously challenged on geological, archaeological, and anthropometric grounds (35). Uranium series analyses indicated ages of 8300 and 9000

Table II. Sunnyvale Skeleton: Radiocarbon Measurements by Carbon Dioxide Gas Proportional Decay Counting and Direct Counting by Tandem Accelerator Mass Spectrometry (37)

<i>Identification</i>	<i>Sample</i>	<i>Sample Size (mg carbon)</i>	<i>Counting Mode</i>	<i>Measured</i>	
				<i>ratio (R)</i>	<i>Radiocarbon Age (¹⁴C years B.P.)</i>
UCR-1437A	Sunnyvale human bone: total acid-soluble organics	250	Decay	—	4390 ± 150
UCR-1437A/ AA-50	Duplicate of UCR-1437A	3	Direct ^a	1.36 ± 0.10	3600 ± 600
UCR-1437B/ AA-52	Sunnyvale human bone: total base-soluble organics	2	Direct ^a	1.16 ± 0.05	4850 ± 400
UCR-1437D/ AA-51	Sunnyvale human bone: total acid-insoluble organics after gelatin conversion with base- soluble organics removed	2	Direct ^a	1.19 ± 0.05	4650 ± 400

^a These values were obtained by using Al₄C₃ mixed with Ag targets.

years B.P. (36). Radiocarbon determinations were needed to resolve the conflict.

Three organic fractions were prepared from postcranial bone of the Sunnyvale skeleton. The recovery of organics was insufficient in two of the three cases to permit standard decay-counting values to be obtained. A decay-counting ^{14}C value could be obtained only on the total acid-soluble fraction (UCR-1437A). The carbon dioxide resulting from the combustion of the two remaining fractions was converted to solid carbon for measurement by the TAMS method (Table II). The ^{14}C values obtained on the Sunnyvale skeleton clearly assign it to a middle Holocene age, probably in the range of 4000 to 5000 ^{14}C years B.P. The direct-counting values on three different organic fractions significantly reduced the possibility that major organic components of the Sunnyvale bone might exhibit significantly older ^{14}C ages.¹ In this case, an age deduced on the basis of an aspartic acid D/L ratio differs by more than an order of magnitude from that indicated by the ^{14}C values (37,38).

We have summarized the status of the important aspects of the operation of the Arizona TAMS system (*see* box on next page). The maximum age attainable in the present configuration can be determined as follows: For a sample count to be greater than the background count at the 95% confidence level, it must be equal to or greater than a critical value (CV) given by

$$\text{CV} = 1.97\sqrt{\sigma_x^2 + \sigma_B^2}$$

where σ_x and σ_B are the standard deviations of the sample count and background count, respectively. Assuming a 0.01 cps (σ) for both sample count and background count, the CV must be 0.0279 cps. Consequently, if the modern count is 4 cps, the maximum age attainable on the basis of a 2- σ criterion is 41,100 years.

Archaeological Perspectives on HEMS ^{14}C Dating

The first direct-counting ^{14}C determination on an archaeologically related sample was published in 1978 (39). In a literal sense, direct counting is currently in an early part of its own "solid carbon" phase, in that all currently operational systems utilize solid carbon sources and, in general, each measurement still requires a considerable degree of special attention and a relatively large commitment of manpower and resources. If the

¹ Preliminary values for the samples measured by the TAMS method were reported at the Eleventh International Radiocarbon Conference, University of Washington, Seattle. These values were calculated with respect to bristlecone pine dendrochronologically dated wood and thus were expressed as a calibrated value in calendar years B.P. The TAMS values listed in Table II reflect a large number of subsequent measurements and are expressed in ^{14}C years B.P. by using the 5568-year half-life (37).

**Current Status of Operating Conditions
University of Arizona TAMS System**

Carbon dioxide employed in conversion to elemental carbon	2-10 cc STP
Typical yields in conversion from carbon dioxide to elemental carbon	90%
Amount of elemental carbon used in target	1-2 mg
Minimum amount of elemental carbon used in target	300 μg
Terminal voltage used for ^{14}C measurements	1.8 MV
Maximum current ($^{12}\text{C}^-$) obtained with spectroscopic grade graphite	25 μA
Average current ($^{12}\text{C}^-$) obtained with Fe_3C	2 μA
Transmission efficiency of $^{12}\text{C}^-$ through accelerator to $^{12}\text{C}^{3+}$	20%
Typical standard deviation of the average of duplicate runs with Fe_3C targets	$\pm 2\%$
Average count rate of 1890 wood converted to elemental carbon and Fe_3C target	2 cps
Radiocarbon age for which the signal is equal to measured background for Fe_3C target prepared from carbon dioxide	$\sim 40,000$ years
Radiocarbon age for which the signal is equal to measured background for blank aluminum	$\sim 60,000$ years

history of the development of the decay-counting method can be used to predict the future course of direct-counting technology and procedures, the HEMS field as applied to ^{14}C measurements will proceed along two parallel but interrelated lines—one focusing on the development and refinements in technical aspects of accelerator hardware and operating conditions and a second dealing with the problems of sample pretreatment and target preparation. The elements of the ^{14}C TAMS technology that initially will probably be of particular interest to archaeologists are the several orders of magnitude reduction in sample size and the extension of the maximum ^{14}C dating range possible with direct counting. Another important feature of TAMS technology is the ability to measure different chemical fractions of the same sample, as illustrated in Table II.

Perhaps the most immediate impact on archaeological applications of ^{14}C dating using TAMS has been the major decrease in the amount of organic materials required for a ^{14}C determination. Even at this stage in the development of the technology, reductions of two or more orders of magnitude have been obtained. Our analysis of the Sunnysvale bone sample vividly illustrated the importance of this characteristic of TAMS ^{14}C technology (Table II). A reduction in sample requirements from 250 to 1–3 mg of carbon permitted two other organic fractions to be measured. Radiocarbon determinations utilizing from 1 to 5 mg of carbon can now be routinely accomplished. With additional effort, a reduction down to 500 μg of carbon has been obtained at the Arizona facility.

An important result of the availability of routine milligram ^{14}C measurement capabilities is that the preparation of specific sample components will increasingly be employed, particularly in cases where the expected ages are in excess of 20,000–30,000 years. The ability to obtain ^{14}C determinations on different chemical or physical fractions of sample materials will provide a more efficient strategy of evaluating the accuracy of a given ^{14}C age estimate. Concordance of ^{14}C values on different fractions of the same sample will significantly increase confidence in the validity of the ^{14}C age estimate. In contrast, a significant anomaly in the ^{14}C age of one fraction might point to a source of contamination in the sample.

In addition to analyzing different chemical fractions, the ability to process milligram-size samples will permit sample materials to be physically or chemically segmented incrementally so that the degree of internal homogeneity can be determined. For example, a much more detailed examination of the degree of isotopic exchange in the carbonate fraction of the surface of shell samples, particularly of Pleistocene age, can now be carried out on a microscale. Where significant surface contamination is present, it might be possible to identify the portion of the shell where the exchange has been severe by noting whether the deviations in ^{14}C activity occur on the surface and then reach a plateau in the

interior of the shell matrix. If so, the plateau ^{14}C values could be considered as more likely to reflect the ^{14}C activity of the unaltered shell. Such an analysis can also be carried out in conjunction with an examination of the ^{14}C activity of the organic fraction of the shell (conchiolin). This type of measurement has heretofore been carried out in only a few instances because of the extremely small amount of conchiolin in the average shell matrix. Analyses suggest that, in some cases, microbacterial activity might contaminate the organic fraction with the increasing age of a shell (40).

The ^{14}C analysis of successive base or solvent extractions from samples suspected of contamination is also now routinely possible with direct counting. For example, at Meadowcroft Rock shelter in Pennsylvania, ^{14}C determinations of up to approximately 17,000 ^{14}C years B.P. on charcoal and carbonized bark (basketry?) associated with strata reportedly containing cultural materials (41,42) have been challenged because of suspected contamination from overlying lignite beds. Haynes (43,44) has suggested the use of successive base extractions of the charcoal samples until similar ^{14}C values are obtained. Measurements of this kind are feasible using an HEMS approach.

Development of methods to prepare various fractions of samples will coincide with unambiguous characterization of each fraction on the basis of a specific criterion, which can be accomplished on several levels. In Table II, for example, the fractions are identified on the basis of nature of the pretreatment applied. Increasingly, however, more specific and detailed chemical data may need to be collected during the preparation of the sample fractions to provide documentation of the nature of the organic components being separated. This process can be particularly well illustrated in the procedures applied to the ^{14}C dating of bone (*see* the following section).

The maximum or "infinite" values currently being reported by various HEMS laboratories for carbon samples that should contain no ^{14}C activity range between 40,000 and 60,000 years. At the Arizona facility, a ^{14}C signal from an aluminum blank currently exhibits an age equivalent to about 60,000 years (*see* box on p. 346). The background responsible for these signals presumably results from either misidentification of ^{14}C at the detector due to scattering in the beam or memory effects from the ion source. Over the next decade, with increasing experience and continuing improvements of HEMS technology, there is a reasonable expectation that instrumental aspects of HEMS operation will result in the reduction of background counts, thus permitting older materials to be studied.

The possibility of being able to secure ^{14}C determinations for the period 50,000 to 100,000 years B.P. is, of course, crucial to archaeologists and paleoanthropologists interested in the emergence of anatomically

modern *Homo sapiens*. Fossil skeletons of modern aspect to not become common in the paleoanthropological record until about 30,000 years ago. What was the nature of the process that gave rise to anatomically modern *H. sapiens* from earlier hominid forms? Did our own species originate in one nuclear region and from there spread rapidly, or did the process occur in a number of separate regions essentially concurrently? Basic to these and similar paleoanthropological questions is the accuracy of the chronological framework for the relevant fossil and archaeological record. The absence of a reliable means to unambiguously assign specific age values to hominid materials known, or thought, to be more than 30,000–40,000 years old and less than a few hundred thousand years old significantly inhibits the ability to reconstruct phylogenetic relationships among the late Pleistocene Hominidae (45). The development of direct ^{14}C counting methods is on the threshold of providing the necessary temporal framework.

However, although there is a reasonable expectation that the instrumental technology will be refined to permit the maximum extensions of direct ^{14}C measurements, the principal roadblock will be the preparation of samples sufficiently free of modern contamination to exploit the full potential of the extended range possible. For samples in excess of about 50,000 years, for example, contamination with modern carbon on the order of a few tenths of a percent can result in reductions in age of up to several thousand years. For materials with expected ages in excess of about 70,000 years, parts per million (ppm) levels of modern contamination can dramatically affect the resultant age. Figure 3 represents a summary of the relationship between the actual and the apparent ages in samples to which have been added varying percentages of contemporary carbon. This plot particularly illustrates the effects of the addition of parts per million levels of modern carbon for samples in the 50,000–100,000 year range. In a sample 75,000 years old, for example, a 100-ppm addition of modern carbon results in an error of approximately 5000 years in the final measured age. Rigorous attention to detail in sample preparation and handling will need to be developed in concert with developments in accelerator technology.

Aspects of the development of the HEMS technology of practical interest to archaeologists include the current and projected relationship of ion ^{14}C counting to conventional decay counting—specifically the question of whether direct counting will replace decay counting in the same way that gas and liquid scintillation systems replaced solid carbon systems more than two decades ago. Also, from a practical perspective, there is the question of the effect of the introduction of routine direct counting on typical processing times and, of course, on costs. These and other similar issues were addressed at a 1981 conference entitled “Radiocarbon Dating in Archaeology: Needs and Priorities in the 1980s” held at the

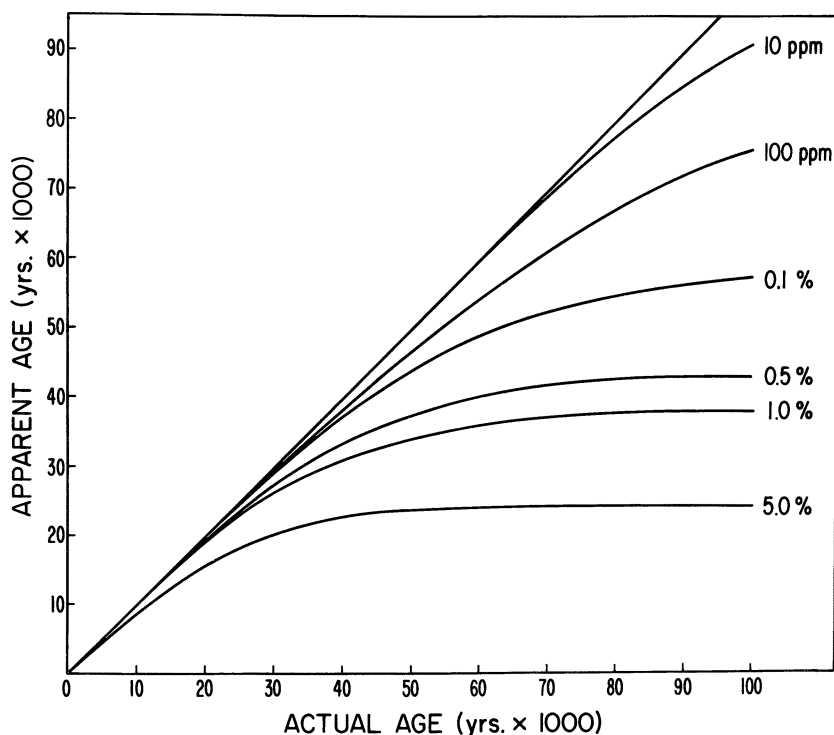


Figure 3. Relationships between actual ages and apparent ages in samples to which varying percentages of modern carbon have been added. (Reproduced with permission from Ref. 50.)

National Science Foundation (46). Present at the discussions were representatives of the professional archaeological community in the United States, laboratory directors of a number of the ^{14}C laboratories involved in archaeological studies, and representatives of several accelerator facilities.

The conferees concluded that, for the immediate future, direct counting will not replace conventional decay counting for most archaeological applications. The principal use of accelerator-based measurements will be where it is either not practical or not possible to employ decay counting because of the limitations in the amount of the sample material available and/or because of the expected age of the sample. The report also concluded that no meaningful cost reductions will be immediately realized when accelerator-based measurements become routinely available. Costs for accelerator determinations are initially estimated to be at least double those for the typical decay-counting analysis. Over the longer term, an increasing percentage of ^{14}C determinations

will be obtained by ion counting. Because the counting times required for equivalent statistics with accelerator-based systems are more than an order of magnitude shorter, "turn around" times can be significantly reduced. However, it is still unclear what the net effect might be for routine processing since, for the immediate future at least, samples too small for dating by conventional methods probably will constitute the vast majority of the samples measured by the HEMS method.

Archaeological Samples for HEMS ^{14}C Dating

The development of HEMS technology will probably have its most important initial impact in archaeological studies as a consequence of its ability to provide ^{14}C determinations on samples in the 1–5-mg range. Materials containing relatively small amounts of organic carbon, for which conventional ^{14}C determinations have been heretofore difficult or impractical, can now be routinely employed. Bone and ceramics are examples of sample types that will see increased attention and utilization as the source of ^{14}C determinations by HEMS.

As Hedges has rightly noted, bone should be the material par excellence for ^{14}C dating (47). The dating of human bone renders moot any question of association between sample and evidence of human activity. In many environments, it constitutes a significant part of the evidence for the reconstruction of paleoenvironments and human paleoecological adaptations. Unfortunately, from the beginning of ^{14}C studies bone was burdened with a marginal status as a sample type. It was missing from the list of sample materials that Libby initially recommended. He and other early researchers discouraged its use because its carbon content and specifically the organic carbon content (dominated by the protein collagen) was low even in modern bone (typically, 10–15% by weight) and because it was a very porous structure potentially subject to contamination (2).

The generally negative reputation of bone was partly reversed in the early 1960s when it was demonstrated that accurate ^{14}C values could be obtained if the inorganic carbonates of the bone were destroyed in acid and the residual acid-insoluble organic fraction (in modern bone, primarily collagen) was utilized in the ^{14}C determination (48). Since that time, a sizable number of bone dates have been measured by utilizing a range of organic preparations—from the acid-soluble to total amino acid fractions. Determinations on bone (e.g., Sunnyside skeleton) have figured predominantly in discussions concerning the antiquity of *Homo sapiens sapiens* in the New World (37,49). Although increasing confidence has been placed in the validity of ^{14}C determinations on bone of Holocene age, this acceptance has been muted when bone samples of Pleistocene age are considered. When relatively large amounts of samples

are available, more confidence can be placed in the integrity of the organic fractions extracted. However, when the organic carbon content of the bone is less than approximately 0.2–0.5%, concern has been expressed as to whether the recoverable organic fraction is actually indigenous to the bone or might include soil humics, bacteria, and fungus (50).

The advent of HEMS ion counting has initiated interest by several groups in developing capabilities to isolate the component amino acids of bone and particularly to isolate a single amino acid, such as hydroxyproline, known to have limited distribution except as a constituent amino acid of collagen. This isolation technique would significantly reduce the chance that the fraction being dated contained organics not indigenous to a bone (47,51) and would, in turn, greatly enhance the possibility of obtaining accurate ^{14}C determinations on bone of Pleistocene age. Thus a more secure temporal framework on which to construct the phylogenetic history of the late Pleistocene hominids would be established. Radiocarbon dating of the constituent amino acids by HEMS should also contribute significantly to resolving such questions as the reliability of amino acid racemization and uranium-series age estimates on bone.

Ceramics constitute one of the best known time-sensitive indicators used by archaeologists in many areas of the world to build local and regional chronologies. Ceramic sequences are particularly important for historic chronologies in ancient Western Asia (52). They also form the backbone of the traditional prehistoric cultural chronologies for many areas in the Western Hemisphere including the southwestern United States, Meso-America, and Peru (53). Radiocarbon determinations on organic components of ceramics have been used to circumvent problems of association between, for example, charcoal samples and ceramics where stratigraphic disturbance has occurred. Sherds should be less likely to become disassociated from their primary context than would single pieces of organic matter such as wood and charcoal.

Initial ^{14}C determinations on ceramic materials indicated that, in several cases, reasonably accurate age estimates could be obtained from the total organics contained in the ceramic fabric following the removal of obvious surface contamination and inorganic carbonates (54). One study, however, showed that the sources of carbon in ceramic materials can be highly variable, thus introducing serious anomalies in the ^{14}C results (55). In all previous studies, kilogram amounts of sherds were generally necessary due to the extremely low organic carbon yields. This sample size limited the ability of the investigators to extract specific chemical components from the ceramic matrix. The advent of HEMS ^{14}C technology will allow a much more detailed analysis of the various organic constituents that are incorporated into different types of ceramics and

will permit the identification of the fractions that would provide most reliable ^{14}C values on a routine basis.

Conclusion

The advent of HEMS technology represents a major step in the development of the ^{14}C method as applied in archaeological and Quaternary studies. It most certainly will have a much greater impact in these areas than did the previous replacement two decades ago of solid-carbon counting systems with systems using gas and liquid scintillation. What we have called the third generation of ^{14}C studies even now provides an order of magnitude adjustment in the conditions under which ^{14}C determinations can be obtained for a number of sample types, particularly those with low organic carbon yields. Therefore, we believe that it is appropriate to talk about the "new" radiocarbon dating in the context of the application of HEMS techniques.

For the archaeologist, the increasing utilization of milligram-sized samples and the potential extension in the practical range of ^{14}C dating will require even more rigorous attention to the collection of samples intended for ^{14}C analysis. A stricture that applies to even current decay-counting applications will become even more important over the next decade as HEMS ^{14}C counting assumes an increasingly important role. We submit that the critical application of ^{14}C data in archaeological studies can most advantageously be implemented when there is a close collaboration between those engaged in archaeological field research studies and those involved in laboratory analysis. In the absence of this collaborative relationship, even the most exacting and careful attention to detail in laboratory procedure may not ensure an accurate temporal assignment of cultural, environmental, or climatic events.

Those groups currently active in the refinements of HEMS instrumentation and in the development of appropriate sample pretreatment and target preparation methods are looking forward to applying this new radiocarbon dating to the widest possible number of important archaeological, historical, geological, and environmental problems. As a result of the development of the HEMS technique, we very much agree with the observation of Haynes (56) that "there is an exciting future ahead for dating the past."

Acknowledgments

Research support for the Radiocarbon Laboratory, University of California, Riverside, has been provided by National Science Foundation Grants BNS 8011764 and 8211804 (anthropology program). The dedicated

laboratory assistance of Louis A. Payen, Christine Prior, and Peter J. Slota, Jr., is gratefully acknowledged. The Regional Accelerator Facility at the University of Arizona is supported by a National Science Foundation Regional Instrumentation Facilities Grant. This is Contribution Number 82/22 of the Institute of Geophysics and Planetary Physics, University of California, Riverside.

Literature Cited

1. Libby, W. F. In "Radiocarbon and Tritium Dating"; Chatters, R. M., and Olson, E. A., Eds.; Clearing House for Federal and Technical Information (Conf. 650652): Springfield, Va., 1965; p. 745.
2. Taylor, R. E. In "Archaeological Chemistry II"; Carter, G. F., Ed.; ADVANCES IN CHEMISTRY SERIES No. 171; American Chemical Society: Washington, D.C., 1978; p. 37.
3. Libby, W. F. *Phys. Rev.* **1964**, *69*, 671-72.
4. Anderson, E. C.; Libby, W. F.; Weinhouse, S.; Reid, A. F.; Kirshenbaum, A. D.; Grosse, A. V. *Science* **1947**, *105*, 576.
5. Libby, W. F. Ph.D. Thesis; Univ. Calif., Berkeley, 1933.
6. Libby, W. F. "Radiocarbon Dating"; Univ. Chicago Press, Chicago, 1952; Chap. 5.
7. Arnold, J. R.; Libby, W. F. *Science* **1949**, *110*, 678-80.
8. Arnold, J. R. *Science* **1954**, *119*, 155-57.
9. McAulay, I. R.; Watts, W. A. *Radiocarbon* **1961**, *3*, 26-38.
10. Stuiver, M. *Science* **1978**, *202*, 881-83.
11. Harbottle, G.; Sayre, E. V.; Stoenner, R. W. *Science* **1979**, *206*, 683-85.
12. Litherland, A. E. *Ann. Rev. Nucl. Part. Sci.* **1980**, *30*, 439.
13. Anbar, M. In "Proceedings of the First Conference on Radiocarbon Dating with Accelerators"; Gove, H. E., Ed.; Univ. Rochester: Rochester, N.Y., 1978; pp. 152-55.
14. Alvarez, L. W. In "Symposium on Accelerator Mass Spectrometry"; Kutschera, W., Ed.; Argonne National Laboratory: Argonne, Ill., 1981; pp. 1-15.
15. Muller, R. A. *Phys. Today* **1979**, *32*, 23-28, 30.
16. Muller, R. A. *Science* **1977**, *196*, 489-94.
17. Nelson, D. E.; Korteling, R. G.; Scott, W. R. *Science* **1977**, *198*, 507-508.
18. Bennett, C. L.; Beukens, R. P.; Clover, M. R.; Gove, H. E.; Liebert, R. B.; Litherland, A. E.; Purser, K. K.; Sondheim, W. E. *Science* **1977**, *198*, 508-509.
19. Gove, H. E., Ed. "Proceedings of the First Conference on Radiocarbon Dating with Accelerators"; Univ. Rochester: Rochester, N.Y., 1978.
20. Kutschera, W., Ed. "Symposium on Accelerator Mass Spectrometry"; Argonne National Laboratory, Argonne, Ill., 1981.
21. Stuiver, M.; Kra, R., Eds.; "Proceedings of the Tenth International Radiocarbon Conference—Heidelberg" *Radiocarbon* **1980**, *22*, 785-852.
22. Stuiver, M.; Kra, R., Eds., "Proceedings of the Eleventh International Radiocarbon Conference—Seattle"; *Radiocarbon* **1983**, *25*, 171-795.
23. Bennett, C. L. *Amer. Sci.* **1979**, *67*, 450-57.
24. Mast, T. S.; Muller, R. A. *Nucl. Sci. Appl.* **1980**, *1*, 7-32.
25. Litherland, A. E. *Ann. Rev. Nucl. Part. Sci.* **1980**, *30*, 437-73.
26. Hedges, R. E. M. *Archaeometry* **1981**, *23*, 3-18.

27. *Ibid.*, p. 6.
28. Mast, T. S.; Muller, R. A. *Nucl. Sci. Appl.* **1980**, *1*, 13.
29. Hedges, R. E. M. *Archaeometry* **1981**, *23*, 6.
30. Muller, R., personal communication.
31. Purser, K. H.; Liebert, R. B.; Litherland, A. E.; Beukens, R. P.; Gove, H. E.; Bennett, C. L.; Clover, M. R.; Sondheim, W. E. *Rev. Phys. Appl.* **1977**, *12*, 1487–92.
32. Donahue, D. J.; Zabel, T. H.; Jull, A. J. T.; Damon, P. E.; Purser, K. H. *Radiocarbon* **1983**, *25*, 719–28.
33. Jull, A. J. T.; Donahue, D. J.; Zabel, T. H. "Nuclear Instruments and Methods"; in press.
34. Bada, J. L.; Helfman, P. M. *World Arch.* **1975**, *7*, 160–73.
35. Lajoie, K. R.; Peterson, E.; Gerow, B. In "Biogeochemistry of Amino Acids"; Hare, P. E.; Hoering, T. C.; King, K., Eds.; Wiley: New York, 1982; pp. 477–89.
37. Taylor, R. E.; Payen, L. A.; Gerow, B.; Donahue, D. J.; Zabel, T. H.; Jull, A. J. T.; Damon, P. E. *Science* **1983**, *220*, 1271–73.
38. Taylor, R. E. *Radiocarbon* **1983**, *25*, 647–54.
39. Muller, R. A.; Stephenson, E. J.; Mast, T. S. *Science* **1978**, *201*, 347–48.
40. Taylor, R. E.; Slota, P. S. In "Radiocarbon Dating"; Berger, R.; Suess, H. E., Eds.; Univ. Calif. Press: Berkeley, 1979; pp. 422–32.
41. Adovasio, J. M.; Gunn, J. D.; Donahue, J.; Stuckenrath, R. In "Peopling of the New World"; Ericson, J. E.; Taylor, R. E.; Berger, R., Eds.; Ballena: Los Altos, 1982; p. 97–131.
42. Adovasio, J. M.; Gunn, J. D.; Donahue, J.; Stuckenrath, R.; Guilday, J. E.; Volman, K. *Amer. Antiq.* **1980**, *45*, 588–95.
43. Haynes, C. V. In "Radiocarbon Dating with Accelerator"; Gove, H. E. Ed.; Univ. Rochester: Rochester, N.Y., 1978; pp. 276–88.
44. Haynes, C. V. *Amer. Antiq.* **1980**, *45*, 582–95.
45. Isaac, G. In "Calibration of Hominoid Evolution"; Bishop, W. W.; Miller, J. A., Eds.; Univ. Toronto Press: Toronto, 1972; p. 381–430.
46. Taylor, R. E., Ed. "Radiocarbon Dating in Archaeology: Needs and Priorities in the 1980's"; report of a conference held at the National Science Foundation, Washington, D.C., June 10–12, 1982. Radiocarbon Laboratory, Univ. Calif.: Riverside, 1981; pp. 6, 17–19.
47. Hedges, R. E. *Archaeometry* **1981**, *23*, 15.
48. Berger, R.; Horney, A. G.; Libby, W. F. *Science* **1964**, *144*, 999–1001.
49. Taylor, R. E.; Payen, L. A. In "Advances in Archaeological Method and Theory"; Schiffer, M. B., Ed.; Academic: New York, 1979; Chap. 8.
50. Taylor, R. E., *Radiocarbon* **1980**, *22*, 969–79.
51. Taylor, R. E. In "Nuclear and Chemical Dating Techniques: Interpreting the Environmental Records"; Currie, L. A., Ed.; ACS SYMPOSIUM SERIES No. 176; American Chemical Society: Washington, D.C., 1982, Chap. 23.
52. Erlick, J., Ed. "Chronologies in Old World Archaeology"; Univ. Chicago Press: Chicago, 1959.
53. Taylor, R. E.; Meighan, C. W., Ed. "Chronologies in New World Archaeology"; Academic: New York, 1978.
54. Taylor, R. E.; Berger, R. *Amer. Antiq.* **1968**, *33*, 363–66.
55. De Atley, S. P. *Radiocarbon* **1980**, *22*, 987–96.

56. Haynes, C. V. In "Proceedings of the First Conference on Radiocarbon Dating with Accelerators"; Gove, H. E., Ed.; Univ. Rochester: Rochester, N. Y., 1978; p. 286.

RECEIVED for review November 2, 1982. ACCEPTED for publication July 12, 1983.

The Analysis of Exudate Plant Gums in Their Artistic Applications: An Interim Report

JOHN W. TWILLEY

University of California, Department of History, Riverside, CA 92521

The rapid unambiguous identification of plant gums used in artistic and ethnographic artifacts has been demonstrated to be feasible through the use of various chromatographic microtechniques. Determination of the monosaccharide ratios for these gums can be accomplished by gas-liquid chromatography of the trimethylsilyl ether derivatives after the monosaccharides have been liberated by hydrolysis. Analysis of a group of gums by these techniques indicates that the precision of such analysis can be 2–3% and that the genus and species of origin may thereby be determined. The taxonomic and geographic origins of the exudate plant gums are discussed briefly along with a historical perspective upon their collection and utilization. The results are presented for a reference group of gums to which unidentified samples may be compared. Included as well are the results of a literature search for species reported to yield exudate plant gums.

Origin, Collection, Utilization

A multidisciplinary study of the various exudate plant gums was undertaken to obtain information concerning their origins, historical uses, properties, and differentiating characteristics in the hope that it might prove possible to identify them unambiguously in artistic and ethnographic applications. The art of miniature painting in Asia has evolved largely with the use of plant gum as its medium. Turkish, Persian, and Indian miniatures share this common material. However, the particular species from which the gum is derived can be any one of dozens of possible plants. The microanalytical techniques presented in this chapter have been developed with the intent that the amount of sample required be held to a minimum—on the order of 1 mg. It is hoped that the Mughal

0065-2393/84/0205-0357\$10.50/0

© 1984 American Chemical Society

Indian miniatures can be studied extensively by the application of these methods to the under-1-mg paint samples available from them (Figure 1).

Most of the present efforts have been directed towards the Mughal period (1526 to the mid-18th century). The methods involved, however, will find application to antiquities from other cultures and periods. Almost every culture on earth has used plant gums in some capacity. Lucas (1) referred to the use of gum arabic in Egypt beginning in the Fourth Dynasty (ca. 2600 B.C.), where it played an important role in the practices of mummification and art (2). In more recent times, the American Indians of the southwestern United States used mesquite gum (*Prosopis juliflora*) in hafting arrows (3). More than 320 species of *Acacia* are said to exist in Australia (4,5), where they are well known to the aborigines who used them as food as well as in tool making. In Europe, gums found some limited use in mucilages, pharmacy, and art. Except for the exudate from the genus *Prunus*, most of these gums were imported rather than indigenously grown. Trade in exudate gums, principally gum arabic, has been carried on from the ports of northern Africa to Europe since the first century A.D. (2,6). In India, gums have been used as the media for ink. A mixture of gum and carbon black is dried into cake form and redissolved in water as needed (7). A multitude of objects from these cultures and others can be subjected to the analytical procedures outlined in this chapter.

Nomenclature. A strict nomenclature should be adhered to in describing plant gums and biopolymers of similar botanical origin. Laxness about proper nomenclature has caused much confusion in the literature. The major plant products of interest in this context and the chemical class to which each belongs are shown in the box below. Exudates that are admixtures of these classes are well known and relatively few in number, for example frankincense and myrrh, the compositions of which are roughly 40% polysaccharides in a terpenoid resin (8). It should be noted that although "adhesives" may have many origins, the term "glue" should be reserved for proteinaceous materials of animal origin.

Chemical Classification of Media Materials

Gums	Polysaccharides
Glues	Proteinaceous materials of animal origin
Resins	Triterpenoids (usually C ₃₀ compounds)
Lacquers	Olefinic and saturated catechols
Oils	Olefinic and saturated triglycerides



Figure 1. Emperor Jahangir Standing on a Globe Shooting Poverty, Mughal ca. 1620; height, 36.8 cm; width, 24.8 cm; opaque watercolors on paper. This work exemplifies the beauty and minute detail of the medium with which we are concerned. Reproduced courtesy of the Museum Associates, Los Angeles County Museum of Art; from the Nasli and Alice Heeramanek Collection, Museum Associates Purchase.

In Mughal art both gums and glues are found in different roles in the same painting. Glue made by boiling horn, hoof, and hide of the water buffalo was used as a size where gold powder was to be applied. For somewhat cheaper paintings, in which gold leaf was substituted for the carefully prepared powder, sugar was added to this glue to promote adhesion to the smooth metallic surface. This mixture was also used when gold powder was sprinkled lightly on the border (7).

Biogenesis of the Exudate Polysaccharides. The exact biochemical pathways leading to the formation of exudates are still being elucidated. However, the similarity of these exudates to cell wall constituents has led to the suggestion that they may represent modifications of crosslinking polysaccharides produced in normal metabolic action (9). These exudates serve to attach adjacent cellulose strands in cell walls. They possess a highly branched structure made of the same group of monosaccharides as that found in gums (10).

Very recently an in-vitro study shed light on the mechanism of gum formation in the species *Albizia julibrissin*. Wood blocks of this species were incubated and examined as gum formation began—presumably in response to being severed from the tree. The gum was observed to be synthesized in vesicles of the parenchyma, which developed remarkably during incubation. The gum was stored in the vessel-side extracytoplasmic space of the parenchyma and then discharged into the vessel lumina through the pittings (11).

Gum exudation ensues in response to stress. The presence of gums is indicative of some pathological condition that has activated a protection mechanism within the plant. At one time, it was thought that gums were produced by fungi that had invaded the open wound. Substantiating evidence for this hypothesis is hard to find, however. No connection between such fungi and exudate gums has ever been proved (12).

Gum arabic will not be produced during the wet season or cold weather; therefore, its primary purpose appears to be the retention of water. The gum forms as a tear or a ribbon at any point of damage to the bark (Figure 2). Here it seals the opening to both the loss of moisture and the invasion of parasites. The largest quantities are produced by plants growing under the most adverse conditions (5,13). Consequently, it has not been worthwhile to cultivate the plants commercially. Members of the genus *Acacia* that experience heavy rain followed by drought and wind are prolific gum yielders. The desiccation of the bark causes shrinkage and cracks. This damage, following a growth surge, produces gum without any sort of artificial tapping by humans.

Collection. Gum collection for purposes other than as a food source has historically been a spare time activity carried out by farmers and herdsman when other work was impossible (13). This activity has been organized only recently as import demand developed in the industrialized



Figure 2. An acacia of undetermined species exudes gum from a natural injury. The nodule shown measures approximately 4 cm across.

countries. This organized collection has been most successfully brought about in Africa (5). Gums have been transported by individual merchants for centuries, however, to be sold in bazaars as a confection, medication, or painting medium. These merchants obtained their goods from individual collectors or nomadic families.

Trees are artificially tapped when a commercial demand for exudate gums exists. An axe is usually used to separate a strip of outer bark from the trunk. The two broken ends of this strip are peeled away from the cut in opposite directions. Gum forms slowly in "tears" along the edges of the cut for several weeks as long as hot weather persists. This mechanism is used in the tapping of *Acacia*, *Cochlospermum*, *Albizia*, and other large plants. The smaller plants such as the various species of *Astragalus* are made to yield gum by pruning the ends of branches, burning off the foliage, or incising the roots. [The formation of gum in the genus *Astragalus* may differ from that described for other genera. It is often seen to exude almost immediately from an incision and sometimes contains starch particles (cellular debris). This cellular material is the basis for occasional reports of glucose as a constituent of gum tragacanth (14,15).] In the latter case, the larger roots are uncovered, punctured, and a small wedge is inserted to hold the slit open (5,13). This particular method of tapping produces the "ribbon" form of gum tragacanth. The small burned twigs produce a rice-shaped exudate called "vermicelli" tragacanth.

With the advent of large-scale international trading of gums (ca. 1850 A.D.), large sorting and packing houses were established. In order to supply material of a quality commensurate with its ultimate use, the gums are sorted into a number of grades based upon clarity, hardness, solubility, color, cleanliness, and uniformity (13). Many gums from unrelated species are indistinguishable physically; yet samples from the same tree may differ greatly in color and clarity (Figure 3). This sorting has made commercial lots very heterogeneous from the botanical standpoint. Therefore, commercial stock cannot be used as reference material for analytical investigations. Botanically authenticated samples from the regions of interest for our work were obtained from the Royal Botanical Gardens in London, England. One interesting aspect of the international trade that developed was the enormous quantity of acacia gum that was exported from the Sudan region of Africa to Bombay and then re-exported to Europe.

Geographical Distribution. It should prove very interesting to look at the possible gum sources for an artifact or artwork whose origins are documented. Local occurrence of the specific plant would be no surprise. If the gum is unavailable locally, three conclusions might be implied. First, the artist or school may have had a preference for this particular type of gum, which will be an aid in authenticating other pieces when

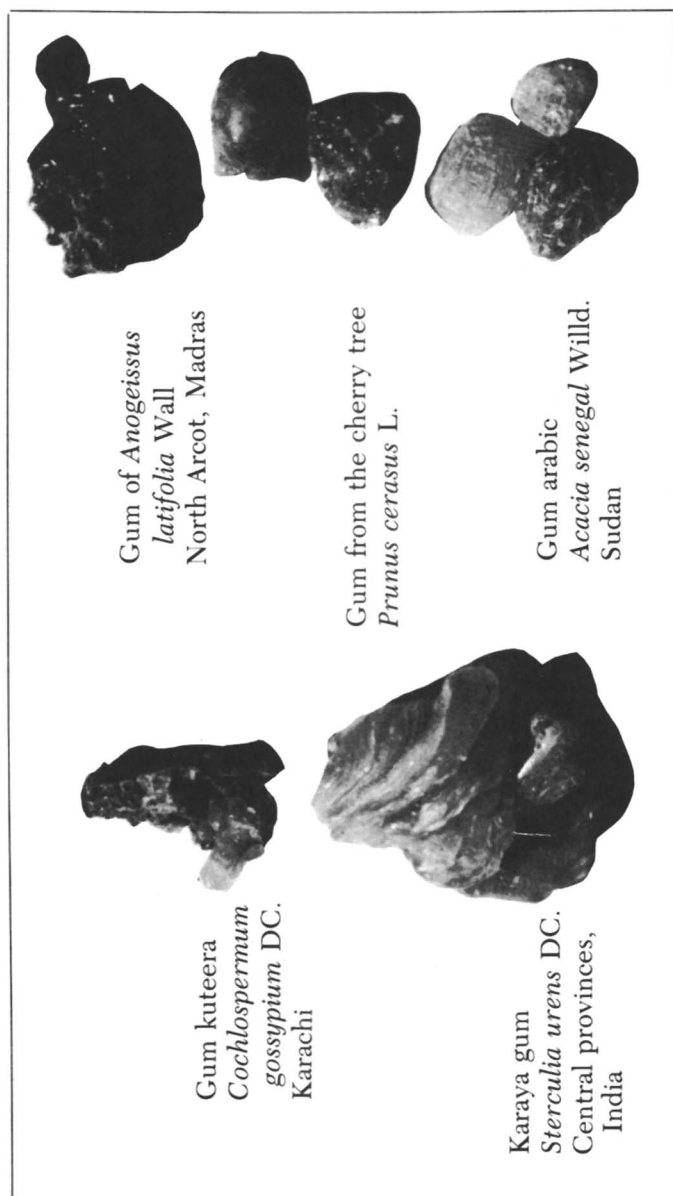


Figure 3. Five gum samples from species of major artistic importance. Note the similarity in shade of the kuteera, karaya, and pale gum arabic tears. All three tears of gum arabic are from the same tree yet one is as dark as the cherry gum. Chemically, the pale and dark samples are identical by monosaccharide analysis. Note the opacity of the sample from *Anogeissus latifolia*.

some doubt exists about their provenance. Second, the more readily obtainable gums may have had inferior properties for the purpose at hand. The artisan's choice of materials may indicate something about his competence or the importance of the work. Third, the presence of gum in an artifact originating far from its source might well indicate the existence of trade between the two points.

The distributions of a few of the more important gum-yielding genera are illustrated in Figure 4. In this map the extent of distribution has been emphasized rather than the depiction of an exhaustive list of all possible gums. An appendix has been added to serve as a more complete reference of individual species. The text of this chapter is restricted to a basic description of each important genus.

Acacia. This very large genus is represented on every continent. More than 320 species exist in Australia, where they are known as "wattles" and provide the majority of the plant exudates that form a segment of the aborigines' diet. For them, the gum is considered a delicacy rather than a last resort for the hungry. Historically, areas where it was collected were subject to the only rudimentary property rights evidenced in aboriginal life (4).

A few species of acacia are found in Indochina, Thailand, and Bengal. In India there are two dozen species. The fact that Africa's primary producer of gum, *Acacia senegal*, extends eastward to Sind but no further into India may be very important if this gum is found in Indian artwork—especially in artwork prior to the Mughal conquest. In arid regions, such as the Middle East, acacias remain confined to the lower elevations. In Africa, acacias occur in great numbers everywhere except in the driest part of the Sahara. The Sudan contains a few areas where large forests consist of a single acacia species (5). This botanic separation is unusual, however, because acacia species may interbreed with the result that over a number of generations the boundary between two species becomes vague. In time a hybrid may become so well defined as to constitute a new species within the genus.

Most acacia gums are entirely soluble in water. They form useful adhesives and binding media for tempera. In solutions they retard settling and stabilize emulsions. Many high quality watercolors are still made from gum arabic, and it is a favorite additive of the processed foods industry.

Various species of locally available acacia gums were the primary media of Mughal painting. A weak solution without pigment is said to have been applied over the paint layer when certain areas (e.g., hair, silken garments, and so forth) were to be enhanced by a glossy surface (7).

Albizzia. This genus contains at least nine gum-yielding species. The gum is not easily soluble and only a few references to its use are made. It occurs in all regions bordering the Indian Ocean.



Figure 4. Distribution of some important gum-yielding genera. Key: 1, *Acacia senegal*; 2, *A. mellifera*; 3, *A. seyal*; 4, *A. karroo*; 5, *A. arabica*; 6, *A. catechu*; 7, *A. modesta*; 8, *Acacias (300 sp.)*; 9, *A. farnesiana*; 10, *Combretum*; 11, *Albizzia*; 12, *Anogeissus latifolia*; 13, *Khaya*; 14, *Astragalus*; 15, *Sterculia urens*; 16, other *Sterculia*; 17, *Bombax malabaricum*; 18, *Cochlospermum gossypium*; 19, *Feronia elephantum*; 20, *Odina wodier*; 21, *Prunus*.

Anogeissus. Chandra (7) states that the gum of *Anogeissus latifolia* is used exclusively with zinc white (presumably in the modern period) and *Peori* ("Indian Yellow"—the flavinoid glycoside derived from mango-fed bovine urine), all other colors in Mughal painting being applied with acacia gums. A solution of gum from *Anogeissus latifolia* curdles when mixed with other pigments.¹ Species of this genus occur outside of India but are rarely put to any use.

Astragalus. This genus is said to contain 1600 species. It is not represented in Australia (5). India contains 70 species. Relatively few of these are reported to yield gum and most of those are in the Middle East. Gum is collected at locations between 4000 and 10,000 ft in elevation. Gum of *Astragalus gummifer*, now known as gum tragacanth, was the original Arabic "kutira." This name was applied to the gum of *Cochlospermum gossypium* by the Mohammadan invaders of India and is now associated exclusively with that species. Because gum is present under slight pressure inside central cavities of the stems, this gum often exudes immediately after an incision is made. Other gum-yielding genera require days or weeks to produce the same amount of gum. Although they are only partially soluble, *Astragalus* gums are highly reputed for their useful properties. They are the primary media of Persian miniatures.

Chandra (7) states that Persian gum tragacanth was only used by the Mughals as a medium for applying mica powder.

Lannea. Gum from *Lannea grandis* (*Odina wodier*) is routinely used in India for a whitewash base because of its availability and large yields.

Prunus. Gums from this genus are often called by the general name cherry gum or the outmoded term Bassora. The latter term has been used to indicate any insoluble or partially soluble gum. *Prunus* gums have not been as widely utilized as the acacias because of their poor solubility. However, their extremely broad geographic distribution and close association with humans requires that they be tested for in any thorough analysis. Birstein has presented evidence for the use of *Prunus*

¹ Moti Chandra's book, "The Technique of Mughal Painting," is an exquisite treatment of the subject. We have found only two technical errors. The first is his statement that acacia gum is obtained from the tree in the form of fine crystals. He was apparently unfamiliar with the gum in its raw form. Tears of the better grades of gum arabic are easily pulverized into what must be the form familiar to the author. The second is a more specific error. After stating that the green pigment, Harābhātā, is a silicate of ferrous oxide, Chandra goes on to state that this is malachite. His further discussion indicates a fair amount of knowledge about malachite, so it is difficult to understand why he assigns this erroneous formula to the mineral. It remains for the accuracy of the pigment usages described by Chandra to be verified by technical examination of the works themselves.

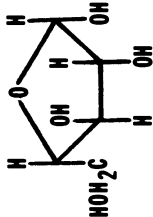
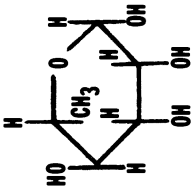
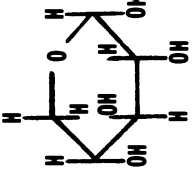
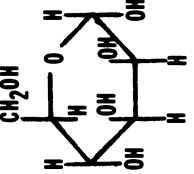
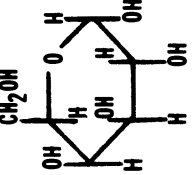
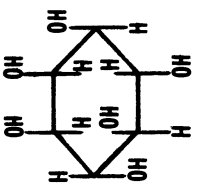
<u>STRUCTURE</u>	<u>NAME</u>	<u>MOL. WT.</u>	<u>TMS MOL. WT.</u>
	L-Arabinofuranose	150	438
	L-Rhamnopyranose	164	452
	D-Xylopyranose	150	438
	D-Mannopyranose	180	540
	D-Galactopyranose	180	540
	Myo-inositol (internal standard)	180	612

Figure 5. Predominant monosaccharides found in plant gums shown in their α configurations.

gums in wall paintings from four locations that span 2000 years of Central Asian history (16).

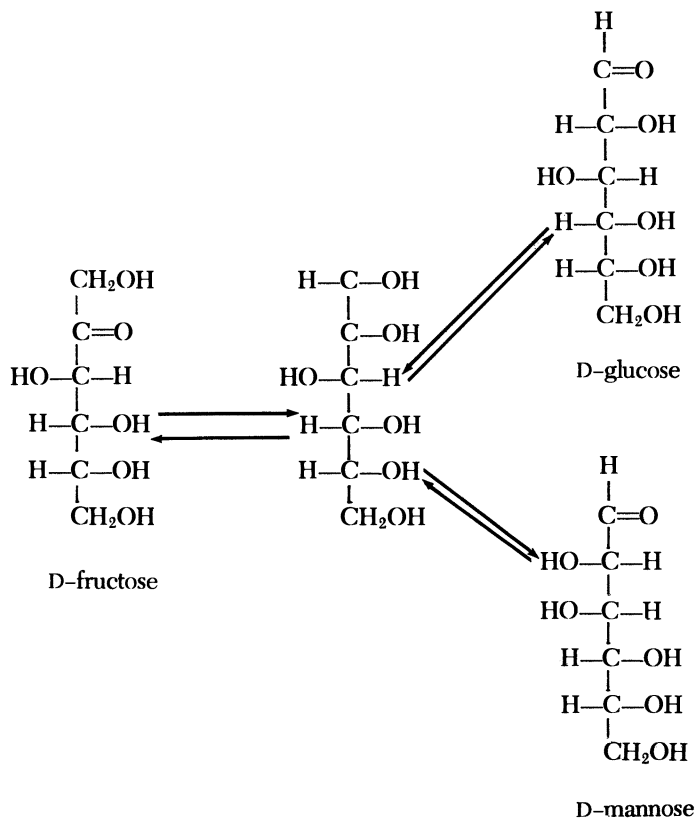
Sterculia. Widely distributed in the Old World, this genus is well known for its gums, which have properties only slightly less desirable than those of acacia. *Sterculia* species generally exude gum rapidly; nodules weighing over a pound each are not unusual.

Chemical Description and Analysis

Monosaccharides. Exudate gums are found to consist of only a small number of possible sugars: L-arabinose, D- or L-galactose, D-mannose, D-glucose, L-rhamnose, D-xylose (Figure 5), and, more rarely, L-fucose, D-fructose, D-glucose, and D-tagatose. D-Glucose, abundant in plant material, is conspicuous by its near absence in gums. In addition to the neutral monosaccharides, there are two sugar acids, D-galacturonic acid and D-glucuronic acid, of which one is always present. Occasionally a modification of one of these is found, namely 4-O-methyl-D-glucuronic acid, wherein the hydroxyl group on C4 has been replaced by the methyl ether.

Although monosaccharides may exist in open chain forms as transitory reaction intermediates, the condensed ring structures shown in Figures 5 and 6 are favored configurations. Cyclization to the six-membered pyranose ring form may occur in two directions to produce the α or β isomers (the hydroxyl on the anomeric carbon either axial or equatorial, respectively, Figure 6). In solution, these isomers will interconvert rapidly to form an equilibrium mixture. The position of this equilibrium is, of course, dependent upon the temperature and the solution pH. A further modification may occur in the formation of a γ component, which was named when the small percentage unaccounted for by the α and β isomers was assumed to be in the open chain configuration. Instead, this γ component is a five-membered ring, the furanose structure, which also has α and β isomers. This total of four structural isomers complicates most gas chromatographic separations. Fortunately, the furanose form is quite unfavorable for most monosaccharides, and one has to deal with only two isomers (17,18). It is important to reproduce experimental conditions very carefully so that the isomer ratio remains constant from one trial to the next. Ordinarily the furanose peaks cannot be measured. A change of 1% or 2% from one ring form to the other will contribute to the quantitative error and may not be observable.

Sugars in solution are also subject to interconversions in the presence of a base. Mannose and glucose will undergo de Bruyn-van Eckenstein transformation as follows:



where the intermediate osazone is common to both the aldose and the ketose. The resulting solution will contain equilibrium amounts of ketose and epimeric aldose (19–21). It is, therefore, necessary to avoid subjecting the monosaccharide solutions to basic conditions for any length of time.

Polysaccharides. Monosaccharides may link into an infinite number of polymeric units. The widely different properties of cellulose and amylopectin (both polymeric glucose) are dependent upon the linear, crystalline nature of the former and the highly branched, amorphous nature of the latter.

Newbauer first identified an acidic substance in gum arabic in 1854 and noted the 2:1 ratio of hydrogen:oxygen. In 1868, Schleibler identified "arabinose" in gum arabic (13); thus plant gums have been studied since the infancy of carbohydrate chemistry. Structural studies of various exudate gums have since shown that, in general, these gums contain a core strand of uronic acid units and one or two types of monosaccharide. Attached to the core are sidechains, usually containing some different

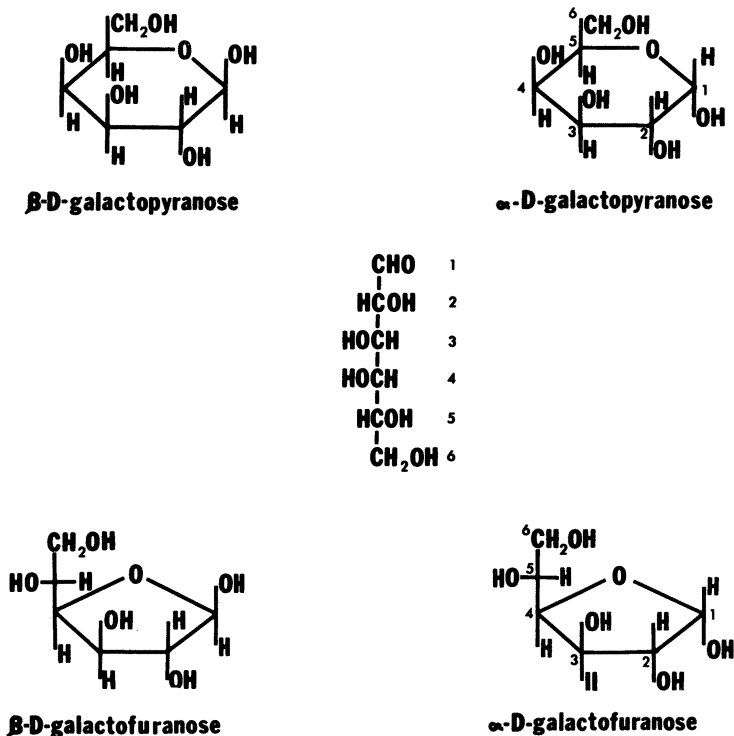


Figure 6. The four structural isomers of *D*-galactose shown in relation to the open chain structure commonly published. This form, once called γ -*D*-galactose, has been proved to exist only as an intermediate in the equilibrium between the other four ring forms. The α , β furanose pair accounts for that remainder once assigned to the open chain structure.

monosaccharides and the same uronic acid. Sidechains may be of two or three different sequences. They are relatively short and contain an average of six units.

A more complex situation is represented by gums that are only partially soluble. These consist of two fractions of differing molecular weight and monosaccharide composition. Often, as in the case of gum tragacanth, the acidic portion is confined to only one of the two fractions.

Due to their uronic acid content, gum solutions exhibit a pH of approximately 5.0. Extended time in solution will lead to autohydrolysis: the self-catalyzed cleavage of the original polymer into shorter units. The most labile groups are normally present in sidechains, and the uronic acid units tend to form part of the backbone of the polymer. Autohydrolytic activity ceases in the dry state. Most gums do not attack a sensitive support such as paper in the absence of aggressive compounds used

as pigments. This inertness may be due to the strong internal hydrogen bonding of the saccharides, which tends to immobilize and isolate the acid units along the backbone when solvent water is unavailable. Any hydrolytic enzyme activity would also be attenuated by drying. Exudate gums have been observed to be stable for at least two millennia.

Polysaccharides are classified on the basis of the units that make up the central strand. In the first group are the galactans, whose core structures consist of 1 → 3 and 1 → 6 linked galactopyranose units. Included in this group are the acacia and mesquite (*Prosopis*) gums. A second group contains a repeating unit of 2-O-(D-glucopyranosyluronic acid)-D-mannose. These gums, including gums of *Prunus* and *Anogeissus*, are referred to as galacturonorhamnans. These may be further subdivided by differences in core structure. The acidic main portion of gum tragacanth (*Astragalus*) is a highly branched polysaccharide containing a core strand of polymeric galacturonic acid. In addition to *Astragalus*, the third group contains *Sterculia*, *Khaya*, and *Cochlospermum* gums. *Sterculia* and *Khaya* produce gums that are partially acetylated, some of their hydroxyl groups being naturally esterified with acetic acid, and they have a slight odor of acetic acid when freshly broken. Many uronic acid units in all gums are present in their salt form with calcium and magnesium counterions.

The stability of the glycosidic bond to acid hydrolysis varies tremendously. Bond strength is dependent upon the two monosaccharides involved and their points of attachment. This dependence has been capitalized upon by structural chemists who carry out partial hydrolysis of the gum into oligosaccharides, characterize the units of these segments, and then assemble a structure based upon a knowledge of relative bond lability (Figure 7). Increasingly severe conditions will provide successively smaller oligosaccharides and segments from the more stable parts of the molecule. (Studies of this type are difficult and one finds some conflicting information in the literature, some of it due to materials obtained from questionable sources. At this time, no single structure can be proved to be correct in every detail.) Bonds to furanose groups, when present, are most easily broken, followed by pyranose and finally glucosiduronic acid bonds. Reaction rates for these hydrolyses vary over three orders of magnitude. The more labile groups, such as arabinofuranose, arabinopyranose, xylopyranose, rhamnopyranose, and fucopyranose, usually occur in the sidechains off of the polysaccharide core. These groups may be liberated by autohydrolysis without a great decrease in the average molecular weight of the polymer. A dramatic decrease would occur if these units were present in the core strand. To hydrolyze the bond between a uronic acid and a neutral monosaccharide (a dimer known as an aldobiuronic acid) requires severe conditions. Fructose may be degraded under these conditions, but that sugar is rarely found in gums

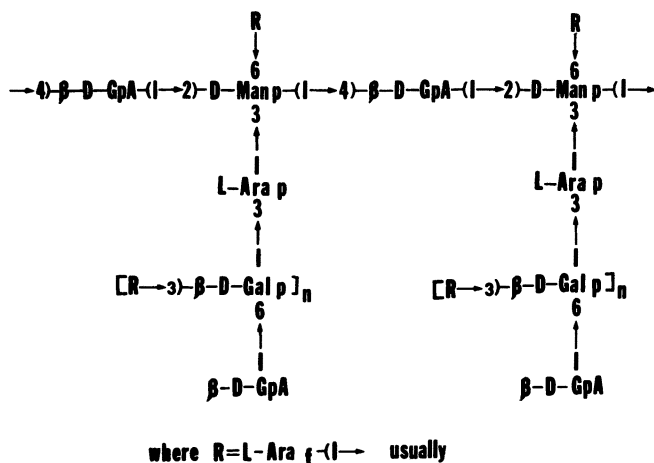


Figure 7. A possible repeating unit in the gum from *Anogeissus latifolia*. Key: GpA, glucopyranosyluronic acid; Man p, mannopyranose; Ara p, arabinopyranose; Ara f, arabinofuranose; and Gal p, galactopyranose. Numbers indicate points of attachment between different units as indicated in Figure 6. The value of n is uncertain.

and never in large amounts. Hydrolysis of the aldobionuronic acid disaccharide almost always involves decomposition of the uronic acid portion.

Average molecular weight may be determined by osmometry by utilizing either membrane or vapor pressure apparatus. Most gums are found to lie in the molecular weight range from about 200,000 to over 1,000,000 (22). This in turn implies that 1100 to over 5500 monomeric units make up each assemblage.

Other techniques have begun to be used more often in structural studies. Immunological precipitation has been used to identify structural attributes of gums by their similarity to virus sheath polysaccharides (8). Gas chromatographic studies have made use of methylated (23), acetylated (16), formylated, trifluoroacetylated, and trimethylsilylated derivatives (19,24).

Since this work began, a gas chromatographic technique has been published that has certain distinct advantages over those previously available for monosaccharides (14). The technique involves the elimination of the asymmetric carbon by mercaptalation of the aldose mixture with ethanethiol prior to silylation. This results in much simpler quantification through the elimination of multiple chromatographic peaks for a single sugar. The problem of small furanose peaks with their low quantitative accuracy is eliminated as well. The main difficulty with this technique lies

in the intensely disagreeable odor of the ethanethiol reagent. High pressure liquid chromatography has also been employed to separate the hydrolysate monosaccharides of plant gums (15).

Analytical Techniques. This investigation was initiated to establish a routine procedure by which an exudate gum source could be identified from a sample of only 1 mg. Initial tests indicated that exudate gums were present in Mughal miniatures (25,26) and were an accepted part of Persian miniatures.

Several investigators have used IR spectroscopy in polysaccharide identification (16,27,28). However, this technique was found to be unsatisfactory in media and artifact identification for a number of reasons:

1. The differences in the spectra of different gums are rather subtle, particularly when the gums are closely related within a structural group (Figure 8). Successful identification is highly dependent upon the operator's ability to optimize test parameters.

2. In many instances gums are not applied as found but are treated to modify their solubility or adhesion. Simple boiling, for instance, will not affect the monosaccharide constituents but will preferentially disrupt certain linkages as hydrolysis takes place, thus altering the IR spectra. Aborigines have used a method of preparing *Acacia pycnantha* gum for hafting stone tools by a base-catalyzed hydrolysis of the gum. The gum is mixed with water and lime sand and then boiled (29). This practice could make any identification procedure more difficult, but IR spectrophotometric methods would be particularly affected. The hydrolysis would be followed by base-catalyzed mutarotation of the liberated monosaccharides (de Bruyn-von Eckenstein transformation).

3. The best resolved IR spectra can be obtained from an evaporated film. However, many gums are not totally soluble. Extraction of only the soluble fraction from a paint layer containing a partially soluble gum could lead to erroneous data.

4. Micropellet techniques would be attractive because of small sample size, but inorganic materials such as pigments will introduce absorptions of their own and reduce the transmittance of the spectral data of interest (16).

5. In an instance involving mixed tempera where a protein-base glue and a plant gum occur together (16), the IR spectra would be much more complex. Thin layer chromatography of the hydrolysate could be more precise.

Spectroscopic analysis did not appear to be suitable. Thin layer chromatographic analysis is useful and may be used to differentiate among the major groups of gums. However, under the best of circumstances it is only semiquantitative. We settled upon gas-liquid partition chromatography (GLC) of the hydrolysate as the best method of identification, as it provides the best information on the monosaccharide profile, in lieu

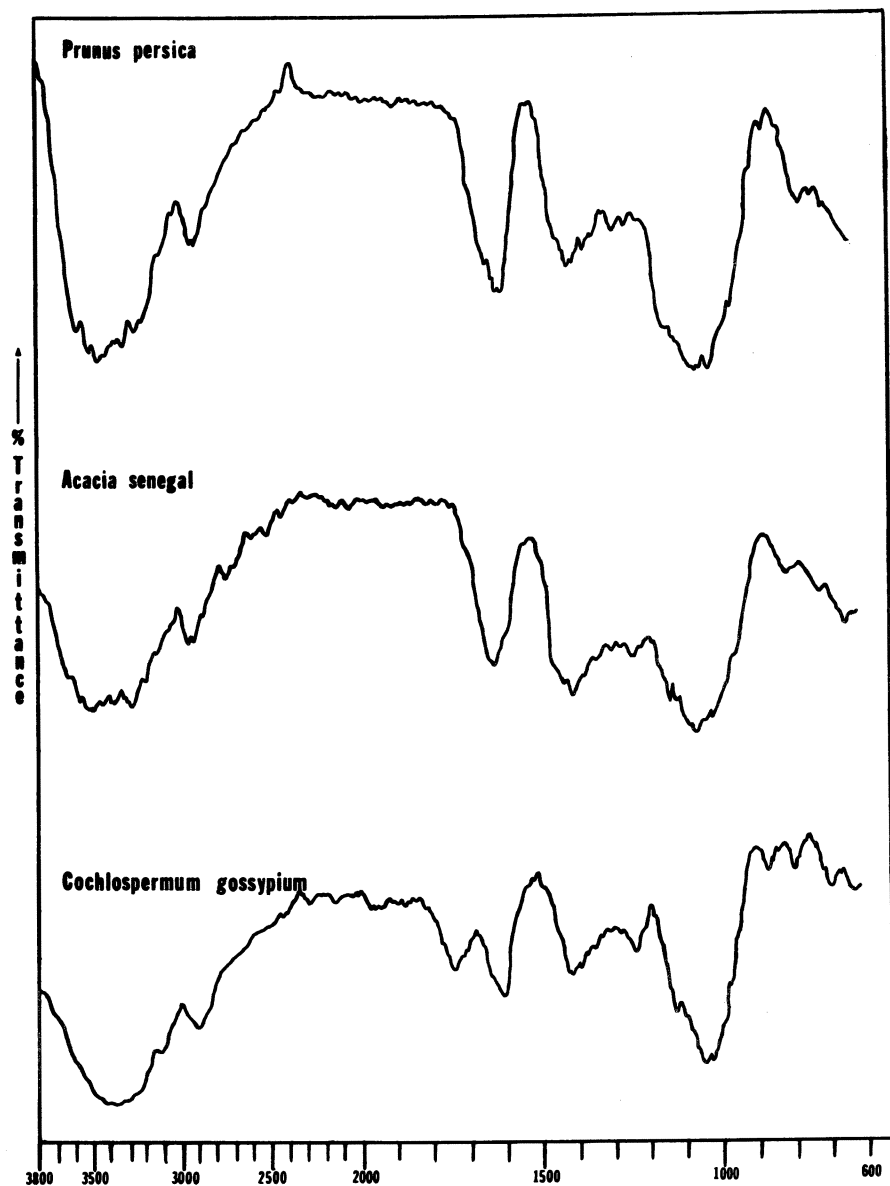
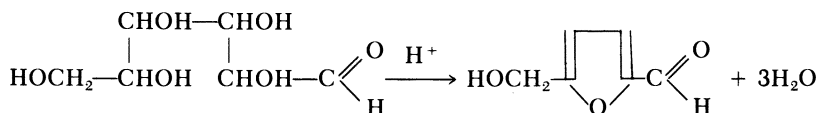


Figure 8. IR spectra illustrating the slight differences in gums that represent each of the main structural groups as defined in the text. The most pronounced difference is the peak at 1750 cm^{-1} in the spectra of *Cochlospermum gossypium*, a naturally acetylated gum. Each of these spectra was produced after maximizing peak resolution for the particular sample. Instrument parameters are not identical for the three recordings.

of establishing the whole structure. The use of a capillary gas chromatograph allows multiple analyses of a very small sample.

The use of gas chromatography requires volatile compounds, of course, and derivatives must be made of the hydrolyzed monosaccharides. Many investigators have used methylation or acetylation to produce these derivatives (10,16). However, both of these methods require more steps than are desirable with a small sample. In addition, the reaction time required for quantitative conversion to the derivative may be a problem. The use of trimethylsilyl ethers makes the derivatization exceedingly simple and relatively fast. Formation of these derivatives in the absence of water has been shown to occur without anomerization and to proceed quantitatively (30,31). The reaction mixture is chromatographed directly (Figure 9).

As mentioned earlier, hydrolysis of the aldobiuronic acid unit usually involves decomposition of the uronic acid portion. Neutral monosaccharides may also decompose by the action of mineral acids. Pentoses and hexoses form furfural and hydroxymethylfurfural, respectively, by the cyclization–dehydration reaction shown below (32).



This reaction is almost quantitative for concentrated hydrochloric acid on cellulose. Under the conditions of our hydrolysis, this reaction occurs to the extent of less than 1%.

Neutralization of the hydrolysate is a problem because of the small sample size—only 1 or 2 drops in the case of a 1-mg paint sample. The solution must be deionized as well as neutralized for analysis by GLC. If sulfuric acid is used, precipitation with barium carbonate is suitable. However, it is difficult to avoid overshooting the end point with such a small sample. Ion exchange with a strongly basic anion exchanger suffers from two shortcomings. Use of such an exchanger can promote de Bruyn–von Eckenstein transformations at localized highly basic functional groups. In addition, these exchangers irreversibly absorb sugars to some extent. The use of a weakly basic anion exchanger in the carbonate form solves both problems (19).

Experimental

Botanical samples are cleaned of all foreign matter (bark, dirt, and the like), and then ground as finely as possible in a mortar. A 50.0-mg portion is dissolved (as completely as possible) in 5.0 mL of 1.0 *N* hydrochloric acid. The liquid is sealed under nitrogen in a partially evacuated ampule and is hydrolyzed at 100 °C for 18 h. At the end of this time, a single drop is removed to test for decom-

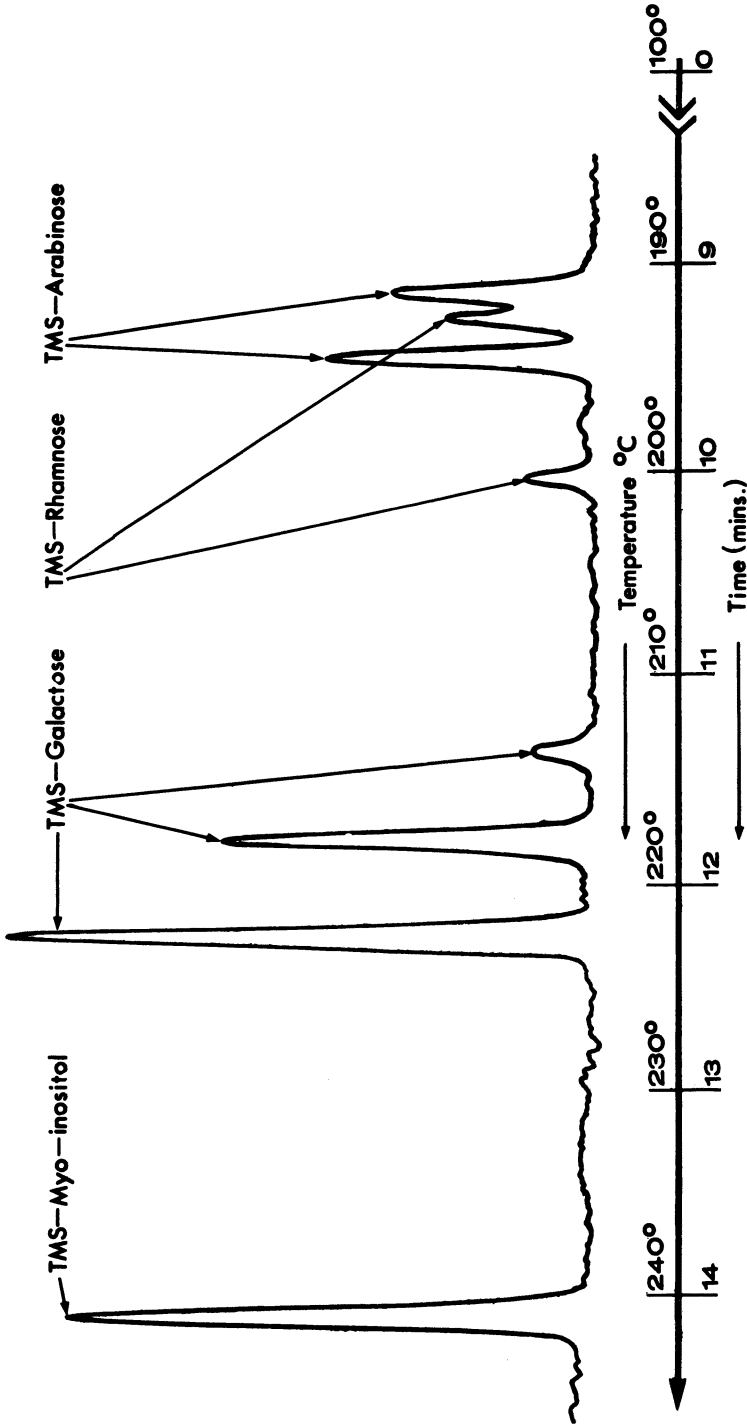


Figure 9. Tracing of an actual chromatograph of the trimethylsilyl ethers of those monosaccharides liberated in the hydrolysis of the gum of *Acacia senegal*.

position. An appropriate spot test for furaldehyde (33) has been made semi-quantitative by testing successive dilutions of furfural (2-furaldehyde) in water. To run this test, a 25-mL ceramic crucible is placed in a tray of water at 40 °C and the drop of hydrolysate is placed at the bottom. A drop of 10% aniline in acetic acid is placed on a piece of filter paper covering the crucible. A watchglass is then used to weight this down. In the presence of furfural vapors this spot will turn bright pink with the formation of a Schiff base. The intensity of this spot and the time required for its appearance are taken as indicative of the concentration of furfural in the hydrolysate. (Within limits, the vapor pressure of furfural over the droplet should be proportional to its concentration in the liquid.) The results appear in Table I. The hydrolysate is then passed through a two-bed ion exchange column. The top layer, consisting of Dowex 50- \times 8 H⁺ form, removes any alkali cations and associated uronic acid anions. The hydrolysate is then neutralized by the exchange of Cl⁻ for CO₃⁼ on the lower bed consisting of Amberlite IRA-45. The monosaccharide solution is then concentrated to about 0.2 mL in a rotary film evaporator. (A somewhat larger volume is left if thin layer separation is to be used. This material is applied directly to the activated plate.) A syringe is used to transfer the concentrate to a sealable vial, where the silylation will ultimately be carried out. Prior to derivatization, the remaining water is removed by freezing the solution and drying over phosphoric anhydride in a vacuum. Silylation is carried out with a commercially prepared reagent mixture containing *N*-trimethylsilylimidazole in pyridine (Tri-Sil Z, Pierce Chemical Co.). This reaction mixture is withdrawn from the septum vial and is injected directly into the gas chromatograph.

Thin layer plates having a 0.25-mm coating of silica gel were developed in a solvent of benzene:1-butanol:pyridine:water; 9:41:25:25 (upper layer). Visualization was accomplished by spraying with 10% sulfuric acid in ethanol or 0.2% 1,3-dihydroxynaphthalene in 10% phosphoric acid in ethanol (34) followed by heating at 100 °C for 10 min. The first reagent merely chars the monosaccharides while the second forms blue-green derivatives. Both methods give slightly different shades with each monosaccharide. R_f values of standard samples are given in Table II for this solvent system when used twice in a multiple development scheme. The plate is developed one-half the distance, removed, dried, and then replaced in the tank to develop the full length. This procedure provides slightly sharper resolution and wider separation of the monosaccharides. GLC is performed on a Perkin-Elmer F-11 capillary gas chromatograph. Detection is performed by flame ionization with a modified amplifier in which the original electrometer has been replaced by a parametric amplifier.

Table I. Decomposition Test

<i>Furaldehyde</i> Concentration (M)	Corresponding Molar Decomposition (%)	Result Observed
1.2×10^{-4}	0.2	Instantaneous bright pink.
1.2×10^{-5}	0.02 ^a	Bright pink after 10 s.
1.2×10^{-6}	0.002 ^a	Pink after 15 s.
1.2×10^{-7}	0.0002	Light pink after 1 min.
1.2×10^{-8}	0.00002	Extremely faint pink after 3 min.

^a Most gum hydrolysates fell into this range.

Table II. R_f Values Derived from Thin Layer Chromatography

Standards		<i>Acacia senegal</i>	<i>Cochlospermum gossypium</i>	<i>Astragalus verus</i>	<i>Sterculia urens</i>
Galactose	0.341	0.338	0.341	0.340	0.343
Arabinose	0.457	0.457	—	—	—
Mannose	0.457	—	—	—	—
Xylose	0.574	—	—	—	—
Rhamnose	0.740	0.733	0.740	0.744	0.742
Uronic Acids					
Glucuronic	0.073	0.073	—	—	—
Galacturonic	0.102	—	0.102	0.099	0.100

Conditions: Solvent: benzene:*n*-butanol:pyridine:water, 1:5:3:3 (upper layer); stationary phase: silica Gel, 0.25 mm thick; development: ascending multiple development (twice), one-half distance (7.0 cm) first run, full length (14.0 cm) second run.

The column, precoated and purchased from Perkin-Elmer, is a support-coated open tubular (SCOT) column made of stainless steel with an inside diameter of 1 mm and a length of 30.8 m. The liquid phase consists of a nonpolar methyl silicone oil, OV-101. Initially, the column had 88,000 theoretical plates, as calculated from the resolution and retention time of trimethylsilyl myoinositol. The carrier gas is helium with a flow rate of 3 mL/min at the detector. In operation, a sample splitter is used that consists of a 0.025-mm i.d. hypodermic needle venting the injection chamber. One microliter of the silylation mixture is injected and a programmed linear temperature increase begins at a rate of 10 °C/min from the initial 100 °C. As the column aged and lost some of its resolution due to column bleed, we were able to compensate by increasing the rate of temperature increase. Over a period of time the combustion of silyl compounds in the detector coats the collector electrode with silica. This coating reduces sensitivity but, within limits, does not seriously affect quantitation. An excellent paper (35) deals with the quantitative aspects of gas chromatography utilizing various detectors and standardizing techniques. The reader is referred to this publication for a background.

Myoinositol was chosen as an internal standard for quantification and to mark the end of the elution of the monosaccharides. The flame ionization detector has an excellent linearity over five orders of magnitude, but response to each compound is slightly different owing to the individual bonding situations of its carbon atoms. In order to establish a common base for quantifying the different monosaccharides, we have prepared a molar response graph from standard mixtures (Figure 10). The slope of the line described by plotting the ratio of the area response for a particular trimethylsilyl monosaccharide to that of trimethylsilyl myoinositol versus the molar ratio of the two is a quantity called the relative molar response (RMR). This value is a characteristic of the monosaccharide and is used to determine the proportion of that monosaccharide in an unknown mixture by the following relations:

$$\frac{A_{S1}}{A_I} \frac{1}{RMR_{S1}} = \frac{\text{moles of S1}}{\text{moles of I}} = B_{S1}$$

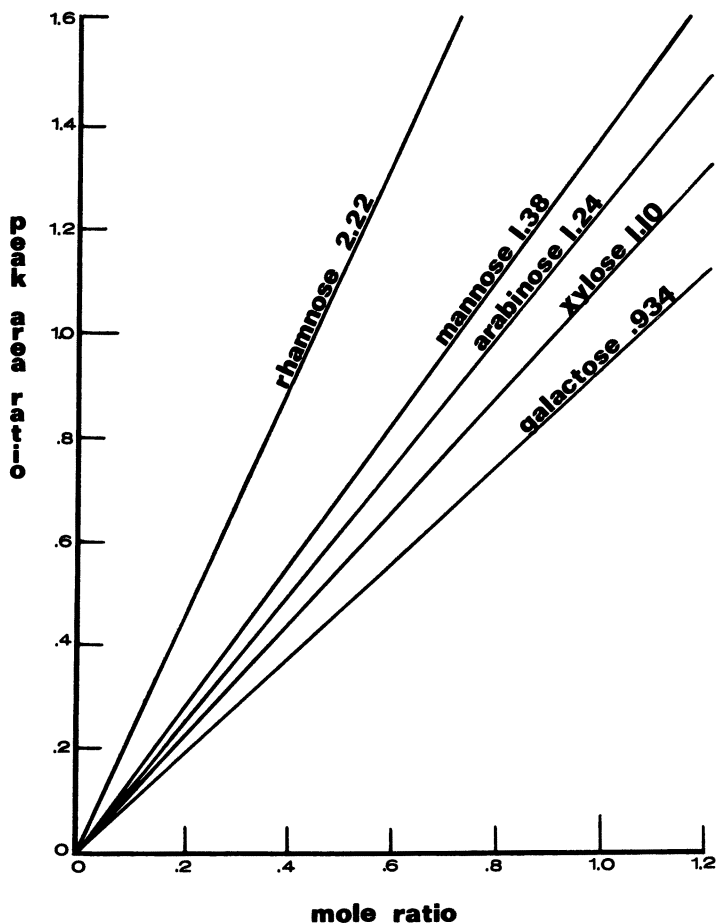


Figure 10. Molar response of trimethylsilyl sugars relative to trimethylsilyl myoinositol. The slopes of these lines make accurate quantification possible from the gas chromatograph by normalizing the detector response for each trimethylsilyl monosaccharide.

and,

$$\frac{B_{S1}}{\sum_{x=1}^y B_{Sx}} = \% S1$$

where A_{S1} is the area sum of all isomers of the trimethylsilyl monosaccharide S1, A_x is the area of trimethylsilyl myoinositol, RMR_{S1} is the relative molar response of the trimethylsilyl monosaccharide, and y is the number of monosaccharides present in the hydrolysate.

We have calculated the peak areas by Simpson's one-half height rule.

IR spectra were obtained from potassium bromide pellets on a Beckman IR-12 spectrophotometer.

Results

Hydrolysis of the gums was often accompanied by the formation of a small amount of fluffy precipitate. Several gums that initially dissolved completely to give crystal clear solutions produced more of this brown residue than did gums that lacked clarity and ready solubility. These precipitates are denatured proteins or tannins often detected in plant gums. In two cases, those of *Anogeissus latifolia* and *Astragalus gummifer*, the hydrolysis was insufficient to cleave the more stable portions of the molecule. Those portions which were initially insoluble remained so but retained a white color quite different from the dark residue found in some other hydrolyses. Decomposition by the pathway shown previously was found to be less than 1% in every case tested.

There are a great many different solvent systems for use with monosaccharides in thin layer chromatography (TLC). Most of them give the same ordering, and all of the ones we tested share the inability to resolve arabinose and mannose under visual examination. The difference in R_f for these two was never greater than 2% of the total solvent travel. Table II shows the R_f values of the standard monosaccharides and four representative gums. It is not necessary to remove uronic acids prior to TLC. D-Glucuronic acid and D-galacturonic acid can be resolved in the usual solvents for neutral monosaccharides if they survive the hydrolysis in sufficient quantities to be detected.

Quantitative monosaccharide profiles obtained via GLC are shown in Table III. In general, they agree well with the data available from the literature that were obtained by classical derivatization procedures. It must be remembered that most data available come from structural studies, which always employ some means of purifying the crude gum to obtain material of uniform molecular weight (36). (Repeated precipitation from water by ethanol is usually used.) This process may eliminate some labile monosaccharides or sidechains that have already been cleaved by autohydrolysis, resulting in legitimate disagreement outside of experimental error. Quantification by internal standardization has been shown to be as much as 1% accurate for compounds of this type (37,38). Prior to substitution of a parametric amplifier for the electrometer, we tested the quantification of the method by chromatographing trimethylsilyl derivatives of a group of three weighted mixtures containing different amounts of five monosaccharides each. Three runs of each were averaged and the standard deviation was calculated. The average percent error was found to be $\pm 3\%$. This amount is roughly the error in weighing plus that

Table III. Composition by Gas-Liquid Chromatography (data given as percentage of neutral monosaccharides)

<i>Species and Origin</i>	<i>Arabinose</i>	<i>Rhamnose</i>	<i>Galactose</i>	<i>Mannose</i>	<i>Xylose</i>
<i>Acacia longifolia</i> (cultivated), Riverside, Calif., native to Australia	~ 6	31.0	44.9	18.1	—
<i>A. nilotica</i> , Lower Umkomanzi, Natal	64.7	Undetermined	35.3	Trace	—
<i>A. senegal</i> , Sudan	29.3	7.3	63.3	—	—
<i>A. seyal</i> , Sudan	36.4	17.7	45.9	—	—
<i>Albizia amara</i> , Salem Forests, Madras	77.4	—	22.6	—	—
<i>A. stipulata</i> , West Bengal	95.9	—	4.1	—	—
<i>Anogeissus latifolia</i> ^a , North Arcot, Madras	88.3	—	—	11.7	—
<i>Astragalus gummifer</i> ^a , Lebanon Grove	85.9	—	14.1	—	—
<i>A. verus</i> , West Persia	—	37.9	62.1	—	—
<i>Cochlospermum gossypium</i> , Karachi, Pakistan	—	25.5	74.5	—	—
<i>Prosopis spicagera</i> , Salem Forests, Madras	72.2	—	22.0	5.8	—
<i>Prunus armeniacum</i> , India	55.2	—	37.8	7.0	—
<i>P. armeniacum</i> , (cultivated), Sacramento, Calif.	63.6	—	32.4	~ 4	—
<i>P. armeniacum</i> ^b (untended), Riverside, Calif.	59.3	—	35.5	5.2	Trace
<i>P. armeniacum</i> , average of above three	59.4	—	35.2	5.4	—
<i>Sterculia cinera</i> , Sudan	—	35.0	65.0	—	—
<i>S. urens</i> , Central India	—	34.7	65.3	—	—
<i>S. villosa</i> , Darjeeling Terai, Bengal	—	30.4	69.6	—	—
<i>Terminalia belerica</i> , West Bengal	72.2	—	27.8	—	—
<i>T. tomentosa</i> , India	81.3	7.0	18.7	—	—

^a See text.

^b Sample showed signs of considerable weathering; portion used in analysis was taken from center of tear.

inherent in the flame ionization detector and peak measurement. After the addition of the parametric amplifier and resulting noise reduction, an independent determination of monosaccharide content from three separate hydrolyses of the same gum sample has shown our method to be reproducible to $\pm 2.3\%$ for the entire process.

The data for *Anogeissus latifolia* suggest that perhaps the gum sample has been altered by time or storage conditions. The literature is unanimous in its description of this gum as soluble and translucent. Our sample was black, opaque, and insoluble (Figure 3). Soaking in water caused the gum to swell to several times its size with no loss of shape.

The utility of the method is clear from the results in Table III. In all cases except those of the three representatives of the genus *Sterculia*,

there is a definite line of demarcation between gums within the same genus. In only one case is there a confusion between genera—*Astragalus verus* is similar to *Sterculia cinerea* in composition. Undoubtedly as more profiles are obtained others will tend to overlap compositionally as well. However, an investigation of geographic availability as described earlier should eliminate most of the ambiguity when applied to a given artifact.

Acknowledgments

We wish to thank the officers of the Royal Botanical Gardens, London, for providing the authentic gum samples for this study. Ben B. Johnson is to be thanked for his observations on the techniques of Mughal painting as he has observed them in the collection of the Los Angeles County Museum of Art. We thank Peter Dammers for his technical assistance in the GC phase of this investigation. The IR spectrophotometer was made available for our use by the research department of Bourns, Inc. Above all, we wish to express our appreciation to Thomas Cairns, formerly of the Los Angeles County Museum of Art, for his role in initiating this work.

Appendix: Compendium of Gum-Yielding Genera

Although certainly not exhaustive, this list has been made as complete as possible from the limited number of references on the subject. All species that are reliably stated to yield gums have been included along with as much information as could be obtained on geographic location and native usage. Only the more common names have been retained for the gums because some also have an endless list of native names and variant spellings (e.g., acacia gum of unknown species has been called Sudan gum, Kordofan gum, Khartoum gum, Turkey gum, Senaar gum, Geddaref gum, Jeddah gum, Sennari gum, Turic gum, Gehzirah gum, Berbera gum, gomme de Galan, gomme de Podor, gomme de Tombouctou, Sunt gum, Suakim gum, and more; most of these names have their origin in some long unused trade route).

<i>Gum-Yielding Genera</i>			
<i>Species</i>	<i>Terminology</i>	<i>Location</i>	<i>Notes</i>
<i>Acacia abyssinia</i> (2,5)	—	Sudan	—
<i>A. albida</i> (2,5)	—	Uganda, Tanganyika, Kenya, northern Rhodesia, Sudan	Edible gum.
<i>A. arabica</i> (2,5,39) (synonym: <i>A. nilotica</i>)	Morocco gum, Mogodor gum, Brown Barbary gum, Amrad gum, Sunt gum	Sudan, Nigeria, Morocco, India, Assam, Burma, Ceylon	Howes says that this gum predominates on local markets in India (5).

<i>Gum-Yielding Genera</i>			
<i>Species</i>	<i>Terminology</i>	<i>Location</i>	<i>Notes</i>
<i>Acacia ataxacantha</i> (2)	—	—	—
<i>A. baileyana</i>	—	South Africa	—
<i>A. bakeri</i> (41,5)	—	Australia	—
<i>A. benthami</i>	—	South Africa	—
<i>A. binervata</i> (2,5)	—	Australia	Contains both a soluble and an insoluble fraction.
<i>A. caffra</i> (2)	—	—	—
<i>A. campylacantha</i> (5)	—	Eastern Africa, Sudan	—
<i>A. catechu</i> (2,5,39)	Khair gum	India, Burma, Ceylon	Locally called Ghatti gum (2).
<i>A. cochlearis</i> (2)	—	—	—
<i>A. cunninghamii</i> (41,5)	—	Australia	—
<i>A. cyanophyllia</i>	—	Eastern Africa, South Africa	—
<i>A. dealbata</i> (41,5)	—	Australia, Java	Gives a very viscous solution.
<i>A. decurrens</i> (2,41)	—	Australia, Java, India, South Africa	—
<i>A. detinens</i> (2)	—	—	—
<i>A. drepanolobium</i> (5)	"Ilula lyapi"	Uganda, Sudan, Tanganyika	—
<i>A. dudgeoni</i> (2)	—	—	—
<i>A. eburnea</i> (2)	—	—	—
<i>A. ebrenbergiana</i> (2)	—	—	—
<i>A. elata</i> (5)	—	Australia, South Africa	—
<i>A. erabescens</i> (2)	—	—	—
<i>A. etbaica</i> (2)	—	—	—
<i>A. farnesiana</i> (2,5,39)	Karachi gum	India, Burma, Australia, Dead Sea Valley, cultivated in Europe, Sudan	—
<i>A. ferruginea</i> (2,5,39)	—	India	—
<i>A. fischeri</i> (5)	—	India, eastern Africa	—
<i>A. flava</i> (5)	—	Sudan	—
<i>A. formicarum</i>	—	Eastern Africa	—
<i>A. giraffae</i> (2,13)	Cape gum	South Africa	—
<i>A. glaucescens</i> (5)	—	Australia	Very good adhesive mucilage.
<i>A. glaucophylla</i> (2)	—	—	—
<i>A. gummifer</i>	Morocco gum, Morador gum, Brown Barbary gum	Morocco	—
<i>A. harpophylla</i> (41)	—	Australia	—
<i>A. homalophylla</i> (2)	—	Australia	Soluble gum.
<i>A. horrida</i> (2,13)	Cape gum	South Africa	—
<i>A. jacquemontii</i> (2,5,39)	—	Australia, India	—
<i>A. karroo</i> (synonym: <i>A. horrida</i>)	Angra Pequena gum, Cape gum	South Africa	—
<i>A. kirkii</i> (2,5)	—	Eastern Africa, Sudan	—
<i>A. krausiana</i> (2)	—	—	—

Continued on next page.

<i>Gum-Yielding Genera</i>			
<i>Species</i>	<i>Terminology</i>	<i>Location</i>	<i>Notes</i>
<i>Acacia latronum</i> (2)	—	—	—
<i>A. leata</i> (2,5)	—	Sudan	—
<i>A. leiophylla</i> (41)	—	Australia	—
<i>A. lenticularis</i> (2)	—	—	—
<i>A. leucophloea</i> (2,5,39)	Gum of Belli Falli	India	Insoluble.
<i>A. longifolia</i>	—	Australia	Soluble.
<i>A. macrostachya</i> (2)	—	—	—
<i>A. maideni</i> (41)	—	Australia	—
<i>A. malacocephala</i> (5)	—	Eastern Africa	—
<i>A. mearnsii</i>	—	South Africa	—
<i>A. mellifera</i> (2)	—	—	—
<i>A. microbotrya</i> (2)	—	—	—
<i>A. modesta</i> (2,5,39)	Armitsar Gum, gum mumrah	Sub-Himalayan areas	—
<i>A. mollissima</i>	—	Australia	Said to be synony- mous with <i>A. de-</i> <i>currens</i> by some authors.
<i>A. orfota</i> (5)	—	Sudan	—
<i>A. oswaldi</i> (41)	—	Australia	—
<i>A. pendula</i> (2,5) (synonym: <i>A. gla-</i> <i>brata</i>)	—	India	Entirely soluble.
<i>A. penninervis</i> (2,41)	—	Australia	—
<i>A. planifrons</i> (2)	—	—	—
<i>A. podalyriaefolia</i>	—	South Africa	—
<i>A. pycnantha</i> (2,39)	—	Australia, India, South Africa	—
<i>A. rehmanniana</i> (2)	—	—	—
<i>A. retinoides</i> (41)	—	Australia	—
<i>A. robusta</i> (2)	—	—	—
<i>A. salicina</i> (41)	—	Australia	—
<i>A. senegal</i> (2,39)	Gum Arabic, kolkol (Nigeria Turkey gum (obsolete, Middle Ages), East India gum, kami (Ancient Egyptian manu- scripts)	Northern and cen- tral Africa. Oc- curs at least as far south as Tangan- yika and extends east to the Sind region of India. Not found in the remainder of the subcontinent.	Predominant yielder north of the Sa- hara. Large stands exist in Senegal and the El Obeid region of Egypt, which are free of other species. Ex- ported to Bom- bay from Africa and then re-ex- ported, known as East India gum.
<i>A. sentis</i> (5)	—	India	Entirely soluble (5).
<i>A. seyal</i> (2,5)	Suakim gum, tahl gum, talca gum, talha, talki	Tanganyika, Sudan	Tapping does not induce gum exu- dation (5).
<i>A. sieberiana</i> (2,5) (synonym: <i>A. ne-</i> <i>fasia</i>)	—	Eastern Africa, Su- dan	—

<i>Gum-Yielding Genera</i>			
<i>Species</i>	<i>Terminology</i>	<i>Location</i>	<i>Notes</i>
<i>Acacia spiricarpa</i> (2,5)	Morocco gum, Mogador gum, Brown Barbary gum	Tanganyika, Sudan	—
<i>A. stenocarpa</i> (5)	Suakim gum, Tolca gum, Talha gum	Tanganyika, Sudan	—
<i>A. striata</i> (2)	—	—	—
<i>A. stublmanii</i> (2,5)	—	Tanganyika, Kenya	—
<i>A. suma</i> (2)	—	India	—
<i>A. sundra</i>	—	India	—
<i>A. thunbergiana</i> (5)	—	Sudan	—
<i>A. tortilis</i> (2)	—	—	—
<i>A. verniciflua</i> (41)	—	India	—
<i>A. vestita</i>	—	Australia	—
<i>A. xanthoploea</i>	Morrua	Eastern Africa	—
<i>A. xiphocarpa</i> (synonym: <i>A. abyssinia</i>)	Aden gum	Eastern Africa	—
<i>Adansonia digitata</i>	Baobob gum	Eastern Africa	Insoluble.
<i>A. gregorii</i> (41)	—	Northwest Australia	Sour Gourd, Cream of Tartar tree.
<i>Adenanthera pavonina</i> (41)	Modatsa gum	Australia, Ceylon, cultivated in eastern Africa	Red Sandalwood.
<i>Aegle marmelos</i> (47)	Bael gum	India	—
<i>Afzelia africana</i>	—	Eastern Africa	—
<i>Ailanthus excelsa</i> (39)	—	India	Insoluble.
<i>Albizzia amara</i> (13)	—	Eastern Africa, India	—
<i>A. antihelmintica</i>	—	Eastern Africa	—
<i>A. brownei</i>	Nongo Gum	Nigeria, Bukedi district of Uganda	Very viscous and only partially soluble.
<i>A. harveyi</i> (synonym: <i>A. hypoleuca</i>)	—	Eastern Africa	—
<i>A. lebbek</i> (2,13) (synonym: <i>Acacias sirissa</i> and <i>speciosa</i>)	Gum shiraz, gum mamrah	Eastern Africa	—
<i>A. odoratissima</i> (13)	Gum khota, gum mamrah	Eastern Africa	—
<i>A. procera</i> (41,13)	—	Northwest Australia, cultivated in eastern Africa	Copious yielder of gum.
<i>A. pruinosa</i> (41)	—	Australia	Stinkwood.
<i>A. stipulata</i> (2,13)	Gum khota (5)	Sub-Himalayan India, cultivated in eastern Africa	Howes says that this gum was used by the Nepalese to size paper made from <i>Daphne</i> leaves but gives no details (5).

Continued on next page.

<i>Gum-Yielding Genera</i>			
<i>Species</i>	<i>Terminology</i>	<i>Location</i>	<i>Notes</i>
<i>Albizia toona</i> (41)	—	Australia	—
<i>Aleurites molluccana</i> (2,41)	—	Australia, India, South Pacific Is- lands	South Sea Islanders eat this gum.
<i>Anacardium occiden- tale</i> (2,13)	Cashew gum, Aca- jou gum	South and Central America. Carried to eastern Africa and India shortly after discovery of the New World.	The gum contains phenolic irritants. It has been used as an insect-repel- lent coating.
<i>Anogeissus latifolia</i> (2,5)	Ghatti gum, Gatty gum	India, Ceylon	This is the true Ghatti gum al- though <i>Acacia ca- techu</i> or anything from the "West- ern Ghats" has been called Ghatti. Said to be 90% dispersible, but our sample was insoluble.
<i>A. schimperi</i>	—	Eastern Africa	Soluble, edible gum.
<i>Astragalus adsendens</i> (5)	—	Southern and south- western Iran	—
<i>A. brachycalyx</i> (5)	—	Iranian Kurdistan and Luristan	—
<i>A. cretious</i> (5)	—	—	—
<i>A. cylleneus</i> (5)	—	—	—
<i>A. eriostylus</i> (5)	—	Luristan	—
<i>A. gummifer</i> (5)	Gum tragacanth, Smyrna traga- canth, Anatolian tragacanth, Per- sian tragacanth	Northern Kurdis- tan, Armenia, Asia Minor, Syria, and eastern Africa	Gum contains two fractions, only one of which is soluble.
<i>A. heratensis</i> (5)	—	Khroason to Af- ghanistan	—
<i>A. kurdicus</i> (5)	—	Southern Kurdistan to Asia Minor and Syria	—
<i>A. leiocladus</i> (5)	—	Western and central Iran	—
<i>A. microcephalus</i> (5)	—	—	—
<i>A. multiceps</i> (39)	—	Simla, Kumaon, Garwal, Western Himalya 10,000- 12,000 ft (39)	Tibetans make a strong paper from the roots (39). Dymock, in "Ma- teria Medica of western India," says that these gums are the an- cient "Sarcocolla" (43).
<i>A. pycnocladus</i> (5)	—	Kermanshab (Shaha and Avroman Mts.)	—

<i>Gum-Yielding Genera</i>			
<i>Species</i>	<i>Terminology</i>	<i>Location</i>	<i>Notes</i>
<i>Astragalus strobiliferus</i> (5)	—	Eastern Iran	—
<i>A. stromatodes</i> (5)	—	—	—
<i>A. verus</i>	—	Western Iran	—
<i>Atalaya hemiglauca</i> (41)	—	Australia	—
<i>Azadirachta indica</i> (2,5) (synonym: <i>Melia azadirachta</i> , <i>M. composta</i> , and <i>Antalaea azadi- rachta</i>)	Neem gum, Go- homba gum	India, Australia	Ancient Indian pharmaceutical (5).
<i>Balanites wilsonia</i>	—	Eastern Africa	—
<i>Bassia longifolia</i> (13)	Mahua gum (13)	India	—
<i>Bauhinia carronii</i> (41)	—	Australia	Heavy yielder of a soluble gum.
<i>B. fassoglensis</i>	—	Eastern Africa	—
<i>B. hookeri</i>	—	Australia	—
<i>B. purpurea</i> (2)	—	India	—
<i>B. retusa</i> (13)	Semla gum	India	—
<i>B. thonningii</i> (syn- onym: <i>B. reticu- lata</i>)	—	Eastern Africa	—
<i>B. variegata</i> (2,13)	Semla gum	India	—
<i>Bombax malabaricum</i> (39,41)	Mocharas gum (5)	India, eastern Af- rica, Australia	Indian Silk Cotton tree.
<i>Brachystegia spicifor- mis</i>	—	Eastern Africa	This species domi- nates woodlands of this genus (42).
<i>Buchanania lanzan</i> (synonym: <i>B. lati- folia</i>)	Peal gum, Pial gum, Chironji gum (13)	India, Burma	—
<i>Butea frondosa</i> (13)	Local adulterant of Karaya	—	—
<i>Capparis nobilis</i> (41)	—	Australia	"Wild lemon."
<i>Cedrela australis</i> (41)	—	Australia	May be synonymous with <i>C. toona</i> of India (37).
<i>C. toona</i>	—	India	—
<i>Ceiba pentandra</i>	—	India	Kapok tree, Indian substitute for ku- tira (5).
<i>Ceratonia siliqua</i>	Carob tree gum, Tragasol gum	Eastern Africa, Mid- dle East	This is not an exu- date gum but a seed mucilage from the pod or "locust bean." It is included owing to its wide utiliza- tion by the an- cients.
<i>Chloroxylan swie- tenia</i> (5)	—	India	—
<i>Chukrasia tabularis</i> (13)	—	India	—
<i>Cochlospermum gossyp- ium</i> (5,39)	Kutira gum, kuteera gum, katira gum,	India, Ceylon, Burma, Thailand,	A partially acety- lated gum which

Continued on next page.

<i>Gum-Yielding Genera</i>			
<i>Species</i>	<i>Terminology</i>	<i>Location</i>	<i>Notes</i>
<i>Cochlospermum gossypium</i> cont'd	Kadaya Gum	Indochina, Malay Peninsula	is insoluble. Persian writers called tragacanth "kutira," "katira," or "kathira"; Mohammedans coming into India with the Mogul conquest called the gum of <i>C. gossypium</i> by these names. Chandra (7) describes the preparation of the insoluble portion of this gum by soaking it and then pressing it through a cloth. The pulp was used as a medium for mica powder.
<i>Cola cordifolia</i>	—	Uganda	Rare species.
<i>Combretum apiculatum</i>	—	Central Africa	Soluble gum.
<i>C. bindersia</i> (synonym: <i>C. collinum</i>)	—	Central Africa	—
<i>C. guienzii</i>	—	Central Africa	—
<i>C. longispecatum</i>	—	Central Africa	—
<i>C. purpureiflorum</i>	—	Central Africa	—
<i>C. zeyheri</i>	—	Central Africa	—
<i>Commiphora iringensis</i>	—	Eastern Africa	This genus yields many important resins such as myrrh but may yield gums from some species.
<i>C. ugogoensis</i>	—	Eastern Africa	See above.
<i>Conocarpus latifolia</i> (43)	—	India	Gum has erroneously been sold as Ghatti.
<i>Cordia gharaf</i> (synonym: <i>C. rothii</i>)	—	Central Africa, India	Soluble astringent gum used as a gargle in India.
<i>Cyamopsis tetragonolobus</i>	Guar gum	Pakistan, India, southwestern United States (since 1900)	Grown as a forage crop. The gum is a seed mucilage rather than an exudate. The endosperm is removed by milling and sold as Guar gum.
<i>C. psoraloides</i>	Guar gum	See above	See above.

<i>Gum-Yielding Genera</i>			
<i>Species</i>	<i>Terminology</i>	<i>Location</i>	<i>Notes</i>
<i>Cycas circinalia</i>	Cycas gum	Cultivated in central Africa	Insoluble.
<i>Delonix elata</i>	—	Central Africa	—
<i>D. regia</i> (2,5)	—	India, central Africa	Good, soluble gum.
<i>Dichrostachys glomerata</i>	—	Central Africa	—
<i>Echinocarpus australis</i> (41)	—	Australia	—
<i>Elaeodendron roxburghii</i> (5)	—	India	Good, soluble gum (5).
<i>Erythrophloeum africana</i>	—	Central Africa	—
<i>Feronia elephantum</i> (2,5) (synonym: <i>F. acidissima</i>)	Ketha gum (8), woodapple gum (5), Gum Sanskrit (43), Dadhittharasa (43)	India, Java	Combined with acacia gums and sold in India. Howes (5) (quoting K. Heyne, 1927) says that the Javanese make ink with this soluble gum.
<i>Ficus glorometa</i>	—	India	Used to prevent tarnishing of brass leaf used in cheap Indian paintings (7).
<i>Flindersia australia</i> (41)	—	Australia	—
<i>F. bennettiana</i> (41)	—	Australia	"Teak."
<i>F. maculosa</i> (41)	—	Australia	Leopard tree.
<i>Grevillea robusta</i>	—	Australia	Australian silk "oak."
<i>Heritiera littoralis</i> (41)	Mendora gum	Ceylon, Australia	Red mangrove.
<i>Hibiscus heterophyllus</i> (41)	—	Eastern Australia	—
<i>Khaya grandifolia</i>	Khaya gum	Western Africa, Uganda	West African "mahogany."
<i>K. senegalensis</i>	Khaya gum	Western Africa	—
<i>Lannea acida</i>	—	Western Africa	Soluble.
<i>L. barteri</i>	—	Uganda	—
<i>L. fruticosa</i>	—	Uganda	—
<i>L. grandis</i> (2) (synonym: <i>Odina woderia</i> (5,39))	Jeol gum (8)	India, Burma, Ceylon, Indochina	Nepalese use this as a paper size (5). This is said to be Bengal's largest producer of gum. It is used in whitewash there. (39)
<i>Leschensultia divaricata</i> (41)	—	Australia	Aborigines extract a root gum to use as a cement.
<i>Lophira alata</i>	—	Central Africa	—
<i>Mangifera indica</i> (2)	—	India	—

Continued on next page.

Gum-Yielding Genera

Species	Terminology	Location	Notes
<i>Melia azedarachta</i> (41,13) (synonym: <i>M. composita</i>)	Neem gum (8)	Introduced to central Africa	—
<i>Moringa pterygasperma</i> (13,39) (synonym: <i>M. oleifera</i>)	Drum Stick (tree) gum (8), Sajna gum (46)	Cultivated throughout India and Burma, central Africa	Horse Radish Tree, "drum stick tree" (39). Gum contains 75% cellulose.
<i>Opuntia fulgida</i>	Cholla gum (8)	Mexico, southwestern United States	This species and other cacti of woodlike structure are yielders of gum.
<i>Pithecellobium dulce</i>	—	India	—
<i>P. saman</i>	—	India	—
<i>Pittosporum phylliroeoides</i> (41) (synonym: <i>P. acacioides</i>)	—	Australia	Useful soluble gum.
<i>Phyllanthus emelica</i>	—	India	Used with soot from mustard oil (<i>Sesamum indica</i>) for ink (41).
<i>Prosopis dulcis</i>	Mesquite gum, Mezquite gum, Sonora gum, "Mexican gum arabic"	Southwestern United States, northern Mexico	The seedpod of this plant (the screwbean) is edible and forms part of the diet of range cattle.
<i>P. glandulosa</i>	See above	See above	See above.
<i>P. juliflora</i>	See above	See above	See above.
<i>P. spicigera</i>	Parambai	India	See above.
<i>Prunus amygdalus</i> (5,39)	Almond tree gum, carmnania gum	Species of <i>Prunus</i> have been transported to all temperate zones of the world. Any distribution must be related to a time period to be meaningful.	None of the <i>Prunus</i> gums is entirely soluble. All have been referred to as "cherry gum."
<i>P. armeniacum</i> (5,39)	Apricot gum	See above	See above.
<i>P. avium</i> (39)	—	Originated in Europe. Grows wild as far as northern Persia, cultivated as far as northwestern Himalaya	Wild cherry, sweet cherry.
<i>P. cerasus</i> (5,39)	Cherry gum	See <i>P. amygdalus</i>	Sour cherry, dwarf cherry.
<i>P. communis</i> (39)	—	See <i>P. amygdalus</i>	Plum.
<i>P. domestica</i> (5,8)	Plum tree gum	—	—
<i>P. eburnea</i> (5)	—	See <i>P. amygdalus</i>	Plum.

Gum-Yielding Genera

<i>Species</i>	<i>Terminology</i>	<i>Location</i>	<i>Notes</i>
<i>Prunus insitia</i> (8)	Damson gum	See <i>P. amygdalus</i>	Plum.
<i>P. mahaleb</i> (39)	—	—	—
<i>P. padus</i> (39)	—	—	Bird cherry.
<i>P. persica</i> (5,39)	Peach gum	China ca. 2000 B.C., spread to India about 1000 B.C. and then to Europe [Watt (39)].	Peach or nectarine; these bear no permanent botanical separation.
<i>P. prostrata</i> (39)	—	—	Scrub brush.
<i>P. puddum</i> (39)	—	Himalaya	Wild Himalayan cherry.
<i>P. virginiana</i> (8)	—	United States	Choke cherry.
<i>Pseudocedrela kotschyi</i>	—	Central Africa	Used as an ingredient in poison for arrow tips, apparently as a thickener (42).
<i>Pterocarpus marsupium</i> (13)	Kino gum	Africa	Various other trees produce forms of resin denoted by the name "kino."
<i>Rhizophora mucronata</i> (41)	—	Pacific Islands	The red sap is used by the Fijians to dye hair. Mixed with the sap from <i>Hibiscus moschatus</i> it is used by potters to paint crockery (41). This is not a true gum.
<i>Saccopetalum tomentosum</i> (39)	—	India	Fairly soluble and adhesive.
<i>Sapindus saponaris</i>	Soap berry	India	Media for water color on hydrophobic surfaces.
<i>S. trifoliatus</i> (13)	Soap, not true gum (13)	—	—
<i>Schefflera volkensii</i>	—	Mountainous central Africa	—
<i>Sclerocarya birrea</i>	—	Central Africa	—
<i>Spondias cytheria</i>	Golden Apple gum (8)	West Indies	—
<i>S. dulcis</i> (44)	—	India	—
<i>S. pinnata</i> (2,45)	—	India, tropical Asia	—
<i>Sterculia acerifolia</i> (5)	—	Australia	—
<i>S. barteri</i> (5)	—	Africa	—
<i>S. caudata</i> (synonym: <i>S. brachychiton</i>)	—	Northwestern Australia	—
<i>S. cinerea</i> (5)	Tartar Gum	Uganda, Kenya, Tanganyika	—
<i>S. companulata</i> (5)	—	India	—

Continued on next page.

<i>Gum-Yielding Genera</i>			
<i>Species</i>	<i>Terminology</i>	<i>Location</i>	<i>Notes</i>
<i>Sterculia foetida</i> (5)	Gum of Temboo	India	—
<i>S. guttata</i> (5)	Gum of Pen Than- aka	India	—
<i>S. hypochroa</i> (5)	—	Indochina	—
<i>S. ornata</i> (5)	—	India	—
<i>S. platanifolia</i> (5)	—	Australia	—
<i>S. quadrifida</i> (41,5)	—	Australia	—
<i>S. scaphigera</i> (5)	—	China	Gum occurs only in the fruit. It is eaten by the Chinese, who call it "ta-hai-tsze" (5).
<i>S. setigera</i> (synonym: <i>S. tomentosa</i>) (5)	Kandi gum, da gum	Nigeria	In contrast to most gum yielders this species produces more when well watered (46).
<i>S. thorelli</i> (5)	—	Indochina	—
<i>S. tragacantha</i> (5)	—	Africa	—
<i>S. urens</i> (5,39)	Karaya gum, Indian tragacanth	North and central India	Occasionally sold as kutira; often exudes immediately upon incision of any part of tree, including the leaves (43).
<i>S. villosa</i> (5)	—	India	—
<i>Stereospermum suaveolens</i> (39)	—	Sub-Himalayan areas	Insoluble.
<i>Swietenia mabogoni</i>	—	India, introduced to Africa	—
<i>Symphonia globulifera</i> (39)	—	West Indies, America	—
<i>Tamarindus indica</i>	—	India	This produces a seed mucilage that is one ingredient in a general-purpose paste used by the Mughal painters (7).
<i>Tarrietia argyrodendron</i> (41)	—	Australia	Ironwood.
<i>Terminalia arjuna</i> (13,39)	Tandra	India	<i>Terminalia</i> gums generally have good properties.
<i>T. belerica</i> (2,13,39)	—	India	—
<i>T. catappa</i> (41,13,39)	India: gum of Jungli Badam	Australia, India	Collected by the aborigines for food.
<i>T. chebula</i> (13,39)	—	India	Used by Mughals in ink containing soot from mustard oil (<i>Sesamum indica</i>) as the pigment (40).

<i>Gum-Yielding Genera</i>			
<i>Species</i>	<i>Terminology</i>	<i>Location</i>	<i>Notes</i>
<i>Terminalia macroptera</i>	—	Uganda	—
<i>T. stublmanni</i>	—	Tanganyika	—
<i>T. tomentosa</i> (13,39)	—	India	—
<i>Virgilia aroboides</i> (8)	—	South Africa	—
<i>V. divaricata</i> (8)	—	South Africa	—

Literature Cited

- Lucas, A. "Ancient Egyptian Materials and Industries"; Arnold: London, 1962; p. 6.
- Caius, J. F.; Radha, K. S. *Bombay Nat. Hist. Soc. J.* 1939, 41, 261-71.
- Bean, Lowell J.; Saubel, Katherine S. "Temalpakh Cahuilla Indian Knowledge and Usage of Plants"; Malki Museum Press: Banning, Calif., 1972.
- Maiden, J. H. *Pharm. J.* 1901, 20, 869-71, 980-82.
- Howes, F. N. In "Chronica Botanica"; Waltham, Mass., 1949.
- Parry, E. J. "Gums and Resins"; Pitman: London, 1920.
- Chandra, Moti "The Technique of Mughal Painting"; U.P. Historical Soc., Provincial Museum: Lucknow, India, 1949.
- Smith, F.; Montgomery, R. "The Chemistry of Plant Gums and Mucilages"; Reinhold: New York, 1959.
- Aspinall, G. O. *Pure Appl. Chem.* 1967, 14, 43.
- Talmadge, K. W.; Kestra, K.; Bauer, W. D.; Albersheim, P. *Plant Physiol.* 1973, 51, 158.
- Fujita, M.; Harada, H.; Kanai, K. *J. Electron. Microsc.* 1981, 30 (3), 244.
- Rosik, J.; Kubala, J.; Stanova, M.; Lacok, P. *Collect. Czech. Chem. Commun.*, 1968, 33, 1943-45.
- Mantell, C. L. "The Water Soluble Gums"; Reinhold: New York, 1947.
- Honda, S.; Yamauchi, N.; Kakehi, K. *J. Chromatogr.* 1979, 169, 287-93.
- Honda, S.; Takahashi, M.; Kakehi, K.; Ganno, S. *Anal. Biochem.* 1981, 113, 130-38.
- Birstein, V. J. *Stud. Conserv.* 1975, 20, 8.
- Isbell, H. S.; Pigman, W. W. In "Polarimetry, Saccharimetry, and the Sugars"; Bates, F. J., Ed.; *Nat. Bur. Stand. (U.S.) Circ.* C440, 1942; Chapter 29.
- Isbell, H. S.; Pigman, W. W. *Adv. Carbohydr. Chem. Biochem.* 1969, 24, 13.
- Rebenfeld, L.; Pacsu, E. *J. Am. Chem. Soc.* 1953, 75, 4370.
- Snowden, J. C. *J. Am. Chem. Soc.* 1954, 76, 4487.
- Blair, M. G.; Sowden, J. C. *J. Am. Chem. Soc.* 1955, 77, 3323.
- Whistler, R. L. "Industrial Gums," 2nd ed.; Academic: New York, 1973.
- Rosik, J.; Zitko, V.; Kubala, J. *Collect. Czech. Chem. Commun.* 1966, 31, 1569.
- Dutton, G. G. S. *Adv. Carbohydr. Chem. Biochem.* 1973, 28, 11-160.
- Johnson, B. B. "The Technique of Indian Miniature Painting"; paper presented at Symposium in Indian Art, Los Angeles County Museum of Art, Los Angeles, 1972.
- Johnson, B. B.; Cairns, T. *Anal. Chem.* 1972, 44 (2), 30A.
- Rosik, J.; Kardosova, A.; Kubala, J. *Carbohydr. Res.* 1971, 18, 151.

28. Masschelein-Kleiner, L.; Tricot-Marckx, F. *Inst. Roy. Patrimoine Artistique—Bull. (Brussels)* **1965**, *8*, 180.
29. Tindale, N. B. "Aboriginal Tribes of Australia"; Univ. Calif. Press: Berkeley, 1974; p. 60.
30. Pierce, A. E. "Silylation of Organic Compounds"; Pierce Chemical Co.: Rockford, Ill., 1968.
31. Sweeley, C. C.; Bentley, R.; Makito, M.; Wells, W. W. *J. Am. Chem. Soc.* **1963**, *85*, 2497.
32. Newth, F. H. *Adv. Carbohydr. Chem.* **19—**, *6*, 83–106.
33. Feigl, F. "Spot Tests in Organic Analysis," 6th ed.; Elsevier: Amsterdam, 1960; p. 474.
34. Stahl, E. "Thin-Layer Chromatography," 2nd ed.; Springer-Verlag: New York, 1967; p. 888.
35. Novak, J. *Adv. Chromatogr.* **1974**, *11*,
36. Aspinall, G. O. "Polysaccharides"; Pergamon: Oxford, 1970.
37. Sowardeker, J. S.; Sloneker, J. H. *Anal. Chem.* **1965**, *37*, 945.
38. Alexander, R. J.; Garbutt, J. T., *Anal. Chem.* **1965**, *37*, 303.
39. Watt, G. "A Dictionary of the Economic Products of India"; Office of the Superintendent of Government Printing: Calcutta, 1889.
40. Brown, P. "Indian Painting under the Mughals"; Oxford, 1949.
41. Maiden, J. H. *R. Soc. New South Wales J. Proc.* **1901**, *35*, 161.
42. Greenway, P. J. *East Afr. Agr. For. J.* **1941**, *6*, 241.
43. Dymock, W.; Warden, C. H. J.; Hooper, D. "Pharmacographia Indica"; Trubner: London, 1889; 3 vols.
44. Basu, Sumanta; Rao, Chintalacharuvu V. N. *Carbohydr. Res.* **1981**, *94*, 215–24.
45. Ghosal, Pradyot K.; Thakur, Swapnadip. *Carbohydr. Res.* **1981**, *98*, 75–81.
46. Bhattacharya, Subhas B.; Das, Asit K.; Banerti, Nilima. *Carbohydr. Res.* **1982**, *102*, 253–62.
47. Mandal, P.; Mukherjee, A. K. *Carbohydr. Res.* **1980**, *84*, 147–59.

RECEIVED for review October 6, 1982. ACCEPTED for publication June 9, 1983.

Technical Examination of Oriental Lacquer

GARY W. CARRIVEAU

Detroit Institute of Arts and Wayne State University, Detroit, MI 48202

Technical examination of objects coated with a protective covering derived from the sap of a shrubby tree produces information that can be used to determine the materials and methods of manufacture. This information sometimes indicates when and where the piece was made. This chapter is intended to present a brief review of the raw material urushi, and the history and study of its use. Analytical techniques have included atomic absorption spectroscopy, thin layer chromatography, differential thermal analysis, emission spectroscopy, x-ray radiography, and optical and scanning electron microscopy; these methods and results are reviewed. In addition, new methods are reported, including the use of energy dispersive x-ray fluorescence, scanning photoacoustical microscopy, laser microprobe and nondestructive IR spectrophotometry.

THE SAP OF A SHRUBBY TREE growing over large areas of Asia has been used to produce a highly durable protective and decorative coating for a wide variety of objects. The finished material, called lacquer, is known to have been used for over 3700 years. It is seen on utilitarian everyday objects such as boxes, trays, and cups, and further serves as a protective and decorative coating on furniture, armor, masks, and sculpture. Furthermore, lacquer ware continues to be used and remains highly prized even today.

The methods of collecting and refining the raw materials and the production of objects are very labor intensive. Even before the final decoration is applied, the manufacture of high-quality lacquer ware involves up to 30 different processes. These include steps in preparation and stabilization of the inner core, application of an undercoating to reinforce the core, and application of the intermediate lacquer layers, each polished and prepared for final decoration. These last decorative procedures may require a great number of multiple layers incorporating a variety of materials.

0065-2393/84/0205-0395\$06.00/0
© 1984 American Chemical Society

The unique qualities of lacquer ware fully justify this effort. Once hardened, the lacquer surface protects from dampness and mold; is relatively scratchproof; and remains unaffected by alcohol, hot water, salt, and alkali solutions. Even with everyday use (employing proper care), lacquered objects can survive in an excellent state for a very long time.

This chapter presents a brief review of the raw material and the history and study of its uses. Technical examination, through the use of a variety of scientific methods, has provided information about the raw material and the film hardening process. Certain diagnostic measurements were used to determine the raw material source (where the trees were grown) and the age of lacquer objects. An extended bibliography is included for those wishing additional details.

Raw Material

Oriental lacquer is produced from the sap of a tree, *Rhus vernicifera*, grown over wide areas of China, Japan, Korea, and other Southeast Asian countries. The evolution of lacquer has been lost in history, but we know that lacquer was used before the Shang dynasty (1751–1112 B.C.) in China. It was employed both in writing and as a protective coating. During the Chou dynasty (1111–256 B.C.), the lacquer craft developed but because of the limited production, most lacquer objects were reserved for royalty and the nobility. In Japan, the earliest known objects are thought to have been produced between the third century B.C. and the fourth century A.D. There is no common agreement among scholars on whether the tree that produces *urushi* is indigenous to Japan or if it was introduced from China. However although the subject matter and style of early Japanese lacquer were first influenced by the neighboring Chinese, the Japanese evolved a different tradition, both stylistically and in manufacture methods.

Use of Lacquer

Lacquer differs entirely from varnish and lac, although the terms may be mistakenly interchanged in the literature. Varnish is a natural resin dissolved in a solvent. After the solution has been applied, the solvent volatilizes, leaving a shiny glaze. Lac is the deposit of the *Coccus lacca* insect, which is collected from certain trees in East India. This deposit is refined and dissolved in a solvent. Both varnish and lac coatings are much less stable than the coating found on oriental lacquer ware.

Raw lacquer is called *urushi*. For our knowledge of the composition of *urushi* and the complex hardening process of the thin film layers, we now rely primarily on the recent work of Kumanotani and his coworkers (1–7). The sap of the Japanese lacquer tree is a latex containing 20–25% water, 65–70% urushic acid (urushiol), approximately 10% gummy sub-

stances, and less than 1% laccase. The amounts vary with the type of tree, where it is grown and cut for release of sap, and the time of year the collection is made. The last component, laccase, is considered to be the enzyme responsible for the hardening process. Chinese lacquer is thought by some to be inferior to Japanese lacquer because it has a smaller amount of urushiol and also because the Chinese often used vegetable oils as extenders.

Urushi, although it forms a thin film in an oxidation process, is unique in that it hardens in the presence of a high relative humidity. Hardening is actually accelerated with an increase in the amount of moisture present. Lacquer will not harden perfectly at normal room temperature and humidity conditions; a good film is only possible in a damp enclosure between 20 and 28 °C.

Many grades of *urushi* are used, depending on the different applications or decorative effects desired. (A detailed description of materials and methods may be found in Reference 8.) The sap, after removal of some water and careful filtration and cleaning, is most often coated onto a prepared core. This core is usually made of wood, but examples of leather, basketry, cloth, paper, metal, pottery, shell, horn, and fish skin may be found. Normally, many lacquer layers are built up on the core, with polishing occurring after each layer has hardened.

Lacquer was probably first used solely as a protective coating; decorative elements have evolved with time. Objects may be simply colored in monochromatic red or black, for example, Chinese bowls and carved boxes. Other objects may be highly ornate, with patterns introduced by using metal flakes or foil to produce decorations on the interior subsurface layers. Some pieces may have designs of inlaid mother of pearl; still others have a combination of metal-flake patterns and mother-of-pearl inlay. It is common for some objects to have 60–100 individual layers. Hardening and polishing each layer takes from several days to months; it might require many years for completion of an article.

When properly produced, a lacquer film is extremely durable. It is unaffected by most acids, bases, alcohol and water at room temperatures. One common usage of lacquer ware is for food storage. Lacquer films are, however, sensitive to UV radiation and extremes of heat; both may cause irreversible discoloration.

History

Early discussions on lacquer ware in occidental publications are rare. An article by Father d'Incarville in 1760 (9) appears to be one of the first containing information on lacquer composition and uses. This is followed in the late 19th century by reports by Wagener (10), Maëda (11), Rein

(12), and Yoshida (13), all of which contain details on the collection, preparation, and uses of this unique material.

Over the past hundred years numerous experimental methods have been used for the study of *urushi* and the finished lacquer ware. The first recorded reports on chemical experiments are those of Ishimatsu (14), Yoshida (13) and Korschelt and Yoshida (15). Miyama gave the name *urushiol* to *urushic acid* (16), and he and Majima and coworkers (17–26) further explored the composition of *urushi*. Work by Sunthanker, Dawson, and Symmes (27,28) helped to determine that it contained three substituted catechol derivatives containing various different side chains. The previously mentioned reports by Kumanotani and coworkers (1–7) have allowed us to understand more of the details of the raw *urushi*, the complex mechanism of film hardening, and some properties of the hardened layers.

More recent papers have recorded results from studies of the actual lacquer manufacturing methods and the decorative materials used. A brief review of selected papers follows, grouped by principal investigator.

Sir Harry Garner has used emission spectroscopy and optical microscopy to study pigments. He found pigments composed of mercury as HgS (cinnabar) in red colors, arsenic as As_2S_3 (orpiment) in yellow colors, and carbon in black colors from a 15th-century Chinese carved box (29). In addition, he has grouped objects according to age by the color of pigments in thin cross sections (29).

Toshikatsu Nakasato also reports on studies using optical microscopy, but he further uses x-ray radiography. His main emphasis has been on correlating the object's age with certain characteristics of metal flakes or foil used in decorations. He argues that information concerning the composition, size, and shape of *maki-e* metal flakes can sometimes be used to determine the age and provenance of decorated objects (30–37). An additional report on the use of x-ray radiography comes from d'Argence (38). He studied the methods used to manufacture the wooden core on medieval Chinese lacquer bowls.

Toshiko Kenjo has used perhaps the greatest number of different methods for studying materials and manufacturing methods. For example, IR spectrophotometry results show that some absorption bands vary in intensity and inverse wavenumber as a function of the source of the *urushi* and the age and hardness of the lacquer layer (39,40). Atomic absorption spectroscopy has been used to measure concentrations of copper, iron, and manganese in lacquer layers (41); Kenjo uses this information in provenance studies. Another tool for provenance investigations is the use of differential thermal analysis (DTA) (42,43). Kenjo has also used DTA to identify unknown thin layers as lacquer. In addition, specific gravity tests have been used to separate lacquer fragments from soil on archaeological excavations (44). Kenjo has also used thin layer

chromatography (45) and IR spectrophotometry (46) to detect the presence of natural vegetable oil extenders such as linseed oil and yam oil.

Even more recently, Burmester reported on the use of pyrolysis mass spectroscopy in lacquer studies (47,48). The results, when used with multivariate data analysis, prove to be a helpful provenance tool. Burmester has also extended the IR work through the use of a Fourier transform instrument and, further, evaluated the efficacy of using carbon-13 NMR measurements (49).

New Analytical Methods

Finally we wish to introduce four new analytical methods for lacquer problems; three are now used in the Detroit Institute of Arts lacquer project and the remaining method is undergoing development for lacquer use. These methods are energy dispersive x-ray fluorescence, laser microprobe, scanning photoacoustical microscopy, and nondestructive IR spectrophotometry.

The first method, x-ray fluorescence, has been used for many years to help solve problems of art and archaeological objects by answering questions concerning their elemental composition. The instrument at the Detroit Institute of Arts, a Kevex Model 0750A Macroanalyzer, is entirely nondestructive (no sample need be taken) and can analyze the surface of an object having any size and shape. Elemental concentrations ranging from sodium to uranium can be detected simultaneously and the sensitivity may be less than 100 ppm, depending on interferences from associated elements.¹ Qualitative and(or) semiquantitative information from lacquer ware may be used to identify metals used in *maki-e* dust, flakes or foil; to classify the pigments used to color lacquer layers; and, with the relatively high sensitivity, to determine trace-element concentrations. This information can be used with other data, such as those relating to style and manufacturing methods, to help answer questions of age, authenticity, provenance, and evidence of repair (52).

As an adjunct to x-ray fluorescence, we use the laser microprobe (53,54). This, of course, is not an entirely nondestructive technique. However, the hole that is produced has dimensions of the order of 10–20 μm , not visible to the unaided eye. The laser microprobe serves as an important supplement to x-ray fluorescence because analysis is not limited only to the upper surface. The laser beam can carefully excavate to lower and lower layers by controlled repeated laser pulses. Analysis can be performed on each individual layer of interest. In addition, the

¹ There are many excellent textbooks for x-ray fluorescence; recent examples are References 50 and 51.

much higher spatial resolution of the laser microprobe enables the study of much finer details than when using x-ray fluorescence.

The two previous methods deal with qualitative and(or) quantitative composition studies. The scanning photoacoustical microscope (55–57) is used to study another facet of lacquer ware problems, that of structural stability. The major conservation problem with lacquer occurs when the thin layers delaminate from the core, which generally happens to objects that are allowed to undergo large variations in relative humidity in storage or display areas. Such variations can periodically shrink or expand the core, placing strains on the core–lacquer interface. Of course, physical abuse can also damage the lacquer layer. The unaided eye, binocular microscope, and(or) x-ray radiography have all been used to study damage and the efficacy of restoration techniques. With its far greater sensitivity, absolute nondestructive nature, and ability to study objects of any size or shape, scanning photoacoustical microscopy offers improvements in the study of damage and repair. We have found that this technique may also be used to determine some methods of manufacture, such as the nature of raw materials and the use of fabrics to strengthen edges and corners.

The final example of new instruments for lacquer analysis uses IR spectrophotometry. Kenjo has pointed out how useful IR spectra can be when used for provenance studies (39,40). M. J. D. Low, of New York University, has recently developed an IR instrument that is nondestructive: no sample taking or preparation is required (58,59). Use of this instrument will prove to be extremely important because of the value of some lacquer ware and the justifiable reluctance of curators to allow samples to be taken. We are currently evaluating this new instrument's performance with lacquer.

Conclusions

This discussion has been intended to provide a review of the technical study of oriental lacquer. This unique material varies greatly in composition, methods of manufacture, and artistic style. Because of this, it offers a wide variety of exciting problems to solve. A bibliography of selected papers has been included as a guide for further study. In addition to this, a detailed annotated bibliography on technical analysis of lacquer, containing in excess of 380 entries, will be published soon (60).

Acknowledgments

We wish to thank R. L. Thomas, L. D. Favro, P. K. Kuo, D. Coleman, and M. J. D. Low for technical and experimental assistance. We also

extend our thanks to S. Mitchell, L. Gorman, S. Weintraub, and B. Roberts for their encouraging and informative comments and support.

Literature Cited

1. Kumanotani, J.; Kato, T.; Hikosaka, A. *J. Polym. Sci., Part C* **1968**, *23*, 519–31
2. Kumanotani, J. *Proc. FATIPEC Congr. 13th, Cannes* **1976**, 360–69
3. Kumanotani, J. *Macromol. Sci. Chem.* **1978**, *179*, 47–61
4. Kumanotani, J. *Kobunshi* **1979**, *28*, 871–73
5. Kumanotani, J.; Achiwa, O.; Ohima, R.; Adachi, K. *Proc. Int. Symp. Cult. Prop. Anal. Chem.* **1979**, 51–62
6. Kumanotani, J. *Proc. 182nd Nat. Meet. Am. Chem. Soc.*, **1981**.
7. Kato, T.; Kumanotani, J. *Bull. Chem. Soc. Jpn.*, **1969**, *42*, 2375.
8. Jahss, M.; Jahss, B. "Intro, and Other Miniature Forms of Japanese Lacquer Art"; Tuttle: Rutland, Vt., 1971; Chap III.
9. d'Incarville, Fr. "Mémoires de Mathématique et la Physique", Vol. III. 1760; pp. 117–42. A free German translation is found in Watins, M. "Kunst des Staffiermalers, Vergolders, Lackiers und Farbenfabrikanten"; Nuer Schaulplatz der Kunst und Harkwerke: Ilmenau, Germany 1824.
10. Wagener, G. *Dinglers Polytech. J.* **1875**, *218*, 361.
11. Maëda, . *Rev. Sci.* **1878**, *7*, 117–28.
12. Rein, J. *Oesterr. Monatsschr. Orient* **1882**, *4*, 5.
13. Yoshida, H. *J. Chem. Soc.* **1883**, 472.
14. Ishimatsu, S. *Mem. Manchester Lit. Philos. Soc.* **1882**, *3*, Ser. 7.
15. Korschelt, O.; Yoshida, H. *Trans. Asiatic Soc. Jpn*, **1885**, *12*, 180–220.
16. Miyama, K. *J. Coll. Eng. (Tokyo)* **1908**, *4*, 89.
17. Majima, R. Cho, S. *Ber. Dtsch. Chem. Ges.* **1907**, *40*, 4390.
18. Majima, R. *Ber. Dtsch. Chem. Ges.* **1909**, *42*, 1418.
19. *Ibid.*, 3664.
20. *Ibid.*, **1912**, *45*, 2727.
21. *Ibid.*, **1913**, *46*, 4080.
22. *Ibid.*, **1915**, *48*, 1593.
23. Majima, R.; Tahara, J. *Ber. Dtsch. Chem. Ges.* **1915**, *48*, 1606.
24. Majima, R.; Takayama, G. *Ber. Dtsch. Chem. Ges.* **1920**, *53*, 1907.
25. Majima, R. *Ber. Dtsch. Chem. Ges.* **1922**, *55*, 172.
26. Majima, R. *Unter. Japanlack*, Iwata Inst. Plant Chem. Tokyo, **1924**.
27. Sunthanker, S. W.; Dawson, C. *J. Am. Chem. Soc.* **1954**, *76*, 5070–74.
28. Symmes, W.; Dawson, R. *J. Am. Chem. Soc.* **1954**, *76*, 2959.
29. Garner, Sir Harry, *Stud. Conserv.* **1963**, *8*, 84–98.
30. Nakasato, T. *Hozon Ryogaku*, **1967**, *3*, 55–69.
31. Nakasato, T. *Sci. Conserv. (Tokyo)* **1972**, *9*, 63–77.
32. Nakasato, T. *Hozon Kagaku*, **1976**, *15*, 56–83.
33. *Ibid.*, **1977**, *16*, 35–44.
34. *Ibid.*, **1978**, *17*, 16–24.
35. *Ibid.*, **1979**, *18*, 73–92.
36. *Ibid.*, **1980**, *19*, 91–105.
37. Nakasato, T. *Proc. Int. Symp. Cult. Prop. Anal. Chem.* **1980**, 113–24.
38. d'Argence, R. *Apollo* **1980**, *112*, 6–19.
39. Kenjo, T. *Hozon Kagaku* **1976**, *15*, 1–8.
40. Kenjo, T. *Sci. Pap. Jpn. Antiq. Art Crafts* **1978**, *23*, 32–39.
41. Kenjo, T. *Int. Symp. Conserv. Restor. Cult. Prop.* (Tokyo) **1978**, 63–69.

42. Kenjo, T. *Hozon Kagaku* 1980, 19, 15–19.
43. Sato, M. *Shikizai Kyokaishi* 1969, 42, 118.
44. Kenjo, T. *Hozon Kagaku* 1978, 17, 6–10.
45. *Ibid.*, 1973, 11, 91–93.
46. *Ibid.*, 1977, 16, 12–16.
47. Burmester, A.; Brandt, K. *Berlin. Beitr. Archaeom.* 1982, 7.
48. Burmester, A. *Archaeometry* 1983, 25 (1), 45–58.
49. Burmester, A. *Proc. 22nd Symp. on Archaeometry*, Bradford, 1982, 184–93.
50. Jenkins, R.; Gould, R.; Gedcke, D. “Quantitative X-ray Spectrometry”; Dekker: New York, 1981.
51. Tertian, R.; Claisse, F. “Principles of Quantitative X-Ray Fluorescence Analysis”; Heyden: London, 1982.
52. Carriveau, G. W. “Technical Examination of Lacquer Using X-ray Fluorescence”; in press.
53. Breck, F.; Young, W. J. In “Application of Science to Works of Art”; Young, W. J., Ed.; Boston Museum of Fine Arts: Boston, 1967.
54. van Deijck, W.; Balke, J.; Maessen, F. *Spectrochim. Acta, Part B* 1979, 34, 359–69.
55. Wong, Y. H.; Thomas, R. L.; Hawkins, G. *Appl. Phys. Lett.* 1978, 32, 538–39.
56. Thomas, R. L.; Pouch, J. J.; Wong, Y. H.; Favro, L. D.; Kuo, P. K.; Rosencwaig, A., *J. Appl. Phys.* 1980, 51, 1152–56.
57. Pouch, J. J.; Thomas, R. L.; Wong, Y. H. *J. Opt. Soc. Am.* 1980, 70, 562–64.
58. Low, M. J. D.; Lacroix, M.; Moterra, C.; Severdia, A. G. *Am. Lab.*, 1982, 14, 16–27.
59. Low, M. J. D.; Lacroix, M.; Moterra, C. *Appl. Spectrosc.* 1982, 36, 582–84.
60. Carriveau, G. W.; Caldwell, R. “An Annotated Bibliography on the Technical Analysis of Oriental Lacquer”; in press.

RECEIVED for review November 3, 1982. ACCEPTED for publication May 16, 1983.

An Examination of the Phenomenon of Textile Fabric Pseudomorphism

KATHRYN A. JAKES and LUCY R. SIBLEY

University of Georgia, CTI Department, Athens, GA 30602

A textile fabric pseudomorph is a mineralized structure formed through a petrification process in which the organic compounds of fibers have been replaced by inorganic compounds while assuming the physical shapes of fibers, yarns, and fabrics. Photomicrographic analysis of a bronze halberd (Shang period, ca. 1300 B.C.) revealed multiple layers of mineralized fabric formations composed of the filament shapes characteristic of silk. x-Ray diffraction, scanning electron microscopy, and energy dispersive analysis of x-rays were employed to identify the mineral composition of the pseudomorphs. A model for the process of silk pseudomorph formation on the bronze halberd is proposed, including solution, transport, and reaction of copper ions. Deposition of the resulting products maintains the outer physical structure of the fiber as a result of the network of polymer chains and the maintenance of some structural integrity during their degradation.

STUDY AND RECONSTRUCTION OF EARLY CULTURES usually rely upon whatever evidence can be recovered from their archaeological contexts. Pottery, stone, and metal artifacts often form the basis for the knowledge of how people lived and worked in the past. Textile fabric products, however, function in much closer associations with people than do the more durable implements. As a result, these products contain valuable information about those who produced, used, and ultimately discarded them. Nevertheless, except in a few rather well-known cases, textile fabrics do not survive the vicissitudes of environmental conditions that follow the final textile use and encourage decay.

Lack of information about textile usage by certain early peoples becomes critical when one finds that their descendants demonstrated mastery of elaborate textile products. For example, the intricacy of silk textiles recovered from Han Dynasty tombs (ca. 206 B.C.–A.D. 220) sug-

0065-2393/84/0205-0403\$06.50/0

© 1984 American Chemical Society

gests a long tradition of textile production and use, but no actual fabrics have been discovered from the earlier Shang period (1600–1100 B.C.). Furthermore, the discovery of a cocoon of the *Bombyx mori*, or cultivated silkworm, at a Yangshao culture site (ca. 3000 B.C.) (1) implies a silk-growing complex far earlier than the Shang period. A key to understanding Han Dynasty silks within the Chinese textile tradition appears to be offered by the earlier Shang Civilization and its sites, which, although devoid of organic textile products, nevertheless yield textile pseudomorphs attached to bronze objects.

The purpose of this work is twofold: to propose a model for the formation of silk pseudomorphs and to evaluate the pseudomorphs as evidence for textiles. The import of the pseudomorph phenomenon to the reconstruction of textile usage by a people will be considered in another paper. A textile fabric pseudomorph is defined herein as a mineralized structure formed through a petrification process in which the organic compounds of fibers have been replaced by inorganic compounds assuming the physical shapes of fibers, yarns, and fabrics (2). The nature of the definition implies that no organic structures remain; that the physical configurations of a fiber, yarn, or fabric are present; and that the pseudomorph resides on a metal artifact. A pseudomorph or "false form" is no longer a textile product, nor can it be considered as such. However, where no fabrics survive and pseudomorphs are formed, the latter shapes may be studied as if they were fragile textiles. It must be realized that the evidence derived will be incomplete, but even incomplete evidence will aid the reconstruction of the Chinese textile tradition.

For this investigation of the pseudomorph phenomenon, a bronze Shang Dynasty *ko*, or halberd, designated Halberd No. 1, on loan from the Museum of Anthropology of the University of Missouri at Columbia (UMC), was studied in detail. Its exact archaeological context is not known, although its general provenance is Honan Province, China. Because the general attributes of the halberd are consistent with those of other Shang bronze weapons, an approximate date of 1300 B.C. has been assigned to it. Such a date places the weapon within the Anyang phase of the Shang period.

Background

Little published information exists about textile fabric pseudomorphs. For the most part, those interested in the phenomenon have been concerned with the pseudomorph as textile evidence rather than with the process of its formation. There is no established methodology for examining the pseudomorph either as mineral or as textile.

As early as 1937, Sylwan (3) noted the presence of textile structures embedded in the corrosion products of Shang bronze artifacts. She ap-

parently assumed that the fibers, yarns, and fabrics observed were still organic and made no attempt to determine their composition.

Biek (4) in 1963 applied the geological term "pseudomorph" to textile shapes clinging to corrosion products of metal objects. Ten years later Carroll (5) used pseudomorph to describe fabric formations attached to a bronze Etruscan bowl, ca. 500–400 B.C., found at Veii and presently owned by the Newark Museum. Vollmer (6) first applied the term to textile structures found on Shang and Han bronzes now located at the Royal Ontario Museum. Although he reported 74 occurrences of pseudomorphs, he did not investigate the replacement process. Of the four authors, Carroll is the only one who included analytical techniques capable of yielding the elemental inorganic composition of the pseudomorphs.

In 1978, Sibley et al. (7) reported the finding of silk pseudomorphs on three Shang Dynasty bronze weapons at the Museum of Anthropology, University of Missouri–Columbia. The authors considered the work to be preliminary and confirmed a lack of organic structure for the formations adhering to the weapons. By using one of the same weapons as the object for study, Sibley and Jakes (2) proposed microenvironmental conditions necessary for mineralization to occur. Included in that work is a more extensive examination and comparison of published and unpublished reports of the phenomenon than is considered here. The reader is referred to the article for detailed discussion of the earlier studies of pseudomorphs.

Experimental Procedures

The UMC halberd exhibits corrosion products along much of its surfaces, and these differ markedly in texture, color, and depth. Dimensions of the halberd are approximately 23.8×5.8 cm (Figure 1). For the purpose of this research, the sides of the blade were designated as side A and side B. The *tang*, or handle, bears an inscription, which has not been translated, as well as the typical hole for insertion of the halberd onto a pole. Sections of the corroded areas on side A exhibit textile fabric pseudomorphs; these are the focus of this research.

Photographs of the halberd were taken with a Nikon F camera with a Nikkor micro lens using Kodachrome type A film. The halberd was placed on a sheet of glass on which was drawn a 1×1 cm grid. The glass, suspended beneath the camera over a grey matboard, was angularly illuminated in a 2:1 lighting ratio in order to eliminate background shadows and to highlight the surface texture of the halberd. To achieve true color, the photographs were developed by the Cibachrome process in lifesize and twice lifesize prints.

A Wild M400 photomicroscope with zoom settings yielding magnifications from $1 \times$ through $20.4 \times$, a Wild MPS55 Electric Control Unit, fiber optics illumination, and Panatomic X and Kodachrome Type A film were used in taking the photomicrographs. The halberd on its 1×1 cm grid was moved by means of microscope positioning screws so that specific locations on the halberd could be found repeatedly.

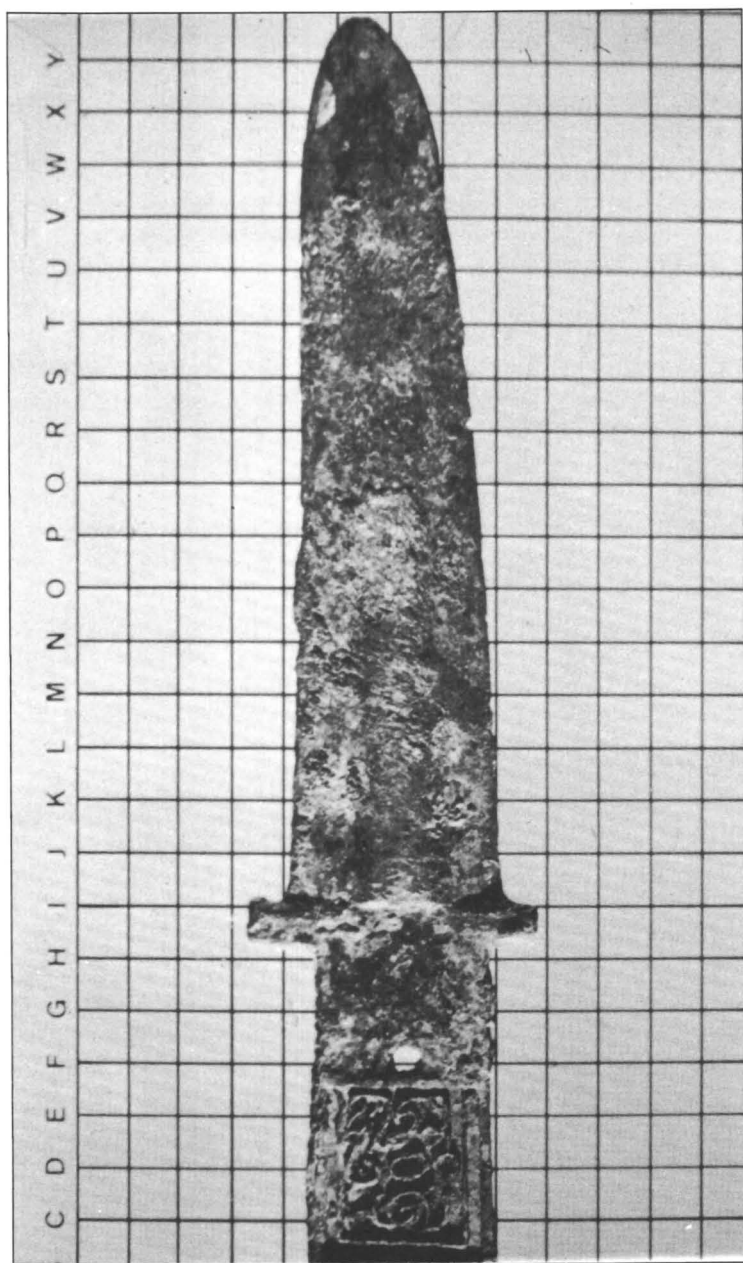


Figure 1. Halberd No. 1, Shang period, Anyang phase.

Samples of green and of black nodules from side B of the blade and of green and of black fiberlike structures from side A of the blade were cut by carefully scraping along the edge of the sample until they became loosened from the corrosion material surrounding them. The pseudomorph samples, although small and brittle, maintained some structural integrity in the cutting process. Although these samples were detached from the other material in which they were embedded, some encrustations on their surfaces could not be removed, and some contamination was expected in the mineralogical analysis. Each sample was ground and collected into a small wax bead or spindle mount for x-ray diffraction.

x-Ray diffraction powder patterns were developed by using a chromium source and a Phillips Debye–Sherrer camera. Due to their small size, the samples from the back of the halberd were irradiated for 12.5 h, and the green pseudomorph sample for 12.3 h. The black pseudomorph sample, larger, was irradiated for only 5 h. The exposed film was measured in accordance with standard procedures (8) and the resulting diffraction spacing values were compared to standard values of known materials (9).

In addition, two samples were cut and mounted on stubs for scanning electron microscopy. One sample was selected from a location near the blade edge and contained more than one fiber pseudomorph. The second sample, without pseudomorphs, was cut from the reverse side of the blade for comparative purposes.

The samples sectioned for scanning electron microscopy were sputter-coated with palladium and then vacuum-coated with gold to insure good coverage of possible porous areas. Micrographs of areas of the samples were taken at magnification levels from $20\times$ to $20,000\times$ by using a Cambridge S-4 Stereoscan electron microscope. Energy-dispersive analysis of x-rays was performed using an energy dispersive analysis of x-rays (EDAX) International model 707B connected to the microscope unit. EDAX counts were taken in both scanning and point-focus modes.

Results of the Analysis of Mineralogical Structure and Composition

Microscopic analysis of the halberd revealed a variation in color and shape of the formations on the surfaces of the blade. Green and black mineral forms are predominant, but some orange, blue, and red structures were also observed. A light-brown grainy substance fills many of the interstices between the mineral formations. The pseudomorph formations are either green or black, and the difference in their composition indicates the possibility of some chemical difference in the original organic material. This point will be discussed in a later section of this chapter.

On side B of the halberd, green nodules typical of malachite are visible, apparently growing on the surface of a blackened, nodular material that thinly covers a large part of the halberd's surface. Scanning electron micrography (SEM) of the green nodules revealed microcrystalline lamellar growths that, in some places, radiate from a nucleating point. Magnification of the black material from side B displayed an amorphous material with a porous character. Study of a fresh-cut surface of the green-colored pseudomorphs from Side A of the halberd showed

crystalline growths similar to those of the green nodule within a more amorphous matrix (Figure 2). Study of a surface of a black pseudomorph showed a solid mass of irregular structure with no apparent microcrystalline growth through $20,000\times$ magnification (Figure 3). The replacement in both types of fiber pseudomorph is solid, completely filling the cross section of the fiber structure. The interstitial light-brown grains appeared to be porous globules of irregular shape under SEM.

EDAX of the green nodules from side B yielded copper and aluminum peaks. In some areas of beam-focused EDAX, the EDAX showed more aluminum relative to copper; but in other loci, the situation was reversed. It could be possible, then, that the copper- and aluminum-containing materials may be mixed physically in the nodule but are not chemically bound to each other. EDAX of the black material from side B also showed almost equivalent aluminum and copper peaks. The EDAX results of the green and black pseudomorphs were similar to those for the green and black material from side B. EDAX of the light-brown interstitial material contained strong silicon and aluminum peaks, as well as peaks for phosphorus, calcium, and iron. A very small peak of copper was apparent but probably not of significant quantity relative to the other components. The color of these interstitial grains, their loose grainy character, and their chemical composition indicate that the material is soil, not a corrosion product of bronze.

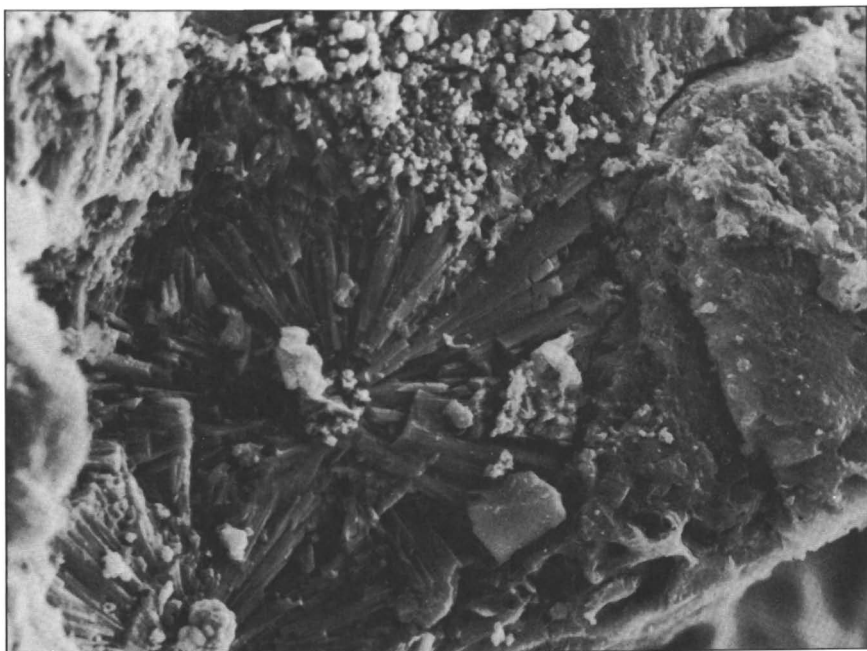


Figure 2. Interior of green pseudomorph, SEM, $1245\times$ magnification.

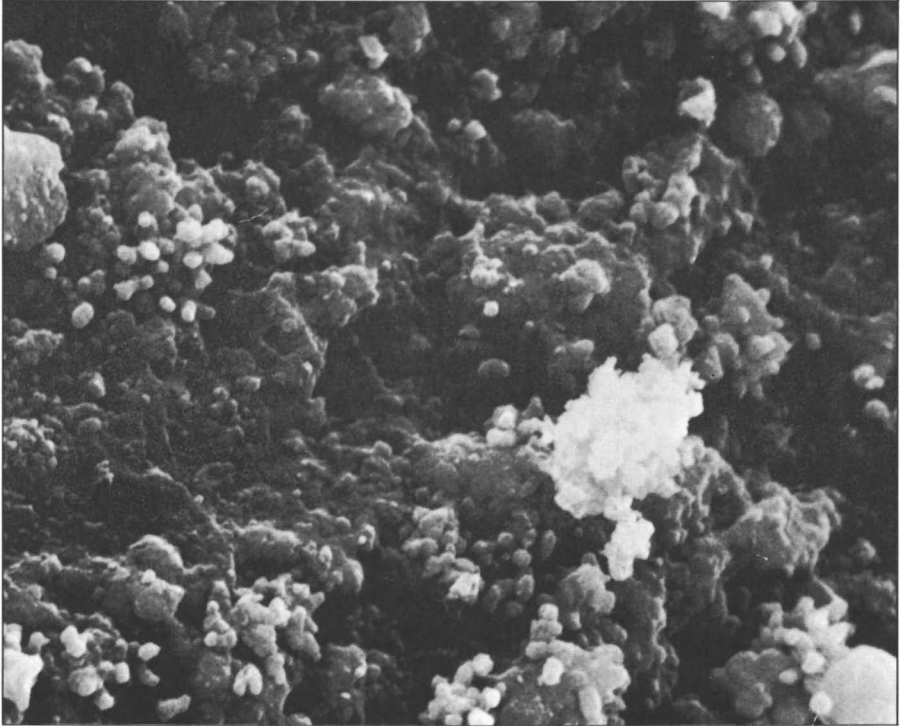


Figure 3. Interior of black pseudomorph, SEM, 1245 \times magnification.

x-Ray diffraction (XRD) of the green material from side B of the halberd produced the powder pattern characteristic of malachite as well as another pattern that was attributed to some aluminum oxide or hydroxide. The exact form of the aluminum material could not be determined conclusively from the data available. XRD analysis of mixtures is difficult and involves more speculation than that of a pure material, particularly in ancient alloys (10). Although the diffraction powder pattern of the green fiber pseudomorphs from side A was not as clear as that of the green nodule from side B, all of the lines apparent in the pattern could be correlated with those of the green nodule. The two must contain the same material, that is, malachite and some aluminum oxide or hydroxide.

The XRD pattern of the black material from side B of the halberd matched that of the black pseudomorphs from side A with the exception of some bands attributable to malachite that were exhibited by the pseudomorphs. Because the black material from side B was scraped clean of any apparent encrustations, it was thought to be a purer sample. The fineness and brittleness of the black pseudomorphs eliminated the possibility of removing encrustations, so that the possibility of contamination

had to be considered. Therefore, although malachite may be contained within the black pseudomorph material, its presence as outgrowths on the surface would also cause the observed XRD results. Micrographs of some of the black fiber pseudomorphs reflect this type of encrustation, with green material deposited irregularly on the surface of a black fiber pseudomorph. The XRD diffraction pattern common to both black samples best fits an aluminum oxide structure.

By compiling the information gained from the SEM, XRD, and EDAX analyses and comparing it with information in mineralogical texts (11,12), some conclusions can be drawn about the chemical composition of the black and green components of sides A and B (Table I).

The green material from both sides must contain malachite. The XRD results of the sample from side B are verified by the characteristic nodular outer structure and the slender, almost needlelike prism crystalline microstructure (11) that both malachite and the green nodule exhibit (Figure 2). Although restricted from forming a nodular outer structure by the physical shape of the silk filament, the inner micro-

Table I. Results of Mineralogical Analyses

	<i>Green Nodule Halberd Side B</i>	<i>Green Pseudo- morphs Hal- berd Side A</i>	<i>Black Material Halberd Side B</i>	<i>Black Pseudo- morphs Hal- berd Side A</i>
SEM	Lamellar to needlelike crystals, radiating from a nucleating point apparent at 1000×	Lamellar to needlelike crystals, similar to side B, with some less ordered areas	Amorphous, porous No microcrystalline structure apparent through 20,000×	Amorphous, solid mass fills fiber cross section
EDAX	Al and Cu	Al and Cu	Al and Cu	Al and Cu
XRD	Malachite Aluminum oxide or hydroxide	Malachite Aluminum oxide or hydroxide Pattern similar to green material, side B	Aluminum oxide or hydroxide Because EDAX demonstrates the presence of Cu, but no XRD pattern for a Cu compound is exhibited, the black material is assumed to contain tenorite, CuO.	Aluminum oxide or hydroxide Malachite Pattern similar to black material, side B

crystalline growths of the green pseudomorph from side A are similar to those of the green nodule, and are thus interpreted to be malachite, also. The XRD and EDAX results also indicate that the green material from both sides of the halberd contains an aluminum compound, probably an oxide or hydroxide.

Analysis of the black material from both sides of the blade yielded similar SEM, XRD, and EDAX data. Micrographs of the two sides show an amorphous material that is more porous on side B and more solid as a fiber replacement on side A. The two have been shown by their XRD patterns to contain aluminum oxide or hydroxide of some form. In addition, the XRD pattern of the black pseudomorphs revealed bands characteristic of malachite, but malachite encrustations on the surface of the pseudomorphs may be the cause, rather than malachite in the internal structure. The EDAX of the interior of the black fiber pseudomorphs, however, reveals the presence of copper as well as aluminum, just as the black material from side B does.

No XRD pattern is apparent for this black, copper-containing material. Perhaps it is so amorphous that a powder pattern is not able to be produced; the SEM micrograph shows an amorphous structure for the black material.

Because both the black and the green materials contain aluminum oxide or hydroxide, a cause for the black color must be found. The amorphous copper material that shows in the EDAX results but not on the XRD pattern may be this cause. A possible source of the black color in corroded bronze is suggested by Gettens (13) in his study of the corrosion of an ancient Chinese fragment. He attributes a black color in the corrosion layers to the presence of tenorite (CuO) and states that because it is so amorphous, it gives "indistinct diffraction patterns or none at all." In a later paper Gettens (14) repeats his belief that the dark product in bronze corrosion is tenorite and stresses the need for further analysis. Plenderleith (15) agrees that the dark material in bronze corrosion is tenorite, but much debate continues as evidenced by a more recently published discussion between corrosion scientists and museum conservators (16).

Tenorite forms black nodular masses that are sometimes shiny (12) or metallic (11). The black material from side B of the halberd was also nodular in structure and appeared almost metallic in its light reflection. Thus it is possible that the black material of both sides A and B contains tenorite, although it is not apparent in the XRD pattern because of its highly amorphous structure.

Pseudomorphs as Evidence for Textile Fabrics

As noted earlier, the UMC Halberd No. 1 displays corrosion over most of its surfaces. Numerous pseudomorph formations were identified on

side A of the halberd; they covered an area between the crosspiece and a point 2.5 cm from the tip of the blade. On side B, only two instances of pseudomorphs were discovered; these were yarn-like structures that measured as follows: (1) 0.23 cm long and 50×10^{-4} cm (50 μm) wide; and (2) 0.13 cm long and 50×10^{-4} cm (50 μm) wide (Figure 4). The remaining corrosion of side B exhibited no evidence of textile pseudomorphs.

Thick formations of pseudomorphs were observed along the straighter edge of side A of the halberd. These occurred approximately 3 cm below the crosspiece and extended for 3 cm. The other edge did not display similar formations.

Generally two types of formations were observed: parallel and paired hair-like strands in one direction and strands of varying sizes moving in two or more directions. The former have been designated yarn-type formations, one yarn consisting of two finer strands; the latter have been stipulated as fabric-type formations because of the presence of two sets of interlacing elements which are perpendicular to each other (Figure 1). Moving in and out of the fabric-type areas are yarn-type formations that are generally parallel to each other. Although these discrete yarns cover much of the pseudomorph area of the blade, there are locations that contain no pseudomorphs either in yarn or fabric shapes (Figure 5).

At approximately 5.5 cm from the crosspiece and at the edge of a "crushed" area, the pseudomorphs change in their geometric relationship with respect to the straight edge of side A. Between the crosspiece and the crushed area, both yarn and fabric formation exhibit a 60° angle

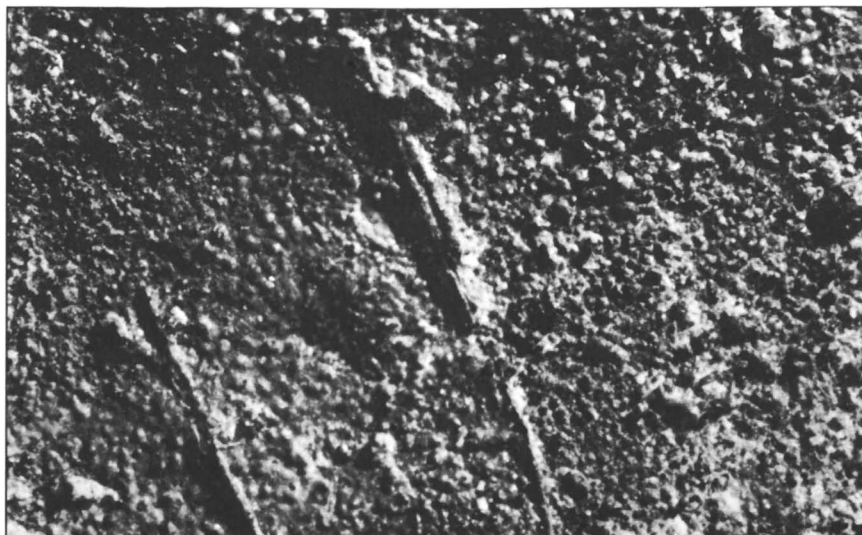


Figure 4. Detail of side B of Halberd No. 1, 36.5 \times magnification.

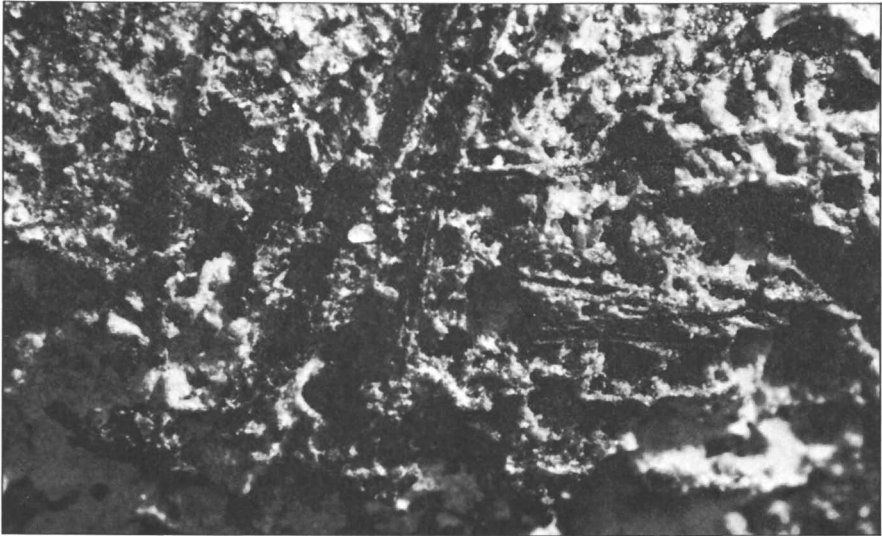


Figure 5. Paired-fiber yarn, side A, Halberd No. 1, 72.5 \times magnification.

relation with the edge, noted above. Between the crushed area and a point 1.5 cm beyond it, the yarn and fabric formations are at a 45° angle with respect to straight edge. This change occurs in the same general zone with the thickest edge formation (Figure 1).

Fiber Evidence. Because analyses reveal no organic structure, the fiber evidence is of physical rather than chemical nature. As noted earlier, the yarn-type formations consist of paired hair-like strands moving parallel to each other (Figure 6). Two hair-like strands are used consistently in each unit, and the strands do not twist around each other. Rather they maintain the same plane or axis. In addition, each formation follows a trajectory that, although following the contours of the blade, is relatively straight. No crimp or waviness was observed.

In searching for a fiber that would exhibit these characteristics, the animal-fiber wool and the seed-hair cotton can be discarded. Both of these fibers lack the above-named attributes, for they have molecular and fiber crimp, which would result in less than straight trajectories. Flax and the other bast fibers may be deleted as well, because the fibers within bundles would vary in number.

The other major natural fiber type, silk, fits the evidence. It is the only natural filament, and as such requires no twisting to be translated into a yarn for weaving. Silk is exuded from two orifices on either side of the silkworm's head and forms single strands called "brins." The two brins then come together as a bave unit which is held in place by sericin (17). A silk filament is smooth and maintains a relatively straight trajectory with no crimp to its structure.

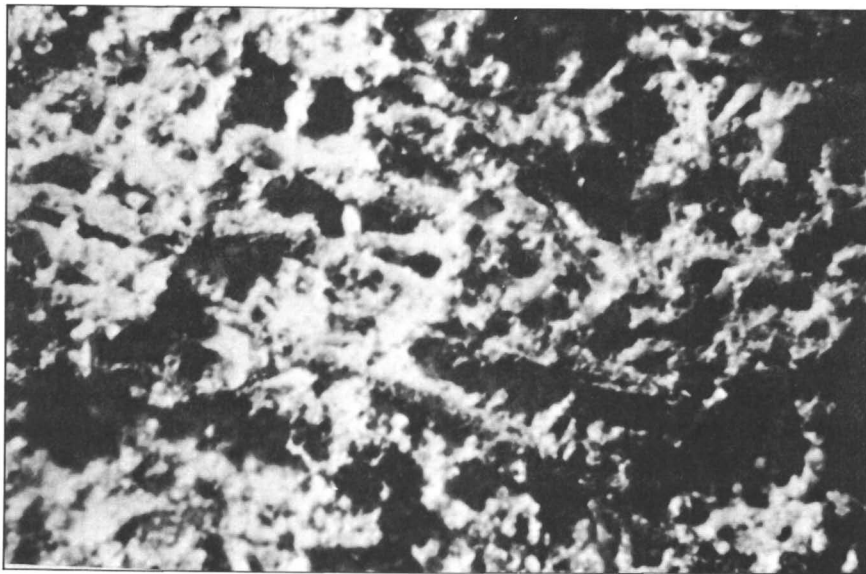


Figure 6. Detail, side A, Halberd No. 1, 37 \times magnification.

Yarn Evidence. Several types of yarn formations were distinguished. The paired-fiber yarn shape evident in the yarn-type formations is present in the fabric-type areas as well (Figure 5). For the most part, this formation is green in color, indicating malachite; however, some of the paired fiber yarn shapes are a dark brown-black in color. These darker entities appear more often in the fabric-type zones than in the yarn-type areas.

Also located in the fabric-type areas are two other types of yarn. These are a single, green yarn shape, possibly a single brin, and a large dark or black yarn configuration (Figure 7). The latter type may be subdivided further, for some of these appear to be twisted and to contain groups of fiber forms. On other dark yarn types of approximately the same size, no twist is evident. These latter shapes may or may not contain paired-fiber-type bundles (Figure 7).

Measurements were obtained from selected yarn pseudomorphs, and the figures indicate a fair amount of consistency for the single-fiber yarn type and the paired-fiber yarn shape. Not as easily measured were yarn pseudomorphs with multiple components, either in the form of a single strand with numerous fiber components or a plied yarn pseudomorph. Because encrustations had formed along the surfaces of the formations, it was difficult to identify clear boundaries for them.

Most of the single-fiber yarn pseudomorphs, green in color and with zero twist, designated 0, ranged from 39 to 50 μm in size; however, one



Figure 7. Detail, side A, Halberd No. 1, $61.2\times$ magnification.

measured $60\ \mu\text{m}$. Two dark single-fiber yarn forms (with 0 twist) were calculated to be $68\ \mu\text{m}$ each. Both types of single fiber shape varied as much as $29\ \mu\text{m}$ in size.

Not surprisingly, paired-fiber yarn formations of both colors ranged from $80\ \mu\text{m}$, a dark yarn with 0 twist, to $107.8\ \mu\text{m}$ for another dark yarn with S-twist, designated (\backslash). All the green, paired-fiber yarn formations measured approximately $100\ \mu\text{m}$ in size.

As noted, the large yarns with multiple components are even more difficult to measure than were the single-fiber and paired-fiber yarn configurations. One black multifiber yarn type was observed with a Z-twist, designated ($/$), and it measured $117.6\ \mu\text{m}$ (Figure 7). Three other large multifiber yarn shapes had similar diameters, but only one displayed a discernible ($/$) twist. In all four of these large formations, no twist was detected for the single strands within the yarn pseudomorphs. One fiber measured $68\ \mu\text{m}$, similar to that of the black single-fiber yarn form.

A three-ply yarn shape was identified and measured (Figure 8). It was dark brown-black in color and was composed of three paired-fiber yarn formations (\backslash) that were plied together in ($/$) direction. The ply yarn was calculated to be $127.45\ \mu\text{m}$ in size; one of the paired-fiber yarn pseudomorphs, to be $107.8\ \mu\text{m}$; and a single fiber, $58.8\text{--}68\ \mu\text{m}$. No green yarns were observed larger than $100\ \mu\text{m}$.

Implications of these findings will be examined in later work. Suffice it to say here that a variety of yarns were observed, and all were related to single and paired-fiber yarns and were either green or black. The evidence of yarn formations is summarized in Table II.

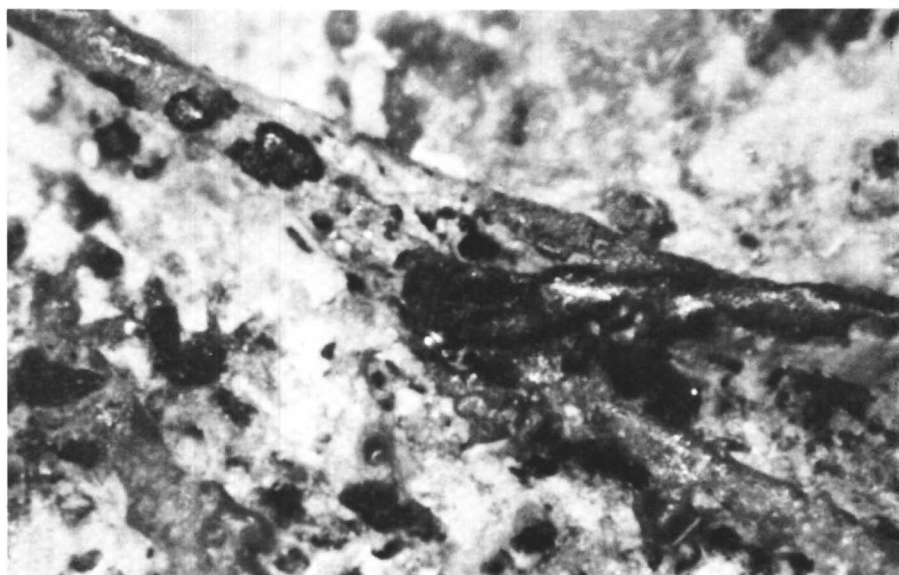


Figure 8. Ply yarn, side A, Halberd No. 1, 74.5× magnification.

Table II. Summary of Yarn Evidence

Type of Yarn	Color	Twist	Size (μm)
Single			
Single-fiber	Green	0	39–50 ^a
	Black	0	49, 68
Paired fiber	Green	0	100
	Black	0	80
	Black	\	107.8 ^b
Single-fiber bundles	Black	0	117.6 ^c
	Black	0	137.2
Ply			
Three-ply	Black	/	127.45 ^d

^a One single green fiber measured 60 μm .

^b One single fiber measured 49 μm .

^c One single fiber measured 68 μm .

^d One paired fiber (\) measured 107.8 μm , and one single fiber measured 58.5–68 μm .

Fabric Evidence. At least five, and possibly six, fabric-type formations were observed on the blade. Most of these occurrences measured less than 2 cm. One large area (approximately 2 × 1 cm), adhering to the raised central section of the weapon's blade, cannot be identified positively as a fabric-type formation because of its present crushed condition.

For all of these formations, at least two different sets of elements, perpendicular to each other, interacted. In all of the fabric type areas, eccentric yarn shapes moving in a curvilinear fashion were identified. No selvages were observed. Single yarn forms do turn back into the formations, but there is no consistency to the movement. Bearing in mind that no positive identification of warp and weft can be made without a selvage, the analyst used the terms "system A" and "system B" to designate those sharing a rectilinear relationship. "System C" indicated yarn shapes that are present in the area but do not interact rectilinearly.

Several layers of fabric-type formations were observed in each location. It is impossible to know whether these pseudomorphs consisted of a single fabric with surface decoration or several layers of the same fabric or even different fabrics (18). The upper or top layers of the fabric formations generally contained large black yarns parallel to each other (system A). Rather consistently, the green, single-fiber yarn and the paired-fiber yarns appeared in both systems A and B or in one (system B) that interlaced with black yarns in the other (system A). Green, paired-fiber yarns also appeared occasionally along the surface in a nonrectilinear situation.

At one point, a green yarn type (system A) floated over three green yarn strands (system B) before interlacing with a fourth green strand from system B. Unfortunately, the mineralization along the yarn-shape surfaces also obscured the rest of the structure.

Two types of nonrectilinear yarn formation were identified, a curvilinear yarn movement and a linear one that moved in a zig-zag, 45° angle relative to the fabric structure (Figures 6, 9). That these were identified along the surfaces of the formations suggests a surface decoration. However, until further study confirms this point, the function of system C yarn formations within the fabric pseudomorphs remains uncertain.

The presence of yarn-type formations from two different systems interlacing in a perpendicular relation to each other confirms a formerly woven-fabric structure for the pseudomorphs. The evidence of the pseudomorphic fibers, yarns, and fabrics confirms the former presence of silk fabrics on a Shang Dynasty bronze weapon. Further discussion and implications of these findings fall outside the purview of this investigation; future work will focus upon an analysis of specific fabric structures present on Shang bronzes.

A Proposed Model for the Process of Silk Pseudomorph Formation

In order to propose a model for the process of silk fabric pseudomorph formation on the Shang bronze halberd, consideration must be given to

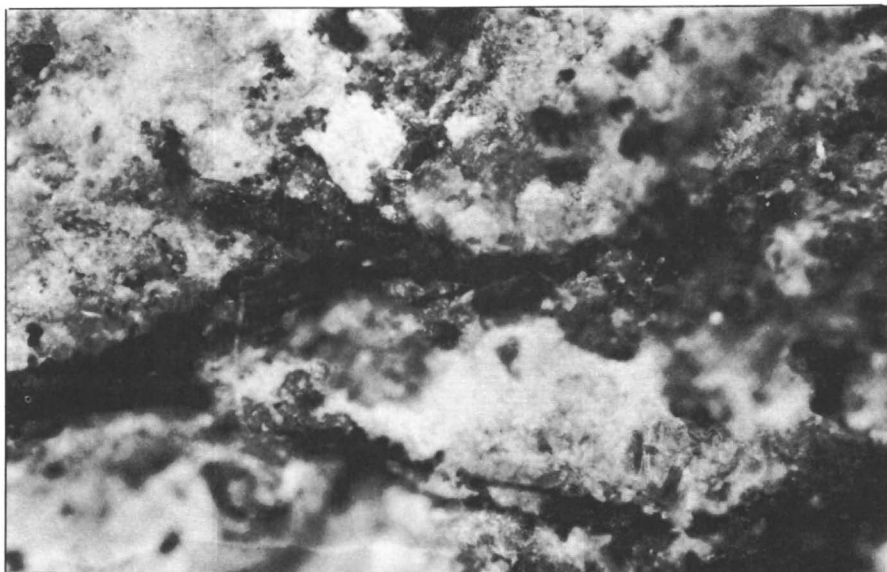


Figure 9. Yarn interaction, side A, Halberd No. 1, 72.5 \times magnification.

the factors pertinent to the conditions to which the halberd was exposed in addition to the results of the mineralogical analyses performed. These factors are (1) the geography, soil, and climate of the area in which the halberd was found; (2) the burial practices of the Shang people; (3) the chemical composition of Shang bronzes; (4) the geological weathering of rock and chemical corrosion of metals; and (5) the decay of silk fibers.

The Geography, Soil, and Climate. An accurate description of soil composition and pH is essential in the analysis of the corrosion of bronze (19). Because we did not have specific site evidence on the halberd studied, a study of the literature was made to obtain a representative description. The halberd probably belongs to the Anyang phase of the Shang period, approximately 1300 B.C. The site of the Anyang culture, near the Yellow River (Huang Ho) in the Honan Province of Northern China, is known to be composed of a rich alkaline loessial soil. The mineral content has been reported by Collins (20) to be 64.22% SiO₂, 18.10% Al₂O₃, 6.31% CaO, 2.09% MgO, and 0.0% Fe₂O₃, FeO, P₂O₅, SO₃, MgCO₃ or CaCO₃. The EDAX analysis of soil particles found on the surface of the halberd indicated the presence of the following elements in descending order of magnitude: silicon, aluminum, potassium \approx calcium, and iron. The soil is very permeable and has a large water-holding capacity. Rainfall in the area varies throughout the year resulting in periods of drought and periods of flooding. The climate is temperate with a large difference in temperature between the warm summers and cold winters (1,20,21).

The Shang Burial Practices. Graves of the Anyang phase Shang Dynasty were constructed by a rammed-earth method. The square or rectangular pits with a north-south orientation had long ramps extending on two or four sides of the pit with the longest ramp extended to the south. Within the pit, a wooden chamber was built which contained the wooden coffin of the deceased and, in various locations, human sacrifices, pottery, bronze ritual vessels, and bronze weapons (1,22). Some of the chambers discovered "had thoroughly disintegrated and were water-logged" (22).

There is no information concerning the burial of the bronze halberd under study; however, it is assumed that it must have been buried in a traditional Shang manner. Silk fabric pseudomorphs were found on the halberd; therefore, it must have been placed in contact with fabric resting either on the ground, on a shelf, or on a body in the burial pit. Each of these three situations could provide a different outlook on the chemical reactions involved in pseudomorph formation. Due to lack of site information, the influence of the placement of the halberd can only be speculated upon.

The Chemical Composition of Shang Bronzes. Early Shang (pre-Anyang) bronzes contain varying levels of copper, tin, and lead, which reflect the early stages of development of bronze metallurgy (23). By the Anyang phase, bronze production became more controlled, and bronzes from this phase contain primarily copper and tin with a smaller proportion of lead (23). Although the bronze of the halberd studied has not yet been analyzed for mineral composition, no lead-containing corrosion products were found on its surface. It is reasonable, therefore, to assume that there is little if any lead in the bronze itself.

The Weathering of Minerals and the Corrosion of Metals. Mineral ores are in a reduced state in the environment beneath the ground water table and remain stable indefinitely if the water does not become oxygenated. If the ores are raised above the level of the water table, oxidation and solution of the metal ions begin to take place (24). Natural surface water has a pH of 5.7 because of dissolved carbonic acid (25), but if decaying organic material is present, the pH may be lower. Acidic natural waters are a better solvent for metal ions than is neutral water. The dissolved ions move with the migrating water, reacting with oxygen or with ions such as carbonate, hydroxyl, silicate, or sulfate, which results in precipitation (24). The reactions that occur and the resulting mineral products are governed by (1) the availability of the ions with which the metals react and (2) the pH and oxidation-reduction potential of the environment.

The corrosion process of bronze metal which is buried in soil is described in a manner similar to the weathering of mineral ores. The factors that affect the corrosion include the "composition of the metal,

the kind and concentration of the chemically active agencies (especially of oxygen and salt anions), pH or degree of acidity or alkalinity, temperature, seasonal changes, and finally the physical character of the products of chemical change" (14). The corrosion process is primarily electrochemical in character; the alloys such as bronze contain small cathodic and anodic points due to their heterogeneous structure. Random deposition of the corrosion products on the metal surface results (20). Water penetrates the intergranular boundaries of the bronze metal, and the copper and tin ions dissolve. Tin oxidizes quickly to form a stable tin oxide essentially in situ, and the oxide precipitates within the dendritic structures of the bronze or as a surface layer in contact with the bronze (13,26). Copper ions migrate with the water and react with available anions to produce oxides, hydroxides, chlorides, sulfates, carbonates, and other complex salts. Each corrosion product is deposited on the bronze in layers or in irregular patterns. Tenorite (CuO) forms a black bumpy layer; cuprite (Cu_2O) a thin red layer; and malachite ($\text{CuCO}_3\text{-Cu(OH)}_2$) grows in nodules. Malachite forms the characteristic and abundant green outer coating seen on bronze objects (13,14,26). Stability of metals and their corrosion products in isolated systems is represented by Pourbaix diagrams [oxidation-reduction potential (Eh) vs. pH]. Construction of such diagrams with emphasis on museum artifacts has been described by Pourbaix (27). Part of the work in progress involves the modification and interpretation of Eh -pH diagrams of copper and its corrosion products with respect to the environmental conditions encountered in weathering environments and the degradation of textile fibers.

Decay of Silk. Silk is a protein fiber, a polymer of α -amino acids. It will degrade in a variety of ways depending on the elements of the environment, including temperature, moisture, pH, Eh , and salinity. In the environment of the burial site described, the silk would at times be exposed to moist, oxidative conditions. The fiber swells as intermolecular bonds are broken, and the polymer chains begin to break at random points. Silk filaments are approximately 20 μm in diameter; the silk filament pseudomorphs vary from 39 to 49 μm . As the degradation proceeds, the fiber deteriorates into its component amino acids and other small molecules such as carbon dioxide, ammonia, and water. The presence of the copper in the adjacent bronze halberd inhibits bacterial degradation, and the alternating wet-and-dry, cold-and-hot conditions provided by seasonal weather variations also slow the degradation process.

Based on a compilation of the preceding information on the probable environment in which the bronze halberd was found, a model can be proposed for the process of silk fabric pseudomorph formation. The presence of an organic material in close proximity to the bronze object alters

the microenvironment of the contact area. Copper ions dissolved in the corrosion solution migrate with the water from the bronze surface, and, because the silk fabric is also wet, the corrosion solution penetrates it as well. The decomposing silk fabric contributes to the acidity of the aqueous solution in contact with the fabric and the bronze. Copper ions within the fiber structure will react in a manner similar to those on the unencumbered bronze surface. The oxidation, hydration, or carbonation products deposited within the fiber structure are restricted by the organic molecular network that remains. Thus a silk fiber, although decomposing ultimately into small water-soluble molecules and some gases, maintains some structural integrity during the process of its decomposition. The long polymer chains, decreasing in size and spreading apart from each other by fiber swelling, form a network with enough association that the degrading fiber maintains its outer physical structure and therefore results in mineral deposition, which also maintains the outer physical structure of that fiber. It is this shape retention in mineral replacement that categorizes these phenomena as pseudomorphs occurring by a petrification process in a manner similar to the formation of certain fossils (28).

Because some aluminum oxide or hydroxide is present in all the types of corrosion studied, general contamination of the bronze by the soil is assumed. Aluminum ions are not abundant in natural water, but aluminum oxides form the second largest component of the soil in the Honan Province. These oxides are only slightly soluble in acid solution but given a long enough period of time, some must migrate into the acidic corrosion solution surrounding the bronze and penetrate the silk fabric.

As previously noted, there are both black and green silk pseudomorphs on the halberd. An example is shown in Figure 7. The mineralogical analysis indicates that the green pseudomorphs are composed of malachite plus some aluminum oxide or hydroxide and the black pseudomorphs are composed of tenorite, some aluminum oxide or hydroxide, and possibly some malachite. Black and green silk filament pseudomorphs of equal size were observed on the same level of corrosion layers on the halberd. Because these pseudomorphs are the same in all respects except color and predominant mineral composition, something different in the chemistry of the fibers must have caused differential mineral replacement. The black and green filaments are not a result of random mineralization processes. There are many areas where green filaments interlace black filaments, and a random process of replacement would result in completely green areas and completely black areas. In addition, study of the pseudomorphs as evidence for textiles showed that large black yarn pseudomorphs occurred along the surface of fabric-type formations, while green pseudomorphs (systems A and B) formed a base structure

for the same fabric layer (Figure 7). This finding raises the possibility that the black pseudomorphs were originally dyed silk and the green pseudomorphs were undyed silk.

The dye could be affecting the mineral replacement process in a number of ways. Perhaps the dye limits the production of carbon dioxide and acids from the silk degradation. In the absence of carbon dioxide and at a pH of approximately 6, the stable form of copper corrosion product is tenorite. In more acidic solutions, malachite production is favored (20,27). In an undyed silk fiber, acidic degradation products and carbon dioxide are produced. As copper ions enter the fiber, they react with HCO_3^- , forming the carbonate (malachite), which precipitates. Perhaps the dye itself degrades to make the solution within the fiber less acidic, again favoring the formation of tenorite. Perhaps the dye, by blocking pore sites in the fiber, restricts moisture transport and slows the degradation of the silk by slowing the replenishment of fresh oxidizing solution. No conclusion can be made without further study of pseudomorphs, particularly those on objects whose corrosion microenvironment is well documented.

Summary

Pseudomorphs on a bronze Shang Dynasty halberd (ca. 1300 B.C.) were subjected to mineralogical analysis to determine their structure and composition. x-Ray diffraction, scanning electron microscopy, and energy dispersive analysis of x-rays were used in these analyses. Photomicrographs of pseudomorphs also were studied for fiber, yarn, and fabric formations that give evidence of textiles. A model describing the process of silk pseudomorph formation was proposed.

Micrographic and mineralogical analysis of both sides of the halberd revealed green and black pseudomorphs on one side of the blade and green and black nodular formations on the reverse side. Both green materials contain malachite with some aluminum oxide or hydroxide impurity. Both black materials contain tenorite plus some oxide or hydroxide of aluminum and perhaps some malachite.

Two categories of pseudomorphic textile fabric formations were identified. One, the yarn type, moves in and out of the second, the fabric type. At least six areas of the latter are apparent.

Observation of single and paired strands moving in relatively straight trajectories, more often without any twist than with twist, confirm silk pseudomorphs on the halberd. In all likelihood, the silk was present in its natural filament form, but the large (0) single yarns of multiple fibers and the three-ply (✓) yarn also indicate the probability of silk staple yarns.

Interaction in the form of a perpendicular interlacing of two yarn systems confirms the presence of woven structures. No selvage was observed; thus the warp system could not be distinguished from the weft system. Both curvilinear and zig-zag trajectories of certain yarns with respect to the interlacing systems were recorded. These may or may not indicate surface decoration in the form of embroidery.

A model for the process of silk pseudomorph formation on bronze is proposed, including solution of copper ions, transport inside the swollen silk, reaction with available anions, and deposition of the resulting products. The maintenance of the outer physical structure of the fiber is attributed to the network of the polymer chains of silk and the maintenance of some structural integrity during degradation. The presence of green and black pseudomorphs of equal size in the same location on the halberd led to a discussion of the possibility of differential replacement of dyed silk fibers and undyed silk fibers.

Questions that remain concerning the process of silk fabric pseudomorph formation on the bronze halberd will be resolved with further study of pseudomorphic formations, particularly on objects whose provenance is documented precisely. A more complete description of the microenvironment of the buried objects as well as a quantitative analysis of the mineral composition of the pseudomorphs is necessary for the development of equations for the chemical equilibria involved. Future work is planned to study pseudomorphs as mineralogical structures and pseudomorphs as evidence of textiles. This work includes examination of two additional Shang bronze objects currently on loan to one of the authors.

Acknowledgments

The authors gratefully acknowledge support received from the Dean, College of Home Economics, the Department of Geology, and the Vice President for Research, University of Georgia. We also wish to thank James W. Morgenthaler for his work in photographing the halberd and producing the enlarged Cibachrome prints, Thomas Kremer for technical assistance in the mineralogical analysis, and the Museum of Anthropology, University of Missouri at Columbia for the loan of the Shang halberd.

Literature Cited

1. Chang, K. C. "The Archaeology of Ancient China"; Yale University Press: New Haven, 1968; p. 92.
2. Sibley, L. R.; Jakes, K. A. *Clothing and Textiles Res. J.* **1982**, *1*, 24–30.
3. Sylwan, V. *Bulletin, Museum of Far-Eastern Antiquities* **1937**, *9*, 119–26.
4. Biek, L. "Archaeology and the Microscope"; Butterworths: London, 1963.
5. Carroll, D. L. *AJA* **1973**, *77*, 334–36.

6. Vollmer, J. In "Proceedings, Irene Emery Roundtable on Museum Textiles"; Textile Museum: Washington, D.C., 1974; pp. 170-74.
7. Sibley, L. R.; Korslund, L.; Rowlett, R. M. In "Combined Proceedings, Association of College Professors of Textiles and Clothing"; Brigham Young University Press: Salt Lake City, 1978; pp. 94-95.
8. Cullity, B. D. "Elements of X-ray Diffraction"; Addison Wesley: Reading, MA, 1978.
9. Joint Committee on Powder Diffraction Standards. "Powder Diffraction File Reference"; Joint Committee on Powder Diffraction Standards: Philadelphia, 1967.
10. Nielsen, N. A., In "Corrosion and Metal Artifacts"; NBS Special Publication, 1977, 479, 17-37.
11. Hana, E. S.; Ford, W. E. "A Textbook of Mineralogy"; Wiley: London, 1922.
12. Read, H. H. "Rutley's Elements of Mineralogy"; Murby: London, 1970.
13. Gettens, R. J. *J. Chem. Ed.* 1951, 28, 67-71.
14. Gettens, R. J. In "Art and Technology, A Symposium on Classical Bronzes"; Doeringer, S., Ed.; MIT Press: Cambridge, 1970; pp. 57-72.
15. Plenderleith, H. J. In "Art and Technology, A Symposium on Classical Bronzes"; Doeringer, S., Ed.; MIT Press: Cambridge, 1970; pp. 95-102.
16. Plenderleith, H. J. In "Corrosion and Metal Artifacts"; NBS Special Publication, 1977, 479, 191-240.
17. Joseph, M. L. "Introductory Textile Science"; Holt, Rinehart and Winston: New York, 1977.
18. King, M. E. *American Antiquity*, 1978, 43, 89-96.
19. Tylecote, R. F. *J. Archaeol. Sci.* 1979, 6, 345-68.
20. Collins, W. F. *J. Inst. Metals* 1931, 45, 23-55.
21. Needham, J. In "Science and Civilization in China"; University Press: Cambridge, 1954; Vol. 1.
22. Thorp, R. L. In "The Great Bronze Age of China"; Fong, W., Ed.; Knopf: New York, 1980; pp. 51-66.
23. Chase, W. T.; Ziebold, T. O. In "Archaeological Chemistry II"; Carter, G. F., Ed.; ADVANCES IN CHEMISTRY No. 171; American Chemical Society: Washington, D.C., 1978; pp. 293-334.
24. Garrells, R. M.; Christ, C. L. "Solutions, Minerals and Equilibria"; Harper and Row: New York, 1965.
25. Krauskopf, K. B. "Introduction to Geochemistry"; McGraw-Hill: New York, 1967.
26. Walker, R. J. *J. Chem. Ed.* 1980, 57, 277-80.
27. Pourbaix, M. In "Corrosion and Metal Artifacts"; NBS Special Publication, 1977, 479, 1-16.
28. Dunbar, C. O.; Waage, K. M. "Historical Geology"; Wiley: New York, 1969.

RECEIVED for review October 6, 1982. ACCEPTED for publication April 18, 1983.

Formation of the Image on the Shroud of Turin by x-Rays: A New Hypothesis

GILES F. CARTER

Eastern Michigan University, Chemistry Department, Ypsilanti, MI 48197

Intensive study of the Shroud of Turin by previous investigators has shown that the image very probably was not formed by painting, dyeing, rubbing, or staining. Indeed no hypothesis satisfactorily explains all attributes of the image, such as its inherent three-dimensional information or its shallow depth. The new hypothesis suggests that x-rays emanated from the elements sodium, silicon, phosphorus, sulfur, chlorine, potassium, and calcium on the surface of the skin. These long-wavelength x-rays, which are easily absorbed by air, apparently account for most attributes of the body-image. Calculations show the x-ray image would be moderately, but not severely, out of focus. Iron, which is present over the entire Shroud in varying concentrations, catalyzes the image formation by x-rays or by scorching.

THE SHROUD OF TURIN is a unique archaeological object believed by many to be the burial cloth of Jesus Christ. Even apart from its religious significance, the Shroud is extremely important. It has already provided a great deal of information on the process of crucifixion.

The Shroud is a piece of fine linen, approximately 1.1 m wide and 4.3 m long, bearing the faint, diffused image of a crucified male (Figure 1). The linen is in a remarkable state of preservation considering its age (it dates at least from A.D. 1357, when it was first displayed publicly, and possibly dates to the first century A.D.) and its function (used to cover a dead body—most shrouds are rather badly decomposed). Its true age may be determined by carbon-14 dating, but this critically important experiment has not yet been performed.

Description of the Image on the Shroud

The image on the Shroud of Turin is a straw color that penetrates only one or two microfibrils or about 125 μm of the linen. When one is close

0065-2393/84/0205-0425\$06.50/0
© 1984 American Chemical Society

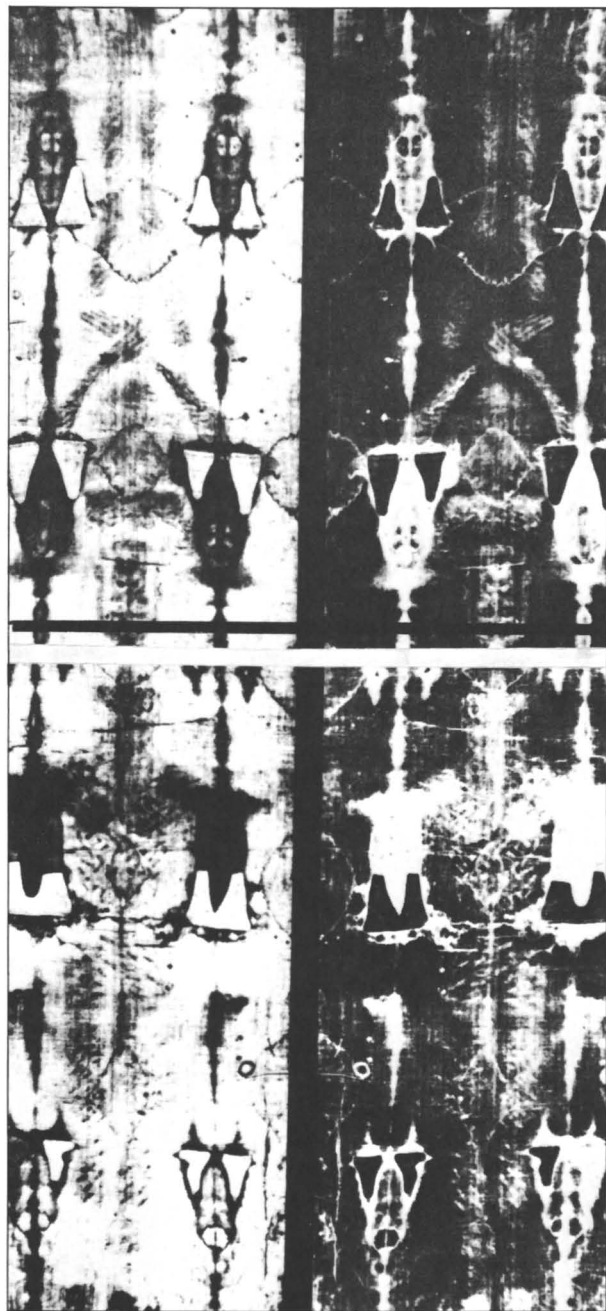


Figure 1. The Shroud of Turin: top, front; bottom, dorsal. The positive has a dark beard and moustache and dark blood; the negative has a light beard, etc. (Reproduced with permission. Copyright 1978, Vernon Miller.)

to the Shroud, the image is difficult to see clearly, but from a distance it becomes fairly clear. Thus the image appears diffuse or somewhat “out of focus.” Jackson et al. have demonstrated that the image contains some three-dimensional information (1,2). The Shroud also has been stained by blood, body fluids, and water used in 1532 to extinguish a fire in which the Shroud was partly burned and scorched in certain areas. The blood stains have been shown by Heller and Adler (3) to be just that—stains caused by contact with blood and body fluids. The image on the Shroud, which is the topic of study in this chapter, is separate from the blood stains and was formed on the linen after deposition of the blood stains (3).

Heller and Adler (3) state that the image on the Shroud has not been applied by humans by painting, staining, dyeing, or rubbing. The quantity of iron oxide present on the Shroud is insufficient to account for the image, and the concentration of iron oxide does not correlate with the image intensity. Heller and Adler’s work disproves that the image on the Shroud was caused by iron oxide, as was claimed by McCrone (4–6), or rubbing, as claimed by Nickell (7). Furthermore, the diffuseness of the image, the shallow penetration of the image into the linen thread, and the three-dimensional information contained in the image are additional evidence that the image was not produced by painting, rubbing, dyeing, or staining.

Other important features of the Shroud image are the minimal distortion and the presence of vertical striations apparently caused by different intensities of the image on different linen threads. These attributes, as well as the ones discussed above, must be accounted for by any satisfactory hypothesis of image formation; these attributes of the image are summarized in the box on the next page.

Hypotheses for Image Formation

It is not the purpose of this chapter to attempt to disprove the various hypotheses that have been advanced to explain the formation of the image on the Shroud. However, it is appropriate to comment briefly on these hypotheses.

1. **Painting.** Insufficient pigments are present to account for the image; the diffuse character, three-dimensional information, lack of brush strokes, and thin surface coloration of the image make this method highly improbable.

2. **Dyeing.** The color of the image is due to dehydrative oxidation of cellulose according to Heller and Adler (3). No evidence for dyes has been found on the Shroud; this method of image formation is highly unlikely.

Attributes of the Image on the Shroud of Turin

1. The intensity of the image is inversely proportional to the distance between the body and the cloth. It appears that no image is formed when the body-cloth distance exceeds 4 cm.
2. Features are usually recognized more clearly in photographic negatives of the image.
3. The image contains some three-dimensional information.
4. The image does not penetrate through the linen; it is about 125 μm deep at most.
5. The image is due to the degradation of cellulose by dehydrative oxidation.
6. Individual fibrils have about the same intensity of color.
7. The image color is straw-yellow.
8. The image was formed after the blood stains were deposited.
9. The intensity of the color in the image varies by roughly a factor of 10.
10. The image is indistinct at close range, but fairly sharp when viewed from a distance (i.e., it appears fuzzy or out of focus).
11. The image is somewhat distorted in some areas such as the hips, suggesting cloth draped over a three-dimensional body form.
12. No brush strokes or directionality of the image has been observed.
13. The image is stable to elevated temperatures (the fire of 1532 did not destroy or alter the image near burned areas).
14. The image is not soluble in water (water was placed on the Shroud to extinguish the fire in 1532; although the blood areas "ran" somewhat, the body image did not).
15. Some threads running the length of the Shroud were colored much more strongly than others. Also, some horizontal threads are deeper or lighter in color than their neighboring threads.

3. Staining. Most of the comments from the two previous hypotheses apply. This method is highly unlikely to have produced the image.

4. Rubbing. The lack of pigment from rubbing essentially rules out this method. It is nearly impossible to prepare a rubbing that would convey three-dimensional information. [Jackson et al. asked police artists to try to duplicate the three-dimensional effect, but they could not do it (2).] No brush strokes or directionality of the image exist.

Pertaining to the four hypotheses, the Shroud of Turin contains physiologically correct information that is counter to popular conceptions

of crucifixion. Nail holes are in the wrist rather than through the hand; blood has run down the arms in two different angles. This information on the Shroud would not likely have been portrayed by a human artist before A. D. 1357. For all the above reasons scientists almost unanimously believe that the image on the Shroud was not painted, dyed, rubbed, or stained.

5. Vapor-Phase Reaction. Perhaps the image was formed by the diffusion of gases, particularly ammonia, from sources such as decomposing sweat or blood, and these gases reacted with burial spices or other compounds on the cloth. However, Jackson et al. (2) found the method cannot account for facial details in the three-dimensional information in the image. The surface-only characteristic of the image is difficult to account for by a vapor phase, which would permeate the cloth. The image would likely be far too diffuse to give the sharpness present in the image. No spices have been found on the cloth. The image of hair is difficult to account for by this hypothesis. This mechanism is unlikely.

6. Physical Contact. The image was perhaps formed through direct contact with a body covered by decomposed sweat, skin, and the like interacting with other chemicals on the cloth, such as spices. However, this process would likely cause much distortion in the image and would not produce gradations in intensity (shading) such as found on the Shroud. The image is uniformly not very deep into the cloth, and direct contact would not be likely to produce a uniform image to limited depth. The intensity of the image would probably be proportional to the pressure on the cloth, but the same approximate intensity exists for frontal and dorsal images. Almost no chemicals are presently on the Shroud. The image appears for parts of the body where little or no contact occurred. The three-dimensional relief of a direct contact image was found by Jackson et al. (2) to be highly distorted. The excellent state of preservation of the linen argues against a centuries-long period of image formation.

7. Scorching with a Hot Statue. Perhaps a statue of a man or a bas-relief (2) was heated, and the cloth was applied to the statue to produce scorching. However, this method is unlikely to produce an image with correct three-dimensional information or an image that is only about 125 μm deep in the linen. Also, the image would be distorted by the bending (drape) of the cloth (8). Experiments have shown that this method would not produce the shading found on the Shroud. The resolution of the image is another difficulty for this method, and it would be exceedingly difficult to obtain the uniformity of image intensities over a large surface. Details, such as the scourge marks covering the body, would be difficult to form by means of a scorch method.

8. High-Intensity Light. Because the image is similar to a scorch, perhaps it was caused by a strong burst of light. High intensities of light are capable of casting images on materials other than photographic film;

for instance the shadow of a valve wheel occurred on concrete due to the atomic bomb explosion in Hiroshima (9). The main difficulty with this hypothesis is the three-dimensional character and diffuseness of the image. Light presumably would be emitted spherically from an array of point sources. This would cause some three-dimensional information (the intensity would decrease laterally on the cloth above a point source because the angular emission, in photons per degree, is constant, but the number of photons striking the cloth would decrease with distance—see Figure 2). However, the image from light alone would likely be too diffuse. This hypothesis would probably account for the degradation of linen to only a relatively small depth. The intensity would be proportional to the distance between the body and the cloth because of geometric dispersion.

9. Corona-Discharge. Perhaps a high potential difference resulted in the emission of ions that were collimated by an electric field (10). Problems with this hypothesis, as outlined by its author, include the following: (1) How was the dorsal image generated if the body rested directly on the cloth? (2) Would there be sufficient potential difference between a body and a linen cloth around and about it? (The natural fibers would tend to short out the potential difference.) (3) An image has not yet been produced by this mechanism.

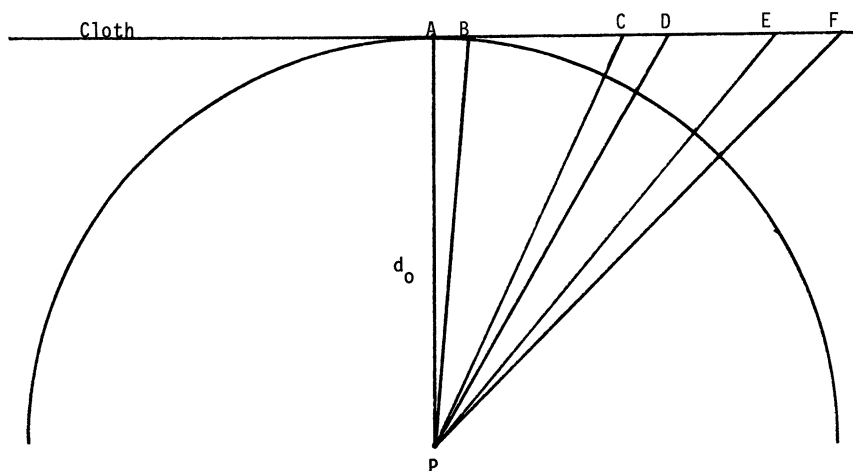


Figure 2. Geometric attenuation of an image from a point source.

P is the point source of x-rays that emanate spherically. The point *A* is defined as ground zero; d_0 is the minimum distance between *P* and the cloth, namely *AP*. Angles *APB*, *CPD*, and *EPF* are each equal to 5° . The same number of x-rays would fall on *AB* as on *CD* or *EF*, assuming that none of the x-rays are absorbed by the intervening space (i.e., the space is a vacuum). Therefore, the number of x-rays per centimeter for *AB* is greater than the x-rays per centimeter for *CD*, which in turn is greater than the x-rays per centimeter for *EF*; *a* is the lateral distance along the cloth, such as *AB*, *AC*, *AD*, or *AE*.

In conclusion, after a large volume of scientific work on the Shroud of Turin no satisfactory mechanism has yet been proposed to account for the formation of the image on the Shroud.

Some Observations of the Image on the Shroud of Turin

Although direct observation of the Shroud of Turin has not been made by the author, many photographs and slides have been studied. Primarily these consist of photographs, including some life-size photographs in the public display on the Shroud prepared by Vernon Miller, the official photographer during the 1978 scientific examination and study of the Shroud.

Many observers have noted the "too-long" fingers in the Shroud image. The fingers are extremely long for a man of 1.73–1.78 m (5'8"–5'10") height (*see* Figure 3). The probability is very small that a man of this height would have such long fingers, yet this remains a possibility (8). Other explanations of the long fingers are that the cloth was moved during image formation or that somehow the image of the fingers was distorted by having their apparent length increased. However, the hand image does not appear to be distorted in this manner, so this appears to be a remote possibility. A disease called Marfan's syndrome could also cause a person to have unusually long fingers but other parts of the body would be similarly affected; however, the Shroud body is muscular and not slender as is found in those afflicted with Marfan's syndrome, and this explanation seems improbable. A further suggestion is that there was much blood in the vicinity of the fingers due to the wrist wound and perhaps due to other wounds on the hands. This suggestion can be checked by further study of the Shroud to determine whether the finger images are due primarily to blood or to the phenomenon that caused the other parts of the image on the Shroud.

The author's suggestion is that the finger images may be due at least in part to x-rays emanating from the bones in the body. Finger bones continue throughout much of the hand, and they could cause the fingers to look too long. In normal bodies, the ratio of the distance from the middle fingertip to the base of the finger divided by the distance from the middle fingertip to the wrist (wound area) is about 0.5. This compares with a ratio of about 0.6 for the image on the Shroud, meaning that the fingers are unusually long and the rest of the hand is grotesquely small. The probability for this to have occurred must be small.

Close inspection of the fingers on both hands reveals still further interesting information. The hand having the visible wrist wound has the tips of the four fingers nearly in a straight line. This is most probably due to the bending of the fingers. As a person cups his or her hand, the fingertips tend to line up. Because this hand probably had its fingers

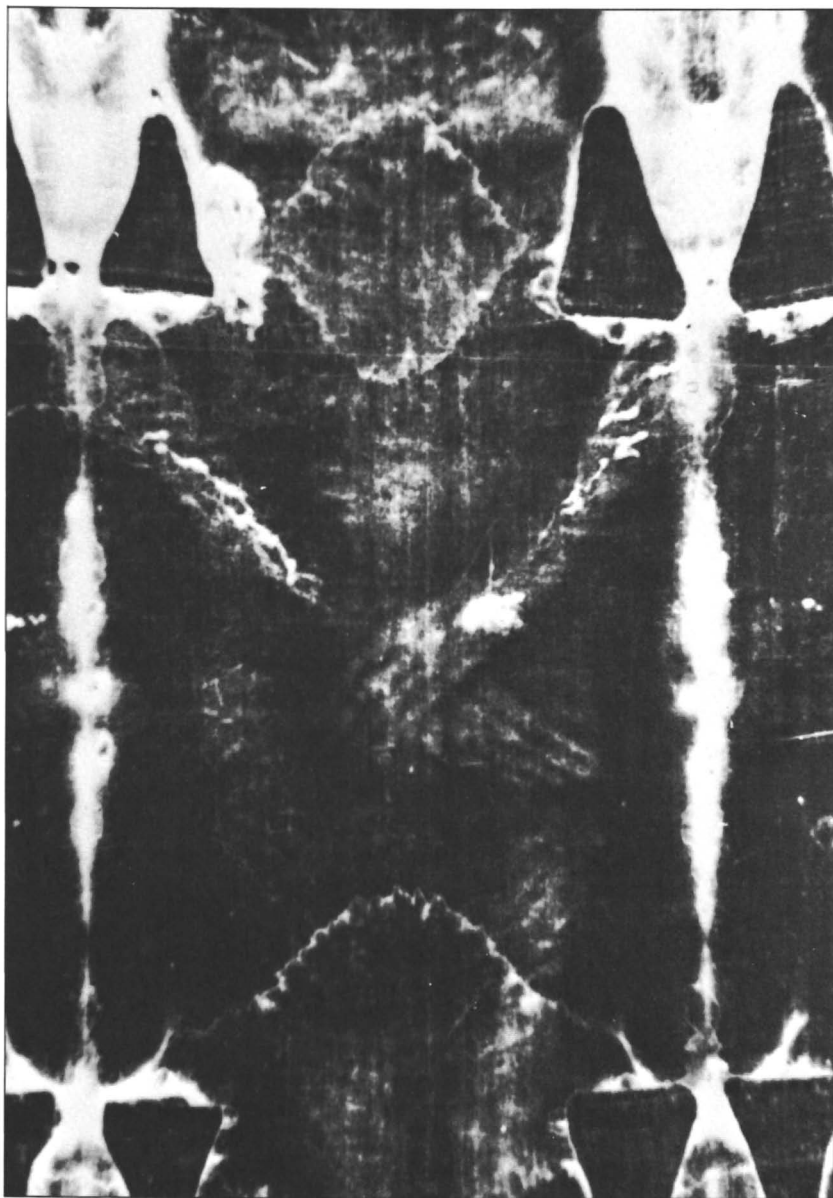


Figure 3. Exceptionally long fingers of the body on the Shroud of Turin. (Reproduced with permission. Copyright 1978, Vernon Miller.)

bent somewhat, the real length of the fingers was somewhat greater than that obtained by directly measuring the Shroud image. This exacerbates the above problem. The other hand apparently has the little finger bent away from the cloth more than the other fingers leading to a highly uneven length of fingers on the Shroud image.

A second curious part of the Shroud image is the mouth area. Close inspection, particularly of slides from a distance, shows the presence of what appear to be eight or more objects, two rows of four or six (*see* Figure 4). Perhaps these could be teeth images, but other observers disagree with this assessment. Because the lips probably covered the teeth of the body of the Shroud, any images of teeth may indicate that x-rays have been involved in the formation of the Shroud image (or perhaps the skin decayed and shrank before the image was completely formed).

A third observation indicating possible image formation by x-rays is the high, pronounced cheekbones. The face is somewhat skull-like, especially in the appearance of the high cheekbones. Part of the backbone may be visible on the dorsal image, but again others have stated that they do not see any bone or teeth images.

x-Ray Hypothesis for Image Formation

If moderately strong x-rays emanated from the bones and teeth of this body or if radiation came from surrounding rocks or soil, then some of the x-rays would have been absorbed by elements at the surface of the body, such as sodium, silicon, phosphorus, sulfur, chlorine, potassium, and calcium, as well as carbon, oxygen, and nitrogen, and characteristic x-rays of relatively long wavelengths would be emitted due to an x-ray fluorescence effect.

These x-rays, many of which were presumably emitted from the surface of the body, would then have interacted with both air and cellulose. Air strongly attenuates x-rays of long wavelengths, and even cellulose absorbs a high percentage of soft x-rays in a few micrometers. However, energetic x-rays (short wavelengths) would not be attenuated by air to any appreciable extent and would largely pass through cellulose (linen) without absorption (*see* Tables I and II).

Table I presents calculations showing the transmittance (the inverse of attenuation) of characteristic x-rays of several elements in air, and Table II shows the transmittance of these soft x-rays in cellulose. There also is a spatial attenuation factor of the x-rays due to the fact that x-rays are spherically generated. Because of this effect, the closer the x-ray source to the cloth, the greater the intensity of x-rays at a small area adjacent to the x-ray source. The lateral x-rays decrease geometrically in number with the number of degrees away from the perpendicular line



Figure 4. Possible teeth images on the Shroud of Turin. (Reproduced with permission. Copyright 1978, Vernon Miller.)

Table I. Transmittance of K_{α} x-Rays of Various Elements Through Air

Element	μ/ρ	Length of Air Path (cm)								
		0.100	0.200	0.300	0.500	1.00	1.50	2.00	2.50	3.00
Na	3088	0.695	0.483	0.335	0.162	0.026	0.004	0.001	N	N
Si	727	0.918	0.842	0.773	0.651	0.424	0.276	0.180	0.117	0.076
P	464	0.947	0.896	0.849	0.761	0.578	0.440	0.335	0.254	0.193
S	317	0.963	0.928	0.894	0.829	0.688	0.571	0.473	0.393	0.326
Cl	219	0.974	0.950	0.925	0.879	0.772	0.679	0.596	0.524	0.461
K	122	0.986	0.972	0.958	0.931	0.866	0.806	0.750	0.698	0.649
Ca	88.8	0.990	0.979	0.969	0.949	0.901	0.855	0.811	0.770	0.730
Fe	18.2	0.998	0.996	0.994	0.989	0.979	0.968	0.958	0.948	0.938
Cu	9.39	0.999	0.998	0.997	0.994	0.989	0.984	0.978	0.973	0.967
Mo	1.12	1.000	1.000	1.000	0.999	0.999	0.998	0.997	0.997	0.996

NOTE: All values above are for transmittance, I/I_0 , calculated from the equation

$$I/I_0 = e^{-\mu/\rho \cdot 0.00118 \cdot \text{air path in cm.}}$$

N = negligible (<0.0005).

Values for μ/ρ were obtained from Reference 11, p. 16. Values were interpolated either graphically or by calculator for the curve of $\ln \mu/\rho$ vs. λ , the wavelength in Å.

$$(\mu/\rho)_{\text{air}} = 0.7803(\mu/\rho)_{\text{N}} + 0.2099(\mu/\rho)_{\text{O}} + 0.0094(\mu/\rho)_{\text{Ar}}$$

to the cloth (*see* Figure 2). Not only is there a geometric attenuation of lateral x-rays, but the air path travelled by the lateral x-rays is greater than that of the x-rays moving almost perpendicular to the cloth, causing greater absorption of lateral x-rays in air. This combination of effects makes the image from x-ray sources reasonably sharp (for details *see* the section on calculations on the dispersion of the image).

Because of the attenuation of x-rays by air, the x-rays interacting with the cloth would convey three-dimensional information. Also because of the emission of x-rays from many point sources, the image is not in sharp focus. Rather the image is diffuse, and it can best be observed from a distance because the eye integrates the intensity of light so that the image then makes sense.

Experimental Formation of x-Ray Images

When linen is placed in an x-ray beam in an x-ray fluorescence spectrometer, it reacts with the x-rays to form a straw-brown color. Upon standing for several hours, the specimens lose some intensity, and the color changes to a straw-yellow color, similar to that of the image on the Shroud of Turin. Specimens of five different linens were used, and all gave similar results, but a recent linen having a chemical brightener gave the most rapid formation of the image. Most experiments were carried out on a linen napkin purchased about 40 years ago. Consequently it was not originally treated with chemical brighteners and crease-resistant ma-

Table II. Transmittance of K_{α} x-Rays of Various Elements Through Cellulose

Element	μ/ρ	Depth in Cellulose (μm)											
		1	5	10	20	35	50	75	100	125	150		
Na	2790	0.669	0.134	0.018	N	N	N	N	N	N	N	N	N
Si	664	0.909	0.620	0.384	0.148	0.035	0.008	0.001	N	N	N	N	N
P	421	0.941	0.739	0.545	0.297	0.120	0.048	0.011	0.002	N	N	N	N
S	294	0.959	0.809	0.655	0.429	0.227	0.120	0.042	0.015	0.005	0.005	0.002	0.002
Cl	204	0.971	0.863	0.745	0.556	0.358	0.230	0.110	0.053	0.025	0.012	0.012	0.012
K	102	0.985	0.930	0.864	0.747	0.600	0.482	0.334	0.232	0.161	0.112	0.112	0.112
Ca	73.8	0.989	0.948	0.899	0.809	0.689	0.588	0.451	0.346	0.265	0.203	0.203	0.203
Fe	15.0	0.998	0.989	0.979	0.958	0.927	0.898	0.850	0.806	0.763	0.723	0.723	0.723
Cu	7.69	0.999	0.994	0.989	0.978	0.962	0.946	0.920	0.895	0.871	0.847	0.847	0.847
Mo	0.63	1.000	1.000	0.999	0.998	0.997	0.995	0.993	0.991	0.989	0.986	0.986	0.986

NOTE: All values above are for transmittance, I/I_0 , calculated from the equation $I/I_0 = e^{-\mu/\rho \cdot 1.44 \cdot \text{path in cellulose in cm}}$.

N = negligible (<0.0005).

Values for μ/ρ were obtained from Reference 11, p. 16. Values were interpolated either graphically or by calculator for the curve of $\ln \mu/\rho$ vs λ , the wavelength in \AA .

Density of cellulose varies from about 1.27 to 1.61 g/cm^3 , or 1.44 g/cm^3 average ($(\mu/\rho)_{\text{cellulose}} = 0.4444(\mu/\rho)_C + 0.0622(\mu/\rho)_H + 0.4934(\mu/\rho)_O$)

terials. Of course, it had been bleached at some point in its manufacture, but it probably approximates satisfactorily ancient linen.

The intensity of the image formed on linen by exposure to x-rays is proportional to the length of the exposure, the current, and the potential used to generate the x-rays. Common exposures were from 10 min to 4 h using 35 keV and 21 mA; the tube target was chromium, and the machine is a Philips spectrometer. The linen was placed normally in the sample chamber and was very close to the x-ray tube. Images were formed over a period of several hours even when the power was set at 8 keV, the lowest possible power setting with this machine. Thus, the x-rays generated tended to have long to moderate wavelengths (the wavelength of Cu K_α x-rays is 0.154 nm, and these x-rays have an energy of 8.047 keV). The intensity of the image formed under vacuum was not significantly different from that of the image formed in air. The temperature of the linen specimen was about 30 °C during irradiation; accurate measurement with a thermocouple was difficult due to radiation hazards—the spectrometer had to be altered to accommodate the thermocouple. A glass capillary containing 4-aminotoluene having a melting point of 43.7 °C was placed in the position of the linen, and the solid did not melt when exposed to x-rays. Also, the glass capillary cast a “shadow” on the linen because the glass absorbed appreciable numbers of x-rays. Hence the temperature of the linen was about 30 °C, and certainly was no more than 44 °C during irradiation.

Once the image fades during the first day after exposure, there is very little, if any, further visual change in the image over at least a period of several months (Figure 5). Because the x-rays have energies that are fairly high due to the excitation voltage of 35 keV, many x-rays penetrate the linen, and the image appears both on the obverse and reverse sides of the linen, but is somewhat weaker on the reverse. The image on the Shroud is about 125 μm deep. The x-rays used in the above experiments had wavelengths shorter than the x-rays postulated to have formed the image on the Shroud. However, calculations in Table II show that x-rays from silicon would form an image on cellulose about 25 μm deep, x-rays from chlorine would form an image about 75 μm deep, and x-rays from calcium about 175 μm deep.

The x-rays that form the image are attenuated by aluminum foil. Using eight thicknesses of foil, or a total thickness of 130 μm , the aluminum absorbed almost all (about 95%) of the x-rays that form the image: only a very weak image forms. Therefore, the x-rays that form the image are at least moderately long in wavelength, namely about 0.22 nm or longer as calculated from the mass absorption coefficient of aluminum. If the specimen is placed relatively far from the x-ray tube, such as at the collimator in the spectrometer after the x-rays have fluoresced from a specimen, the intensity of the x-rays is too low to form a visible image

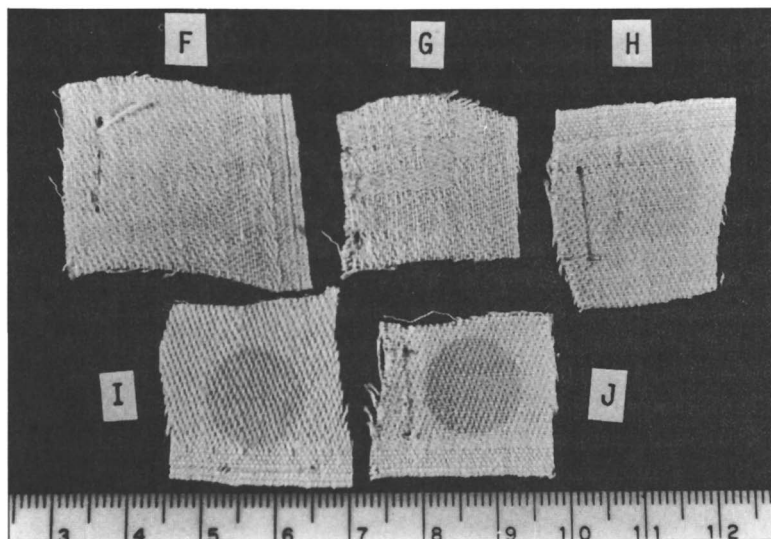


Figure 5A. Linen specimens exposed to x-rays. All specimens treated at 35 keV and 21 mA; centimeter scale used.

Key: F, 5 min; G, 10 min; H, 20 min; I, 40 min; and J, 80 min. Subtle differences in shade do not show in black and white photographs. Very slight images are actually present on specimens F and G.

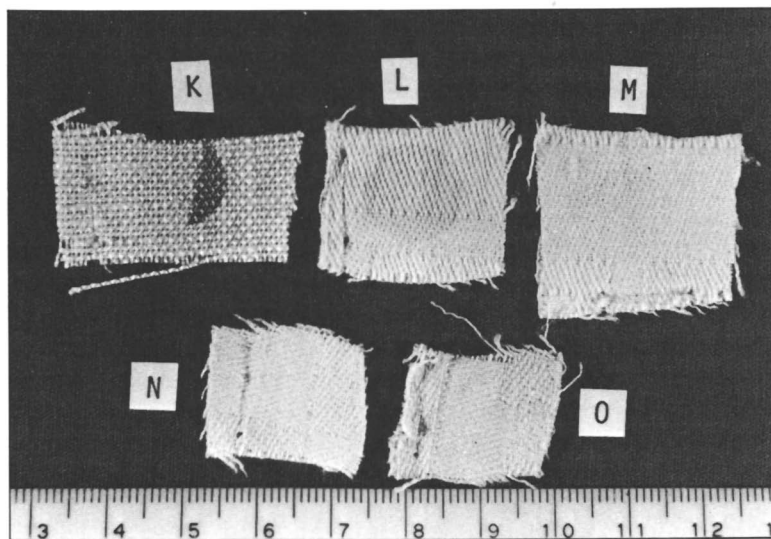


Figure 5B. Linen specimens exposed to x-rays. All specimens treated at 35 keV and 21 mA; centimeter scale used.

Key: K, 6-h exposure, 127 μm of aluminum covered half the exposed area, absorbing nearly all the image-forming x-rays. L, linen treated in 10^{-3} M Fe^{3+} and dried; 15 min in x-ray beam. M, same as L except no treatment in Fe^{3+} solution. N, no iron pretreatment; scorched by heating at 195 $^{\circ}\text{C}$ for 30 min. O, pretreated for 1 min. in 10^{-3} M Fe^{3+} solution; scorched along side of specimen N for 30 min at 195 $^{\circ}\text{C}$.

even after several hours of irradiation. Either an intense x-ray source is needed to form an image, or a weaker source over a long period of time.

Photographs of linen specimens exposed to x-rays for various lengths of time appear in Figure 5. When the x-ray exposure is excessive, such as for about 10 h, the image is very pronounced, yellow-orange in color, and the linen becomes brittle and cracks easily when flexed. Probably the reason why x-rays of short wavelengths do not contribute appreciably to image formation is that cellulose is essentially transparent to these x-rays, and therefore too few of the x-rays are absorbed by the cellulose to cause image formation. For example, refer to Table II, which shows that fewer than 2% of molybdenum K_{α} x-rays are absorbed in 150 μm of cellulose.

The Role of Iron in the Image Formation

The Shroud of Turin has many vertical and horizontal strands or threads that have an image intensity much greater than that of adjacent strands. Any hypothesis for the formation of the image must explain why various threads of linen, which are very close to one another, differ in the intensity of image.

It is known from x-ray fluorescence analyses of the Shroud (11) that iron, calcium, and strontium are the only elements having an atomic number greater than 18 that are present in detectable concentrations throughout the Shroud. There is no evidence for any other metallic species on the body image fibrils at a level that would produce color evident to the eye (3). Heller and Adler (3) found three types of iron on the Shroud: a cellulose-bound chelated form; heme-bound forms; and iron oxide (Fe_2O_3). The predominant form was the cellulose-bound form. The iron oxide occurs primarily in the water-stain margins and charred blood areas, and it constitutes a small percentage of the total iron found on the Shroud. Heller and Adler explain the presence of cellulose-bound iron as due to the retting process, in which flax was fermented by submerging the material in water for 7–21 days. Retting enables separation of the cellulose from noncellulosic materials and was used until recent times. During the retting process, the natural ion exchange properties of cellulose cause calcium and iron to bind to the cellulose (3). Linen makers tried to avoid using iron-containing water because it stains linen.

This discussion is pertinent to the image formation by x-rays because iron, but apparently not calcium, catalyzes the image formation. Concentrations of 0.01 *M* ferric nitrate indeed cause linen to stain due to the binding of iron by cellulose. Washing the linen with a strong detergent causes some of the iron to be lost, whereas washing with water causes essentially no loss of iron. If the linen is placed in a dilute iron

solution for 20 h, it binds up to several times as much iron as in a treatment of only 1 min. Solutions of ferric nitrate as dilute as 10^{-4} M still cause an easily detectable (using x-ray fluorescence analysis) pick-up of iron by the linen.

Even in concentrations as low as 10^{-4} M Fe^{3+} , linen reacts with sufficient iron to catalyze the image formation. The increase in image intensity is dependent somewhat on the iron concentration. Of course, linen fibers having relatively high iron contents are stained already by the iron.

The vertical striations in the Shroud of Turin probably represent threads of linen that have higher iron contents than do their neighbors. This prediction could be verified by experiment. The increased image intensity is probably due to the iron acting as a catalyst and possibly due to the natural color of iron bound to cellulose. Very low iron concentrations (probably less than 0.01% Fe on the linen) catalyze the image formation. Calcium by itself does not seem to catalyze the image formation. Presumably, the linen threads have different concentrations of iron due to varying conditions during retting, such as the concentration of iron in the water or the time of immersion of the flax in water, or due to different concentrations of iron in the soil in which the flax was grown.

When linen was heated for 15 min at 195 °C, light scorching occurred. However, when the linen was treated for 1 min in 10^{-4} M Fe^{3+} and then heated 15 min at 195 °C, a somewhat darker image formed. It appears that the presence of iron on linen not only catalyzes the image formation due to x-rays but also catalyzes image formation from other means as well. Incidentally, rather regularly spaced, vertical striations are visible on the sides of the Shroud, and these may have "developed" during the fire of 1532, or they may have developed due to the absorption of x-rays.

Calculations on the Dispersion of the Image

If the image on the Shroud were produced by spherical emission of x-rays from a group of point sources, two factors would have caused the attenuation of the x-rays: geometric dispersion and attenuation due to the length of the air path. x-Rays are transmitted through any medium according to the equation

$$I/I_0 = e^{-\mu/\rho \cdot \rho \cdot d}$$

where I/I_0 is the transmittance, μ/ρ is the mass absorption coefficient of elements in the medium for various wavelengths of x-rays, ρ is the density of the medium through which the x-rays pass, and d is the length of the distance the x-rays travel in the medium. For chlorine K_{α} x-rays in air

at 23°C the mass absorption coefficient is 219 (calculated from data in Reference 12 for air containing 78.0% N, 21.0% O, and 0.94% Ar) and for silicon K_{α} x-rays, it is 727. The density of moist air at 23°C is 0.00118 g/cm³. The distance in air, d , travelled by the x-rays from the point source to the cloth is $d = d_0/\cos \theta$, where d_0 is the minimum distance between the point source and the cloth, and θ is the angle between the perpendicular from the point source to the cloth and the line from the point source to the cloth at some point. "Ground zero" is defined as the point on the cloth through which the perpendicular line between the cloth and x-ray point source passes. The resulting equations for transmittance of x-rays through air follow:

$$I/I_0 = e^{-219 \cdot 0.00118 \cdot d_0/\cos \theta}$$

for chlorine K_{α} x-rays and

$$I/I_0 = e^{-727 \cdot 0.00118 \cdot d_0/\cos \theta}$$

for silicon K_{α} x-rays.

It is interesting to calculate the transmittance for chlorine and silicon x-rays as a function of both d_0 and θ . These calculations appear in Table III.

Visually, intensity is seen as the effect of the number of x-rays/cm² that interacted with the cloth. Therefore the number of x-rays/cm² striking the cloth must be calculated as a function of distance from ground zero. This value was approximated by calculating the number of x-rays per centimeter falling on a straight line passing through ground zero.

The calculations were made by using data from Table III and by assuming 100 x-rays for each degree. For example, when d_0 , the distance between the x-ray point source and ground zero, equals 10 mm, the number of silicon x-rays striking the cloth within a 1.0-mm radius of ground zero was found as follows (*see* Table III): for $a = 1.0$ mm, θ ranges from 0° to 5.71°, because $a = d_0 \tan \theta$, and therefore $\theta = \arctan (a/d_0) = \arctan (1.0/10.0) = 5.71^\circ$. The problem is to determine the number of x-rays striking the cloth between 0° and 5.71°. For 0° to 5.71° the average I/I_0 is estimated and inserted into the equation (Table IV).

$$I = 5.71 \cdot 100 \cdot 0.4235 = 242 \text{ x-rays}$$

In general the relative intensity of x-rays striking the cloth is

$$I = \text{average } I/I_0 \cdot 100 \text{ x-rays deg}^{-1} \cdot \left(\arctan a/d_0 - \arctan \frac{a - 1.0 \text{ mm}}{d_0} \right)$$

Table III. Transmittance of Silicon and Chlorine K_{α} x-Rays Through Air

	d_0 (cm)	θ							
		0°	5°	10°	20°	30°	45°	60°	75°
Si I/I_0	0.10	0.918	0.917	0.917	0.913	0.906	0.886	0.842	0.718
Cl I/I_0	0.10	0.974	0.974	0.974	0.973	0.971	0.964	0.950	0.905
a (cm)	0.10	0.000	0.009	0.018	0.036	0.058	0.100	0.173	0.373
Si I/I_0	0.20	0.842	0.842	0.840	0.833	0.820	0.785	0.710	0.515
Cl I/I_0	0.20	0.950	0.949	0.949	0.946	0.942	0.930	0.902	0.819
a (cm)	0.20	0.000	0.017	0.035	0.073	0.115	0.200	0.346	0.746
Si I/I_0	0.30	0.773	0.772	0.770	0.760	0.743	0.695	0.598	0.370
Cl I/I_0	0.30	0.925	0.925	0.924	0.921	0.914	0.896	0.856	0.741
a (cm)	0.30	0.000	0.026	0.053	0.109	0.173	0.300	0.520	1.12
Si I/I_0	0.50	0.651	0.650	0.647	0.634	0.609	0.545	0.424	0.191
Cl I/I_0	0.50	0.879	0.878	0.877	0.872	0.861	0.833	0.772	0.607
a (cm)	0.50	0.000	0.044	0.088	0.182	0.289	0.500	0.866	1.87
Si I/I_0	0.70	0.549	0.547	0.543	0.528	0.500	0.428	0.301	0.098
Cl I/I_0	0.70	0.835	0.834	0.832	0.825	0.811	0.774	0.696	0.497
a (cm)	0.70	0.000	0.061	0.123	0.255	0.404	0.700	1.21	2.61
Si I/I_0	1.00	0.424	0.423	0.418	0.401	0.371	0.297	0.180	0.036
Cl I/I_0	1.00	0.772	0.772	0.769	0.760	0.742	0.694	0.596	0.368
a (cm)	1.00	0.000	0.087	0.176	0.364	0.577	1.00	1.73	3.73
Si I/I_0	1.60	0.253	0.252	0.248	0.232	0.205	0.144	0.064	0.005
Cl I/I_0	1.60	0.661	0.660	0.657	0.644	0.620	0.557	0.437	0.202
a (cm)	1.60	0.000	0.140	0.282	0.582	0.924	1.60	2.77	5.97
Si I/I_0	2.40	0.128	0.127	0.124	0.112	0.093	0.054	0.016	0
Cl I/I_0	2.40	0.538	0.537	0.533	0.517	0.489	0.416	0.289	0.091
a (cm)	2.40	0.000	0.210	0.423	0.874	1.39	2.40	4.16	8.96

NOTE: For silicon: $I/I_0 = e^{-727 \cdot 0.00118 \cdot d_0 / \cos \theta}$
 For chlorine: $I/I_0 = e^{-219 \cdot 0.00118 \cdot d_0 / \cos \theta}$

where a and d_0 are in millimeters, and the number of 100 x-rays per degree is purely arbitrary. Calculations of the relative intensities, based on 100 x-rays per degree, appear in Table IV for silicon K_{α} x-rays and Table V for chlorine K_{α} x-rays.

Assume that intensities of about 400 x-rays/mm are the lowest number leading to a visible image. This assumption appears reasonable in that the strongest image formed on the linen would be produced from (relatively) 4090 x-rays/mm, or 10 times the intensity of the faintest image. It has been estimated that the most intense part of the visible image on the Shroud of Turin is roughly 7 times the weakest visible portion of the image (13). Only 15 shades of gray were distinguished photographically (14). Hence the above assumption is reasonable.

When Table V is studied to determine the fuzziness of the image from a point source as a function of d_0 , the maximum value of a for which even a faint image would be present is about 4.7 mm (d_0 is the minimum distance between the point source of x-rays and the cloth; a is the lateral distance in the plane of the cloth from ground zero). When d_0 is 1.0 mm, most of the x-rays reach the cloth, but because of the proximity of

Table IV. Relative Intensities of Silicon K_{α} x-Rays as a Function of a and d_o

d_o (mm)	a (mm)								
	1.0	2.0	3.0	4.0	5.0	6.0	7.0	8.0	9.0
1.0	4090	1580	646	326	180	(116)	N	N	N
2.0	2210	1480	860	504	310	204	(139)	N	N
3.0	1420	1140	810	547	372	257	182	N	N
5.0	734	669	566	456	355	275	209	162	N
7.0	445	422	384	334	284	236	194	N	N
10.0	242	235	222	205	186	165	N	N	N
16.0	(90)	(89)	(87)	(84)	N	N	N	N	N
24.0	(31)	(30)	N	N	N	N	N	N	N

NOTE: N = negligible (<150). Numbers in parentheses are negligible, but nevertheless are instructive.

All values are numbers of x-rays/mm, calculated from Table III using the equation $I = \text{ave. } I/I_o \cdot 100 \text{ x-rays deg}^{-1} \cdot (\text{arc tan } \frac{a}{d_o} - \text{arc tan } \frac{a - 1.0 \text{ mm}}{d_o})$, where a and d_o are millimeters.

a is the lateral distance between ground zero and the point where x-rays strike the cloth.

d_o is the perpendicular distance between the point source of x-rays on the body and the cloth.

the point source of x-rays to the cloth, the image is fairly sharp (the maximum a is about 3.7 mm). When d_o is 3.0 mm, then the maximum radius, a , for a visible image is about 4.7 mm. When d_o is 4.0 mm or greater, the value of maximum a for which the image is visible decreases. This is due to the increasing absorption of silicon x-rays by longer air paths. Finally, when d_o exceeds about 7 mm, no visible image is found anywhere because most of the silicon x-rays are absorbed in air. The net result of the calculations is that regardless of d_o , the image from silicon

Table V. Relative Intensities of Chlorine K_{α} x-Rays as a Function of a and d_o

d_o (mm)	a (mm)									
	1.0	2.0	3.0	4.0	5.0	6.0	7.0	8.0	9.0	10.0
1.0	4370	1760	758	387	240	(159)	N	N	N	N
2.0	2520	1730	1040	641	419	290	209	N	N	N
3.0	1700	1400	1020	722	512	373	279	215	N	N
5.0	992	917	793	657	533	429	345	277	227	N
7.0	678	649	598	534	467	403	344	293	249	N
10.0	441	431	413	388	359	327	296	265	234	N
16.0	236	234	230	224	216	208	N	N	N	N
24.0	(128)	(128)	(127)	N	N	N	N	N	N	N

NOTE: N = negligible (<200). Numbers in parentheses are negligible, but nevertheless are instructive.

All values are numbers of x-rays per millimeter. See note, Table IV.

x-rays is only moderately out of focus. This gives the appearance that the image is largely unidirectional from the body, almost as if the x-rays were travelling primarily in lines perpendicular to the plane of the body. Of course, the image on a cloth from x-rays emanating from a surface results from x-rays coming from many point sources. However, each of these point sources results in a tiny spot on the cloth. The maximum radius of the spot is 4–5 mm.

Consider the image formed on the cloth when placed parallel to an x-ray source 10 mm in diameter. The image on the cloth would comprise a central area 2 mm in diameter of maximum intensity. From a radius of 1–5 mm the intensity would decrease slightly. However, near 5 mm the intensity would begin to decrease rapidly, and at 9 mm the intensity would be zero. The net effect would be an image whose boundary would be indistinct, but the object would still be identifiable as circular; when viewed from a distance, the outer boundary would appear reasonably well defined. This corresponds to the description of the image on the Shroud of Turin.

One might believe that the fair resolution of image from silicon x-rays is due only to their rather high mass absorption coefficient. However, Table V presents calculations for chlorine K_{α} x-rays having a mass absorption coefficient less than a third of that of silicon x-rays. However, the calculations for chlorine surprisingly show only a modest increase in dispersion compared with that of silicon x-rays. The maximum value of a for chlorine is 6.2 mm compared with 4.7 mm for silicon, meaning that the resolution is slightly worse than that of silicon x-rays. If there were no absorption of the radiation by air ($I/I_0 = 1$), there would still be a reasonable sharpness when the emitting surface is very close to the cloth, namely from 0 to about 2 mm. However, if the air does not absorb the radiation and if the radiation is emitted spherically, then at distances greater than roughly 5 mm the image would be garbled because of the poor resolution.

The above calculations show that an x-ray image on cellulose arising from x-rays from elements such as silicon or chlorine would form an image only moderately out of focus, similar to the image on the Shroud. However, these calculations are in conflict with an experiment by Jackson et al. (2). This ingenious experiment simulates radiation processes in which radiation is absorbed by the medium between the body surface and the cloth. In this experiment, Jackson et al. covered a three-dimensional face with phosphorescent paint. Photographic film was then contoured over the face to simulate the drape of a cloth. Finally, the intervening space between the face and a clear plastic sheet simulating cloth drape was filled with a green solution as the light-attenuating medium. The three-dimensional relief obtained by image analysis provided a poorly resolved face with a lack of facial details such as found on the Shroud.

These authors concluded that “radiation from a full body shape is probably unable to account for the Shroud image.”

The above experiment did not exactly simulate the postulated x-ray mechanism for forming the image on the Shroud for the following reasons: (1) The experiment employed a liquid having an absorbance that was lower than needed to simulate the x-ray hypothesis, and (2) the experiment used only one value for the absorbance. Because several x-rays having different wavelengths presumably contributed to the image on the Shroud, the experiment should be repeated using various absorbances for the liquid with a partial exposure for each different absorbance. Perhaps performing the experiment in this way would resolve the difference in conclusions between the authors who performed the reported experiment and calculations based on x-rays made in this section.

Possible Sources of x-Rays

Some explanations for how x-rays could have been emitted from the surface of the body of the man of the Shroud of Turin follow.

1. This person could have lived in a cave whose walls were radioactive due to their mineral content or he could have been a shepherd exposed to radiation from minerals, or he may have consumed food grown in soil enriched with natural radioactivity. If radioactive materials were stored in his bones, such as ^{226}Ra having a half-life of about 1600 years, then after death it is possible that over a long period of time the x-rays emanating from the body could have produced the image on the Shroud. In a long period of time most of the skin would decompose, and x-rays emitted by the bones could form the image. However, the tip of the nose should be less intense than it appears on the Shroud, and preliminary calculations show that the number of x-rays produced by ^{40}K or by ^{226}Ra are likely to be far too few even over a period of 1000 years to account for the image on the Shroud. This source of x-rays is unlikely.

2. Possibly the man of the Shroud was buried in a radioactive tomb (or in radioactive soil). The radioactivity may have interacted with heavy elements in the bones and teeth to produce short-wavelength x-rays, which would produce some fluorescent x-rays from elements such as chlorine, silicon, and calcium on the surface of the skin (or bones after decomposition of the skin). Another possibility is that surrounding radioactivity may have interacted directly with light elements on the skin to produce fluorescing x-rays. This process would likely require a strong source of radioactivity and a long period of time, say a thousand years.

3. Another explanation, which should not be automatically rejected by scientists, is that perhaps the Shroud of Turin is in reality the Shroud of Jesus Christ, and perhaps some unknown process resulted in the resurrection, and the energy released by this process was partly in the

form of x-rays, which then reacted with the linen Shroud as described above.

Conclusion

The hypothesis that low-energy x-rays caused some or all of the image on the Shroud of Turin is in good agreement with published and other observations of the image. It is known that x-rays of moderate energy easily cause a coloration on linen similar to that found on the Shroud of Turin. However, it is unknown whether silicon, phosphorus, sulfur, chlorine, calcium, or potassium x-rays will cause a similar discoloration of linen. Further, it is unknown whether the image formed is microscopically and chemically identical to that of the Shroud image.

Acknowledgments

I appreciate the donation by C. Blake of a fine linen napkin for experimental purposes. Helpful conversations were held with Eric Jumper, Alan Adler, John Heller, K. Rengan, Mel Usselman, Carroll Osborn, and Vernon Miller.

Literature Cited

1. Jackson, J.; Jumper, E.; Mottern, R.; Stevenson, K. *Proc. U. S. Conf. on the Shroud of Turin*, Bronx, N.Y., 1977.
2. Jackson, J. P.; Jumper, E. J.; Ercoline, W. R. *Proc. IEEE Int. Conf. Cybernetics Soc.*, Seattle, Wash., 1982.
3. Heller, J. H.; Adler, A. D. *J.-Can. Soc. Forensic Sci.* 1981, 14, 81-103.
4. McCrone, W. *Microscope* 1980, 28, 105-13.
5. *Ibid.*, 115-28.
6. *Ibid.*, 1981, 29, 19-38.
7. Nickell, J. *Humanist* 1978, 6, 30-33.
8. Ercoline, W. R.; Downs, R. C.; Jackson, J. P. In *Proc. IEEE Int. Conf. Cybernetics Soc.*, Seattle, Wash., 1982.
9. Hershey, J. "Hiroshima", Penguin, New York, 1946.
10. Mills, A. A., personal communication.
11. Morris, R.; Schwalbe, L.; London, J. *X-Ray Spectrom.* 1980, 9, 40-47.
12. Muller, R. O. "Spectrochemical Analysis by X-ray Fluorescence"; Plenum: New York, 1972.
13. Jackson, J. P.; Jumper E. J. *Symp. on the Shroud of Turin*, New London, Conn., 1981.
14. Miller, V. *Symp. on the Shroud of Turin*, New London, Conn., 1981

RECEIVED for review November 23, 1982. ACCEPTED for publication April 11, 1983.

A Comprehensive Examination of the Various Stains and Images on the Shroud of Turin

ERIC J. JUMPER—Air Force Institute of Technology, Department of Aeronautics and Astronautics, Wright-Patterson Air Force Base, OH 45433

ALAN D. ADLER—Western Connecticut State University, Department of Chemistry, Danbury, CT 06810

JOHN P. JACKSON—University of Colorado at Colorado Springs, Department of Electrical Engineering and Computer Science, Colorado Springs, CO 80907

SAMUEL F. PELLICORI—Santa Barbara Research Center, Goleta, CA 93117

JOHN H. HELLER—The New England Institute, Ridgefield, CT 06877

JAMES R. DRUZYK—Los Angeles County Museum of Art, Conservation Center, Los Angeles, CA 90036

The chemistry of the various stains and images on the Shroud of Turin is presented. The chemical conclusions were drawn from all the data and observations, both physical and chemical, collected by direct investigation of the Shroud in 1978. The conclusions are that the body image is made up of yellowed surface fibrils of the linen that are at more advanced stages of degradation than the non-image linen. The chromophore is a conjugated carbonyl. No evidence was found in the body image of any added substances that could have contributed to the yellow color of the fibrils that form the image. The blood images on the cloth are made of blood. The data, taken together, do not support the hypothesis that the images on the Shroud are due to an artist.

A TEAM OF SCIENTISTS AND TECHNICIANS known as the Shroud of Turin Research Project (STURP) took part in direct physical testing on the Shroud of Turin in October 1978. The object of their efforts was a piece of ancient linen measuring approximately 4.3 m × 1.1 m presently kept in the Chapel of the Holy Shroud in the north Italian city of Turin. The cloth's value stems from the presence of the frontal and dorsal image

American Chemical
Society Library
0065-2038/84/0001-0147\$08.50/0
© 1984 American Chemical Society
1155 16th St., N.W.
Washington, D.C. 20036

In Archaeological Chemistry—III; Lambert, J.;

Advances in Chemistry; American Chemical Society: Washington, DC, 1984.

of a man purported to be that of the dead Jesus of Nazareth. A major goal of the testing was to gather data that could be used to determine the chemical composition of these images. Some background information as it was known before the 1978 testing can be found in Reference 1.

During the 1978 test program, members of STURP performed photographic imaging; visible, UV, and IR spectroscopy; IR thermography; x-ray fluorescence analysis; and x-radiographic imaging. They also collected microscopic samples of the various kinds of images and marks on the Shroud for chemical testing (2). Details of these tests with results can be found elsewhere (3–10). Results of chemical testing can be found in References 11 and 12.

The previously cited references do not deal with a comprehensive picture of the chemistry of the marks and images on the Shroud, nor do they propose a satisfactory explanation for how the body image got on the cloth. However, Pellicori and Evans (7) have proposed direct contact as a candidate with full recognition of its drawbacks. A series of three articles by McCrone (13–15) are not so cautious; these conclude that the Shroud is simply a clever painting. Although some of McCrone's visual observations are consistent with those reported by others, we find his conclusion to be inconsistent with the chemical picture presented here. Further, it will be clear to the reader that one of the few causes of the body image that can be ruled out is a painting. It is, however, not our intention in this chapter to directly address the question of image formation but rather to bring together the results of all the previous work in an attempt to arrive at a definitive description of the chemistry of the images and marks on the Shroud. The reader is directed to Reference 16, where various hypotheses for image formation are examined.

In order to consider in detail each kind of image/mark on the Shroud, it is essential to describe these images and stains, thereby establishing unambiguous meanings and reference points. Figure 1 shows a photograph of the Shroud with pointers indicating the various types of stains and images. First note the frontal and dorsal image of what appears to be a nude adult male, labeled A. Superimposed on these "body" images are what appear to be wounds in "blood," labeled B. In this chapter, images in category A will be referred to as body-only images, that is, these are only body images and not body images that are "contaminated" by the superimposed blood images. The "blood" images will then be referred to simply as blood images.

Because other stains/images on the cloth (which are of known origin) are important for comparison, we will also refer to some of these, as we will to extraneous pieces of cloth that are presently attached to the Shroud in one way or another. The most obvious marks are those resulting from a fire in A.D. 1532. These can be classified as burns (labeled C), marks actually composed in part of charred linen, and scorches (labeled D),

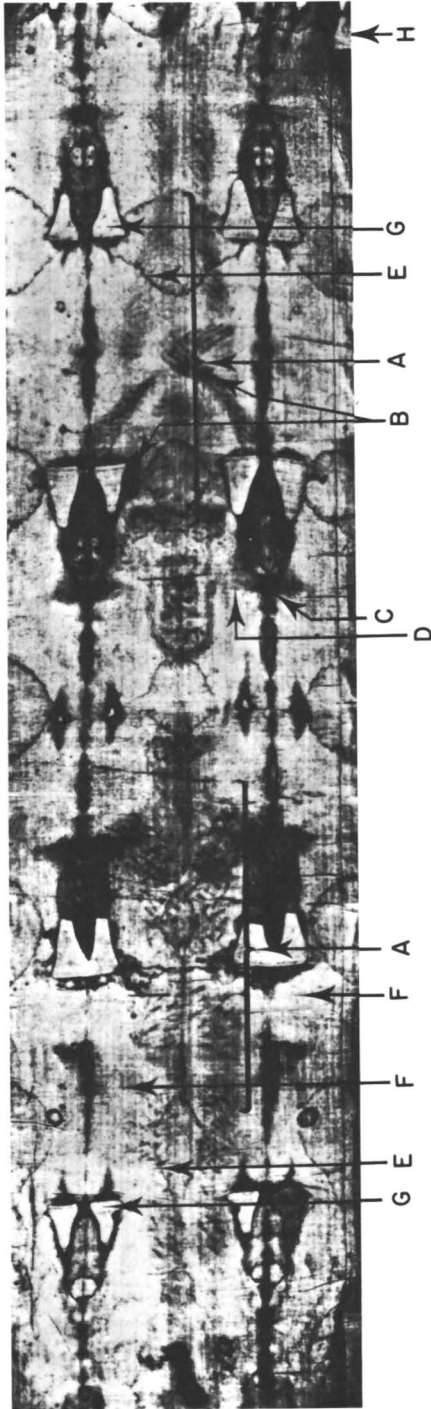


Figure 1. Photograph of the Shroud showing examples of the various types of marks and images. Key: A, body-only image; B, blood image; C, burn mark; D, scorch mark; E, water-stain mark; F, clear area; G, patches; and H, Holland cloth. (Reproduced with permission. Copyright 1978, Vernon Miller.)

where the linen is noticeably discolored but not actually reduced to char. These scorches vary in optical density from barely noticeable when compared to the background to optical densities that approach those of the charred or "burn" areas. Also important are the water-stain marks (labeled E) that were produced at the time of the 1532 fire, when water was poured on the silver container in which the Shroud was kept. The clear areas (i.e., non-image areas) also have some bearing on the identification of the chemistry of the other marks on the Shroud and as such are identified in Figure 1 (labeled F). For the sake of completeness we will also make reference to the patches (labeled G) and the Holland cloth backing cloth, which was attached to the Shroud in 1534 in an attempt to restore structural integrity lost in the 1532 fire. Because the Holland cloth is attached to the back of the Shroud it only appears where portions of the Shroud are missing in Figure 1 (labeled H).

Body-Only Images

The first type image we will discuss is the body-only type (labeled A in Figure 1). First the macroscopic characteristics will be discussed, then the microscopic characteristics, and finally the chemical characteristics.

Macroscopic Characteristics. COMPOSITION. As can be noted in Figure 1, that portion of the Shroud showing visible front and back images of a man is composed of a continuous range of optical densities from background density to its darkest density in areas like that of the tip of the nose. It is important, for comparison purposes, to note that the shading density of the body-only images falls in the same density range as the scorches, D, and not the burns, C. On close examination, the surface fibrils of the threads composing the weave of the cloth here are yellow. With both aided and unaided eye, we find that the densities above background making up the body-only image are composed of groups of these yellow fibrils residing only on the uppermost portions of the threads (7). These groups of fibrils are not cemented to one another as was demonstrated by probing with a dissecting needle. Thus, no pigment "binder" appears to be present. Further, with few exceptions, we find that the yellow coloration of the fibrils is interrupted as the thread goes beneath a crossing thread in the weave pattern. Those few exceptions where the yellowing appears to pass under the crossing thread seem due to mechanical stretching of the cloth, because these are usually accompanied by a region of uncolored fibrils at the opposite end of the exposed thread where it comes up from beneath a crossing thread. The yellowed fibrils are not yellowed continuously over their entire length. We observed a fibril that was yellow only on the part that was on the uppermost portion of the thread but lost its coloring as it left the upper portion of

the thread in its normal course of following the twist to the lower portion of the thread. In examining the cause of the differing integrated densities of the body-only image as seen by the eye, we found that the darker portions of the image were not due to a variation of the degree of the yellowing of the fibrils, but rather to the presence of more yellowed fibrils per unit area (7). Thus, the extent of yellowing of a given fibril was the same, to within 10% (of full scale) of any other yellowed fibril on the basis of microdensitometric measurements of the color photomicrographs. The shading of the body-only image, then, is much like that of a halftone. In this regard, it should be noted that there are ubiquitous examples of yellowed fibrils lying adjacent to unyellowed fibrils. Thus, body-only image to the unaided eye (also, to the aided eye to 50 \times) appears as a striping of uniformly yellowed fibrils on the uppermost portions of the uppermost threads of the cloth and exhibits no cementing between fibrils.

SPATIAL DISTRIBUTION. The spatial distribution of the optical densities that make up the body-only image appear to correlate with a well-defined mapping function (17). Considerable work has been done on the frontal image of the man on the Shroud. These studies show that a relationship exists between the shading density of the image and expected cloth-body distances obtained by enfolded volunteer human subjects in a full scale model of the Shroud. Two points should be noted: first, this characteristic of the image is not obtained by considering it to arise from a reflectance of an albedo image of its "source;" and secondly, it accounts for the "reversed" nature of the tonal scale as perceived by the eye, that is, its so-called negativity (*see* Figure 2).

Extensive study of the back image has not yet been undertaken; however, there appear to be striking similarities between the frontal and dorsal body-only images. We find, for example, that the maximum optical densities of the dorsal image are nearly the same as those for the frontal image. Further, qualitatively, the optical density of the dorsal image falls off from peak density to that of the background over anatomical distances (e.g., in the region of the calf) suggesting a similar correlation to cloth-body distance as exists for the frontal image. However, other portions of the dorsal image might be interpreted as characteristic of a contact mechanism (17). A more definitive statement must await further study.

There are areas on the body-only image that are relatively lower in optical density than other areas in relation to the background. Most noticeably these areas appear as stripes running longitudinally on the Shroud and are due to the different lots of thread used in the manufacture of the cloth. The most notable example of this phenomenon is seen bordering the face. Two of these stripes, measuring approximately 2.5 cm each, run along the sides of the face (*see* Figure 2) and have often



Figure 2. Pictures of the face on the Shroud. The right-hand picture is photographically reversed; arrows on the left-hand picture indicate the 2.5-cm stripes along the face. (Reproduced with permission. Copyright 1978, Vernon Miller.)

been referred to as due to a "chin bandage" in popular writings on the Shroud (1). This interpretation is mistaken, as these are part of the same lighter bands that can be seen to run the length of the Shroud.

COLOR. In white light, the color of the body-only image is yellow [c.f. spectra (4,6)]. It is interesting that the image has been described prior to the 1978 testing as a monotonic sepia color; however, the perceptual judgement of color is extremely sensitive to lighting and the distance from the cloth to the observer. Under low color temperature lighting, it is possible that the color could be mistaken for sepia because the yellow is due to a broad absorption of the blues (shorter wavelengths in the visible spectra) (4,6,7). It should be noted that the color of the body-only image is distinctly different from that of the blood images (c.f. later section). The color of the body-only image (as viewed in the visible) when irradiated by UV light (390–420 nm) is neutral gray or black (10).

THERMOGRAPHY. Accetta and Baumgart viewed the image in the IR both at 3–5 μm and at 8–14 μm (5). In the 3–5 μm range no discernible image was evidenced. In the 8–14 μm range a clearly discernible emission image was visible. They could find no apparent differences in spatial distribution between the IR and visible image (5) (unlike the case for most paintings).

Microscopic Characteristics. At 50 \times magnification, the body-only image is composed of yellow fibrils (c.f. above) on the uppermost portions of the uppermost threads (7). At higher magnifications, up to 1000 \times , two types of "red" particles identified as either iron oxide or "blood" are occasionally present on some of the yellow fibrils (12,13); however, it is clear that these particles do not account for the yellow color of the fibrils or the image itself for several reasons. x-Ray fluorescence analysis of the Shroud shows that there is no correspondence of the body-only image density to the concentration of high-Z elements (particularly note, Fe) within the resolution of the analysis (3). The spectral characteristics of body-only image are different from those of iron oxide (4,6). Further, one would expect that an image of comparable optical density to that of the visual body-only image on the Shroud, if made from iron oxide pigments, would have appeared on the x-radiographs. The water-stain margins, which do contain iron oxide (12), are present on the x-rays; the body images do not appear on the x-rays (9) (c.f. below).

In a more definitive sense, examinations of samples taken on sticky tape (12,13) have shown that the color of the yellow fibrils does not arise from any inorganic pigments (12). Both oxidative and reductive reversal of color back to "new"-linen white readily demonstrates that the color of the fibrils cannot be due to the presence of iron oxides. Thus the body-only image is due solely to the distribution of the yellow fibrils.

We turn, then, to the cause of the body-only image fibrils' being yellow. We have already mentioned that the yellow fibrils are not ce-

mented to one another as would be expected in the presence of a pigment binder. At magnifications of up to $1000\times$, these fibrils do not appear to have any coating. This is most clearly demonstrated by observations made at the joint locations of the linen fibrils. These joints exhibit no meniscus, but are clearly and sharply defined with no evidence of a coating. Further, under phase contrast microscopy, these fibrils not only appear uncoated, but show "corroded" surfaces as would be expected for an oxidatively degraded cellulosic material (12). Although protein-covered fibrils can be readily demonstrated in blood image areas (c.f. later section), the body-only image fibrils test negative for protein to the nanogram level (12). Several tests were used, including the amido black test (14), the more sensitive fluorescamine test, and protease digestion (12). That this conclusion is contrary to previously reported results (13–15), seems to arise from a failure of those investigators to discriminate between body-only image and blood image fibrils. They have apparently concluded by visual inspection only that the yellow-appearing fibrils from these two disparate types of locations are identical. Chemical observations do not agree with this assumption. Blood image fibrils do test positive for protein. Further, the "yellow-coated" fibrils found in the blood-image areas are yellowed by a distinctly different cause, that is, serum proteins (12). A further possible contribution to the misidentification of protein on fibrils from the body-only image areas (14) is due to the use of only the amido black test as a confirmatory test for protein. Amido black is not a metachromatic stain, that is, it does not show a color change on its staining interaction with protein. Amido black, being a basic dye, also stains oxidized cellulose in the same fashion, as is readily demonstrated by its staining rayon (i. e., regenerated cellulose that is completely protein free) (12). Therefore, positive amido black tests without proper controls do not demonstrate the presence of protein as claimed in Reference 14.

Schwalbe and Rogers note that in removing the tape samples, the tape pulled up more easily from the body-image areas than from the non-image areas. The linen fibrils seen on the body-image tapes are shorter and more fractured than are those from non-image areas (16). Both of these observations suggest that the body-image fibrils are more chemically degraded than are those from the non-image areas.

Explanation for the Yellow Color of the Fibrils. It seems clear that the cause of the body-only image is the yellow fibrils and that the yellow color is not due to inorganic pigments. We turn, then, to considering other possible causes of the yellow color of the fibrils.

One possible explanation might be an organic stain or dye. The body-only image exhibits broad nonspecific absorption in the shorter visible wavelengths (4,6), unlike many naturally occurring dyes (16). Further, many natural dyes are soluble in water and would have migrated at the time the water marks were made (c.f. below). As Schwalbe and

Rogers point out, the body-only images were unaffected by such water (16). Further, most organic dyes are affected by temperature, and the Shroud body-only images exhibit no color change in areas where scorch marks from the 1532 fire intersect body-only images (16). Many organic chromophores are fluorescent in the visible when excited by UV light, and the body-only images are nonfluorescing (10).

All the foregoing suggests that the yellow color is not due to a stain or dye; however, to test further the possibility of the presence of a stain or dye, the microsamples were subjected to a battery of tests (12): the color is not extractable in various organic solvents covering the entire range of solubility classes; the color does not change on treatment with strong acids and(or) bases; the color was not bleached by weak oxidants (even under UV irradiation), nor by weak reductants; and a wide range of specific metallic elements and chromophoric organic groups were not evidenced by specific chemical tests. This battery of tests showed that the only ubiquitous microdetectable metal species present were calcium and iron, and their presence was shown to be consistent with their having been deposited in the cloth as coordinate covalently bound species during the original retting process in the manufacture of the linen (c.f. below). These observations agree with the findings of Morris et al. (3). It should be noted here that the iron oxide particles occasionally seen on and also in the medulla of fibrils could have been formed during this same retting process or even possibly at the time of the water staining during the 1532 fire by a process similar to the production of "mineral khaki" (12).

We can also rule out the possibility that the yellow color arises from diffraction and/or dichroic phenomena; there is no evident angular dependence for the apparent color, as is required by such mechanisms.

Selective scattering by the cellulose structure is also ruled out because the surface structures in both the body-only image areas and the background areas are essentially the same. Scattering from both areas is due to the fibrils, but the body-only image areas have enhanced density of "yellow" color over background areas that are pale straw color to the eye. The slightly rougher fibril appearance in the body-only image areas is at a scale size orders of magnitude greater than the wavelengths in question, and therefore does not contribute selectively to the color.

Finally, microchemical tests (12), mass spectroscopy (16), and laser-microprobe Raman spectroscopy (16) all fail to show the presence of any added materials on the yellow body-only image fibrils to within their limits of detection. We conclude that no material has been added to these yellowed fibrils to produce the color (12,16).

What then is the cause of the fibrils' yellow color? The nature of the absorption curve (4) demonstrates that the yellow color is similar to the light scorches. Miller and Pellicori point out the similarity is not complete, because the body-only image does not show the same UV-

stimulated, orange-red fluorescence as the scorch-image areas (D) (10) (c.f. discussion on high vs. ambient temperature decomposition below). The case for the yellow color being due to chemistry similar to that of a light scorch or ambient temperature process goes further, however. The physical properties of the cloth in the areas of the body-only image (the microscopically corroded appearance, the lack of migration of the image with water, the lower tensile strength of the colored fibrils, and the lack of color change in the presence of elevated temperatures) are all consistent with this sort of chemistry (16).

These suggestions have been given corroborative support from the microchemistry results (12) (c.f. above). Organic functional groups that are characteristic of dehydratively oxidized, degraded cellulose have been found. Further, such groups have also been found in the "ghost" patterns on the sticky tape after the fibrils have been removed. The absence of products expected from a high-temperature cellulose degradation, however, suggests that the process that formed the final chemistry took place at lower temperatures (less than 200 °C), because no pyrolytic compounds were found (6,12). The fluorescence of the scorch image areas, however, demonstrates the presence of high-temperature pyrolytic products in these areas (10). The cause, then, of the yellowing is chemically altered cellulose consisting of structures formed by dehydration, oxidation, and conjugation products of the linen itself. Heller and Adler have postulated that the most probable chromophores are conjugated carbonyls (12). Possible chemical schemes for forming such structures are shown in Figure 3 and in the box on the page that follows it.

This conclusion is supported by laboratory simulations using controlled accelerated aging processes that produce the same spectral reflectance curves as the body-only image areas and the background areas on the Shroud (6). The changes in cellulose known to be the result of aging are the same dehydrative and oxidative processes described above (18,19). Such chromophores result in a broad UV absorption decreasing monotonically toward longer wavelengths. Further, the conjugation of such chromophores in varying chain lengths results in the observed broad gradual nature of the absorption (4,12).

It is important to note that this chemistry is similar to the chemistry that causes the yellowing of linen with age. The fact that we can see the body image tells us that the body image is due to a more advanced decomposition process than the normal aging rate of the background linen itself. For this reason, we will from this point on refer to the chemistry of the body-only image as advanced decomposition. Later in this chapter we will briefly address possible causes for catalyzing the decomposition process. It will suffice to close this section with the simple statement that the body-only image is due to a yellowing of the uppermost fibrils of the linen threads of the cloth, the darkness of the image being

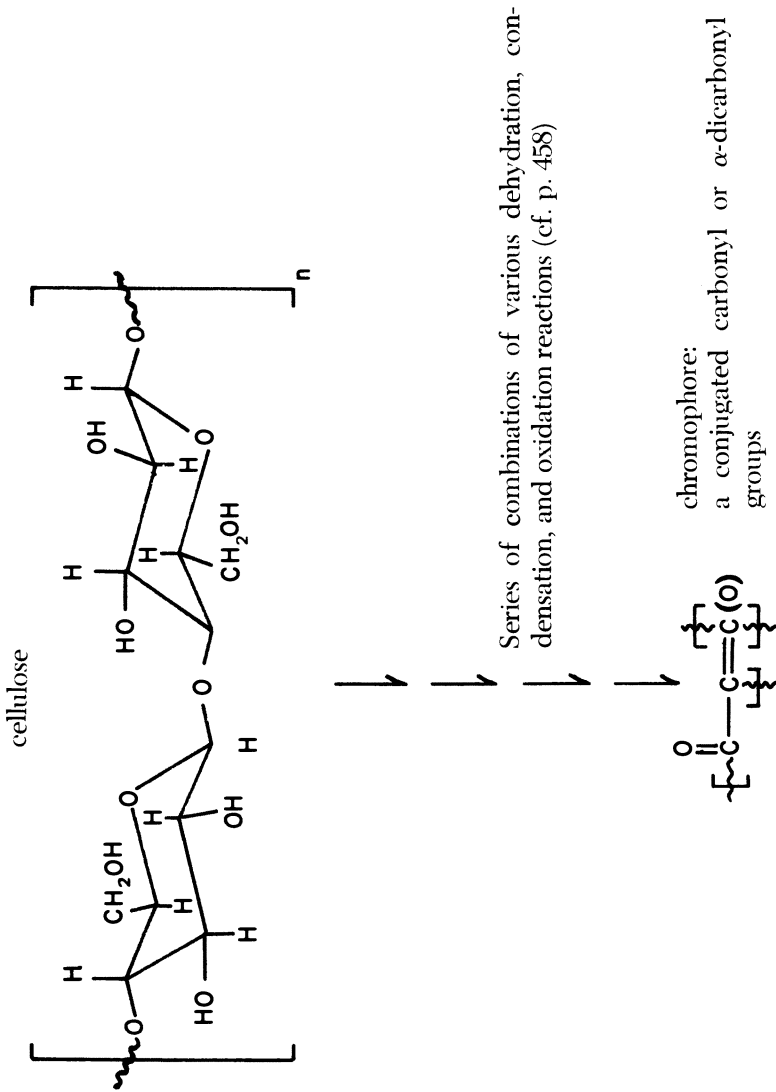


Figure 3. Generation of chromophoric groups from cellulose structure of the linen of the Shroud.

Cellulose Reactions Pertinent to the Formation of the Chromophore* of the Shroud Body-Only Image

A. Condensation Reactions (internal and cross-linking)

1. acetal + water \rightleftharpoons hemiacetal
2. hemiacetal \rightleftharpoons linear saccharide (free carbonyl group)
3. aldol condensation (intra and inter)
4. esterification (intra and inter)
5. double bond addition (e.g., ionization-produced radical polymerization)
6. radical polymerization (e.g., ionizing conditions)

B. Dehydration Reactions

1. alcohol dehydration \rightarrow alkene + water (e.g., pyrolytic conditions)
2. α,β -diol dehydration \rightleftharpoons enol + water (e.g., anhydroglucose formation)
3. aldol dehydration \rightarrow α,β -unsaturated carbonyl* + water

C. Oxidation Reactions

1. primary alcohol + [O] \rightarrow aldehyde (e.g., 6-OH groups)
2. aldehyde + [O] \rightarrow carboxylic acid
3. secondary alcohol + [O] \rightarrow ketone
4. ketone + [O] \rightarrow 2-carboxylic acids
5. alkene + [O] \rightarrow 2-carbonyls
6. enol + [O] \rightarrow aldehyde + carboxylic acid (e.g., dehydrative)
7. α,β -diol + [O] \rightarrow 2-carboxylic acids (ionizing conditions)
8. α,β -unsaturated carbonyl \rightarrow carbonyl + α -dicarbonyl*

*Conjugated carbonyl.

due to a greater number of these fibrils, and the yellowing of these fibrils being due to dehydration, oxidation, and conjugation of the cellulose of the fibril itself (advanced decomposition).

Blood Images

The next major type of image is the blood image labeled B on Figure 1. Again we will consider this image type by examining the macroscopic, microscopic, and chemical descriptions.

Macroscopic Characteristics. COMPOSITION. The blood images appear as three major types: areas that might be termed wounds, on the wrists, for example; areas of blood flow, along the small of the back, for example; and "scourge" marks that are ubiquitous over the torso and legs. All of these types bear certain similarities and differences. On close examination one sees that blood flows have gone onto the cloth as viscous liquids penetrating the cloth through to the back, and diffusively seeping

along threads near the edges of the stains demonstrating some limited capillary flow. Menisci are clearly visible at the edges of the stains. Heavily colored portions of the stains have not diffused very far, which suggests high viscosity. The color of the darker portions of the blood images is quite red. The color is not uniform, however, and the color ranges from a brown through red to orange. In general, the color has a crimson appearance as would be expected for old blood stains composed of a solid-phase mixture of methemoglobin (brown) and its degradation products [e.g., bilidienes, such as rubins (orange)], both of which have been demonstrated to be present in these blood images (6,11,12). In some areas there is evidence of some apparently colorless fluid bordering or diffusing farther out than the darker fluid (one could thus conclude that this fluid would be thinner than the darker fluid, c.f. below). All blood stains appeared to have had the upper portions of the dried stain removed as if abraded by mechanical wear; the most intact stain is seen in the interstices of the weave of the cloth. Repeated folding of the cloth has apparently translocated some of this abraded material to other locations. Therefore, the material comprising the stains is absent on the crowns of the threads and is most abundant between threads and penetrating between the fibrils of the thread (c.f. figures in Refs. 7 and 20). In those parts of the stain where the darker material has been removed, one can see "yellow" fibrils that appear to be coated and cemented together. These coated yellow fibrils are also a deeper yellow color than those in the body-only areas (6), and are not confined to the first layer of fibrils as are those in the body-only areas. Fibrils in the blood areas are clearly cemented together, even in areas where there appears to be a thinner fluid progressing beyond the edges of the darker portion of the stain. The appearance of the cemented fibrils has been described as appearing matted together in some areas (16). In those areas where the water stains have intersected the blood areas, there is a clear indication that the presence of the blood images has impeded the progress of the diffusion of the water through the cloth. Before moving to the specific types of blood stains, it should be emphasized that the blood images are distinctly different in appearance from the body-only images (c.f., previous section). Finally, at 50 \times the cementing of fibrils, coating of the fibrils, capillarity, and variation of color are more clearly seen (6,7).

WOUNDS. These images appear to be located at distinct and clearly identifiable parts of the anatomy of the man on the Shroud, which would suggest they are wounds. While there is no mistaking the location of the major wounds, there are some examples of blood images that do not coincide with any particular anatomical detail, for example the apparent trace of blood off the right elbow as seen in the frontal image. There are also other examples of the blood image being off-register with respect to the anatomical detail upon which it is clearly associated, for example,

on the right foot as seen on the dorsal image of the man on the Shroud. Bucklin has made an extensive investigation of the correlation of these locations to specific types of injuries (21). It is interesting to point out that many of these wound images appear to have a border encircling the darkly colored area where body image is absent, a halo of sorts that can clearly be seen as such in the UV photography (10). These are the areas where the flow pattern suggests a thinner fluid was present in the cloth as we have noted above (10). This absence of body image on the wound image margins suggests that the blood images were present on the cloth before the body image was "placed," "appeared," or perhaps "developed." This suggestion is consistent with the chemistry of the body-only image, because this thinner fluid could have coated these margin fibrils sealing them and preventing the advanced decomposition reaction. This conclusion is supported by microscopic examination of the fibrils from the blood areas after removing the serum coating by protease digestion. Fibrils, so treated, more closely resemble those from the off-image clear areas than those from the body-only image areas when viewed by phase contrast microscopy (12).

BLOOD FLOW. In these areas, the fluid seems to have flowed along contours of the cloth such as folds. The clearest area of this happening is in the region corresponding to the area of the small of the back above the buttocks.

SCOURGE MARKS. These appear to be somewhat different from the other two types of blood images. Under UV fluorescence, they appear to be darker than the image and, also, to be much more sharply defined than they appear in visible light (10), as would be expected on the basis of the known spectral characteristics of iron porphyrin compounds (11). The geometric similarity of groups of these dumbbell-shaped marks is also quite striking (21). Fine "scratches" from the distal ends of these dumbbell-shaped marks appear in the UV-stimulated fluorescence photographs (10).

Microscopic Characteristics. At magnifications of $250\times$ to $1000\times$, the fibrils in the blood areas are clearly coated. Joints of the linen fibril are filled with some substance. Samples of ca. 300-year-old Spanish linen were treated with partially clotted blood and allowed to sit for 18 months (11,12). Microscopic samples of this treated linen made with sticky tape in the same manner as the Shroud samples appeared to be very similar to the Shroud samples. Amorphous globs colored orange to orange-red to yellow to yellow-red were observed in the Shroud samples and appeared similar to those from samples taken from such treated linen. In other words, microscopically the Shroud samples taken from the blood areas looked like blood as seen on a simulacrum (12).

Also present on the Shroud samples was a significantly high number of nonbirefringent red particles identified as blood and decomposed blood

materials (12) and not as protein "cemented" iron oxide (13–15). These particles were ubiquitous in the blood areas. This finding is in distinct contrast to the limited quantity of nonbirefringent and birefringent red particles present in body-only and off-body clear areas on the Shroud. The relative quantities of all such red particles in these off-blood areas were several orders of magnitude less than those in the blood areas. These blood image particles are clearly associated with blood materials and are present only incidentally in other regions of the cloth where they are occasionally observed due to translocation (c.f. background section). Some of the blood-image red particles near scorch intersections have darkened and test as charred blood (12).

A mechanical description of the blood image areas can be divided into that for the fibril coatings and that for the globs, particulates, and "shards" (12). The nonbirefringent, red-coated fibrils test positively for the presence of heme materials and proteins (12). The yellow-coated fibrils test positively for protein with fluorescamine and also positively for serum albumin with bromocresol green indicating that they are blood serum coated (12). Suggestions (14) that this protein coating is a "collagen-type" animal glue used in medieval times as a paint binder are inconsistent with positive selective tests for serum albumin. The identification of the albumin (12) has now been immunochemically confirmed. Further, the suggestion that the body-only image was formed by such "yellowed" collagen is also unjustified as no protein can be detected by the fluorescamine and protease tests on such fibrils. Also, Miller and Pellicori found that both laboratory-prepared animal-glue collagen as well as glue used as a binder in a bible (ca. A.D. 1400) fluoresced brightly in the visible range when excited by UV radiation (365 nm); both the Shroud blood images and body-only images were nonfluorescing under the same conditions (10).

The globs, shards, and particulates range in size and color. They can be variously shown to contain proteins, hemes (11) and/or bile pigments, small black carbon particles, and only relatively small amounts of iron (12). Iron can only be identified in these materials after oxidative degradation. This finding is consistent with the globs, shards, and particulates being derived from the blood itself in various stages of decomposition, even including "charred" blood near scorch areas. Birefringent red particles identified as iron oxide are occasionally seen only in these scorch blood areas. Such birefringent red iron oxide particles are only prevalent in the water stain margins (c.f., below).

In closing this section we can state that the blood image areas appear to be composed of blood. Whether the blood is of human origin we cannot definitively say. However, we have recently confirmed the Italian immunochemical tests (22) suggesting that it is, in fact, human blood on the basis of positive tests involving human antiglobulin. Our tests em-

ployed human antialbumin and anti-whole sera. However, the problem of cross-serological interactions of other primate bloods prevents an absolute identification of the blood as human at this time. There seems ample evidence to explain all the red particles on the Shroud as originating from either the blood itself, the retting process, or, possibly, the water of the 1532 fire incident (c.f. above); we reject the hypothesis (13–15) requiring that an artist had to have touched up an earlier image. We, therefore, strengthen our statement on the blood to say that all of what we see in the blood area is derivable from blood itself or its products (12).

Burns and Scorches

We turn now to the burns and scorches identified in Figure 1 as C and D, respectively.

Macroscopic Characteristics. In white light, the scorches and burns vary from a light brown shading into a darker brown and finally into black. As indicated previously, the light scorch marks resemble the body-only image in the visible spectrum (4), but not under fluorescence (10).

At 50× magnification, the color gradations appear to range from a few yellowed fibrils to a complete black char. Under UV light (335–375 nm), an orange fluorescence is seen in the darkest areas (10). This observation is compatible with combustion of linen in a limited oxygen environment and at elevated temperatures rather than an ambient temperature oxidation process, which does not produce an orange fluorescence (10). In this regard, the more intensely burned areas showed the expected differences in spectral characteristics from those of the body-only image areas (4–6,10).

Microscopic Characteristics. At 500× to 1000× magnification with transmitted or reflected lighting, the fibrils range from yellow to brown to black. There are translocations of charred and scorched fibrils to other areas of the Shroud. This observation confirms the folding-contact mechanism mentioned earlier as that which translocated occasional blood particles to other locations.

The chemistry of the lightly scorched fibrils is very similar to the chemistry and appearance of the body-only image fibrils (12). This similarity is also evident in the IR spectra (5). In the more heavily scorched and charred areas, both chemistry and surface appearance begin to diverge from that of the body-only image areas (5,12). Indeed, it appears that a graded series of these fibrils can be made. If a series is made of off-image fibrils, body-only image fibrils, light scorch, to char, the number of aldehyde groups and carboxyls increases along with the corroded appearance, evidencing an increasing state of dehydrative oxidation. It should also be noted that the difference in the UV spectra and fluorescence characteristics between scorch and body-only image noted earlier

can be explained by the presence of pyrolytic products that form at higher temperatures. This explanation indicates an upper limit to the temperature of reaction during the formation of the body-only image.

Water Marks

The water marks are labeled E in Figure 1.

Macroscopic Characteristics. The water marks are interesting as they are the only marks (other than added material like the patches) that show up distinctly in the x-radiographs (9). Clearly, the density of heavy elements in the water-mark boundaries is sufficiently great to be apparent on these x-radiographs. These images conform closely to the water marks seen by the unaided eye in white light. These roughly diamond-shaped water marks derive from the extinguishing of the 1532 fire (when the molten silver of the Shroud's container burned through the folded layers of the Shroud, scorching it).

At $50\times$ magnification there is little that is remarkable other than the observation that neither the body-only images nor blood images migrated, although loose debris from them can be seen in the boundaries of the water marks. However, the blood did pose a barrier to the migration of the water, as would be expected of aged clotted blood. This can be best seen at the side wound blood flow. However, the body-only image did not impede nor facilitate the migration of the water through the cloth.

Microscopic Characteristics. At $500\times$ to $1000\times$ magnification it can be easily seen that virtually everything "movable" on the Shroud migrated to the boundaries of the water marks: blood coated fibrils, blood particulates, blood shards, off-image fibrils, body image fibrils, charred and burned fibrils, pollen, insect parts. Most interesting is the presence of birefringent red particles, which, although observed occasionally in other locations such as blood/scorch, are only prevalent in this area.

Chemistry. Since, as mentioned above, virtually everything movable on the Shroud can be found in this area, the chemistry of this debris need not be discussed here (having been discussed earlier) with one exception: the birefringent red particles. These red particles were found to be ferric oxide (Fe_2O_3) (12). Further, no manganese, nickel, or cobalt could be detected in these particles, confirming their origin from a "khaki-like" chromatographic process (c.f. above), rather than from an "ore-derived" pigment (12,14).

Clear Off-Image Area

The clear off-image, labeled F in Figure 1, served as a basic control for virtually all the observations on the Shroud.

Macroscopic Characteristics. Under white light, the linen is seen to be slightly yellow-tan with age. The material feels remarkably supple, considering it is at least six centuries old. The threads are seen in the x-radiographs to be inhomogeneous and the weave is somewhat uneven, as would be expected of a hand-spun, hand-loomed linen (9). As was indicated in the body-only image section, inhomogeneous lots of thread have resulted in the apparent effect of stripes appearing to run laterally and longitudinally the length of the cloth. The stripes are undoubtedly due to the fact that different lots of thread will show different degrees of degradation. We know that the body-only image is due to advanced degradation of the cellulose. Hence, it is perfectly consistent that the body-only image also reflects these same differentials. There are no extensive patches of mildew, although there are large numbers of mildew spores present. Earlier speculation that the lack of mildew is due to *Saponaria* is not borne out by chemical tests (12). Under UV light (335–375 nm), the off-image fluoresces a greenish-yellow (10). x-Ray fluorescence and microchemical tests both showed the presence of calcium and iron, which is consistent with that expected due to the normal retting process (c.f. below).

The weave of the cloth is seen to be a 3-to-1 herringbone twill (7) [supposedly typical of near-Eastern cloths of antiquity (23)]. The fibrils on the surface show mechanical wear indicative of many flexions and aging degradation.

Microscopic Characteristics. At 500× to 1000× magnification, the fibrils have the typical morphology of linen, but their surfaces are only lightly corroded (oxidized) although clearly less than body-only image fibrils as seen by phase microscopy. There are, also, fewer broken and crushed fibrils than in the body-only image areas, showing less degradation in further support of the arguments presented in the body-only image chemistry. Scanning electron micrographic images show pollen, spores, insect parts, and mites (24). Normal microscopic observations also reveal the presence of red silk, pink nylon, green polyester, and microdebris of the ages.

It is important to note that there are also charred linen fibrils, body-only image fibrils, blood particulates, globs, and shards occasionally present on these off-image areas. To our mind, this observation is best explained by the translocation mechanism referred to earlier. This explanation was proposed by Jackson et al. (17) who attribute numerous foldings of the cloth as the most dominant mechanism. There appear to be at least four distinct fold patterns that are identifiable in the permanent-fold patterns that are on the Shroud. Jackson performed an experiment in which he deposited ferric oxide in locations corresponding to the blood images on the Shroud on a clean piece of cloth of the dimensions of the Shroud. After just four foldings he took sticky tape

samples on his laboratory cloth in the same manner as samples made on the Shroud and found that the ferric oxide had migrated to every location where blood debris has been occasionally found on the Shroud. Because, as stated earlier, there is clear evidence that material is missing from the blood-image areas, the translocation model explains how the occasional blood particles, and other particles as well, could have been relocated to all parts of the cloth including the off-image areas. This translocation mechanism coupled with the water-caused migration at the time of the 1532 fire explains why various "atypical occasional" objects are found in various locations on the Shroud.

Chemistry. The fibrils all give a strong positive calcium reaction and a positive reaction for iron (even at test reagent conditions, pH 4.5, and even where Fe_2O_3 particles are not visible), indicating that ion exchanged (chelated) bound iron is present. It is of interest to note that only when the ferric oxide particles are present on a fibril does the iron test become "stronger" than the calcium test (12). Our estimate is that at least 90% of the iron present on the Shroud is of the ion exchange bound type. In the manufacture of linen from flax at that time, the linen was subjected to a process called retting. Retting involved submerging the linen an extended time in natural bodies of water while it underwent a fermentative process. During retting the linen can act as an ion exchange resin and selectively take up iron and calcium. Subsequently, some of this iron could become converted to ferric oxide in the water-stain margins by a process similar to the production of "mineral khaki." Of possible interest is the finding that we have similar positive tests for calcium and iron in the 300-year-old Spanish linen, some Coptic funerary linen (ca. A.D. 350), and some Pharaonic funerary linen (ca. 1500 B.C.).

Iron oxide particles found on the Shroud are chemically pure to the level of 99+%, as would be expected if they were formed by a "khaki-like" process from the iron taken up by the original retting. The only other source of iron on the Shroud is from blood, which is also pure as of biological origin. In contrast, earth pigments (13–15) such as Venetian red or ocher from medieval or older European, North African, or Middle Eastern sources are always contaminated with elements such as manganese, nickel, or cobalt above the level of 1% (unless pure hematite crystals were employed by the artist, which, although possible, is highly unlikely). Examination of medieval Venetian red and ocher demonstrates that these contaminants are omnipresent above the 1% level. Indeed, electron microprobe of late medieval ferric oxide-derived paints or even modern ones shows such contaminants. In contrast, electron microprobe analysis of Shroud samples shows uncontaminated iron—with no detectable manganese, nickel, or cobalt.

Microchemical analysis of large numbers of ferric oxide particles from the waterstain margins also shows contaminating impurity elements

not to be present. It is of interest to note that the method of making "khaki" depends upon steeping linen in a soluble iron salt, adding base, and dehydrating it. An experiment was carried out producing such "khaki" linen fibrils containing iron oxide on the linen and occasionally, also, inside the lumen of the linen fibril. Photomicrographs of these fibrils on sticky tape were indistinguishable from the red birefringent particle-coated Shroud fibrils from the water-stain margins (12).

One further observation should be made. There are occasional tiny black irregular specks (and one larger one) that are only found in scorch areas. These specks give a positive silver reaction and are undoubtedly due to the molten silver splatter at the time of the 1532 fire (12). No lead was detectable, but a possible positive copper contaminant was seen in the large silver particle.

Patches and Holland Cloth

For the sake of completeness, we mention the patches, labeled G on Figure 1, and also the Holland cloth. As these are of known origin (sewn on in 1534 to repair damage caused in the 1532 fire), they are of little interest to the investigation of the Shroud and will not be pursued to any depth here; however, two interesting points should be mentioned. First, debris of all sorts found on the Shroud were also found on these areas (including blood debris) and even on the back of the Holland backing cloth. This finding underscores the extent of the translocation action.

Secondly, a series of transmission photographs were made where the Shroud was illuminated from behind while the photographs were taken from the front. Although these were made primarily to be used in correlating the x-radiographs, they revealed an interesting fact. From reflectance photographs we know that the patches appear to be approximately the same optical density as the Shroud, suggesting that they may have aged approximately as much as the Shroud; however, in transmission the patches are much lighter than the Shroud. No doubt some of the difference can be accounted for by the thickness differences in the cloths used for the patches and the Shroud, but this will not adequately explain the difference in the transmission coloration. This is an indirect indication that the Shroud is a great deal older than the patches and implies that the Shroud probably has a history prior to the known A.D. 1350 date. Some corroborating evidence of the disparate ages of the Shroud and the Holland cloth backing can be found in a location where a triangular piece of the Shroud was removed in 1973. Here the surface of the Holland cloth appears "whiter" than the Shroud, although the portion of the backing cloth exposed prior to 1973 looks the same color as the Shroud. Although this observation indicates that the Shroud is quite old, we urge caution in interpreting it and strongly encourage judgment be withheld until such time as a carbon-14 dating is performed.

Conclusions

We have attempted to assemble from various studies all the known facts that bear on the chemistry of the images on the Shroud. This chapter reveals the self-consistency of the chemical conclusions with all the physical observations made since 1978. In these concluding statements we will attempt to highlight our major conclusions.

First, let us turn to the blood images. These are clearly made of blood, likely human; however, we cannot state absolutely that the blood is of human origin. It is in these blood areas that we [and others (22)] find proteins present of the types associated with blood serum. Finally, there is nothing unaccounted for in the blood areas that would lead one to suspect that anything but blood formed the blood images (12). We therefore do not agree that there has been an attempt to artistically enhance a "preexisting" blood image (13–15); nor do we feel that these are "painted" blood images.

The body-only image posed a more difficult problem of identification, because the final coloring of the image is only a more advanced stage of the natural aging-type decomposition present over the entire cloth. Iron (entirely of the chelated type) is present incidentally, but only at levels that match (and sometimes are even less than) those of off-image areas. There is no evidence of the ubiquitous presence of any stains, dyes, or pigments in these body-only image areas. Although occasional particles, possibly identifiable as artist's pigments, have been reported in Shroud studies (13–15), they are not seen in consistent or adequate enough amounts to account for any of the images—blood or body-only images. The Shroud is known to have been reproduced by several artists since the 14th century and therefore to have been exposed to pigment "debris." This is sufficient explanation for such incidental appearances. However, the observed concentrations of these materials are not sufficient, by many orders of magnitude, to account for what is observed visually. All observations confirm that the body-only image is visible because the topmost fibrils of the linen are yellowed to a greater extent than the non-image linen. This yellowing is due to the natural process of dehydration, oxidation, and conjugation typical of low-temperature cellulose decomposition; the chromophore is some form of conjugated carbonyl groups.

The large amounts of iron present on the cloth (along with Ca) are consistent with the retting process in common use in the preparation of linen throughout the ages. We estimate that 90% of the iron exists in the cellulosic chelated state. Only a small amount of the iron found exists as ferric oxide, and this is found in the largest amounts in the fronts or margins of the water stains. These findings lead us to believe that the iron oxide was water transported (i.e., "chromatographed") at the time of the 1532 fire, and then deposited in the manner of a method for making

“mineral khaki.” Smaller amounts of ferric oxide found in the scorch-blood-image area can be attributed to charred blood, and it can be readily demonstrated that ferric oxide can be formed by heating whole blood. The purity of the iron oxide, wherever located, in itself tends to rule out any connection with naturally occurring earth pigments, thereby supporting our suggestions as to its origins. Iron is also present in the blood areas in heme forms that one expects to find in blood. In short, the iron forms present on the Shroud are as expected and natural, rather than “painted” onto it.

Epilog

Although this chapter was not meant to address the specific question of how the images got on the Shroud, it does seem appropriate to conclude with a brief discussion of those things that seem obvious. To begin this discussion let us take one last look at the most widely publicized explanation for the Shroud images, the painting hypothesis. This hypothesis, detailed in References 13, 14, and 15, proposes that both the body images and blood images are composed of the same substance, a gelatin-based paint whose pigment consists of iron oxides and mercuric sulfide (iron earths and vermilion). It is obvious that the chemistry presented in this chapter is inconsistent with this explanation; however, the hypothesis can be tested without resorting to the detailed chemistry reported here. Figures 4–7 show the same area of the Shroud from four different perspectives. The first, Figure 4, shows a normal reflectance photograph of the side-wound area on the Shroud. The arrows point out water stains and a heavy blood flow. Figure 5 shows the same area in a transmission photograph (i. e., lit from behind). Figure 6 is an x-ray image of the same area. Finally, Figure 7 is the same area in UV fluorescence. Recall that our analysis shows that the water marks are rich in calcium and iron and, in particular, rich in very pure ferric oxide; in other words, these water stains are not untypical of common iron- and calcium-rich hard water stains. In addition, the visual appearance of these water stains is enhanced by organic debris from the fire. The x-ray image of Figure 6 is an absorption image. This x-ray image is a direct consequence of areal density (i. e., the density in grams per cubic centimeter integrated along the path length of the x-radiation so that the units become grams per square centimeter, that is to say the mass density between the x-ray source and the x-ray plate). The heavier the atomic weight, the more absorption and the lighter the x-ray image. In the first two images, it is clear that the blood stain is both darker and denser than the water stains. If the blood image were the result of iron oxides and mercuric sulfide, it would show up far more distinctly on the x-ray than the water stains, but quite the opposite is true. As reported in Reference 9, none of the blood marks

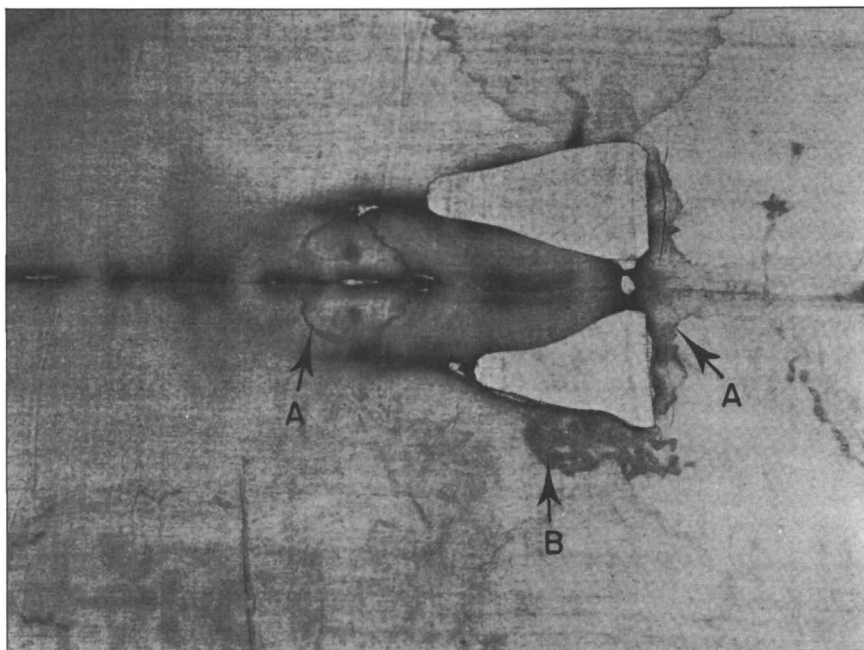


Figure 4. Reflectance photograph of side-wound area. Key: A, water stains; B, blood flow.

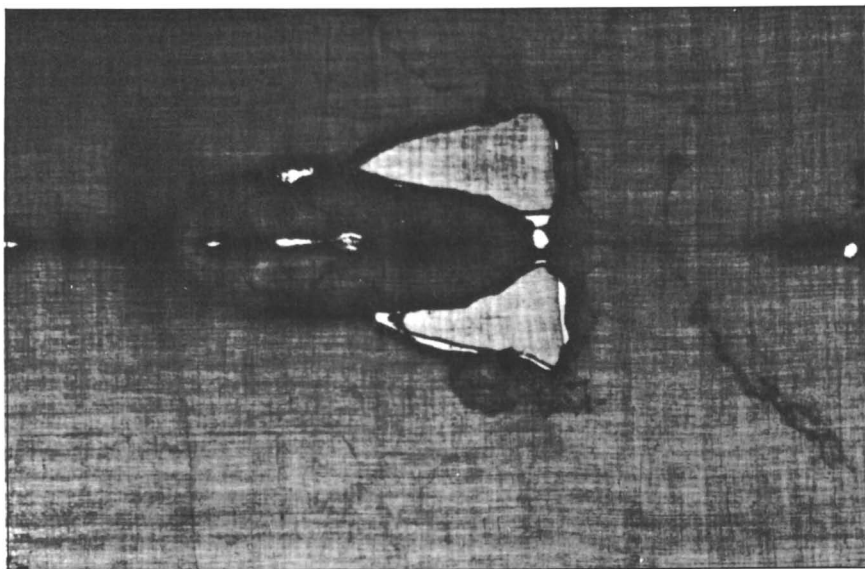


Figure 5. Transmission photograph of side-wound area.

showed up on the x-rays, while all the water marks were clearly visible. Further, the extensively darker appearance of the blood mark compared to the water stains in Figure 7 can be explained by the nature of porphyrin (heme) compounds, which are highly absorbing in the UV region. The point is that one need not look far to find inconsistencies in the painting hypothesis.

This kind of exercise is typical of many such exercises that can be performed; they tell us what the Shroud is not, but not what it is. In fact, Reference 16 is devoted to these kinds of exercises. Because we have not been able to propose a mechanism that explains all the characteristics of the Shroud, a viable hypothesis remains undiscovered. This is not to say that our findings have not led to some implications about the origin of the images.

First, the blood images present no mystery; all evidence suggests that the blood went on as one would expect for a cloth in contact with wounds or the normal secretions of such wounds. We therefore suggest that the blood images are the natural consequences of the linen being in contact with wounds.

If the blood images were made by contact with wounds, it follows that the cloth was used to enfold a body. We have independent evidence that the cloth was used in this way. The mapping function, which maps body-only image density to expected cloth-body distance and the two-dimensional placement of the image on the cloth, offers a consistent argument that the Shroud enfolded a human-body shape. If we couple this argument with the testimony of the forensic pathologists, we can say more: not only was it a human form, but further, it was a human body.

Because the yellow fibrils comprising the body-only image are confined to the uppermost portions of the threads of the cloth, mechanisms that would evidence migration by capillary action can be excluded. Our attempts to reproduce this surface quality of the image have been most successful with various catalyzed-decomposition contact mechanisms. Laboratory simulations (8) have produced very convincing results both in chemistry and appearance (*see* Figure 8).

The Shroud's mapping relationship, however, poses the strongest objection to a contact mechanism. Contact mechanisms have not been able to produce a convincing cloth-body distance relationship. In fact, taken alone, this mapping function seems to suggest some kind of "projection" mechanism, because there seems to be image present even where it does not appear to have been possible that the cloth was in contact with the body. We are left to identify what kind of "projection" mechanism, and this we have been unable to do. Simple molecular diffusion and "radiation" models, for example, fail to account for the apparent resolution of the image as we understand it.

Whatever the body-image production mechanism, it appears that it was prevented from acting by the presence of the blood/serum. This

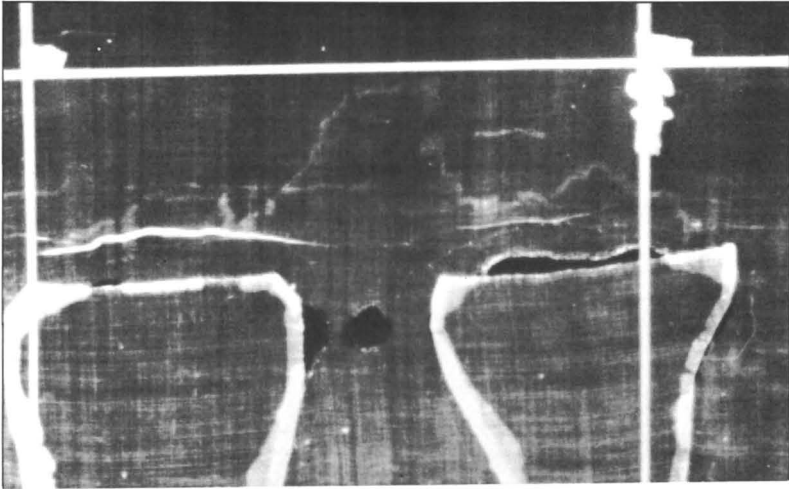


Figure 6A. x-Ray of side-wound area.

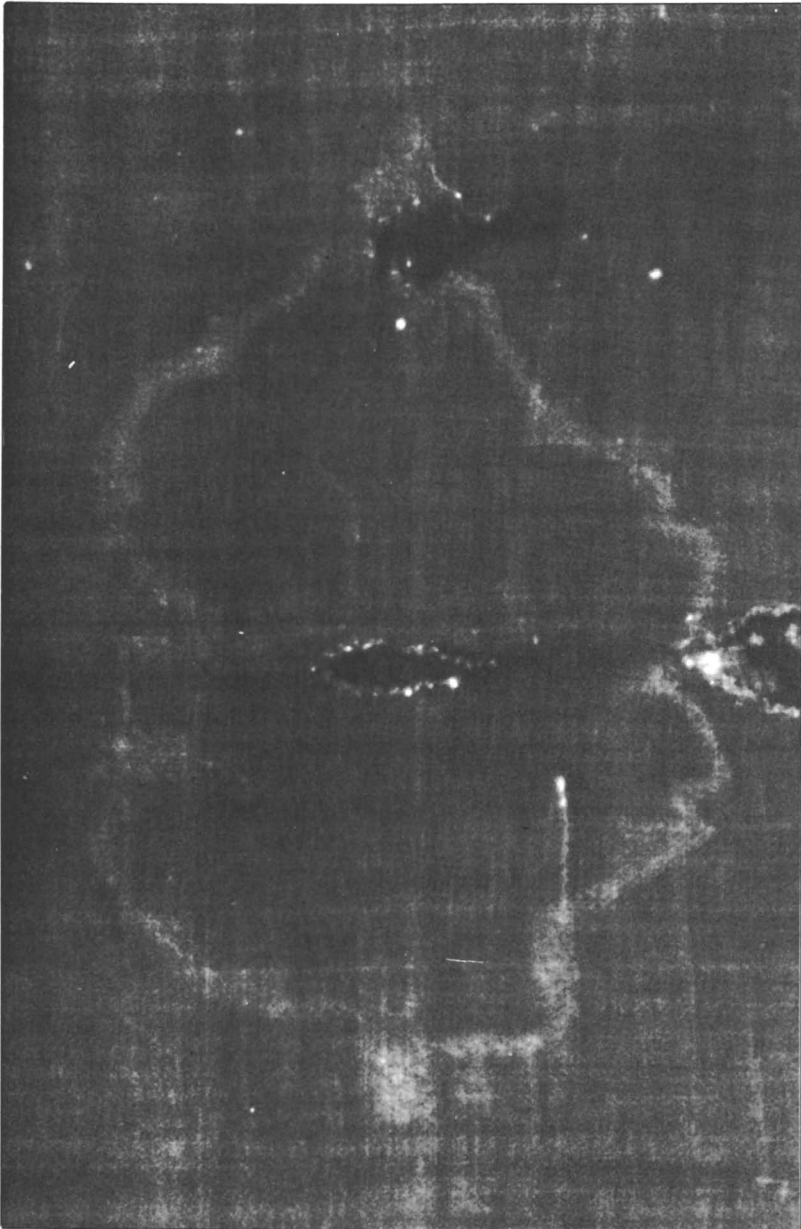


Figure 6B. Detail of left water stain.



Figure 6C. Detail of right water stain.

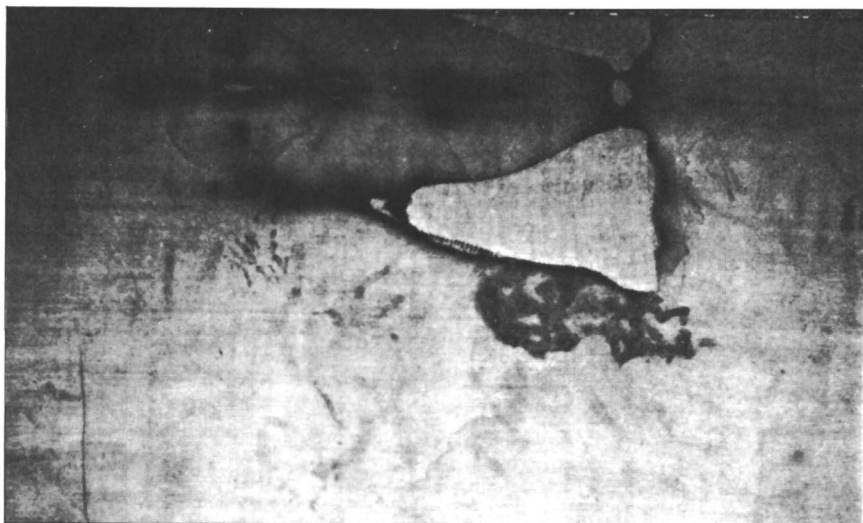


Figure 7. UV fluorescence photograph of side-wound area.

observation is suggested by both the presence of the “halo” around the heavy blood areas and the less degraded nature of the linen fibrils in the blood and serum areas.

We really do not have a satisfactory, simple explanation for how the body image got on the cloth. We think this fact is underscored by the fact that to our knowledge no other image on any cloth—grave cloth or art form—like the body image on the Shroud is known to exist today. If another example were to exist, our task of identifying the origin of the body image would be much simplified.

In the end, the question of the authenticity of the Shroud as the burial cloth of Jesus of Nazareth remains open-ended. We should all keep in mind that science is really not in a position to ever prove categorically that the Shroud is authentic (i. e., Jesus’ burial cloth). We have, however, examined the probability that the Shroud was artistically produced and find it improbable. The question is left so that those who wish to believe it authentic are not hindered with scientific objection to doing so. However, without proof of authenticity, those who choose to believe the Shroud is not authentic are also free to do so without scientific objection, provided they do not assert a production mechanism that is excluded by the information now available.

The case for carbon-14 dating of the Shroud now seems to be more critical than ever. If we had discovered categorical proof that the Shroud was the work of a clever forger, there would be no need to pursue the question further. Lacking such evidence, the Shroud should be put to this further test. With the advent of accelerator carbon dating methods, little enough sample need be sacrificed to put the Shroud to this test

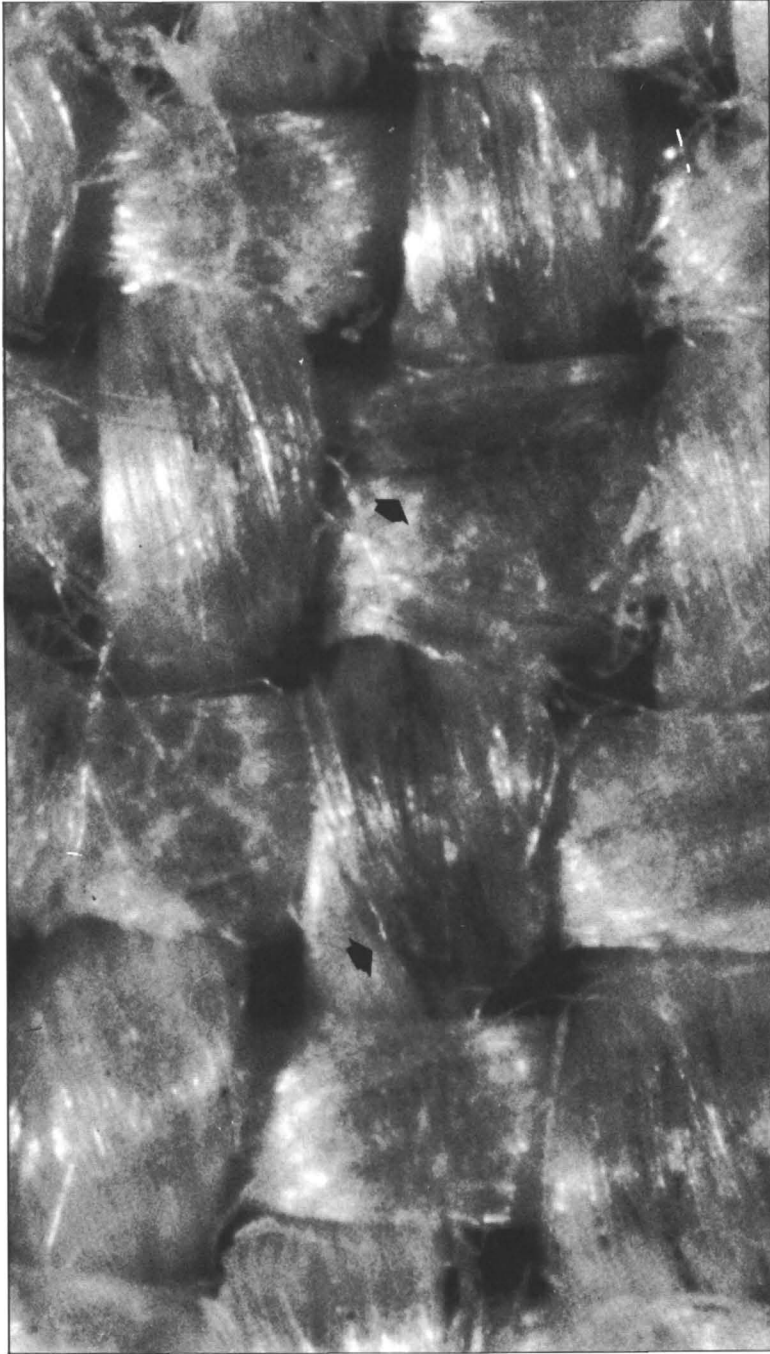


Figure 8. Photomicrograph of laboratory simulation by Pellicori (~40X). Arrows indicate placement of image on thread which matches Shroud body-only image.

(which if "negative," i.e., not first century, can prove lack of authenticity, but cannot prove authenticity).

Acknowledgments

We would like to acknowledge our indebtedness to Cardinal Ballestrero for allowing us access to the Shroud and to his knowledgeable and patient representative Luigi Gonella of the Turin Polytechnic for his kindness and support. Also, to all the members of STURP, too numerous to mention here, and to all those cooperating participants who were not directly involved in STURP, we acknowledge their part in this research. We owe a great deal of thanks also to the spouses of STURP members for their unending patience and understanding. Finally, to two silent members of STURP whose agonizing efforts made the scientific work possible through their management skills, we give special thanks to Thomas D'Muhala and George Markoski.

Literature Cited

1. Culliton, B. J. *Science* **1978**, *201*, 235–39.
2. Jumper, E. J.; Mottern, R. W. *Appl. Opt.* **1980**, *19*, 1909–12.
3. Morris, R. A.; Schwalbe, L. A.; London, J. R. *x-Ray Spectrom.* **1980**, *9*, 40–47.
4. Gilbert, R.; Gilbert M. M. *Appl. Opt.* **1980**, *19*, 1930–36.
5. Accetta, J. S.; Baumgart, J. S. *Appl. Opt.* **1980**, *19*, 1921–29.
6. Pellicori, S. F. *Appl. Opt.* **1980**, *19*, 1913–20.
7. Pellicori, S. F.; Evans, M. S. *Archaeology* **1981**, *34*, 34–43.
8. Pellicori, S. F.; Chandos, R. A. *Industrial Res./Dev.* **1981**, February, 186–89.
9. Mottern, R. W.; London, R. J.; Morris, R. A. *Mater. Eval.* **1980**, *38*(12), 39–44.
10. Miller, V. D.; Pellicori, S. F. *J. Biol. Photogr. Assoc.* **1981**, *49*, 71–85.
11. Heller, J. H.; Adler, A. D. *Appl. Opt.* **1980**, *19*, 2742–44.
12. Heller, J. H.; Adler, A. D. *Can. Soc. Forensic Sci. J.* **1981**, *14*, 81–103.
13. McCrone, W. C.; Skirius, C. *Microscope* **1980**, *28*, 105–14.
14. McCrone, W. C. *Microscope* **1980**, *28*, 115–28.
15. *Ibid.*, **1981**, *29*, 19–38.
16. Schwalbe, L. A.; Rogers, R. N. *Anal. Chim. Acta* **1982**, *135*, 3–49.
17. Jackson, J. P.; Jumper, E. J.; Ercoline, W. R. In *Proc. IEEE Int. Conf. Cybernetics Soc.*, Seattle, Wash.; 1982.
18. Ott, E.; Spurlin, H.; Grafflin, M. "Cellulose and Cellulose Derivatives"; Pts. I–III; Interscience: New York, 1954.
19. Pigman, W., Ed. "The Carbohydrates"; Academic: New York, 1967.
20. Weaver, K. F. *National Geographic* **1980**, *157*, 730–53.
21. Bucklin, R. In *Leg. Med. Annu.* **1981**.
22. Bollone, Pierluigi Baima. Private communication. Also c.f., *Sindon*, *30*, December 1981.
23. Wilson, I. "The Shroud of Turin"; Doubleday: New York, 1978.
24. Riggi, Giovanni. Private communication.

RECEIVED for review October 6, 1982. ACCEPTED for publication April 11, 1983.

AUTHOR INDEX

- Adler, Alan D., 447
Allen, Ralph, 3, 51
Allert, James, 273
Arie, Ana W., 193
Bimson, M., 215
Blackman, M. James, 19
Buikstra, Jane E., 97
Cabelli, Diane E., 243
Carriveau, Gary W., 395
Carter, Giles F., 311, 425
Charles, Douglas K., 97
Coatsworth, L. L., 295
Cowell, M. R., 215
Damon, P. E., 333
Davis, A. M., 79
Donahue, Douglas J., 333
Druzik, James R., 447
Fitzhugh, William, 3
Hamroush, Hany, 3, 51
Hancock, R. C. V., 79
Heller, John H., 447
Henrickson, Eiler, 273
Jackson, John P., 447
Jakes, Kathryn A., 403
Jull, A. J. T., 333
Jumper, Eric J., 447
Kronberg, B. I., 295
Lambert, Joseph B., 97
Lo, K. K. N., 133
Maggetti, Marino, 151
Mathews, Thomas F., 243
McKenna, P., 133
McLean, G., 133
McNeil, Roderick J., 255
Nagle, Christopher, 3
Olin, Jacqueline S., 151
Orna, Mary Virginia, O.S.U., 243
Ottaway, J. M., 133
Pellicori, Samuel F., 447
Perlman, I., 117
Rapp, George, Jr., 273
Sandoval, Beatriz, 193
Sibley, Lucy R., 403
Simpson, Sharon Vlasak, 97
Stimmell, C. A., 79
Taylor, R. E., 333
Tennent, N. H., 133
Tite, M. S., 215
Torres, Luis M., 193
Twilley, John W., 357
Usselman, M. C., 295
Westley, Harold, 151
Woods, William I., 67
Zabel, T. H., 333

SUBJECT INDEX

A

- Acacia* gum-yielding genera, 364, 382*t*-85*t*
Acacia senegal gum
 chromatograph of hydrolysate, 376*f*
 IR spectra, 374*f*
Accelerator mass spectrometry (AMS or
 HEMS), 338, 339
 basic principles, 338
 development, 337
 electrostatic accelerator systems, 339-45
 radiocarbon dating, 337-54
 samples for radiocarbon dating, 351-53
Albizia gum-yielding genera, 364, 385*t*,
 386*t*
Alkali oxides in Egyptian Blue, 219, 220
Amido black protein test, image on Shroud
 of Turin, 454, 461, 462
Amphibole
 in clay mixtures, 173, 174
 in volcanic clays, 173
Anogeissus gum-yielding genus, 366, 386*t*
Anogeissus latifolia gum, repeating
 unit, 372*f*
Antimony in copper sources, 290*t*
Aqua regia, W. H. Wollaston's
 preparation, 302, 304
Armenian manuscripts
 analysis of medieval pigments, 243-53
 description, 244, 246
Arsenic in copper sources, 287*t*
Artifact-source correlation, statistical
 analyses, 275-85

AUTHOR INDEX

- Adler, Alan D., 447
Allen, Ralph, 3, 51
Allert, James, 273
Arie, Ana W., 193
Bimson, M., 215
Blackman, M. James, 19
Buikstra, Jane E., 97
Cabelli, Diane E., 243
Carriveau, Gary W., 395
Carter, Giles F., 311, 425
Charles, Douglas K., 97
Coatsworth, L. L., 295
Cowell, M. R., 215
Damon, P. E., 333
Davis, A. M., 79
Donahue, Douglas J., 333
Druzik, James R., 447
Fitzhugh, William, 3
Hamroush, Hany, 3, 51
Hancock, R. C. V., 79
Heller, John H., 447
Henrickson, Eiler, 273
Jackson, John P., 447
Jakes, Kathryn A., 403
Jull, A. J. T., 333
Jumper, Eric J., 447
Kronberg, B. I., 295
Lambert, Joseph B., 97
Lo, K. K. N., 133
Maggetti, Marino, 151
Mathews, Thomas F., 243
McKenna, P., 133
McLean, G., 133
McNeil, Roderick J., 255
Nagle, Christopher, 3
Olin, Jacqueline S., 151
Orna, Mary Virginia, O.S.U., 243
Ottaway, J. M., 133
Pellicori, Samuel F., 447
Perlman, I., 117
Rapp, George, Jr., 273
Sandoval, Beatriz, 193
Sibley, Lucy R., 403
Simpson, Sharon Vlasak, 97
Stimmell, C. A., 79
Taylor, R. E., 333
Tennent, N. H., 133
Tite, M. S., 215
Torres, Luis M., 193
Twilley, John W., 357
Usselman, M. C., 295
Westley, Harold, 151
Woods, William I., 67
Zabel, T. H., 333

SUBJECT INDEX

A

- Acacia* gum-yielding genera, 364, 382*t*-85*t*
Acacia senegal gum
 chromatograph of hydrolysate, 376*f*
 IR spectra, 374*f*
Accelerator mass spectrometry (AMS or
 HEMS), 338, 339
 basic principles, 338
 development, 337
 electrostatic accelerator systems, 339-45
 radiocarbon dating, 337-54
 samples for radiocarbon dating, 351-53
Albizia gum-yielding genera, 364, 385*t*,
 386*t*
Alkali oxides in Egyptian Blue, 219, 220
Amido black protein test, image on Shroud
 of Turin, 454, 461, 462
Amphibole
 in clay mixtures, 173, 174
 in volcanic clays, 173
Anogeissus gum-yielding genus, 366, 386*t*
Anogeissus latifolia gum, repeating
 unit, 372*f*
Antimony in copper sources, 290*t*
Aqua regia, W. H. Wollaston's
 preparation, 302, 304
Armenian manuscripts
 analysis of medieval pigments, 243-53
 description, 244, 246
Arsenic in copper sources, 287*t*
Artifact-source correlation, statistical
 analyses, 275-85

Astragalus gum-yielding genus, 366, 386, 387*t*
 Atomic absorption spectrometry
 chemical interference, 136–38
 of Egyptian Blue, 216
 of medieval stained glass, 133–48
 Auger electrons, definition, 258
 Auger transitions, energies, 258–60
 Aztec majolica sherds, oxide
 concentrations, 192*t*, 193*t*

B

Bassora, 366, 368, 391*t*
 Beisamoun obsidian, provenance
 determination, 126
 Biogenesis of exudate
 polysaccharides, 360
 Black Earth site, soil analysis, 72–75
 Blood flow on Shroud of Turin, 460
 Blood image areas, description, Shroud of
 Turin, 460–62
 Blue glasses, composition, 146
 Bone, buried, effect on soil
 composition, 97–112
 Bone, radiocarbon dating by AMS, 351,
 352
 Brass, ancient glass colorant, 146, 147
 Bronze weapons, Shang Dynasty, silk
 pseudomorphs, 404–23
 Burial mound construction, 106, 107
 Burns on Shroud of Turin, 462

C

Cadmium in copper sources, 287*t*
 Calcitic matrix for majolica temper, 161
 Calcium
 and diet determination, 99, 111
 in Fine Orange ware, 205, 209*f*
 in soil and population estimation, 74
 Calcium analysis in soil, 69–74
 Calcium oxide in Egyptian Blue, 217*f*, 218
 Calcsilicates
 in clay mixtures, 173–76
 in majolica, 163, 164
 in marl, 172
 in volcanic clays, 173
 Caligulan coins, comparison with Claudian
 quadrantes, 317–20
 Castillo polychrome, majolica, oxide
 concentrations, 188*t*, 189*t*
 Centennial cluster composition
 comparisons, 285*t*
 Ceramic figurines, Fine Orange Maya,
 provenance determination, 193–211
 Ceramic sample analysis, Jomon, 93, 94
 Ceramic samples, ancient,
 description, 184*t*–86*t*
 Ceramics, fine paste, 198
 Ceramics, tin-glazed—*See* Majolica
 Cerium in copper sources, 288*t*
 Cesium in copper sources, 288*t*
 Champion cluster composition
 comparisons, 285*t*

Cherry gum, 366, 368, 391*t*
 Chlorine x-rays
 relative intensities, 443*t*
 transmittance through air, 442*t*
 Chromium in copper sources, 288*t*
 Chromopore formation from Shroud of
 Turin, 457*f*, 458
 Chronology of Eastern Terra Sigillata in
 Israel, 129, 130
 Cilician manuscripts
 12th and 13th centuries, palette, 248–50
 hue of pigments, 249*t*
 Clay composition, modern majolica
 production, 169, 170
 Clay majolica samples, description, 187*t*
 Clay mixture, mineralogical changes during
 firing, 175*f*, 177*f*
 Clay pretreatment, ancient Mexican
 majolica production, 171, 172
 Clay sources
 ancient Mexican majolica
 production, 171, 172
 Jonuta, 200, 201
 Cluster analysis
 artifact–source correlation, 275, 281–85
 obsidian source samples, 26–28
 parameters, 25*t*
 Cluster composition
 Illinois copper, 282*t*
 Snake River copper, 282*t*
 Cluster composition comparisons
 Champion and Centennial, 284*t*
 midwestern copper localities, 283*t*
 Clustering
 obsidian artifacts, 32*f*, 33*f*
 obsidian source samples, 33*f*
 Cobalt
 ancient glass colorant, 146, 147
 in copper sources, 287*t*
 in Egyptian Blue, 220
Cochlospermum gossypium gum, IR
 spectra, 374*f*
 Color evaluation of Egyptian Blue, 223,
 234, 235, 240*t*, 241*t*
 Colorants for ancient glasses, 146, 147
 Columbia Gun Metal majolica, 166
 oxide concentrations, 190*t*, 191*t*
 Columbia Plain majolica, oxide
 concentrations, 192*t*, 193*t*
Combretum gum-yielding genera, 388*t*
 Computer-assisted REE pattern
 recognition, 12, 13*t*
 Copper, ancient glass colorant, 146, 147
 Copper analysis in soil, 69–74
 Copper artifacts and sources, elemental
 concentration, 278
 Copper-based Roman coins, chemical
 compositions, 311–23
 Copper oxide in Egyptian Blue, 217*f*, 218
 Copper sources
 element concentration
 intervals, 287*t*–292*t*
 trace element discrimination, 273–92
 Correlation coefficients, Pearson, Fine
 Orange ceramic samples, 205, 207*t*

- Corrosion of metals and pseudomorph formation on bronze halberd, 419, 420
 Counting error, NAA, 122
 Cristobalite in volcanic clays, 173
 Cyclotron systems, radiocarbon dating, 338, 339

D

- Dandara sediments, 57
 Data base of trace element analyses, NAA, 275*t*
 Dating of manuscript inks
 intrasample error, 264
 by regression analysis, 266*f*
 by SAM, 255-69
 Decay counting for radiocarbon dating, 335, 336*t*
 Decomposition test, plant gums, 377*t*
 Dibeira-Jer formation sediments, 57
 Diet determination and strontium, 98, 111
 Diopside
 in clay mixtures, 173, 174
 in majolica sherds, 178
 Direct current plasma-optical emission spectrometry of majolica, 153-55
 Discriminant function in artifact-source correlation, 275-81
 Document preparation for SAM, 267
 Dorset culture and soapstone, 16

E

- Eastern Terra Sigillata, 128, 129
 elemental concentrations, 126*t*
 in Israel, provenance determination, 129-32
 Egyptian Blue
 analysis, 215-36
 color evaluation, 223, 234, 235, 240*t*, 241*t*
 elemental analyses, 240*t*
 glass phase, 228, 229
 hardness measurements, 223, 233, 234, 240*t*, 241*t*
 laboratory reproduction, 221-23
 manufacture, 216
 implications from analyses, 218-20
 microstructure, 222-34
 samples
 chemical compositions, 216-21, 240*t*, 241*t*
 description, 238*t*, 239*t*
 Electrostatic accelerator systems, radiocarbon dating, 339-45
 Element concentration intervals, copper source localities, 287*t*-292*t*
 Elemental analyses
 Egyptian Blue, 240*t*, 241*t*
 medieval stained glass, 141*t*
 Mexican majolica, 151-91
 obsidian artifacts, 23-26
 stained glass with flame AAS, 133-48
 stained glass standards, 139*t*, 140*t*

- Elemental compositions of Fine Orange ware, 206
 Elemental concentrations
 copper artifacts and sources, 278
 Eastern Terra Sigillata, 130*t*
 Hierakonpolis pottery, 60*t*
 Nile silts, 60*t*
 obsidian
 artifact and source groups, 34*t*
 artifacts samples, 46*t*-49*t*
 source samples, 42*t*-45*t*
 soil units, 88*t*
 Elgin Cathedral glass
 painted designs on fragments, 145*f*
 potash and magnesia levels, 146*f*
 "Emperor Jahangir Standing on a Globe Shooting Poverty," Mughal miniature, 359*f*
 Energy dispersive analysis of x-rays (EDAX) of pseudomorphs, 407-11
 Eskimo soapstone trade, 16
 Europium anomaly, 10, 60, 92
 Europium in copper sources, 288*t*
 Exudate polysaccharides, biogenesis, 360

F

- Fabric evidence from pseudomorphs, 416, 417
 Fabric pseudomorphism—*See* Pseudomorphism
 Fiber evidence from pseudomorphs, 413
 Fig Springs polychrome majolica, oxide concentrations, 188*t*-190*t*
 Fine Orange Maya ceramics
 archaeological background, 197-99
 figurines, 193-211
 sample preparation, 201, 204, 205
 Firing temperatures, ancient Mexican majolica production, 172-79
 Flame atomic absorption spectrometry of ceramic figurines, 193-211
 comparison with NAA, 208*t*, 210*f*
 Fleur de Lys soapstone quarry, 8, 10, 16-19
 Fort de Chartres 1 site, 68-72

G

- D-Galactose, structural isomers, 370*f*
 Gamma-ray interferences, 120*t*
 Gas chromatography, polysaccharide identification, 372, 373
 Gas-liquid chromatography
 plant gum monosaccharide identification, 380-82
 polysaccharide identification, 373, 375
 Gehlenite
 in clay mixtures, 173, 174
 in majolica sherds, 178
 Glass, ancient, colorants, 146, 147
 Glass fragments
 igmimbritic, 162*f*, 163*f*
 painted designs, 144*f*

- Glass-making, medieval, 142, 143, 147, 148
 Glass manufacture compared with
 Egyptian Blue manufacture, 218–20
 Glass phase in Egyptian Blue, 228, 229
 Glasshouse, 15th century Bohemian, 145f
 Glycosidic bond stability in plant
 gums, 371, 372
 Gold in copper sources, 287t
 Goldschmidt's rule, 7
 Göllü Dag obsidian source, 126
 samples, 23–49
 Gospel manuscripts, Cilician Armenian,
 description, 244, 246
 Grain size analysis of Nile silts, 57
 Gum arabic
 production, 360
 samples, 363f
 Gum nodule on acacia, 361f

H

- Hafnium in copper sources, 289t
 Halberd, bronze, Shang Dynasty, 406f
 description, 406f
 pseudomorph analysis, 407–11
 pseudomorph sample preparation, 407
 Hardness measurements of Egyptian
 Blue, 223, 233, 234, 240t, 241t
 Hassan Dag obsidian source
 samples, 23–49
 Hematite in majolica sherds, 176, 178
 Hierakonpolis, Predynastic Egyptian
 site, 52, 59f
 High energy mass spectrometry—*See*
 Accelerator mass spectrometry
 Hotnis Dag obsidian source
 samples, 23–49, 125, 126
 Houska Point copper artifacts, 280, 281
 Human activity
 and soil pH, 53, 54
 and soil phosphate, 53, 54

I

- Illinois copper, cluster composition, 282t
 Image on the Shroud of Turin, formation
 hypotheses, 427–31, 433, 435
 Indium in copper sources, 289t
 Inks, manuscript, 260
 SAM analytical methods, 260–64
 SAM dating, 255–69
 SAM profile, 261f
 spectrum from 1722 document, 259
 Ion migration, secondary, of manuscript
 ink, 255, 256
 IR spectroscopy, polysaccharide
 identification, 373, 374f
 Iridium in copper sources, 289t
 Iron, ancient glass colorant, 146, 147
 Iron in
 copper sources, 288t
 Fine Orange ware, 209f
 manuscript inks, 256, 257
 Nile silts, 60, 61

- Iron—*Continued*
 the Shroud of Turin, 439, 455,
 465–68
 soil, 69–74

J

- Jaina
 ceramic samples, 201–203
 figurines, internal correlation, 206–209
 geography and climate, 199
 Jomon
 ceramic sample analysis, 93, 94
 occupations, 80–82
 period of Japanese prehistory, 80–82
 Jonuta
 ceramic samples, 200–203
 geography and climate, 199

K

- K-means cluster analysis, copper
 artifact-source correlation, 281–85
 Kaferi Phase, 37, 38
 Karaya gum samples, 363f
 Khatchatur of Khizan, Cilician priest, 252
 Kuteera gum samples, 363f

L

- Lacquer, Oriental,
 analysis, 395–400
 history, 397–99
 uses, 396, 397
 Lake Sevan, obsidian source
 samples, 23–49
Lannea gum-yielding genus, 366, 390t
 Laser microprobe lacquer
 analysis, 399–400
 Leaching effects from buried
 bone, 99–110
 Lead, ancient glass colorant, 146, 147
 Linens exposed to x-rays, 438f
 Lithic artifacts, 3–5
 Lutecium in copper sources, 289t

M

- Magnesia in Elgin Cathedral glass, 146f
 Magnesium
 in Fine Orange ware, 209f
 in soil, 69–74
 Magnesium oxide in Egyptian Blue, 220,
 221f
 Majolica
 American, 166–68
 composition, comparison of
 techniques, 157t
 European, 165
 Mexican, provenance
 determination, 151–91
 Mexico City, 168, 176, 178
 oxide concentrations, 188t, 189t

Majolica—*Continued*

- modern, oxide concentration, 192*t*, 193*t*
- phase associations, 165*t*, 166*f*
- production, 152, 168, 169
 - ancient technique, 170–79
 - modern technique, 169, 170
- sample preparation, 153
- samples, modern, description, 187*t*
- sherds, 155, 158–63
 - classification, 167*t*
 - firing conditions from
 - mineralogy, 176–79
 - mineralogical composition, 165–68
 - oxide concentrations, 188*t*–193*t*
 - Plutonic temper, 163
 - sources, 152, 153
 - temper classification, 159–63
 - from Triana, Spain 192*t*, 193*t*
 - x-ray diffraction, 158, 163, 164
- Malachite in pseudomorphs on bronze weapons, 407–11
- Marl, mineralogical changes during firing, 174*f*, 177*f*
- Masmas formation, REE distributions, 61*f*
- Mass spectrometry and historical metallurgy, 295–309
- Maya ceramic figurines, provenance determination, 193–211
- Medieval pigments from Cilician Armenia, analysis, 243–53
- Mercury in copper sources, 289*t*
- Metallurgy, historical, and mass spectrometry, 295–309
- Microscopy, scanning auger, dating of manuscript inks, 255–69
- Microstructure of Egyptian Blue, 222–33
- Midden deposits, soil analysis, 72–75
- Middle Eastern obsidian
 - interlaboratory analyses
 - correlation, 28–31
 - provenance studies, 19–41
- Mineral composition
 - of majolica sherds, 165–68
 - and sedimentary units, 57–60
- Mineralogy of majolica sherds, 172–79
 - deduction of firing conditions, 176–79
- Miniature painting plant gum
 - medium, 357, 358
- Monosaccharides in plant gums, 368, 369
 - identification by gas-liquid chromatography, 380–82
 - identification by thin layer chromatography, 377–80
 - R_f values, 378*t*
- Montmorillonite
 - in clay mixtures, 173–76
 - in marl, 172
 - in volcanic clays, 173
- Mughal Indian miniatures, 357–60
- Mullite in volcanic clays, 173

N

- Nahal Lavan obsidian, provenance determination, 126

- Natron
 - definition, 220
 - in Egyptian Blue manufacture, 219, 220
- Nemrud Dag obsidian source
 - samples, 23–49
- Neronian coins, comparison with Claudian quadrantes, 317–20
- Neutron activation analysis
 - of ceramic figurines, 208*t*, 210*f*
 - data base, 275
 - of majolica, 153–55
 - for obsidian provenance, 123–26
 - of pottery, 117–22
 - of soapstone samples, 7–16
 - of soil, 87, 88*t*
 - uncertainty minimization, 122, 123
- Nickel in copper sources, 290*t*
- Nile silts, composition, 56–63
- Nitrogen analysis in soil, 69–74
- Nondestructive IR spectrophotometry
 - lacquer analysis, 399

O

- Obsidian
 - artifacts
 - and archaeological sites, 20–22
 - characterization, 22
 - comparison with sources, 126, 127
 - manufacture, 22
 - source assignments, 31–35
 - distribution patterns, 38, 39
 - exchange network, 36–39
 - from Iran, provenance, 19–41
 - provenance determination, 123–26
 - source sampling, 125*t*
 - Optical microscopy of majolica sherds, 155, 158–63
 - Organic carbon
 - in soil, 69–74, 83
 - and soil color, 86
 - Oriental lacquers, provenance studies, 398, 399
 - Oxide concentrations
 - of Fine Orange ware, 208
 - of majolica sherds, 188*t*–93*t*

P

- Palette of Cilician manuscripts, 12th and 13th centuries, 248–50, 253
 - and Armenian tradition, 251, 252
- Particle accelerators, radiocarbon dating, 333–154
- Particle size analysis in soil, 83
- Peabody Point soapstone, 13, 16*t*
- pH analysis in soil, 69–74, 83
- Phosphate in soil, 69–74
 - source, 53
- Phosphorus in medieval stained glass, AAS determination, 142
- Phosphorus in soil, 83
 - and allophane, 86
 - and population estimation, 74

- Pigments**
 in Chinese lacquered artifacts, 398
 in Cilician manuscripts, hue, 249*f*
 medieval, from Cilician Armenia,
 analysis, 243–53
 samples
 analysis, 247, 248
 hue and location, 248*f*
 preparation, 246, 247
See also Egyptian Blue
- Plagioclase**, 161–64
 in clay mixtures, 173–76
 in majolica sherds, 178
 in marl, 172
 in volcanic clays, 173
- Plant gum media**, chemical
 classification, 358*f*
- Plant gums**
 analytical techniques, 373, 375
 in artistic artifacts analysis, 357–82
 biogenesis, 360
 collection, 360, 362
 decomposition test, 377*f*
 geographical distribution, 362–68
 glycosidic bond stability, 371, 372
 historic uses, 358
 monosaccharides, 368, 269
 R_f values, 378*f*
 nomenclature, 358, 360
 polysaccharides in, 368–73
 sample analysis, 377–80
 sample preparations, 375, 377
- Platinum as a new noble metal**, 297, 298
- Platinum**
 alluvial, elemental composition, 299*f*
 hardness and malleability, 301
 historical availability, 295–309
 Knight's purification procedure
 elemental composition, 300*f*
 malleability, 298–301
 reconstruction, 306
 sample preparation, 306
 Wollaston's purification procedures
 elemental composition, 303*f*, 305*f*
 malleability, 295, 296, 301–19
 reconstruction, 306, 307
- Pleistocene bone**, radiocarbon dating, 352
- Plum Red ware**, untempered, 62, 63
- Plutonic temper** of majolica sherds, 163
- Polysaccharides in plant gums**, 369–73
 gas chromatography, 372, 373
 gas-liquid chromatography, 373, 375
 IR spectroscopy, 373, 374*f*
- Population parameters from soil**
 analysis, 72–75
- Portlandite**
 in clay mixtures, 173–76
 in marl, 172
 in volcanic clays, 173
- Potash glasses**, 143–45
- Potash level in Elgin Cathedral glass**, 146*f*
- Potassium**
 in Fine Orange ware, 209*f*
 in soil, 69–74
- Potassium oxide in Egyptian Blue**, 219,
 220
- Pottery**
 classification, 117–19
 cyprriot, provenance determination, 130,
 131
 manufacture at Hierakonpolis, 62
 neutron activation analysis, 117–22
 provenance determination,
 methodology, 119–23
 as source material, 130, 131
See also Plum Red ware, Untempered
 straw ware, and Eastern Terra
 Sigillata
- Pottery repertory**, 117–19
- Predynastic Period of Egypt**, 52
- Preform**, soapstone, 15, 16
- Protein testing**, image on Shroud of
 Turin, 454, 461, 462
- Provenance determination**, general
 requirements, 194, 195
- Provenance postulate**, 194
- Prunus* gum-yielding genus**, 366, 368, 391*f*
- Prunus persica* gum**, IR spectra, 374*f*
- Pseudomorph sample preparation**, 407
- Pseudomorph**
 background, 404, 405
 black, SEM, 409*f*
 silk
 mineralogical structure and
 composition, 407–11
 proposed formation, 417–22
 Shang Dynasty bronze
 weapons, 404–23
 textile fabric, definition, 403–23
- Pseudomorphism**, textile fabric, 403–23
- Puebla majolica**, 168, 178
 oxide concentrations, 188*f*, 189*f*
- Purification of platinum**, 296–98
- Pyroclastic deposits**, Oshima
 Peninsula, 83*f*
- Pyroxenes**, 161, 162
 in clay mixtures, 173, 174
 in majolica sherds, 178

Q

- Quadrantes**
 Augustan, chronology, 312
 background, 312, 313
 Claudian, 315*f*, 316*f*
 chemical compositions, 311–23,
 326*f*–328*f*
 chemical properties, 314–17
 physical properties, 313, 314,
 321*f*–325*f*
- Quarry-soapstone artifacts**
 correlation, 8–18
- Quartz**
 in clay mixtures, 173–76
 in majolica sherds, 178
 in marl, 172
 in volcanic clays, 173

R

- Radiocarbon dating**
 method development, 333–35

- Radiocarbon dating—*Continued*
 by particle accelerators, 333–54
 Sunnyvale skeleton, 343–45
 TAMS
 archaeological applications, 347–51
 range limitations, 348, 349
 sample size, 347, 348
- Radiocarbon measurements, third generation, 337, 338
- Rare earth element concentrations
 of soil units, 89–94
 in Yagi ceramics, 94*t*
- distribution
 in Nile silts, 61
 in soapstone, 7–8, 10*f*, 12*f*
 in Yagi soils, 91*f*, 93*f*
 in soapstone, 3–20
- Realgar, orange pigment, 252
- Red ink spectrum, 268
- Remote sensing of archaeological sites, 69–72
- Romita Sgraffito majolica, 168, 176
 oxide concentrations, 192*t*, 193*t*
- Ruthenium in copper sources, 290*t*
- S
- Sahaba formation
 REE distributions, 61*f*
 sediments, 57
- “St. Matthew, the Evangelist,” illuminated manuscript, 247
- Sample–source correlation, Fine Orange ware, 205–11
- San Elizano polychrome majolica, oxide concentrations, 188*t*, 189*t*
- Scandium in copper sources, 290*t*
- Scanning electron micrography (SAM) of pseudomorphs, 407–11
- Scanning photoacoustical microscopy lacquer analysis, 399
- Scorches on Shroud of Turin, 463
- Scourge marks on Shroud of Turin, 460
- Secondary ion migration of manuscript ink, 255, 256
- Sedimentary temper of majolica sherds, 159, 160*f*
- Sedimentary units
 identification, 56–63
 and stratigraphic studies, 54–56
- Sedimentological units of the Nile Valley, 63*t*
- Selenium in copper sources, 290*t*
- Sevilla White majolica, oxide concentrations, 190*t*, 191*t*
- Shang burial practices and pseudomorph formation on bronze halberd, 419
- Shroud of Turin
 background of cloth
 chemistry, 465, 466
 macroscopic characteristics, 464
 microscopic characteristics, 464, 465
 blood flow, 420
 blood images
 discussion, 467
- Shroud of Turin—*Continued*
 macroscopic characteristics, 458–60
 microscopic characteristics, 460–62
 body images
 discussion, 467
 macroscopic characteristics, 450–53
 microscopic characteristics, 453, 454
 yellow fibrils explanation, 454–58
 burns and scorches
 chemistry, 462, 463
 macroscopic characteristics, 462
 microscopic characteristics, 462
 dispersion of the image, 440–45
 facial images, 452*f*
 finger images, 431–33
 image description, 425, 427, 428, 448
 image formation and iron, 439, 440
 image formation hypotheses, 427–31
 mouth images, 433, 434*f*
 scourge marks, 460
 side-wound area, 469*f*, 471*f*, 474*f*
 vertical striations, 440
 water marks
 chemistry, 463
 macroscopic characteristics, 463
 microscopic characteristics, 463
 water stains, 472*f*, 473*f*
 wound images, 459, 460
 x-ray hypothesis for image formation, 433–46
- Silica in Egyptian Blue, 217*f*, 218
- Siliceous matrix for majolica temper, 162, 163
- Silicon x-rays
 relative intensities, 443*t*
 transmittance through air, 442*t*
- Silk decay and pseudomorph formation on bronze halberd, 420–22
- Silver in copper sources, 287*t*
- Smalt, blue pigment, 252
- Snake River copper, cluster composition, 282*t*
- Snake River fingerprint copper source, 278–80
- Soapstone
 artifacts, manufacture, 16
 outcrops, Labrador coast, 3
 INAA data, 9*t*
 sampling, 4
 structure, 4
 utilization and procurement, REE analysis, 3–20
- Sodium oxide in Egyptian Blue, 219–21
- Soil
 analysis
 for burials, 101*t*–105*t*
 F-test for burials, 100, 106–108
 in Illinois, 67–76
 in Japan, 79–95
 of Predynastic Egypt, 51–63
 and site boundary detection, 70–72
 and stratigraphic studies, 54
 from Woodland burials, 97–112
 color and organic carbon, 86
 composition and buried bone, 97–112
 pH and human activity, 53, 54

- Soil—*Continued*
 phosphate and human activity, 53, 54
 sample preparation, 69*t*, 87, 99
 unit classification and element concentrations, 87, 89
- Source material, pottery as, 130, 131
- Spatial distribution, image on Shroud of Turin, 451, 453
- Stained glass
 fragments, 143*f*
 medieval, flame AAS analysis, 133–48
 sample dissolution, 137
 sample preparation, 135, 136
- Standards for majolica analysis, 153, 154
 composition, 152*f*
- Standards for stained glass analysis, 135, 138–40
- Statistical analyses, 273–83
- Sterculia* gum-yielding genus, 368, 392*t*
- Stratigraphic studies and soil analysis, 54
- Stratigraphy, archaeological vs.
 pedological, 84, 85
- Straw tempered ware, 62
- Strontium and diet determination, 98, 111
- Sunnyvale skeleton, radiocarbon dating, 343–45
- Suphan Dag obsidian source samples, 23–49
- T**
- Tal-e Malyan
 archaeological site, 20, 35–39
 obsidian artifact-to-source assignments, 35*t*
- Tandem accelerator mass spectrometry (TAMS), 341*f*, 342*f*
 ion source, 340
 operating conditions, 346
 radiocarbon dating measurement procedure, 343
 radiocarbon dating of Sunnyvale skeleton, 343–45
- Tandem electrostatic accelerators, 339, 340
- Tantalum in copper sources, 291*t*
- Tellurium in copper sources, 291*t*
- Temper classification of majolic sherds, 159–63
- Tepe Yahya
 archaeological site, 20–22, 35–39
 obsidian artifact-to-source assignments, 35*t*
- Terminalia* gum-yielding genera, 393*t*
- Textile fabric pseudomorphism—*See* Pseudomorphism
- Textile fabrics, pseudomorphs as evidence, 410–17
- Textile usage by early peoples, 403, 404
- Thermography of image on Shroud of Turin, 453
- Thin layer chromatography, plant gum monosaccharide identification, 377–80
- Thorium in copper sources, 291*t*
- Tiberian coins, comparison with Claudian quadrantes, 317–20
- Tin
 as ancient glass colorant, 146, 147
 in copper sources, 291*t*
 in Egyptian Blue, 218, 219
- Trace element discrimination, copper sources, 273–92
- Trace elements
 in Nile silts, 60–62
 in rocks and minerals, 273, 274
- Tungsten in copper sources, 291*t*
- Turin, Shroud—*See* Shroud of Turin
- U**
- Ultramarine in Cilician palette, 251
- Uronic acid in plant gum solutions, 370, 371, 375
- Urushi*, raw lacquer, 396–99
- V**
- Valle Ware majolica, 168, 171, 176
 oxide concentrations, 190*t*–193*t*
- Vellum surface, letter “O” from 1722 document, 256*f*–258*f*
- Volcanic clay, mineralogical changes during firing, 174*f*, 177*f*
- Volcanic episodes during Jomon occupations, 82
- Volcanic temper of majolica sherds, 159–63
- W**
- Water marks on Shroud of Turin, 463
- Water stains on Shroud of Turin, 472*f*, 473*f*
- Weathering of minerals and pseudomorph formation on bronze halberd, 419, 420
- Wollaston, William Hyde, platinum production, 295–309
- Wollastonite in majolica sherds, 178
- Wound images on Shroud of Turin, 459, 460
- Writing supports, regression plot, 265
- X**
- X-ray diffraction
 majolica sherds, 158, 163, 164
 pseudomorphs, 409–11
- X-ray fluorescence analysis
 lacquer, 399
 Shroud of Turin, 453
- X-ray images, experimental formation, 435–39
- X-ray sources, image formation on Shroud of Turin, 445
- X-ray transmittance
 by copper coins, 313*t*

X-ray transmittance—*Continued*

- elements
- through air, 435*t*
- through cellulose, 436*t*
- silicon and chlorine
- through air, 442
- relative intensities, 442

Y

- Yagi ceramics, REE concentrations, 94*t*
- Yagi site
- description, 80-82
- soil description, 84-87

Yarn evidence from

- pseudomorphs, 414-16
- Yayal blue-on-white majolica, oxide
- concentrations, 192*t*, 193*t*
- Yellow fibrils in Shroud of Turin, 450, 451, 453-62
- Ytterbium in copper sources, 292*t*

Z

Zinc

- as ancient glass colorant, 146, 147
- in copper sources, 292*t*
- in Fine Orange ware, 205
- in soil, 69-74